frontiers | Research Topics

New numerical and analytical methods for nonlinear partial differential equations with applications in quantum physics

Edited by
Mustafa Inc, Xiao-Jun Yang and Devendra Kumar

Published in
Frontiers in Physics
Frontiers in Applied Mathematics and Statistics

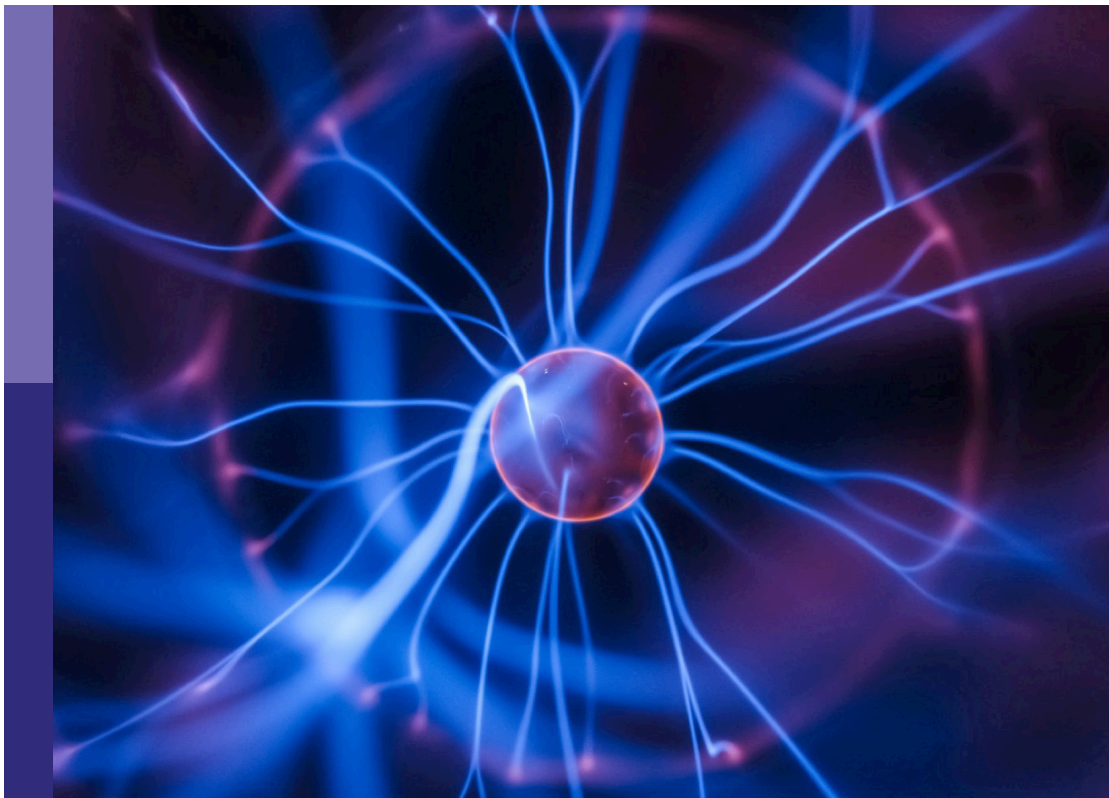

ISSN 1664-8714
ISBN 978-2-8325-3943-9
DOI 10.3389/978-2-8325-3943-9

About Frontiers

Frontiers is more than just an open access publisher of scholarly articles: it is a pioneering approach to the world of academia, radically improving the way scholarly research is managed. The grand vision of Frontiers is a world where all people have an equal opportunity to seek, share and generate knowledge. Frontiers provides immediate and permanent online open access to all its publications, but this alone is not enough to realize our grand goals.

Frontiers journal series

The Frontiers journal series is a multi-tier and interdisciplinary set of open-access, online journals, promising a paradigm shift from the current review, selection and dissemination processes in academic publishing. All Frontiers journals are driven by researchers for researchers; therefore, they constitute a service to the scholarly community. At the same time, the *Frontiers journal series* operates on a revolutionary invention, the tiered publishing system, initially addressing specific communities of scholars, and gradually climbing up to broader public understanding, thus serving the interests of the lay society, too.

Dedication to quality

Each Frontiers article is a landmark of the highest quality, thanks to genuinely collaborative interactions between authors and review editors, who include some of the world's best academicians. Research must be certified by peers before entering a stream of knowledge that may eventually reach the public - and shape society; therefore, Frontiers only applies the most rigorous and unbiased reviews. Frontiers revolutionizes research publishing by freely delivering the most outstanding research, evaluated with no bias from both the academic and social point of view. By applying the most advanced information technologies, Frontiers is catapulting scholarly publishing into a new generation.

What are Frontiers Research Topics?

Frontiers Research Topics are very popular trademarks of the *Frontiers journals series*: they are collections of at least ten articles, all centered on a particular subject. With their unique mix of varied contributions from Original Research to Review Articles, Frontiers Research Topics unify the most influential researchers, the latest key findings and historical advances in a hot research area.

Find out more on how to host your own Frontiers Research Topic or contribute to one as an author by contacting the Frontiers editorial office: frontiersin.org/about/contact

New numerical and analytical methods for nonlinear partial differential equations with applications in quantum physics

Topic editors

Mustafa Inc — Firat University, Türkiye

Xiao-Jun Yang — China University of Mining and Technology, China

Devendra Kumar — University of Rajasthan, India

Citation

Inc, M., Yang, X.-J., Kumar, D., eds. (2023). *New numerical and analytical methods for nonlinear partial differential equations with applications in quantum physics*. Lausanne: Frontiers Media SA. doi: 10.3389/978-2-8325-3943-9

Table of contents

frontiers in Physics

ORIGINAL RESEARCH
published: 21 November 2019
doi: 10.3389/fphy.2019.00197

Complex and Real Optical Soliton Properties of the Paraxial Non-linear Schrödinger Equation in Kerr Media With M-Fractional

Wei Gao[1]*, *Hajar F. Ismael*[2,3], *Sizar A. Mohammed*[4], *Haci Mehmet Baskonus*[5] and *Hasan Bulut*[3]

[1] School of Information Science and Technology, Yunnan Normal University, Kunming, China, [2] Department of Mathematics, Faculty of Science, University of Zakho, Zakho, Iraq, [3] Department of Mathematics, Faculty of Science, Firat University, Elâzig, Turkey, [4] Department of Mathematics, College of Basic Education, University of Duhok, Duhok, Iraq, [5] Department of Mathematics and Science Education, Harran University, Sanliurfa, Turkey

In this paper, we use the modified exponential function method in terms of $K^{f(x)}$ instead of $e^{f(x)}$and the extended sinh-Gordon method to find some new family solution of the M-fractional paraxial non-linear Schrödinger equation. The novel complex and real optical soliton solutions are plotted in 2-D, 3-D with a contour plot. Moreover, the dark exact solutions, singular soliton solutions, kink-type soliton solution, and periodic dark-singular soliton solutions for M-fractional paraxial non-linear Schrödinger equation are constructed. We guarantee that all solutions are new and verified the main equation of the M-fractional paraxial wave equation. For existence, the constraint condition is also added.

Keywords: paraxial wave equation, complex soliton, extended sinh-Gordon method, soliton structures, contour surfaces

OPEN ACCESS

Edited by:
Xiao-Jun Yang,
China University of Mining and Technology, China

Reviewed by:
Zakia Hammouch,
Moulay Ismail University, Morocco
Carlo Cattani,
Università degli Studi della Tuscia, Italy

***Correspondence:**
Wei Gao
gaowei@ynnu.edu.cn

Specialty section:
This article was submitted to Mathematical Physics, a section of the journal Frontiers in Physics

Received: *21 September 2019*
Accepted: *06 November 2019*
Published: *21 November 2019*

Citation:
Gao W, Ismael HF, Mohammed SA, Baskonus HM and Bulut H (2019) Complex and Real Optical Soliton Properties of the Paraxial Non-linear Schrödinger Equation in Kerr Media With M-Fractional. Front. Phys. 7:197. doi: 10.3389/fphy.2019.00197

INTRODUCTION

The breaking up and moving away from ultrashort pulses of a field related to electricity-producing magnetic fields or radiation into a medium is a multidimensional important physical phenomenon. The interaction between different physical procedures such as breaking up/spreading out, material breaking up or spreading out, diffraction, and non-linear response affects the pulse patterns of relationships, movement, or sound. According to the interaction of breaking up or spreading out, diffraction and non-linearity, a non-dispersive, and non-diffractive wave packet called soliton is created. Solitons have many uses in optical microscopy, optical information storage, laser caused particle increasing speed, Bose-Einstein (a liquid that forms from a gas/change from gas to liquid), and bright and sharp signal transmission.

In the research papers, researchers have been noted several computational methods for solving NPDEs, building separate solitons, and other alternatives for distinct types of NPDEs such as, the Haar wavelet method [1], the homotopy perturbation method [2], the Adomian decomposition method [3, 4], the shooting method [5–8], the sine-Gordon expansion method [9–12], the inverse scattering method [13], the sinh-Gordon expansion method [14–16], the $\tan(\phi(\xi)/2)$-expansion method [17, 18], the inverse mapping method [19], modified $\exp(-\varphi(\xi))$-expansion function method [20–23], the decomposition-Sumudu-like-integral-transform method [24], a functional variable method [25], the Bernoulli sub-equation function method [26–28], modified exponential function method [29], the modified auxiliary expansion method [30], the Riccati-Bernoulli sub-ODE method [31], the extended trial equation method [32, 33], and tanh function method [34, 35].

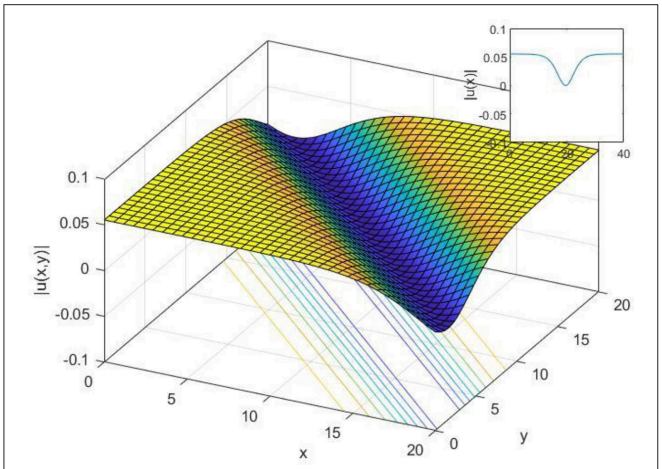

FIGURE 1 | 2-D, 3-D, and contour plot of dark soliton solution Equation (20) when $\lambda = 3, \mu = 2, \beta = 0.6, \alpha = 0.9, \varepsilon = 0.2, c = 0.3, t = 2, \gamma = 3$ and $z = 2$ for 2-D.

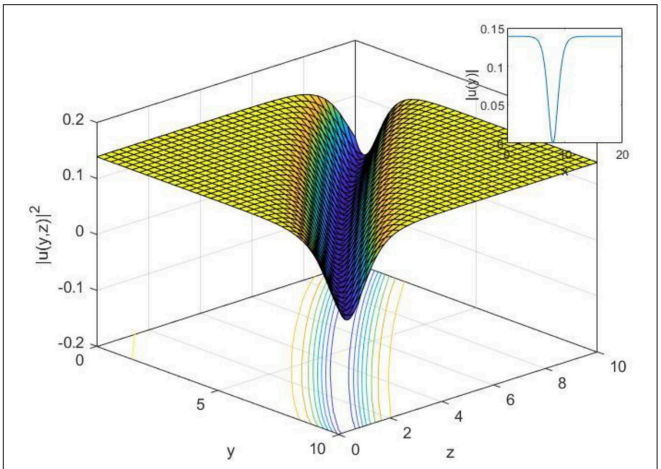

FIGURE 3 | 2-D, 3-D, and contour plot of dark soliton solution Equation (22) when $\lambda = 3, \mu = 1, \beta = 0.1, \alpha = 0.9, \varepsilon = 0.2, c = 0.3, t = 2, \gamma = 3$, $a_0 = 1, b_0 = 2$ and $z = 2$ for 2-D.

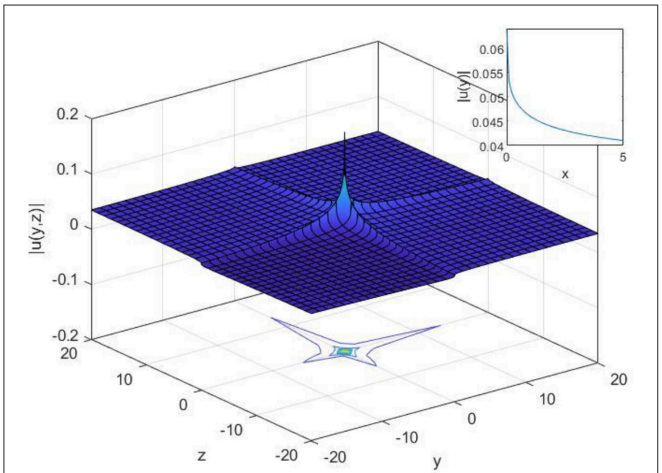

FIGURE 2 | 2-D, 3-D, and contour plot of singular soliton solution Equation (21) when $\lambda = 0.3, \mu = 0, \beta = 0.6, \alpha = 1/3, \varepsilon = 2, c = -0.3, t = 2, \gamma = 3$ and $z = 2$ for 2-D.

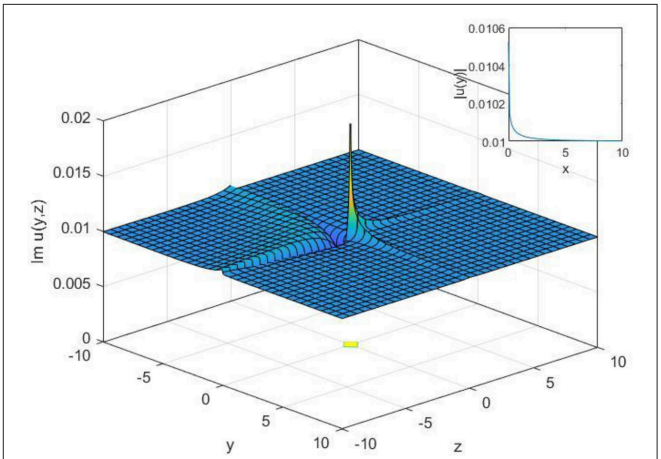

FIGURE 4 | 2-D, 3-D, and contour plot of singular soliton solution Equation (23) when $\lambda = 1, \mu = 0, \beta = 0.6, \alpha = \frac{1}{3}, \varepsilon = 2, c = 0.3, t = 2, \gamma = 0.3$, $a_0 = 0.1, b_0 = 1$ and $z = 2$ for 2-D.

Also, different methods have been used to solve fractional differential equation such as, the finite difference method [36], the improved Adams–Bashforth algorithm [37, 38], Adams-Bashforth-Moulton method [39], the extended fractional sinh-Gordon expansion method [40], the Laplace transforms [41], the q-homotopy analysis transform method [42], local fractional series expansion method [43], the wavelets method [44], Local fractional homotopy perturbation method [45], and many other techniques [46, 47].

In this paper, we will construct some new complex and real soliton solutions of M-fractional paraxial non-linear Schrödinger equation in Kerr media by using a modified expansion function method as well as by the extended sinh-Gordon method. Over the previous two centuries, the field of fractional calculus has drawn many researchers' attention. They are used for modeling multiple non-linear features such as biological procedures, fluid mechanics, chemical processes, etc. Fractional order partial differential equations serve as the generalization of partial differential equations in the classical integer-order. The literature contains several definitions of fractional derivatives, such as the Hadamard derivative (1892) [48], the Weyl derivative [49], Caputo, Riesz derivative [50], Riemann-Liouville, Grunwald-Letnikov definitions, Atangana-Baleanu derivative in the context of Caputo, Atangana-Baleanu fractional derivative in the context of Riemann-Liouville [51, 52], Erdelyi-Kober [53], and the conformable fractional derivative [54]. Atangana et al. provided the conformable fractional derivative with some new characteristics [55]. Sousa and Oliveira in [56] have recently been created the new truncated M-fractional derivative.

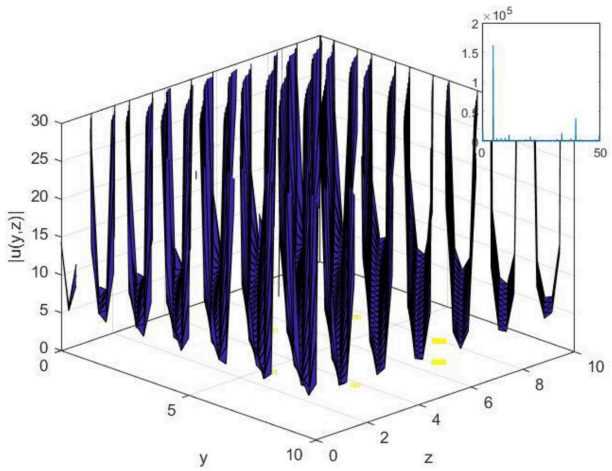

FIGURE 5 | 2-D, 3-D, and contour plot of periodic singular soliton solution Equation (24) when $\lambda = 0.1, \mu = 0.3, \beta = 0.6, \alpha = 0.9, \varepsilon = 0.1, c = 0.3, t = 2, \gamma = 0.3, a_0 = 0.5, b_1 = 0.2$ and $z = 2$ for 2-D.

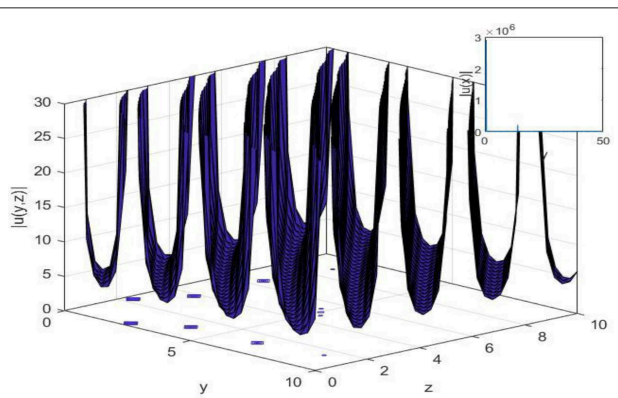

FIGURE 6 | 2-D, 3-D, and contour plot of periodic singular soliton solution Equation (25) when $\lambda = 1, \mu = 1, \beta = 0.6, \alpha = 0.9, \varepsilon = 0.1, c = 3, t = 2, \gamma = 3a_0 = 0.5, b_0 = 0.2$ and $z = 2$ for 2-D.

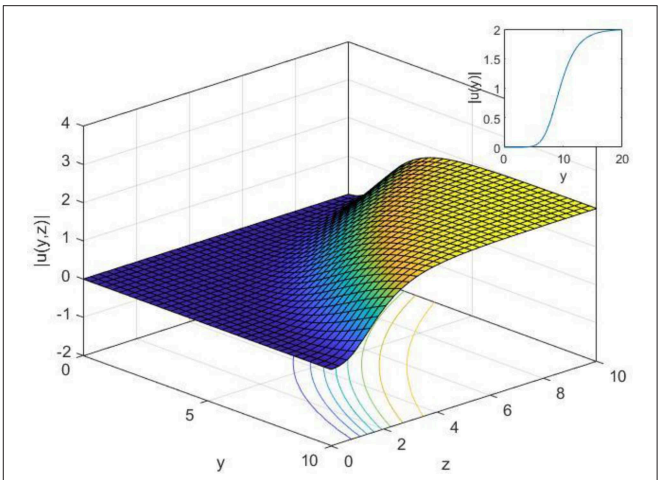

FIGURE 7 | 2-D, 3-D, and contour plot of Equation (27), when $t = 2, c = 3, \gamma = 2, \alpha = 0.5, \beta = 0.6$ and $z = 2$ for 2-D.

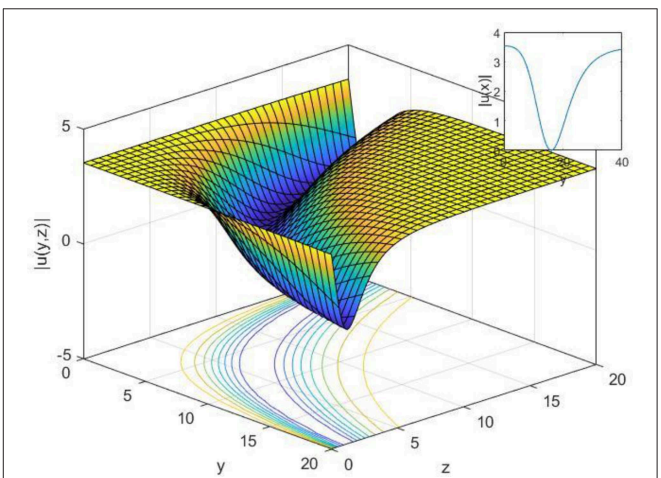

FIGURE 8 | 2-D, 3-D, and contour plot of Equation (28), when $t = 2, c = 3, \gamma = 0.2, \alpha = \frac{1}{3}, \beta = 0.6$ and $z = 2$ for 2-D.

THE TRUNCATED M-FRACTIONAL DERIVATIVE

In this section, we give some definitions, theorems, and properties of the truncated M-fractional derivative of order α.

Definition 1. If the function $f : (0, \infty) \to \mathbb{R}$, then, the new truncated M-fractional derivative of function of order α is defined as,

$$D_M^{\alpha,\beta} f(t) = \lim_{\varepsilon \to 0} \frac{f\left(t\epsilon_\beta\left(\varepsilon t^{1-\alpha}\right)\right) - f(t)}{\varepsilon}, \quad \text{for all } t > 0,\ 0 < \alpha \leq 1,\ \beta > 0,$$

where $\epsilon_\beta(.)$ is a truncated Mittag-Leffler function of one parameter [56].

Theorem 1. Let $\alpha \in (0, 1]$, $\beta > 0$ and $f = f(t), g = g(t)$ be α-differentiable at a point $t > 0$, then:

I $D_M^{\alpha,\beta}(af + bg) = aD_M^{\alpha,\beta} f + bD_M^{\alpha,\beta} g$, for all $a, b \in \mathbb{R}$.

II $D_M^{\alpha,\beta}(c) = 0$, for all $c \in \mathbb{R}$.

III $D_M^{\alpha,\beta}(f.g) = gD_M^{\alpha,\beta}(f) + fD_M^{\alpha,\beta}(g)$.

IV $D_M^{\alpha,\beta}\left(\frac{f}{g}\right) = \frac{gD_M^{\alpha,\beta}(f) - fD_M^{\alpha,\beta}(g)}{g^2}$.

Furthermore; if the function f is a differentiable function; then $D_M^{\alpha,\beta}(f(t)) = \frac{t^{1-\alpha}}{\Gamma(\beta+1)} \frac{df}{dt}$.

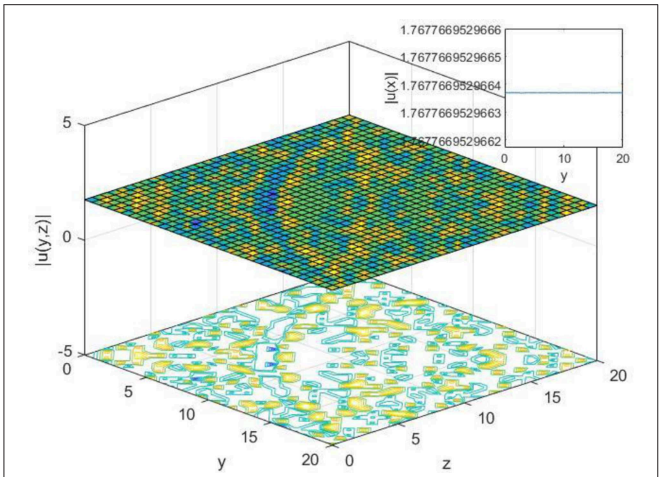

FIGURE 9 | 2-D, 3-D, and contour plot of Equation (29), when $t = 2, c = 0.3$, $\gamma = 0.2, \alpha = 0.5, \beta = 0.6$ and $z = 2$ for 2-D.

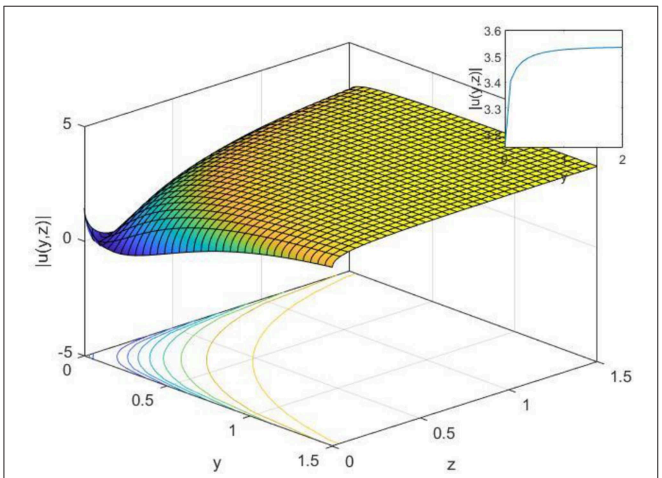

FIGURE 10 | 2-D, 3-D, and contour plot of Equation (30), when $t = 2, c = 0.3$, $\gamma = 0.2, \alpha = 0.5, \beta = 0.6$ and $z = 2$ for 2-D.

GENERAL FORM OF METHODS

Modified Expansion Function Method

Step 1. Suppose that, we have the following non-linear partial differential equation (NLPDE)

$$P\left(u, D_{M,x}^{\alpha,\beta}u, u^2 D_{M,x}^{\alpha,\beta}u, D_{M,t}^{\alpha,\beta}u, D_{M,t}^{2\alpha,\beta}u, \ldots\right) = 0. \tag{1}$$

To find explicit exact solutions of Equation (1), we use the following transformation

$$u\left(x, y, t\right) = U\left(\xi\right), \xi = \frac{\Gamma\left(\beta+1\right)}{\alpha}\left(x^{\alpha} - \nu\, t^{\alpha}\right), \tag{2}$$

where ν is arbitrary constant and ξ is the symbol of the wave variable. Substituting Equation (2) to Equation (1), the result is a non-linear ordinary differential equation (NLODE) as follow

$$N\left(U, U^2, U', U'', \ldots\right) = 0. \tag{3}$$

Step 2. Now the trial equation of solution for Equation (3) is defined a

$$U\left(\xi\right) = \frac{\sum_{i=1}^{n} a_i\left(K^{-i\Phi(\xi)}\right)^i}{\sum_{j=1}^{m} b_i\left(K^{-\Phi(\xi)}\right)^j} = \frac{a_0 + a_1 K^{-\phi(\xi)} + a_2 K^{-2\phi(\xi)} + \ldots + a_n K^{-n\phi(\xi)}}{b_0 + b_1 K^{-\phi(\xi)} + b_2 K^{-2\phi(\xi)} + \ldots + b_n K^{-m\phi(\xi)}}, \tag{4}$$

where a_i and b_i, $\left(0 \le i \le n, 0 \le j \le m\right)$ are non-zero constants and $\Phi\left(\xi\right)$ is the auxiliary ODE given by

$$\Phi'\left(\xi\right) = \frac{K^{-\Phi(\xi)} + \mu\, K^{\Phi(\xi)} + \lambda}{\ln\left(K\right)}, \tag{5}$$

where μ, λ are constants and $K > 0$, $K \neq 1$. The auxiliary ODE has the general solution as follows:

I When $\lambda^2 - 4\mu > 0$, then $f\left(\xi\right) = \log_K\left(-\lambda - \sqrt{\lambda^2 - 4\mu}\tanh\left(\frac{1}{2}\sqrt{\lambda^2 - 4\mu}\left(\xi + \varepsilon\right)\right)\right)$.

II When $\lambda^2 - 4\mu < 0$, then $f\left(\xi\right) = \log_K\left(-\lambda + \sqrt{-\lambda^2 + 4\mu}\tan\left(\frac{1}{2}\sqrt{-\lambda^2 + 4\mu}\left(\xi + \varepsilon\right)\right)\right)$.

III When $\lambda^2 - 4\mu > 0$ and $\mu = 0$, then $f\left(\xi\right) = \log_K\left(\frac{\lambda}{-1+\cosh(\lambda(\xi+\varepsilon))+\sinh(\lambda(\xi+\varepsilon))}\right)$.

IV When $\lambda^2 - 4\mu = 0, \lambda \neq 0$ and $\mu \neq 0$, then $f\left(\xi\right) = \log_K\left(\frac{-2-\lambda(\xi+\varepsilon)}{2\mu(\xi+\varepsilon)}\right)$.

V When $\lambda^2 - 4\mu = 0, \lambda = 0$ and $\mu = 0$, then $f\left(\xi\right) = \log_K\left(\xi + \varepsilon\right)$.

Extended Sinh-Gordon Expansion Method

Step 1. The same structure of step 1 of MEFM is valid.

Step 2. The trial solution of Equation (3) is expressed in the form [19],

$$U\left(w\right) = \sum_{i=1}^{n}\left[b_i \sinh\left(w\right) + a_i \cosh\left(w\right)\right]^i + a_0, \tag{6}$$

where $a_0, a_i, b_i\ (i = 1, 2, \cdots, n)$ are constants and to find it's value later, w is a function of ξ that satisfies the following equation

$$w' = \sinh\left(w\right). \tag{7}$$

The solution of Equation (7) possess the following solutions

$$\sinh\left(w\left(\xi\right)\right) = \pm\,\mathrm{csch}\left(\xi\right) \text{ or } \sinh\left(w\left(\xi\right)\right) = \pm i\,\mathrm{sech}\left(\xi\right), \tag{8}$$

and

$$\cosh\left(w\left(\xi\right)\right) = \pm\coth\left(\xi\right) \text{ or } \cosh\left(w\left(\xi\right)\right) = \pm\tanh\left(\xi\right), \tag{9}$$

where $i = \sqrt{-1}$.

Step 3. By putting Equation (7) and the derivatives of Equation (6) into Equation (3), we obtain a polynomial equation in $w'^l \sinh^i\left(w\right)\cosh^j\left(w\right)\left(l = 0, 1 \text{ and } i, j = 0, 1, 2, \ldots\right)$. As the

result the obtained non-linear algebraic equations by equating the coefficients of $w'^{l}\sinh^{i}(w)\cosh^{j}(w)$ to zero, we can find the coefficients.

Step 4. Using Equation (9) and Equation (10), we get the following solutions of Equation (1)

$$U(\xi)=\sum_{i=1}^{n}\left[\pm b_i\,\mathrm{sech}(\xi)\pm a_i\tanh(\xi)\right]^{i}+a_0, \tag{10}$$

$$U(\xi)=\sum_{i=1}^{n}\left[\pm ib_i\,\mathrm{csch}(\xi)\pm a_i\coth(\xi)\right]^{i}+a_0, \tag{11}$$

where the value of n will finds by using the principal homogeneous balance.

GOVERNING EQUATION AND ITS APPLICATIONS

Application on MEFM

The paraxial NLSE in Kerr media is given by [57]

$$iD_{M,z}^{\alpha,\beta}u+\frac{a}{2}D_{M,t}^{2\alpha,\beta}u+\frac{b}{2}D_{M,y}^{2\alpha,\beta}u+\gamma|u|^2u=0, \tag{12}$$

where $u=u(y,z,t)$ is the complex wave envelope function. The constants a, b and γ are the symbols of the dispersion, diffraction, and Kerr non-linearity, respectively. In Equation (12) if $ab>0$ we get elliptic non-linear Schrödinger equation and if $ab<0$, Equation (12) becomes hyperbolic non-linear Schrödinger equation. Now assume the following wave transformations:

$$u(x,y,t)=U(\xi)e^{i\theta},\xi=\frac{\Gamma(\beta+1)}{\alpha}(y+z-ct),\quad \theta=\frac{\Gamma(\beta+1)}{\alpha}\kappa(y+z-ct). \tag{13}$$

Inserting Equation (13) into Equation (12), and separate the result into the real and imaginary part, we get

$$-\left(c^2a+b\right)U''+\left(b\kappa^2+a\kappa^2c^2+2\kappa\right)U-2\gamma U^3=0, \tag{14}$$

$$\left(1+b\kappa+a\kappa c^2\right)U'=0. \tag{15}$$

Now, we know that $U'\neq 0$, therefore

$$b=\frac{-1-a\kappa c^2}{\kappa}. \tag{16}$$

Putting Equation (16) into Equation (14) to get the closed solution, we get

$$U''+\kappa^2U-2\gamma U^3=0. \tag{17}$$

Finding the principal balance between U'' and U^3, we find the following relation between n and m

$$n=m+1. \tag{18}$$

Let $m=1$, then $n=2$. Putting the value of $m=1$ and $n=2$ into Equation (4), the Equation (4) can be written as the following

$$U(\xi)=\frac{\sum_{i=1}^{2}a_i\left(K^{-i\Phi(\xi)}\right)^{i}}{\sum_{j=1}^{1}b_i\left(K^{-\Phi(\xi)}\right)^{j}}=\frac{a_0+a_1K^{-\phi(\xi)}+a_2K^{-2\phi(\xi)}}{b_0+b_1K^{-\phi(\xi)}}. \tag{19}$$

Where a_0,a_1,a_2,b_0,b_1 are constants and $b_2\neq 0$ & $a_1\neq 0$. Using Equation (19) and its second derivative with Equation (17), we analyze the following cases and solutions:

Case 1. When $a_0=0,a_1=\frac{ib_1\lambda\left(\lambda^2-4\mu\right)^{1/4}}{2^{3/4}\sqrt{\gamma\left(\lambda^2-4\mu\right)}},a_2=\frac{i2^{1/4}b_1\left(\lambda^2-4\mu\right)^{1/4}}{\sqrt{\gamma\left(\lambda^2-4\mu\right)}},\kappa=-\frac{\sqrt{\lambda^2-4\mu}}{\sqrt{2}},b_0=0$, we get the following solutions:

Solution 1. When $\lambda^2-4\mu>0,\lambda\neq 0,\mu\neq 0$, then

$$u(y,z,t)=\frac{ie^{-\frac{i\sqrt{\lambda^2-4\mu}\xi}{\sqrt{2}}}\left(\lambda^2-4\mu\right)^{1/4}\left(\lambda^2-4\mu+\lambda\sqrt{\lambda^2-4\mu}\tanh\left(\frac{1}{2}\sqrt{\lambda^2-4\mu}(\varepsilon+\xi)\right)\right)}{2^{3/4}\sqrt{\gamma\left(\lambda^2-4\mu\right)}\left(\lambda+\sqrt{\lambda^2-4\mu}\tanh\left(\frac{1}{2}\sqrt{\lambda^2-4\mu}(\varepsilon+\xi)\right)\right)}. \tag{20}$$

Solution 2. When $\lambda^2-4\mu>0,\mu=0$, then

$$u(y,z,t)=\frac{ie^{-\frac{i\sqrt{\lambda^2}\xi}{\sqrt{2}}}\lambda\left(\lambda^2\right)^{1/4}\coth\left(\frac{1}{2}\lambda(\epsilon+\xi)\right)}{2^{3/4}\sqrt{\gamma\lambda^2}}. \tag{21}$$

Case 2. When $a_1=a_0\left(\frac{b_1}{b_0}+\frac{2}{\lambda}\right),a_2=\frac{2a_0b_1}{b_0\lambda},\kappa=\frac{\sqrt{\lambda^2-4\mu}}{\sqrt{2}},\gamma=\frac{{b_0}^2\lambda^2}{2\sqrt{2}{a_0}^2\sqrt{\lambda^2-4\mu}}$, then we get the following solutions

Solution 1. When $\lambda^2-4\mu>0,\lambda\neq 0,\mu\neq 0$, then

$$u(y,z,t)=\frac{a_0e^{\frac{i\sqrt{\lambda^2-4\mu}\xi}{\sqrt{2}}}\left(\lambda^2-4\mu+\lambda\sqrt{\lambda^2-4\mu}\tanh\left(\frac{1}{2}\sqrt{\lambda^2-4\mu}(\varepsilon+\xi)\right)\right)}{b_0\lambda\left(\lambda+\sqrt{\lambda^2-4\mu}\tanh\left(\frac{1}{2}\sqrt{\lambda^2-4\mu}(\varepsilon+\xi)\right)\right)}. \tag{22}$$

Solution 2. When $\lambda^2-4\mu>0,\mu=0$, then

$$u(y,z,t)=\frac{a_0e^{\frac{i\sqrt{\lambda^2}\xi}{\sqrt{2}}}\coth\left(\frac{1}{2}\lambda(\epsilon+\xi)\right)}{b_0}. \tag{23}$$

Case 3. When $a_1 = \frac{a_0\lambda}{\mu}, a_2 = \frac{a_0}{\mu}, b_0 = \frac{b_1\lambda}{2}, \kappa = -\sqrt{-\lambda^2+4\mu}, \gamma = -\frac{{b_1}^2\mu^2}{{a_0}^2\sqrt{-\lambda^2+4\mu}}$, we get the following solution

$$u\left(y,z,t\right) = -\frac{2a_0 e^{-i\sqrt{-\lambda^2+4\mu}\xi}\left(\lambda^2-4\mu\right)\sec^2\left(\frac{1}{2}\sqrt{-\lambda^2+4\mu}\left(\varepsilon+\xi\right)\right)}{b_1\left(\lambda-\sqrt{-\lambda^2+4\mu}\tan\left(\frac{1}{2}\sqrt{-\lambda^2+4\mu}\left(\varepsilon+\xi\right)\right)\right)\left(\lambda^2-4\mu-\lambda\sqrt{-\lambda^2+4\mu}\tan\left(\frac{1}{2}\sqrt{-\lambda^2+4\mu}\left(\varepsilon+\xi\right)\right)\right)}, \quad (24)$$

where $\lambda^2 - 4\mu < 0$.

Case 4. When $a_1 = \frac{a_0\lambda}{\mu}, a_2 = \frac{a_0}{\mu}, b_1 = \frac{2b_0}{\lambda}, \kappa = -\sqrt{-\lambda^2+4\mu}, \gamma = -\frac{4{b_0}^2\mu^2}{{a_0}^2\lambda^2\sqrt{-\lambda^2+4\mu}}$ we get the following solutions

$$\mathrm{u}\left(y,z,t\right) = -\frac{i}{2^{1/4}\sqrt{\gamma}} e^{-\frac{i\sqrt{2}\Gamma(1+\beta)\left(-ct^\alpha+y^\alpha+z^\alpha\right)}{\alpha}} \coth\left(\frac{\Gamma\left(1+\beta\right)\left(-ct^\alpha+y^\alpha+z^\alpha\right)}{\alpha}\right)$$

$$u\left(y,z,t\right) = -\frac{a_0 e^{-i\sqrt{-\lambda^2+4\mu}\xi}\lambda\left(\lambda^2-4\mu\right)\sec^2\left(\frac{1}{2}\sqrt{-\lambda^2+4\mu}\left(\varepsilon+\xi\right)\right)}{b_0\left(\lambda-\sqrt{-\lambda^2+4\mu}\tan\left(\frac{1}{2}\sqrt{-\lambda^2+4\mu}\left(\varepsilon+\xi\right)\right)\right)\left(\lambda^2-4\mu-\lambda\sqrt{-\lambda^2+4\mu}\tan\left(\frac{1}{2}\sqrt{-\lambda^2+4\mu}\left(\varepsilon+\xi\right)\right)\right)}, \quad (25)$$

where $\lambda^2 - 4\mu < 0$.

Application on Extended Sinh-Gordon Method

In this subsection, we apply the extended sinh-Gordon method to the M-fractional paraxial wave equation that labeled Equation (12). Consider the Equation (17) and applying the principal homogeneous balance between the between U'' and U^3, we find $n = 1$. Using the value of $n = 1$and substituting it into Equation (6), we get

$$U\left(w\right) = b_1\sinh\left(w\right) + a_1\cosh\left(w\right) + a_0 \quad (26)$$

Putting Equation (26) and its derivatives into Equation (17), we get the polynomial equation includes for $\left(i,j = 0,1,2,...\right)$. Equating its coefficients to zero, and using Mathematica package, one can investigate the following cases.

Case 5. When $A_0 = 0, A_1 = 0, B_1 = \frac{(-1)^{1/4}}{\sqrt{\gamma}}, \kappa = -\mathrm{i}$, we get

$$u\left(y,z,t\right) = \frac{(-1)^{3/4}}{\sqrt{\gamma}} e^{\frac{\Gamma(1+\beta)\left(-ct^\alpha+y^\alpha+z^\alpha\right)}{\alpha}} sech\left(\frac{\Gamma\left(1+\beta\right)\left(-ct^\alpha+y^\alpha+z^\alpha\right)}{\alpha}\right) \quad (27)$$

or

$$u\left(y,z,t\right) = \frac{(-1)^{1/4}}{\sqrt{\gamma}} e^{\frac{\Gamma(1+\beta)\left(-ct^\alpha+y^\alpha+z^\alpha\right)}{\alpha}} csch\left(\frac{\Gamma\left(1+\beta\right)\left(-ct^\alpha+y^\alpha+z^\alpha\right)}{\alpha}\right),$$

providing that $\gamma > 0$.

Case 6. When $A_0 = 0, A_1 = -\frac{\mathrm{i}}{2^{1/4}\sqrt{\gamma}}, B_1 = 0, \kappa = -\sqrt{2}$, we get

$$\mathrm{u}\left(y,z,t\right) = -\frac{i}{2^{1/4}\sqrt{\gamma}} e^{-\frac{i\sqrt{2}\left(-ct^\alpha+y^\alpha+z^\alpha\right)\Gamma(1+\beta)}{\alpha}} \tanh\left(\frac{\Gamma\left(1+\beta\right)\left(-ct^\alpha+y^\alpha+z^\alpha\right)}{\alpha}\right) \quad (28)$$

or

providing that $\gamma > 0$.

Case 7. When $A_0 = 0, A_1 = 0, B_1 = -\frac{(-1)^{1/4}}{\sqrt{\gamma}}, \kappa = -\mathrm{i}$, we get

$$\mathrm{u}\left(y,z,t\right) = -\frac{(-1)^{3/4}}{\sqrt{\gamma}} e^{\frac{\Gamma(1+\beta)\left(-ct^\alpha+y^\alpha+z^\alpha\right)}{\alpha}} sech\left(\frac{\Gamma\left(1+\beta\right)\left(-ct^\alpha+y^\alpha+z^\alpha\right)}{\alpha}\right) \quad (29)$$

or

$$\mathrm{u}\left(y,z,t\right) = e^{\frac{i\Gamma(1+\beta)\left(-ct^\alpha+y^\alpha+z^\alpha\right)}{\sqrt{2}\alpha}}\left(\frac{\coth\left(\frac{\Gamma(1+\beta)\left(-ct^\alpha+y^\alpha+z^\alpha\right)}{\alpha}\right)}{2^{3/4}\sqrt{\gamma}} + \frac{csch\left(\frac{\Gamma(1+\beta)\left(-ct^\alpha+y^\alpha+z^\alpha\right)}{\alpha}\right)}{2^{3/4}\sqrt{\gamma}}\right),$$

providing that $\gamma > 0$.

Case 8. When $A_0 = 0, A_1 = \frac{1}{2^{1/4}\sqrt{\gamma}}, B_1 = 0, \kappa = \sqrt{2}$, we get

$$u\left(y,z,t\right) = \frac{e^{\frac{i\sqrt{2}\Gamma(1+\beta)\left(-ct^\alpha+y^\alpha+z^\alpha\right)}{\alpha}}\tanh\left(\frac{\Gamma(1+\beta)\left(-ct^\alpha+y^\alpha+z^\alpha\right)}{\alpha}\right)}{2^{1/4}\sqrt{\gamma}},$$

$$u\left(y,z,t\right) = \frac{e^{\frac{i\sqrt{2}\Gamma(1+\beta)\left(-ct^\alpha+y^\alpha+z^\alpha\right)}{\alpha}}\coth\left(\frac{\Gamma(1+\beta)\left(-ct^\alpha+y^\alpha+z^\alpha\right)}{\alpha}\right)}{2^{1/4}\sqrt{\gamma}} \quad (30)$$

providing that $\gamma > 0$.

CONCLUSION

In this article, the modified exponential function method in a new trial solution and the extended sinh-Gordon expansion method are used to construct some new soliton solutions of M-fractional paraxial non-linear Schrödinger equation. The new exact solutions are included in the hyperbolic function and trigonometric function. **Figures 1**, **3**, **8**, **10** are expressing dark

wave solutions, **Figures 2**, **4** are expressing the singular wave, **Figure 7** is the kink-type soliton solution, **Figure 9** is a surface solution and **Figures 5**, **6** are the periodic dark-singular soliton solutions as well as 2D, 3D with a contour plot of all new solutions are plotted. We guarantee that all solutions are new and verified the main equation of M-fractional paraxial wave equation after it substituted to the main equation labeled Equation (6). All our new solutions of (2+1)-dimensional M-fractional paraxial wave equation might be useful and applicable in the optical fiber industry.

DATA AVAILABILITY STATEMENT

The datasets generated for this study are available on request to the corresponding author.

AUTHOR CONTRIBUTIONS

All authors listed have made a substantial, direct and intellectual contribution to the work, and approved it for publication.

REFERENCES

1. Oruç Ö, Bulut F, Esen A. Numerical solution of the KdV equation by Haar wavelet method. *Pramana.* (2016) **87**:94. doi: 10.1007/s12043-016-1286-7
2. Yousif MA, Mahmood BA, Ali KK, Ismael HF. Numerical simulation using the homotopy perturbation method for a thin liquid film over an unsteady stretching sheet. *Int J Pure Appl Math*. (2016) **107**:289–300. doi: 10.12732/ijpam.v107i2.1
3. Ismael HF, Ali KK. MHD casson flow over an unsteady stretching sheet. *Adv Appl Fluid Mech.* (2017) **20**:533–41. doi: 10.17654/FM020040533
4. Bulut H, Ergüt M, Asil V, Bokor RH. Numerical solution of a viscous incompressible flow problem through an orifice by Adomian decomposition method. *Appl Math Comput.* (2004) **153**:733–41. doi: 10.1016/S0096-3003(03)00667-2
5. Ismael HF, Arifin NM. Flow and heat transfer in a maxwell liquid sheet over a stretching surface with thermal radiation and viscous dissipation. *JP J Heat Mass Transf.* (2018) **15**:847–66. doi: 10.17654/HM015040847
6. Ali KK, Ismael HF, Mahmood BA, Yousif MA. MHD Casson fluid with heat transfer in a liquid film over unsteady stretching plate. *Int J Adv Appl Sci.* (2017) **4**:55–8. doi: 10.21833/ijaas.2017.01.008
7. Ismael HF. Carreau-Casson fluids flow and heat transfer over stretching plate with internal heat source/sink and radiation. *Int J Adv Appl Sci J.* (2017) **6**:81–6. doi: 10.21833/ijaas.2017.07.003
8. Zeeshan, Ismael HF,Yousif MA, Mahmood T, Rahman SU. Simultaneous effects of slip and wall stretching/shrinking on radiative flow of magneto nanofluid through porous medium. *J Magn.* (2018) **23**:491–8. doi: 10.4283/JMAG.2018.23.4.491
9. Bulut H, Sulaiman TA, Baskonus HM, Aktürk T. On the bright and singular optical solitons to the (2 + 1)-dimensional NLS and the Hirota equations. *Opt Quant Electron.* (2018) **50**:134. doi: 10.1007/s11082-018-1411-6
10. Baskonus HM, Sulaiman TA, Bulut H. On the novel wave behaviors to the coupled nonlinear Maccari's system with complex structure. *Optik.* (2017) **131**:1036–43. doi: 10.1016/j.ijleo.2016.10.135
11. Baskonus HM,Bulut H, Sulaiman TA. New complex hyperbolic structures to the lonngren-wave equation by using sine-gordon expansion method. *Appl Math Nonlinear Sci.* (2019) **4:**141–50. *doi: 10.2478/AMNS.2019.1.00013*
12. Eskitaşçioglu EI,Aktaş MB, Baskonus HM. New complex and hyperbolic forms for ablowitz–kaup–newell–segur wave equation with fourth order. *Appl Math Nonlinear Sci.* (2019) 4:105–12. doi: 10.2478/AMNS.2019.1.00010
13. Vakhnenko VO,Parkes EJ, Morrison AJ. A Bäcklund transformation and the inverse scattering transform method for the generalised Vakhnenko equation. *Chaos Solitons Fract.* (2003) **17**:683–92. doi: 10.1016/S0960-0779(02)00483-6
14. Cattani C, Sulaiman TA, Baskonus HM, Bulut H. On the soliton solutions to the Nizhnik-Novikov-Veselov and the Drinfel'd-Sokolov systems. *Opt Quant Electron.* (2018) **50**:138. doi: 10.1007/s11082-018-1406-3
15. Seadawy R, Kumar D, Chakrabarty AK. Dispersive optical soliton solutions for the hyperbolic and cubic-quintic nonlinear Schrödinger equations via the extended sinh-Gordon equation expansion method. *Eur Phys Plus J.* (2018) **133**:182. doi: 10.1140/epjp/i2018-12027-9
16. Bulut H, Sulaiman TA, Baskonus HM. Dark, bright optical and other solitons with conformable space-time fractional second-order spatiotemporal dispersion. *Optik.* (2018) **163**:1–7. doi: 10.1016/j.ijleo.2018.02.086
17. Manafian J, Lakestani M, Bekir A. Study of the analytical treatment of the (2+1)-dimensional zoomeron, the duffing and the SRLW equations via a new analytical approach. *Int J Appl Comput Math.* (2016) **2**:243–68. doi: 10.1007/s40819-015-0058-2
18. Hammouch Z, Mekkaoui T, Agarwal P. Optical solitons for the Calogero-Bogoyavlenskii-Schiff equation in (2 + 1) dimensions with time-fractional conformable derivative. *Eur Phys Plus J.* (2018) **133**:248. doi: 10.1140/epjp/i2018-12096-8
19. Dewasurendra M, Vajravelu K. On the method of inverse mapping for solutions of coupled systems of nonlinear differential equations arising in nanofluid flow, heat and mass transfer. *Appl Math Nonlinear Sci.* (2018) **3**:1–14. doi: 10.21042/AMNS.2018.1.00001
20. Ilhan OA,Esen A, Bulut H, Baskonus HM. Singular solitons in the pseudo-parabolic model arising in nonlinear surface waves. *Results Phys.* (2019) **12**:1712:5. doi: 10.1016/j.rinp.2019.01.059
21. Yokus, Baskonus HM,Sulaiman TA, Bulut H. Numerical simulation and solutions of the two-component second order KdV evolutionarysystem. *Numer. Methods Partial Differ Equ.* (2018) **34**:211–27. doi: 10.1002/num.22192
22. Cattani STA, Baskonus HM, Bulut H. Solitons in an inhomogeneous Murnaghan's rod. *Eur Phys Plus J.* (2018) **133**:228. doi: 10.1140/epjp/i2018-12085-y
23. Houwe A, Justin M, Jerome D, Betchewe G, Doka SY. TimoleonCrepin, K. Soliton solutions, kink and antikink of the Gerdjikov-Ivanov equation. *Preprints* **2018**:2018090284 doi: 10.20944/preprints201809.0284.v1
24. Yang X, Yang Y, Cattani C, Zhu CM. A new technique for solving the 1-D Burgers equation. *Therm Sci.* (2017) **21**:S129–36. doi: 10.2298/TSCI17S1129Y
25. Hammouch Z, Mekkaoui T. Traveling-wave solutions of the generalized Zakharov equation with time-space fractional derivatives. *J MESA*. (2014) **5**:489–98. doi: 10.20944/preprints201903.0114.v1
26. Baskonus HM, Yel G, Bulut H. Novel wave surfaces to the fractional Zakharov-Kuznetsov-Benjamin-Bona-Mahony equation. In: *AIP Conference Proceedings*. Istanbul (2017). doi: 10.1063/1.4992767
27. Baskonus HM, Bulut H. Exponential prototype structures for (2+1)-dimensional Boiti-Leon-Pempinelli systems in mathematical physics. *Waves Random Complex Media*. (2016) **26**:189–96. doi: 10.1080/17455030.2015.1132860
28. Baskonus HM, Bulut H. An effective schema for solving some nonlinear partial differential equation arising in nonlinear physics. *Open Phys.* (2015) **13**:280–89. doi: 10.1515/phys-2015-0035
29. Bulut H. Application of the modified exponential function method to the Cahn-Allen equation. In: *AIP Conference Proceedings*. Istanbul (2017). doi: 10.1063/1.4972625
30. Wei G, Ismael HF, Bulut H, Baskonus HM. Instability modulation for the (2+1)-dimension paraxial wave equation and its new optical soliton solutions in Kerr media. *Phys Scr.* (2019). doi: 10.1088/1402-4896/ab4a50
31. Yang XF, Deng ZC, Wei Y. A riccati-bernoulli sub-ODE method for nonlinear partial differential equations and its application. *Adv Differ Equat.* (2015) 2015:117. doi: 10.1186/s13662-015-0452-4
32. Manafian J, Foroutan M, Guzali A. Applications of the ETEM for obtaining optical soliton solutions for the Lakshmanan-Porsezian-Daniel model. *Eur. Phys. Plus J.* (2017) **132**:494. doi: 10.1140/epjp/i2017-11762-7

33. Biswas, Ekici M, Sonmezoglu A, Alqahtani RT. Optical solitons with differential group delay for coupled Fokas–Lenells equation by extended trial function scheme. *Optik*. (2018) **165**:102–10. doi: 10.1016/j.ijleo.2018.03.102
34. Li HM, Xu YS, Lin J. New optical solitons in high-order dispersive cubic-quintic nonlinear Schrodinger equation. *Commun. Theor. Phys.* (2004) **41**:6. doi: 10.1088/0253-6102/41/6/829
35. Jawad JM, Abu-AlShaeer MJ, Biswas A, Zhou Q, Moshokoa S, Belic M. Optical solitons to Lakshmanan-Porsezian-Daniel model for three nonlinear forms. *Optik*. (2018) **160**:197–202. doi: 10.1016/j.ijleo.2018.01.121
36. Yokuş A, Gülbahar S. Numerical solutions with linearization techniques of the fractional harry dym equation. *Appl. Math. Nonlinear Sci.* (2019) **4**:35–42. doi: 10.2478/AMNS.2019.1.00004
37. Baskonus H, Mekkaoui T, Hammouch Z, Bulut H. Active control of a chaotic fractional order economic system. *Entropy*. (2015) **17**:5771–83. doi: 10.3390/e17085771
38. Baskonus HM, Hammouch Z, Mekkaoui T, Bulut H. Chaos in the fractional order logistic delay system: circuit realization and synchronization. In: *AIP Conference Proceedings*. Greece (2016). doi: 10.1063/1.4952077
39. Baskonus HM, Bulut H. On the numerical solutions of some fractional ordinary differential equations by fractional Adams-Bashforth-Moulton method. *Open Math.* (2015) **13**:547–56. doi: 10.1515/math-2015-0052
40. Esen A, Sulaiman TA, Bulut H, Baskonus HM. Optical solitons to the space-time fractional (1+ 1)-dimensional coupled nonlinear Schrödinger equation. *Optik*. (2018) **167**:150–6. doi: 10.1016/j.ijleo.2018.04.015
41. Subashini R, Ravichandran C, Jothimani K, Baskonus HM. Existence results of Hilfer integro-differential equations with fractional order. *Discret. Contin. Dyn. Syst.* (2019) **911**:911–23. doi: 10.3934/dcdss.2020053
42. Veeresha P, Prakasha DG, Baskonus HM. New numerical surfaces to the mathematical model of cancer chemotherapy effect in Caputo fractional derivatives. *Chaos An Interdiscip. J Nonlinear Sci.* (2019) **29**:13119. doi: 10.1063/1.5074099
43. Yang AM, Zhang YZ, Cattani C, Xie GN, Rashidi MM, Zhou YJ, et al. Application of local fractional series expansion method to solve Klein-Gordon equations on cantor sets. *Abstr Appl Anal.* (2014) **2014**:372741. doi: 10.1155/2014/372741
44. Heydari MH, Hooshmandasl MR, Ghaini FMM, Cattani C. Wavelets method for solving fractional optimal control problems. *Appl. Math. Comput.* (2016) **286**:139–54. doi: 10.1016/j.amc.2016.04.009
45. Zhang Y, Cattani C, Yang J-X. Local fractional homotopy perturbation method for solving non-homogeneous heat conduction equations in fractal domains. *Entropy*. (2015) **170**:6753–64. doi: 10.3390/e17106753
46. Brzezinski DW. Review of numerical methods for NumILPT with computational accuracy assessment for fractional calculus. *Appl Math Nonlinear Sci.* (2019) **3**:487–502. doi: 10.2478/AMNS.2018.2.00038
47. Brzezinski DW. Comparison of fractional order derivatives computational accuracy-right hand vs left hand definition. *Appl Math Nonlinear Sci.* (2017) **2**:237–48. doi: 10.21042/AMNS.2017.1.00020
48. Machado JT, Kiryakova V, Mainardi F. Recent history of fractional calculus. *Commun Nonlinear Sci Numer Simulat*. (2011) **16**:1140–53. doi: 10.1016/j.cnsns.2010.05.027
49. Weyl H. Bemerkungen zum begriff des differentialquotienten gebrochener ordnung. *Zürich. Naturf. Ges.* (1917) **62**:296–302.
50. Riesz M. L'intégrale de Riemann-Liouville et le problème de Cauchy pour l'équation des ondes. *Bull. la Société Mathématique Fr.* (1939) **67**:153–70. doi: 10.24033/bsmf.1309
51. Podlubny I. An introduction to fractional derivatives, fractional differential equations, to methods of their solution and some of their applications. *Math. Sci. Eng.* (1999) **198**:24–340.
52. Atangana A, Baleanu D. New fractional derivatives with non-local and non-singular kernel: Theory and application to heat transfer model. *Therm. Sci.* (2016) **20**:763–69. doi: 10.2298/TSCI160111018A
53. Miller S, Ross B. *An Introduction to the Fractional Calculus and Fractional Differential Equations*. New York, NY: Wiley (1993).
54. Khalil R, Al Horani M, Yousef A, Sababheh M. A new definition of fractional derivative. *J Comput Appl Math.* (2014) **264**:65–70. doi: 10.1016/j.cam.2014.01.002
55. Atangana A, Baleanu D, Alsaedi A. New properties of conformable derivative. *Open Math.* (2015) **13**:889–98. doi: 10.1515/math-2015-0081
56. Sousa JVC, Oliveira EC. A new truncated M-fractional derivative type unifying some fractional derivative types with classical properties. *Int. J. Anal. Appl.* (2018) 16:83–96.
57. Choi S, Howell JC. Paraxial ray optics cloaking. *Opt. Exp*. (2014) **22**:29465–78. doi: 10.1364/OE.22.029465

Conflict of Interest: The authors declare that the research was conducted in the absence of any commercial or financial relationships that could be construed as a potential conflict of interest.

frontiers in Physics

ORIGINAL RESEARCH
published: 04 December 2019
doi: 10.3389/fphy.2019.00193

Fractional Approach for Equation Describing the Water Transport in Unsaturated Porous Media With Mittag-Leffler Kernel

D. G. Prakasha[1], *P. Veeresha*[2] *and Jagdev Singh*[3]*

[1] Department of Mathematics, Faculty of Science, Davangere University, Davangere, India, [2] Department of Mathematics, Karnatak University, Dharwad, India, [3] Department of Mathematics, JECRC University, Jaipur, India

In this paper, we find the solution for a fractional Richards equation describing the water transport in unsaturated porous media using the *q-homotopy analysis transform method* (*q*-HATM). The proposed technique is to use graceful amalgamations of the Laplace transform technique with the q-homotopy analysis scheme as well as the fractional derivative that is defined with the Atangana-Baleanu (AB) operator. The fixed point hypothesis is considered in order to demonstrate the existence and uniqueness of the obtained solution for the proposed fractional order model. In order to validate and illustrate the efficiency of the future technique, we analyze the projected model in terms of fractional order. Meanwhile, the physical behavior of the *q*-HATM solutions are captured in terms of plots for diverse fractional order and the numerical simulation is also demonstrated. The achieved results illuminate that the future algorithm is easy to implement, highly methodical, effective, and very accurate in its analysis of the behavior of non-linear differential equations of fractional order that arise in the connected areas of science and engineering.

Keywords: Laplace transform, Atangana-Baleanu derivative, Richards equation, *q*-homotopy analysis method, fixed point theorem

OPEN ACCESS

Edited by:
Devendra Kumar,
University of Rajasthan, India

Reviewed by:
Haci Mehmet Baskonus,
Harran University, Turkey
Francisco Gomez,
Centro Nacional de Investigación y Desarrollo Tecnológico, Mexico

***Correspondence:**
Jagdev Singh
jagdevsinghrathore@gmail.com

Specialty section:
This article was submitted to Mathematical Physics, a section of the journal Frontiers in Physics

Received: *18 October 2019*
Accepted: *05 November 2019*
Published: *04 December 2019*

Citation:
Prakasha DG, Veeresha P and Singh J (2019) Fractional Approach for Equation Describing the Water Transport in Unsaturated Porous Media With Mittag-Leffler Kernel. Front. Phys. 7:193. doi: 10.3389/fphy.2019.00193

INTRODUCTION

Fractional calculus (FC) was originated in Newton's time, but, lately, it has fascinated and captured the attention of many scholars. For the last 30 years, the most intriguing leaps in scientific and engineering applications have been found within the framework of FC. The concept of the fractional derivative has been industrialized due to the complexities associated with a heterogeneous phenomenon. The fractional differential operators are capable of capturing the behavior of multifaceted media as they have diffusion processes. It has been a very essential tool, and many problems can be illustrated more conveniently and more accurately with differential equations having an arbitrary order. Due to the swift development of mathematical techniques that use computer software, many researchers started to work on generalized calculus to present their viewpoints while analyzing many complex phenomena.

Numerous pioneering directions are prescribed for the diverse definitions of fractional calculus by many senior researchers, and these have prearranged the foundation [1–6]. Calculus with fractional order is associated with practical ventures and is extensively employed within nanotechnology [7], optics [8], human diseases [9], chaos theory [10], and other areas [11–39]. The numerical as well as analytical solutions for these equations illustrate that these models have an important role in portraying the nature of non-linear problems within connected areas of science.

In order to illustrate the importance of the novel fractional order derivative and future scheme, we, in the present framework, consider the Richards equation, which plays a vital role in describing the nature of the porous medium as well as the penetration of unsaturated regions in the soil. In 1931, *Lorenzo A. Richards* was the first person to pioneer work on the unsaturated porous material in order to model water movement. Later, he derived an equation based on continuum mechanics, which govern the water flow in the soil [40]. In the proposed model for the momentum equation, the continuity equation is an amalgam with Darcy's law, and is defined in a one-dimensional form as follows, with soil water diffusivity symbolized by ρ and hydraulic conductivity by σ for unsaturated soil moisture content u

$$\frac{\partial u}{\partial t} = \frac{\partial}{\partial z}\left(\rho \frac{\partial u}{\partial z} - \sigma\right), \tag{1}$$

where z designates the elevation above a vertical datum. Recently, many authors employed numerical as well as analytical techniques in order to analyze and predict the suitable models for parameters in the equation and solve the governing equation of unsaturated flow in soils. Meanwhile, three models are generally applied, namely (i) the exponential model, (ii) the van Genuchten model, and (iii) the Brook-Coreysmodel (BCM). Among these models, BCM is extensively applied due to its well-defined configuration and because it is associated with the largest pore size. The following equations describe the complete wet ability of the BC model [41, 42]:

$$\begin{aligned} \sigma(u) &= \sigma_0 u^k, \\ \rho(u) &= \rho_0 (n+1) u^n, \end{aligned} \tag{2}$$

where $\sigma_0, k,\ \rho_0$, and n are constants denoting particle shape, pore-size distribution and many other soil properties. For $n = 0$ and $k = 2$, Equation (2) simplified it to the classic Burgers equation [43, 44], and some particular values signify the generalized Burgers equation, which is essential to describing the important physical phenomena. In the present study, we consider that BCM employed the RC equation. In this case, for the (n, 1) order, the RC equation coincides with the Burgers equation, and this is presented here [45, 46]:

$$u_t + a\left(u^n\right)_x + bu_{xx} = 0,\ \ a,\ b \neq 1,\ n \geq 1. \tag{3}$$

The analytical solution for the above equation is presented:

$$u(x,t) = \left(\frac{c}{2a}\left(1 + \tanh\left(\frac{c(n-1)}{2b}(x - ct)\right)\right)\right)^{\frac{1}{n-1}}. \tag{4}$$

In the present scenario, many important and non-linear models are methodically and effectively analyzed with the help of fractional calculus. There have been diverse definitions that have been suggested by many senior research scholars like, Riemann, Liouville, Caputo, and Fabrizio. However, these definitions have their own limitations. The Riemann-Liouville derivative is unable to explain the importance of the initial conditions; the Caputo derivative has overcome this shortcoming but cannot explain the singular kernel of the phenomena. In 2015, Caputo and Fabrizio solved the above issues [47], and many researchers consult this derivative in order to analyze and find the solution for diverse classes of non-linear complex problems. Some issues, however, were pointed out in the CF derivative; non-singular kernel and non-local properties are very essential in describing the physical behavior and nature of the non-linear problems. In 2016, Atangana and Baleanu introduced and natured a novel fractional derivative, namely the AB derivative. This novel derivative was defined with the aid of Mittag-Leffler functions [48]. This fractional derivative buried all the above-cited issues and helps us to understand the natural phenomena in the systematic and effective way.

In this framework, we consider the fractional RC equation of the form

$${}_{a}^{ABC}D_t^{\alpha} u(x,t) + a\left(u^n\right)_x + bu_{xx} = 0, \tag{5}$$

where α is fractional order of the system and defined with AB fractional operator, u is the water content with depth x. The fractional order is introduced in order to incorporate the memory effects and hereditary consequence in the system, and these properties aid us in capturing the essential physical properties of the complex problems.

Recently, many mathematicians and physicists have developed very effective and more accurate methods in order to find and analyze solutions for complex and non-linear problems that have arisen in science and technology. In connection with this is the homotopy analysis method (HAM) proposed by Chinese Mathematician *Liao Shijun* [49, 50]. HAM has been profitably and effectively applied to study the behavior of non-linear problems without perturbation or linearization. But, for computational work, HAM requires significant time and computer memory. To overcome this, there is a possibility of using an amalgamation of the considered method and well-known transformation techniques.

In the present investigation, we analyzed the nature of the q-homotopy analysis transform method (q-HATM) solution for the FCDG equation by applying q-HATM. The future algorithm is the combination of q-HAM with LT [51]. The method of the considered scheme is merging two strong methods to solve linear and non-linear fractional differential equations both analytically as well as numerically. The future technique has many sturdy properties, including a non-local effect, straight forward solution procedure, and a promising large convergence region; moreover, it is free from any assumptions, discretization, and perturbation. Recently, due to its reliability and efficacy, the considered method has been exceptionally applied by many researchers to understand physical behavior in diverse classes of complex problems [52–60]. The novelty of the future method is that it aids a modest algorithm to evaluate the solution, and it is natured by the homotopy and axillary parameters, which provide the rapid convergence of the obtained solution for a non-linear portion of the given problem. Meanwhile, it has prodigious generality because it plausibly contains the results obtained by many algorithms like q-HAM, HPM, ADM and some other

traditional techniques. The considered method can preserve great accuracy while decreasing the computational time and work in comparison with other methods.

The considered non-linear model recently caught the attention of researchers from different areas of science. Since RC equation plays a significant role in portraying several complex phenomena, many authors have found and analyzed the solution using analytical as well as numerical schemes; for instance, authors in [61] considered analytical techniques and found solutions for the considered model with arbitrary surface boundary conditions, and authors in [62] presented the compression approximation and infiltration of the RC equation with an analytical solution, authors in [45] applied the Adomian decomposition scheme, and authors in [46] applied HAM in order to find the approximated analytical solution. In this paper, we made an attempt to find the solution for the FRC equation using q-HATM.

PRELIMINARIES

Recently, many authors considered these derivatives to analyze a diverse class of models in comparison with classical order as well as other fractional derivatives, and they prove that the AB derivative is more effective while analyzing the nature and physical behavior of the models [63, 64]. Here, we define the basic notion of Atangana-Baleanu derivatives and integrals [48].

Definition 1. The fractional Atangana-Baleanu-Caputo derivative for a function $f \in H^1(a, b)\ (b > a,\ \alpha \in [0, 1])$ is presented:

$$ {}^{ABC}_{a}D^{\alpha}_{t}\left(f(t)\right) = \frac{\mathcal{B}[\alpha]}{1-\alpha}\int_a^t f'(\vartheta)\, E_{\alpha}\left[\alpha\frac{(t-\vartheta)^{\alpha}}{\alpha-1}\right]d\vartheta. \quad (6) $$

Definition 2. The AB derivative of fractional order for a function $f \in H^1(a, b)$, $b > a$, $\alpha \in [0, 1]$ in the Riemann-Liouville sense is presented:

$$ {}^{ABR}_{a}D^{\alpha}_{t}\left(f(t)\right) = \frac{\mathcal{B}[\alpha]}{1-\alpha}\frac{d}{dt}\int_a^t f(\vartheta)\, E_{\alpha}\left[\alpha\frac{(t-\vartheta)^{\alpha}}{\alpha-1}\right]d\vartheta. \quad (7) $$

Definition 3. The fractional AB integral related to the non-local kernel is defined by

$$ {}^{AB}_{a}I^{\alpha}_{t}\left(f(t)\right) = \frac{1-\alpha}{\mathcal{B}[\alpha]}f(t) + \frac{\alpha}{\mathcal{B}[\alpha]\,\Gamma(\alpha)}\int_a^t f(\vartheta)\,(t-\vartheta)^{\alpha-1}\,d\vartheta. \quad (8) $$

Definition 4. The Laplace transform (LT) of AB derivative is defined by

$$ L\left[{}^{ABR}_{0}D^{\alpha}_{t}\left(f(t)\right)\right] = \frac{\mathcal{B}[\alpha]}{1-\alpha}\frac{s^{\alpha}L\left[f(t)\right] - s^{\alpha-1}f(0)}{s^{\alpha} + \left(\alpha/(1-\alpha)\right)}. \quad (9) $$

Theorem 1. The following Lipschitz conditions, respectively, hold true for both Riemann-Liouville and AB derivatives defined in Equations (6) and (7) [48],

$$ \left\| {}^{ABC}_{a}D^{\alpha}_{t}f_1(t) - {}^{ABC}_{a}D^{\alpha}_{t}f_2(t)\right\| < K_1\left\|f_2(x) - f_2(x)\right\|, \quad (10) $$

and

$$ \left\| {}^{ABC}_{a}D^{\alpha}_{t}f_1(t) - {}^{ABC}_{a}D^{\alpha}_{t}f_2(t)\right\| < K_2\left\|f_1(x) - f_2(x)\right\|. \quad (11) $$

Theorem 2. The time-fractional differential equation ${}^{ABC}_{a}D^{\alpha}_{t}f_1(t) = s(t)$ has a unique solution, which is defined as [48]

$$ f(t) = 1 - \frac{\alpha}{\mathcal{B}[\alpha]}s(t) + \frac{\mu}{\mathcal{B}[\alpha]\,\Gamma(\alpha)}\int_a^t s(\varsigma)\,(t-\varsigma)^{\alpha-1}\,d\varsigma. \quad (12) $$

FUNDAMENTAL IDEA OF THE PROPOSED SCHEME

Here, we consider the arbitrary order differential equation in order to demonstrate the basic solution procedure [65, 66]

$$ {}^{ABC}_{a}D^{\alpha}_{t}v(x,t) + \mathcal{R}v(x,t) + \mathcal{N}v(x,t) = f(x,t), \quad n-1 < \alpha \le n, \quad (13) $$

with the initial condition

$$ v(x,0) = g(x), \quad (14) $$

where ${}^{ABC}_{a}D^{\alpha}_{t}v(x,t)$ symbolize the AB derivative of $v(x,t)$. On using the LT on Equation (13), we have after simplification

$$ \mathcal{L}[v(x,t)] - \frac{g(x)}{s} + \frac{1}{\mathcal{B}[\alpha]}\left(1-\alpha+\frac{\alpha}{s^{\alpha}}\right)\left\{\mathcal{L}[\mathcal{R}v(x,t)] + \mathcal{L}[\mathcal{N}v(x,t)] - \mathcal{L}\left[f(x,t)\right]\right\} = 0. \quad (15) $$

The non-linear operator is presented as

$$ \mathcal{N}\left[\varphi(x,t;q)\right] = \mathcal{L}\left[\varphi(x,t;q)\right] - \frac{g(x)}{s} + \frac{1}{\mathcal{B}[\alpha]}\left(1-\alpha+\frac{\alpha}{s^{\alpha}}\right)\left\{\mathcal{L}\left[\mathcal{R}\,\varphi(x,t;q)\right] + L\left[\mathcal{N}\varphi(x,t;q)\right] - L\left[f(x,t)\right]\right\}. \quad (16) $$

Here, $\varphi(x,t;q)$ is the real valued function with respect to x, t and $\left(q \in \left[0, \frac{1}{n}\right]\right)$. Now, we define a homotopy as follows

$$ (1-nq)\,\mathcal{L}\left[\varphi(x,\ t;q) - v_0(x,t)\right] = \hbar q\mathcal{N}\left[\varphi(x,\ t;q)\right], \quad (17) $$

where L is signifies LT, $q \in \left[0, \frac{1}{n}\right]$ $(n \ge 1)$ is the embedding parameter and $\hbar \ne 0$ is an auxiliary parameter. For $q = 0$ and $q = \frac{1}{n}$, the results given below are hold true

$$ \varphi(x,t;0) = v_0(x,t), \quad \varphi\left(x,t;\frac{1}{n}\right) = v(x,t). \quad (18) $$

Now, by intensifying q from 0 to $\frac{1}{n}$, then $\varphi(x,t;q)$ varies from $v_0(x,t)$ to $v(x,t)$. By using the Taylor theorem near to q, we define $\varphi(x,t;q)$ in series form and then we get

$$ \varphi(x,t;q) = v_0(x,t) + \sum\nolimits_{m=1}^{\infty} v_m(x,t)\,q^m, \quad (19) $$

where

$$v_m(x,t) = \frac{1}{m!}\frac{\partial^m \varphi(x,\ t;\ q)}{\partial q^m}|_{q=0}. \tag{20}$$

The series (16) converges at $q = \frac{1}{n}$ for the proper chaise of $v_0(x,t)$, n and $\hbar$. Then

$$v(x,t) = v_0(x,t) + \sum\nolimits_{m=1}^{\infty} v_m(x,t)\left(\frac{1}{n}\right)^m. \tag{21}$$

On m-times differentiating Equation (17) with q and lately dividing by $m!$ and then substituting $q = 0$, we get

$$\mathcal{L}[v_m(x,t) - k_m v_{m-1}(x,t)] = \hbar \Re_m\left(\overrightarrow{v}_{m-1}\right), \tag{22}$$

where the vectors are defined as

$$\overrightarrow{v}_m = \{v_0(x,t), v_1(x,t), \ldots, v_m(x,t)\}. \tag{23}$$

On employing the inverse LT on Equation (22), we have

$$v_m(x,t) = \mathsf{k}_m v_{m-1}(x,t) + \hbar\mathcal{L}^{-1}\left[\Re_m\left(\overrightarrow{v}_{m-1}\right)\right], \tag{24}$$

where

$$\begin{aligned}\Re_m\left(\overrightarrow{v}_{m-1}\right) =\ & L[v_{m-1}(x,t)] - \left(1-\frac{\mathsf{k}_m}{n}\right)\\ & \left(\frac{g(x)}{s} + \frac{1}{\mathcal{B}[\alpha]}\left(1-\alpha+\frac{\alpha}{s^\alpha}\right)L\left[f(x,t)\right]\right)\\ & + \frac{1}{\mathcal{B}[\alpha]}\left(1-\alpha+\frac{\alpha}{s^\alpha}\right)L\left[Rv_{m-1} + \mathcal{H}_{m-1}\right],\end{aligned} \tag{25}$$

and

$$\mathsf{k}_m = \begin{cases} 0, & m \le 1, \\ n, & m > 1. \end{cases} \tag{26}$$

In Equation (25), $\mathcal{H}_m$ signifies a homotopy polynomial and presented as follows

$$\begin{aligned}\mathcal{H}_m =\ & \frac{1}{m!}\left[\frac{\partial^m \varphi\left(x,\ t;\ q\right)}{\partial q^m}\right]_{q=0} \text{ and } \varphi\left(x,\ t;\ q\right)\\ =\ & \varphi_0 + q\varphi_1 + q^2\varphi_2 + \ldots.\end{aligned} \tag{27}$$

By the aid of Equations (24) and (25), one can get

$$\begin{aligned}v_m(x,t) =\ & (\mathsf{k}_m + \hbar)\, v_{m-1}(x,t) - \left(1-\frac{\mathsf{k}_m}{n}\right)\mathcal{L}^{-1}\\ & \left(\frac{g(x)}{s} + \frac{1}{\mathcal{B}[\alpha]}\left(1-\alpha+\frac{\alpha}{s^\alpha}\right)L\left[f(x,t)\right]\right)\\ & + \hbar\mathcal{L}^{-1}\left\{\frac{1}{\mathcal{B}[\alpha]}\left(1-\alpha+\frac{\alpha}{s^\alpha}\right)L\left[Rv_{m-1} + \mathcal{H}_{m-1}\right]\right\}.\end{aligned} \tag{28}$$

Then, the terms of $v_m(x,t)$ we can obtain using the Equation (28). The q-HATM series solution is presented as

$$v(x,t) = \sum_{m=0}^{\infty} v_m(x,t). \tag{29}$$

SOLUTION FOR FRC EQUATION

In order to present the solution procedure and efficiency of the future scheme, in this segment we consider the DSW equation of fractional order with two distinct cases. Further, by the help of obtained results we made an attempt to capture the behavior of q-HATM solution for different fractional order. By the help of Equation (5) for the function of cubic water content and constant, we have

$${}_a^{ABC}D_t^\alpha u(x,t) + u^2 u_x - u_{xx} = 0, \qquad 0 < \alpha \le 1, \tag{30}$$

with initial conditions

$$u(x,0) = u_0(x,t). \tag{31}$$

Taking LT on Equation (29) and then using Equation (30), we get

$$\begin{aligned}L[u(x,t)] =\ & \frac{1}{s}(u_0(x,t))\\ & + \frac{1}{\mathcal{B}[\alpha]}\left(1-\alpha+\frac{\alpha}{s^\alpha}\right)L\left\{u^2u_x - u_{xx}\right\}.\end{aligned} \tag{32}$$

The non-linear operator N is presented with the help of future algorithm as below

$$\begin{aligned}N\left[\varphi(x,t;q)\right] =\ & L\left[\varphi(x,t;q)\right] - \frac{1}{s}(u_0(x,t))\\ & + \frac{1}{\mathcal{B}[\alpha]}\left(1-\alpha+\frac{\alpha}{s^\alpha}\right)\\ & L\left\{\varphi(x,t;q)\frac{\partial\varphi}{\partial x}(x,t;q) - \varphi(x,t;q)\right\}.\end{aligned} \tag{33}$$

The deformation equation of m-th order by the help of q-HATM at $\mathcal{H}(x,t) = 1$, is given as follows

$$L[u_m(x,t) - \mathsf{k}_m u_{m-1}(x,t)] = \hbar\Re_m\left[\overrightarrow{u}_{m-1}\right], \tag{34}$$

where

$$\begin{aligned}\Re_m\left[\overrightarrow{u}_{m-1}\right] =\ & L[u_{m-1}(x,t)] - \left(1-\frac{\mathsf{k}_m}{n}\right)\left\{\frac{1}{s}(u_0(x,t))\right\}\\ & + \frac{1}{\mathcal{B}[\alpha]}\left(1-\alpha+\frac{\alpha}{s^\alpha}\right)\\ & L\{\sum\nolimits_{j=0}^{i}\sum\nolimits_{i=0}^{m-1} u_j u_{i-j}\frac{\partial u_{m-1-i}}{\partial x} - \frac{\partial^2 u_{m-1}}{\partial x^2}\}.\end{aligned} \tag{35}$$

On applying inverse LT on Equation (34), it reduces to

$$u_m(x,t) = \mathsf{k}_m u_{m-1}(x,\ t) + \hbar L^{-1}\left\{\Re_m\left[\overrightarrow{u}_{m-1}\right]\right\}. \tag{36}$$

On simplifying the above equation systematically by using $u_0(x,t)$, we can evaluate the terms of the series solution

$$u(x,t) = u_0(x,t) + \sum_{m=1}^{\infty} u_m(x,t)\left(\frac{1}{n}\right)^m. \tag{37}$$

EXISTENCE OF SOLUTIONS FOR THE FUTURE MODEL

Here, we considered the fixed-point theorem in order to demonstrate the existence of the solution for the proposed model. Since the considered model cited in Equation (30) is non-local as well as complex, there are no particular algorithms or methods that exist to evaluate the exact solutions. However, under some particular conditions, the existence of the solution is assured. Now, Equation (30) is considered:

$$ {}_{0}^{ABC}D_{t}^{\alpha}\left[u\left(x,t\right)\right]=\mathcal{G}\left(x,t,\ u\ \right). \tag{38}$$

The foregoing system is transformed to the Volterra integral equation using the Theorem 2 as follows

$$\begin{aligned} u\left(x,t\right)-u\left(x,0\right) &= \frac{\left(1-\alpha\right)}{\mathcal{B}\left(\alpha\right)}g\left(x,t,u\right) \\ &+\frac{\alpha}{\mathcal{B}\left(\alpha\right)\Gamma\left(\alpha\right)}\int_{0}^{t}g\left(x,\zeta,u\right)\left(t-\zeta\right)^{\alpha-1}d\zeta. \end{aligned} \tag{39}$$

Theorem 3. The kernel g satisfies the Lipschitz condition and contraction if the condition $0 \leq \left(\delta\left(a^2+b^2+ab\right)-\delta^2\right) < 1$ holds.

Proof. In order to prove the required result, we consider the two functions u and u_1, then

$$\begin{aligned} \left\|g\left(x,t,\ u\right)-g\left(x,t,\ u_1\right)\right\| &= \left\|\left[u^2\left(x,t\right)\frac{\partial u\left(x,t\right)}{\partial x}-u^2\left(x,t_1\right)\frac{\partial u\left(x,t_1\right)}{\partial x}\right]\right. \\ &\left.-\left[\frac{\partial^2 u\left(x,t\right)}{\partial x^2}-\frac{\partial^2 u\left(x,t_1\right)}{\partial x^2}\right]\right\| \\ &= \left\|\left[\frac{1}{3}\frac{\partial}{\partial x}\left(u^3\left(x,t\right)-u^3\left(x,t_1\right)\right)\right]\right. \\ &\left.-\left[\frac{\partial^2 u\left(x,t\right)}{\partial x^2}-\frac{\partial^2 u\left(x,t_1\right)}{\partial x^2}\right]\right\| \\ &\leq \left\|\delta\left(a^2+b^2+ab\right)-\delta^2\right\| \\ &\quad \left\|u\left(x,t\right)-u(x,t_1)\right\| \\ &\leq \left(\delta\left(a^2+b^2+ab\right)-\delta^2\right) \\ &\quad \left\|u\left(x,t\right)-u\left(x,t_1\right)\ \right\|, \end{aligned}$$

where $a=\|u\|$ and $b=\|u_1\|$ (since u and u_1 are the bounded functions). Putting $\eta = \delta\left(a^2+b^2+ab\right)-\delta^2$ in the above inequality, then we have

$$\left\|g\left(x,t,\ u\right)-g\left(x,t,\ u_1\right)\right\| \leq \eta\left\|u\left(x,t\right)-u(x,t_1)\ \right\|. \tag{40}$$

The Lipschitz condition is thus obtained for $\mathcal{G}$. Further, we can see that if $0 \leq \left(\delta\left(a^2+b^2+ab\right)-\delta^2\right) < 1$, then it implies the contraction. The recursive form of Equation (36) is defined as

$$\begin{aligned} u_n\left(x,t\right) &= \frac{\left(1-\alpha\right)}{\mathcal{B}\left(\alpha\right)}g\left(x,t,u_{n-1}\right) \\ &+\frac{\alpha}{\mathcal{B}\left(\alpha\right)\Gamma\left(\alpha\right)}\int_{0}^{t}g\left(x,\zeta,u_{n-1}\right)\left(t-\zeta\right)^{\alpha-1}d\zeta. \end{aligned} \tag{41}$$

The associated initial condition is

$$u\left(x,0\right)=u_0\left(x,t\right). \tag{42}$$

The successive difference between the terms is presented as

$$\begin{aligned} \phi_n\left(x,t\right) &= u_n\left(x,t\right)-u_{n-1}\left(x,t\right) \\ &= \frac{\left(1-\alpha\right)}{\mathcal{B}\left(\alpha\right)}\left(g_1\left(x,t,u_{n-1}\right)-g\left(x,t,u_{n-2}\right)\right) \\ &+\frac{\alpha}{\mathcal{B}\left(\alpha\right)\Gamma\left(\alpha\right)}\int_{0}^{t}g\left(x,\zeta,u_{n-1}\right)\left(t-\zeta\right)^{\alpha-1}d\zeta \end{aligned} \tag{43}$$

Notice that

TABLE 1 | Numerical simulation presented for $u\left(x,\ t\right)$ of FR equation consider in Case 1 at $n=1,\ \hbar=-1$ and $\alpha=1$.

x	t	$\left\|u_{Exact}-u^{(3)}_{q-HATM}\right\|$	$\left\|u_{Exact}-u^{(4)}_{q-HATM}\right\|$	$\left\|u_{Exact}-u^{(5)}_{q-HATM}\right\|$
2.5	0.25	6.50636×10^{-7}	1.84782×10^{-8}	1.01181×10^{-10}
	0.50	5.35446×10^{-6}	2.97193×10^{-7}	3.15969×10^{-9}
	0.75	1.85802×10^{-5}	1.51192×10^{-6}	2.33755×10^{-8}
	1	4.52584×10^{-5}	4.80032×10^{-6}	9.57906×10^{-8}
5	0.25	3.86055×10^{-7}	8.87727×10^{-10}	5.42849×10^{-11}
	0.50	3.08044×10^{-6}	1.50958×10^{-8}	1.76075×10^{-9}
	0.75	1.03664×10^{-5}	8.10613×10^{-8}	1.35526×10^{-8}
	1	2.44931×10^{-5}	2.71248×10^{-7}	5.78869×10^{-8}
7.5	0.25	2.68674×10^{-7}	1.50440×10^{-9}	2.57157×10^{-12}
	0.50	2.16147×10^{-6}	2.41095×10^{-8}	8.01731×10^{-11}
	0.75	7.33582×10^{-6}	1.22240×10^{-7}	5.92186×10^{-10}
	1	1.74857×10^{-5}	3.86892×10^{-7}	2.42301×10^{-9}
10	0.25	1.26101×10^{-7}	8.43873×10^{-10}	4.16169×10^{-12}
	0.50	1.01562×10^{-6}	1.35692×10^{-8}	1.33829×10^{-10}
	0.75	3.45096×10^{-6}	6.90365×10^{-8}	1.01990×10^{-9}
	1	8.23569×10^{-6}	2.19278×10^{-7}	4.31168×10^{-9}

TABLE 2 | Numerical simulation presented for $u\left(x,\ t\right)$ of FR equation consider in Case 2 at $n=1,\ \hbar=-1$ and $\alpha=1$.

x	t	$\left\|u_{Exact}-u^{(3)}_{q-HATM}\right\|$	$\left\|u_{Exact}-u^{(4)}_{q-HATM}\right\|$	$\left\|u_{Exact}-u^{(5)}_{q-HATM}\right\|$
2.5	0.25	3.32962×10^{-7}	5.38964×10^{-9}	1.86945×10^{-11}
	0.50	2.70710×10^{-6}	8.65185×10^{-8}	5.83456×10^{-10}
	0.75	9.28381×10^{-6}	4.39361×10^{-7}	4.31477×10^{-9}
	1	2.23573×10^{-5}	1.39264×10^{-6}	1.76784×10^{-8}
5	0.25	9.75190×10^{-8}	5.33186×10^{-10}	1.16072×10^{-11}
	0.50	7.75698×10^{-7}	8.72022×10^{-9}	3.74948×10^{-10}
	0.75	2.60229×10^{-6}	4.51222×10^{-8}	2.87429×10^{-9}
	1	6.12959×10^{-6}	1.45752×10^{-7}	1.22274×10^{-8}
7.5	0.25	9.03607×10^{-8}	2.66049×10^{-10}	2.09943×10^{-13}
	0.50	7.25010×10^{-7}	4.25260×10^{-9}	7.54358×10^{-12}
	0.75	2.45406×10^{-6}	2.15062×10^{-8}	6.08009×10^{-11}
	1	5.83395×10^{-6}	6.78929×10^{-8}	2.69468×10^{-10}
10	0.25	5.17685×10^{-8}	1.88526×10^{-10}	2.13869×10^{-10}
	0.50	4.15714×10^{-7}	3.07483×10^{-9}	3.36348×10^{-9}
	0.75	1.40835×10^{-6}	1.56930×10^{-8}	1.69010×10^{-8}
	1	3.35098×10^{-6}	4.98643×10^{-8}	5.31486×10^{-8}

$$u_n(x,t) = \sum_{i=1}^{n} \phi_i(x,t). \tag{44}$$

By using Equation (39) after applying the norm on the Equation (43), one can get

$$\|\phi_n(x,t)\| \leq \frac{(1-\alpha)}{\mathcal{B}(\alpha)}\eta \left\|\phi_{(n-1)}(x,t)\right\| + \frac{\alpha}{\mathcal{B}(\alpha)\Gamma(\alpha)}\eta \int_0^t \left\|\phi_{(n-1)}(x,\zeta)\right\| d\zeta. \tag{45}$$

We prove the following theorem by using the above result.

Theorem 4. The solution for the Equation (30) will exist, and if we have specific t_0, then

$$\frac{(1-\alpha)}{\mathcal{B}(\alpha)}\eta + \frac{\alpha}{\mathcal{B}(\alpha)\Gamma(\alpha)}\eta < 1.$$

Proof. Let us consider the bounded function $u(x,t)$ satisfying the Lipschitz condition. Then, by Equation (43), we have

$$\|\phi_i(x,t)\| \leq \|u_n(x,0)\| \left[\frac{(1-\alpha)}{\mathcal{B}(\alpha)}\eta + \frac{\alpha}{\mathcal{B}(\alpha)\Gamma(\alpha)}\eta\right]^n. \tag{46}$$

Therefore, the continuity as well as existence of the obtained solution is proved. Subsequently, in order to show the Equation (46) is a solution for the Equation (29), we consider

$$u(x,t) - u(x,0) = u_n(x,t) - \mathcal{K}_n(x,t). \tag{47}$$

In order to obtain require a result, we consider

$$\begin{aligned}\|\mathcal{K}_n(x,t)\| &= \|\frac{(1-\alpha)}{\mathcal{B}(\alpha)}\left(g(x,t,u) - \mathcal{G}\Leftarrow x,t,\ u_{n-1})\right) \\ &+ \frac{\alpha}{\mathcal{B}(\alpha)\Gamma(\alpha)}\int_0^t (t-\zeta)^{\mu-1}\left(g(x,\zeta,u) - g(x,\zeta,u_{n-1})\right)d\zeta\| \\ &\leq \frac{(1-\alpha)}{\mathcal{B}(\alpha)}\left\|g(x,\zeta,u) - g(x,\zeta,u_{n-1})\right\| \\ &+ \frac{\alpha}{\mathcal{B}(\alpha)\Gamma(\alpha)}\int_0^t \left\|g(x,\zeta,u) - g(x,\zeta,u_{n-1})\right\| d\zeta \\ &\leq \frac{(1-\alpha)}{\mathcal{B}(\alpha)}\eta_1\|u-u_{n-1}\| + \frac{\alpha}{\mathcal{B}(\alpha)\Gamma(\alpha)}\eta_1\|u-u_{n-1}\|t. \end{aligned} \tag{48}$$

Similarly, at t_0 we can obtain

$$\|\mathcal{K}_n(x,t)\| \leq \left(\frac{(1-\alpha)}{\mathcal{B}(\alpha)} + \frac{\alpha t_0}{\mathcal{B}(\alpha)\Gamma(\alpha)}\right)^{n+1}\eta^{n+1}M. \tag{49}$$

As n approaches to ∞, we can see that form Equation (49), $\|\mathcal{K}_n(x,t)\|$ tends to 0.

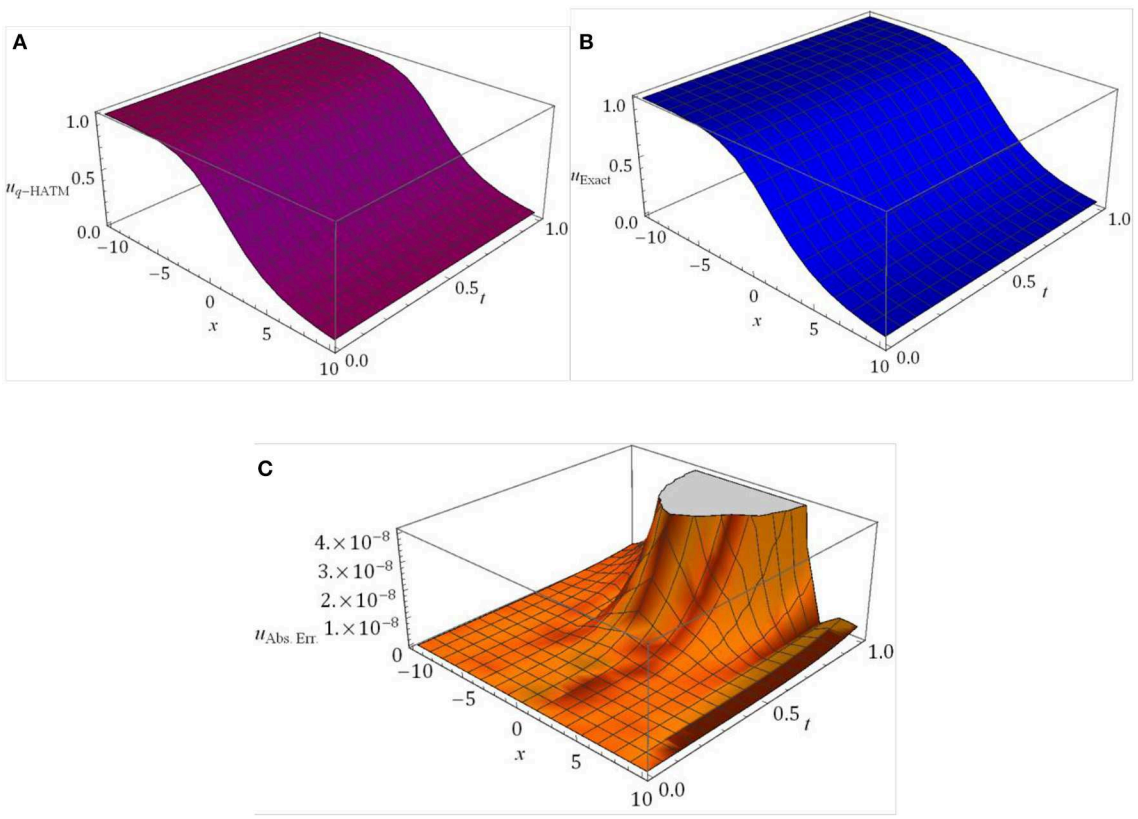

FIGURE 1 | Surfaces of **(A)** u_{q-HATM}, **(B)** u_{Exact} **(C)** $u_{Abs.\ Err.} = |u_{Exact} - u_{q-HATM}|$ for FR equation considered in Case 1 at $\hbar = -1$, $n = 1$ and $\alpha = 1$.

Next, it is a necessity to demonstrate uniqueness for the solution of the considered model. Suppose $u^*(x,t)$ is the other solution, then we have

$$u(x,t) - u^*(x,t) = \frac{(1-\alpha)}{\mathcal{B}(\alpha)}\left(g(x,t,u) - g(x,t,u^*)\right) + \frac{\alpha}{\mathcal{B}(\alpha)\Gamma(\alpha)}\int_0^t \left(g(x,\zeta,u) - g(x,\zeta,u^*)\right)d\zeta. \tag{50}$$

On applying norm, the Equation (50) simplifies to

$$\begin{aligned}\left\|u(x,t) - u^*(x,t)\right\| &= \left\|\frac{(1-\alpha)}{\mathcal{B}(\alpha)}\left(g(x,t,u) - g(x,,t,u^*)\right)\right. \\ &\left. + \frac{\alpha}{\mathcal{B}(\alpha)\Gamma(\alpha)}\int_0^t \left(g(x,\zeta,u) - g(x,\zeta,u^*)\right)d\zeta\right\| \\ &\leq \frac{(1-\alpha)}{\mathcal{B}(\alpha)}\eta\left\|u(x,t) - u^*(x,t)\right\| \\ &+ \frac{\alpha}{\mathcal{B}(\alpha)\Gamma(\alpha)}\eta t\left\|u(x,t) - u^*(x,t)\right\|. \end{aligned} \tag{51}$$

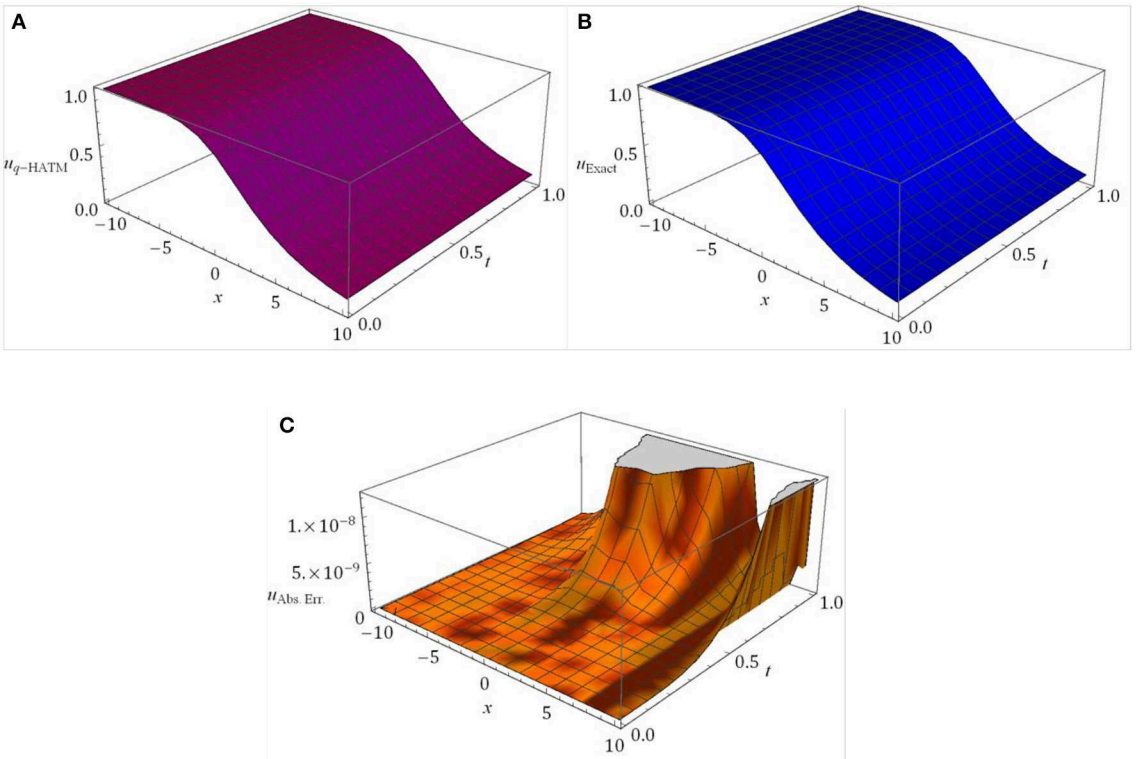

FIGURE 2 | Surfaces of **(A)** u_{q-HATM}, **(B)** u_{Exact} **(C)** $u_{Abs.\ Err.} = \left|u_{Exact} - u_{q-HATM}\right|$ for FR equation considered in Case 2 at $\hbar = -1$, $n = 1$ and $\alpha = 1$.

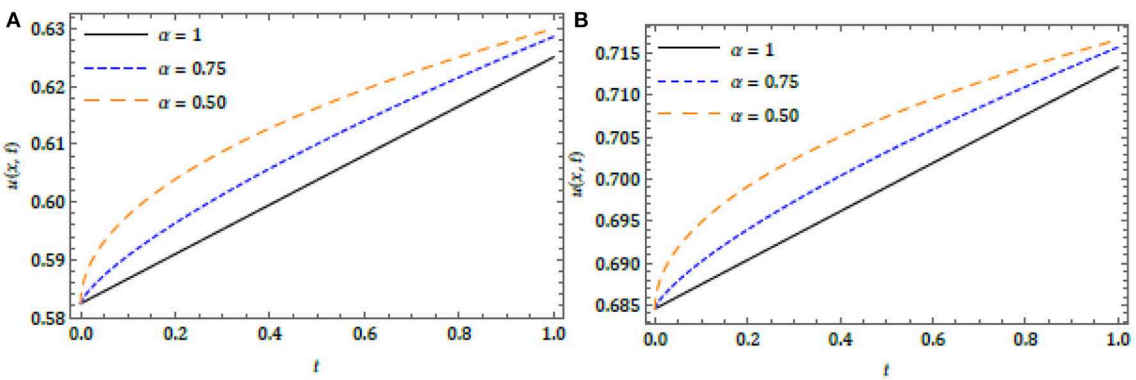

FIGURE 3 | Nature of the*q*-HATM solution for **(A)** Case 1 and **(B)** Case 2 with distinct α at $\hbar = -1$, $n = 1$ and $x = 1$.

On simplification

$$\left\| u\left(x,t\right) - u^{*}\left(x,t\right) \right\| \left(1 - \frac{\left(1-\alpha\right)}{\mathcal{B}\left(\alpha\right)}\eta - \frac{\alpha}{\mathcal{B}\left(\alpha\right)\Gamma\left(\alpha\right)}\eta t \right) \leq 0. \tag{52}$$

From the above condition, it is clear that $u\left(x,t\right) = u^{*}\left(x,t\right)$, if

$$\left(1 - \frac{\left(1-\alpha\right)}{\mathcal{B}\left(\alpha\right)}\eta - \frac{\alpha}{\mathcal{B}\left(\alpha\right)\Gamma\left(\alpha\right)}\eta t \right) \geq 0. \tag{53}$$

Hence, Equation (53) proves our essential result.

Theorem 5. Suppose $u_n\ (x,\ t)$ and $u\ (x,\ t)$ are defined in the Banach space $(\mathfrak{B}\left[0,\ T\right],\ \|\cdot\|)$. The series solution defined in Equation (29) converges to the solution of the Equation (13), if $0 < \lambda < 1$.

Proof: Consider the sequence $\{\mathcal{S}_n\}$, which is the partial sum of the Equation (29), and we have to prove $\{\mathcal{S}_n\}$ is the Cauchy sequence in $(\mathfrak{B}\left[0,\ T\right],\ \|\cdot\|)$. Now consider

$$\begin{aligned}
&\left\| \mathcal{S}_{n+1}\left(x,t\right) - \mathcal{S}_n\left(x,t\right) \right\| = \left\| u_{n+1}\left(x,t\right) \right\| \\
&\leq \lambda \left\| u_n\left(x,t\right) \right\| \\
&\leq \lambda^2 \left\| u_{n-1}\left(x,t\right) \right\| \leq \ldots \leq \lambda^{n+1} \left\| u_0\left(x,t\right) \right\|.
\end{aligned}$$

Now, we have for every $n,\ m \in N\ (m \leq n)$

$$\begin{aligned}
&\left\| \mathcal{S}_n - \mathcal{S}_m \right\| = \left\| \left(\mathcal{S}_n - \mathcal{S}_{n-1}\right) + \left(\mathcal{S}_{n-1} - \mathcal{S}_{n-2}\right) \right. \\
&\left. + \ldots + \left(\mathcal{S}_{m+1} - \mathcal{S}_m\right) \right\| \\
&\leq \left\| \mathcal{S}_n - \mathcal{S}_{n-1} \right\| + \left\| \mathcal{S}_{n-1} - \mathcal{S}_{n-2} \right\| + \ldots + \left\| \mathcal{S}_{m+1} - \mathcal{S}_m \right\| \\
&\leq \left(\lambda^n + \lambda^{n-1} + \ldots + \lambda^{m+1}\right) \left\| u_0 \right\| \\
&\leq \lambda^{m+1} \left(\lambda^{n-m-1} + \lambda^{n-m-2} + \ldots + \lambda + 1\right) \left\| u_0 \right\| \\
&\leq \lambda^{m+1} \left(\frac{1-\lambda^{n-m}}{1-\lambda} \right) \left\| u_0 \right\|.
\end{aligned} \tag{54}$$

But $0 < \lambda < 1$, therefore $\left\| \mathcal{S}_n - \mathcal{S}_m \right\| = 0$. Hence, $\{\mathcal{S}_n\}$ is the Cauchy sequence. This proves the required result.

NUMERICAL RESULTS AND DISCUSSION

In the present investigation, we have found the solution for equation describing the water transport in unsaturated porous media using q-HATM with the help of Mittag-Leffler law. Here, we consider two distinct cases to present the effectiveness of the proposed method.

Case 1: In this case, we consider the conductivity term as a function of cubic water content and constant $\sigma = \frac{u^3}{3} cm/h$ and $\rho = 1\ cm^{2/h}$. At $a = c = \frac{1}{3}$, $n = 3$ and $b = -1$, Equation (4) becomes

$$\underset{a}{^{ABC}}D_t^a u(x,t) + u^2 u_x - u_{xx} = 0, \qquad 0 < \alpha \leq 1, \tag{55}$$

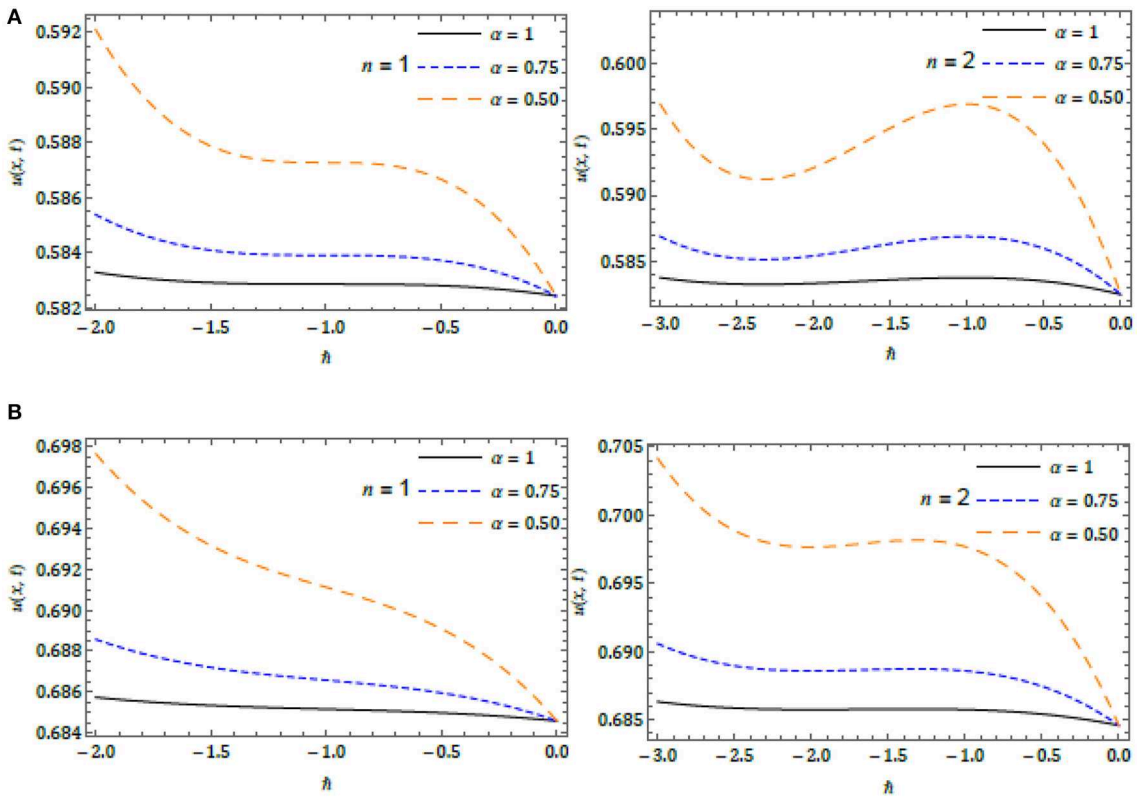

FIGURE 4 | $\hbar$-curves for **(A)** Case 1 **(B)** Case 2 with distinct α at $x = 1$ and $t = 0.01$ with $n = 1$ and 2.

with initial condition

$$u(x,0) = \sqrt{\frac{1}{2}\left(1+\tanh\left(-\frac{x}{3}\right)\right)}. \tag{56}$$

Case 2: In this segment, we consider the conductivity term as a function of quadric water content and constant $\sigma = \frac{u^4}{4} cm/h$ and $\rho = 1\ cm^{2/h}$. At $a = c = \frac{1}{1}$, $n = 1$ and $b = -1$, the Equation (4) becomes

$${}^{ABC}_{a}D^{\alpha}_{t}u(x,t) + u^3 u_x - u_{xx} = 0, \qquad 0 < \alpha \leq 1, \tag{57}$$

with initial condition

$$u(x,0) = \sqrt[3]{\frac{1}{2}\left(1+\tanh\left(-\frac{3x}{8}\right)\right)}. \tag{58}$$

Here, we demonstrate the numerical simulation for the considered non-linear. In **Tables 1** and **2**, the error analysis has been validated. From the tables we can see that the proposed scheme is more accurate, and we confirm that the iterations increase the q-HATM solutions so that they get closer to the analytical solution.

The surfaces of the obtained solution and the exact solution in comparison with absolute error have been captured, respectively, in **Figures 1** and **2** for Case 1 and Case 2. The behavior of the obtained solution for different orders is presented in **Figure 3** for both the cases in terms of 2D plots. In order to analyze the variations of the obtained solution for the FRC equation cited in Case 1 and Case 2 with respect to the homotopy parameter ($\hbar$), and the ($\hbar$) curves are drawn for diverse μ and presented in **Figure 4** with distinct n. In the plots, the horizontal line signifies the convergence region of the q-HATM solution and these curves aid us to adjust and handle the convergence province of the solution. For an appropriate value of $\hbar$, the achieved solution quickly tends to the exact solution. The small deviation in the physical behavior of the complex models stimulates the enormous new results to analyze and understand the nature in a better and systematic manner. Moreover, from all the plots we can see that the proposed method is more accurate and very effective in its analysis of the considered non-linear fractional order equations.

Since every non-linear differential equation does not have an exact solution we look for an approximated analytical solution thorugh which we can prove the exactness or accuracy of the proposed scheme, as opposed to an exact solution. As we mentioned earlier, the q-HATM is a modified algorithm of HAM, and it thus does not require perturbation, dissertation, linearization, or any assumptions. More importantly, the future method generalizes many traditional techniques, such as HAM, HPM, FRDTM, and others, because these are a special case of q-HATM ($n = 1$, $\hbar = 1$). In connection with this, we capture the physical behavior of q-HATM solution to illustrate the accuracy. Further, we noticed that the considered non-linear phenomenon is highly dependent on a fractional operator. In order to illustrate the computational level and computational cost, the numerical simulation has been presented. From the table, it shows that as a number of series terms increases the solution converges to an analytical solution.

CONCLUSION

In this paper, the q-HATM is applied profitably to find the solution for an arbitrary order RC equation describing the water transport in the unsaturated porous media. Since AB derivatives and integrals having fractional order are defined with the help of generalized Mittag-Leffler function as the non-local kernel and non-singular, the present investigation illuminates the effectiveness of the considered derivative. The existence and uniqueness of the obtained solution is demonstrated by the fixed point hypothesis. The results obtained by the future scheme are more stimulating as compared to results available in the literature. Further, the proposed algorithm finds the solution of the non-linear problem without considering any discretization, perturbation or transformations.

The behavior of the obtained series solution has been captured in terms of 2D and 3D plots for distinct fractional order. These plots show that the q-HATM solution is more accurate and also conformed with the help of numerical simulation, and this is cited in the tables. Further, we confirm that, as the order of the solution increases, the obtained solutions converge to the exact solution. The present investigation illuminates how the considered complex non-linear phenomena noticeably depend on the time history and the time instant, which can be proficiently analyzed by applying the concept of calculus to fractional order. The present investigation helps the researchers to study the behavior of non-linear problems, and this gives very interesting and useful consequences. The proposed derivative provides non-singular kernel and non-local properties; these properties are very essential in describing the physical behavior and nature of the non-linear problems, and hence researchers can consider the AB derivative to solve many non-linear complex problems. Lastly, we can conclude the projected method is extremely methodical, effective and very accurate, and that it can be applied to the analysis of the diverse classes of non-linear problems that exist in science and technology.

DATA AVAILABILITY STATEMENT

All datasets generated for this study are included in the article/supplementary material.

AUTHOR CONTRIBUTIONS

All the authors have worked equally in this manuscript. All the authors have read and approved the final manuscript.

REFERENCES

1. Liouville J. Memoire surquelques questions de geometrieet de mecanique, etsur un nouveau genre de calcul pour resoudreces questions. *JEcolePolytech*. (1832) **13**:1–69.
2. Riemann GFB. *Versuch Einer Allgemeinen Auffassung der Integration und Differentiation*. Leipzig: Gesammelte Mathematische Werke (1896).
3. Caputo M. *Elasticita e Dissipazione*. Bologna: Zanichelli (1969).
4. Miller KS, Ross B. *An Introduction to Fractional Calculus and Fractional Differential Equations*. New York, NY: Wiley (1993).
5. Podlubny I. *Fractional Differential Equations*. New York, NY: Academic Press (1999).
6. Kilbas AA, Srivastava HM, Trujillo JJ. *Theory and Applications of Fractional Differential Equations*. Amsterdam: Elsevier (2006).
7. Baleanu D, Guvenc ZB, Tenreiro Machado JA. *New Trends in Nanotechnology and Fractional Calculus Applications*. London; New York, NY: Springer Dordrecht Heidelberg (2010). doi: 10.1007/978-90-481-3293-5
8. Esen S, Sulaiman TA, Bulut H, Baskonus HM. Optical solitons and other solutions to the conformable space-time fractional Fokas-Lenells equation. *Optik*. (2018) **167**:150–6. doi: 10.1016/j.ijleo.2018.04.015
9. Veeresha P, Prakasha DG, Baskonus HM. Solving smoking epidemic model of fractional order using a modified homotopy analysis transform method. *Math Sci.* (2019) **13**:115–28. doi: 10.1007/s40096-019-0284-6
10. Baleanu D, Wu GC, Zeng SD. Chaos analysis and asymptotic stability of generalized Caputo fractional differential equations. *Chaos Solitons Fractals*. (2017) **102**:99–105. doi: 10.1016/j.chaos.2017.02.007
11. Veeresha P, Prakasha DG, Baskonus HM. New numerical surfaces to the mathematical model of cancer chemotherapy effect in Caputo fractional derivatives *Chaos*. (2019) **29**:013119. doi: 10.1063/1.5074099
12. Baskonus HM, SulaimanTA, Bulut H. On the new wave behavior to the Klein-Gordon-Zakharov equations in plasma physics. *Indian J Phys.* (2019) **93**:393–9. doi: 10.1007/s12648-018-1262-9
13. Prakasha DG, Veeresha P, Baskonus HM. Analysis of the dynamics of hepatitis E virus using the Atangana-Baleanu fractional derivative, *Eur Phys J Plus*. (2019) **134**:1–11. doi: 10.1140/epjp/i2019-12590-5
14. Veeresha P, Prakasha DG, Baleanu D. An efficient numerical technique for the nonlinear fractional Kolmogorov-Petrovskii-Piskunov equation. *Mathematics*. (2019) **7**:1–18. doi: 10.3390/math7030265
15. Yokuş A, Gülbahar S. Numerical solutions with linearization techniques of the fractional Harry Dym equation. *Appl Math Nonlinear Sci*. (2019) **4**:35–42. doi: 10.2478/AMNS.2019.1.00004
16. Cattani C. Haar wavelet-based technique for sharp jumps classification. *Math Comp Model*. (2004) **39**:255–78. doi: 10.1016/S0895-7177(04)90010-6
17. Yang A-M, Zhang Y-Z, Cattani C, Xie G-N, Rashidi MM, Zhou Y-J, et al. Application of local fractional series expansion method to solve Klein-Gordon equations on Cantor sets. *Abstr Appl Anal*. (2014) **2014**:372741. doi: 10.1155/2014/372741
18. Zhang Y, Cattani C, Yang X-J. Local fractional homotopy perturbation method for solving non-homogeneous heat conduction equations in fractal domains. *Entropy*. (2015) **17**:6753–64. doi: 10.3390/e17106753
19. Prakasha DG, Veeresha P, Baskonus HM. Residual power series method for fractional Swift–Hohenberg equation. *Fractal Fract*. (2019) **3**:1–9. doi: 10.3390/fractalfract3010009
20. Singh J, Kumar D, Hammouch Z, Atangana A. A fractional epidemiological model for computer viruses pertaining to a new fractional derivative. *Appl Math Comput*. (2018) **316**:504–15. doi: 10.1016/j.amc.2017.08.048
21. Asif NA, Hammouch Z, Riaz MB, Bulut H. Analytical solution of a Maxwell fluid with slip effects in view of the Caputo-Fabrizio derivative. *Eur Phys J Plus*. (2018) **133**:272. doi: 10.1140/epjp/i2018-12098-6
22. Veeresha P, Prakasha DG, Magesh N, Nandeppanavar MM, Christopher AJ. Numerical simulation for fractional Jaulent–Miodek equation associated with energy-dependent Schrödinger potential using two novel techniques. *Waves Random Complex Media*. (2019). doi: 10.1080/17455030.2019.1651461. [Epub ahead of print].
23. Baskonus HM, Mekkaoui T, Hammouch Z, Bulut H. Active control of a chaotic fractional order economic system. *Entropy*. (2015) **17**:5771–83. doi: 10.3390/e17085771
24. Ravichandran C, Jothimani K, Baskonus HM, Valliammal N. New results on nondensely characterized integrodifferential equations with fractional order, *EurPhys J Plus*. (2018) **133**:1–10. doi: 10.1140/epjp/i2018-11966-3
25. Gao W, Ghanbari B, Baskonus HM. New numerical simulations for some real world problems with Atangana-Baleanu fractional derivative. *Chaos Solitons Fractals*. (2019) **128**:34–43. doi: 10.1016/j.chaos.2019.07.037
26. Atangana A, Koca I. Chaos in a simple nonlinear system with Atangana–Baleanu derivatives with fractional order. *Chaos Solitons Fractals*. (2016) **89**:447–54. doi: 10.1016/j.chaos.2016.02.012
27. Abro KA, Mirbhar MN, Gómez-Aguilar JF. Functional application of Fourier sine transform in radiating gas flow with non-singular and non-local kernel. *J Braz Soc Mech Sci Eng*. (2019) **41**:400. doi: 10.1007/s40430-019-1899-0
28. Abro KA, Khan I, Gómez-Aguilar JF. Thermal effects of magnetohydrodynamic micropolar fluid embedded in porous medium with Fourier sine transform technique. *J Braz Soc Mech Sci Eng*. (2019) **41**:174. doi: 10.1007/s40430-019-1671-5
29. Abro KA, Gómez-Aguilar JF. A comparison of heat and mass transfer on a Walter's B fluid via Caputo-Fabrizio versus Atangana-Baleanu fractional derivatives using the Fox-H function. *Eur Phys J Plus*. (2019) **134**:101. doi: 10.1140/epjp/i2019-12507-4
30. Gómez-Aguilar1 JF, Yépez-Martínez H, Torres-Jiménez J, Córdova-Fraga T, Escobar-JiméneRF, Olivares-Peregrino VH. Homotopy perturbation transform method for nonlinear differential equations involving to fractional operator with exponential kernel. *Adv Diff Equ*. (2017) **2017**:68. doi: 10.1186/s13662-017-1120-7
31. Yepez-Martineza H, Gomez-Aguilar JF, Sosaa IO, Reyesa JM, Torres-Jimenez J. The Feng's first integral method applied to the nonlinear mKdV space-time fractional partial differential equation. *Rev Mex Fís*. (2016) **62**:310–6. doi: 10.1155/2016/7047126
32. Gómez-Aguilar JF, Torres L, Yépez-Martínez H, Baleanu D, Reyes JM, Sosa IO. Fractional Liénard type model of a pipeline within the fractional derivative without singular kernel. *Adv Diff Equ*. (2016) **2016**:173. doi: 10.1186/s13662-016-0908-1
33. Morales-Delgado VF, Taneco-Hernández MA, Gómez-Aguilar JF. On the solutions of fractional order of evolution equations. *Eur Phys J Plus*. (2017) **132:**47. doi: 10.1140/epjp/i2017-11341-0
34. Singh J, Kumar D, Baleanu D. New aspects of fractional Biswas-Milovic model with Mittag-Leffler law. *Math Model Nat Phenom*. (2019) **14**:1–23. doi: 10.1051/mmnp/2018068
35. Bhatter S, Mathur A, Kumar D, Singh J. A new analysis of fractional Drinfeld–Sokolov–Wilson model with exponential memory. *Phys A*. (2020) **537**:122578. doi: 10.1016/j.physa.2019.122578
36. Kumar D, Singh J, Baleanu D. On the analysis of vibration equation involving a fractional derivative with Mittag-Leffler law. *Math Methods Appl Sci*. (2019). doi: 10.1002/mma.5903. [Epub ahead of print].
37. Goswami A, Singh J, Kumar D, Sushila. An efficient analytical approach for fractional equal width equations describing hydro-magnetic waves in cold plasma. *Phys A*. (2020) **524**:563–75. doi: 10.1016/j.physa.2019.04.058
38. Kumar D, Singh J, Qurashi MA, Baleanu D. A new fractional SIRS-SI malaria disease model with application of vaccines, anti-malarial drugs, and spraying. *Adv Diff Equ*. (2019) **2019**:278. doi: 10.1186/s13662-019-2199-9
39. Veeresha P, Prakasha DG, Kumar D. An efficient technique for nonlinear time-fractional Klein–Fock–Gordon equation. *Appl Math Comput*. (2020) **364**:124637. doi: 10.1016/j.amc.2019.124637
40. Richards LA. Capillary conduction of liquids through porous medium. *Physics*. (1931) **1**:318–33. doi: 10.1063/1.1745010
41. Brooks RH, Corey AT. *Hydraulic Properties of Porous Media*. Hydrol Paper 3. Fort Collins, CO: Colorado State University (1964).
42. Corey AT. *Mechanics of Immiscible Fluids in Porous Media*. Highlands Ranch, CO: Water Resource Publications (1994).
43. Whitam GB. *Linear and Nonlinear Waves*. New York, NY: Wiley. (1974).
44. Basha HA. Burgers' equation: a general nonlinear solution of infiltration and redistribution. *Water Resour Res*. (2002) **38**:1–9. doi: 10.1029/2001WR000954
45. Nasseri M, Shaghaghian MR, Daneshbod Y, Seyyedian H. An analytic solution of water transport in unsaturated porous media. *J Porous Media*. (2008) **11**:591–601. doi: 10.1615/JPorMedia.v11.i6.60
46. Jafari H, Firoozjaee MA. Application of homotopy analysis method for water transport in unsaturated porous media. *Stud Nonlinear Sci*. (2010) **1**:8–13.

47. Caputo M. Fabrizio M. A new definition of fractional derivative without singular kernel. *Prog Fract Diff Appl.* (2015) **1**:73–85. doi: 10.12785/pfda/010201
48. Atangana A, Baleanu D. New fractional derivatives with non-local and non-singular kernel theory and application to heat transfer model. *Therm Sci.* (2016) **20**:763–9. doi: 10.2298/TSCI160111018A
49. Liao SJ. Homotopy analysis method and its applications in mathematics. *J Basic Sci Eng*. (1997) **5**:111–25.
50. Liao SJ. Homotopy analysis method: a new analytic method for nonlinear problems. *Appl Math Mech.* (1998) **19**:957–62. doi: 10.1007/BF02457955
51. Singh J, Kumar D, SwroopR. Numerical solution of time- and space-fractional coupled Burgers' equations via homotopy algorithm. *Alexandria Eng J.* (2016) **55**:1753–63. doi: 10.1016/j.aej.2016.03.028
52. Srivastava HM, Kumar D, Singh J. An efficient analytical technique for fractional model of vibration equation. *Appl Math Model.* (2017) **45**:192–204. doi: 10.1016/j.apm.2016.12.008
53. Prakasha DG, Veeresha P, Baskonus HM. Two novel computational techniques for fractional Gardner and Cahn-Hilliard equations, *Comp Math Methods*. (2019) **1**:1–19. doi: 10.1002/cmm4.1021
54. Bulut H, Kumar D, Singh J, Swroop R, Baskonus HM. Analytic study for a fractional model of HIV infection of CD4+T lymphocyte cells. *Math Nat Sci*. (2018) **2**:33–43. doi: 10.22436/mns.02.01.04
55. Veeresha P, Prakasha DG. Solution for fractional Zakharov-Kuznetsov equations by using two reliable techniques. *Chinese J Phys*. (2019) **60**:313–30. doi: 10.1016/j.cjph.2019.05.009
56. Kumar D, Agarwal RP, Singh J. A modified numerical scheme and convergence analysis for fractional model of Lienard's equation. *J Comput Appl Math*. (2018) **399**:405–13. doi: 10.1016/j.cam.2017.03.011
57. Prakash A, Prakasha DG, Veeresha P. A reliable algorithm for time-fractional Navier-Stokes equations via Laplace transform. *Nonlinear Eng*. (2019). **8**:695–701. doi: 10.1515/nleng-2018-0080
58. Veeresha P, Prakasha DG, Baskonus HM. Novel simulations to the time-fractional Fisher's equation. *Math Sci*. (2019) **13**:33–42. doi: 10.1007/s40096-019-0276-6
59. Prakash A, Veeresha P, Prakasha DG, Goyal M. A homotopy technique for fractional order multi-dimensional telegraph equation via Laplace transform. *Eur Phys J Plus*. (2019) **134**:19. doi: 10.1140/epjp/i2019-12411-y
60. Singh J, Kumar D, Baleanu D, Rathore S. An efficient numerical algorithm for the fractional Drinfeld–Sokolov–Wilson equation. *Appl Math Comput*. (2018) **335**:12–24. doi: 10.1016/j.amc.2018.04.025
61. Parlang J-Y, Barry DA, Parlange MB, Hogarth WL, Haverkamp R, Ross PJ, et al. New approximate analytical technique to solve Richards equation for arbitrary surface boundary conditions. *Water Resour Res*. (1997) **33**:903–6. doi: 10.1029/96WR03846
62. Parlang J-Y, Hogarth WL, Barry DA, Parlange MB, Haverkamp R, Ross PJ, et al. Analytical approximation to the solutions of Richards' equation with applications to infiltration, ponding, and time compression approximation. *Adv Water Resour*. (1999) **23**:189–94. doi: 10.1016/S0309-1708(99)00022-6
63. Atangana A, Alkahtani BT. Analysis of the Keller-Segel model with a fractional derivative without singular kernel. *Entropy*. (2015) **17**:4439–53. doi: 10.3390/e17064439
64. Alkahtani BT, Atangana A. Analysis of non-homogenous heat model with new trend of derivative with fractional order. *Chaos Solitons Fractals*. (2016) **89**:566–71. doi: 10.1016/j.chaos.2016.03.027
65. Singh J, Kumar D, Swroop R, Kumar S. An Efficient computational approach for time-fractional Rosenau-Hyman equation. *Neural Comput Appl*. (2018) **30**:3063–70. doi: 10.1007/s00521-017-2909-8
66. Veeresha P, Prakasha DG. A novel technique for (2 + 1)-dimensional time-fractional coupled Burgers equations. *Math Comput Simulation*. (2019) **166**:324–45. doi: 10.1016/j.matcom.2019.06.005

Conflict of Interest: The authors declare that the research was conducted in the absence of any commercial or financial relationships that could be construed as a potential conflict of interest.

frontiers in Physics

ORIGINAL RESEARCH
published: 17 January 2020
doi: 10.3389/fphy.2019.00220

Numerical Analysis of the Susceptible Exposed Infected Quarantined and Vaccinated (SEIQV) Reaction-Diffusion Epidemic Model

Nauman Ahmed[1,2], *Mehreen Fatima*[3], *Dumitru Baleanu*[4,5], *Kottakkaran Sooppy Nisar*[6], *Ilyas Khan*[2*], *Muhammad Rafiq*[7], *Muhammad Aziz ur Rehman*[1] and *Muhammad Ozair Ahmad*[8]

[1] Department of Mathematics, University of Management and Technology, Lahore, Pakistan, [2] Department of Mathematics, College of Science Al-Zulfi, Majmaah University, Al-Majma'ah, Saudi Arabia, [3] Department of Electrical Engineering, University of Lahore, Lahore, Pakistan, [4] Department of Mathematics, Cankaya University, Ankara, Turkey, [5] Institute of Space Sciences, Măgurele, Romania, [6] Department of Mathematics, College of Arts and Sciences, Wadi Aldawaser, Prince Sattam Bin Abdulaziz University, Al-Kharj, Saudi Arabia, [7] Faculty of Engineering, University of Central Punjab, Lahore, Pakistan, [8] Department of Mathematics and Statistics, University of Lahore, Lahore, Pakistan

In this paper, two structure-preserving nonstandard finite difference (NSFD) operator splitting schemes are designed for the solution of reaction diffusion epidemic models. The proposed schemes preserve all the essential properties possessed by the continuous systems. These schemes are applied on a diffusive SEIQV epidemic model with a saturated incidence rate to validate the results. Furthermore, the stability of the continuous system is proved, and the bifurcation value is evaluated. A comparison is also made with the existing operator splitting numerical scheme. Simulations are also performed for numerical experiments.

Keywords: splitting methods, NSFD schemes, positivity, epidemic model, stability, bifurcation value

OPEN ACCESS

Edited by:
Devendra Kumar,
University of Rajasthan, India

Reviewed by:
Yudhveer Singh,
Amity University Jaipur, India
Vinod Gill,
Government Post Graduate College, Hisar, India

***Correspondence:**
Ilyas Khan
ilyaskhan@tdtu.edu.vn

Specialty section:
This article was submitted to Mathematical Physics, a section of the journal Frontiers in Physics

Received: *06 October 2019*
Accepted: *28 November 2019*
Published: *17 January 2020*

Citation:
Ahmed N, Fatima M, Baleanu D, Nisar KS, Khan I, Rafiq M, Rehman MA and Ahmad MO (2020) Numerical Analysis of the Susceptible Exposed Infected Quarantined and Vaccinated (SEIQV) Reaction-Diffusion Epidemic Model. Front. Phys. 7:220. doi: 10.3389/fphy.2019.00220

1. INTRODUCTION

Mathematical modeling has a prominent role in describing physical phenomena in various disciplines of mathematics, physical sciences, social sciences, engineering, life sciences, and many more [1–6]. The transmission of infectious diseases and the control of their spread can be studied effectively by constructing mathematical models for various strategies like vaccination and quarantine. The word quarantine denotes forced isolation or being cut off from interactions with others. Quarantine is an effective intervention process for restraining the spread of infection by isolating individuals who are affected by the disease. Such isolation has been adopted to decrease the communication of infectious diseases like dengue, measles, smallpox, cholera, leprosy, tuberculosis, and many more.

Epidemic models, that is, mathematical models of infectious diseases, are a simplified way to illustrate the transmission dynamics of the complicated nonlinear processes and complex behavior of an infectious disease in individuals within a population. These are deterministic models that are used to allocate the population to different subclasses or compartments, describing a particular stage of the epidemic. The incidence rate, which is proportional to the number of susceptible and infected persons, is an important parameter of compartment-based epidemic models. The mathematical models of infectious diseases are often based on bilinear incidence rate βSI, but a more concise approach to use the saturated incidence rate rather than the bilinear incidence rate. In the saturated incidence rate $\frac{\beta SI}{1+\alpha I}$, if number of infected individuals I becomes very large, $\frac{\beta SI}{1+\alpha I}$ approaches the saturation level. The infection force is measured by βI, which describes

the penetration of the disease into a fully susceptible population. $\frac{1}{1+\alpha I}$ is used to measure the inhibition effect of behavioral change of susceptible persons. Liu and Yang [7] proposed the SEIQV epidemic model, which uses the saturated incidence rate. The model is expressed as:

$$\frac{dS(t)}{dt} = b - \frac{\beta S(t)I(t)}{1+\alpha I(t)} - \left(\omega + \mu + q_3\right) S(t) \tag{1}$$

$$\frac{dE(t)}{dt} = \frac{\beta S(t)I(t)}{1+\alpha I(t)} - \left(\mu + \sigma + q_2\right) E(t) \tag{2}$$

$$\frac{dI(t)}{dt} = \sigma E(t) - \left(\mu + \epsilon + \gamma + q_1\right) I(t) \tag{3}$$

$$\frac{dQ(t)}{dt} = q_3 S(t) + q_2 E(t) + q_1 I(t) - (\mu + \phi)\, Q(t) \tag{4}$$

$$\frac{dV(t)}{dt} = \omega S(t) + \phi Q(t) + \gamma I(t) - \mu V(t) \tag{5}$$

The variables and parameters of the model are defined as:
$S(t)$ = Susceptible persons at time t,
$E(t)$ = Exposed persons at time t,
$I(t)$ = Infected persons at time t,
$Q(t)$ = Quarantined persons at time t,
$V(t)$ = Vaccinated persons at time t,
b = Rate of recruitment,
β = Rate of transmission,
μ = Rate of natural death,
ϵ = Rate of death due to disease in infected compartment,
α = Parameter that measures psychological or inhibitory effects,
γ = Rate at which infected individuals are being vaccinated infected persons,
σ = Rate at which exposed persons become infected,
ω = Rate at which infected individuals are being vaccinated susceptible persons,
ϕ = Rate at which infected individuals are being vaccinated quarantined persons,
q_1, q_2, q_3 = Effective quarantine probabilities.

The above model (1)–(5) assumes a homogeneous population, where the population mixes in such a way that there is no difference between person in one place and person in another place. However, in actual scenarios, the disease may spread faster in one place than in another because of different circumstances like different weather conditions, etc. Hence, it is essential for the variables to depend on space also. Therefore, we extend system (1)–(5) to make it a reaction-diffusion system by adding a diffusion term.

$$\frac{\partial S(x,t)}{\partial t} = b - \frac{\beta S(x,t)I(x,t)}{1+\alpha I(x,t)} - \left(\omega + \mu + q_3\right) S(x,t) + d_1 \frac{\partial^2 S(x,t)}{\partial x^2} \tag{6}$$

$$\frac{\partial E(x,t)}{\partial t} = \frac{\beta S(x,t)I(x,t)}{1+\alpha I(x,t)} - \left(\mu + \sigma + q_2\right) E(x,t) + d_2 \frac{\partial^2 E(x,t)}{\partial x^2} \tag{7}$$

$$\frac{\partial I(x,t)}{\partial t} = \sigma E(x,t) - \left(\mu + \epsilon + \gamma + q_1\right) I(x,t) + d_3 \frac{\partial^2 I(x,t)}{\partial x^2} \tag{8}$$

$$\frac{\partial Q(x,t)}{\partial t} = q_3 S(x,t) + q_2 E(x,t) + q_1 I(x,t) - (\mu + \phi)\, Q(x,t) + d_4 \frac{\partial^2 Q(x,t)}{\partial x^2} \tag{9}$$

$$\frac{\partial V(x,t)}{\partial t} = \omega S(x,t) + \phi Q(x,t) + \gamma I(x,t) - \mu V(x,t) + d_5 \frac{\partial^2 V(x,t)}{\partial x^2} \tag{10}$$

with the initial conditions:

$$S(x,0) = g_1(x) \qquad 0 \le x \le L \tag{11}$$

$$E(x,0) = g_2(x) \qquad 0 \le x \le L \tag{12}$$

$$I(x,0) = g_3(x) \qquad 0 \le x \le L \tag{13}$$

$$Q(x,0) = g_4(x) \qquad 0 \le x \le L \tag{14}$$

$$V(x,0) = g_5(x) \qquad 0 \le x \le L \tag{15}$$

The boundary conditions are no flux,

$$S_x(0,t) = S_x(L,t) = 0 \tag{16}$$

$$E_x(0,t) = E_x(L,t) = 0 \tag{17}$$

$$I_x(0,t) = I_x(L,t) = 0 \tag{18}$$

$$Q_x(0,t) = Q_x(L,t) = 0 \tag{19}$$

$$V_x(0,t) = V_x(L,t) = 0 \tag{20}$$

Epidemic models always demonstrate two equilibrium points: the disease-free equilibrium (DFE) point and the endemic equilibrium (EE) point. The DFE point exists if $R_0 < 1$, where R_0 is the reproductive number, which basically measures the occurrence of disease. The EE point exists if $R_0 > 1$. This implies that the SEIQV reaction-diffusion system (6–10) always converges to the DFE point or EE point if $R_0 < 1$ or $R_0 > 1$, respectively. Analytical solution of the SEIQV epidemic system is not possible, so we have to use numerical techniques to find its solution. Note that the numerical technique must show the same behavior as is possessed by the continuous SEIQV reaction-diffusion epidemic system.

In this work, we propose two operator-splitting NSFD methods, one explicit and one implicit. These methods are used to solve the SEIQV epidemic model with diffusion. As S, E, I, Q, and V are population sizes and evaluated in absolute scale, we propose NSFD methods because they give a positive solution. Also, the convergence of the proposed NSFD operator splitting methods toward the equilibrium points is the same as the convergence of continuous an SEIQV reaction-diffusion epidemic system. The proposed splitting methods are designed with the aid of rules given by Mickens [8]. In the recent era, positivity preserving FD methods have gained importance, as many physical dynamical systems possess the positivity property [9–11]. The NSFD method presented by Mickens [8, 12, 13] has becomes an effective and important structure-preserving FD method for solving differential equations. In epidemic models, population dynamics and population size cannot be negative, so the numerical technique must be a positivity-preserving technique. Various authors have used different positivity-preserving numerical techniques for the approximate solution of epidemic models: see, for example [14–22].

In this work, we also show the numerical stability of the SEIQV epidemic model with diffusion and evaluate the bifurcation value of the vaccination parameter ω with the aid of the Routh-Hurwitz method.

2. EQUILIBRIUM POINTS

The model (6–10) has two equilibrium points [7], the DFE point and EE point. The DFE point is:

$$\begin{aligned} DFE &= (S_0, E_0, I_0, Q_0, V_0) \\ &= \left(\frac{b}{\omega+\mu+q_3}, 0, 0, \frac{q_3 S_0}{\mu+\phi}, \frac{\omega S_0 + \phi Q_0}{\mu}\right) \end{aligned} \tag{21}$$

and the EE point is:

$$EE = (S_*, E_*, I_*, Q_*, V_*) \tag{22}$$

where,

$$\begin{aligned} S_* &= \frac{(\mu+\sigma+q_2)(\mu+\epsilon+\gamma+q_1)(1+\alpha I)}{\gamma\beta} \\ E_* &= \frac{(\mu+\epsilon+\gamma+q_1) I}{\sigma} \\ Q_* &= \frac{q_3 S + q_2 E + q_1 I}{\mu+\phi} \\ V_* &= \frac{\omega S + \phi Q + \gamma I}{\mu} \\ I* &= \frac{\sigma\beta b - (\omega+\mu+q_3)(\mu+\sigma+q_2)(\mu+\epsilon+\gamma+q_1)}{(\mu+\sigma+q_2)(\mu+\epsilon+\gamma+q_1)(\beta+\alpha(\omega+\mu+q_3))} \end{aligned}$$

Reproductive number R_0 is given as:

$$\begin{aligned} R_0 &= \frac{\sigma\beta b}{(\omega+\mu+q_3)(\mu+\sigma+q_2)(\mu+\epsilon+\gamma+q_1)}, \\ &\text{when, } d_1 = d_2 = d_3 = d_4 = d_5 = 0 \end{aligned}$$

R_0 is the reproductive value. Now, if $R_0 < 1$, the model acquires a DFE point, and if $R_0 > 1$, the model acquires an EE point.

3. NUMERICAL STABILITY OF THE SEIQV MODEL AT EQUILIBRIUM POINT

We evaluated the small perturbation $S_1(x,t)$, $E_1(x,t)$, $I_1(x,t)$, $Q_1(x,t)$, and $V_1(x,t)$ so that (6)–(10) is linearized at the EE point $(S_*, E_*, I_*, Q_*, V_*)$, as discussed in Chakrabrty et al. [23].

$$\frac{\partial S_1}{\partial t} = a_{11}S_1 + a_{12}E_1 + a_{13}I_1 + a_{14}Q_1 + a_{15}V_1 + d_1\frac{\partial^2 S_1}{\partial x^2} \tag{23}$$

$$\frac{\partial E_1}{\partial t} = a_{21}S_1 + a_{22}E_1 + a_{23}I_1 + a_{24}Q_1 + a_{25}V_1 + d_2\frac{\partial^2 E_1}{\partial x^2} \tag{24}$$

$$\frac{\partial I_1}{\partial t} = a_{31}S_1 + a_{32}E_1 + a_{33}I_1 + a_{34}Q_1 + a_{35}V_1 + d_3\frac{\partial^2 I_1}{\partial x^2} \tag{25}$$

$$\frac{\partial Q_1}{\partial t} = a_{41}S_1 + a_{42}E_1 + a_{43}I_1 + a_{44}Q_1 + a_{45}V_1 + d_4\frac{\partial^2 Q_1}{\partial x^2} \tag{26}$$

$$\frac{\partial V_1}{\partial t} = a_{51}S_1 + a_{52}E_1 + a_{53}I_1 + a_{54}Q_1 + a_{55}V_1 + d_5\frac{\partial^2 V_1}{\partial x^2} \tag{27}$$

Suppose a Fourier series solution is demonstrated for Equations (23)–(27) of the form:

$$S_1(x,t) = \sum_k S_k e^{\lambda t} cos(kx) \tag{28}$$

$$E_1(x,t) = \sum_k E_k e^{\lambda t} cos(kx) \tag{29}$$

$$I_1(x,t) = \sum_k I_k e^{\lambda t} cos(kx) \tag{30}$$

$$Q_1(x,t) = \sum_k Q_k e^{\lambda t} cos(kx) \tag{31}$$

$$V_1(x,t) = \sum_k V_k e^{\lambda t} cos(kx) \tag{32}$$

Here, $k = n\pi/2, (n = 1, 2, 3, ...)$ exhibits the value of the wave number for the node n. Substituting Equations (28)–(32) in the system (23)–(27), the system is converted into:

$$\sum_k (a_{11} - d_1k^2 - \lambda)S_k + \sum_k a_{12}E_k + \sum_k a_{13}I_k + \sum_k a_{14}Q_k + \sum_k a_{15}V_k = 0 \tag{33}$$

$$\sum_k a_{21}S_k + \sum_k (a_{22} - d_2k^2 - \lambda)E_k + \sum_k a_{23}I_k + \sum_k a_{24}Q_k + \sum_k a_{25}V_k = 0 \tag{34}$$

$$\sum_k a_{31}S_k + \sum_k a_{32}E_k + \sum_k (a_{33} - d_3k^2 - \lambda)I_k + \sum_k a_{34}Q_k + \sum_k a_{35}V_k = 0 \tag{35}$$

$$\sum_k a_{41}S_k + \sum_k a_{42}E_k + \sum_k a_{43}I_k + \sum_k (a_{44} - d_4k^2 - \lambda)Q_k + \sum_k a_{45}V_k = 0 \tag{36}$$

$$\sum_k a_{51}S_k + \sum_k a_{52}E_k + \sum_k a_{53}I_k + \sum_k a_{54}Q_k + \sum_k (a_{55} - d_5k^2 - \lambda)V_k = 0 \tag{37}$$

The variational matrix $\mathcal{V}$ for the system (33)–(37) is:

$$\mathcal{V} = \begin{pmatrix} a_{11} - d_1k^2 & a_{12} & a_{13} & a_{14} & a_{15} \\ a_{21} & a_{22} - d_2k^2 & a_{23} & a_{24} & a_{25} \\ a_{31} & a_{32} & a_{33} - d_3k^2 & a_{34} & a_{35} \\ a_{41} & a_{42} & a_{43} & a_{44} - d_4k^2 & a_{45} \\ a_{51} & a_{52} & a_{53} & a_{54} & a_{55} - d_5k^2 \end{pmatrix} \tag{38}$$

where,

$$a_{11} = -\frac{\beta I_*}{(1+\alpha I_*)} - (\omega+\mu+q_3), a_{12} = 0, a_{13} = -\frac{\beta S_*}{(1+\alpha I_*)^2}$$

TABLE 1 | Values of parameters.

Cases	b	μ	σ	β	γ	ω	q_1
1	0.7[a]	0.06[a]	0.7[a]	0.35[a]	0.15[a]	0.06[a]	0.2[a]
2	0.7	0.06	0.7	0.35	0.15	0.07	0.2
4	0.7	0.06	0.7	0.35	0.15	0.09	0.2
5	0.7	0.06	0.7	0.35	0.15	0.10	0.2

q_2	q_3	ϕ	ϵ	α
0.2[a]	0.1[a]	0.4[a]	0.05[a]	2[a]
0.2	0.1	0.5	0.05	2
0.2	0.1	0.6	0.05	2
0.2	0.1	0.7	0.05	2
0.2	0.1	0.8	0.05	2

[a]*Liu et al. [7].*

$$a_{14} = 0, a_{15} = 0, a_{21} = \frac{\beta I_*}{(1+\alpha I_*)}, a_{22} = -(\sigma+\mu+q_2)$$
$$a_{23} = \frac{\beta S_*}{(1+\alpha I_*)^2}, a_{24} = 0, a_{25} = 0, a_{31} = 0, a_{32} = \sigma$$
$$a_{33} = -(\mu+\epsilon+\gamma+q_1), a_{34} = 0, a_{35} = 0, a_{41} = q_3, a_{42} = q_2,$$
$$a_{43} = q_1$$
$$a_{44} = -(\mu+\phi), a_{45} = 0, a_{51} = \omega, a_{52} = 0, a_{53} = \gamma, a_{54} = \phi,$$
$$a_{55} = -\mu$$

The characteristics equation for matrix $\mathcal{V}$ is:

$$\lambda^5 + \xi_1\lambda^4 + \xi_2\lambda^3 + \xi_3\lambda^2 + \xi_4\lambda + \xi_5 = 0$$

The expressions for ξ_1, ξ_2, ξ_3, ξ_4, and ξ_5 with diffusion and without diffusion are mentioned in Islam and Haider [24].

The Routh-Hurwitz stability criterion gives:

$$\xi_1 > 0, \xi_2 > 0, \xi_3 > 0, \xi_4 > 0, \xi_5 > 0$$

$$t_1 = \xi_1\xi_2\xi_3 - \xi_3^2 - \xi_1^2\xi_4 > 0$$

and

$$t_2 = (\xi_1\xi_4 - \xi_5)(\xi_1\xi_2\xi_3 - \xi_3^2 - \xi_1^2\xi_4) - \xi_5(\xi_1\xi_2 - \xi_3)^2 - \xi_1\xi_5^2 > 0.$$

The **Table 2** reflects the numerical stability of the equilibrium point against the various cases, as discussed in **Table 1**.

4. BIFURCATION VALUE OF VACCINATION PARAMETER ω INDEPENDENT OF DIFFUSION

Considering the vaccination parameter ω, to find its bifurcation value, a_{11}, a_{12}, are used instead of S_*, E_*, I_*, Q_*, and V_*.

$$a_{11} = -0.6893640968\omega - 0.2309369724,$$
$$a_{13} = -1.1198107335\omega - 0.3751365957$$

TABLE 2 | Stability of equilibrium point.

Case	Point of equilibrium	n	ξ_1	ξ_2
1	(2.5707, 0.1400, 0.2131, 0.7124, 7.8528)	1	2.4122	1.8086
2	(2.5072, 0.1285, 0.1955, 0.5634, 8.1091)	1	2.5191	2.0081
3	(2.4468, 0.1175, 0.1787, 0.4605, 8.3142)	1	2.6259	2.2090
4	(2.3892, 0.1070, 0.1628, 0.3854, 8.4867)	1	2.7328	2.4112
5	(2.3343, 0.0970, 0.1475, 0.3283, 8.6366)	1	2.8397	2.6149

ξ_3	ξ_4	ξ_5	t_1	t_2	Stability
0.5585	0.0715	0.0030	1.7083	0.2457	Stable
0.6450	0.0833	0.0035	2.3180	0.4095	Stable
0.7318	0.0944	0.0040	3.0585	0.6444	Stable
0.8191	0.1048	0.0043	3.9434	0.9685	Stable
0.9067	0.1146	0.0046	4.9869	1.4018	Stable

$$a_{21} = 0.0709369724 - 0.3106359032\omega, a_{22} = -0.96$$
$$a_{23} = 1.1198107335\omega + 0.3751365957, a_{32} = 0.7,$$
$$a_{33} = -0.46, a_{41} = 0.1, a_{42} = 0.2$$
$$a_{43} = 0.2, a_{44} = -0.46, a_{51} = \omega, a_{53} = 0.15, a_{54} = 0.4,$$
$$a_{55} = -0.06$$
$$a_{12} = a_{14} = a_{15} = a_{24} = a_{25} = a_{31} = a_{34} = a_{35} = a_{45} = a_{52} = 0$$

The Routh-Hurwitz criterion for stability gives:

$$\begin{aligned}
\xi_1 &= 0.6893640968\omega + 2.1709369724 = f_1(\omega)\\
\xi_2 &= 0.5534988343\omega + 1.3930221095 = f_2(\omega)\\
\xi_3 &= -0.7838675135\omega^2 + 0.0368505571\omega\\
&\quad + 0.3691384683 = f_3(\omega)\\
\xi_4 &= -0.4076111070\omega^2 - 0.0380846274\omega\\
&\quad + 0.0451739663 = f_4(\omega)\\
\xi_5 &= -0.0216347434\omega^2 - 0.0023071181\omega\\
&\quad + 0.00165507 = f_5(\omega)\\
\xi_1\xi_2\xi_3 - \xi_3^2 - \xi_1^2\xi_4 &= -0.7198363952\omega^4 - 0.3846861900\omega^3\\
&\quad + 0.4409094061\omega^2 + 0.9265604777\omega\\
&\quad + 0.7671683354 = f_6(\omega)
\end{aligned}$$

$$\begin{aligned}
(\xi_1\xi_4 - \xi_5)(\xi_1\xi_2\xi_3 - \xi_3^2 - \xi_1^2\xi_4) - \xi_5(\xi_1\xi_2 - \xi_3)^2 - \xi_1\xi_5^2\\
= 0.2022686014\omega^7 + 0.7777858386\omega^6 + 0.3637035355\omega^5\\
- 0.4633365077\omega^4 - 0.8380985505\omega^3 - 0.5245415951\omega^2\\
+ 0.0491674986\omega + 0.0622935244 = f_7(\omega)
\end{aligned}$$

where the values of $\xi_1, \xi_2, \xi_3, \xi_4$, and ξ_5 are obtained from the expression of the characteristic equation (without diffusion) given in paper [24].

$f_5(\omega) = 0$ gives the value of bifurcation for ω. This value transfers the stability of a continuous model from stable to unstable. $f_5(\omega) = 0$ provides the bifurcation value $\omega = 0.228360507$. The EE point is stable for ω less than $\omega = 0.228360507$.

5. BIFURCATION VALUE OF VACCINATION PARAMETER ω WITH DIFFUSION

For the bifurcation value of vaccination parameter ω, the values of S_*, E_*, I_*, Q_*, and V_* are replaced into a_{11}, a_{12}, to

$$\begin{aligned}
a_{11} &= -0.6893640968\omega - 0.2309369724,\\
a_{13} &= -1.1198107335\omega - 0.3751365957\\
a_{21} &= 0.0709369724 - 0.3106359032\omega, a_{22} = -0.96\\
a_{23} &= 1.1198107335\omega + 0.3751365957, a_{32} = 0.7, a_{33} = -0.46,\\
a_{41} &= 0.1\\
a_{42} &= 0.2, a_{43} = 0.2, a_{44} = -0.46, a_{51} = \omega, a_{53} = 0.15,\\
a_{54} &= 0.4, a_{55} = -0.06\\
a_{14} &= a_{12} = a_{15} = a_{24} = a_{25} = a_{31} = a_{34} = a_{35}\\
&= a_{45} = a_{52} = 0
\end{aligned}$$

The Routh-Hurwitz criterion for stability gives:

$$\begin{aligned}
\xi_1 &= 0.6893640968\omega + 2.3707964615 = f_1(\omega)\\
\xi_2 &= 0.60622790397\omega + 1.7722067841 = f_2(\omega)\\
\xi_3 &= -0.7838675135\omega^2 - 0.0208144715\omega\\
&\quad + 0.5625469972 = f_3(\omega)\\
\xi_4 &= -0.4462934183\omega^2 - 0.0884716755\omega\\
&\quad + 0.0784487226 = f_4(\omega)\\
\xi_5 &= -0.0321693682\omega^2 - 0.0070094221\omega\\
&\quad + 0.0035676470 = f_5(\omega)\\
\xi_1\xi_2\xi_3 - \xi_3^2 - \xi_1^2\xi_4 &= -0.7299468904\omega^4 - 0.6247499708\omega^3\\
&\quad + 0.5281660018\omega^2 + 1.6725898825\omega\\
&\quad + 1.6061706299 = f_6(\omega)
\end{aligned}$$

$$\begin{aligned}
&(\xi_1\xi_4 - \xi_5)(\xi_1\xi_2\xi_3 - \xi_3^2 - \xi_1^2\xi_4) - \xi_5(\xi_1\xi_2 - \xi_3)^2 - \xi_1\xi_5^2\\
&= 0.2245744816\omega^7 + 1.0320435772\omega^6 + 0.8416645931\omega^5\\
&\quad -0.5793147772\omega^4 - 1.7894315920\omega^3 - 1.3916904163\omega^2\\
&\quad +0.0896889602\omega + 0.2457209648 = f_7(\omega)
\end{aligned}$$

$f_5(\omega) = 0$ gives $\omega = 0.24144152$. The EE point is stable therefore for any value less than $\omega = 0.24144152$.

It can be seen that the value of bifurcation of ω for the system with diffusion is greater than value of bifurcation of ω for the system without diffusion.

6. NUMERICAL METHODS

In this section, we apply two proposed and classical splitting methods to the SEIQV reaction-diffusion epidemic model with diffusion. Operator-splitting techniques very effectively handle the nonlinearity and complexity of reaction-diffusion equations. Therefore, these techniques are used frequently by several researchers for the solution of nonlinear differential equations [23, 25–33]. The SEIQV epidemic model with diffusion is split in two ways. The nonlinear reaction equations are split in the first step as,

$$\frac{1}{2}\frac{\partial S}{\partial t} = b - \frac{\beta SI}{1+\alpha I} - \left(\omega + \mu + q_3\right) S \tag{39}$$

$$\frac{1}{2}\frac{\partial E}{\partial t} = \frac{\beta SI}{1+\alpha I} - \left(\mu + \sigma + q_2\right) E \tag{40}$$

$$\frac{1}{2}\frac{\partial I}{\partial t} = \sigma E - \left(\mu + \epsilon + \gamma + q_1\right) I \tag{41}$$

$$\frac{1}{2}\frac{\partial Q}{\partial t} = q_3 S + q_2 E + q_1 I - (\mu + \phi)\, Q \tag{42}$$

$$\frac{1}{2}\frac{\partial V}{\partial t} = \omega S + \phi Q + \gamma I - \mu V \tag{43}$$

and the diffusion equations are split in the second step as:

$$\frac{1}{2}\frac{\partial S}{\partial t} = d_1\frac{\partial^2 S}{\partial x^2} \tag{44}$$

$$\frac{1}{2}\frac{\partial E}{\partial t} = d_2\frac{\partial^2 E}{\partial x^2} \tag{45}$$

$$\frac{1}{2}\frac{\partial I}{\partial t} = d_3\frac{\partial^2 I}{\partial x^2} \tag{46}$$

$$\frac{1}{2}\frac{\partial Q}{\partial t} = d_4\frac{\partial^2 Q}{\partial x^2} \tag{47}$$

$$\frac{1}{2}\frac{\partial V}{\partial t} = d_5\frac{\partial^2 V}{\partial x^2} \tag{48}$$

Now, we apply forward and backward Euler methods with operator splitting on the system (6)–(7).

$$\overline{S}_i^{m+\frac{1}{2}} = S_i^m + \tau\left(b - \frac{\beta S_i^m I_i^m}{1+\alpha I_i^m} - \left(\omega + \mu + q_3\right) S_i^m\right) \tag{49}$$

$$\overline{E}_i^{m+\frac{1}{2}} = E_i^m + \tau\left(\frac{\beta S_i^m I_i^m}{1+\alpha I_i^m} - \left(\mu + \sigma + q_2\right) E_i^m\right) \tag{50}$$

$$\overline{I}_i^{m+\frac{1}{2}} = I_i^m + \tau\left(\sigma E_i^m - \left(\mu + \epsilon + \gamma + q_1\right) I_i^m\right) \tag{51}$$

$$\overline{Q}_i^{m+\frac{1}{2}} = Q_i^m + \tau\left(q_3 S_i^m + q_2 E_i^m + q_1 I_i^m - (\mu + \phi)\, Q_i^m\right) \tag{52}$$

$$\overline{V}_i^{m+\frac{1}{2}} = V_i^m + \tau\left(\omega S_i^m + \phi Q_i^m + \gamma I_i^m - \mu V_i^m\right) \tag{53}$$

where $S_i^m, E_i^m, I_i^m, Q_i^m$ and V_i^m at $m\tau, m = 0, 1, ...$ and $0 + ih, i = 0, 1, ...$ reflects difference approximations of S, E, I, Q, and V. The values of $\overline{S}_i^{m+\frac{1}{2}}$, $\overline{E}_i^{m+\frac{1}{2}}$, $\overline{I}_i^{m+\frac{1}{2}}$, $\overline{Q}_i^{m+\frac{1}{2}}$, and $\overline{V}_i^{m+\frac{1}{2}}$ are the values at the half time step. Both forward and backward Euler methods have same process at first step, but, at the second half step of time, they have different procedures. Since the forward Euler operator splitting method is explicit, we use:

$$S_i^{m+1} = \overline{S}_i^{m+\frac{1}{2}} + \lambda_1\left(\overline{S}_{i-1}^{m+\frac{1}{2}} - 2\overline{S}_i^{m+\frac{1}{2}} + \overline{S}_{i+1}^{m+\frac{1}{2}}\right) \tag{54}$$

$$E_i^{m+1} = \overline{E}_i^{m+\frac{1}{2}} + \lambda_2\left(\overline{E}_{i-1}^{m+\frac{1}{2}} - 2\overline{E}_i^{m+\frac{1}{2}} + \overline{E}_{i+1}^{m+\frac{1}{2}}\right) \tag{55}$$

$$I_i^{m+1} = \overline{I}_i^{m+\frac{1}{2}} + \lambda_3\left(\overline{I}_{i-1}^{m+\frac{1}{2}} - 2\overline{I}_i^{m+\frac{1}{2}} + \overline{I}_{i+1}^{m+\frac{1}{2}}\right) \tag{56}$$

$$Q_i^{m+1} = \overline{Q}_i^{m+\frac{1}{2}} + \lambda_4 \left(\overline{Q}_{i-1}^{m+\frac{1}{2}} - 2\overline{Q}_i^{m+\frac{1}{2}} + \overline{Q}_{i+1}^{m+\frac{1}{2}} \right) \quad (57)$$

$$V_i^{m+1} = \overline{V}_i^{m+\frac{1}{2}} + \lambda_5 \left(\overline{V}_{i-1}^{m+\frac{1}{2}} - 2\overline{V}_i^{m+\frac{1}{2}} + \overline{V}_{i+1}^{m+\frac{1}{2}} \right) \quad (58)$$

For the backward Euler method, we use:

$$-\lambda_1 S_{i-1}^{m+1} + (1+2\lambda_1)\, S_i^{m+1} - \lambda_1 S_{i-1}^{m+1} = \overline{S}_i^{m+\frac{1}{2}} \quad (59)$$

$$-\lambda_2 E_{i-1}^{m+1} + (1+2\lambda_2)\, E_i^{m+1} - \lambda_2 E_{i-1}^{m+1} = \overline{E}_i^{m+\frac{1}{2}} \quad (60)$$

$$-\lambda_3 I_{i-1}^{m+1} + (1+2\lambda_3)\, I_i^{m+1} - \lambda_3 I_{i-1}^{m+1} = \overline{I}_i^{m+\frac{1}{2}} \quad (61)$$

$$-\lambda_4 Q_{i-1}^{m+1} + (1+2\lambda_4)\, Q_i^{m+1} - \lambda_4 Q_{i-1}^{m+1} = \overline{Q}_i^{m+\frac{1}{2}} \quad (62)$$

$$-\lambda_5 V_{i-1}^{m+1} + (1+2\lambda_5)\, V_i^{m+1} - \lambda_5 V_{i-1}^{m+1} = \overline{V}_i^{m+\frac{1}{2}} \quad (63)$$

For the proposed NSFD operator splitting methods, we implement the rules constructed by Mickens [8]. The technique for both explicit and implicit schemes is similar at the first half time step:

$$\overline{S}_i^{m+\frac{1}{2}} = \frac{S_i^m + \tau b}{1 + \frac{\tau \beta I_i^m}{1+\alpha I_i^m} + \tau\left(\omega + \mu + q_3\right)} \quad (64)$$

$$\overline{E}_i^{m+\frac{1}{2}} = \frac{E_i^m + \frac{\tau \beta S_i^m I_i^m}{1+\alpha I_i^m}}{1 + \tau(\mu + \sigma + q_2)} \quad (65)$$

$$\overline{I}_i^{m+\frac{1}{2}} = \frac{I_i^m + \tau \sigma E_i^m}{1 + \tau(\mu + \epsilon + \gamma + q_1)} \quad (66)$$

$$\overline{Q}_i^{m+\frac{1}{2}} = \frac{Q_i^m + \tau(q_3 S_i^m + q_2 E_i^m + q_1 I_i^m)}{1 + \tau(\mu + \phi)} \quad (67)$$

$$\overline{V}_i^{m+\frac{1}{2}} = \frac{V_i^m + \tau(\omega S_i^m + \phi Q_i^m + \gamma I_i^m)}{1 + \tau\mu} \quad (68)$$

A positive solution desires that if:

$$\begin{aligned} &S_i^m \geq 0, E_i^m \geq 0, I_i^m \geq 0, Q_i^m \geq 0, V_i^m \geq 0 \\ \Longrightarrow\ &\overline{S}_i^{m+\frac{1}{2}} \geq 0, \overline{E}_i^{m+\frac{1}{2}} \geq 0, \overline{I}_i^{m+\frac{1}{2}} \geq 0, \overline{Q}_i^{m+\frac{1}{2}} \geq 0, \overline{V}_i^{m+\frac{1}{2}} \geq 0 \end{aligned} \quad (69)$$

The techniques for the implicit and explicit NSFD schemes are not similar for the second half of the time step. The procedure for the explicit NSFD scheme is as follows:

$$S_i^{m+1} = (1-2\lambda_1)\, \overline{S}_i^{m+\frac{1}{2}} + \lambda_1 \left(\overline{S}_{i-1}^{m+\frac{1}{2}} + \overline{S}_{i+1}^{m+\frac{1}{2}} \right) \quad (70)$$

$$E_i^{m+1} = (1-2\lambda_2)\, \overline{E}_i^{m+\frac{1}{2}} + \lambda_2 \left(\overline{E}_{i-1}^{m+\frac{1}{2}} + \overline{E}_{i+1}^{m+\frac{1}{2}} \right) \quad (71)$$

$$I_i^{m+1} = (1-2\lambda_3)\, \overline{I}_i^{m+\frac{1}{2}} + \lambda_3 \left(\overline{I}_{i-1}^{m+\frac{1}{2}} + \overline{I}_{i+1}^{m+\frac{1}{2}} \right) \quad (72)$$

$$Q_i^{m+1} = (1-2\lambda_4)\, \overline{Q}_i^{m+\frac{1}{2}} + \lambda_4 \left(\overline{Q}_{i-1}^{m+\frac{1}{2}} + \overline{Q}_{i+1}^{m+\frac{1}{2}} \right) \quad (73)$$

$$V_i^{m+1} = (1-2\lambda_5)\, \overline{V}_i^{m+\frac{1}{2}} + \lambda_5 \left(\overline{V}_{i-1}^{m+\frac{1}{2}} + \overline{V}_{i+1}^{m+\frac{1}{2}} \right) \quad (74)$$

We use an implicit procedure for the second NSFD method at the second half of the time step:

$$-\lambda_1 S_{i-1}^{m+1} + (1+2\lambda_1)\, S_i^{m+1} - \lambda_1 S_{i-1}^{m+1} = \overline{S}_i^{m+\frac{1}{2}} \quad (75)$$

$$-\lambda_2 E_{i-1}^{m+1} + (1+2\lambda_2)\, E_i^{m+1} - \lambda_2 E_{i-1}^{m+1} = \overline{E}_i^{m+\frac{1}{2}} \quad (76)$$

$$-\lambda_3 I_{i-1}^{m+1} + (1+2\lambda_3)\, I_i^{m+1} - \lambda_3 I_{i-1}^{m+1} = \overline{I}_i^{m+\frac{1}{2}} \quad (77)$$

$$-\lambda_4 Q_{i-1}^{m+1} + (1+2\lambda_4)\, Q_i^{m+1} - \lambda_4 I_{i-1}^{m+1} = \overline{Q}_i^{m+\frac{1}{2}} \quad (78)$$

$$-\lambda_5 V_{i-1}^{m+1} + (1+2\lambda_5)\, V_i^{m+1} - \lambda_5 V_{i-1}^{m+1} = \overline{V}_i^{m+\frac{1}{2}} \quad (79)$$

where,

$$\lambda_1 = d_1 \frac{\tau}{h^2}, \lambda_2 = d_2 \frac{\tau}{h^2}, \lambda_3 = d_3 \frac{\tau}{h^2}, \lambda_4 = d_4 \frac{\tau}{h^2}, \lambda_5 = d_5 \frac{\tau}{h^2}$$

6.1. Stability and Accuracy of Splitting Schemes

In finite difference operator splitting techniques, the step involving the reaction term is unconditionally stable because it is solved exactly [25, 26]. On the other hand, the step involving the diffusion term has different stability in different techniques. The explicit procedure has conditional stability in the region:

$$\lambda_i \leq \frac{1}{2}, (i = 1, 2, 3, 4, 5). \quad (80)$$

while the implicit procedure has unconditionally stability [25, 26]. The accuracy of both schemes is $O(\tau)$ and $O(h^2)$ for all the methods under study.

6.2. Positivity of Proposed Schemes

Equations (64)–(65) in the reaction step of both proposed methods preserve the property of positivity depicted by the continuous SEIQV model, as there is no negative term involved in (64)–(65).

As far as the diffusion step is concerned, the proposed explicit scheme (70)–(74) demonstrates the positivity of the solution if:

$$1 - 2\lambda_i \geq 0, i = 1, 2, 3, 4, 5$$

so,

$$\lambda_i \leq \frac{1}{2}, (i = 1, 2, 3, 4, 5)$$

which is the condition of stability for the explicit operator-splitting NSFD scheme (70)–(74). This verifies that the explicit NSFD scheme retains the positive solution in the region of stability. M matrix theory has been used for the verification of the positivity of the implicit NSFD method (75)–(79). For more details [34] is referred.

6.2.1. Theorem [21, 22]

For any positive τ and h, the system described by (75)–(79) is also positive, i.e., $S^m > 0, E^m > 0, Q^m > 0$ and $V^m > 0$, $\forall m = 0, 1, 2...$

Proof
Equations (75)–(79) can be written as:

$$AS^{m+1} = S^m \tag{81}$$
$$BE^{m+1} = E^m \tag{82}$$
$$CI^{m+1} = I^m \tag{83}$$
$$DQ^{m+1} = Q^m \tag{84}$$
$$GV^{m+1} = V^m \tag{85}$$

In Equations (81)–(85), the letters A, B, C, D, and G represent the square matrices. Where,

$$A = \begin{pmatrix} a_3 & a_1 & 0 & \cdots & \cdots & \cdots & \cdots & 0 \\ a_2 & a_3 & a_2 & \ddots & & & & \vdots \\ 0 & a_2 & a_3 & a_2 & \ddots & & & \vdots \\ \vdots & \ddots & \ddots & \ddots & \ddots & \ddots & & \vdots \\ \vdots & & \ddots & \ddots & \ddots & \ddots & \ddots & \vdots \\ \vdots & & & \ddots & a_2 & a_3 & a_2 & 0 \\ \vdots & & & & \ddots & a_2 & a_3 & a_2 \\ 0 & \cdots & \cdots & \cdots & \cdots & 0 & a_1 & a_3 \end{pmatrix} \tag{86}$$

$$B = \begin{pmatrix} b_3 & b_1 & 0 & \cdots & \cdots & \cdots & \cdots & 0 \\ b_2 & b_3 & b_2 & \ddots & & & & \vdots \\ 0 & b_2 & b_3 & b_2 & \ddots & & & \vdots \\ \vdots & \ddots & \ddots & \ddots & \ddots & \ddots & & \vdots \\ \vdots & & \ddots & \ddots & \ddots & \ddots & \ddots & \vdots \\ \vdots & & & \ddots & b_2 & b_3 & b_2 & 0 \\ \vdots & & & & \ddots & b_2 & b_3 & b_2 \\ 0 & \cdots & \cdots & \cdots & \cdots & 0 & b_1 & b_3 \end{pmatrix} \tag{87}$$

$$C = \begin{pmatrix} c_3 & c_1 & 0 & \cdots & \cdots & \cdots & \cdots & 0 \\ c_2 & c_3 & c_2 & \ddots & & & & \vdots \\ 0 & c_2 & c_3 & c_2 & \ddots & & & \vdots \\ \vdots & \ddots & \ddots & \ddots & \ddots & \ddots & & \vdots \\ \vdots & & \ddots & \ddots & \ddots & \ddots & \ddots & \vdots \\ \vdots & & & \ddots & c_2 & c_3 & c_2 & 0 \\ \vdots & & & & \ddots & c_2 & c_3 & c_2 \\ 0 & \cdots & \cdots & \cdots & \cdots & 0 & c_1 & c_3 \end{pmatrix} \tag{88}$$

$$D = \begin{pmatrix} d_3 & d_1 & 0 & \cdots & \cdots & \cdots & \cdots & 0 \\ d_2 & d_3 & d_2 & \ddots & & & & \vdots \\ 0 & d_2 & d_3 & d_2 & \ddots & & & \vdots \\ \vdots & \ddots & \ddots & \ddots & \ddots & \ddots & & \vdots \\ \vdots & & \ddots & \ddots & \ddots & \ddots & \ddots & \vdots \\ \vdots & & & \ddots & d_2 & d_3 & d_2 & 0 \\ \vdots & & & & \ddots & d_2 & d_3 & d_2 \\ 0 & \cdots & \cdots & \cdots & \cdots & 0 & d_1 & d_3 \end{pmatrix} \tag{89}$$

$$G = \begin{pmatrix} g_3 & g_1 & 0 & \cdots & \cdots & \cdots & \cdots & 0 \\ g_2 & g_3 & g_2 & \ddots & & & & \vdots \\ 0 & g_2 & g_3 & g_2 & \ddots & & & \vdots \\ \vdots & \ddots & \ddots & \ddots & \ddots & \ddots & & \vdots \\ \vdots & & \ddots & \ddots & \ddots & \ddots & \ddots & \vdots \\ \vdots & & & \ddots & g_2 & g_3 & g_2 & 0 \\ \vdots & & & & \ddots & g_2 & g_3 & g_2 \\ 0 & \cdots & \cdots & \cdots & \cdots & 0 & g_1 & g_3 \end{pmatrix} \tag{90}$$

The off-diagonal entries of A are $a_1 = -2\lambda_1$, $a_2 = -\lambda_1$, and the diagonal entries are $a_3 = 1 + 2\lambda_1$. The entries of B in the off-diagonal are $b_1 = -2\lambda_1$, $b_2 = -\lambda_1$, and the diagonal entries are $b_3 = 1 + 2\lambda_2$. The entries of C in the off-diagonal are $c_1 = -2\lambda_3$, $c_2 = -\lambda_3$, and the diagonal entries are $c_3 = 1 + 2\lambda_3$. The off-diagonal entries of D are $d_1 = -2\lambda_4$, $d_2 = -\lambda_4$, and the diagonal entries are $d_3 = 1 + 2\lambda_4$. The off-diagonal entries of G are $g_1 = -2\lambda_5$, $g_2 = -\lambda_5$, and the diagonal entries are $g_3 = 1 + 2\lambda_5$. Thus, A, B, C, D, and G are M-matrices, and Equations (81), (82), (83), (84), and (85) are:

$$S^{m+1} = A^{-1}S^m \tag{91}$$
$$E^{m+1} = B^{-1}E^m \tag{92}$$
$$I^{m+1} = C^{-1}I^m \tag{93}$$
$$Q^{m+1} = D^{-1}I^m \tag{94}$$
$$V^{m+1} = G^{-1}I^m \tag{95}$$

If we consider that $S^m > 0$, $E^m > 0, I^m > 0, Q^m > 0$, and $V^m > 0$, then the M-matrix along with (60) implies that the values of all of the state variables, i.e., S^{m+1}, E^{m+1}, I^{m+1}, $Q^{m+1}0$, and V^{m+1} are positive. Hence, the theorem is done by using the principle of mathematical induction.

This theorem is applied for drawing the conclusion that the proposed scheme, which is implicit in nature, guarantees the positive solution unconditionally.

7. NUMERICAL EXPERIMENT AND SIMULATIONS

A numerical test is performed on both the points of equilibrium for all the schemes under consideration.

The set of parametric values considered for the test problem at disease-free equilibrium point [7] is given as:

$b = 0.7, \mu = 0.06, \sigma = 0.7, \beta = 0.35, \gamma = 0.15, \omega = 0.3, q_1 = 0.2, q_2 = 0.2, q_3 = 0.1, \phi = 0.4, \epsilon = 0.05, \alpha = 2, d_1 = 0.05, d_2 = 0.01, d_3 = 0.001, d_4 = 0.01, d_5 = 0.01.$

For the endemic equilibrium point, the following parametric values are used:

$b = 0.7, \mu = 0.06, \sigma = 0.7, \beta = 0.35, \gamma = 0.15, \omega = 0.06, q_1 = 0.2, q_2 = 0.2,$
$q_3 = 0.1, \phi = 0.4, \epsilon = 0.05, \alpha = 2, d_1 = 0.05, d_2 = 0.01, d_3 = 0.001, d_4 = 0.01, d_5 = 0.01.$

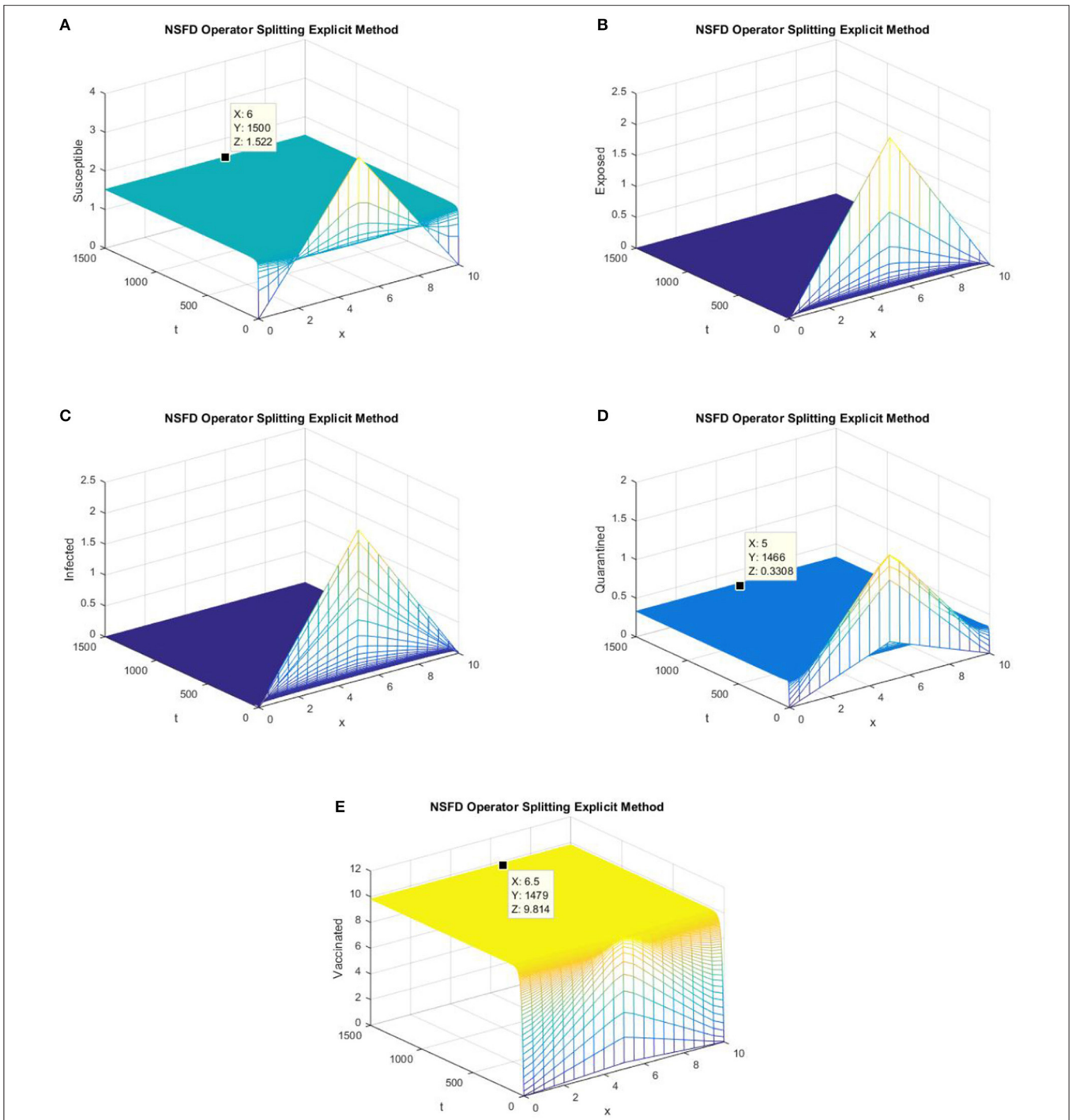

FIGURE 1 | The explicit operator splitting NSFD scheme is used to simulate the graphs **(A–E)**. **(A)** Mesh graph of *S*; **(B)** Mesh graph of *E*; **(C)** Mesh graph of *I*; **(D)** Mesh graph of *Q*; **(E)** Mesh graph of *V*.

The initial condition for the model (6)–(10) is:

$$S(x,0) = \begin{cases} 0.7x & \text{if } x \in [0, 0.5) \\ 0.7\,(10 - x) & \text{if } x \in [0.5, 1] \end{cases} \tag{96}$$

$$E(x,0) = \begin{cases} 0.5x & \text{if } x \in [0, 0.5) \\ 0.5\,(10 - x) & \text{if } x \in [0.5, 1] \end{cases} \tag{97}$$

$$I(x,0) = \begin{cases} 0.3x & \text{if } x \in [0, 0.5) \\ 0.3\,(10 - x) & \text{if } x \in [0.5, 1] \end{cases} \tag{98}$$

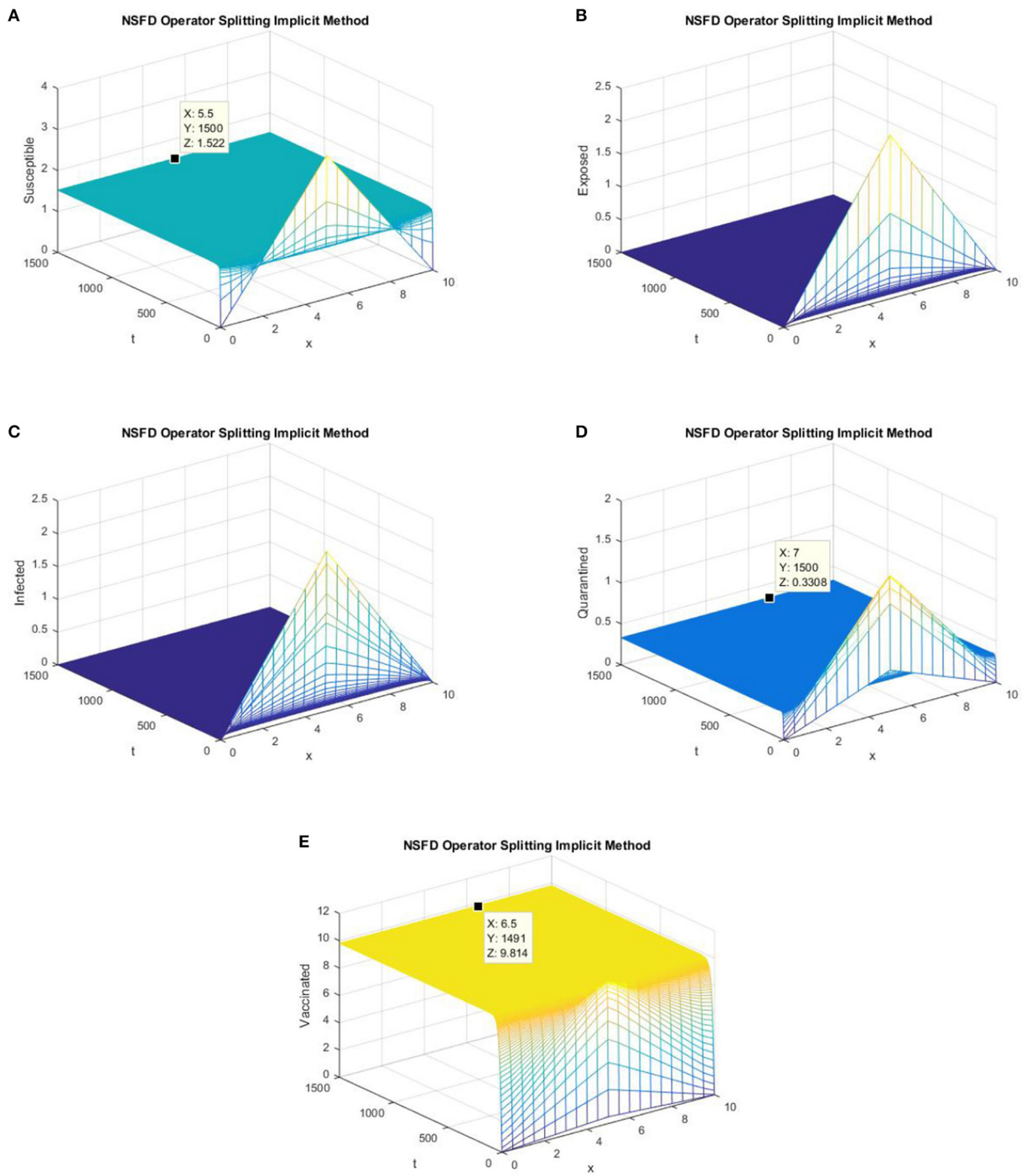

FIGURE 2 | The implicit operator splitting NSFD scheme is used to simulate graphs **(A–E)**. **(A)** Mesh graph of S; **(B)** Mesh graph of E; **(C)** Mesh graph of I; **(D)** Mesh graph of Q; **(E)** Mesh graph of V.

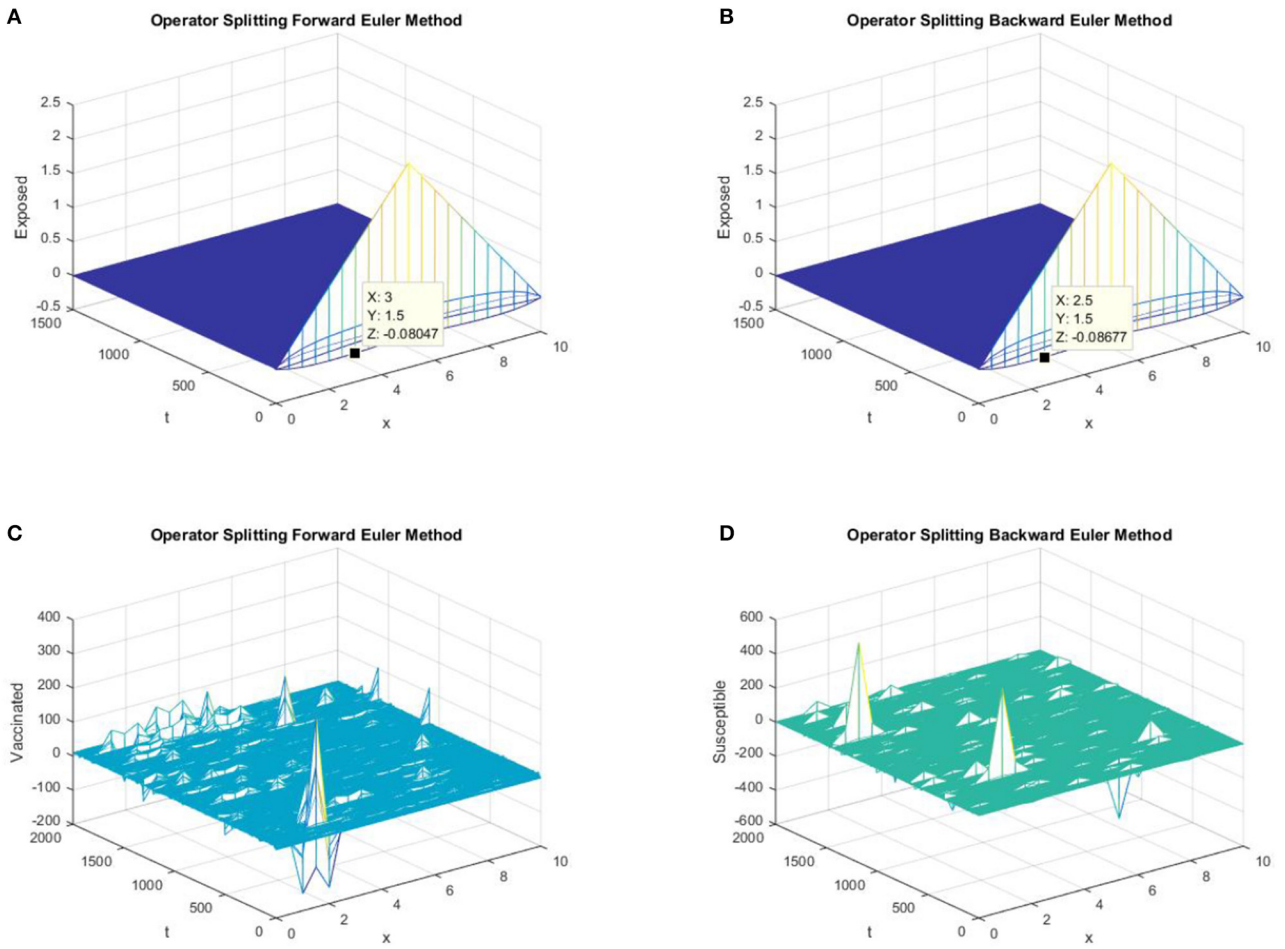

FIGURE 3 | (A) The forward Euler FD operator splitting method is used to simulate the graph of exposed persons for the DFE point at $h = 0.5, \lambda_1 = 0.3$. **(B)** The backward Euler FD operator splitting method is used to simulate the graph of susceptible persons for the DFE point at $h = 0.5, \lambda_1 = 0.3$. **(C)** The forward Euler FD operator splitting method is used to simulate the graph of susceptible persons for the DFE point at $h = 0.5, \lambda_1 = 0.4$. **(D)** The backward Euler FD operator splitting method is used to simulate the graph of susceptible persons for the DFE point at $h = 0.5, \lambda_1 = 0.4$.

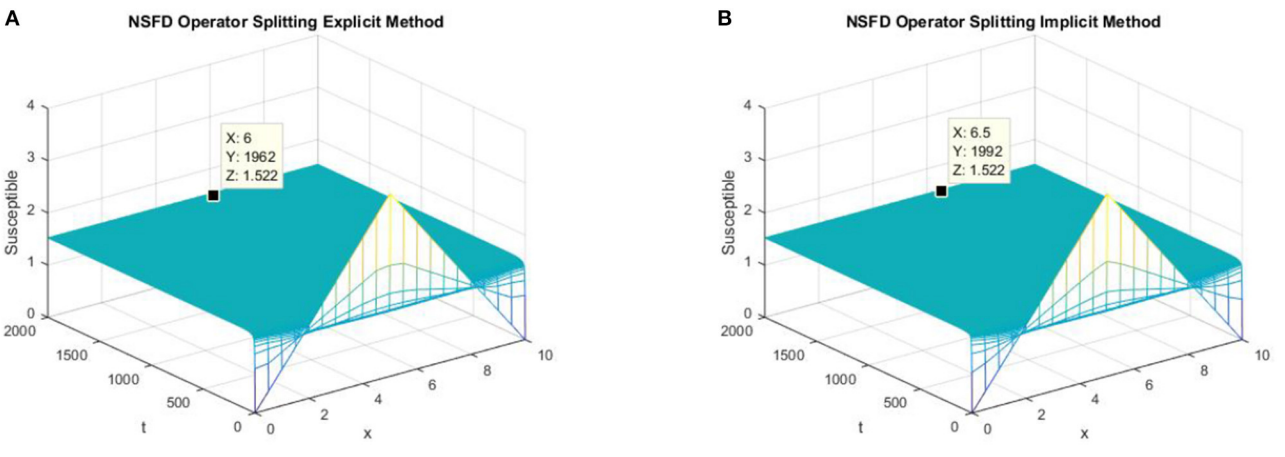

FIGURE 4 | (A) The explicit operator splitting NSFD method is used to simulate the graph of susceptible persons for the DFE point at $h = 0.5, \lambda_1 = 0.3$. **(B)** The implicit operator splitting NSFD method is used to simulate the graph of susceptible persons for the DFE point at $h = 0.5, \lambda_1 = 0.4$.

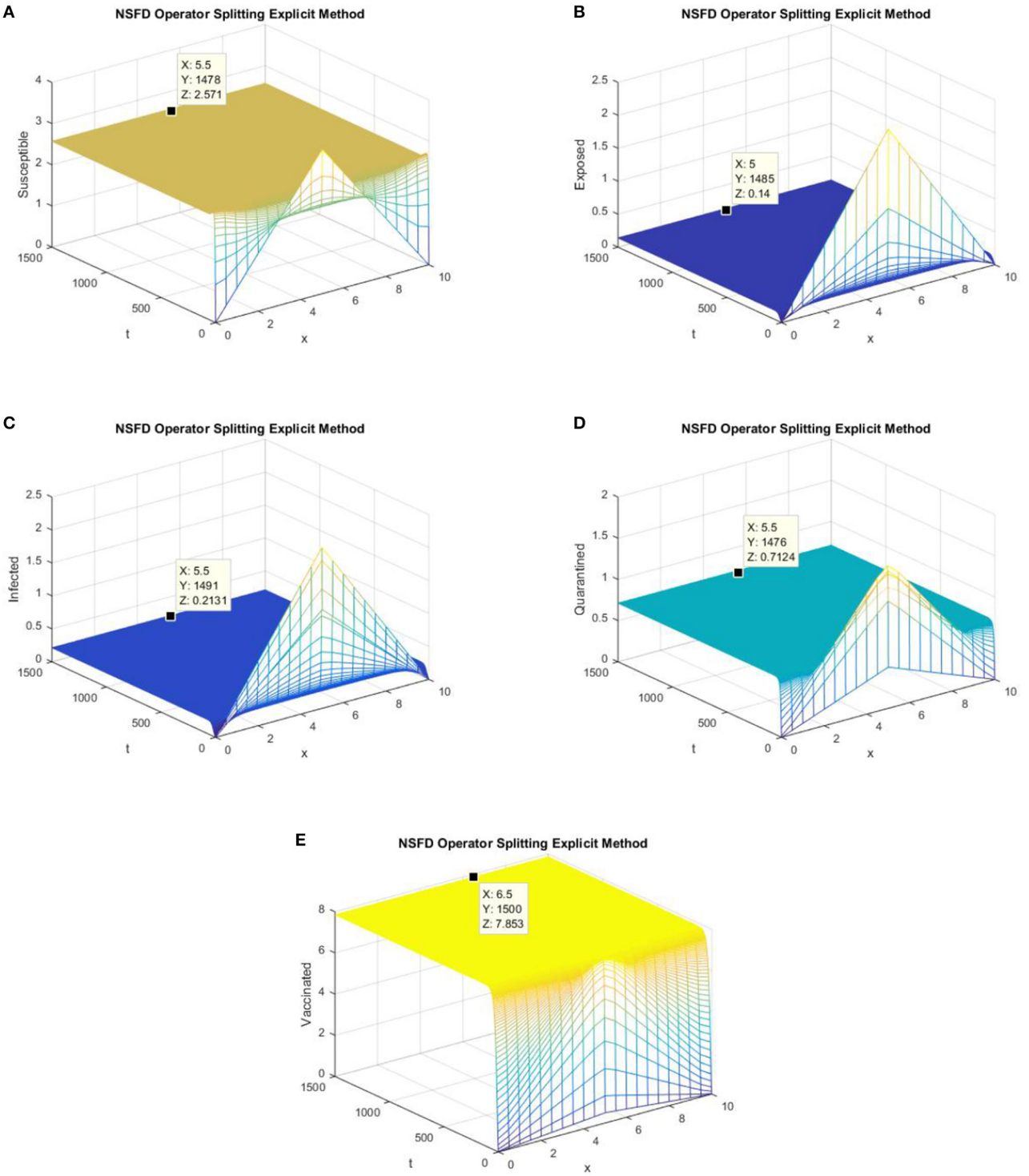

FIGURE 5 | (A) The explicit operator splitting NSFD scheme is used to simulate graphs **(A–E)**. **(A)** Mesh graph of S; **(B)** Mesh graph of E; **(C)** Mesh graph of I; **(D)** Mesh graph of Q; **(E)** Mesh graph of V.

$$Q(x,0) = \begin{cases} 0.1x & \text{if } x \in [0, 0.5) \\ 0.1\,(10 - x) & \text{if } x \in [0.5, 1] \end{cases} \tag{99}$$

$$V(x,0) = \begin{cases} 0.1x & \text{if } x \in [0, 0.5) \\ 0.1\,(10 - x) & \text{if } x \in [0.5, 1] \end{cases} \tag{100}$$

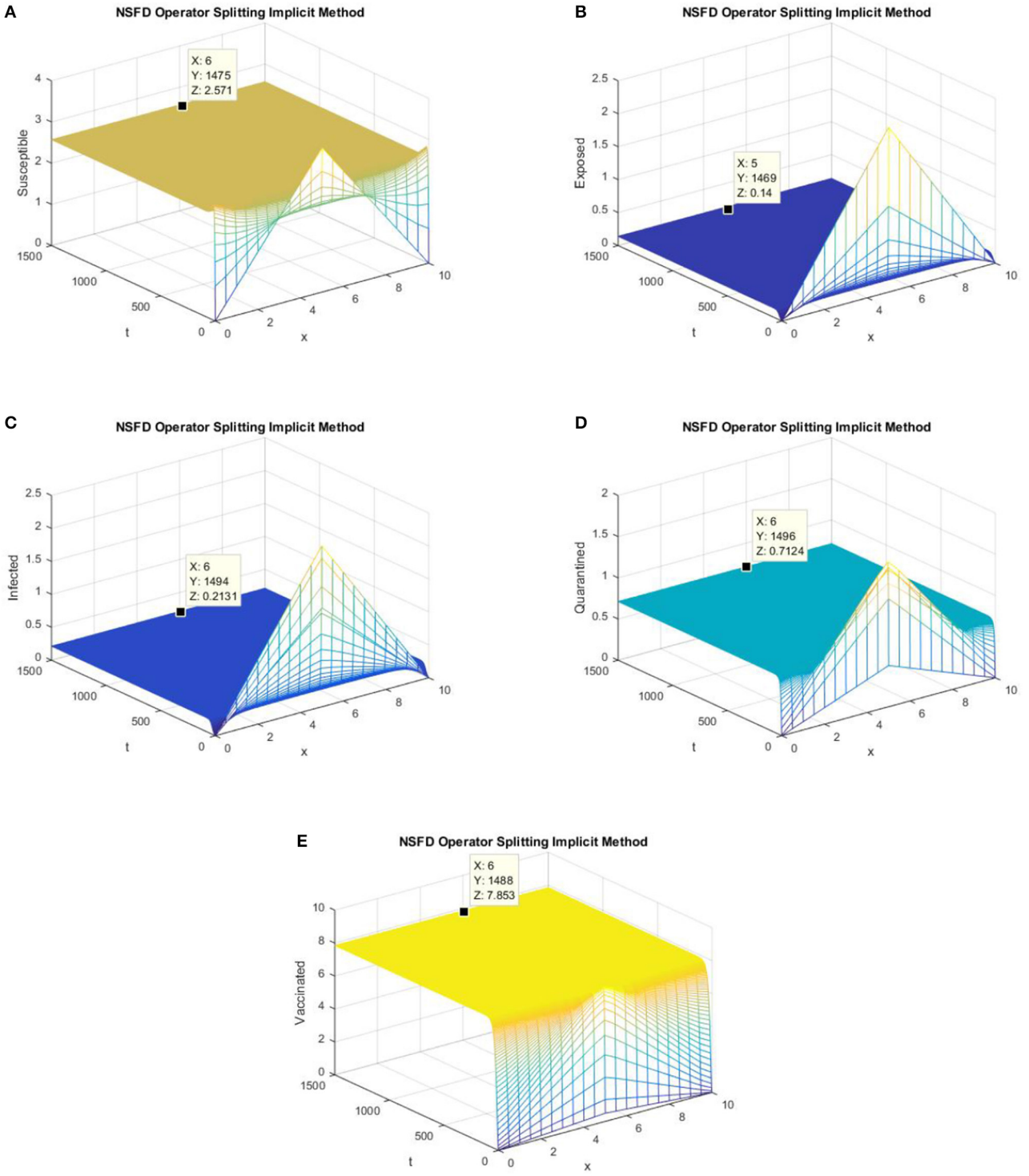

FIGURE 6 | The implicit operator splitting NSFD scheme is used to simulate graphs **(A–E)**. **(A)** Mesh graph of S; **(B)** Mesh graph of E; **(C)** Mesh graph of I; **(D)** Mesh graph of Q; **(E)** Mesh graph of V.

7.1. Disease-Free Equilibrium Point

In this section, graphs of all the state variables against time are presented (for DFE) to illustrate the behavior of the schemes. In **Figures 1**, **2**, we consider $h = 0.5$, $\lambda_1 = 0.3$, $\lambda_2 = 0.06$, $\lambda_3 = 0.006$, $\lambda_4 = 0.06$, and $\lambda_5 = 0.06$.

Figures 1, **2** validate the preservation of the positivity property in both of the proposed operator splitting NSFD schemes. Also,

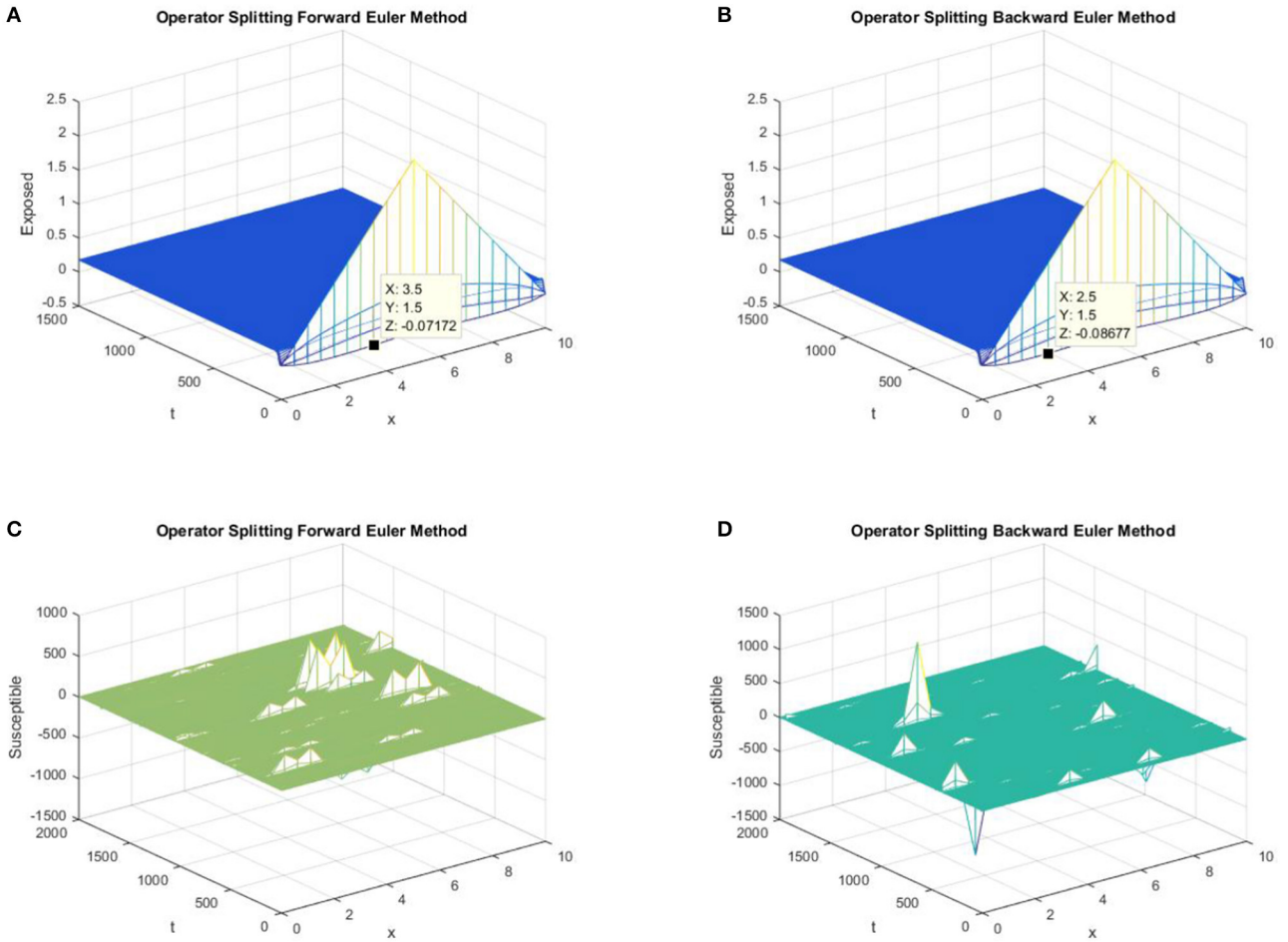

FIGURE 7 | (A) The forward Euler FD operator splitting method is used to simulate the graph of exposed persons for the DFE point at $h = 0.5, \lambda_1 = 0.3$. **(B)** The backward Euler FD operator splitting method is used to simulate the graph of exposed persons for the DFE point at $h = 0.5, \lambda_1 = 0.3$. **(C)** The forward Euler FD operator splitting method is used to simulate the graph of susceptible persons for the DFE point at $h = 0.5, \lambda_1 = 0.4$. **(D)** The backward Euler FD operator splitting method is used to simulate the graph of susceptible persons for the DFE point at $h = 0.5, \lambda_1 = 0.4$.

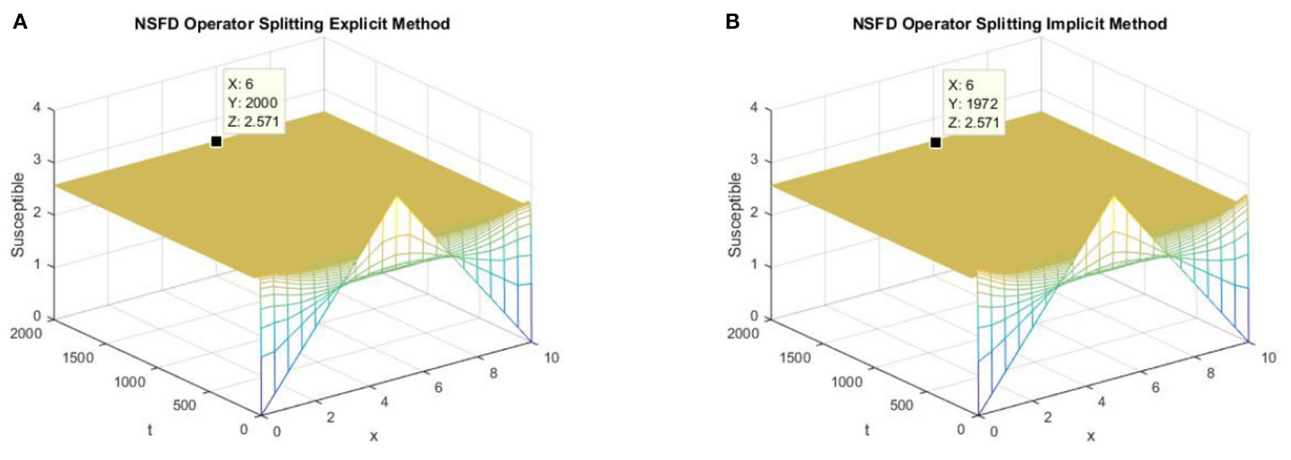

FIGURE 8 | (A) The explicit operator splitting NSFD method is used to simulate the graph of susceptible persons for the DFE point at $h = 0.5, \lambda_1 = 0.4$. **(B)** The implicit operator splitting NSFD method is used to simulate the graph of susceptible persons for the DFE point at $h = 0.5, \lambda_1 = 0.4$.

all the graphs in **Figures 1**, **2** show that both proposed NSFD schemes achieve convergence to the DFE point. Next, we examine the behavior of forward Euler and backward Euler splitting schemes at different values of h and τ.

In parts (a) and (b) of **Figure 3**, we take the same values of h and τ as in **Figures 1**, **2** for the graphs of forward Euler operator splitting scheme and backward Euler operator splitting scheme. The graphs clearly show the failure of the positivity property of both classic schemes. In parts (c) and (d) of **Figure 3**, both existing splitting schemes converge to the false DFE equilibrium point for susceptible individuals.

In parts (a) and (b) of **Figure 4**, we take the same values of h and τ as given in parts (c) and (d) of **Figure 3** for the explicit and implicit NSFD operator splitting schemes, respectively. The graphs clearly show that both of the proposed NSFD schemes not only preserve the positivity property but also achieve convergence to the true equilibrium point.

7.2. Endemic Equilibrium Point

In this section, we present simulations of the SEIQV epidemic model at the EE point using all of the operator splitting FD schemes. In **Figures 5**, **6**, we consider $h = 0.5$, $\lambda_1 = 0.3$, $\lambda_2 = 0.06$, $\lambda_3 = 0.006$, $\lambda_4 = 0.06$, and $\lambda_5 = 0.06$.

Figures 5, **6** depict the graphs of susceptible, exposed, infected, quarantined, and vaccinated individuals for the EE point using the explicit operator splitting NSFD scheme and implicit operator splitting NSFD scheme, respectively. All the graphs in **Figures 5**, **6** demonstrate that both of the proposed operator splitting NSFD schemes preserve the property of positivity. These graphs also show that both proposed schemes converge to the EE point.

Again, both the forward and backward Euler FD schemes fail to preserve the positivity property and converge to the false EE point, as shown in **Figure 7**.

Figure 8 shows that the proposed NSFD operator splitting methods are consistent with the continuous reaction-diffusion system as they not only preserve the positivity property but converge to the EE point.

8. CONCLUSION

In this work, we consider the SEIQV reaction-diffusion epidemic model. The stability of the SEIQV model is guaranteed numerically by using criteria defined by Routh-Hurwitz. We also find the bifurcation value of the important vaccination parameter ω of SEIQV epidemic systems with diffusion and without diffusion. We design two novel and efficient operator splitting NSFD schemes for the SEIQV reaction-diffusion system. The NSFD schemes put forth, which are technically operator splitting schemes, possess the same behavior as is possessed by the SEIQV epidemic system. To conclude regarding the designed methods, we present two novel numerical schemes, one of which is explicit and the other of which is implicit in nature. The explicit scheme is more computationally efficient than the implicit scheme, but it has conditional stability while the implicit scheme is stable unconditionally. Both schemes employ structural splitting, due to which they deal adroitly with the nonlinearity of the reaction-diffusion system. These schemes avoid the false chaos that is a part of many existing methods. The positive solution of the SEIQV model is sustained by both schemes. Also, the nature of the stability of equilibria is preserved effectively by the proposed NSFD schemes. It is also shown that classical schemes, in parallel to our proposed schemes, produce chaos, leading to inconsistencies and instabilities numerically. The currently designed schemes are a valuable contribution for finding the solutions of nonlinear dynamical systems comprising differential equations. These NSFD schemes will become very efficient for the solution of one- and multi-dimensional reaction-diffusion population models, auto-catalytic chemical reaction models, and many more.

AUTHOR CONTRIBUTIONS

NA, MR, and MAR designed the study. NA, MF, and MR developed the methodology. NA and MF collected the data. NA, DB, KN, and IK performed the analysis. NA, MF, DB, MA, and IK wrote the manuscript.

ACKNOWLEDGMENTS

The authors are grateful to the referees for their suggestions and useful comments on this paper.

REFERENCES

1. Ahmed N, Wei Z, Baleanu D, Rafiq M, Rehman MA. Spatio-temporal numerical modeling of reaction-diffusion measles epidemic system. *Chaos.* (2019) **29**:103101. doi: 10.1063/1.5116807
2. Abro KA, Khan I, Nisar KS. Novel technique of Atangana and Baleanu for heat dissipation in transmission line of electrical circuit. *Chaos Solitons Fractals.* (2019) **129**:40–5 doi: 10.1016/j.chaos.2019.08.001
3. Ahmed N, Rafiq M, Baleanu D, Rehman MA. Spatio-temporal numerical modeling of auto-catalytic Brusselator model. *Roman J Phys.* (2019) **64**:110.
4. Gill V, Singh J and Singh Y. Analytical solution of generalized space-time fractional advection-dispersion equation via coupling of sumudu and fourier transforms. *Front Phys.* (2019) **6**:151. doi: 10.3389/fphy.2018.00151
5. Kumar D, Singh J, Al Qurashi M, Baleanu D. A new fractional SIRS-SI malaria disease model with application of vaccines, antimalarial drugs, and spraying. *Adv Differ Equ.* (2019) **278**. doi: 10.1186/s13662-019-2199-9
6. Saqib M, Khan I, Shafie S. Application of fractional differential equations to heat transfer in hybrid nanofluid: modeling and solution via integral transforms. *Adv Differ Equ.* (2019) **52**: doi: 10.1186/s13662-019-1988-5
7. Liu X, Yang L. Stability analysis of an SEIQV epidemic model with saturated incidence rate. *Nonlinear Anal Real World Appl.* (2012) **13**:2671–9. doi: 10.1016/j.nonrwa.2012.03.010
8. Mickens RE. Nonstandard finite difference models of differential equations world scientific (1994).

9. Ahmed N, Rafiq M, Rehman MA, Iqbal MS, Ali M. Numerical modelling of three dimensional Brusselator reaction diffusion system. *AIP Adv.* (2019) **9**:015205. doi: 10.1063/1.5070093
10. Mickens RE. Dynamic consistency: a fundamental principle for constructing nonstandard finite difference schemes for differential equations. *J Differ Equ Appl.* (2005) **11**:645–53. doi: 10.1080/10236190412331334527.
11. Macias-Diaz JE, Puri A. An explicit positivity-preserving finite-difference scheme for the classical Fisher-Kolmogorov-Petrovsky-Piscounov equation. *Appl Math Comput.* (2012) **218**:5829–37. doi: 10.1016/j.amc.2011.11.064
12. Mickens RE. A nonstandard finite difference scheme for a Fisher PDE having nonlinear diffusion. *Comput Math Appl.* (2003) **45**:429–36. doi: 10.1016/S0898-1221(03)80028-7
13. Mickens RE. A nonstandard finite difference scheme for an advection-reaction equation *J Diff Eq Appl.* (2004) **10**:307–1312. doi: 10.1080/10236190410001652838
14. Ahmed N, Rafiq M, Rehman MA, Ali M, Ahmad MO. Numerical modeling of SEIR measles dynamics with diffusion. *Commun Math Appl.* (2018) **9**:315–26.
15. Ahmed N, Shahid N, Iqbal Z, Jawaz M, Rafiq M, Tahira SS, et al. Numerical modeling of SEIQV epidemic model with saturated incidence rate. *J Appl Environ Biol Sci.* (2018) **8**:67–82.
16. Ahmed N, Jawaz M, Rafiq M, Rehman MA, Ali M, Ahmad MO. Numerical treatment of an epidemic model with spatial diffusion. *J Appl Environ Biol Sci.* (2018) **8**:17–29.
17. Chinviriyasit S, Chinviriyasit W. Numerical modeling of SIR epidemic model with diffusion. *Appl Math Comp.* (2010) **216**:395–409. doi: 10.1016/j.amc.2010.01.028
18. Fatima U, Ali M, Ahmed N, Rafiq M. Numerical modeling of susceptible latent breaking-out quarantine computer virus epidemic dynamics. *Heliyon.* (2018) **4**:e00631. doi: 10.1016/j.heliyon.2018.e00631
19. Jansen H, Twizell EH. An unconditionally convergent discretization of the SEIR model. *Math Comput Simulat.* (2002) **58**:147–58. doi: 10.1016/S0378-4754(01)00356-1
20. Rafiq M. *Numerical modeling of infectious diseases dynamics*. Ph.D. thesis, Lahore, Pakistan: University of Engineering and Technology (2016).
21. Qin W, Wang L, Ding X. A non-standard finite difference method for a hepatitis B virus infection model with spatial diffusion. *J Differ Equ Appl.* (2014) **20**:1641–51. doi: 10.1080/10236198.2014.968565
22. Manna K, Chakrabarty SP. Global stability and a non-standard finite difference scheme for a diffusion driven HBV model with capsids. *J Differ Equ Appl.* (2015) **21**:918–33. doi: 10.1080/10236198.2015.1056524
23. Chakrabrty A, Singh M, Lucy B, Ridland P. Predator-prey model with prey- taxis and diffusion. *Math Comput Model.* (2007) **46**:482–98. doi: 10.1016/j.mcm.2006.10.010
24. Islam S, Haider N. Numerical solution of compartmental model by meshless finite difference methods. *Appl Math Comput.* (2014) **238**:408–35. doi: 10.1016/j.amc.2014.04.014
25. Harwood RC. (2011) *Operator splitting method and applications for semilinear parabolic partial differential equations*. Ph.D. dissertation. Pullman, WA: Dept. Math., Washington State Univ.
26. Harwood RC, Manoranjan VS, Edwards DB. Lead-acid battery model under discharge with a fast splitting method. *IEEE Trans Energy Convers.* (2011) **26**:1109–17. doi: 10.1109/TEC.2011.2162093
27. Yanenko NN. The method of fractional steps. Berlin; Heidelberg: Springer-Verlag (1971).
28. Zharnitsky V. Averaging for split-step scheme. *Nonlinearity.* (2003) **16**:1359–66. doi: 10.1088/0951-7715/16/4/310
29. Ansarizadeh F, Singh M, Richards D. Modelling of tumor cells regression in response to chemotherapeutic treatment. *Appl Math Model.* (2017) **48**:96–112. doi: 10.1016/j.apm.2017.03.045
30. Naheed A, Singh M, Lucy D. Numerical study of SARS epidemic model with the inclusion of diffusion in the system. *Appl Math Comput.* (2014) **229**:480–98. doi: 10.1016/j.amc.2013.12.062
31. Naheed A, Singh M, Lucy D. Effect of treatment on transmission dynamics of SARS epidemic. *J Infect Non Infect Dis.* (2016) 2:16. doi: 10.24966/INID-8654/100016
32. Samsuzzoha MD. *A Study on numerical solutions of epidemic models*. Ph.D. thesis, Australia: Swinburne University of Technology (2012).
33. Wang, H. Q., Numerical studies on the split-step finite difference method for nonlinear Schrödinger equations. *Appl Math Comput.* (2005) **170**:17–35. doi: 10.1016/j.amc.2004.10.066
34. Fujimoto T, Ranade R. Two characterizations of inverse-positive matrices: the Hawkins-Simon condition and the Le Chatelier-Braun principle. *Electron J Linear Algebra.* (2004) **11**:59–65. doi: 10.13001/1081-3810.1122

Conflict of Interest: The authors declare that the research was conducted in the absence of any commercial or financial relationships that could be construed as a potential conflict of interest.

frontiers in Physics

ORIGINAL RESEARCH
published: 17 January 2020
doi: 10.3389/fphy.2019.00214

Time-Dependent MHD Flow of Non-Newtonian Generalized Burgers' Fluid (GBF) Over a Suddenly Moved Plate With Generalized Darcy's Law

Aisha M. Alqahtani[1] *and Ilyas Khan*[2]*

[1] Mathematical Sciences Department, College of Science, Princess Nourah Bint Abdulrahman University, Riyadh, Saudi Arabia, [2] Faculty of Mathematics and Statistics, Ton Duc Thang University, Ho Chi Minh City, Vietnam

Time-dependent magnetohydrodynamic (MHD) motion of a generalized Burgers' fluid (GBF) is investigated in this article. GBF is a highly complicated non-Newtonian fluid and is of highest degree in the class of rate type fluids. GBF is taken electrically conducting by using the restriction of small magnetic Reynolds number. Darcy's law has been used here in its generalized form using the GBF constitutive relation; hence, the medium is made porous. The impulsive motion in the fluid is induced due to sudden jerk of the plate. Exact expressions for velocity as well as for shear stress fields are obtained using the Laplace transform method. The solutions for hydrodynamic fluid (absence of MHD) in a non-porous medium as well as those for a Newtonian fluid (NF) executing a similar motion are also recovered. Results are sketched in terms of several plots and discussed for embedded parameters. It is found that the Hartmann number and porosity of the medium have strong influence on the velocity and shear stress fields.

Keywords: time-dependent flow, MHD, generalized Burgers' fluid, generalized Darcy's law, Laplace transform

OPEN ACCESS

Edited by:
Devendra Kumar,
University of Rajasthan, India

Reviewed by:
Muhammad Mubashir Bhatti,
Shanghai University, China
Najeeb Khan,
University of Karachi, Pakistan

***Correspondence:**
Ilyas Khan
ilyaskhan@tdtu.edu.vn

Specialty section:
This article was submitted to Mathematical Physics, a section of the journal Frontiers in Physics

Received: *28 September 2019*
Accepted: *21 November 2019*
Published: *17 January 2020*

Citation:
Alqahtani AM and Khan I (2020) Time-Dependent MHD Flow of Non-Newtonian Generalized Burgers' Fluid (GBF) Over a Suddenly Moved Plate With Generalized Darcy's Law. Front. Phys. 7:214. doi: 10.3389/fphy.2019.00214

INTRODUCTION

Most of the fluid problems (published literature), or fluid problems with heat transfer or heat and mass transfer together, are computed numerically due to the difficult nature of these problems. Indeed, the exact solutions for these problems are either not possible or quite difficult to obtain. These difficulties further increase if one is interested to solve such a problem using the integral transform techniques such as Laplace transform, Fourier transform, etc. In the Laplace transform, particularly the most difficult job is how to take the inversion. Therefore, some of the researchers are then using numerical inversion to somehow solve the inversion problem. However, such solutions are then not the so-called pure exact solutions. Among the interesting studies on exact solutions and, of course, the pioneering work includes the work of Rajagopal [1], where he studied non-Newtonian second-grade fluid for different flow motions and obtained exact solutions for each flow case. The flow was unsteady unidirectional and one-dimensional. Eight different flow cases were discussed. This work was then extended in 2007 by Hayat et al. [2] for the case of MHD flow and porous medium. More exactly, the fluid was taken electrically conducted and passing through a porous medium. They discussed seven different flow situations and obtained exact solution either by perturbation method or Fourier transform method. Other interesting studies on exact solutions include the work of Erdogan [3], Erdogan and Imrak [4], and Tan and Masuoka [5, 6]. Hayat et al. [7, 8] established for rotating flows exact analytic solutions for two different types of non-Newtonian fluids, namely, the second-grade fluid and the Maxwell fluid. They considered transient problems in both cases with combined effects of MHD and porosity.

The obtained exact solutions were discussed for various embedded parameters and concluded. Fetecau et al. [9] in a short note investigated analytically the Stokes' second problem (SSP) for Newtonian fluids (NF) flow. Fetecau and Fetecau [10] considered an unsteady problem of a Maxwell fluid (MF, non-Newtonian) over a rigid plate moved due to a sudden jerk. In another paper, Fetecau and Fetecau [11] extended the idea of MF to an Oldroyd-B fluid (OBF, non-Newtonian) and examined exact solutions for the first problem of Stokes'. Vieru et al. [12] also determined exact solution for the flow situation of an OBF over an infinite rigid plate.

In the group of viscoelastic fluids, Burgers' fluids and the corresponding generalized Burgers' fluids (GBFs) are less studied in the literature compared to other fluids in that group. Indeed, the resulting equations based on their complicated constitutive relations are not easy to handle. The exact solutions for these fluids problems are not possible unless we impose several assumptions. Even then, the exact solutions for these fluid problems are limited to certain well-known problems. Some famous fluid problems for Burgers or GBFs have been studied in Ravindran et al. [13], Hayat et al. [14], Khan et al. [15], Tong and Shan [16], Xue and Nie [17], Hayat et al. [18], Vieru et al. [19], Khan et al. [20–22], Fetecau et al. [23] and related references therein. However, for several other problems, such solutions are either too much complicated or even not possible. Such a complication even increases if the problem under consideration is composed of fractional differential equations, such as the problem considered in these articles on different aspects of sciences and engineering [24–36]. Some other related studies regarding fluid dynamics problems can be seen in Waqas et al. [37], Marin et al. [38], Jamil [39], and Jamil et al. [40, 41]. Roberts and Kaufman [42] is used for some of the Laplace inversion formulas needed for this work.

The main purpose of the present article is to study the time-dependent flow of GBF (incompressible) over an infinite (in horizontal-direction) rigid plate given sudden jerk. Simultaneous effects of MHD and porosity are also taken into consideration.

Exact analytic solutions are obtained for the dimensionless fluid velocity and non-trivial shear stress exerted by the fluid on the plate. Laplace transform is indeed a suitable method to solve this problem. Clearly, these solutions satisfy the given imposed conditions [initial and boundary conditions (IBCs)] and can produce other exact analytic solutions for other non-Newtonian fluids problems such as Burgers' fluids, OBFs, and Maxwell fluids performing a similar type of motion. Exact solutions for Newtonian fluids performing the same motion can also be obtained as a special case by vanishing all other non-Newtonian parameters. Graphical results are plotted and discussed for embedded parameters. Solutions for other fluids (generalized Burger fluids without MHD and porosity effects, Newtonian fluids) in limiting sense are also recovered.

PROBLEM FORMULATION AND INTEGRAL TRANSFORM SOLUTION

The problem formulation states that an incompressible flow strongly depends on time (unsteady flow) of a highly non-Newtonian fluid known as GBF lies in a semi-infinite porous space $y > 0$; i.e., the fluid is over a rigid plate kept at $y = 0$. The axes ($x-$axis and $y-$axis) are taken perpendicular to each other; i.e., the $x-$axis is taken in the flow direction while the $y-$axis is chosen normal to the direction of the flow. MHD effect is considered under which the fluid behaves like an electrically conducting liquid under the influence of an applied magnetic field such that the induced magnetic field is $v(0, t) = V, \quad v(y, t) \to 0 \text{ as } y \to \infty; \quad t > 0$, neglected assuming that magnetic Reynolds number is too small. GBF is initially taken at rest (for time $t = 0$); however, for time $t > 0$, the plate is give a sudden jerk (impulsive motion of the plate) and the fluid starts with the same impulsive motion. The scenario stated above is formulated in the form of partial differential equation with physical boundary and initial conditions as given below (for detailed analysis of the governing equation, one may refer to Xue and Nie [17] and Hayat et al. [18]):

$$\rho\left(1+\lambda\frac{\partial}{\partial t}+\gamma\frac{\partial^2}{\partial t^2}\right)\frac{\partial v}{\partial t} = \mu\left(1+\lambda_r\frac{\partial}{\partial t}+\gamma_1\frac{\partial^2}{\partial t^2}\right)\frac{\partial^2 v}{\partial y^2} - \delta B_0^2\left(1+\lambda\frac{\partial}{\partial t}+\gamma\frac{\partial^2}{\partial t^2}\right)v - \frac{\mu\varphi}{k}\left(1+\lambda_r\frac{\partial}{\partial t}+\gamma_1\frac{\partial^2}{\partial t^2}\right)v, \quad (1)$$

$$\left(1+\lambda\frac{\partial}{\partial t}+\gamma\frac{\partial^2}{\partial t^2}\right)T(y,t) = \mu\left(1+\lambda_r\frac{\partial}{\partial t}+\gamma_1\frac{\partial^2}{\partial t^2}\right)\frac{\partial v(y,t)}{\partial y}, \quad (2)$$

$$v(0, t) = V, \quad v(y, t) \to 0 \text{ as } y \to \infty; \quad t > 0, \quad (3)$$

$$v(y, 0) = \frac{\partial v(y, 0)}{\partial t} = \frac{\partial^2 v(y, 0)}{\partial t^2} = 0; \quad y > 0. \quad (4)$$

in which v is the velocity component in $x-$ direction, ρ is the fluid density, μ is the dynamic viscosity, δ is the finite electrical conductivity of the fluid, $\varphi\,(0 < \varphi < 1)$ is the porosity, $k > 0$ is the permeability of the porous medium, λ and $\lambda_r\,(< \lambda)$ are respectively the relaxation and retardation times, γ and γ_1 are the material constants having the dimensions as the square of time, and V denotes the reference velocity.

The problem described by Equations (1)–(3), after using non-dimensional quantities, takes the following form:

$$\left(1+\frac{\partial}{\partial\tau}+\beta\frac{\partial^2}{\partial\tau^2}\right)\frac{\partial u(\xi,\tau)}{\partial\tau} = \begin{bmatrix}\left(1+\alpha\frac{\partial}{\partial\tau}+\beta_1\frac{\partial^2}{\partial\tau^2}\right)\frac{\partial^2 u(\xi,\tau)}{\partial\xi^2} - M^2\left(1+\frac{\partial}{\partial\tau}+\beta\frac{\partial^2}{\partial\tau^2}\right)u(\xi,\tau)\\ -\frac{1}{K}\left(1+\alpha\frac{\partial}{\partial\tau}+\beta_1\frac{\partial^2}{\partial\tau^2}\right)u(\xi,\tau), \quad \xi,\tau>0,\end{bmatrix} \quad (5)$$

$$\left(1+\frac{\partial}{\partial\tau}+\beta\frac{\partial^2}{\partial\tau^2}\right)s = \left(1+\alpha\frac{\partial}{\partial\tau}+\beta_1\frac{\partial^2}{\partial\tau^2}\right)\frac{\partial u}{\partial\tau}, \quad \xi,\tau>0, \quad (6)$$

$$u(0,\tau) = 1, \quad u(\xi,\tau) \to 0 \text{ as } \xi \to \infty \quad \tau > 0, \quad (7)$$

$$u(\xi, 0) = \frac{\partial u(\xi, 0)}{\partial \tau} = \frac{\partial^2 u(\xi, 0)}{\partial \tau^2} = 0, \quad \xi > 0, \tag{8}$$

where

$$\tau = \frac{t}{\lambda}, \ \xi = \frac{y}{c\lambda}, \ u = \frac{v}{V}, \ s = \frac{T}{\rho c V}, \ c = \sqrt{\frac{\mu}{\rho\lambda}}, \tag{9}$$

$$\alpha = \frac{\lambda_r}{\lambda}, \ \beta = \frac{\gamma}{\lambda^2}, \ \beta_1 = \frac{\gamma_1}{\lambda^2}, \ M^2 = \frac{\delta B_0^2 \lambda}{\rho}, \ \frac{1}{K} = \frac{\mu\varphi\lambda}{\rho k}. \tag{10}$$

In the transformed $q-$plane, Equations (5)–(8) give

$$\frac{d^2\overline{u}(\xi, q)}{d\xi^2} - \frac{\beta q^3 + a_0 q^2 + b_0 q + c_0}{\beta_1 q^2 + \alpha q + 1}\overline{u}(\xi, q) = 0, \tag{11}$$

$$\overline{u}(0, q) = \frac{1}{q}, \quad \overline{u}(\xi, q) \to 0 \text{ as } \xi \to \infty, \tag{12}$$

in which q is a Laplace transform parameter and

$$a_0 = M^2\beta + \frac{\beta_1}{K} + 1, \quad b_0 = 1 + M^2 + \frac{\alpha}{K}, \quad c_0 = M^2 + \frac{1}{K}, \tag{13}$$

$$\overline{u}(\xi, q) = L^{-1}\{u(\xi, \tau)\} = \int_0^\infty e^{-q\tau} u(\xi, \tau) \, d\tau.$$

The transformed solution of Equation (11) under the boundary conditions (12) gives

$$\overline{u}(\xi, q) = \frac{1}{q} \exp\left[-\xi\sqrt{\frac{\beta q^3 + a_0 q^2 + b_0 q + c_0}{\beta_1 q^2 + \alpha q + 1}}\right]. \tag{14}$$

In obtaining $u(\xi, \tau) = L^{-1}\{\overline{u}(\xi, q)\}$, we write Equation (14) as

$$\overline{u}(\xi, q) = \overline{u}_1(q) \ \overline{u}_2(\xi, q), \tag{15}$$

with

$$\overline{u}_1(q) = \frac{1}{q}, \tag{16}$$

$$\overline{u}_2(\xi, q) = \exp\left(-\xi\sqrt{w(q)}\right);$$
$$w(q) = \frac{\beta q^3 + a_0 q^2 + b_0 q + c_0}{\beta_1 q^2 + \alpha q + 1}. \tag{17}$$

Expressing $u_1(\tau) = L^{-1}\{\overline{u}_1(q)\}$, $u_2(\xi, \tau) = L^{-1}\{\overline{u}_2(\xi, q)\}$, Equation (16) after Laplace inversion gives

$$u_1(\tau) = 1. \tag{18}$$

To find $u_2(\xi, \tau) = L^{-1}\{\overline{u}_2(\xi, q)\}$, using the inversion formula for compound functions

$$L^{-1}\{F[w(q)]\} = \int_0^\infty f(u) \, g(u, \tau) \, du, \tag{19}$$

where $f(\tau) = L^{-1}\{F(q)\}$ and $g(u, \tau) = L^{-1}\{e^{-uw(q)}\}$. Choosing $f(\xi, q) = e^{-\xi\sqrt{q}}$, then

$$f(\xi, \tau) = L^{-1}\{e^{-\xi\sqrt{q}}\} = \frac{\xi}{2\tau\sqrt{\pi\tau}} \exp\left(\frac{-\xi^2}{4\tau}\right); \quad \xi > 0 \tag{20}$$

and

$$u_2(\xi, \tau) = L^{-1}\{\overline{u}_2(\xi, q)\} = \int_0^\infty f(\xi, u) \, g(u, \tau) \, du$$
$$= \frac{\xi}{2\sqrt{\pi}} \int_0^\infty \frac{1}{u\sqrt{u}} \exp\left(\frac{-\xi^2}{4u}\right) g(u, \tau) \, du. \tag{21}$$

In order to find $g(u, \tau) = L^{-1}\{e^{-uw(q)}\}$, we express $w(q)$ as follows

$$w(q) = b_1 + a_1 q + \frac{\eta_1}{q - q_1} + \frac{\eta_2}{q - q_2}, \tag{22}$$

$$a_1 = \frac{\beta}{\beta_1}, \ b_1 = \left(a_0 - \frac{\alpha\beta}{\beta_1}\right)\frac{1}{\beta_1}, \ c_1 = b_0 - \frac{\beta}{\beta_1} - \frac{\alpha}{\beta_1}\left(a_0 - \frac{\alpha\beta}{\beta_1}\right),$$
$$d_1 = c_0 + \left(a_0 - \frac{\alpha\beta}{\beta_1}\right)\frac{1}{\beta_1}, \ \eta_1 = \frac{c_1 q_1 + d_1}{q_1 - q_2}, \ \eta_2 = -\frac{c_1 q_2 + d_1}{q_1 - q_2}, \tag{23}$$

where q_1 and q_2 are the roots of the equation $\beta_1 q^2 + \alpha q + 1 = 0$. Thus,

$$g(u, \tau) = e^{-u\eta_0} L^{-1}\left\{\exp\left(-\frac{ua}{d}q\right)\left[1 - H_1(q) - H_2(q) + H_1(q) \ H_2(q)\right]\right\},$$

with

$$H_1(q) = 1 - \exp\left(-\frac{u\eta_1}{q - q_1}\right) \quad \text{and}$$
$$H_2(q) = 1 - \exp\left(-\frac{u\eta_2}{q - q_2}\right).$$

Let us denote

$$h_1(\tau) = L^{-1}\{H_1(q)\} = \sqrt{\frac{\eta_1 u}{\tau}} e^{q_1\tau} J_1\left(2\sqrt{\eta_1 u\tau}\right), \tag{24}$$

and

$$h_2(\tau) = L^{-1}\{H_2(q)\} = \sqrt{\frac{\eta_2 u}{\tau}} e^{q_2\tau} J_1\left(2\sqrt{\eta_2 u\tau}\right), \tag{25}$$

where $J_1(\cdot)$ denotes the Bessel function of first kind of order one and then finally one has

$$\begin{aligned} g(u,\tau) = {} & \delta(\tau - ua_1)\, e^{-ub_1} \\ & -\sqrt{\eta_1 u}\int_0^\tau \frac{\delta(s-ua_1)}{\sqrt{\tau-s}} e^{q_1(\tau-s)} J_1\left(2\sqrt{\eta_1 u(\tau-s)}\right) \mathrm{d}s \\ & -\sqrt{\eta_2 u}\int_0^\tau \frac{\delta(s-ua_1)}{\sqrt{\tau-s}} e^{q_2(\tau-s)} J_1\left(2\sqrt{\eta_2 u(\tau-s)}\right) \mathrm{d}s \\ & +u\sqrt{\eta_1\eta_2}\int_0^\tau\int_0^s \\ & \times \frac{\delta(\tau-s-ua_1)}{\sqrt{\sigma(s-\sigma)}} e^{q_1\sigma+q_2(s-\sigma)} J_1\left(2\sqrt{\eta_1 u\sigma}\right) \\ & J_1\left(2\sqrt{\eta_2 u(s-\sigma)}\right) \mathrm{d}s\,\mathrm{d}\sigma \end{aligned} \tag{26}$$

and $L^{-1}\{e^{-\alpha q}\} = \delta(\tau-\alpha)$. Here $\delta(\cdot)$ indicates the Dirac delta function.

Insertion of Equation (26) into Equation (21) leads to the following result:

$$\begin{aligned} u_2(\xi,\tau) = {} & \frac{\xi}{2\sqrt{\pi}}\int_0^\infty \frac{\delta(\tau-ua_1)}{u\sqrt{u}} \exp\left(\frac{-\xi^2}{4u} - b_1 u\right) \mathrm{d}u \\ & -\frac{\sqrt{\eta_1}\xi}{2\sqrt{\pi}}\int_0^\tau\int_0^\infty \frac{\delta(s-ua_1)}{u\sqrt{\tau-s}} \\ & \times \exp\left(\frac{-\xi^2}{4u} + q_1(\tau-s) - b_1 u\right) \\ & J_1\left(2\sqrt{\eta_1 u(\tau-s)}\right) \mathrm{d}u\,\mathrm{d}s \\ & -\frac{\sqrt{\eta_2}\xi}{2\sqrt{\pi}}\int_0^\tau\int_0^\infty \frac{\delta(s-ua_1)}{u\sqrt{(\tau-s)}} \\ & \exp\left(\frac{-\xi^2}{4u} + q_2(\tau-s) - b_1 u\right) \\ & J_1\left(2\sqrt{\eta_2 u(\tau-s)}\right) \mathrm{d}u\,\mathrm{d}s \\ & +\frac{\sqrt{\eta_1\eta_2}\xi}{2\sqrt{\pi}}\int_0^\tau\int_0^s\int_0^\infty \frac{\delta(\tau-s-ua_1)}{\sqrt{u\sigma(s-\sigma)}} \\ & \exp\left(\frac{-\xi^2}{4u} + q_1\sigma + q_2(s-\sigma) - b_1 u\right) \\ & \times J_1\left(2\sqrt{\eta_1 u\sigma}\right) J_1\left(2\sqrt{\eta_2 u(s-\sigma)}\right) \mathrm{d}u\,\mathrm{d}s\,\mathrm{d}\sigma. \end{aligned} \tag{27}$$

Taking into consideration Equations (27) and (18), one obtains

$$\begin{aligned} u(\xi,\tau) = {} & \frac{\xi}{2\sqrt{\pi}}\int_0^\tau\int_0^\infty \frac{\delta(s-ua_1)}{u\sqrt{u}} \exp\left(\frac{-\xi^2}{4u} - b_1 u\right) \mathrm{d}u\,\mathrm{d}s \\ & -\frac{\sqrt{\eta_1}\xi}{2\sqrt{\pi}}\int_0^\tau\int_0^s\int_0^\infty \frac{\delta(\sigma-ua_1)}{u\sqrt{s-\sigma}} \\ & \exp\left(\frac{-\xi^2}{4u} + q_1(s-\sigma) - b_1 u\right) \\ & J_1\left(2\sqrt{\eta_1 u(s-\sigma)}\right) \mathrm{d}u\,\mathrm{d}s\,\mathrm{d}\sigma \\ & -\frac{\sqrt{\eta_2}\xi}{2\sqrt{\pi}}\int_0^\tau\int_0^s\int_0^\infty \frac{\delta(\sigma-ua_1)}{u\sqrt{s-\sigma}} J_1\left(2\sqrt{\eta_2 u(s-\sigma)}\right) \\ & \exp\left(\frac{-\xi^2}{4u} + q_2(s-\sigma) - b_1 u\right) \mathrm{d}u\,\mathrm{d}s\,\mathrm{d}\sigma \\ & +\frac{\sqrt{\eta_1\eta_2}\xi}{2\sqrt{\pi}}\int_0^\tau\int_0^s\int_0^\sigma\int_0^\infty \frac{\delta(s-\sigma-ua_1)}{\sqrt{u\eta(\sigma-\eta)}} \\ & J_1\left(2\sqrt{\eta_1 u\eta}\right) J_1\left(2\sqrt{\eta_2 u(\sigma-\eta)}\right) \\ & \times \exp\left(\frac{-\xi^2}{4u} + q_1\eta + q_2(\sigma-\eta) - b_1 u\right) \mathrm{d}u\,\mathrm{d}s\,\mathrm{d}\sigma\,\mathrm{d}\eta. \end{aligned} \tag{28}$$

Setting $u = dv/a$ into Equation (28) and using the following property:

$$\int_a^b f(x)\,\delta(x-x_0)\,dx = \begin{cases} f(x_0) & \text{for } x \in [a,b), \\ 0 & \text{for } x \notin [a,b) \end{cases} \tag{29}$$

we arrive at the following result:

$$\begin{aligned} u(\xi,\tau) = {} & \frac{\xi\sqrt{a_1}}{2\sqrt{\pi}}\int_0^\tau \frac{1}{s\sqrt{s}} \exp\left(\frac{-a_1\xi^2}{4s} - \frac{b_1 s}{a_1}\right) \mathrm{d}s \\ & -\frac{\sqrt{\eta_1}\xi}{2\sqrt{\pi}}\int_0^\tau\int_0^s \frac{1}{\sigma\sqrt{s-\sigma}} \\ & \exp\left(\frac{-a_1\xi^2}{4\sigma} + q_1(s-\sigma) - \frac{b_1\sigma}{a_1}\right) \\ & \times J_1\left(2\sqrt{\frac{\eta_1}{a_1}\sigma(s-\sigma)}\right) \mathrm{d}s\,\mathrm{d}\sigma \\ & -\frac{\sqrt{\eta_2}\xi}{2\sqrt{\pi}}\int_0^\tau\int_0^s \frac{\exp\left(\frac{-a_1\xi^2}{4\sigma} + q_2(s-\sigma) - \frac{b_1\sigma}{a_1}\right)}{\sigma\sqrt{s-\sigma}} \\ & \times J_1\left(2\sqrt{\frac{\eta_2}{a_1}\sigma(s-\sigma)}\right) \mathrm{d}s\,\mathrm{d}\sigma \\ & +\frac{\sqrt{\eta_1\eta_2}\xi}{2\sqrt{a_1}\pi}\int_0^\tau\int_0^s\int_0^\sigma \frac{J_1\left(2\sqrt{\frac{\eta_1}{a_1}\eta(s-\sigma)}\right)}{\sqrt{\eta(s-\sigma)(\sigma-\eta)}} \\ & \times \exp\left(\frac{-a_1\xi^2}{4(s-\sigma)} + q_1\eta + q_2(\sigma-\eta) - \frac{b_1}{a_1}(s-\sigma)\right) \\ & J_1\left(2\sqrt{\frac{\eta_2}{a_1}(s-\sigma)(\sigma-\eta)}\right) \mathrm{d}s\,\mathrm{d}\sigma\,\mathrm{d}\eta. \end{aligned} \tag{30}$$

Now, the expression for the shear stress can be easily found from Equation (6) and hence finally we get.

$$\begin{aligned} s(\xi,\tau) = {} & \sqrt{\frac{a_1}{\pi\tau}} \exp\left(\frac{-a_1\xi^2}{4\tau} - \frac{b_1\tau}{a_1}\right) \\ & -\frac{\sqrt{\eta_1}}{a_1\sqrt{\pi}}\int_0^\tau \frac{1}{\sqrt{\tau-s}} \end{aligned}$$

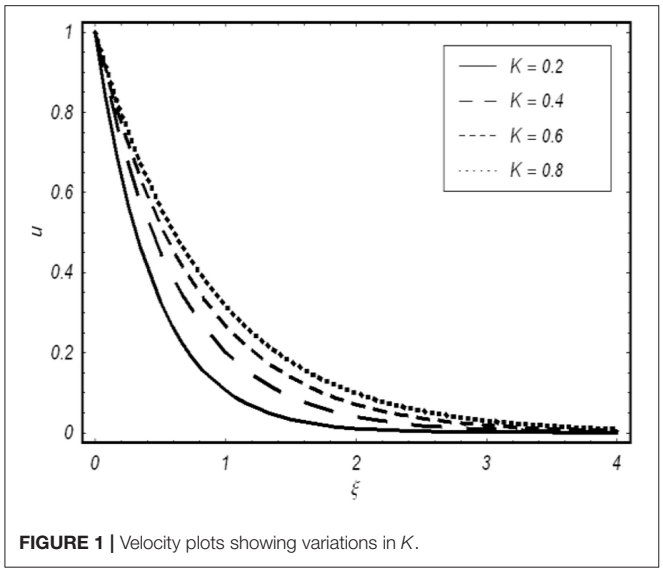

FIGURE 1 | Velocity plots showing variations in K.

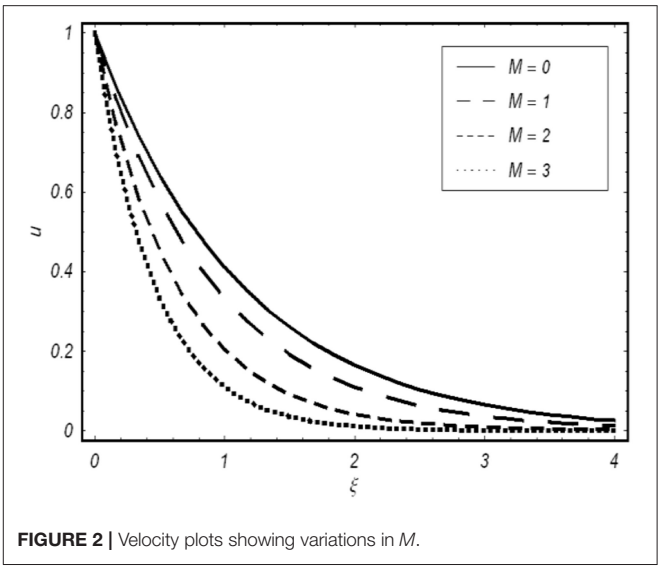

FIGURE 2 | Velocity plots showing variations in M.

$$
\begin{aligned}
&\exp\left(\frac{-a_1\xi^2}{4s}+q_1(\tau-s)-\frac{b_1 s}{a_1}\right) J_1\left(2\sqrt{\frac{\eta_1}{a_1}s(\tau-s)}\right)\mathrm{d}s\\
&-\frac{\sqrt{\eta_2}}{a_1\sqrt{\pi}}\int_0^\tau \frac{1}{\sqrt{\tau-s}}\exp\left(\frac{-a_1\xi^2}{4s}+q_2(\tau-s)-\frac{b_1 s}{a_1}\right)\\
&J_1\left(2\sqrt{\frac{\eta_2}{a_1}s(\tau-s)}\right)\mathrm{d}s\\
&+\frac{\sqrt{\eta_1\eta_2}}{a_1\sqrt{a_1\pi}}\int_0^\tau\int_0^s \frac{\sqrt{\tau-s}}{\sqrt{\sigma(s-\sigma)}}\\
&\exp\left(\frac{-a_1\xi^2}{4(\tau-s)}+q_1\sigma+q_2(s-\sigma)-\frac{b_1}{a_1}(\tau-s)\right)\\
&\times J_1\left(2\sqrt{\frac{\eta_1}{a_1}\sigma(\tau-s)}\right) J_1\left(2\sqrt{\frac{\eta_2}{a_1}(\tau-s)(s-\sigma)}\right)\mathrm{d}s\,\mathrm{d}\sigma.
\end{aligned}
\tag{31}
$$

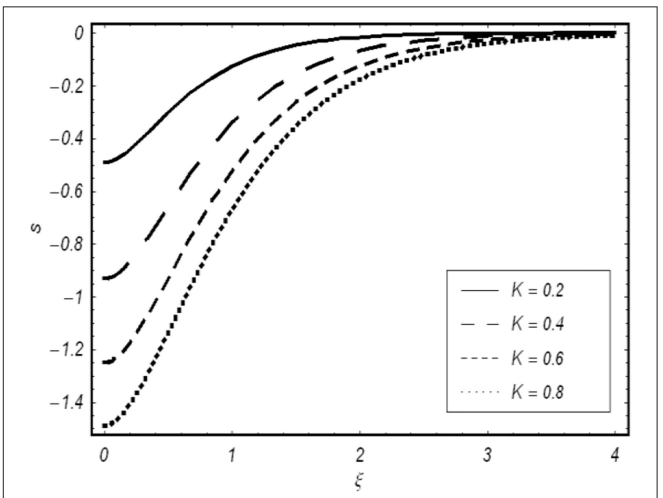

FIGURE 3 | Shear stress plots showing variations in K.

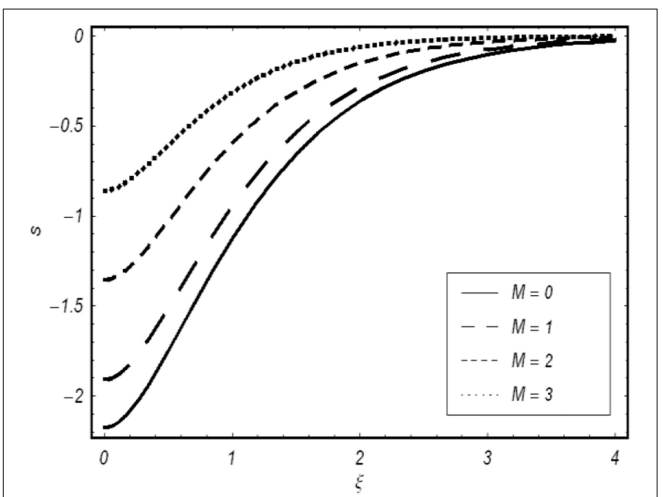

FIGURE 4 | Shear stress plots showing variations in M.

LIMITING CASES

Absence of MHD and Porosity

In limiting sense, when the magnetic effect is absent ($M = 0$) and the medium is non-porous, then the above solutions take the following forms:

$$
\begin{aligned}
u(\xi,\tau) = &\frac{\xi\sqrt{\beta}}{2\sqrt{\beta_1\pi}}\int_0^\tau \frac{1}{s\sqrt{s}}\exp\left(\frac{-\beta\xi^2}{4\beta_1 s}-\left(\frac{1}{\beta}-\frac{\alpha}{\beta_1}\right)s\right)\mathrm{d}s\\
&-\frac{\sqrt{\eta_3}\xi}{2\sqrt{\pi}}\int_0^\tau\int_0^s \frac{1}{\sigma\sqrt{s-\sigma}}\\
&\exp\left(\frac{-\beta\xi^2}{4\beta_1\sigma}+q_1(s-\sigma)-\left(\frac{1}{\beta}-\frac{\alpha}{\beta_1}\right)\sigma\right)\\
&\times J_1\left(2\sqrt{\frac{\beta_1\eta_3}{\beta}\sigma(s-\sigma)}\right)\mathrm{d}s\,\mathrm{d}\sigma\\
&-\frac{\sqrt{\eta_4}\xi}{2\sqrt{\pi}}\int_0^\tau\int_0^s \frac{1}{\sigma\sqrt{s-\sigma}}J_1\left(2\sqrt{\frac{\beta_1\eta_4}{\beta}\sigma(s-\sigma)}\right)\\
&\times\exp\left(\frac{-\beta\xi^2}{4\beta_1\sigma}+q_2(s-\sigma)-\left(\frac{1}{\beta}-\frac{\alpha}{\beta_1}\right)\sigma\right)\mathrm{d}s\mathrm{d}\sigma
\end{aligned}
$$

$$+\frac{\sqrt{\beta_1\eta_3\eta_4}\xi}{2\sqrt{\beta\pi}}\int_0^\tau\int_0^s\int_0^\sigma \exp\left(\frac{-\beta\xi^2}{4\beta_1(s-\sigma)}+q_1\eta+q_2(\sigma-\eta)-\left(\frac{1}{\beta}-\frac{\alpha}{\beta_1}\right)(s-\sigma)\right)\frac{}{\sqrt{\eta(s-\sigma)(\sigma-\eta)}} \times J_1\left(2\sqrt{\frac{\beta_1\eta_3}{\beta}\eta(s-\sigma)}\right) J_1\left(2\sqrt{\frac{\beta_1\eta_4}{\beta}(s-\sigma)(\sigma-\eta)}\right) \mathrm{d}s\,\mathrm{d}\sigma\,\mathrm{d}\eta. \quad (32)$$

$$\begin{aligned} s(\xi,\tau) = {} & \sqrt{\frac{\beta}{\beta_1\pi\tau}}\exp\left(\frac{-\beta\xi^2}{4\beta_1\tau}-\left(\frac{1}{\beta}-\frac{\alpha}{\beta_1}\right)\tau\right) \\ & -\frac{\beta_1\sqrt{\eta_3}}{\beta\sqrt{\pi}}\int_0^\tau\frac{1}{\sqrt{\tau-s}}\exp\left(\frac{-\beta\xi^2}{4\beta_1 s}+q_1(\tau-s)\right. \\ & \left.-\left(\frac{1}{\beta}-\frac{\alpha}{\beta_1}\right)s\right) \\ & \times J_1\left(2\sqrt{\frac{\beta_1\eta_3}{\beta}s(\tau-s)}\right)\mathrm{d}s \\ & -\frac{\beta_1\sqrt{\eta_4}}{\beta\sqrt{\pi}}\int_0^\tau\frac{1}{\sqrt{\tau-s}}J_1\left(2\sqrt{\frac{\beta_1\eta_4}{\beta}s(\tau-s)}\right)\mathrm{d}s \\ & \times\exp\left(\frac{-\beta\xi^2}{4\beta_1 s}+q_2(\tau-s)-\left(\frac{1}{\beta}-\frac{\alpha}{\beta_1}\right)s\right) \\ & +\frac{\beta_1\sqrt{\beta_1\eta_3\eta_4}}{\beta\sqrt{\beta\pi}}\int_0^\tau\int_0^s\frac{\sqrt{\tau-s}}{\sqrt{\sigma(s-\sigma)}} \\ & \times\exp\left(\frac{-\beta\xi^2}{4\beta_1(\tau-s)}+q_1\sigma+q_2(s-\sigma)\right. \\ & \left.-\left(\frac{1}{\beta}-\frac{\alpha}{\beta_1}\right)(\tau-s)\right) \\ & J_1\left(2\sqrt{\frac{\beta_1\eta_3}{\beta}\sigma(\tau-s)}\right) \\ & J_1\left(2\sqrt{\frac{\beta_1\eta_4}{\beta}(\tau-s)(s-\sigma)}\right)\mathrm{d}s\,\mathrm{d}\sigma, \end{aligned} \quad (33)$$

with the following expressions for η_3 and η_4:

$$\begin{aligned} \eta_3 &= \frac{\left(1-\frac{\beta}{\beta_1}-\frac{\alpha}{\beta_1}+\frac{\alpha^2\beta}{\beta_1^2}\right)q_1+\frac{\alpha\beta}{\beta_1^2}-\frac{1}{\beta_1}}{q_1-q_2}, \\ \eta_4 &= -\frac{\left(1-\frac{\beta}{\beta_1}-\frac{\alpha}{\beta_1}+\frac{\alpha^2\beta}{\beta_1^2}\right)q_2+\frac{\alpha\beta}{\beta_1^2}-\frac{1}{\beta_1}}{q_1-q_2}. \end{aligned} \quad (34)$$

It is important to note that if we put $M = \frac{1}{K} = 0$ into the governing Equation (6) and solve along with Equation (7) with the prescribed boundary and initial conditions, we get the same expressions for velocity and shear stress as given above.

Newtonian Fluid

For Newtonian fluid, we make λ, λ_r, γ, and γ_1 equal to zero or equivalently $\lambda = \lambda_r = \gamma = \gamma_1$, then the solutions (30) and (31) reduce to

$$u(\xi,\tau) = \frac{\xi}{2\sqrt{\pi}}\int_0^\tau\frac{1}{s\sqrt{s}}\exp\left(\frac{-\xi^2}{4s}-\left(M^2+\frac{1}{K}\right)s\right)\mathrm{d}s, \quad (35)$$

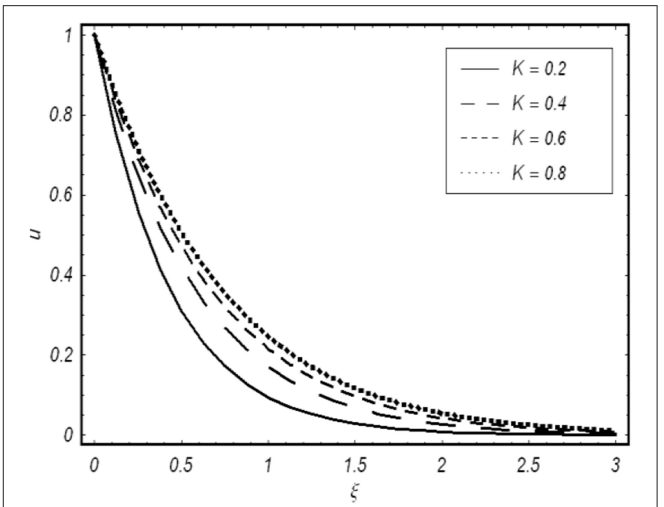

FIGURE 5 | Velocity plots showing variations in K (Newtonian fluid).

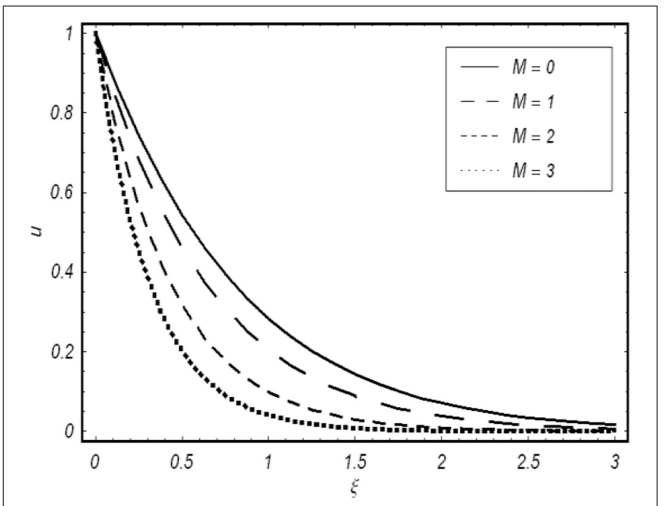

FIGURE 6 | Velocity plots showing variations in M (Newtonian fluid).

$$s(\xi,\tau) = \frac{1}{\sqrt{\pi\tau}}\exp\left(\frac{-\xi^2}{4\tau}-\left(M^2+\frac{1}{K}\right)\tau\right). \quad (36)$$

Now, taking $\lambda = \lambda_r = \gamma = \gamma_1$ in the governing Equation (6) and solving the resulting equations with the given boundary and initial conditions, we get

$$\overline{u}(\xi,q) = \frac{1}{q}\exp\left(-\xi\sqrt{q}\right) = \overline{u_1}(q)\,\overline{u_2}(\xi,q) \quad (37)$$

where

$$\overline{u_1}(q) = \frac{1}{q} \text{ and } \overline{u_2}(\xi,q) = \exp\left(-\xi\sqrt{q+M^2+\frac{1}{K}}\right). \quad (38)$$

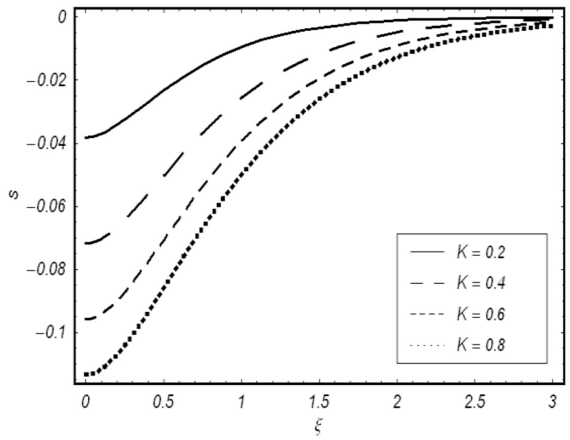

FIGURE 7 | Shear stress plots showing variations in K (Newtonian fluid).

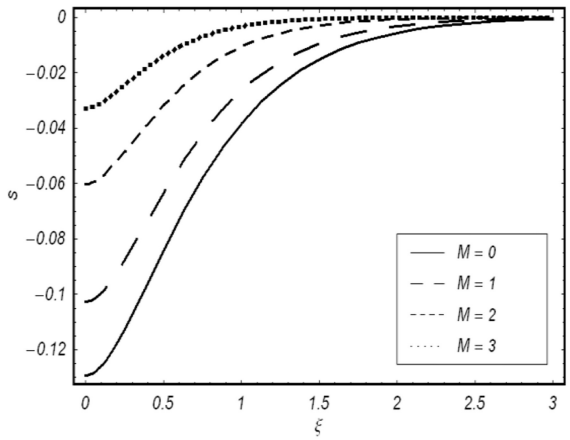

FIGURE 8 | Shear stress plots showing variations in M (Newtonian fluid).

Taking the Laplace inverse of Equation (38), we get

$$u_1(\tau) = 1, \quad u_2(\xi, \tau) = \frac{\xi}{2\tau\sqrt{\pi\tau}} \exp\left(\frac{-\xi^2}{4\tau} - \left(M^2 + \frac{1}{K}\right)\right). \quad (39)$$

The convolution product of $u_1(\tau) = 1$ and $u_2(\xi, \tau)$ gives

$$u(\xi, \tau) = \frac{\xi}{2\sqrt{\pi}} \int_0^\tau \frac{1}{s\sqrt{s}} \exp\left(\frac{-\xi^2}{4\tau} - \left(M^2 + \frac{1}{K}\right) s\right) \mathrm{d}s. \quad (40)$$

The corresponding shear stress can be easily found by using Equation (6); i.e.,

$$\bar{s}(\xi, q) = -\frac{\exp\left(-\xi\sqrt{w(q)}\right)}{\sqrt{w(q)}}; \quad w(q) = q + M^2 + \frac{1}{K}. \quad (41)$$

Using a similar method as in the case of velocity, the final expression for the shear stress is given as follows:

$$s(\xi, \tau) = \frac{1}{\sqrt{\pi\tau}} \exp\left(\frac{-\xi^2}{4\tau} - \left(M^2 + \frac{1}{K}\right)\tau\right). \quad (42)$$

Here, we noted that in both cases, i.e., from the final solutions given by Equations (30) and (31) and from the governing Equations (5) and (6), we obtained the same exact results for velocity and shear stress given by Equations (35), (36), (40), and (42), respectively. Indeed, this provides a useful check of correctness.

NUMERICAL RESULTS AND DISCUSSION

Figure 1 is plotted for $K = 0.2, 0.4, 0.6, 0.8$ when $M = 0.2$, $\alpha = 0.9$, $\beta_1 = 0.5$, $\beta = 0.8$ and $\tau = 0.5$, whereas **Figures 2**, **4** are sketched for $M = 0, 1, 2, 3$ when $K = 2$, $\alpha = 0.9$, $\beta_1 = 0.5$, $\beta = 0.8$, and $\tau = 0.5$. **Figures 1–4** have been displayed to see the influence of Hartmann number M and porosity parameters K on the fluid velocity and the corresponding shear stress of a GBF. To check the effects of M and K on the fluid velocity and related shear stress for a Newtonian fluid, **Figures 5–8** are sketched. **Figures 5**, **7** are plotted for different values of K when $M = 0.2$ and $\tau = 0.5$, whereas **Figures 6**, **8** are prepared for various values of M when $K = 2$ and $\tau = 0.5$. Note that **Figures 1–8** provide a comparison of velocity field and the related shear stress for the case of GBF with that of a Newtonian fluid. **Figure 1** shows the influence of K on the Burgers' fluid velocity; it can be noticed that velocity increases with the increasing values of K, due to the decrease in opposing forces. In **Figure 2**, the impact of M is shown on fluid velocity; from this figure, it is noticed that velocity is a decreasing function of M. This is because the greater values of M enhance the Lorentz forces, which are the opposing forces. The same behavior is noticed in **Figures 5**, **6** for Newtonian fluid. **Figure 3** is plotted in order to show the effect of K on shear stress; the shear stress decreases with the increasing values of K. The behavior of shear stress is noticed for different values of M in **Figure 4**. It is observed that the shear stress increases with the increasing values of M. **Figures 7**, **8** also show the same behavior of shear stress for Newtonian fluid.

DATA AVAILABILITY STATEMENT

All datasets generated for this study are included in the article/supplementary material.

AUTHOR CONTRIBUTIONS

AA formulated the problem. IK solved the problem and discussed results.

FUNDING

This research was funded by Deanship of Scientific Research at Princess Nourah bint Abdulrahman University (Grant No. 39/S/269: ٣٩/ص/٢٦٩).

REFERENCES

1. Rajagopal KR. A note on unsteady unidirectional flows of a non-Newtonian fluid. *Int J Non Linear Mech*. (1982) **17**:369–73.
2. Hayat T, Khan I, Ellahi R, Fetecau C. Some MHD flows of a second grade fluid through the porous medium. *J Porous Media*. (2008) **11**:389–400. doi: 10.1615/JPorMedia.v11.i4.50
3. Erdogan ME. A note on an unsteady flow of a viscous fluid due to an oscillating plane wall. *Int J Non Linear Mech*. (2000) **35**:1–6. doi: 10.1016/S0020-7462(99)00019-0
4. Erdogan ME, Imrak CE. On some unsteady flows of a non-Newtonian fluids. *Appl Math Model*. (2007) **31**:70–180. doi: 10.1016/j.apm.2005.08.019
5. Tan WC, Masuoka T. Stokes first problem for a second grade fluid in a porous half space with heated boundary. *Int J Non-Linear Mech*. (2005) **40**:515–22. doi: 10.1016/j.ijnonlinmec.2004.07.016
6. Tan WC, Masuoka T. Stokes first problem for an Oldroyd-B fluid in a porous half space. *Phys Fluid*. (2005) **17**:023101–7. doi: 10.1063/1.1850409
7. Hayat T, Fetecau C, Sajid M. Analytical solution for MHD transient rotating flow of a second grade fluid in a porous space. *Non Linear Anal Real World Appl*. (2008) **9**:1619–27. doi: 10.1016/j.nonrwa.2007.04.006
8. Hayat T, Fetecau C, Sajid M. On MHD transient flow of a Maxwell fluid in a porous medium and rotating frame. *Phys Lett A*. (2008) **372**:1639–44. doi: 10.1016/j.physleta.2007.10.036
9. Fetecau C, Vieru D, Fetecau C. A note on the second problem of Stokes' for Newtonian fluids. *Int J Non Linear Mech*. (2008) **43**:451–7. doi: 10.1016/j.ijnonlinmec.2007.12.022
10. Fetecau C, Fetecau C. A new exact solution for the flow of a Maxwell fluid past an infinite plate. *Int J Non Linear Mech*. (2002) **38**:423–7. doi: 10.1016/S0020-7462(01)00062-2
11. Fetecau C, Fetecau C. The first problem of Stokes' for an Oldroyd-B fluid. *Int J Non-Linear Mech*. (2003) **38**:1539–44. doi: 10.1016/S0020-7462(02)00117-8
12. Vieru D, Nazar M, Fetecau C, Fetecau C. New exact solutions corresponding to the first problem of Stokes' for Oldroyd-B fluids. *Appl Math Comput*. (2008) **55**:1644–52. doi: 10.1016/j.camwa.2007.04.040
13. Ravindran P, Krishnan JM, Rajagopal KR. A note on the flow of Burgers' fluid in an orthogonal rheometer. *Int J Eng Sci*. (2004) **42**:1973–85. doi: 10.1016/j.ijengsci.2004.07.007
14. Hayat T, Fetecau C, Asghar S. Some simple flows of a Burgers' fluid. *Int J Eng Sci*. (2006) **44**:1423–31. doi: 10.1016/j.ijengsci.2006.08.008
15. Khan M, Maqbool K, Hayat T. Influence of Hall current on the flows of a generalized Oldroyd-B fluid in the porous space. *Acta Mech*. (2006) **184**:1–13. doi: 10.1007/s00707-006-0326-7
16. Tong D, Shan L. Exact solutions for generalized Burgers' fluid in an annular pipe. *Meccanica*. (2009) **44**:427–31. doi: 10.1007/s11012-008-9179-6
17. Xue C, Nie J. Exact solutions of Stokes first problem for heated generalized Burgers' fluid in a porous half space. *Non Linear Anal Real World Appl*. (2008) **9**:1628–37. doi: 10.1016/j.nonrwa.2007.04.007
18. Hayat T, Khan SB, Khan M. Exact solution for rotating flows of a generalized Burgers' fluid in a porous space. *Appl Math Model*. (2008) **32**:749–60. doi: 10.1016/j.apm.2007.02.011
19. Vieru D, Hayat T, Fetecau C, Fetecau C. On the first problem of Stokes' for Burgers' fluid, II: the Cases $\gamma = \lambda^2/4$ and $\gamma > \lambda^2/4$. *Appl Math Comput*. (2008) **197**:76–86. doi: 10.1016/j.amc.2007.07.033
20. Khan M, Ali SH, Fetecau C. Exact solutions of accelerated flows for a Burgers' fluid. I. The case $\gamma < \lambda^2/4$. *Appl Math Comput*. (2008) **203**:881–94. doi: 10.1016/j.amc.2008.05.121
21. Khan M, Ali SH, Fetecau C. Exact solutions of accelerated flows for a Burgers' fluid. II. The cases $\gamma = \lambda^2/4$ and $\gamma > \lambda^2/4$, Z. *Angew Math Phys*. (2009) **60**:701–22. doi: 10.1007/s00033-008-7155-6
22. Khan M, Anjum A, Fetecau C. On exact solutions of Stokes second problem for a Burgers' fluid, I. The case $\gamma < \lambda^2/4$, Z. *Angew Math Phys*. (2009) **61**:697–720. doi: 10.1007/s00033-009-0025-z
23. Fetecau C, Vieru D, Hayat T, Fetecau C. On the first problem of Stokes for Burgers' fluid, I: Case $\gamma < \lambda^2/4$. *Int J Non-Linear Anal*. (2009) **10**:2183–94. doi: 10.1016/j.nonrwa.2008.04.002
24. Kumar D, Singh J, Baleanu D. Analytic study of Allen-Cahn equation of fractional order. *J Math Anal Appl*. (2017) **9**:31–40.
25. Gupta S, Kumar D, Singh J. An efficient computational approach for generalized Hirota-Satsuma coupled KdV equations arising in shallow water waves. *Waves Wavelets Fractals Adv Anal*. (2017) **3**:14–30. doi: 10.1515/wwfaa-2017-0002
26. Kumar D, Singh J, Baleanu D. Modified Kawahara equation within a fractional derivative with non-singular kernel. *Therm Sci*. (2018) **22**:789–96. doi: 10.2298/TSCI160826008K
27. Singh J, Kumar D, Baleanu D. On the analysis of fractional diabetes model with exponential law. *Adv Diff Equ*. (2018) **2018**:231. doi: 10.1186/s13662-018-1680-1
28. Kumar D, Singh J, Baleanu D. A new fractional model for convective straight fins with temperature-dependent thermal conductivity. *Therm Sci*. (2018) **22**:2791–802. doi: 10.2298/TSCI170129096K
29. Prakash A, Verma V, Kumar D, Singh J. Analytic study for fractional coupled Burger's equations via sumudu transform method. *Nonlinear Eng*. (2018) **7**:323–32. doi: 10.1515/nleng-2017-0090
30. Kumar D, Singh J, Baleanu D, Rathore S. Analysis of a fractional model of Ambartsumian equation. *Eur Phys J Plus*. (2018) **133**:259. doi: 10.1140/epjp/i2018-12081-3
31. Kumar D, Tchier F, Singh J, Baleanu D. An efficient computational technique for fractal vehicular traffic flow. *Entropy*. (2018) **20**:259. doi: 10.3390/e20040259
32. Kumar D, Singh J, Tanwar K, Baleanu D. A new fractional exothermic reactions model having constant heat source in porous media with power, exponential and Mittag-Leffler Laws. *Int J Heat Mass Transf*. (2019) **138**:1222–7. doi: 10.1016/j.ijheatmasstransfer.2019.04.094
33. Kumar D, Singh J, Purohit SD, Swroop R. A hybrid analytical algorithm for nonlinear fractional wave-like equations. *Math Model Nat Pheno*. (2019) **14**:304. doi: 10.1051/mmnp/2018063
34. Kumar D, Singh J, Al Qurashi M, Baleanu D. A new fractional SIRS-SI malaria disease model with application of vaccines, anti-malarial drugs, and spraying. *Adv Differ Equ*. (2019) **2019**:278. doi: 10.1186/s13662-019-2199-9
35. Yang XJ, Tenreiro Machado JA. A new fractal nonlinear Burgers' equation arising in the acoustic signals propagation. *Math Method Appl Sci*. (2019) 14:304. doi: 10.1002/mma.5904
36. Yang XJ, Tenreiro Machado JA, Baleanu D. Exact traveling-wave solution for local fractional boussinesq equation in fractal domain. *Fractals*. (2017) **25**:1–19. doi: 10.1142/S0218348X17400060
37. Waqas H, Khan SU, Imran M, Bhatti MM. Thermally developed Falkner–Skan bioconvection flow of a magnetized nanofluid in the presence of a motile gyrotactic microorganism: buongiorno's nanofluid model. *Physica Scripta*. (2019) **94**:115304. doi: 10.1088/1402-4896/ab2ddc
38. Marin M, Vlase S, Ellahi R, Bhatti MM. On the partition of energies for the backward in time problem of thermoelastic materials with a dipolar structure. *Symmetry*. (2019) **11**:863. doi: 10.3390/sym11070863
39. Jamil M. First problem of Stokes for generalized Burgers' fluids. *ISRN Math Phys*. (2012) **2012**:831063. doi: 10.5402/2012/831063
40. Jamil M, Rauf A, Zafar AA, Khan NA. New exact analytical solutions for Stokes' first problem of Maxwell fluid with fractional derivative approach. *Comput Math Appl*. (2011) **62**:1013–23. doi: 10.1016/j.camwa.2011.03.022
41. Jamil M, Khan NA, Imran MA. New exact solutions for an Oldroyd-B Fluid with Fractional Derivatives: Stokes' first problem. *Int J Nonlinear Sci Num Simul*. (2013) **14**:443–51. doi: 10.1515/ijnsns-2011-024
42. Roberts GE, Kaufman H. *Table of Laplace Transforms*. Philadelphia, PA: W.B. Saunders Company (1968).

Conflict of Interest: The authors declare that the research was conducted in the absence of any commercial or financial relationships that could be construed as a potential conflict of interest.

NOMENCLATURE

v (m/s)	Velocity component in the $x-$ direction
λ (s)	Relaxation time
ρ (kg/m^3)	Fluid density
λ_r ($< \lambda$) (s)	Retardation time
μ (kg/m s)	Dynamic viscosity
γ (s^2) and γ_1 (s^2)	Material constants having the dimensions as the square of time
δ (s^{3}A^2/kg m^3)	Finite electrical conductivity
V (m/s)	Reference velocity
φ ($0 < \varphi < 1$)	Porosity
B_0 (kg/s^{2}A)	Applied magnetic field
$k > 0$ (m^2)	The permeability of the porous medium
$v(y, t)$ (m/s)	Fluid velocity
$T(y, t)$ (kg/s^{2}m)	Shear tress
$u(\xi, \tau)$ (m/s) ands (ξ, τ) (Pa)	Dimensionless fluid velocity and shear stress

frontiers in Physics

BRIEF RESEARCH REPORT
published: 21 January 2020
doi: 10.3389/fphy.2019.00242

Lump-Type and Bell-Shaped Soliton Solutions of the Time-Dependent Coefficient Kadomtsev-Petviashvili Equation

Aliyu Isa Aliyu[1], Yongjin Li[1]*, Liu Qi[1], Mustafa Inc[2], Dumitru Baleanu[3,4] and Ali S. Alshomrani[5]*

[1] Department of Mathematics, Sun Yat-sen University, Guangzhou, China, [2] Department of Mathematics, Firat University, Elâziğ, Turkey, [3] Department of Mathematics, Cankaya University, Ankara, Turkey, [4] Institute of Space Sciences, Măgurele, Romania, [5] Department Mathematics, Faculty of Science, King Abdulaziz University, Jeddah, Saudi Arabia

In this article, the lump-type solutions of the new integrable time-dependent coefficient (2+1)-dimensional Kadomtsev-Petviashvili equation are investigated by applying the Hirota bilinear technique and a suitable ansatz. The equation is applied in the modeling of propagation of small-amplitude surface waves in large channels or straits of slowly varying width, depth and non-vanishing vorticity. Applying the Bell's polynomials approach, we successfully acquire the bilinear form of the equation. We firstly find a general form of quadratic function solution of the bilinear form and then expand it as the sums of squares of linear functions satisfying some conditions. Most importantly, we acquire two lump-type and a bell-shaped soliton solutions of the equation. To our knowledge, the lump type solutions of the equation are reported for the first time in this paper. The physical interpretation of the results are discussed and represented graphically.

Keywords: Bell's polynomials, Hirota bilinear form, bell-type solutions, lump-type solutions, (2+1)-dimensional Kadomtsev-Petviashvili equation

OPEN ACCESS

Edited by:
Carlo Cattani,
Universitá degli Studi della Tuscia, Italy

Reviewed by:
Kazuharu Bamba,
Fukushima University, Japan
Marin I. Marin,
Transilvania University of Braşov, Romania

****Correspondence:***
Aliyu Isa Aliyu
aliyu@mail.sysu.edu.cn
Yongjin Li
stslyj@mail.sysu.edu.cn

Specialty section:
This article was submitted to Mathematical Physics, a section of the journal Frontiers in Physics

Received: *16 October 2019*
Accepted: *18 December 2019*
Published: *21 January 2020*

Citation:
Aliyu AI, Li Y, Qi L, Inc M, Baleanu D and Alshomrani AS (2020) Lump-Type and Bell-Shaped Soliton Solutions of the Time-Dependent Coefficient Kadomtsev-Petviashvili Equation. Front. Phys. 7:242. doi: 10.3389/fphy.2019.00242

1. INTRODUCTION

Nonlinear equations (NLEs) have been the subject of concentrate in different parts of numerical physical sciences, for example, material science, science, and so forth. The explanatory arrangements of such conditions are of essential significance since a great deal of scientific physical models are depicted by NLEs [1]. Among the conceivable answers for NLEs, certain unique frame arrangements may depend just on a solitary blend of factors, for example, solitons. In soliton theory [2], optical solitons, painleve analysis, investigation of integrability of systems of equations, Hamiltonian structure, Bell's polynomials, Backlaund transformations, etc. are the hot topics in recent time. Lump solutions are important models to used to describe certain complicated physical phenomena in science [3]. Lump solution is a kind of special rational function solutions localized along all directions in the space. Lump solitons have been intensively studied and some of the results have been reported in [4–6]. The be integrable time-dependent coefficient (2+1)-dimensional Kadomtsev-Petviashvili model that will be studied in this work is given by Wazwaz [7]:

$$(\psi_t + \psi\psi_x + \psi_{xxx})_x + 3\psi_{yy} + g(t)\psi_{xx} = 0, \tag{1}$$

where $\psi(x,t,y)$ is a function of the temporal variable t and two scaled spatial variables x and y. $g(t)$ is a functions of t. The equation is applied in the modeling of propagation of small-amplitude surface waves in large channels or straits of slowly varying width, depth and non-vanishing vorticity. (1) was proposed by WazWaz in [7] where the integrability property of the equation were explicitly demonstrated and the multiple complex and multiple real soliton solutions of the equation were reported. Variable-coefficients KP equations have been investigated thoroughly in the literature [8–11].

To our knowledge, the lump soliton solutions to (1) have not been studied using the Hirota Bilinear methods. In this article, by applying the concept of Bell polynomials [3, 4] and Hirota Bilinear approach [12–14], the lump soliton solutions of (1) will be derived. In addition, a Bell-shaped soliton solution will also be derived using an efficient ansatz [15].

2. BELL POLYNOMIAL

In this part, we recall some important terminologies about the Bell polynomials [12–14].

Let $f = f(y_1, y_2, ..., y_n)$ be a $\mathbb{C}^\infty$ function, the multi-dimensional Bell polynomials are defined by the following:

$$Y_{n_1y_1,...,m_ry_r}(f) \equiv Y_{m_1,...,m_r}(f_{l_1y_1}, ..., f_{l_ry_r}) = e^{-f}\partial_{y_1}^{m_1}...\partial_{y_r}^{m_r}e^{f}, \quad (2)$$

where $(f_{l_1y_1}, ..., f_{l_ry_r}) = \partial_{y_1}^{l_1}...\partial_{y_r}^{l_r}(0 \le l_i \le m_i, \quad i = 1, 2, ...r)$. Taking $m = 1$, Bell polynomials is given by:

$$Y_{my}(f) \equiv Y_m(f_1, ..., f_m)\sum \frac{m!}{s_1!...s_m!(1!)^{s_1}...(m!)^{s_m}} f_1^{s_1}...f_n^{s_m}, \qquad m = \sum_{k=1}^{m} ks_k. \quad (3)$$

The multi-dimensional Bell polynomials can be represented by Gilson et al. [14]:

$$\mathscr{Y}_{m_1y_1,...m_ry_r}(v,w) = Y_{m_1,...,m_r}(f)|_{f_{l_1y_1},...,f_{l_ry_r}} = \begin{cases} v_{l_1y_1}, ..., f_{l_ry_r}, & l_1 + ...l_r \quad \text{is odd} \\ w_{l_1y_1}, ..., f_{l_ry_r}, & l_1 + ...l_r \quad \text{is even} \end{cases} \quad (4)$$

$$\mathscr{Y}_y = v_y, \ \mathscr{Y}_{2y}(v,w) = v_x^2 + w_{2y}, \ \mathscr{Y}_{y,t}(v,w) = v_yv_t + w_{yt}, \ \mathscr{Y}_{3y}(v,w) = v_{3y} + 3v_yw_{2y} + v_y^2, ... \quad (5)$$

The conjunction between $\mathscr{Y}$-polynomials and the Hirota bilinear operator are related by the following identity:

$$\mathscr{Y}_{m_1y_1,...,m_ry_r}\left(v = \ln F/G, \quad w = \ln FG\right).\left(FG\right)^{-1} D_{y_1}^{m_1}...D_{y_r}^{m_r}F.G, \quad (6)$$

where F and G are functions of y and t. Setting $F = G$, the identity (6) becomes:

$$F^{-2}D_{y_1}^{m_1}...D_{y_r}^{m_r}F.F = \mathscr{Y}(0, 2\ln F) = \begin{cases} 0, & m_1 + ...m_r \ \text{is odd} \\ \mathscr{Y}_{m_1y_1,...m_ry_r}(q), & m_1 + ...m_r \ \text{is even.} \end{cases} \quad (7)$$

The first few $\mathscr{P}$-polynomials can be represented by the following:

$$\mathscr{P}_{2y}(q) = q_{2y}, \quad \mathscr{P}_{yt}(q) = q_{yt}, \quad \mathscr{P}_{4y}(q) = q_{4y} + 3q_{2y}^2, \quad \mathscr{P}_{6y}(q) = q_{6y} + 15q_{2y}q_{4y} + 15q_{2y}^3, ... \quad (8)$$

The Bell polynomials $\mathscr{Y}_{m_1y_1,...m_ry_r}(v,w)$ can be separated into certain polynomials and $\mathscr{Y}$-polynomials:

$$(FG)^{-1}D_{y_1}^{m_1}...D_{y_r}^{m_r}F.G = \mathscr{Y}_{m_1y_1,...m_ry_r}(v,w)|_{v=\ln F/G, w=\ln FG)} = \sum_{m_1+...+m_r=\text{even}} \sum_{l_1=0}^{m_1} ... \sum_{l_r=0}^{m_r} \prod_{i=0}^{r} \binom{m_i}{l_i} P_{l_1y_1,...,l_ry_r}(q)Y_{(m_r-l_r)y_r}(v). \quad (9)$$

The main property of the Bell polynomials:

$$\mathscr{Y}_{m_1y_1,...n_ry_r}(v)|_{v=\ln \ \psi = \psi_{m_1y_1,...,m_ry_r}/\psi} \quad (10)$$

means that the binary Bell polynomials $\mathscr{Y}_{m_1y_1,...m_ry_r}(v,w)$ can be linearized by applying the Hopf-Cole transformation $v = \ln\psi$, that is $\psi = F/G$

Theorem 1. *By applying the transformation,*

$$\psi = 12(lnf)_{xx}, \quad (11)$$

(1) bilinearized into

$$(D_x^4 + g(t)D_x^2 + D_tD_x + 3D_y^2).f.f = 0, \quad (12)$$

where $f = f(x,t,y)$.

Proof: Introducing the potential field variable q on setting

$$\psi = h(t)q_{xx}, \quad (13)$$

where $h = h(t)$ is a function of t. Substituting (13), we can obtain

$$\frac{1}{2}h(t)q_{xx}^2 + g(t)q_{xx} + 3q_{yy} + q_{xxxx} + q_{xt} = 0. \quad (14)$$

Integrating (14) with respect to x, setting $h(t) = 6$ and by means of formula (8), (14) can be converted to $\mathscr{P}$-polynomials represented by:

$$3\mathscr{P}_{2y}(q) + g(t)\mathscr{P}_{2x}(q) + \mathscr{P}_{4x}(q) + \mathscr{P}_{xt}(q) = 0. \quad (15)$$

By applying (10), we obtain:

$$\psi = 2\ln f \iff \psi = h(t)q_{xx} = 12(\ln f)_{xx}. \quad (16)$$

3. LUMP-TYPE SOLITONS TO (1)

The Hirota bilinear form (12) of (1) is equivalent to the following:

$$3ff_{yy}-2g(t)f_x{}^2+2fg(t)f_{xx}+6f_{xx}^2-8f_xf_{xxx}+2ff_{xxxx}-2f_xf_t+2ff_{xt}=0. \tag{17}$$

To derive the lump-type soliton of (1), we consider f in the following form [3]

$$f = X^T BX + f_0, \tag{18}$$

where $B = (a_{ij})_{4\times 4}$ is a symmetric matrix, $X = (1, x, y, t)^T$, a_{ij} and f_0 are constants. (18) can be expanded as:

$$f = a_{22}x^2 + a_{44}t^2 + a_{33}y^2 + 2a_{12}x + 2a_{13}y + 2a_{14}t + a_{23}xy + 2a_{24}tx + 2a_{34}ty + a_{11} + f_0. \tag{19}$$

Putting (19) into (12) and performing all the necessary algebraic calculations by symbolic computations, we acquire the following system of algebraic expressions:

$$\begin{aligned}
&6f_0a_{33} + 6a_{11}a_{33} - 8a_{12}a_{14} + 24a_{22}^2 + 4g(t)(-2a_{12}^2 \\
&+ (f_0 + a_{11})a_{22}) + 4f_0a_{24} + 4a_{11}a_{24} = 0, && (20)\\
&-2\,a_{22}(2g(t)a_{22} + 2a_{24} - 3a_{33}) = 0, && (21)\\
&(-8g(t)a_{12}a_{22} - 8a_{14}a_{22} + 12a_{12}a_{33}) = 0, && (22)\\
&(-4a_{14}a_{23} + 8g(t)(a_{13}a_{22} - a_{12}a_{23}) \\
&+ 8a_{13}a_{24} + 12a_{13}a_{33} - 8a_{12}a_{34}) = 0, && (23)\\
&(-4g(t)a_{22}a_{23} + 6a_{23}a_{33} - 8a_{22}a_{34}) = 0, && (24)\\
&(4a_{24}a_{33} + 6a_{33}^2 - 2g(t)(a_{23}^2 - 2a_{22}a_{33}) - 4a_{23}a_{34}) = 0, && (25)\\
&4\,(2g(t)(a_{14}a_{22} - 2a_{12}a_{24}) + 3a_{14}a_{33} - 2a_{12}a_{44}) = 0, && (26)\\
&(-8g(t)a_{22}a_{24} + 12a_{24}a_{33} - 8a_{22}a_{44}) = 0, && (27)\\
&(12a_{33}a_{34} + g(t)(-8a_{23}a_{24} + 8a_{22}a_{34}) - 4a_{23}a_{44}) = 0, && (28)\\
&(2(-2a_{24} + 3a_{33})a_{44} + g(t)(-8a_{24}^2 + 4a_{22}a_{44})) = 0. && (29)
\end{aligned}$$

Solving (20) to (29), we acquire the following soliton parameters:

$$\begin{cases}
a_{22} = \dfrac{a_{24}^2 a_{33}}{a_{34}^2},\\
a_{13} = \dfrac{a_{14}a_{33}}{a_{34}},\\
a_{12} = \dfrac{a_{14}a_{24}a_{33}}{a_{34}^2},\\
a_{44} = \dfrac{a_{34}^2}{a_{33}},\\
a_{23} = \dfrac{2a_{24}a_{33}}{a_{34}},\\
g(t) = -\dfrac{\left(2a_{24}a_{33} - 3a_{33}^2\right)a_{34}^2}{2a_{24}^2a_{33}^2},\\
f_0 = -a_{11} + \dfrac{a_{33}\left(-2a_{24}^4 + a_{14}^2a_{34}^2\right)}{a_{34}^4}.
\end{cases} \tag{30}$$

where $a_{33} \neq 0, a_{24} \neq 0, a_{34} \neq 0$ are necessary and sufficient conditions which must be satisfied for the solution to exist. From (30), we obtain the following solution of f under the general quadratic function:

$$\begin{aligned}
f = \frac{1}{a_{34}^4}\Bigg\{ &-2a_{24}^4a_{33} + a_{24}^2a_{33}a_{34}^2x^2\\
&+ 2a_{24}a_{34}^2(a_{14}a_{33}x + a_{34}(a_{33}y + ta_{34}))\\
&+ \frac{a_{34}^2(a_{14}a_{33} + a_{34}(a_{33}y + a_{34}t))^2}{a_{33}}\Bigg\}.
\end{aligned} \tag{31}$$

Using (30), under the transformation (11), we acquire the following lump-type solution of (1).

$$\begin{aligned}
\psi(x,t,y) &= \frac{12(ff_{xx} - f_x^2)}{f^2}\\
&= \frac{12}{f^2a_{34}^6}\Bigg\{2a_{24}^2(2a_{24}^4a_{33}^2 + x^2a_{24}^2a_{33}^2a_{34}^2\\
&+ 2xa_{24}a_{33}a_{34}^2(a_{14}a_{33} + a_{34}(ya_{33} + ta_{34}))\\
&+ a_{34}^2(a_{14}a_{33} + a_{34}(ya_{33} + ta_{34}))^2)\Bigg\}.
\end{aligned} \tag{32}$$

It should be noted that the positiveness of f cannot be guaranteed. To tackle this problem, we expand (18) as the sums of squares of linear function f and introduce the following theorem:

Theorem 2. *(Cholesky Decomposition Theorem [3]). Let $B = (a_{ij})$ be a real symmetric positive matrix, then it can be simplified into the following:*

$$B = RR^T, \tag{33}$$

where $R = (r_{ij})$ is a triangular matrix. The relationship between elements in B and elements in R is given below:

$$r_{ij} = \begin{cases}
(a_{ii} - \sum_{k=1}^{i-1} r_{ik}^2)^2, & (i = j),\\
\frac{1}{r_{ii}}(a_{ii} - \sum_{k=1}^{i-1} r_{ik}r_{jk}), & (i > j),\\
0, & (i < j).
\end{cases} \tag{34}$$

In accordance with Theorem 2, (18) can be rewritten as:

$$\begin{aligned}
f = X^TRR^TX + f_0 = (R^TX)^T(R^TX) + f_0 =\\
(r_{11} + r_{12}x + r_{13}y + r_{14}t)^2 + (r_{22}x + r_{23}y + r_{24}t)^2\\
+(r_{33}y + r_{34}t)^2 + r_{44}^2t^2 + f_0.
\end{aligned} \tag{35}$$

(35) guarantees the positive definiteness of f. Putting (35) into (12) and solving the result, we obtain the following soliton coefficients:

$$\begin{cases} r_{23}=0, \\ r_{22}=0, \\ r_{33}=0, \\ r_{31}=0, \\ r_{24}=\sqrt{-r_{34}^2-r_{44}^2}, \\ g(t)=\frac{3r_{13}^2-2r_{12}r_{14}}{2r_{12}^2}, \\ f_0=-\frac{2r_{12}^4}{r_{13}^2}. \end{cases} \tag{36}$$

Where $r_{23}\neq 0, r_{22}\neq 0$ are necessary and sufficient conditions which must be satisfied for the solutions to exist. From (36), we obtain the solution of f as:

$$f=-\frac{2r_{12}^4}{r_{13}^2}t^2+\left(r_{11}+r_{12}x+r_{13}y+r_{14}t\right)^2 +r_{34}^2t^2+t^2r_{44}^2+\left(-r_{34}^2-r_{44}^2\right). \tag{37}$$

Putting (36) into (35) using (11), we acquire the following lump-type solution of (1) under positive quadratic function:

$$\psi(x,t,y)=\frac{12(ff_{xx}-f_x^2)}{f^2}=12\Bigg\{-\frac{4r_{12}^2(r_{11}+xr_{12}+yr_{13}+tr_{14})^2}{(-\frac{2r_{12}^4}{r_{13}^2}+(r_{11}+xr_{12}+yr_{13}+tr_{14})^2+t^2r_{34}^2+t^2r_{44}^2+t^2(-r_{34}^2-r_{44}^2))^2}+ \frac{2r_{12}^2}{-\frac{2r_{12}^4}{r_{13}^2}+(r_{11}+xr_{12}+yr_{13}+tr_{14})^2+t^2r_{34}^2+t^2r_{44}^2+t^2(-r_{34}^2-r_{44}^2)}\Bigg\}. \tag{38}$$

4. LUMP SOLITONS TO (1)

4.1. Lump Solitons to (1) Using (32)

Setting the following soliton parameters $a_{24}=1, a_{33}=2, a_{14}=1, a_{34}=3$ in (32), we obtain the following lump solution to (1):

$$\psi(x,t,y)=-\frac{864\left(8+36x^2+36x(2+3(3t+2y))+9(2+3(3t+2y))^2\right)}{\left(-8+36x^2+36x(2+3(3t+2y))+9(2+3(3t+2y))^2\right)^2}. \tag{39}$$

4.2. Lump Solitons to (1) Using (38)

Setting the following soliton parameters: $r_{11}=1, r_{12}=2, r_{13}=-1, r_{44}=1, r_{34}=3, r_{14}=1$ in (38), we acquire the following lump solution to (1)

$$\psi(x,t,y)=12\left\{\frac{8}{-32+(1+t+2x-y)^2}-\frac{16(1+t+2x-y)^2}{(-32+(1+t+2x-y)^2)^2}\right\}. \tag{40}$$

5. BELL-SHAPED SOLITON TO (1)

The bell-shaped soliton solution of (1) may be derived using:

$$\psi(x,t,y)=\rho\,\mathrm{sech}^p\sigma, \tag{41}$$

where $\sigma=\eta(x+y-vt)$. Putting (41) into (1) yields:

$$\begin{aligned} &p\nu\eta^2\rho\,\mathrm{sech}(\sigma)^p-p\eta^4\rho\,\mathrm{sech}(\sigma)^p+2p(1+p)\eta^4\rho\,\mathrm{sech}(\sigma)^p- \\ &p(1+p)\nu\eta^2\rho\,\mathrm{sech}(\sigma)^{2+p}\sinh(\sigma)^2+p(1+p)\eta^4\rho\,\mathrm{sech}(\sigma)^{2+p} \\ &\sinh(\sigma)^2-2p(1+p)^2\eta^4\rho\,\mathrm{sech}(\sigma)^{2+p}\sinh(\sigma)^2 \\ &+p^2\eta^2\rho^2\,\mathrm{sech}(\sigma)^{2+2p}\sinh(\sigma)^2+3(-p\eta^2\rho\,\mathrm{sech}(\sigma)^p \\ &+p(1+p)\eta^2\rho\,\mathrm{sech}(\sigma)^{2+p}\sinh(\sigma)^2)+g(t)(-p\eta^2\rho\,\mathrm{sech}(\sigma)^p \\ &+p(1+p)\eta^2\rho\,\mathrm{sech}(\sigma)^{2+p}\sinh(\sigma)^2)+\rho\,\mathrm{sech}(\sigma)^p \\ &(-p\eta^2\rho\,\mathrm{sech}(\sigma)^p+p(1+p)\eta^2\rho\,\mathrm{sech}(\sigma)^{2+p}\sinh(\sigma)^2)-p\eta^2\rho\cosh(\sigma) \\ &(-(1+p)\eta^2\mathrm{sech}(\sigma)^{1+p}+(1+p)(2+p)\eta^2\mathrm{sech}(\sigma)^{3+p}\sinh(\sigma)^2) \\ &-p\eta\rho\sinh(\sigma)(-(1+p)\eta^3\mathrm{sech}(\sigma)^{2+p}\sinh(\sigma) \\ &+2(1+p)(2+p)\eta^3\mathrm{sech}(\sigma)^{2+p}\sinh(\sigma) \\ &-(1+p)\eta\mathrm{sinh}(\sigma)(-(2+p)\eta^2\mathrm{sch}(\sigma)^{2+p} \\ &+(2+p)(3+p)\eta^2\mathrm{sech}(\sigma)^{4+p}\sinh(\sigma)^2)=0. \end{aligned} \tag{42}$$

Equating the exponents $4+p=2+2p$, we obtain $p=1$. Plugging the obtained value of p into (42) yields:

$$\begin{aligned} &2\eta^2\rho(-3+\nu+8\eta^2-\rho-g(t))\mathrm{sech}(\sigma)^2 \\ &+6\eta^2\rho(3-\nu-20\eta^2+2\rho+g(t))\mathrm{sech}(\sigma)^2\tanh(\sigma)^2 \\ &+10\eta^2(12\eta^2-\rho)\rho\,\mathrm{sech}(\sigma)^2\tanh(\sigma)^4=0. \end{aligned} \tag{43}$$

Equating the coefficients of linearly independent terms in (43) to zero, we get:

$$\begin{aligned} 2\eta^2\rho(-3+\nu+8\eta^2-\rho-g(t))=0, \\ 6\eta^2\rho(3-\nu-20\eta^2+2\rho+g(t))=0, \\ 10\eta^2(12\eta^2-\rho)\rho=0. \end{aligned} \tag{44}$$

Solving (44) yields:

$$\eta=\frac{1}{2}\sqrt{\frac{\rho}{3}}, g(t)=\frac{1}{3}(-9+3\nu-\rho). \tag{45}$$

The bell-shaped soliton is represented by:

$$\psi(x,t,y)=\rho\,\mathrm{sech}^2\left[\frac{1}{2}\sqrt{\frac{\rho}{3}}(x+y-vt)\right]. \tag{46}$$

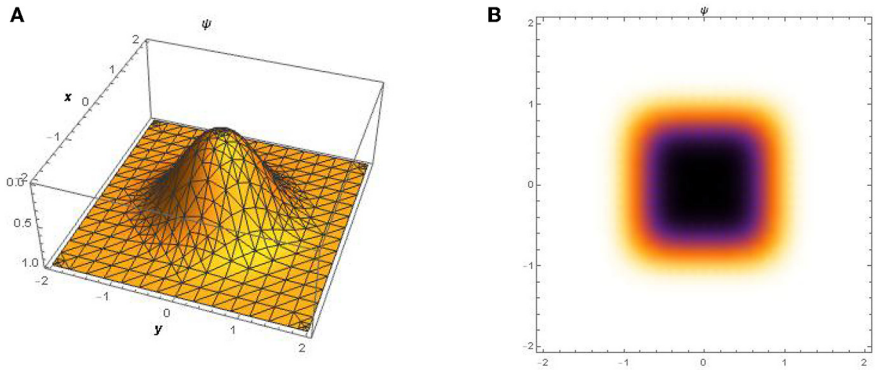

FIGURE 1 | Perspective view of the lump soliton (39) at $t = 0$. **(A)** 3D plot **(B)** Density plot.

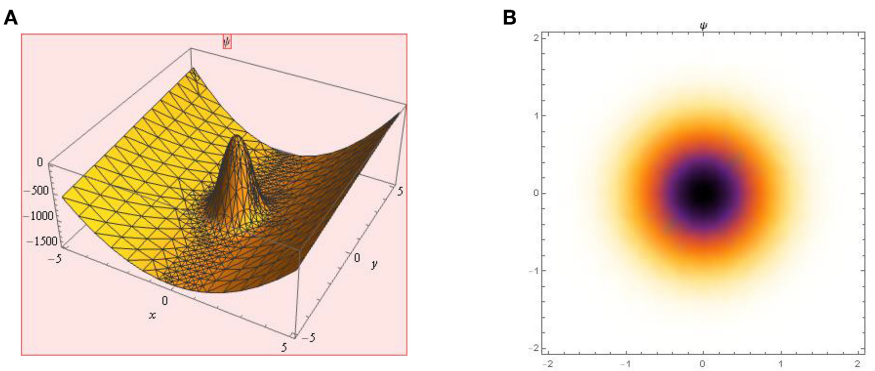

FIGURE 2 | Perspective view of the lump soliton (40) at $t = 0$. **(A)** 3D plot **(B)** Density plot.

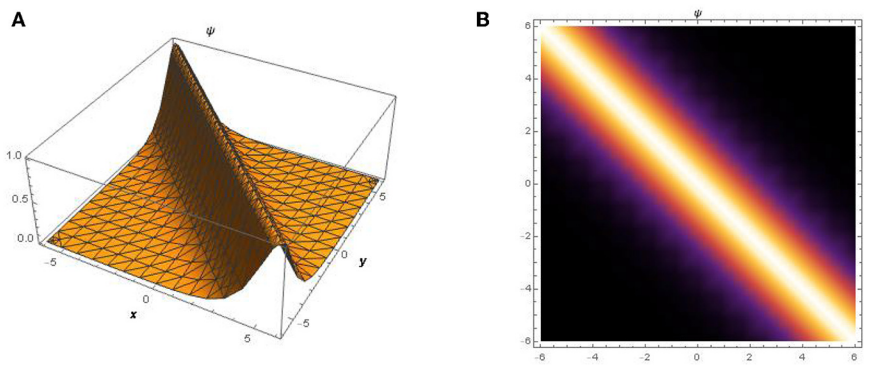

FIGURE 3 | Perspective view of the bell-shaped soliton (46) at $t = 0$. **(A)** 3D plot **(B)** Density plot.

Specifically, for the soliton (46) to exist, the condition $\rho > 0$ must hold.

6. PHYSICAL INTERPRETATION OF RESULTS

It is worth to mention that at for every t, the solution $\psi = 12(\ln f)_{xx}$ will approach 0 whenever (x, y) approach infinity in both solutions. The 3D and the density plot for the lump soliton (39) for $t = 0$ is shown in **Figure 1**. The 3D and the density plot for the lump soliton (40) for $t = 0$ is shown in **Figure 2**. The lump solitons (39) and (40) admits a pattern with one high peak and a deep hole hidden beneath the plane wave. Finally, the 3D and the density plot for the bell-shaped soliton (46) for $t = 0$ is shown in **Figure 3**.

7. CONCLUDING REMARKS

In this paper, with the aid of the Bell-polynomials approach, we have successfully derived the bilinear forms of an integrable time-dependent coefficient (2+1)-dimensional Kadomtsev-Petviashvili. We also studied the positive quadratic function solution to the model. Several constraint conditions that are necessary for the existence of the polynomial solutions were reported. Upon expanding the polynomials as sums of squares of linear functions, we acquire a lump-type solution possessing some arbitrary constraints. With the choice of different solution parameters, we have reported two forms of lump soliton solutions. We also utilized a suitable ansatz approach to derive a one soliton bell-shaped solution. To our knowledge, the results reported in this paper are new and introduced for the first time in the literature. Figures were given to describe the dynamics of the obtained results.

AUTHOR CONTRIBUTIONS

All authors participated in the preparation and presentation of the manuscript.

FUNDING

This work was supported by the National Natural Science Foundation of China (11571378, 11971493).

REFERENCES

1. Whitham GB. *Linear and Nonlinear Waves*. New York, NY: John Whiley (1974).
2. Hesegawa A, Kodama Y. *Solitons in Optical Communication*. Oxford: Oxford University Press (1995).
3. Li Q, Chaolu T, Wanga YH. Lump-type solutions and lump solutions for the (2+1)-dimensional generalized Bogoyavlensky-Konopelchenko equation. *Comput Math Appl.* (2019) **77**:2077–85. doi: 10.1016/j.camwa.2018.12.011
4. Yong X, Li X, Huang Y. General lump-type solutions of the (3+1)-dimensional Jimbo-Miwa equation. *Appl Math Lett.* (2018) **86**:222–8. doi: 10.1016/j.aml.2018.07.001
5. Ma WX, Qin ZY, Lu X. Lump solutions to dimensionally reduced p-gKP and p-gBKP equations. *Nonlinear Dynam.* (2016) **84**:923–31. doi: 10.1007/s11071-015-2539-6
6. Ma WX, You Y. Solving the Korteweg-de Vries equation by its bilinear form: Wronskian solutions. *Trans Amer Math Soc.* (2005) **357**:1 753–78.
7. Wazwaz AM. Two new integrable Kadomtsev-Petviashvili equations with time-dependent coefficients: multiple real and complex soliton solutions. *Waves Complex Random Media.* (2018). doi: 10.1080/17455030.2018.1559962. [Epub ahead of print].
8. Kadomtsev BB, Petviashvili VI. On the stability of solitary waves in weakly dispersive media. *Sov Phys Dokl.* (1970) **15**:539–41.
9. Tian FS, Zhang HQ. On the integrability of a generalized variable-coefficient forced Korteweg-de Vries equation in fluids. *Stud Appl Math.* (2013) **132**:212–46. doi: 10.1111/sapm.12026
10. Wazwaz AM. Multiple real and multiple complex soliton solutions for the integrable Sine-Gordon equation. *Optik.* (2013) **172**:622–7. doi: 10.1016/j.ijleo.2018.07.080
11. Wazwaz AM. Negative–order KdV equation and negative-order KP equation: multiple soliton solutions. *Proc Natl Acad Sci Indian Sect A.* (2017) **87**:291–6. doi: 10.1007/s40010-017-0349-6
12. Bell ET. Exponential polynomials. *Ann Math.* (1934) **35**:258–77.
13. Zhang TT, Ma PL, Xu MJ, Zhang XY, Tian SF. On Bell polynomials approach to the integrability of a (3 + 1)-dimensional generalized Kadomtsev Petviashvili equation. *Modern Phys Lett B.* (2015) **29**:1550051. doi: 10.1142/S0217984915500517
14. Gilson G, Lambert F, Nimmo JJC, Willox R. On the combinatorics of the Hirota D-operators. *Proc R Soc Lond A.* (1996) **452**:223–34.
15. Aliyu AI, Li Y, Baleanu D. Invariant subspace and classification of soliton solutions of the coupled nonlinear Fokas-Liu system. *Front Phys.* (2018) 7:39. doi: 10.3389/fphy.2019.00039

Conflict of Interest: The authors declare that the research was conducted in the absence of any commercial or financial relationships that could be construed as a potential conflict of interest.

frontiers in Physics

ORIGINAL RESEARCH
published: 23 January 2020
doi: 10.3389/fphy.2019.00230

Approximate Simulations for the Non-linear Long-Short Wave Interaction System

Haiyong Qin[1,2]*, *Mostafa M. A. Khater*[3]*, *Raghda A. M. Attia*[3,4] *and Dianchen Lu*[3]

[1] School of Mathematics, Qilu Normal University, Jinan, China, [2] School of Control Science and Engineering, Shandong University, Jinan, China, [3] Department of Mathematics, Faculty of Science, Jiangsu University, Zhenjiang, China, [4] Department of Basic Science, Higher Technological Institute, 10th of Ramadan City, Egypt

This research paper studies the semi-analytical and numerical solutions of the non-linear long-short wave interaction system. This represents an optical field that does not change through multiplication due to a sensitive balance being struck between linear and non-linear impacts in an elastic medium, defined as a medium that can adjust its shape as a consequence of deforming stress and return to its original form when the force is eliminated. In this medium, a wave is produced by vibrations that are a consequence of acoustic power, known as a sound wave or acoustic wave. The Adomian decomposition method and the cubic and septic B-spline methods are applied to the suggested system to obtain distinct types of solutions that are used to explain the novel physical properties of this system. These novel features are described by different types of figures that show more of the physical properties of this model. Also, the convergence between the obtained solutions is discussed through tables that show the values of absolute error between them.

Keywords: nonlinear long-short wave interaction system, adomian decomposition method, cubic B-spline method, septic B-spline method, semi-analytical and numerical solutions

OPEN ACCESS

Edited by:
Mustafa Inc,
Firat University, Turkey

Reviewed by:
Syed Tauseef Mohyud-Din,
HITEC University, Pakistan
Abdullahi Yusuf,
Federal University, Dutse, Nigeria

***Correspondence:**
Haiyong Qin
qhymath@hotmail.com
Mostafa M. A. Khater
mostafa.khater2024@yahoo.com

Specialty section:
This article was submitted to Mathematical Physics, a section of the journal Frontiers in Physics

Received: *16 October 2019*
Accepted: *10 December 2019*
Published: *23 January 2020*

Citation:
Qin H, Khater MMA, Attia RAM and Lu D (2020) Approximate Simulations for the Non-linear Long-Short Wave Interaction System. Front. Phys. 7:230. doi: 10.3389/fphy.2019.00230

1. INTRODUCTION

Optical study is considered as one of the most important methodologies in this age due to its different and important applications in several fields. To develop a deeper understanding of this type of study, mathematicians have derived many analytical, semi-analytical, and numerical schemes to obtain distinct types of solutions that are used to characterize the physical properties of optical soliton waves. The optical soliton constitutes an optical field that does not alter through multiplication due to a sensitive balance being struck between linear and non-linear impacts in the medium [1–5]. Optical soliton can be of two types:

- Spatial solitons: the non-linear influence balances the diffraction. The electromagnetic field can alter the refraction index of the medium while propagating, thus establishing an architecture identical to a graded-index fiber [6–10].
- Temporal solitons: if the electromagnetic field is already spatially restricted, it is feasible to transmit pulses that will not alter their form, as the non-linear impacts will be in equilibrium with the dispersion [11–15].

The non-linear long-short wave interaction system describes the interaction between one short transverse wave and one long longitudinal wave propagating in a generalized elastic medium. This system has the following form:

$$\begin{cases} i\,\Phi_t + \Phi_{xx} - \Phi\,\Psi = 0, \\ \Psi_t + \Psi_x + \left(|\Phi|^2\right)_x. \end{cases} \tag{1}$$

where $\Phi(x,t)$ represents the slowly varying envelope of the short transverse wave, $\Psi(x,t)$ discriminates the long longitudinal wave, (x) is the locational harmonization, and (t) is the time. Waves in plasmas are defined as an interrelated set of particles and fields that disseminate in a periodically duplicating fashion. A plasma is a quasi-neutral, electrically conductive fluid. Plasma waves have an EM character of two types, electrostatic and electromagnetic. Electrostatic and electromagnetic waves have oscillating species in electrons and ions. Some examples of the dispersion relationships of plasma waves in electrostatic and electromagnetic terms are as follows:

- Plasma oscillation: rapid oscillations of the electron intensity in conducting media such as plasmas or metals in the ultraviolet zone
- Upper hybrid oscillation: a form of oscillation of magnetized plasma
- Ion acoustic wave: one kind of longitudinal oscillation of the ions and electrons in a plasma
- Electrostatic ion cyclotron wave: a longitudinal wobble of the ions in a magnetized plasma, with dissemination nearly perpendicular to the magnetic field
- Langmuir wave
- Lower hybrid oscillation: a longitudinal fluctuation of ions and electrons in a magnetized plasma
- Light wave: a wave made of oscillating magnetic and electric fields; comprises radio waves, microwaves, ultraviolet, visible light, infrared, gamma rays, and X-rays
- O wave
- X wave
- R wave (whistler-mode)
- L wave
- Alfvén wave: a kind of magnetohydrodynamic wave in which ions oscillate in response to a restoration strength presented by an effective tension on the magnetic field lines; this kind of wave was named after Hannes Alfvén
- Magnetosonic wave: a longitudinal wave of ions in a magnetized plasma disseminating perpendicular to the stationary magnetic field.

All of the properties and abilities of the non-linear partial differential equations are used to describe these natural phenomena. According to these properties, many mathematicians have developed methods and are still trying to find new general methods to obtain exact and single traveling wave solutions for these models. For more details about these methods, please see [16–36].

The rest of this paper is arranged as follows. In section 2, the Adomian decomposition method [37–40] and Cubic and septic B-spline method [41–50] are used to obtain approximate solutions of the non-linear long-short wave interaction system. In section 4, the conclusion is given.

2. APPLICATION

This section applies the Adomian decomposition method as the semi-analytical scheme and the cubic & septic B–spline methods as numerical schemes to the non-linear long-short wave interaction system [51–55] that is given by:

$$\begin{cases} i\,\Phi_t + \Phi_{xx} - \Phi\,\Psi = 0, \\ \Psi_t + \Psi_x + \left(|\Phi|^2\right)_x. \end{cases} \tag{2}$$

Using the wave transformation $\Phi(x,t) = e^{i\eta}\,\Lambda(\varepsilon)$, $\Psi(x,t) = \varphi(\varepsilon)$ where $\eta = (\rho\,x + c\,t)$, $\varepsilon = (a\,x + b\,t)$ transforms the non-linear partial differential equation (2) into the following ordinary differential equation:

$$\begin{cases} \left(b + 2\,a\,\rho\right)\,i\,\Lambda - \left(\rho^2 + c\right)\,\Lambda + a^2\,\Lambda'' - \Lambda\,\varphi = 0, \\ (a+b)\,\varphi' + a\,\left(\Lambda^2\right)' = 0. \end{cases} \tag{3}$$

Equating the complex term to zero leads to

$$b = -2\,a\,\rho. \tag{4}$$

Integrating the second equation of the system (3) with zero constant of integration yields:

$$\varphi = \frac{-a}{a+b}\,\Lambda^2. \tag{5}$$

Substituting (4) and (5) into the first equation in the system (3) yields:

$$a^2\,\Lambda'' - \left(\rho^2 + c\right)\,\Lambda + \frac{1}{1-2\,\rho}\,\Lambda^3 = 0. \tag{6}$$

According to the analytical solutions obtained in Raghda et al. [Submitted], the exact solution of Equation (6) takes the following formula

$$\Lambda(\varepsilon) = 8\,\tanh\left(\frac{\varepsilon}{2}\right). \tag{7}$$

2.1. Semi-analytical Solution

This section applies the Adomian decomposition method to Equation (6) by using its exact solution (6) with the following conditions:

$$\Lambda(0) = 0,\ \Lambda'(0) = 4,$$

where $\left[\sigma = 6,\ a = 4,\ \alpha = 1,\ \beta = 5,\ \rho = 4.5\right]$. Implementation of the Adomian decomposition method on Equation (6) yields

$$\Lambda_0 = 4\,\varepsilon, \tag{8}$$

$$\Lambda_1 = 0.025\,\varepsilon^5 - 1.17708\,\varepsilon^3, \tag{9}$$

$$\Lambda_2 = 0.000416667\,\varepsilon^{10} - 0.031529\,\varepsilon^8 - 0.00105097\,\varepsilon^7 + 0.103914\,\varepsilon^5, \tag{10}$$

$$\Lambda_3 = 0.000618538\,\varepsilon^{10} + 0.00196005\,\varepsilon^9 - 0.0148781\,\varepsilon^7 - 0.0000501598\,\varepsilon^{11} - 5.5733112373737385 \times 10^{-6}\,\varepsilon^{12} + 3.7560096153846164 \times 10^{-7}\,\varepsilon^{13}, \tag{11}$$

According to (8–11), we get

$$\Lambda_{\text{Semi-analytical}} = 3.7560096153846164 \times 10^{-7}\,\varepsilon^{13} - 5.5733112373737385 \times 10^{-6}\,\varepsilon^{12} - 0.0000501598\,\varepsilon^{11} + 0.0010352\,\varepsilon^{10} + 0.00196005\,\varepsilon^9 - 0.031529\,\varepsilon^8 - 0.0159291\,\varepsilon^7 + 0.128914\,\varepsilon^5 - 1.17708\,\varepsilon^3 + 4\,\varepsilon + \ldots \tag{12}$$

2.2. Numerical Solutions

This section studies the numerical solutions of the modified BBM equation by applying the cubic and septic B-spline techniques, which are considered as the most accurate numerical tools for getting this type of solution.

2.2.1. Cubic-Spline

According to the cubic B–spline, the numerical solution of the modified BBM equation (6) is given by

$$\Lambda(\varepsilon) = \sum_{i=-1}^{n+1} \lambda_i\,\beta_i, \tag{13}$$

where λ_i, β_i fulfill the conditions:

$$L\,\Lambda(\varepsilon) = \emptyset(\varepsilon_i, \Lambda(\varepsilon_i)) \text{ where } (i = 0, 1, ..., n)$$

and

$$\beta_i(\varepsilon) = \frac{1}{6\,h^3}\begin{cases} (\varepsilon - \varepsilon_{i-2})^3, & \varepsilon \in [\varepsilon_{i-2}, \varepsilon_{i-1}], \\ -3\,(\varepsilon - \varepsilon_{i-1})^3 + 3\,h\,(\varepsilon - \varepsilon_{i-1})^2 + 3\,h^2\,(\varepsilon - \varepsilon_{i-1}) + h^3, & \varepsilon \in [\varepsilon_{i-1}, \varepsilon_i], \\ -3\,(\varepsilon_{i+1} - \varepsilon)^3 + 3\,h\,(\varepsilon_{i+1} - \varepsilon)^2 + 3\,h^2\,(\varepsilon_{i+1} - \varepsilon) + h^3, & \varepsilon \in [\varepsilon_i, \varepsilon_{i+1}], \\ (\varepsilon_{i+2} - \varepsilon)^3, & \varepsilon \in [\varepsilon_{i+1}, \varepsilon_{i+2}], \\ 0, & \text{otherwise}, \end{cases} \tag{14}$$

where $i \in [-2, n+2]$, so that the numerical formula of the solution is given as

$$\Lambda_i(\varepsilon) = \lambda_{i-1} + 4\,\lambda_i + \lambda_{i+1}. \tag{15}$$

Substituting Equation (15) into (6), leads to a system of equations. Solving this system of equations gives the value of λ_i. Replacing the values of λ_i, β_i into Equation (13) gives the data shown in **Table 2**.

TABLE 1 | Computational, semi-analytical, and absolute error values obtained by using the Adomian decomposition method.

Value of ε	Analytical value	Semi-analytical value	Value of absolute error
0.000	0.000	0.000	0.0000000000
0.001	0.004	0.004	8.4375×10^{-10}
0.002	0.008	0.008	6.75×10^{-9}
0.003	0.012	0.012	2.27812×10^{-8}
0.004	0.0160000	0.0159999	5.39999×10^{-8}
0.005	0.0200000	0.0199999	1.05468×10^{-7}
0.006	0.0239999	0.0239997	1.82249×10^{-7}
0.007	0.0279999	0.0279996	2.89405×10^{-7}
0.008	0.0319998	0.0319994	4.31997×10^{-7}
0.009	0.0359998	0.0359991	6.15088×10^{-7}
0.010	0.0399997	0.0399988	8.4374×10^{-7}

TABLE 2 | Computational, numerical, and absolute error values obtained by using the cubic B–spline scheme.

Value of ε	Val. Com.	Val. Nu.	Value of abs. error
0.000	0.0000000	0.0000000000	0.0000000000
0.001	0.004	0.0040001	8.35327×10^{-8}
0.002	0.008	0.0080002	1.62003×10^{-7}
0.003	0.012	0.0120002	2.30348×10^{-7}
0.004	0.0160000	0.0160003	2.83505×10^{-7}
0.005	0.0200000	0.0200003	3.16411×10^{-7}
0.006	0.0239999	0.0240003	3.24004×10^{-7}
0.007	0.0279999	0.0280002	3.01222×10^{-7}
0.008	0.0319998	0.0320001	2.43003×10^{-7}
0.009	0.0359998	0.0359999	1.44283×10^{-7}
0.010	0.0399997	0.0399997	6.93889×10^{-18}

TABLE 3 | Computational, numerical, and absolute error value obtained by using the septic B–spline scheme.

Value of ε	Val. Com.	Val. Nu.	Value of abs. error
0.000	0.0000000	0.0000000000	0.0000000000
0.001	0.0040000	0.0040001	7.5153×10^{-8}
0.002	0.0080000	0.0080002	1.70905×10^{-7}
0.003	0.0120000	0.0120002	2.31487×10^{-7}
0.004	0.0160000	0.0160003	2.88889×10^{-7}
0.005	0.0200000	0.0200003	3.19377×10^{-7}
0.006	0.0239999	0.0240003	3.3083×10^{-7}
0.007	0.0279999	0.0280002	3.01294×10^{-7}
0.008	0.0319998	0.0320001	2.59145×10^{-7}
0.009	0.0359998	0.0359999	1.26976×10^{-7}
0.010	0.0399997	0.0399997	6.93889×10^{-18}

2.2.2. Septic-Spline

Based on the septic B-spline, the suggested solution of the ordinary differential form of the modified BBM equation (6) is given as follows:

$$\Lambda(\varepsilon) = \sum_{i=-1}^{n+1} \lambda_i \beta_i, \tag{16}$$

where λ_i, β_i satisfies the conditions

$$L\,\Lambda(\varepsilon) = \emptyset(\varepsilon_i, \Lambda(x_i)) \text{ where } (i = 0, 1, ..., n)$$

and

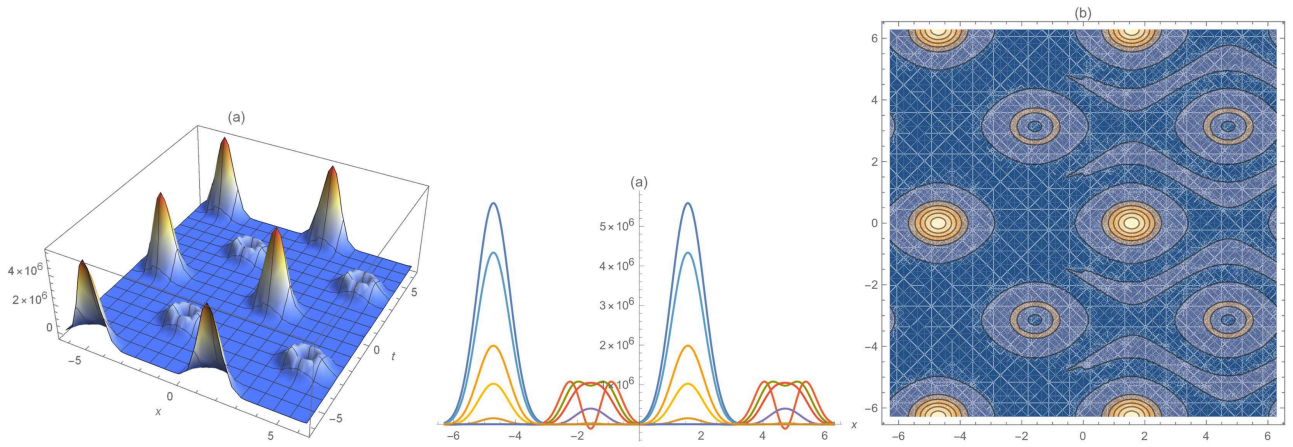

FIGURE 1 | Three, two-dimensional, and contour plots of Equation (12), respectively.

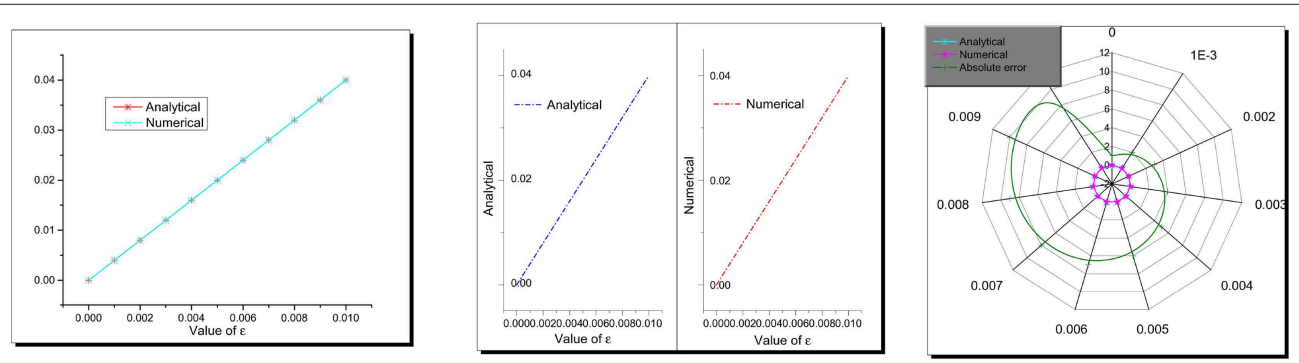

FIGURE 2 | Combined, separated, and radar plots of analytical (7) and semi-analytical solutions (12) of Equation (6), respectively.

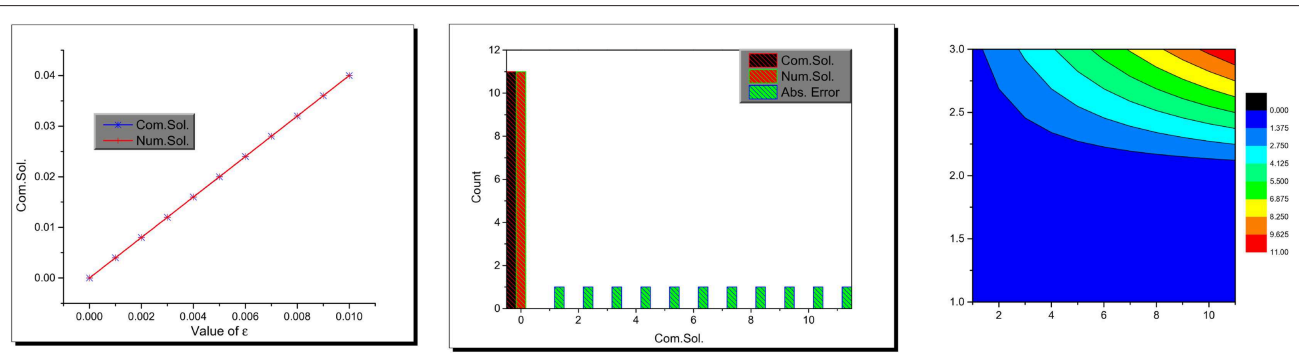

FIGURE 3 | Combined, bar, and contour plots of the computational, numerical, and absolute error values.

$$\beta_i(\varepsilon) = \frac{1}{h^5}\begin{cases} (\varepsilon-\varepsilon_{i-4})^7, & \varepsilon\in[\varepsilon_{i-4},\varepsilon_{i-3}],\\ (\varepsilon-\varepsilon_{i-4})^7-8(\varepsilon-\varepsilon_{i-3})^7, & \varepsilon\in[\varepsilon_{i-3},\varepsilon_{i-2}],\\ (\varepsilon-\varepsilon_{i-4})^7-8(\varepsilon-\varepsilon_{i-3})^7+28\varepsilon(\varepsilon-\varepsilon_{i-2})^7, & \varepsilon\in[\varepsilon_{i-2},\varepsilon_{i-1}],\\ (\varepsilon-\varepsilon_{i-4})^7-8(\varepsilon-\varepsilon_{i-3})^7+28(\varepsilon-\varepsilon_{i-2})^7+56(\varepsilon-\varepsilon_{i-1})^7, & \varepsilon\in[\varepsilon_{i-1},\varepsilon_i],\\ (\varepsilon_{i+4}-\varepsilon)^7-8(\varepsilon_{i+3}-\varepsilon)^7+28(\varepsilon_{i+2}-\varepsilon)^7+56(\varepsilon_{i+1}-\varepsilon)^7, & \varepsilon\in[\varepsilon_i,\varepsilon_{i+1}],\\ (\varepsilon_{i+4}-\varepsilon)^7-8(\varepsilon_{i+3}-\varepsilon)^7+28(\varepsilon_{i+2}-\varepsilon)^7, & \varepsilon\in[\varepsilon_{i+1},\varepsilon_{i+2}],\\ (\varepsilon_{i+4}-\varepsilon)^7-8(\varepsilon_{i+3}-\varepsilon)^7, & \varepsilon\in[\varepsilon_{i+2},\varepsilon_{i+3}],\\ (\varepsilon_{i+4}-\varepsilon)^7, & \varepsilon\in[\varepsilon_{i+3},\varepsilon_{i+4}],\\ 0, & \text{otherwise}, \end{cases} \tag{17}$$

where $i \in [-3, n+3]$. Thus, the approximate solution is given by:

$$v_i(\varepsilon) = \lambda_{i-3} + 120\,\lambda_{i-2} + 1191\,\lambda_{i-1} + 2416\,\lambda_i + 1191\,\lambda_{i+1} + 120\,\lambda_{i+2} + \lambda_{i+3}. \tag{18}$$

Substituting Equation (18) into Equation (6) produces a system of equations. Solving this system gives the data shown in **Table 3**.

3. RESULTS AND DISCUSSION

This section details a comparison between the numerical solutions obtained in our paper to determine which one of them is the more accurate.

The comparison between the numerical solutions depends on showing which one of the schemes obtains the smallest value of the absolute value of error. To find these values, the obtained values of the total value of error in each method used are plotted in **Figure 5**, which shows that all the methods used are accurate and have almost the same amount of absolute failure.

4. CONCLUSION

This research paper succeeded in the application of the Adomian decomposition method and the cubic and septic B–spline

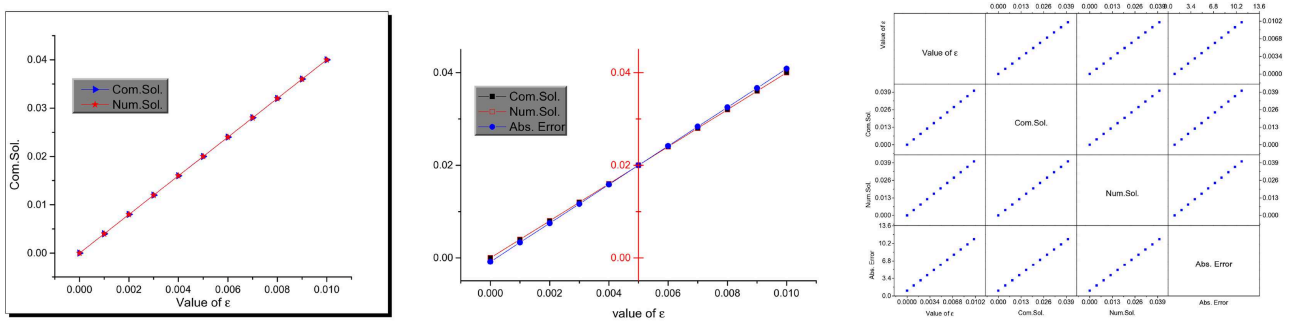

FIGURE 4 | Combined and scattering matrix plots of the computational, numerical, and absolute error values.

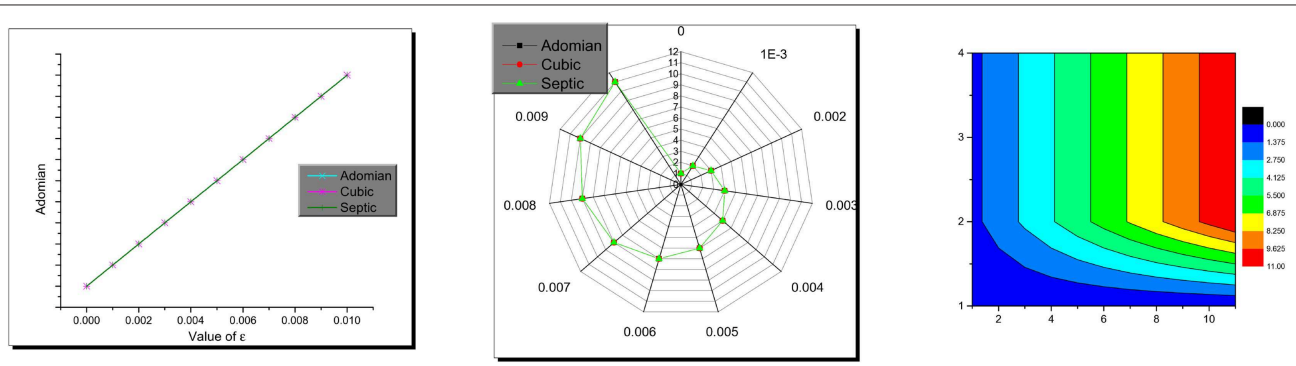

FIGURE 5 | Combined, radar, and contour plots of the absolute value of error for the Adomian, cubic, and septic schemes.

method to the non-linear long-short wave interaction system and in obtaining semi-analytical and numerical solutions for this system. Moreover, a comparison between the distinct types of solutions obtained is detailed, and the absolute values of error between them are shown in **Tables 1–3** and **Figures 1–5**. Both semi–computational and numerical schemes are shown to be powerful, effective, and able to be applied to many and various forms of non-linear evolution equations.

DATA AVAILABILITY STATEMENT

All datasets generated for this study are included in the article/supplementary material.

AUTHOR CONTRIBUTIONS

All authors conceived of the study, participated in its design and coordination, drafted the manuscript, participated in the sequence alignment, and read and approved the final manuscript.

ACKNOWLEDGMENTS

This research is supported by a Project of Shandong Province Higher Educational Science and Technology Program (Grant No. J17KB121), Shandong Provincial Natural Science Foundation (Grant No. ZR2016AB04), Foundation for Young Teachers of Qilu Normal University (Grant Nos. 2016L0605, 2015L0603, 2017JX2311, and 2017JX2312), Scientific Research Foundation for University Students of Qilu Normal University (Grant Nos. XS2017L01 and XS2017L05).

REFERENCES

1. Mena-Contla A, Serkin V, Belyaeva T, Peña-Moreno R, Agüero M, Hernandez-Tenorio C, et al. Extreme nonlinear waves in external gravitational-like potentials: possible applications for the optical soliton supercontinuum generation and the ocean coast line protection. *Optik*. (2018) **161**:187–95. doi: 10.1016/j.ijleo.2018.01.031
2. Kippenberg TJ, Gaeta AL, Lipson M, Gorodetsky ML. Dissipative Kerr solitons in optical microresonators. *Science*. (2018) **361**:eaan8083. doi: 10.1126/science.aan8083
3. Trocha P, Karpov M, Ganin D, Pfeiffer MH, Kordts A, Wolf S, et al. Ultrafast optical ranging using microresonator soliton frequency combs. *Science*. (2018) **359**:887–91. doi: 10.1126/science.aao3924
4. Li BQ, Ma YL, Yang TM. Stable optical soliton in the ring-cavity fiber system with carbon nanotube as saturable absorber. *Superlattices Microstruct*. (2018) **113**:366–72. doi: 10.1016/j.spmi.2017.11.016
5. Biswas A, Zhou Q, Triki H, Ullah MZ, Asma M, Moshokoa SP, et al. Resonant optical solitons with parabolic and dual-power laws by semi-inverse variational principle. *J Mod Opt*. (2018) **65**:179–84. doi: 10.1080/09500340.2017.1382597
6. Cyprych K, Jung PS, Izdebskaya Y, Shvedov V, Christodoulides DN, Krolikowski W. Anomalous interaction of spatial solitons in nematic liquid crystals. *Opt Lett*. (2019) **44**:267–70. doi: 10.1364/OL.44.000267
7. Jung PS, Karpierz M, Trippenbach M, Christodoulides D, Krolikowski W. Supermode spatial solitons via competing nonlocal nonlinearities. *Photon Lett Pol*. (2018) **10**:33–5. doi: 10.4302/plp.v10i2.827
8. Rubin S, Fainman Y. Nonlocal and nonlinear surface plasmon polaritons and optical spatial solitons induced by the thermocapillary effect. *Phys Rev Lett*. (2018) **120**:243904. doi: 10.1103/PhysRevLett.120.243904
9. Salgueiro JR, Ferrando A. Spatial solitons in nonlinear photonic crystal fibers. In: *Nonlinear Systems*, Vol. 2. Springer (2018). p. 139–71.
10. Perumbilavil S, Piccardi A, Kauranen M, Assanto G. Directional random laser by combining cavity-less lasing and spatial solitons in liquid crystals. In: *Nonlinear Photonics*. Optical Society of America (2018). p. NpW2C–4.
11. Obrzud E, Brasch V, Lecomte S, Herr T. Temporal cavity solitons in synchronously driven Fabry-Perot microresonators. In: *Laser Resonators, Microresonators, and Beam Control XX*. Vol. 10518. *International Society for Optics and Photonics*. (2018).
12. Lilienfein N, Hofer C, Högner M, Saule T, Trubetskov M, Pervak V, et al. Temporal solitons in free-space femtosecond enhancement cavities. *Nat Photon*. (2019) **13**:214. doi: 10.1038/s41566-018-0341-y
13. Spiess C, Yang Q, Dong X, Bucklew VG, Renninger WH. Chirped temporal solitons in driven optical resonators. *arXiv preprint* arXiv:190612127 (2019).
14. Xue X, Zheng X, Zhou B. Super-efficient temporal solitons in mutually coupled optical cavities. *Nat Photon*. (2019) **13**:616–22. doi: 10.1038/s41566-019-0436-0
15. Shtyrina O, Kivshar Y, Turitsyn S, Yarutkina I, Fedoruk M. Stability of spatio-temporal solitons in multi-mode fibers. In: *Nonlinear Photonics*. Optical Society of America (2018). p. JTu5A–45.
16. Rezazadeh H, Korkmaz A, Khater MM, Eslami M, Lu D, Attia RA. New exact traveling wave solutions of biological population model via the extended rational Sinh–Cosh method and the modified Khater method. *Mod Phys Lett B*. (2019) **33**:1950338. doi: 10.1142/S0217984 91950338X
17. Khater M, Attia RA, Lu D. Explicit lump solitary wave of certain interesting (3+ 1)-dimensional waves in physics via some recent traveling wave methods. *Entropy*. (2019) **21**:397. doi: 10.3390/e21040397
18. Khater MM, Lu D, Attia RA. Dispersive long wave of nonlinear fractional Wu–Zhang system via a modified auxiliary equation method. *AIP Adv*. (2019) **9**:025003. doi: 10.1063/1.5087647
19. Khater MM, Lu D, Attia RA. Lump soliton wave solutions for the (2+ 1)-dimensional Konopelchenko–Dubrovsky equation and KdV equation. *Mod Phys Lett B*. (2019) **33**:1950199. doi: 10.1142/S0217984919 501999
20. Khater MM, Attia RA, Lu D. Numerical solutions of nonlinear fractional Wu–Zhang system for water surface versus three approximate schemes. *J Ocean Eng Sci*. (2019). doi: 10.1016/j.joes.2019.03.002
21. Attia RA, Lu D, Khater MMA. Chaos and relativistic energy-momentum of the nonlinear time fractional Duffing equation. *Math Comput Appl*. (2019) **24**:10. doi: 10.3390/mca24010010
22. Khater M, Attia R, Lu D. Modified auxiliary equation method versus three nonlinear fractional biological models in present explicit wave solutions. *Math Comput Appl*. (2019) **24**:1. doi: 10.3390/mca24010001
23. Elghobashi S. Direct numerical simulation of turbulent flows laden with droplets or bubbles. *Annu Rev Fluid Mech*. (2019) **51**:217–44. doi: 10.1146/annurev-fluid-010518-040401
24. Nasiri H, Jamalabadi MYA, Sadeghi R, Safaei MR, Nguyen TK, Shadloo MS. A smoothed particle hydrodynamics approach for numerical simulation of nano–fluid flows. *J Therm Anal Calorimetry*. (2019) **135**:1733–41. doi: 10.1007/s10973-018-7022-4
25. Knab O, Riedmann H, Ivancic B, Höglauer C, Frey M, Aichner T. Consequences of modeling demands on numerical rocket thrust chamber flow simulation tools. *EUCASS Proc Ser*. (2019) **11**:317–46. doi: 10.1051/eucass/201911317
26. Khan U, Ellahi R, Khan R, Mohyud-Din ST. Extracting new solitary wave solutions of Benny–Luke equation and Phi-4 equation of fractional order by using (G'/G)-expansion method. *Opt Quant Electron*. (2017) **49**:362. doi: 10.1007/s11082-017-1191-4
27. Sikander W, Khan U, Ahmed N, Mohyud-Din ST. Optimal solutions for homogeneous and non–homogeneous equations arising in physics. *Results Phys*. (2017) **7**:216–24. doi: 10.1016/j.rinp.2016.12.018

28. Sikander W, Khan U, Mohyud-Din ST. Optimal solutions for the evolution of a social obesity epidemic model. *Eur Phys J Plus*. (2017) **132**:257. doi: 10.1140/epjp/i2017-11512-y
29. Mohyud-Din ST, Irshad A, Ahmed N, Khan U. Exact solutions of (3+ 1)-dimensional generalized KP equation arising in physics. *Results Phys*. (2017) **7**:3901–9. doi: 10.1016/j.rinp.2017.10.007
30. Mohyud-Din ST, Noor MA, Noor KI. Some relatively new techniques for nonlinear problems. *Math Probl Eng*. (2009) **2009**:234849. doi: 10.1155/2009/234849
31. Tauseef Mohyud-Din S, Yildirim A, Demirli G. Analytical solution of wave system in R n with coupling controllers. *Int J Numer. Methods Heat Fluid Flow*. (2011) **21**:198–205. doi: 10.1108/09615531111105399
32. Nazir A, Ahmed N, Khan U, Mohyud-din ST. On stability of improved conformable model for studying the dynamics of a malnutrition community. *Physica A Stat Mech Appl*. (2020) **537**:122664. doi: 10.1016/j.physa.2019.122664
33. Shakeel M, Mohyud-Din ST, Iqbal MA. Modified extended exp-function method for a system of nonlinear partial differential equations defined by seismic sea waves. *Pramana*. (2018) **91**:28. doi: 10.1007/s12043-018-1601-6
34. Tchier F, Yusuf A, Aliyu AI, Inc M. Soliton solutions and conservation laws for lossy nonlinear transmission line equation. *Superlattices Microstruct*. (2017) **107**:320–36. doi: 10.1016/j.spmi.2017.04.003
35. Al Qurashi MM, Yusuf A, Aliyu AI, Inc M. Optical and other solitons for the fourth–order dispersive nonlinear Schrödinger equation with dual-power law nonlinearity. *Superlattices Microstruct*. (2017) **105**:183–97. doi: 10.1016/j.spmi.2017.03.022
36. Yusuf A, Inc M, Bayram M. Invariant and simulation analysis to the time fractional Abrahams–Tsuneto reaction diffusion system. *Phys Script*. (2019) **94**:125005. doi: 10.1088/1402-4896/ab373b
37. Keskin AÜ. Adomian Decomposition Method (ADM). In: *Boundary Value Problems for Engineers*. Springer (2019). p. 311–59.
38. Hamoud AA, Ghadle KP. Modified adomian decomposition method for solving fuzzy volterra-fredholm integral equation. *J Indian Math Soc*. (2018) **85**:53–69. doi: 10.18311/jims/2018/16260
39. Ali N, Ahmad S, Aziz S, Zaman G. The adomian decomposition method for solving Hiv infection model of latently infected cells. *Matrix Sci Math*. (2019) **3**:5–8. doi: 10.26480/msmk.01.2019.05.08
40. Moradweysi P, Ansari R, Hosseini K, Sadeghi F. Application of modified Adomian decomposition method to pull–in instability of nano–switches using nonlocal Timoshenko beam theory. *Appl Math Model*. (2018) **54**:594–604. doi: 10.1016/j.apm.2017.10.011
41. Goss A, Schmidt M, Erdogan E, Görres B, Seitz F. High-resolution vertical total electron content maps based on multi-scale B-spline representations. *Ann Geophys*. (2019). **37**. doi: 10.5194/angeo-2019-32
42. Penner A. ODF Using a 5-Point B-Spline. In: *Fitting Splines to a Parametric Function*. Springer (2019). p. 37–42.
43. Edwards MC, Meyer R, Christensen N. Bayesian nonparametric spectral density estimation using B-spline priors. *Stat Comput*. (2019) **29**:67–78. doi: 10.1007/s11222-017-9796-9
44. Gavriil K, Schiftner A, Pottmann H. Optimizing B–spline surfaces for developability and paneling architectural freeform surfaces. *Comput Aid Design*. (2019) **111**:29–43. doi: 10.1016/j.cad.2019.01.006
45. Hepson OE, Korkmaz A, Dag I. Exponential B–spline collocation solutions to the Gardner equation. *Int J Comput Math*. (2019) 1–14. doi: 10.1080/00207160.2019.1594791
46. Karakoc SBG, Ucar Y, Yağmurlu N. Numerical solutions of the MRLW equation by cubic B–spline Galerkin finite element method. *Kuwait J Sci*. (2019) **42**:141–59.
47. Massarwi F, Elber G. A B–spline based framework for volumetric object modeling. *Comput Aid Design*. (2016) **78**:36–47. doi: 10.1016/j.cad.2016.05.003
48. Qiao B, Zhang X, Luo X, Chen X. A force identification method using cubic B–spline scaling functions. *J Sound Vibr*. (2015) **337**:28–44. doi: 10.1016/j.jsv.2014.09.038
49. Donatelli M, Garoni C, Manni C, Serra-Capizzano S, Speleers H. Symbol–based multigrid methods for Galerkin B–spline isogeometric analysis. *SIAM J Numer Anal*. (2017) **55**:31–62. doi: 10.1137/140988590
50. Fey M, Eric Lenssen J, Weichert F, Müller H. SplineCNN: Fast geometric deep learning with continuous B–spline kernels. In: *Proceedings of the IEEE Conference on Computer Vision and Pattern Recognition*. (2018). p. 869–77.
51. Baskonus HM, Bulut H, Belgacem FBM. Analytical solutions for nonlinear long–short wave interaction systems with highly complex structure. *J Comput Appl Math*. (2017) **312**:257–66. doi: 10.1016/j.cam.2016.05.035
52. Aghdaei MF, Adibi H. On some new analytical solutions for the nonlinear long–short wave interaction system. *Opt Quant Electron*. (2018) **50**:100. doi: 10.1007/s11082-018-1361-z
53. Chan HN, Ding E, Kedziora DJ, Grimshaw R, Chow KW. Rogue waves for a long wave–short wave resonance model with multiple short waves. *Nonlinear Dyn*. (2016) **85**:2827–41. doi: 10.1007/s11071-016-2865-3
54. Inc M, Aliyu AI, Yusuf A, Baleanu D. On the classification of conservation laws and soliton solutions of the long short-wave interaction system. *Mod Phys Lett B*. (2018) **32**:1850202. doi: 10.1142/S0217984918502020
55. Baskonus HM, Sulaiman TA, Bulut H. On the exact solitary wave solutions to the long-short wave interaction system. In: *ITM Web of Conferences. Vol. 22*. EDP Sciences (2018). p. 01063.

Conflict of Interest: The authors declare that the research was conducted in the absence of any commercial or financial relationships that could be construed as a potential conflict of interest.

frontiers in Physics

ORIGINAL RESEARCH
published: 31 January 2020
doi: 10.3389/fphy.2019.00241

Shape-Preservation of the Four-Point Ternary Interpolating Non-stationary Subdivision Scheme

*Pakeeza Ashraf[1], Mehak Sabir[1], Abdul Ghaffar[2], Kottakkaran Sooppy Nisar[3] and Ilyas Khan[4]**

[1] Department of Mathematics, Government Sadiq College Women University, Bahawalpur, Pakistan, [2] Faculty of Mathematics and Statistics, Ton Duc Thang University, Ho Chi Minh City, Vietnam, [3] Department of Mathematics, College of Arts and Sciences, Prince Sattam bin Abdulaziz University, Wadi Aldawaser, Saudi Arabia, [4] Faculty of Mathematics and Statistics, Ton Duc Thang University, Ho Chi Minh City, Vietnam

In this paper, we present the shape-preserving properties of the four-point ternary non-stationary interpolating subdivision scheme (the four-point scheme). This scheme involves a tension parameter. We derive the conditions on the tension parameter and initial control polygon that permit the creation of positivity- and monotonicity-preserving curves after a finite number of subdivision steps. In addition, the outcomes are generalized to determine conditions for positivity- and monotonicity-preservation of the limit curves. Convexity-preservation of the limit curve of the four-point scheme is also analyzed. The shape-preserving behavior of the four-point scheme is also shown through several numerical examples.

Keywords: interpolating, non-stationary, shape-preservation, subdivision scheme, ternary

OPEN ACCESS

Edited by:
Mustafa Inc,
Firat University, Turkey

Reviewed by:
Amin Jajarmi,
University of Bojnord, Iran
Sunil Kumar,
National Institute of Technology, Jamshedpur, India

***Correspondence:**
Ilyas Khan
ilyaskhan@tdtu.edu.vn

Specialty section:
This article was submitted to Mathematical Physics, a section of the journal Frontiers in Physics

Received: *16 October 2019*
Accepted: *18 December 2019*
Published: *31 January 2020*

Citation:
Ashraf P, Sabir M, Ghaffar A, Nisar KS and Khan I (2020) Shape-Preservation of the Four-Point Ternary Interpolating Non-stationary Subdivision Scheme. Front. Phys. 7:241. doi: 10.3389/fphy.2019.00241

1. INTRODUCTION

Subdivision Schemes (SS) are iterative algorithms for constructing smooth curves/surfaces from a given control polygon/mesh. The advantages of such schemes are that they are easy to use, simple to investigate, and highly flexible. The popularity of SS is increasing in various applications such as in computer-aided geometric design, computer graphics, computer animation, signal processing, and commercial industry due to their attractive properties. Shape-preservation of the subdivision curve has significant importance in geometric shape design. Shape-preserving SS are extensively used in the design of curves to manage and predict their shape according to the shape of initial control points. Differential equations are used for mathematical modeling of many phenomena. Different techniques are being used to solve boundary value problems [1] and non-linear problems [2]. In the same way, SS can also be used to solve fractional differential equations such as [3–7].

Rham [8] was the first to present an SS with C^0 continuity to attain a smooth curve. Afterward, Chaikin [9] introduced a corner-cutting approximating scheme with C^1 continuity. Dyn et al. [10] developed a four-point binary interpolating scheme that is capable of generating a C^1-continuous limit curve. Dyn et al. [11] formulated the convexity-preserving property of the famous four-point interpolatory scheme [10] by taking into account that the initial control points are convex. Kuijt and Damme [12] presented a series of local non-linear interpolating schemes that preserve monotonicity. With time, the research community started taking an interest in ternary SS because, by increasing arity from binary to ternary, one can improve the order of continuity of the limit curve without significantly increasing support width [see Beccari et al. [13]]. Hassan et al. [14] constructed a four-point ternary interpolatory scheme with a tension parameter. Cai [15] derived conditions

on this parameter to ensure convexity preservation of the limit curve. Pitolli [16] examined the shape-preserving properties of a ternary scheme with bell-shaped masks.

Most of the SS offered in literature are stationary, but this limits the application of the schemes. To reproduce conics, spirals, and polynomial curves, one has to opt for non-stationary schemes. Beccari et al. [17] presented a C^1 four-point binary non-stationary interpolating scheme. Akram et al. [18] analyzed the shape-preserving properties of this scheme [17]. Beccari et al. [19] also offered a four-point ternary non-stationary interpolatory scheme with a tension parameter. They showed that the proposed scheme can generate a variety of curves within the C^2-continuous range of its tension parameter. Ghaffar et al. [20, 21] introduced odd and even point non-stationary binary SS with a shape parameter for curve design. Ghaffar et al. [22] also presented a new class of $2m-$point non-stationary SS with some attractive properties such as torsion, continuity, monotonicity, curvature, and convexity preservation.

This research aims to completely explore the shape-preserving properties of the four-point ternary non-stationary interpolatory scheme [19] (the four-point scheme). We formulate the necessary conditions on the tension parameter of the scheme and initial control points that permit the creation of positivity- and monotonicity-preserving curves after finite iteration levels. Beccari et al. [19] visually demonstrated that, for an initial convex control polygon, the four-point scheme did not generate convex curves. In this regard, we establish the conditions on the tension parameter that prove that the four-point scheme does not generate convexity-preserving limit curves.

The rest of the paper is designed as follows. In section 2, we present the four-point scheme and recall some of its important results. The positivity-preserving and monotonicity-preserving properties of the four-point scheme are proved in sections 3 and 4, respectively. In section 5, the convexity-preserving property of the four-point scheme is discussed. Some numerical examples are given in section 6 to analyze and demonstrate the shape-preserving properties of the four-point scheme. Conclusions are drawn in the last section.

2. THE FOUR-POINT SCHEME

Beccari et al. [19] presented a four-point scheme involving a tension parameter. For given initial control polygon $\{(x_i^0, p_i^0) \in \mathbb{R}\}_{i\in\mathbb{Z}}$ and for the set of control points at the j^{th} refinement level $\{(x_i^j, p_i^j)\}_{i\in\mathbb{Z}}, j \in \mathbb{N}_0 := \mathbb{N} \cup \{0\}$, the control points at the $(j+1)^{th}$ refinement level can be obtained by the rules:

$$\begin{cases} p_{3i}^{j+1} = p_i^j, \\ p_{3i+1}^{j+1} = \frac{1}{60}((-90\gamma_i^{j+1} - 1)p_{i-1}^j + (90\gamma_i^{j+1} + 43)p_i^j \\ \qquad +(90\gamma_i^{j+1} + 17)p_{i+1}^j + (-90\gamma_i^{j+1} + 1)p_{i+2}^j), \\ p_{3i+2}^{j+1} = \frac{1}{60}((-90\gamma_i^{j+1} + 1)p_{i-1}^j + (90\gamma_i^{j+1} + 17)p_i^j \\ \qquad +(90\gamma_i^{j+1} + 43)p_{i+1}^j + (-90\gamma_i^{j+1} - 1)p_{i+2}^j), \end{cases} \tag{1}$$

where,

$$\gamma_i^{j+1} = -\frac{1}{3(1-(\beta^{j+1})^2)(1+\beta^{j+1})}, \tag{2}$$

and,

$$\beta^{j+1} = \sqrt{2+\beta^j}, \beta^j \geq -2\ (\beta^j \neq -1) \forall j \in \mathbb{N}_0. \tag{3}$$

The four-point scheme (1) generates C^2-continuous limit curves for any choice of the initial tension parameter β_0 in the interval $[-2, +\infty[\backslash\{-1\}$. For the initial parameter $\beta^0 \in [-2, +\infty[\backslash\{-1\}$, the recurrence relation in (3) satisfies the property:

$$\lim_{j\to+\infty} \beta^j = 2. \tag{4}$$

Proposition 1.
Given the initial parameter $\beta^0 \in [-2, +\infty[\backslash\{-1\}$, the parameter γ_i^{j+1} given in (2) satisfies the property:

$$\lim_{j\to+\infty} \gamma_i^{j+1} = \frac{1}{27}. \tag{5}$$

3. POSITIVITY PRESERVATION

In this section, we discuss the positivity-preserving property of the four-point scheme (1), which can be obtained by taking $f_i^j = \frac{p_{i+1}^j}{p_i^j}$ and $F^j = max_i\{f_i^j, \frac{1}{f_i^j}\}, j \in \mathbb{N}_0$.

Lemma 2.
Let the initial control points $\{(x_i^0, p_i^0) : i \in \mathbb{Z}\}$ be positive, i.e., $p_i^0 > 0, i \in \mathbb{Z}$, for any $j \in \mathbb{N}_0$, such that:

$$F^0 < \frac{1}{\gamma_i^{j+1}} = \alpha^j \tag{6}$$

then $p_i^j > 0$, $F^j < \alpha^j$, $j \in \mathbb{N}_0$, $i \in \mathbb{Z}$, i.e., the control points generated by the four-point scheme (1) at the j^{th} refinement level are also positive.

Proof.
As $\gamma_i^{j+1} \in (1, \infty) \forall j \in \mathbb{N}_0$, we have:

$$\alpha^j = \frac{1}{\gamma_i^{j+1}} > 0.$$

The proof of Lemma 2 is obtained by induction on j.

- By hypothesis, the holds for $j = 0$, i.e., $p_i^0 > 0, F^0 < \alpha^j, i \in \mathbb{Z}$.
- Suppose, by induction hypothesis $p_i^j > 0$ and $F^j < \alpha^j, i \in \mathbb{Z}$ and for some $j \in \mathbb{N}$. Now, we prove that $p_i^{j+1} > 0$ and $F^{j+1} < \alpha^j$.

Obviously, $\frac{1}{\alpha^j} < f_i^j < \alpha^j$ and $\frac{1}{\alpha^j} < \frac{1}{f_i^j} < \alpha^j$.
By the definition of the four-point scheme (1), we have:

$$p_{3i}^{j+1} > 0. \tag{7}$$

Consider

$$\begin{aligned}
p_{3i+1}^{j+1} &= \frac{1}{60}((-90\gamma_i^{j+1}-1)p_{i-1}^j + (90\gamma_i^{j+1}+43)p_i^j \\
&\quad +(90\gamma_i^{j+1}+17)p_{i+1}^j + (-90\gamma_i^{j+1}+1)p_{i+2}^j) \\
&= \frac{p_i^j}{60}\left(-(90\gamma_i^{j+1}+1)\frac{1}{f_{i-1}^j} + 90\gamma_i^{j+1} + 43\right. \\
&\quad \left.+(90\gamma_i^{j+1} - 90\gamma_i^{j+1}f_{i+1}^j)f_i^j + (17+f_{i+1}^j)f_i^j\right) \\
&> \frac{p_i^j}{60}\left(-(90\gamma_i^{j+1}+1)\alpha^j + 90\gamma_i^{j+1} + 43 + (90\gamma_i^{j+1}\right. \\
&\quad \left.-90\gamma_i^{j+1}\alpha^j)\frac{1}{\alpha^j} + \left(17+\frac{1}{\alpha^j}\right)\frac{1}{\alpha^j}\right) \\
&= \frac{p_i^j}{60(\alpha^j)^2}(-90\gamma_i^{j+1}(\alpha^j)^3 - (\alpha^j)^3 + 43(\alpha^j)^2 \\
&\quad +90\gamma_i^{j+1}\alpha^j + 17\alpha^j + 1) \\
&= \frac{p_i^j}{\frac{60}{(\gamma_i^{j+1})^2}}\left(\frac{-90\gamma_i^{j+1}}{(\gamma_i^{j+1})^3} - \frac{1}{(\gamma_i^{j+1})^3} + \frac{43}{(\gamma_i^{j+1})^2}\right. \\
&\quad \left.+\frac{90\gamma_i^{j+1}}{\gamma_i^{j+1}} + \frac{17}{\gamma_i^{j+1}} + 1\right) \\
&= \frac{p_i^j}{60\gamma_i^{j+1}}\left(91(\gamma_i^{j+1})^3 + 17(\gamma_i^{j+1})^2 - 47\gamma_i^{j+1} - 1\right),
\end{aligned}$$

As we know that $p_i^j > 0$, it is also clear that $\frac{1}{60\gamma_i^{j+1}}[91(\gamma_i^{j+1})^3 + 17(\gamma_i^{j+1})^2 - 47\gamma_i^{j+1} - 1] > 0$, for $\gamma_i^{j+1} > 0$. This implies that:

$$p_{3i+1}^{j+1} > 0. \tag{8}$$

In the same way, we can get $p_{3i+2}^{j+1} > 0$, so we have $p_i^{j+1} > 0$.
In order to prove $F^{j+1} < \alpha^j$, we show that $f_i^{j+1} < \alpha^j$ and $\frac{1}{f_i^{j+1}} < \alpha^j$. For this, consider:

$$\begin{aligned}
f_{3i}^{j+1} &= \frac{p_{3i+1}^{j+1}}{p_{3i}^{j+1}} \\
&= \frac{1}{60}(-(90\gamma_i^{j+1}+1)\frac{1}{f_{i-1}^j} + 90\gamma_i^{j+1} + 43 \\
&\quad +(90\gamma_i^{j+1} - 90\gamma_i^{j+1}f_{i+1}^j)f_i^j + (17+f_{i+1}^j)f_i^j).
\end{aligned}$$

So, we have:

$$\begin{aligned}
f_{3i}^{j+1} - \alpha^j &= \frac{1}{60}\left(-(90\gamma_i^{j+1}+1)\frac{1}{f_{i-1}^j} + 90\gamma_i^{j+1} + 43\right. \\
&\quad \left.+(90\gamma_i^{j+1} - 90\gamma_i^{j+1}f_{i+1}^j)f_i^j + (17\right. \\
&\quad \left.+f_{i+1}^j)f_i^j - 60\alpha^j\right) \\
&< \frac{1}{60}\left(-(90\gamma_i^{j+1}+1)\frac{1}{\alpha^j} + 90\gamma_i^{j+1} + 43\right. \\
&\quad + \left(90\gamma_i^{j+1} - \frac{90\gamma_i^{j+1}}{\alpha^j}\right)\alpha^j + (17 \\
&\quad \left.+\alpha^j)\alpha^j - 60\alpha^j\right) \\
&= \frac{1}{60\alpha^j}(-90\gamma_i^{j+1} - 1 + 90\gamma_i^{j+1}\alpha^j + 43\alpha^j \\
&\quad +90\gamma_i^{j+1}(\alpha^j)^2 - 90\gamma_i^{j+1}\alpha^j + 17(\alpha^j)^2 \\
&\quad +(\alpha^j)^3 - 60(\alpha^j)^2) \\
&= \frac{1}{60(\gamma_i^{j+1})^2}(-90(\gamma_i^{j+1})^4 - (\gamma_i^{j+1})^3 \\
&\quad +133(\gamma_i^{j+1})^2 - 43\gamma_i^{j+1} + 1).
\end{aligned}$$

Since $\frac{1}{60(\gamma_i^{j+1})^2} > 0$, it is also clear that $[-90(\gamma_i^{j+1})^4 - (\gamma_i^{j+1})^3 + 133(\gamma_i^{j+1})^2 - 43\gamma_i^{j+1} + 1] < 0$, for $\alpha^j = \frac{1}{\gamma_i^{j+1}}$ and $\gamma_i^{j+1} > 0$. This implies that $f_{3i}^{j+1} - \alpha^j < 0$. Thus, we have:

$$f_{3i}^{j+1} < \alpha^j. \tag{9}$$

Similarly, we can have $f_{3i+1}^{j+1} < \alpha^j$ and $f_{3i+2}^{j+1} < \alpha^j$. Thus, it shows that $f_i^{j+1} < \alpha^j$. In the same way, it can be shown that $\frac{1}{f_i^{j+1}} < \alpha^j$ when $\frac{1}{f_{3i}^{j+1}} < \alpha^j$, $\frac{1}{f_{3i+1}^{j+1}} < \alpha^j$ and $\frac{1}{f_{3i+2}^{j+1}} < \alpha^j$. Since, $F^{j+1} = max_i\{f_i^{j+1}, \frac{1}{f_i^{j+1}}\}$, so $F^{j+1} < \alpha^j$.

Lemma 2 examines the positivity-preservation of the four-point scheme (1) for the finite number of j subdivision steps. Henceforth, Theorem 3 is given to build up the positivity-preserving condition in the limiting case, as $j \to \infty$. It can be observed that the parameter γ_i^{j+1} given in (2) fulfills $\lim_{j\to\infty}\gamma_i^{j+1} = \frac{1}{27}$. Thus, $\lim_{j\to\infty}\alpha^j = 27$ in Theorem 3, and the proof can be followed from Lemma 2 easily.

Theorem 3.
Suppose that the initial control points $\{(x_i^0, p_i^0) : i \in \mathbb{Z}\}$ are positive, with the end goal that:

$$F^0 < 27,$$

at that point, the limit curves generated by the four-point scheme (1) are positive.

4. MONOTONICITY PRESERVATION

The monotonicity-preservation property of the four-point scheme (1) which can be obtained by defining the first-order divided difference by $D_i^j = p_{i+1}^j - p_i^j$ and taking $q_i^j = \frac{D_{i+1}^j}{D_i^j}$, $Q^j = max\{q_i^j, \frac{1}{q_i^j}\}, j \in \mathbb{N}_0, i \in \mathbb{Z}$ examined in this section.

The next lemma is given to build the monotonicity-preserving condition for the finite number of j subdivision steps.

Lemma 4.
For $j \in \mathbb{N}$, suppose that the initial control points $\{(x_i^0, p_i^0) : i \in \mathbb{Z}\}$ are strictly monotonically increasing, i.e., $D_i^0 > 0, i \in \mathbb{Z}$, such that:

$$Q^0 \leq \frac{1}{\gamma_i^{j+1}} = \eta^j. \tag{10}$$

Then $D_i^j > 0, Q^j \leq \eta^j, i \in \mathbb{Z}, j \in \mathbb{N}$, *i.e.*, the control points generated by the four-point scheme (1) at the j^{th} subdivision step are still strictly monotonically increasing.

Proof.
First-order divided differences for the four-point scheme (1) can be obtained as:

$$\begin{aligned}
D_{3i}^{j+1} &= \left(\frac{3}{2}\gamma_i^{j+1} + \frac{1}{60}\right) D_i^j + \frac{3}{10} D_{i+1}^j \\
&\quad + \left(-\frac{3}{2}\gamma_i^{j+1} + \frac{1}{60}\right) D_{i+2}^j, \\
D_{3i+1}^{j+1} &= -\frac{1}{30} D_i^j + \frac{2}{5} D_{i+1}^j - \frac{1}{30} D_{i+2}^j, \\
D_{3i+2}^{j+1} &= \left(-\frac{3}{2}\gamma_i^{j+1} + \frac{1}{60}\right) D_i^j + \frac{3}{10} D_{i+1}^j \\
&\quad + \left(\frac{3}{2}\gamma_i^{j+1} + \frac{1}{60}\right) D_{i+2}^j.
\end{aligned}$$

As $\gamma_i^{j+1} \in (1, \infty), \forall j \in \mathbb{Z}_+$, so it gives

$$\eta^j = \frac{1}{\gamma_i^{j+1}} > 0.$$

The proof of Lemma 4 proceeds by induction on j.

- By hypothesis, the assertion holds for $j = 0$, i.e., $D_i^0 > 0, Q^0 \leq \eta^j, i \in \mathbb{Z}$.
- Suppose by induction hypothesis $D_i^j > 0$ and $Q^j \leq \eta^j, i \in \mathbb{Z}$ and for some $j \in \mathbb{N}$. Now we prove that $D_i^{j+1} > 0$ and $Q^{j+1} \leq \eta^j$.

To prove $D_i^{j+1} > 0$, we show that:

$$D_{3i}^{j+1} > 0, \quad D_{3i+1}^{j+1} > 0 \quad \text{and} \quad D_{3i+2}^{j+1} > 0.$$

For this consider,

$$\begin{aligned}
D_{3i}^{j+1} &= \left(\frac{3}{2}\gamma_i^{j+1} + \frac{1}{60}\right) D_i^j + \frac{3}{10} D_i^j q_i^j + \left(-\frac{3}{2}\gamma_i^{j+1} \right. \\
&\quad \left. + \frac{1}{60}\right) q_i^j q_{i+1}^j D_i^j \\
&> \frac{D_i^j}{60}\left(90\gamma_i^{j+1} + 1 + \frac{1}{\eta^j}(18 - 90\gamma_i^{j+1}\eta^j) \right. \\
&\quad \left. + \frac{1}{(\eta^j)^2}\right) \\
&= \frac{D_i^j}{60(\eta^j)^2}[(\eta^j)^2 + 18\eta^j + 1] \\
&= \frac{D_i^j}{\frac{60}{(\gamma_i^{j+1})^2}}\left(\frac{1}{(\gamma_i^{j+1})^2} + \frac{18}{\gamma_i^{j+1}} + 1\right) \\
&= \frac{D_i^j}{60}((\gamma_i^{j+1})^2 + 18\gamma_i^{j+1} + 1).
\end{aligned}$$

As we know that $D_i^j > 0$, and it is also clear that $\frac{1}{60}[(\gamma_i^{j+1})^2 + 18\gamma_i^{j+1} + 1] > 0$, for $\eta^j = \frac{1}{\gamma_i^{j+1}}$ and $\gamma_i^{j+1} > 0$. This implies that,

$$D_{3i}^{j+1} > 0. \tag{11}$$

In the same way, it can be proved that $D_{3i+1}^{j+1} > 0$ and $D_{3i+2}^{j+1} > 0$. This implies that we have $D_i^{j+1} > 0$. Moreover, to verify $Q^{j+1} \leq \eta^j$, we show that $q_i^{j+1} \leq \eta^j$ and $\frac{1}{q_i^{j+1}} \leq \eta^j$. For this, consider:

$$\begin{aligned}
q_{3i}^{j+1} &= \frac{D_{3i+1}^{j+1}}{D_{3i}^{j+1}} \\
&= \frac{-2 + 24q_i^j - 2q_i^j q_{i+1}^j}{90\gamma_i^{j+1} + 1 + 18q_i^j - 90\gamma_i^{j+1} q_i^j q_{i+1}^j + q_i^j q_{i+1}^j},
\end{aligned}$$

thus,

$$\begin{aligned}
q_{3i}^{j+1} - \eta^j &= \frac{-2 + 24q_i^j - 2q_i^j q_{i+1}^j}{90\gamma_i^{j+1} + 1 + 18q_i^j - 90\gamma_i^{j+1} q_i^j q_{i+1}^j + q_i^j q_{i+1}^j} \\
&\quad -\eta^j, \\
q_{3i}^{j+1} - \eta^j &= \frac{N_{m_1}}{D_{m_1}}.
\end{aligned} \tag{12}$$

Using (11), as $D_{m_1} = 90\gamma_i^{j+1} + 1 + 18q_i^j - 90\gamma_i^{j+1} q_i^j q_{i+1}^j + q_{i+1}^j q_i^j > 0$. Further, N_{m_1} of (12) fulfills

$$\begin{aligned}
N_{m_1} &= -2 + 24q_i^j - 2q_i^j q_{i+1}^j - 90\gamma_i^{j+1}\eta^j - \eta^j - 18q_i^j\eta^j \\
&\quad + 90\gamma_i^{j+1} q_i^j q_{i+1}^j \eta^j - q_i^j q_{i+1}^j \eta^j \\
&\leq -2 + \eta^j\left(24 - \frac{2}{\eta^j}\right) - 90\gamma_i^{j+1}\eta^j - \eta^j - \frac{18\eta^j}{\eta^j} \\
&\quad + \eta^j\left(90\gamma_i^{j+1}(\eta^j)^2 - \frac{\eta^j}{\eta^j}\right) \\
&= 90\gamma_i^{j+1}(\eta^j)^3 - 90\gamma_i^{j+1}\eta^j + 22\eta^j - 22 \\
&= \frac{90\gamma_i^{j+1}}{(\gamma_i^{j+1})^3} - \frac{90\gamma_i^{j+1}}{\gamma_i^{j+1}} + \frac{22}{\gamma_i^{j+1}} - 22 \\
&= \frac{1}{(\gamma_i^{j+1})^2}(-112(\gamma_i^{j+1})^2 + 22\gamma_i^{j+1} + 90),
\end{aligned}$$

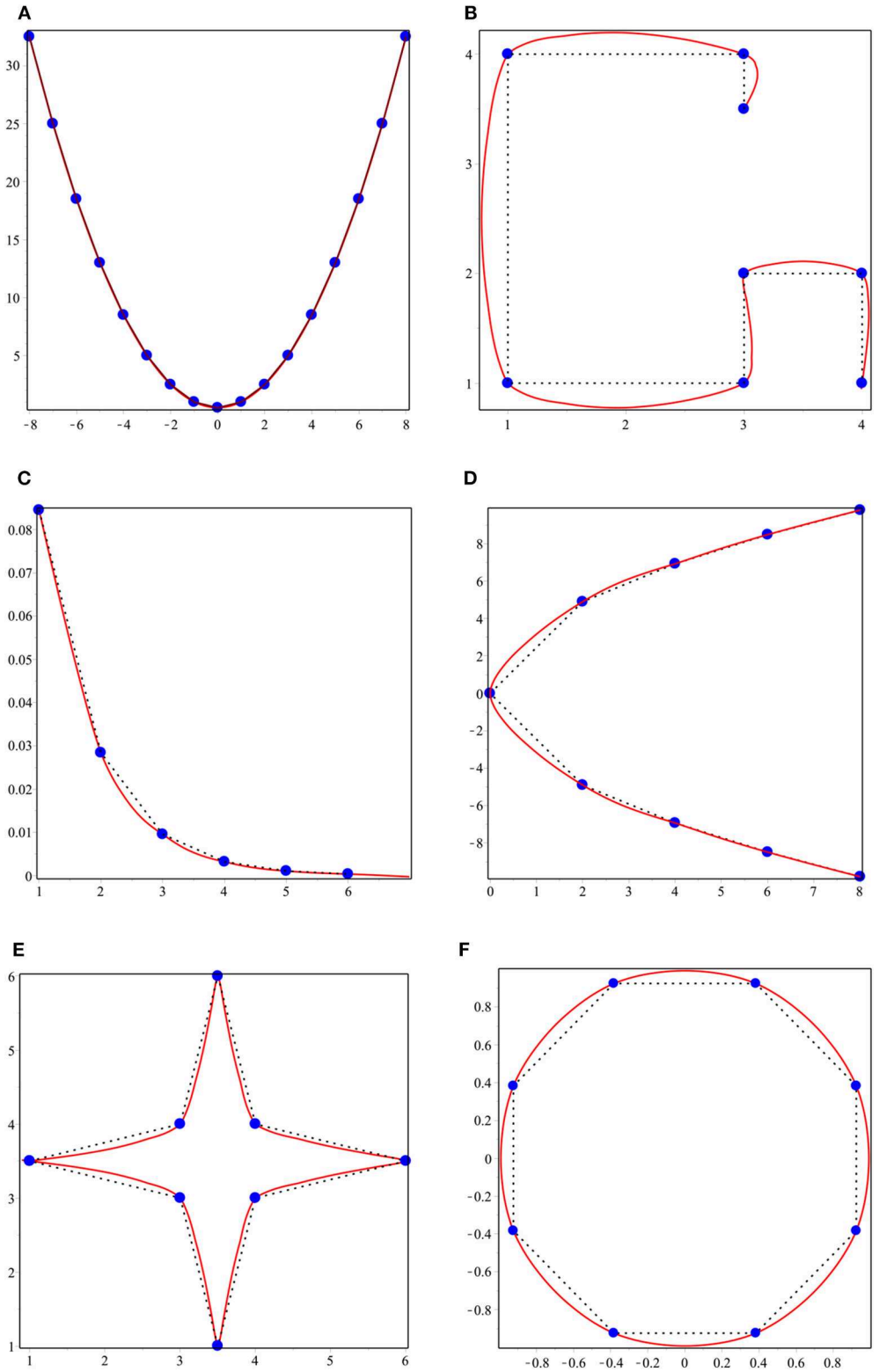

FIGURE 1 | The convexity-preserving limit curves generated by the proposed scheme with the control polygon.

Since $\frac{1}{(\gamma_i^{j+1})^2} > 0$, and it is clear that $(-112(\gamma_i^{j+1})^2 + 22\gamma_i^{j+1} + 90) < 0$, for $\eta^j = \frac{1}{\gamma_i^{j+1}}$ and $\gamma_i^{j+1} > 0$. Thus, from (12), we have $q_{3i}^{j+1} - \eta^j \leq 0$. This implies that:

$$q_{3i}^{j+1} \leq \eta^j. \tag{13}$$

Similarly, it is easy to show that $q_{3i+1}^{j+1} \leq \eta^j$ and $q_{3i+2}^{j+1} \leq \eta^j$, which leads to $q_i^{j+1} \leq \eta^j$.

In the same way, it can be proved that $\frac{1}{q_i^{j+1}} \leq \eta^j$ by showing that $\frac{1}{q_{3i}^{j+1}} \leq \eta^j$, $\frac{1}{q_{3i+1}^{j+1}} \leq \eta^j$ and $\frac{1}{q_{3i+2}^{j+1}} \leq \eta^j$. Since $Q^{j+1} = max_i\{q_i^{j+1}, \frac{1}{q_i^{j+1}}\}$, thus $Q^{j+1} \leq \eta^j$. So, by induction $D_i^j > 0$ and $Q^j \leq \eta^j, i \in \mathbb{Z}$, for some $j \in \mathbb{N}$.

Lemma 4 examines the monotonicity preservation of the four-point scheme (1) for the finite number of j subdivision steps. Henceforth, Theorem 5 is given to build up the monotonicity-preserving condition in the limiting case, as $j \to \infty$. It can be observed that the parameter γ_i^{j+1} given in (2) fulfills $\lim_{j\to\infty} \gamma_i^{j+1} = \frac{1}{27}$. Thus, $\lim_{j\to\infty} \eta^j = 27$ in Theorem 5 and note that the proof can be followed from Lemma 4.

Theorem 5.

Assume that the initial control points $\{(x_i^0, p_i^0) : i \in \mathbb{Z}\}$ are strictly monotonicallly increasing, with the end goal that

$$Q^0 \leq 27,$$

at that point, the limit curves generated by the four-point scheme (1) are strictly monotonically increasing.

5. CONVEXITY PRESERVATION

In this section, we examine the convexity-preserving property of the four-point scheme (1). Basically, a subdivision scheme satisfies the convexity-preserving property if, for an initial convex control polygon, the limit curves generated by the scheme preserve the convexity of the initial data. For a subdivision scheme, the convexity-preserving property is attained if, at each refinement level, the second-order divided differences of the scheme are all positive. Specifically, for a given *jth*-level sequence of real values $\{p_i^j, i \in \mathbb{Z}\}$ located at regularly spaced parameter values $\{x_i^j = \frac{i}{3^j}, i \in \mathbb{Z}\}$, the second-order divided difference of

TABLE 1 | Wind data (positive data) [23].

i	0	1	2	3	4	5	6
x_i	0	0.25	0.5	1	1.2	1.8	2
f_i	2	0.8	0.5	0.1	1	0.5	1

TABLE 2 | Positive data from Sarfraz et al. [24].

i	0	1	2	3	4	5	6
x_i	2	3	7	8	9	13	14
f_i	10	2	3	7	2	3	10

TABLE 3 | Positive data from Butt and Brodlie [25].

i	0	1	2	3	4	5	6
x_i	0	2	4	10	28	30	32
f_i	20.8	8.8	4.2	0.5	3.9	6.3	9.6

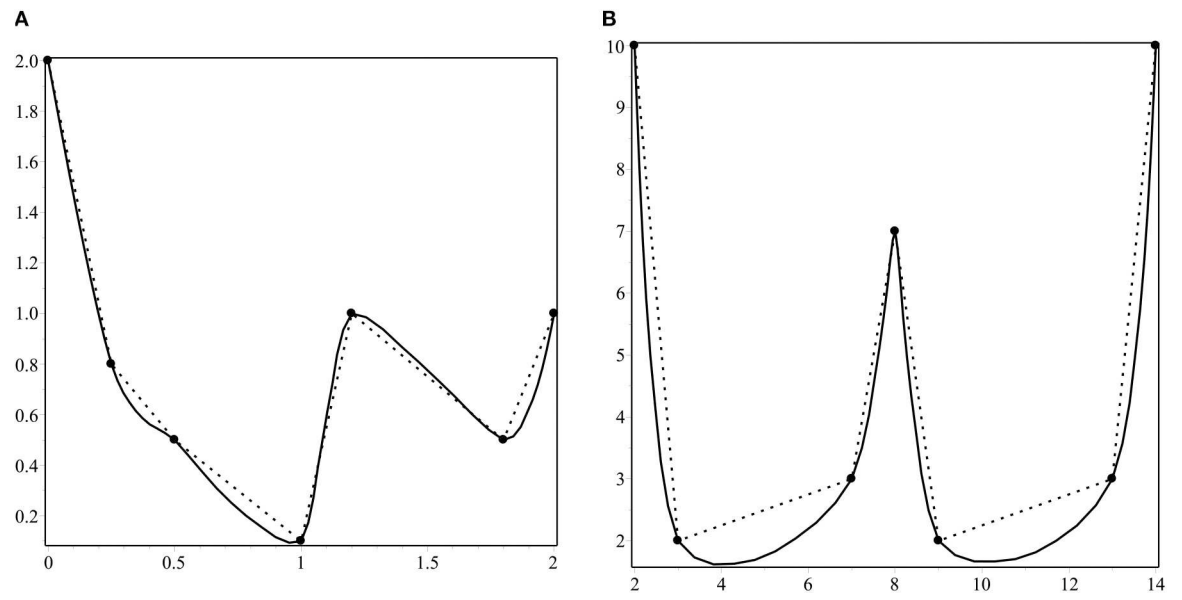

FIGURE 2 | The positivity-preserving curves generated by the four-point scheme (1) for positive initial data.

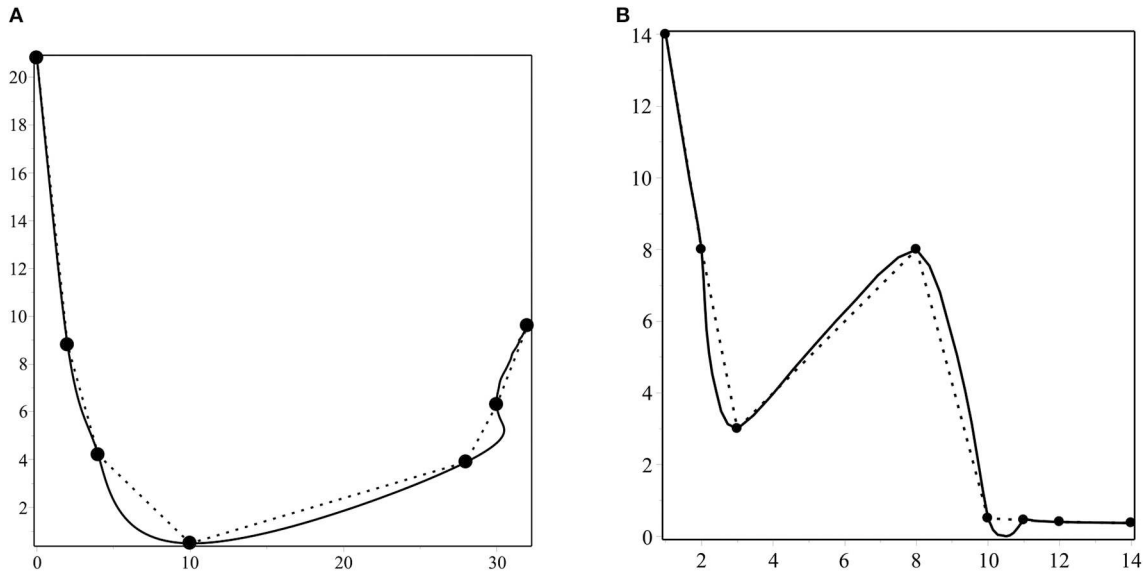

FIGURE 3 | The positivity-preserving curves generated by the four-point scheme (1) for positive initial data.

TABLE 4 | Positive data from Hussain and Ali [26].

i	0	1	2	3	4	5	6
x_i	2	3	7	8	9	13	14
f_i	10	2	3	7	2	3	10

TABLE 5 | Monotonic data.

i	0	1	2	3	4	5	6
x_i	–5.89	–4.56	–3.39	–2.47	–1.66	0	0.898
f_i	2.62	2.36	2.10	1.86	1.63	1	0.33

the scheme is defined by $d_i^j = \frac{3^{2j}}{2}(p_{i-1}^j - 2p_i^j + p_{i+1}^j)$ and, for convexity preservation, $\{d_i^j > 0, i \in \mathbb{Z}, j \in \mathbb{N}_0\}$ holds.

Beccari et al. [19] showed that, for an initial convex control polygon, the four-point scheme (1) fails to generate a convex limit curve when choosing different values of the initial tension parameter β_0 in the interval $[-2, +\infty[\backslash\{-1\}$. In **Figures 1A–D**, dotted lines show the initial convex polygon and solid lines represent curves generated by the four-point scheme (1) after one iteration level. It is clear from the figure that the scheme does not preserve convexity.

Now, we check whether the condition $\{d_i^j > 0, i \in \mathbb{Z}, j \in \mathbb{N}_0\}$ is satisfied by the four-point scheme (1) or not. By taking $y_i^j = \frac{d_{i+1}^j}{d_i^j}$, $Y^j = max\{y_i^j, \frac{1}{y_i^j}\}, j \in \mathbb{N}_0, i \in \mathbb{Z}$, we establish the following result.

Proposition 6.
For $j \in \mathbb{N}$, suppose that the initial control points $\{(x_i^0, p_i^0) : i \in \mathbb{Z}\}$ are strictly convex, i.e., $d_i^0 > 0, i \in \mathbb{Z}$, such that

$$Y^0 \leq \frac{1}{\gamma_i^{j+1}} = \delta^j \tag{14}$$

then $d_i^j \leq 0$, i.e., the points generated by the four-point scheme (1) at the j^{th} subdivision step are not strictly convex.

Proof.
The second-order divided difference of the four-point scheme (1) can be obtained as:

$$\begin{cases} d_{3i}^{j+1} = \left(\frac{3}{2}\gamma_i^{j+1} + \frac{1}{20}\right) d_i^j + \left(\frac{3}{2}\gamma_i^{j+1} - \frac{1}{20}\right) d_{i+1}^j, \\ d_{3i+1}^{j+1} = \left(\frac{3}{2}\gamma_i^{j+1} - \frac{1}{20}\right) d_i^j + \left(\frac{3}{2}\gamma_i^{j+1} + \frac{1}{20}\right) d_{i+1}^j, \\ d_{3i+2}^{j+1} = \left(-\frac{3}{2}\gamma_i^{j+1} + \frac{1}{60}\right) d_i^j + \left(-3\gamma_i^{j+1} + \frac{3}{10}\right) d_{i+1}^j \\ \qquad + \left(-\frac{3}{2}\gamma_i^{j+1} + \frac{1}{60}\right) d_{i+2}^j. \end{cases}$$

As $\gamma_i^{j+1} \in (1, \infty), \forall j \in \mathbb{N}$, so it gives $\delta^j = \frac{1}{\gamma_i^{j+1}} > 0$. The proof of Proposition 6 proceeds by induction on j.

- By hypothesis, the assertion holds for $j = 0$, i.e., $d_i^0 > 0, Y^0 \leq \delta^j, i \in \mathbb{Z}$.
- Suppose by induction hypothesis $d_i^j > 0$ and $Y^j \leq \delta^j, i \in \mathbb{Z}$ and for some $j \in \mathbb{N}$. Now we show that $d_i^{j+1} > 0$. Also, simply, we have $\frac{1}{\delta^j} \leq y_i^j \leq \delta^j$ and $\frac{1}{\delta^j} \leq \frac{1}{y_i^j} \leq \delta^j$.

To prove $d_i^{j+1} > 0$, it is sufficient to show that:

$$d_{3i}^{j+1} > 0, \quad d_{3i+1}^{j+1} > 0 \quad \text{and} \quad d_{3i+2}^{j+1} > 0.$$

From (15), we have:

$$\begin{aligned} d_{3i}^{j+1} &= \frac{3}{2}\gamma_i^{j+1} d_i^j + \frac{1}{20} d_i^j + \frac{3}{2}\gamma_i^{j+1} y_i^j d_i^j - \frac{1}{20} y_i^j d_i^j \\ &> \frac{d_i^j}{60}[90\gamma_i^{j+1} + 3 + 90\gamma_i^{j+1}\frac{1}{\delta^j} - 3\delta^j] \end{aligned}$$

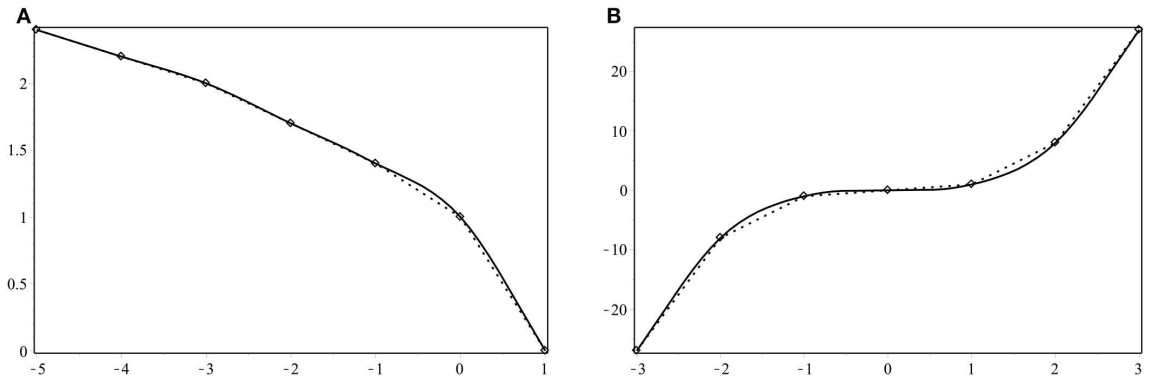

FIGURE 4 | The monotonicity-preserving curves generated by the four-point scheme (1) with monotonic initial data.

TABLE 6 | Monotonic data.

i	0	1	2	3	4	5	6
x_i	–3.89	–2.56	–1.39	0	1.47	2.66	3.89
f_i	-58.86	–16.78	-2.56	0	3.18	18.82	58.86

$$= \frac{d_i^j}{60\gamma_i^{j+1}}[90(\gamma_i^{j+1})^3 + 90(\gamma_i^{j+1})^2 + 3(\gamma_i^{j+1}) - 3].$$

As we know that $d_i^j > 0$, and it is also clear that $\frac{1}{60\gamma_i^{j+1}}[90(\gamma_i^{j+1})^3 + 90(\gamma_i^{j+1})^2 + 3(\gamma_i^{j+1}) - 3] > 0$, for $\delta^j = \frac{1}{\gamma_i^{j+1}}$ and $\gamma_i^{j+1} > 0$. So, we have:

$$d_{3i}^{j+1} > 0. \tag{15}$$

Now consider from (15)

$$\begin{aligned} d_{3i+1}^{j+1} &= \left(\frac{3}{2}\gamma_i^{j+1} - \frac{1}{20}\right) d_i^j + \left(\frac{3}{2}\gamma_i^{j+1} + \frac{1}{20}\right) y_i^j d_i^j \\ &> \frac{d_i^j}{60}\left(90\gamma_i^{j+1} - 3 + 90\gamma_i^{j+1}\frac{1}{\delta^j} + 3\frac{1}{\delta^j}\right) \\ &= \frac{d_i^j \gamma_i^{j+1}}{60}\left(90 - \frac{3}{\gamma_i^{j+1}} + 90\gamma_i^{j+1} + 3\right) \\ &= \frac{d_i^j}{60}(90(\gamma_i^{j+1})^2 + 93\gamma_i^{j+1} - 3). \end{aligned}$$

As we know that $d_i^j > 0$, and it is clear that $\frac{1}{60}[90(\gamma_i^{j+1})^2 + 93\gamma_i^{j+1} - 3] > 0$, for $\delta^j = \frac{1}{\gamma_i^{j+1}}$ and $\gamma_i^{j+1} > 0$. This implies that:

$$d_{3i+1}^{j+1} > 0. \tag{16}$$

Now consider,

$$\begin{aligned} d_{3i+2}^{j+1} &= \left(-\frac{3}{2}\gamma_i^{j+1} + \frac{1}{60}\right) d_i^j + \left(-3\gamma_i^{j+1} + \frac{3}{10}\right) d_i^j y_i^j \\ &\quad + \left(-\frac{3}{2}\gamma_i^{j+1} + \frac{1}{60}\right) d_i^j y_i^j y_{i+1}^j \\ &> \frac{d_i^j}{60}\left(-90\gamma_i^{j+1} + 1 + \left(-180\gamma_i^{j+1} + \frac{1}{\delta^j}\right)\frac{1}{\delta^j} \right. \\ &\quad \left. + (18 - 90\gamma_i^{j+1}\delta^j)\frac{1}{\delta^j}\right) \\ &= \frac{d_i^j}{60}(-179(\gamma_i^{j+1})^2 - 162\gamma_i^{j+1} + 1), \end{aligned}$$

As we know that $d_i^j > 0$, and it is also clear that $\frac{d_i^j}{60}[-179(\gamma_i^{j+1})^2 - 162\gamma_i^{j+1} + 1] < 0$, for $\delta^j = \frac{1}{\gamma_i^{j+1}}$ and $\gamma_i^{j+1} > 0$. This implies that:

$$d_{3i+2}^{j+1} < 0. \tag{17}$$

By combining (15), (16), and (17), we have $d_i^{j+1} \leq 0$, which shows that the four-point scheme (1) does not preserve strict convexity. Some numerical examples are presented to verify and examine the conditions of shape preserving for the 4-point ternary scheme (1). In Examples $1 - 4$, the initial set of values is displayed by dotted line segments while the limit curves are marked by solid lines, such that the limit curves generated by the four-point scheme (1) satisfy the shape-preserving condition.

Example 1.
There are several important meteorological data parameters that scientists use for dealing with different climate challenges. Wind velocity data (WVD) is one of them. These data always have a positive value, and the minimum value is ∼0. In this example, we choose WVD from Wu et al. [23], as given in **Table 1**. We use these WVD to demonstrate the positivity-preserving property of the four-point scheme (1). In **Figure 2A**, the dotted line represents WVD (which is positive) and the solid curve is generated by the four-point scheme (1), which is also positive.

Example 2.
In this example, we consider experimental data that are quoted from Sarfraz et al. [24]. The proposed data are positive and represent the volume of NaOH vs. HCl in a beaker, as stated in the

experimental procedures. These experimental data are presented in **Table 2**. **Figure 2B** presents the positivity preservation of the curve generated by the four-point scheme (1). In this figure, the dotted line represents the positive data (which are given in **Table 2**) and the solid curve is generated by the four-point scheme (1). It is clear that the curve generated by the scheme is also positive.

Example 3.

The data given in **Table 3** are also experimental data. These data represent the oxygen level from an experiment conducted in the laboratory and are quoted from Butt and Brodlie [25]. We use the proposed data in **Figure 3A**. In this figure, we find that, by imposing the condition of positivity on the initial data, the four-point scheme (1) is capable of producing a positive curve.

Example 4.

The data in **Table 4** are obtained from Hussain and Ali [26]. These data represent the depreciation of the valuation of the market price of computers installed at City Computer Center. The x-coordinate corresponds to the time in years, and the y-coordinate corresponds to the computer price in Rs. 10,000. **Figure 3B** generated by the four-point scheme (1) indicates the positivity preservation of the curve generated by the scheme.

Example 5.

The data given in **Table 5** represents monotonic data that are obtained from a monotonic function. From **Figure 4A** we find that by imposing the condition of monotonicity on the initial data, the four-point scheme (1) is capable of producing a monotonically increasing curve.

Example 6.

In this example, we again consider monotonic data from a monotonic function. These data are presented in **Table 6**. **Figure 4B** displays the curve generated by the four-point scheme (1). It is clear from the figure that, for an initial monotonic dataset, the scheme produces a monotonic curve.

6. CONCLUSION

In this paper, we have presented the shape-preserving properties of the four-point scheme (1). We have derived the necessary conditions on the initial control points and tension parameter of the scheme to show that the four-point scheme (1) generates positivity- and monotonicity-preserving curves after a finite number of subdivision steps. We have also shown that, for initial convex data, the proposed scheme does not generate a convex curve. Further, we have generalized these results for the positivity- and monotonicity-preservation of the limit curves. Finally, the discussion is followed by several numerical examples. By using this technique, one can analyze the shape-preserving properties of higher arity interpolation and also approximating schemes.

DATA AVAILABILITY STATEMENT

All datasets generated for this study are included in the article/supplementary files.

AUTHOR CONTRIBUTIONS

PA, AG, and KN: conceptualization. PA, MS, AG, and KN: writing the original manuscript: MS and IK: formal analysis: IK: methodology and supervision: KN and IK: writing review and editing: PA, MS, AG, KN, and IK: software.

REFERENCES

1. Kanwal G, Ghaffar A, Hafeezullah MM, Manan SA, Rizwan M, Rahman G. Numerical solution of 2-point boundary value problem by subdivision scheme. *Commun Math Appl.* (2019) **10**:1–11. doi: 10.26713/cma.v10i1.980
2. Tassaddiq A, Khalid A, Naeem MN, Ghaffar A, Khan F, Karim SAA, et al. A new scheme using Cubic B-Spline to solve non-linear differential equations arising in visco-elastic flows and hydrodynamic stability problems. *Mathematics.* (2019) **7**:1078. doi: 10.3390/math7111078
3. Goufo EFD, Kumar S, Mugisha SB. Similarities in a fifth-order evolution equation with and with no singular kernel. *Chaos Solit Fractals.* (2020) **130**:109467. doi: 10.1016/j.chaos.2019.109467
4. Zaid O, Kumar S. A robust computational algorithm of homotopy asymptotic method for solving systems of fractional differential equations. *J. Comput. Nonlinear Dynam.* (2019) **14**:081004. doi: 10.1115/1.4043617
5. Ahmad E, Oqielat MN, Al-Zhour Z, Kumar S, Momani S. Solitary solutions for time-fractional nonlinear dispersive PDEs in the sense of conformable fractional derivative. *Chaos Interdiscip J Nonlinear Sci.* (2019) **29**:093102. doi: 10.1063/1.5100234
6. Kumar S, Kumar A, Momani S, Aldhaifallah M, Nisar KS. Numerical solutions of nonlinear fractional model arising in the appearance of the stripe patterns in two-dimensional systems. *Adv Diff Equ.* (2019) **2019**:413. doi: 10.1186/s13662-019-2334-7
7. Sharma B, Kumar S, Cattani C, Baleanu D. Nonlinear dynamics of Cattaneo-Christov heat flux model for third-grade power-law uid. *J Comput Nonlinear Dynam* (2019) **15**:9. doi: 10.1115/1.4045406
8. de Rham G. Sur une courbe plane. *J de Mathmat Pures et Appl.* (1956) **35**:25–42.
9. Chaikin GM. An algorithm for high-speed curve generation. *Comput Graph Image Proc.* (1974) **3**:346–9.
10. Dyn N, Levin D, Gregory JA. A 4-point interpolatory subdivision scheme for curve design. *Comput Aided Geom Des.* (1987) **4**:257–68.
11. Dyn N, Kuijt F, Levin D, van Damme R. Convexity preservation of the four-point interpolatory subdivision scheme. *Comput Aided Geom Des.* (1999) **16**:789–92.
12. Kuijt F, van Damme R. Monotonicity preserving interpolatory subdivision schemes. *J Comput Appl Math.* (1999) **101**:203–29.
13. Beccari C, Casciola G, Romani L. Shape controlled interpolatory ternary subdivision. *Appl Math Comput.* (2009) **215**:916–27. doi: 10.1016/j.amc.2009.06.014
14. Hassan MF, Ivrissimitzis IP, Dodgson NA, Sabin MA. An interpolating 4-point C^2 ternary stationary subdivision scheme. *Comput Aided Geom Des.* (2002) **19**:1–18. doi: 10.1016/S0167-8396(01)00084-X
15. Cai Z. Convexity preservation of the interpolating four-point C^2 ternary stationary subdivision scheme. *Comput Aided Geom Des.* (2009) **26**:560–65. doi: 10.1016/j.cagd.2009.02.004
16. Pitolli F. Ternary shape-preserving subdivision schemes. *Math Comput Simul.* (2014) **106**:185–94. doi: 10.1016/j.matcom.2013.04.003
17. Beccari C, Casciola G, Romani L. A non-stationary uniform tension controlled interpolating 4-point scheme reproducing conics. *Comput Aided Geom Des.* (2007) **24**:1–9. doi: 10.1016/j.cagd.2006.10.003
18. Akram G, Bibi K, Rehan K, Siddiqi SS. Shape preservation of 4-point interpolating non-stationary subdivision scheme. *J Comput Appl Math.* (2017) **319**:480–92. doi: 10.1016/j.cam.2017.01.026
19. Beccari C, Casciola G, Romani L. An interpolating 4-point C^2 ternary non-stationary subdivision scheme with tension control. *Comput Aided Geom Des.* (2007) **24**:210–19. doi: 10.1016/j.cagd.2007.02.001
20. Ghaffar A, Ullah Z, Bari M, Nisar KS, Baleanu D. Family of odd point non-stationary subdivision schemes and their applications. *Adv Diff Equ.* (2019) **2019**:171. doi: 10.1186/s13662-019-2105-5

21. Ghaffar A, Bari M, Mudassar I, Nisar KS, Baleanu D. A new class of 2*q*-point nonstationary subdivision schemes and their applications. *Mathematics.* (2019) **7**:639. doi: 10.3390/math7070639
22. Ghaffar A, Ullah Z, Bari M, Nisar KS, Qurashi AL, Baleanu D. A new class of 2m-point binary non-stationary subdivision schemes. *Adv Diff Equ.* (2019) **2019**:325. doi: 10.1186/s13662-019-2264-4
23. Wu J, Zhang X, Peng L. Positive approximation and interpolation using compactly supported radial basis functions. *Math Problem Eng.* (2010) **10**:964528. doi: 10.1155/2010/964528
24. Sarfraz M, Hussain MZ, Nisar A. Positive data modeling using spline function. *Appl Math Comput.* (2010) **216**:2036–49. doi: 10.1016/j.amc.2010.03.034
25. Butt S, Brodlie KW. Preserving positivity using piecewise cubic interpolation. *Comput Graph.* (1993) **17**:55–64.
26. Hussain MZ, Ali JM. Positivity preserving piecewise rational cubic interpolation. *Matematika.* (2006) **22**:147–53. doi: 10.11113/matematika.v22.n.183

Conflict of Interest: The authors declare that the research was conducted in the absence of any commercial or financial relationships that could be construed as a potential conflict of interest.

frontiers in Physics

ORIGINAL RESEARCH
published: 04 February 2020
doi: 10.3389/fphy.2019.00255

Rogue Wave Solutions and Modulation Instability With Variable Coefficient and Harmonic Potential

Safdar Ali[1†] *and Muhammad Younis*[2*†]

[1] Department of Mathematics and Statistics, The University of Lahore, Lahore, Pakistan, [2] Punjab University College of Information Technology, University of the Punjab, Lahore, Pakistan

This article studies the propagation of rogue waves with a nonautonomous NLSE in the presence of external potential. This model is considered to be an important model for many physical phenomena in quantum mechanics and optical fiber. The obtained waves are of first and second order and are investigated using similarity transformation. The nonlinear dynamic behavior of these waves is also demonstrated with different parameter values for the magnetic and gravity fields. The results show the influence of these fields over density, width, and peak heights. Moreover, the modulation instability is also discussed.

Keywords: rogue wave solutions, modulation instability, similarity transformation, NLSE, harmonic potential

OPEN ACCESS

Edited by:
Mustafa Inc,
Firat University, Turkey

Reviewed by:
Aly R. Seadawy,
Taibah University, Saudi Arabia
Abdullahi Yusuf,
Federal University, Dutse, Nigeria

***Correspondence:**
Muhammad Younis
younis.pu@gmail.com

[†] *These authors have contributed equally to this work*

Specialty section:
This article was submitted to Mathematical Physics, a section of the journal Frontiers in Physics

Received: *21 October 2019*
Accepted: *31 December 2019*
Published: *04 February 2020*

Citation:
Ali S and Younis M (2020) Rogue Wave Solutions and Modulation Instability With Variable Coefficient and Harmonic Potential. Front. Phys. 7:255. doi: 10.3389/fphy.2019.00255

1. INTRODUCTION

One of the interesting known models with a time-dependent coefficient is the nonautonomous NLSE with a harmonic potential. This is expressed as:

$$iq_t + \frac{\alpha(t)}{2}q_{xx} + \left(- i\gamma(t) + \frac{\omega(t)r^2}{2} + \beta(t)|q|^2 \right)q = 0. \tag{1}$$

The function q is a wave profile in a homogeneous nonlinear medium, $\alpha(t)$ is the dispersion coefficient, $\beta(t)$ is the measure of the Kerr nonlinearity, $\gamma(t)$ is considered as the distributed gain/loss coefficient, and the harmonic potential is given by $\omega(t)r^2/2$. This model describes many physical phenomena in nonlinear sciences.

This article studies the first- and second-order rogue wave solutions. It is a single giant wave whose amplitude is two to three times higher than those of the surrounding waves. The interesting fact regarding this wave is that it appears from nowhere and disappears without a trace. The similarity transformation (ST) is utilized to construct the solutions. These waves are also found in deep and shallow water and, beyond oceanic expanses, in optical fibers [1–8], super fluids, and so on [9–18]. In recent times, the theoretical study of these kinds of waves has become an interesting part of the field of nonlinear sciences [19–34]. The following section deals with the extraction of wave solutions with ST.

2. ROGUE WAVE SOLUTIONS

The envelope field q is considered in the following form [33]:

$$q = (q_R + iq_I)e^{i\phi}, \tag{2}$$

where q_R, q_I, q, and ϕ are all dependent functions of x and t, while the intensity is defined by:

$$|q|^2 = |q_R|^2 + |q_I|^2. \tag{3}$$

The use of Equations (2)–(3) in (1) yields an equation with variable coefficients. After solving and simplification, we can split this equation into its real and imaginary equations. For the real functions q_R, q_I, and ϕ, which depend on x and t, the variables $\xi(x,t)$ and $\tau(t)$ are introduced. Thus, the new transformations for q_R, q_I, and ϕ are constructed in this manner: $q_R = A(t) + B(t)P(\xi(x,t),\tau(t))$, $q_I = C(t) + D(t)Q(\xi(x,t),\tau(t))$, and $\phi = \zeta(x,t) + \lambda\ \tau(t)$, where λ is a constant. Substituting this new transformation into the real and imaginary part equations, the following equations are obtained:

$$\begin{aligned}
&-2(A+BP)(\zeta_t+\lambda\tau_t)-2(C_t+D_tQ+DQ_\xi\xi_t+DQ_\tau\tau_t)\\
&-\alpha(t)(C+DQ)\zeta_{xx}-\alpha(t)(A+BP)\zeta_x^2-2\alpha(t)DQ_\xi\xi_x\zeta_x\\
&+\alpha(t)(BP_{\xi\xi}\xi_x^2+BP_\xi\xi_{xx})+2\beta(t)((A+BP)^2\\
&+(C+DQ)^2)(A+BP)+2\gamma(t)(C+DQ)\\
&+\omega(t)x^2(A+BP)=0,
\end{aligned} \tag{4}$$

$$\begin{aligned}
&-2(C+DQ)(\zeta_t+\lambda\tau_t)+2(A_t+B_tP+BP_\xi\xi_t+BP_\tau\tau_t)\\
&+\alpha(t)(A+BP)\zeta_{xx}-\alpha(t)(C+DQ)\zeta_x^2+2\alpha(t)BP_\xi\xi_x\zeta_x\\
&+\alpha(t)(DQ_{\xi\xi}\xi_x^2+DQ_\xi\xi_{xx})+2\beta(t)((A+BP)^2\\
&+(C+DQ)^2)(C+DQ)-2\gamma(t)(A+BP)\\
&+\omega(t)x^2(C+DQ)=0.
\end{aligned} \tag{5}$$

Simplifying the above equations, we perform the similarity reduction in the following way.

$$\xi_{xx}=0, \tag{6}$$

$$\xi_t+\alpha(t)\xi_x\zeta_x=0, \tag{7}$$

$$\omega(t)x^2-2\zeta_t-\alpha(t)\zeta_x^2=0, \tag{8}$$

$$2\sigma_t+(\alpha(t)\zeta_{xx}-2\gamma(t))\sigma=0, \text{for } (\sigma=A,B,C,D), \tag{9}$$

$$\begin{aligned}
&-2(A+BP)\lambda\tau_t-2DQ_\tau\tau_t+\alpha(t)BP_{\xi\xi}\xi_x^2\\
&+2\beta(t)(A+BP)(|A+BP|^2+|C+DQ|^2)=0,
\end{aligned} \tag{10}$$

$$\begin{aligned}
&-2(C+DQ)\lambda\tau_t+2BP_\tau\tau_t+\alpha(t)DQ_{\xi\xi}\xi_x^2\\
&+2\beta(t)(C+DQ)(|A+BP|^2+|C+DQ|^2)=0.
\end{aligned} \tag{11}$$

where $\xi(x,t), \zeta(x,t), A(t), B(t), C(t), D(t), P(\xi,\tau)$, and $Q(\xi,\tau)$ are different functions and are determined later. After algebraic computation, the above equations produce the following results.

$$\xi = \delta(t)x+\delta_0(t), \tag{12}$$

$$\omega = \frac{2\zeta_t+\alpha(t)\zeta_x^2}{x^2}, \tag{13}$$

$$\zeta_{(x,t)} = -\frac{1}{\alpha(t)}\left(\frac{\delta(t)_t}{2\delta(t)}x^2+\frac{\delta_0(t)}{\delta(t)}x\right), \tag{14}$$

$$\begin{aligned}
A(t) &= a_0\exp\left[\frac{1}{2}\int_0^t\left(\frac{\delta(k)_k}{\delta(k)}+2\gamma(k)\right)dk\right],\\
B(t) &= bA,\ D(t)=dA,
\end{aligned} \tag{15}$$

where a_0, b, and d are constants, and $C = 0$. The variables $\tau(t)$ and $\beta(t)$ are given by

$$\tau(t) = \frac{1}{2}\int_0^t\alpha(k)\delta^2(k)dk, \tag{16}$$

$$\beta(t) = \frac{\alpha(t)\delta^2}{2A^2}. \tag{17}$$

To further reduce to Equations (4) and (5) to the partial differential equations, we require

$$\begin{aligned}
&-2(1+bP)\lambda-2dQ_\tau+\alpha(t)bP_{\xi\xi}\\
&+2\beta(t)(1+bP)(|1+bP|^2+|1+dQ|^2)=0,
\end{aligned} \tag{18}$$

$$\begin{aligned}
&-2(c+dQ)\lambda+2bP_\tau+\alpha(t)dQ_{\xi\xi}\\
&+2\beta(t)(c+dQ)(|1+bP|^2+|1+dQ|^2)=0.
\end{aligned} \tag{19}$$

According to the direct method, we obtain the first-order rational solution

$$P(\xi,\tau) = -\frac{4}{R_1(\xi,\tau)b},\ Q(\xi,\tau) = -\frac{8\tau}{R_1(\xi,\tau)d}, \tag{20}$$

where $R_1 = 1+2\xi^2+4\tau^2$. Moreover, the second-order solution is obtained as

$$P(\xi,\tau) = \frac{P_1(\xi,\tau)}{R_2(\xi,\tau)b},\ Q(\xi,\tau) = \frac{Q_1(\xi,\tau)\tau}{R_2(\xi,\tau)d}, \tag{21}$$

$$P_1(\xi,\tau) = \frac{3}{8}-9\tau^2-\frac{3\xi^2}{2}-6\xi^2\tau^2-10\tau^4-\frac{\xi^4}{2}, \tag{22}$$

$$Q_1(\xi,\tau) = -\frac{15}{4}+2\tau^2-3\xi^2+4\xi^2\tau^2+4\tau^4+\xi^4, \tag{23}$$

$$\begin{aligned}
R_2 = {}& \frac{3}{32}+\frac{33}{8}\tau^2+\frac{9\xi^2}{16}-\frac{3\xi^2\tau^2}{2}+\frac{9\tau^4}{2}+\frac{\xi^4}{8}\\
&\frac{2\xi^6}{3}+\xi^2\tau^6+\frac{\xi^4\tau^2}{2}+\frac{\xi^6}{12}.
\end{aligned} \tag{24}$$

The direct reduction solution is considered in the following form:

$$q = A(1+bP+idQ)e^{i(\zeta+\tau)}, \tag{25}$$

where $\xi(x,t), \zeta(x,t), A(t), \tau(t), P(\xi,\tau)$, and $Q(\xi,\tau)$ are expressed by the relations given in Equations (12), (14)–(16), and (20), respectively.

The rogue wave solution of first order to Equation (1) can be obtained using Equations (20) and (25); thus, after simplification, we may have the following form:

$$\begin{aligned}
q = {}& a_0\left(\frac{-3+2\xi^2+4\tau^2-8i\tau}{1+2\xi^2+4\tau^2}\right)\\
&\times\exp\left[\frac{1}{2}\int_0^t\left(\frac{\delta(k)_k}{\delta(k)}+2\gamma(k)\right)dk\right]e^{i(\zeta,\tau)},
\end{aligned} \tag{26}$$

whose amplitude can be written as

$$|q|^2 = a_0^2\frac{[-3+2(\delta(t)x+\delta_0(t))^2+4\tau^2]^2+64\tau^2(t)}{[1+2(\delta(t)x+\delta_0(t))^2+4\tau^2(t)]^2}$$

$$\times \exp\left[\int_0^t \left(\frac{\delta(k)_k}{\delta(k)} + 2\gamma(k)\right)dk\right]. \tag{27}$$

The rogue wave (rational-like) solution of second order to Equation (1) can be obtained using Equations (21) and (25); thus, after simplification, we may have the following form:

$$\begin{aligned} q = a_0\Bigg(1 - \frac{4(-3+4\xi^4+72\tau^2+80\tau^4+12\xi^2(1+4\tau^2))}{3+18\xi^2+4\xi^4+24\xi^6+4(33+4\xi^2(-3+\xi^2))\tau^2+144\tau^4+32\xi^2\tau^6} \\ +i\frac{8\tau(4\xi^2(-3+\xi^2+4\tau^2)+(-5+8t^2))}{3+18\xi^2+4\xi^4+24\xi^6+4(33+4\xi^2(-3+\xi^2))\tau^2+144\tau^4+32\xi^2\tau^6}\Bigg) \\ \times \exp\left[\frac{1}{2}\int_0^t \left(\frac{\delta(k)_k}{\delta(k)} + 2\gamma(k)\right)dk\right]e^{i(\zeta+\tau)}, \end{aligned} \tag{28}$$

whose intensity is written as

$$\begin{aligned} |q|^2 = a_0^2\Bigg[\Bigg(1 - \Bigg(4(-3+4\xi^4+72\tau^2+80\tau^4+12\xi^2(1+4\tau^2))/(3+18\xi^2 \\ +4\xi^4+24\xi^6+4(33+4\xi^2(-3+\xi^2))\tau^2+144\tau^4+32\xi^2\tau^6\Bigg)\Bigg)^2 \\ +\Bigg(8\tau(4\xi^2(-3+\xi^2+4\tau^2)+(-5+8t^2))/(3+18\xi^2+4\xi^4 \\ +24\xi^6+4(33+4\xi^2(-3+\xi^2))\tau^2+144\tau^4+32\xi\tau^6\Bigg)^2\Bigg] \\ \times \exp\left[\int_0^t \left(\frac{\delta(k)_k}{\delta(k)} + 2\gamma(k)\right)dk\right], \end{aligned} \tag{29}$$

The following section discusses the dynamical behavior of waves.

3. DYNAMICAL BEHAVIOR OF WAVES

The behavior of constructed waves is demonstrated using the relation $\delta(t) = b + l\cos(\omega t)$. The first term on the right-hand side

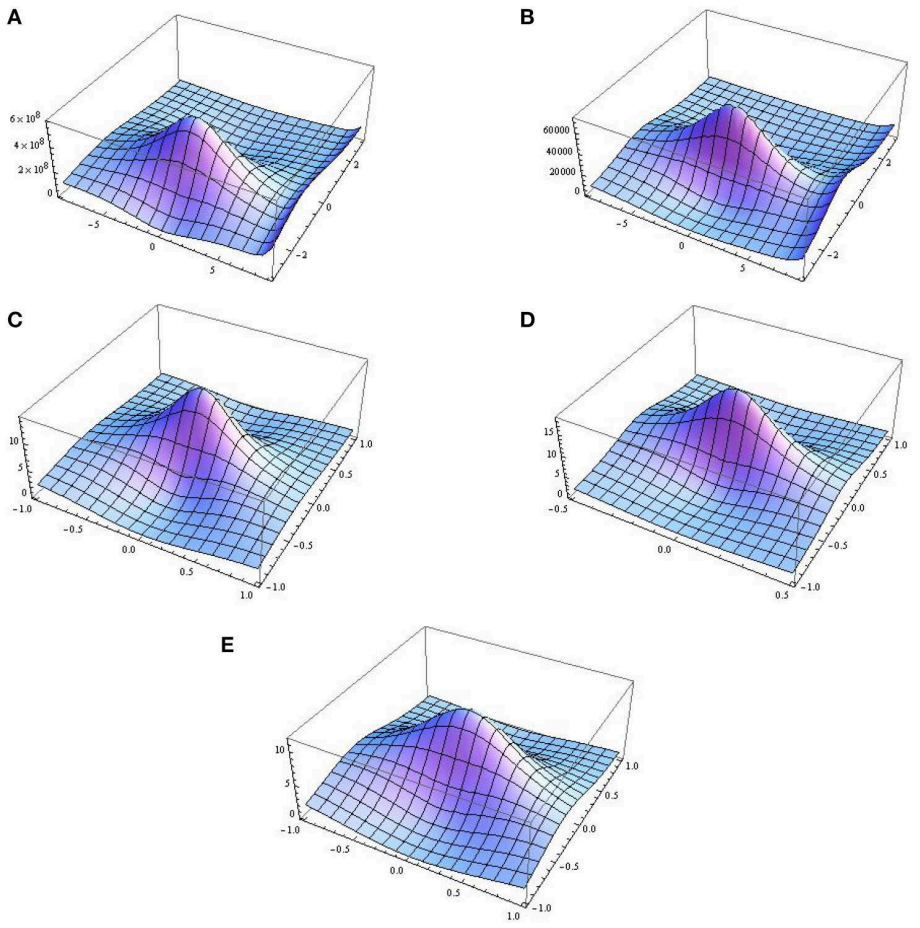

FIGURE 1 | 3D graphical representations of first-order rogue waves. **(A)** $b = 0.5$ and $\delta_0(t) = 0.5$, **(B)** $b = 0.79$ and $\delta_0(t) = 0.61$, **(C)** $\delta_0(t) = 0.5t^2$ and $\delta(t) = 0.7 + 0.9\cos(0.1t)$, **(D)** $\delta_0(t) = 0.35t^2$ and $\delta(t) = 0.86 + 1.2\cos(0.1t)$, and **(E)** $\delta_0(t) = 0.35t^2$, $\delta(t) = 0.1 + 1.2\cos(0.1t)$, and $\delta_0(t) = 0.35t^2$.

represents the gravity field (GF) $b = \delta mg$ with the real parameter δ, and the second term on the same side is the external magnetic field (EMF) and is given by $l\cos(\omega t)$.

There are two possibilities for the occurrence of the waves in the presence of GF. The first is that when the GF (i.e., $b \neq 0$ and $l = 0$) is acting, and the second is that when both the GF and EMF are present (i.e., $b \neq 0$ and $l \neq 0$).

Now, we discuss the first possibility for nonlinear dynamical behavior, when there is only the GF. Say $\delta(t) = b$, and the amplitude (corresponding to $l = 0$) is given by the following relation:

$$|q|^2 = a_0^2 \frac{[-3 + 2(bx + \delta_0(t))^2 + 4\tau^2]^2 + 64\tau^2(t)}{[1 + 2(bx + \delta_0(t))^2 + 4\tau^2(t)]^2} \times \exp\left[\int_0^t \left(\frac{\delta(k)_k}{\delta(k)} + 2\gamma(k)\right)dk\right]. \quad (30)$$

The behavior of the second-order rogue wave is considered when there is only the GF. Then, the value of $\delta(t) = b$, so the amplitude (corresponding to $l = 0$) is given by

$$\begin{aligned}|q|^2 = a_0^2\Bigg[\Bigg(1 - \Bigg(&4(-3 + 4(bx + \delta_0(t))^4 + 72\tau^2 + 80\tau^4 \\ &+12(bx + \delta_0(t))^2(1 + 4\tau^2))/(3 + 18(bx + \delta_0(t))^2 \\ &+4(bx + \delta_0(t))^4 + 24(bx + \delta_0(t))^6 + 4(33 + 4(bx \\ &+\delta_0(t))^2(-3 + (bx + \delta_0(t))^2))\tau^2 + 144\tau^4 + 32(bx \\ &+\delta_0(t))^2\tau^6\Bigg)\Bigg)^2 + \Bigg(8\tau(4(bx + \delta_0(t))^2(-3 + (bx \\ &+\delta_0(t))^2 + 4\tau^2) + (-5 + 8t^2))/(3 + 18(bx + \delta_0(t))^2 \\ &+4(bx + \delta_0(t))^4 + 24(bx + \delta_0(t))^6 \\ &+4(33 + 4(bx + \delta_0(t))^2(-3 + (bx + \delta_0(t))^2))\tau^2 + 144\tau^4 \\ &+32(bx + \delta_0(t))\tau^6\Bigg)^2\Bigg] \\ &\times \exp\left[\int_0^t \left(\frac{\delta(k)_k}{\delta(k)} + 2\gamma(k)\right)dk\right]. \end{aligned} \quad (31)$$

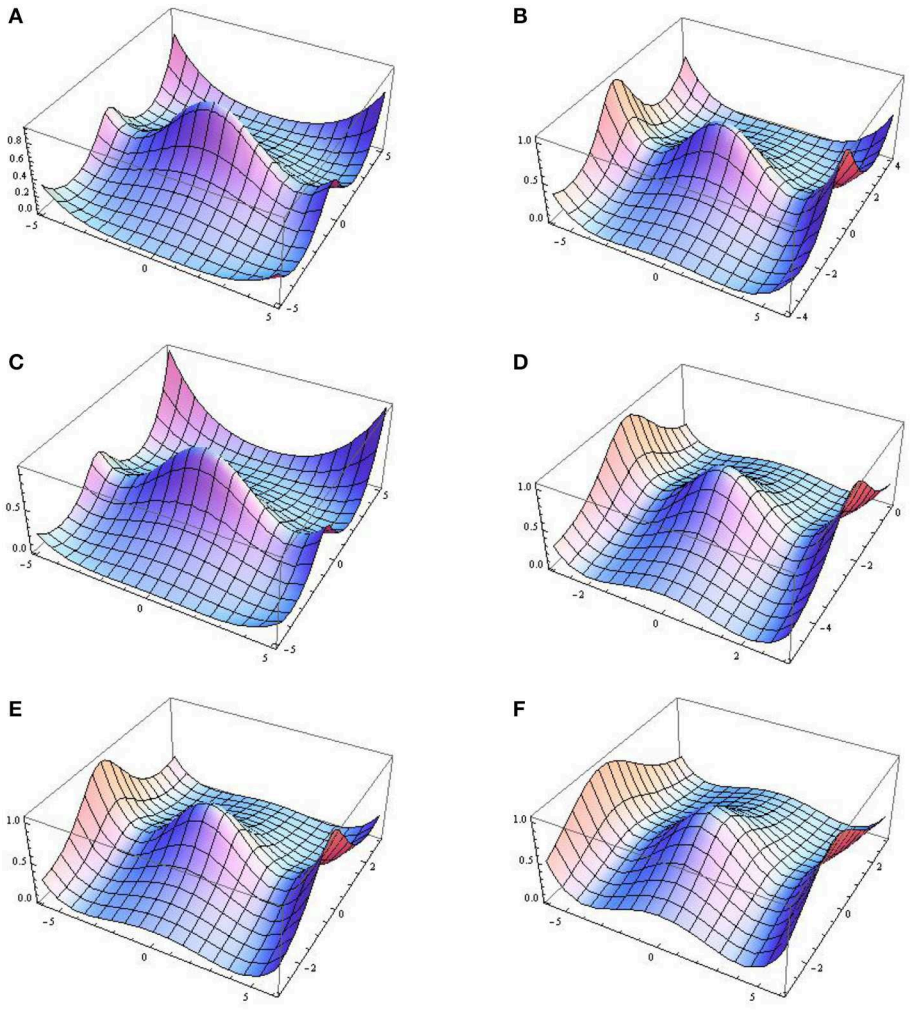

FIGURE 2 | 3D graphical representations of second-order waves. **(A)** $\delta(t) = 0.5$ and $\delta_0(t) = 0.1$, **(B)** $\delta(t) = 0.4$ and $\delta_0(t) = 0.1$, **(C)** $\delta(t) = 0.7$ and $\delta_0(t) = 0.2\exp(sech(0.2t))$, **(D)** $\delta(t) = 0.5sech(0.2t)$ and $\delta_0(t) = 0.5\exp(sech(0.2t))$, **(E)** $\delta(t) = 0.5 + 1.2\cos(0.005t)$ and $\delta_0(t) = 0.35t^2$, and **(F)** $\delta(t) = 0.1 + 1.2\cos(0.1t)$ and $\delta_0(t) = 0.35t^2$.

4. ANALYSIS OF MODULATION INSTABILITY

In this section, we study the modulation instability (MI). The linear stability analysis technique [34] has been applied, and we suppose that Equation (1) has the perturbed steady-state (PSS) solution in the following form:

$$q(x,t) = \{\sqrt{P} + \chi(x,t)\} \times e^{(i\varphi_{NL})},\ \varphi_{NL} = \beta P x, \tag{32}$$

where $\chi << P, P$ is the incident optical power, and φ_{NL} is the phase component. The perturbation $\chi(x,t)$ is examined by using linear stability analysis. Now, we substitute Equation (32) into Equation (1) and, after linearizing it, we obtain

$$i\frac{\partial \chi}{\partial t} + \frac{1}{2}\alpha(t)\frac{\partial^2 \chi}{\partial x^2} + \beta(t)P(\chi + \chi^*) + \left(- i\gamma(t) + \frac{\omega(t)x^2}{2}\right)\chi = 0, \tag{33}$$

where "$*$" denotes a complex conjugate. Consider that the solution of Equation (33) has of the form

$$\chi(x,t) = \eta_1 e^{i(kx-\nu t)} + \eta_2 e^{-i(kx-\nu t)}, \tag{34}$$

where ν and k are the frequency of perturbation and normalized wave number, respectively. After putting Equation (34) into Equation (33) and by separating the obtained equation into its real and imaginary parts, we get the dispersion relation:

$$-\nu^2 + \alpha\nu k^2 - 2i\gamma\nu - \frac{\alpha^2}{4}k^4 + i\alpha\gamma k^2 + \beta P\omega r^2 + \gamma^2 + \frac{\omega^2 r^4}{4} = 0. \tag{35}$$

The dispersion relation given in Equation (35) has the following solutions in terms of frequency ν after taking the modulus of the above equation. We have

$$\nu = \frac{1}{2}\alpha k^2 \pm \frac{1}{2}\sqrt{-4\gamma^2 + \omega^2 r^4 + 4\beta P r^2 \omega \pm 4\sqrt{-\gamma^2\omega^2 r^4 - 4\beta P r^2 \omega\gamma^2}}. \tag{36}$$

The above dispersion relation determines the PSS stability, and that depends on the harmonic potential or distributed gain (loss) coefficient of the model. If the frequency ν has an imaginary part, the PSS solution is unstable since the perturbations grow exponentially. On the other hand, if ν is real, then the PSS solution is stable against small

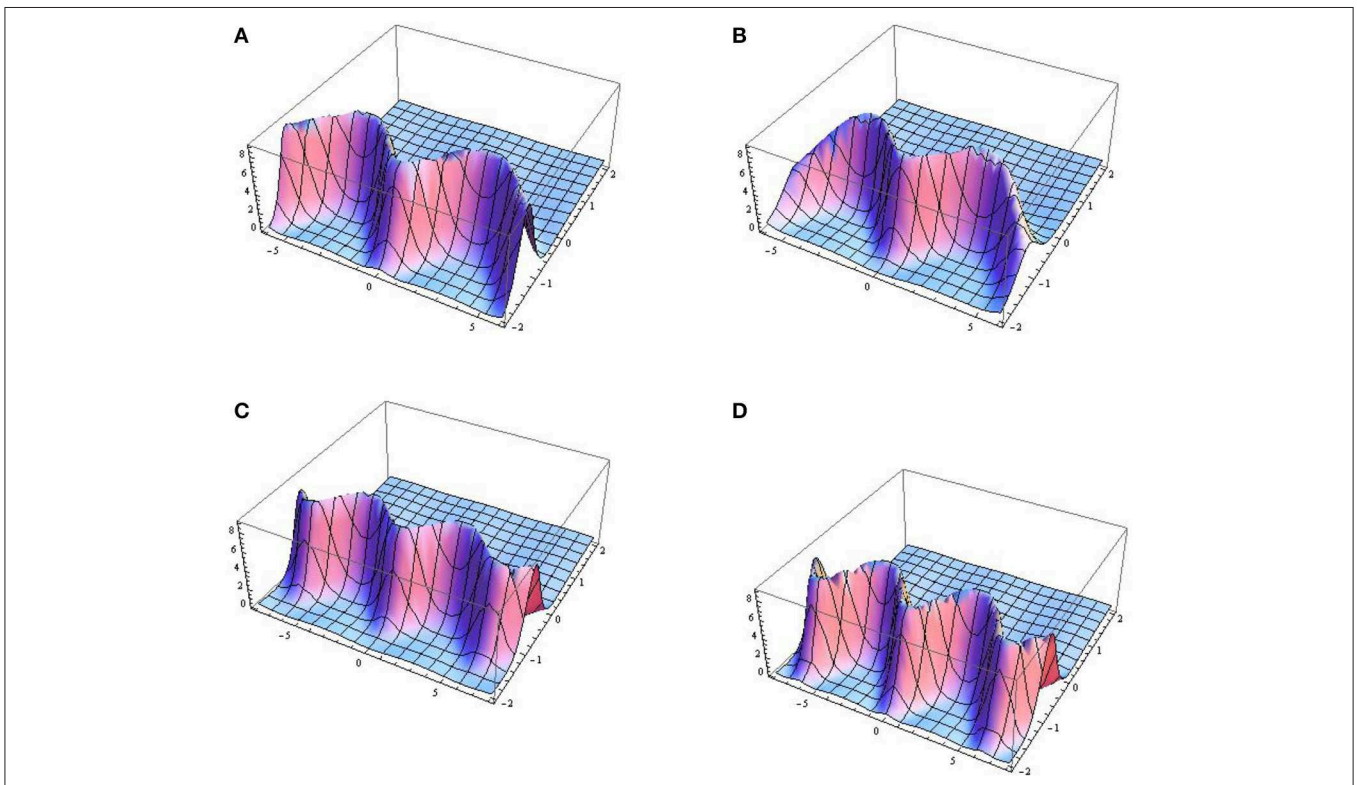

FIGURE 3 | 3D graphical representations of first-order rogue waves. The figures correspond with **(A)** $b = 1.3, \delta_0(t) = \exp(0.5 + 0.5\cos t)$ and $\alpha = \tan^2(0.02t)$, **(B)** $b = 1.5, \delta_0(t) = \exp(0.05 + 0.5\cos t)$ and $\alpha = \tan^2(0.02t)$, **(C)** $\delta(t) = 1.4 + 0.05\cos t, \delta_0(t) = \exp(0.002 + 0.4\cos t)$ and $\alpha = \tan^2(0.02t)$, and **(D)** $\delta(t) = 1.3 + 0.01\cos t, \delta_0(t) = \exp(0.05 + 0.5\cos t)$, and $\alpha = \tan^2(0.02t)$.

perturbations. The necessary condition for the existence of MI is

$$\gamma^2\omega r^2(\omega r^2 + 4\beta P) > 0, \tag{37}$$

or

$$\left(-4\gamma^2 + \omega^2 r^4 + 4\beta P r^2 \omega \pm 4\sqrt{-\gamma^2\omega^2 r^4 - 4\beta P r^2 \omega \gamma^2} \right) < 0. \tag{38}$$

The MI gain spectrum is given as

$$g(\nu) = 2Im(\nu) = \sqrt{-4\gamma^2 + \omega^2 r^4 + 4\beta P r^2 \omega \pm 4\sqrt{-\gamma^2\omega^2 r^4 - 4\beta P r^2 \omega \gamma^2}}. \tag{39}$$

The MI is significantly affected by P. If P is increased, the growth rate of MI will appear to disperse.

5. GRAPHICAL RESULTS AND DISCUSSION

The graphical representation of the amplitude defined by Equation (30) considering $a_0 = 1, \alpha = t$, and $\gamma(t) = \sin^3(0.005t)$ is depicted in **Figures 1A,B**, with the values of only GF b (0.5 and 0.79) and δ_0 (0.5 and 0.61). The graph with the maximum peak can be obtained at $b = 0.5$ and $\delta_0 = 0.5$. For the second possibility, when the GF and the EMF are both present, we discuss the graphical behavior of the solutions. For this, let us consider $\delta(t) = 0.7 + 0.9\cos(0.1t), \delta_0(t) = 0.5t^2$, $\delta(t) = 0.86 + 1.2\cos(0.1t), \delta_0(t) = 0.35t^2$ and $\delta_0(t) = 0.35t^2$, and $\delta(t) = 0.1 + 1.2\cos(0.1t)$ and $\delta_0(t) = 0.35t^2$. The graphical representations are demonstrated in **Figures 1C–E**, respectively.

The results show that there are no different effects of GF on first- and second-order rogue waves. Graphical representations of the amplitude given by Equation (31) at $a_0 = 1$ and $\gamma(t) = \sin^3(0.005t)$ with different values of GF and $\delta_0(t)$ is depicted in **Figures 2A–C**. Six small peaks appear around the one high peak of the second-order solution. Graphical representations of second-order rogue waves with both GF and EMF are also shown in **Figures 2D–F**.

Graphical representations of the amplitudes given by equation (30) at $a_0 = 1$ and $\gamma(t) = t$ are depicted in **Figures 3A–D** with the different parameter values. The curves in **Figures 3A,B** are formed under the GF, and those in **Figures 3C,D** are formed when both the GF and EMF are present.

Graphical representations of the amplitude given by Equation (31) at $a_0 = 1$ and $\gamma(t) = t$ with different values of GF and $\delta_0(t)$ are depicted in **Figures 4A,B**. Small lumps appear in the graph of the second-order solution. Graphical demonstrations of second-order rogue waves with both GF and EMF are shown in **Figures 4C,D**.

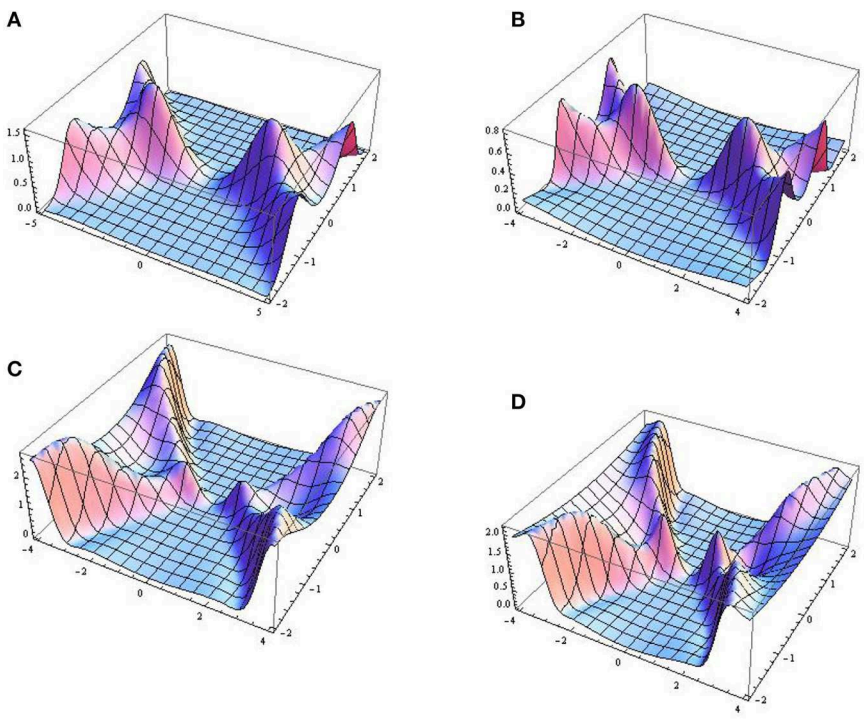

FIGURE 4 | 3D graphical representations of second-order rogue waves. These are constructed with **(A)** $b = 0.9, \delta_0(t) = 0.001t$ and $\alpha = 5\tan^2(0.05t)$, **(B)** $b = 0.9, \delta_0(t) = 0.001t$ and $\alpha = 5\tan^2(0.05t)$, **(C)** $\delta(t) = 1.5 + 0.4\cos t, \delta_0(t) = 0.001t$ and $\alpha = 25\tan^2(0.05t)$, and **(D)** $\delta(t) = 1.5 + 0.001\cos t, \delta_0(t) = 0.001t$ and $\alpha = 35\tan^2(0.05t)$.

6. CONCLUSION

This article studies the construction of rogue waves in NLSE with a variable coefficient in the presence of harmonic potential. The graphical demonstration shows that the dynamical behavior of waves under the influence of gravity and magnetic fields in linear potential. It is observed that in the presence of GF, the density remains constant, while peak height and width remain invariant. The obtained solutions are of first and second order and are constructed using the ST approach. Moreover, the MI is calculated and is significantly affected by incident optical power.

AUTHOR CONTRIBUTIONS

All authors listed have made a substantial, direct and intellectual contribution to the work, and approved it for publication.

REFERENCES

1. Akhmediev N, Ankiewicz A, Soto CJM, Rogue waves and rational solutions of the nonlinear Schrödinger equation. *Phys Rev E.* (2009) **80**:026601. doi: 10.1103/PhysRevE.80.026601
2. Ali S, Younis M, Ahmad MO, Rizvi STR. Rogue wave solutions in nonlinear optics with coupled Schrdinger equations. *Opt Quant Electr.* (2018) **50**:266. doi: 10.1007/s11082-018-1526-9
3. Younas B, Younis M, Ahmed MO, Rizvi STR. Exact optical solitons in (n + 1)-dimensions under anti-cubic law of nonlinearity. *Optik.* (2018) **156**:479–86. doi: 10.1016/j.ijleo.2017.11.148
4. Seadawy AR. Nonlinear wave solutions of the three-dimensional Zakharov-Kuznetsov-Burgers equation in dusty plasma. *Physica A.* (2015) **439**:124–31. doi: 10.1016/j.physa.2015.07.025
5. Seadawy AR. Three-dimensional nonlinear modified Zakharov-Kuznetsov equation of ion-acoustic waves in a magnetized plasma. *Comput Math Appl.* (2016) **71**:201–12. doi: 10.1016/j.camwa.2015.11.006
6. Seadawy AR, Two-dimensional interaction of a shear flow with a free surface in a stratified fluid and its solitary-wave solutions via mathematical methods. *Eur Phys J Plus.* (2017) **132**:518. doi: 10.1140/epjp/i2017-11755-6
7. Seadawy AR. Three-dimensional weakly nonlinear shallow water waves regime and its traveling wave solutions. *Int J Comput Methods.* (2018) **15**:1850017. doi: 10.1142/S0219876218500172
8. Zabusky NJ, Galvin CJ. Shallow-waterwaves, the korteweg-de-vries equation and solitons. *J. Fluid Mech.* (1971) **47**:811–24. doi: 10.1017/S0022112071001393
9. Seadawy AR, Rashidy KE, Nonlinear Rayleigh–Taylor instability of the cylindrical fluid flow with mass and heat transfer. *Pramana J Phys.* (2016) **87**:20. doi: 10.1007/s12043-016-1222-x
10. Seadawy AR. Stability analysis solutions for nonlinear three-dimensional modified Korteweg-de Vries-Zakharov-Kuznetsov equation in a magnetized electron-positron plasma. *Physica A.* (2016) **455**:44–51. doi: 10.1016/j.physa.2016.02.061
11. Seadawy AR. Ion acoustic solitary wave solutions of two-dimensional nonlinear Kadomtsev-Petviashvili-Burgers equation in quantum plasma. *Math Methods Appl Sci.* (2017) **40**:1598–607. doi: 10.1002/mma.4081
12. Seadawy AR, Alamri SZ. Mathematical methods via the nonlinear two-dimensional water waves of Olver dynamical equation and its exact solitary wave solutions. *Results Phys.* (2018) **8**:286–91. doi: 10.1016/j.rinp.2017.12.008
13. Seadawy AR. Solitary wave solutions of two-dimensional nonlinear Kadomtsev-Petviashvili dynamic equation in dust-acoustic plasmas. *Pramana J Phys.* (2017) **89**:1–11. doi: 10.1007/s12043-017-1446-4
14. Seadawy AR. Stability analysis for Zakharov-Kuznetsov equation of weakly nonlinear ion-acoustic waves in a plasma. *Comput Math Appl.* (2014) **67**:172–80. doi: 10.1016/j.camwa.2013.11.001
15. Seadawy AR. Stability analysis for two-dimensional ion-acoustic waves in quantum plasmas. *Phys Plasmas.* (2014) **21**:052107. doi: 10.1063/1.4875987
16. Ali S, Rizvi STR, Younis M. Traveling wave solutions for nonlinear dispersive water wave systems with time dependent coefficients. *Nonliner Dyn.* (2015) **82**:1755–62. doi: 10.1007/s11071-015-2274-z
17. Yue WY, Qing DC. Spatiotemporal Rogue Waves for the Variable-Coefficient (3 + 1)-dimensional nonlinear Schrödinger equation. *Commun Theor Phys.* (2012) **58**:255–60. doi: 10.1088/0253-6102/58/2/15
18. Cheemaa N, Younis M. New and more general traveling wave solutions for nonlinear Schrdinger equation. *Waves Random Comp Media.* (2016) **26**:30–41. doi: 10.1080/17455030.2015.1099761
19. Wang XB, Tian SF, Qin CY, Zhang TT. Dynamics of the breathers, rogue waves and solitary waves in the (2+1)-dimensional Ito equation. *Appl Math Lett.* (2017) **68**:40–7. doi: 10.1016/j.aml.2016.12.009
20. Feng LL, Tian SF, Wang XB, Zhang TT. Rogue waves, homoclinic breather waves and soliton waves for the (2+1)-dimensional B-type Kadomtsev-Petviashvili equation. *Appl Math Lett.* (2017) **65**:90–7.
21. Younis M, Rizvi STR, Ali S. Analytical and soliton solutions: nonlinear model of nanobioelectronics transmission lines. *Appl Math Comput.* (2015) **265**:994–1002. doi: 10.1016/j.amc.2015.05.121
22. Rizvi STR, Ali K, Bashir S, Younis M, Ashraf R, Ahmad MO. Exact soliton of (2+1)-dimensional fractional Schrödinger equation. *Superlatt Microstruct.* (2017) **107**:234–9. doi: 10.1016/j.spmi.2017.04.029
23. Xia T, Chen X, Chen D. Darboux transformation and soliton-like solutions of nonlinear Schrödinger equations. *Chaos Soltons Fract.* (2005) **26**:889–96. doi: 10.1016/j.chaos.2005.01.030
24. Wang XB, Tian SF, Qin CY, Zhang TT. Characteristics of the breathers, rogue waves and solitary waves in a generalized (2+1)-dimensional Boussinesq equation. *Europhys Lett.* (2016) **115**:10002. doi: 10.1209/0295-5075/115/10002
25. Agrawal GP, Baldeck PL, Alfano RR. Modulation instability induced by cross-phase modulation in optical fibers. *Phys Rev A.* (1989) **39**:3406–413. doi: 10.1103/PhysRevA.39.3406
26. Tchier F, Yusuf A, Aliyu AI, Inc M. Soliton solutions and conservation laws for lossy nonlinear transmission line equation. *Superlatt Microstruct.* (2017) **107**:320–36. doi: 10.1016/j.spmi.2017.04.003
27. Inc M, Yusuf A, Aliyu AI, Baleanu D. Fractional optical solitons for the conformable space-time nonlinear Schro-dinger equation with Kerr law nonlinearity. *Opt Quant Elect.* (2018) **50**:139. doi: 10.1007/s11082-018-1410-7
28. Inc M, Yusuf A, Aliyu AI, Hashemi MS. Soliton solutions, stability analysis and conservation laws for the brusselator reaction diffusion model with time- and constant-dependent coefficients. *Eur Phys J Plus.* (2017) **133**:168. doi: 10.1140/epjp/i2018-11989-8
29. Yusuf A, Inc M, Bayram M. Invariant and simulation analysis to the time fractional Abrahams- Tsuneto reaction diffusion system. *Phys Script.* (2019) **94**:125005. doi: 10.1088/1402-4896/ab373b
30. Yusuf A, Inc M, Baleanu D. Optical solitons with M-truncated and beta derivatives in nonlinear optics. *Front Phys.* (2019) **7**:126. doi: 10.3389/fphy.2019.00126
31. Inc M, Aliyu AI, Yusuf A, Baleanu D. Optical solitary waves, conservation laws and modulation instability analysis to the nonlinear Schrödingers equation in compressional dispersive Alven waves. *Optik.* (2017) **155**:257–66. doi: 10.1016/j.ijleo.2017.10.109
32. Inc M, Aliyu AI, Yusuf A, Baleanu D. Dispersive optical solitons and modulation instability analysis of Schrödinger-Hirota equation

with spatio-temporal dispersion and Kerr law nonlinearity. *Superlatt Microstruct.* (2018) **113**:319–27. doi: 10.1016/j.spmi.2017.11.010

33. Yan ZY. *Constructive Theory and Applications of Complex Nonlinear Waves*. Beijing: Science Press (2007).
34. Inc M, Aliyu AI, Yusuf A, Baleanu D. Novel optical solitary waves and modulation instability analysis for the coupled nonlinear Schröodinger equation in monomode step-index optical fibers. *Superlatt Microstruct.* (2018) **113**:745–53. doi: 10.1016/j.spmi.2017.12.010

Conflict of Interest: The authors declare that the research was conducted in the absence of any commercial or financial relationships that could be construed as a potential conflict of interest.

frontiers in Physics

ORIGINAL RESEARCH
published: 28 February 2020
doi: 10.3389/fphy.2020.00033

Generalized Mittag-Leffler Type Function: Fractional Integrations and Application to Fractional Kinetic Equations

*Kottakkaran Sooppy Nisar**

Department of Mathematics, College of Arts and Sciences, Prince Sattam Bin Abdulaziz University, Wadi Aldawaser, Saudi Arabia

The generalized fractional integrations of the generalized Mittag-Leffler type function (GMLTF) are established in this paper. The results derived in this paper generalize many results available in the literature and are capable of generating several applications in the theory of special functions. The solutions of a generalized fractional kinetic equation using the Sumudu transform is also derived and studied as an application of the GMLTF.

Keywords: The Mittag-Leffler type function, fractional calculus, fractional kinetic equations; MSC [2000]: 33C05; 33C20; 33E12; 26A33; 44A20; 35Qxx, riemam-liouville derivative, special function

OPEN ACCESS

Edited by:
Devendra Kumar,
University of Rajasthan, India

Reviewed by:
Haci Mehmet Baskonus,
Harran University, Turkey
Yudhveer Singh,
Amity University Jaipur, India

***Correspondence:**
Kottakkaran Sooppy Nisar
n.sooppy@psau.edu.sa

Specialty section:
This article was submitted to Mathematical Physics, a section of the journal Frontiers in Physics

Received: *21 December 2019*
Accepted: *05 February 2020*
Published: *28 February 2020*

Citation:
Nisar KS (2020) Generalized Mittag-Leffler Type Function: Fractional Integrations and Application to Fractional Kinetic Equations. Front. Phys. 8:33. doi: 10.3389/fphy.2020.00033

1. INTRODUCTION

The Pochhammer symbol $(\varpi)_n$ is defined by (for $\varpi \in \mathbb{C}$)[see ([1], p. 2 and p. 5)]:

$$(\varpi)_n := \begin{cases} 1 & (n=0) \\ \varpi(\varpi+1)\dots(\varpi+n-1) & (n \in \mathbb{N}) \end{cases} = \frac{\Gamma(\varpi+n)}{\Gamma(\varpi)} \quad (\varpi \in \mathbb{C} \setminus \mathbb{Z}_0^-). \tag{1}$$

The familiar generalized hypergeometric function ${}_pF_q$ is defined as follows (see [2]):

$${}_pF_q\left[\begin{matrix}(\varpi_p);\\(\chi_q);\end{matrix} x\right] = \sum_{n=0}^{\infty} \frac{\Pi_{j=1}^{p}(\varpi_j)_n}{\Pi_{j=1}^{q}(\chi_j)_n} \frac{x^n}{n!}, \tag{2}$$

$$(p \le q, x \in \mathbb{C}; p = q+1, |x| < 1),$$

where $(\varpi_j)_n$ and $(\chi_j)_n$ given in (1) and χ_i can not be a negative integer or zero. Here p or q or both are permitted to be zero. For all finite x, the series (2) is absolutely convergent if $p \le q$ and for $|x| < 1$ if $p = q+1$. When $p > q+1$, then the series diverge for $x \neq 0$ and the series does not terminate.

In particular, if $p = 2$ and $q = 1$, (2) reduces to the Gaussian hypergeometric function

$${}_2F_1(\varpi_1, \varpi_2; \varpi_3; x) = \sum_{k=0}^{\infty} \frac{(\varpi_1)_n(\varpi_2)_n}{(\varpi_3)_n} \frac{x^n}{n!}. \tag{3}$$

The function ${}_r\Psi_s(z)$ is the generalized Wright hypergeometric series which is given by

$$ {}_r\Psi_s(z) = {}_r\Psi_s\left[\begin{matrix}(\mathfrak{a}_i, \varpi_i)_{1,r}\\(\mathfrak{b}_j, \chi_j)_{1,s}\end{matrix}\middle| z\right] = \sum_{k=0}^{\infty} \frac{\prod_{i=1}^{r}\Gamma(\mathfrak{a}_i + \varpi_i k)}{\prod_{j=1}^{s}\Gamma(\mathfrak{b}_j + \chi_j k)}\frac{z^k}{k!}, \quad (4) $$

where $\mathfrak{a}_i, \mathfrak{b}_j \in \mathbb{C}$, and real $\varpi_i, \chi_j \in \mathbb{R}$ $(i = 1, 2, \ldots, r; j = 1, 2, \ldots, s)$. The asymptotic behavior of (4) for large values of argument of $z \in \mathbb{C}$ were mentioned in [3, 4] (also, see [5, 6]).

To proceed our study, we need the definitions of the Mittag-Leffler functions (MLF) denoted by $E_{\varpi}(z)$ (see [7]) and $E_{\varpi,\chi}(x)$ [8], respectively:

$$ E_{\varpi}(x) = \sum_{n=0}^{\infty} \frac{x^n}{\Gamma(\varpi n + 1)} \quad (x, \varpi \in \mathbb{C}; |x| < 0, \Re(\varpi) > 0). \quad (5) $$

$$ E_{\varpi,\chi}(x) = \sum_{n=0}^{\infty} \frac{x^n}{\Gamma(\varpi n + \chi)} \quad (x, \varpi, \chi \in \mathbb{C}; \Re(\varpi) > 0, \Re(\chi) > 0). \quad (6) $$

Many more generalizations and extensions of MLF widely studied recently [9, 10]. Also, the MLF performs an important role in physics and engineering problems. The derivations of physical problems of exponential nature could be governed by the physical laws through the MLF (power-law) [11–13].

Very recently, Nisar [14] defined a generalized Mittag-Leffler type function which is defined as follows

For $\rho, \sigma, \varsigma \in \mathbb{C}, \Re(\kappa) > 0, \delta \neq 0, -1, -2, \cdots, (\kappa)_s$ and $(\omega)_s$ denotes the Pochammer symbol.

$$ {}_p\mathsf{E}_{q;\delta}^{\rho,\sigma;\varsigma}(z) = {}_p\mathsf{E}_{q,\delta}^{\rho,\sigma,\varsigma}\left(\kappa_1, \kappa_2, \cdots, \kappa_p; \omega_1, \omega_2, \cdots, \omega_q; z\right) = \sum_{s=0}^{\infty} \frac{(\kappa_1)_s (\kappa_2)_s \cdots (\kappa_p)_s}{(\omega_1)_s (\omega_2)_s \cdots (\omega_q)_s} \frac{(\varsigma)_s z^s}{(\delta)_s \Gamma(\rho s + \sigma)}. \quad (7) $$

By assuming particular values for various parameters in (7), we get many of the popular functions in the literature. For example, ${}_p\mathsf{E}_{q;1}^{\rho,\sigma;\varsigma}(z)$ gives the $K-$ function [15] and ${}_0\mathsf{E}_{0;1}^{\rho,\sigma;\varsigma}(z)$ turns to $E_{\rho,\sigma}^{\varsigma}(z)$ [16]. Also, ${}_0\mathsf{E}_{0;\delta}^{\rho,\sigma;\varsigma}(z)$ reduces to $E_{\rho,\sigma}^{\varsigma,\delta}(z)$ [17] and ${}_0\mathsf{E}_{0;1}^{\rho,\sigma;1}(z)$ gives the Mittag-Leffler function $E_{\rho,\sigma}(z)$ [8]. Similar way, ${}_0\mathsf{E}_{0;1}^{\rho,1;1}(z)$ turns to the Mittag-Leffler functions $E_{\rho}(z)$ [7]. For more details one can be referred to Nisar [14].

2. GENERALIZED FRACTIONAL INTEGRATION OF GMLTF

Fractional calculus is one of the prominent branch of applied mathematics that deals with non-integer order derivatives and integrals (including complex orders), and their applications in almost all disciplines of science and engineering [18–22]. In this line, the use of special functions in connection with fractional calculus also studied widely [23–27]. For the basics of fractional calculus and its related literature, interesting readers can be referred to as Kiryakova [28], Miller and Ross [29], and Srivastava et al. [30]. In this paper, we studied the generalized fractional calculus of more generalized function given in (7). The generalized fractional integral operators (FIOs) involving the Appell functions F_3 are given for $\varpi, \varpi', \tau, \tau', \epsilon \in \mathbb{C}$ with $\Re(\epsilon) > 0$ and $x \in \mathbb{R}^+$as follows:

$$ \left(I_{0+}^{\varpi,\varpi',\tau,\tau',\epsilon} f\right)(x) = \frac{x^{-\varpi}}{\Gamma(\epsilon)} \int_0^x (x-t)^{\epsilon-1} t^{-\varpi'} F_3\left(\varpi, \varpi', \tau, \tau'; \epsilon; 1 - \frac{t}{x}, 1 - \frac{x}{t}\right) f(t)\, \mathrm{d}t \quad (8) $$

and

$$ \left(I_{-}^{\varpi,\varpi',\tau,\tau',\epsilon} f\right)(x) = \frac{x^{-\varpi'}}{\Gamma(\epsilon)} \int_x^{\infty} (t-x)^{\epsilon-1} t^{-\varpi} F_3\left(\varpi, \varpi', \tau, \tau'; \epsilon; 1 - \frac{t}{x}, 1 - \frac{x}{t}\right) f(t)\, \mathrm{d}t. \quad (9) $$

The integral operators of the types (8) and (9) have been introduced by Marichev [31] and later extended and studied by Saigo and Maeda [32]. Recently, many researchers (see [33–35]) have studied the image formulas for MSM FIOs involving various special functions.

The corresponding fractional differential operators (FDOs) have their respective forms:

$$ \left(D_{0+}^{\varpi,\varpi',\tau,\tau',\epsilon} f\right)(x) = \left(\frac{\mathrm{d}}{\mathrm{d}x}\right)^{[\Re(\epsilon)]+1} \left(I_{0+}^{-\varpi',-\varpi,-\tau'+[\Re(\epsilon)]+1,-\tau,-\epsilon+[\Re(\epsilon)]+1} f\right)(x) \quad (10) $$

and

$$ \left(D_{-}^{\varpi,\varpi',\tau,\tau',\epsilon} f\right)(x) = \left(-\frac{\mathrm{d}}{\mathrm{d}x}\right)^{[\Re(\epsilon)]+1} \left(I_{-}^{-\varpi',-\varpi,-\tau',-\tau+[\Re(\epsilon)]+1,-\epsilon+[\Re(\epsilon)]+1} f\right)(x). \quad (11) $$

Here, we recall the following results (see [32, 36]).

LEMMA 2.1. *Let* $\varpi, \varpi', \tau, \tau', \epsilon, \sigma \in \mathbb{C}$ *be such that* $\Re(\epsilon) > 0$ *and*

$$ \Re(\sigma) > \max\{0, \Re(\varpi + \varpi' + \tau - \epsilon), \Re(\varpi' - \tau')\}. $$

Then there exists the relation

$$ \left(I_{0+}^{\varpi,\varpi',\tau,\tau',\epsilon}\, t^{\sigma-1}\right)(x) = \frac{\Gamma(\sigma)\Gamma\left(\sigma + \epsilon - \varpi - \varpi' - \tau\right)}{\Gamma\left(\sigma + \tau' - \varpi'\right)} \frac{\Gamma\left(\sigma + \tau' - \varpi'\right)}{\Gamma\left(\sigma + \tau'\right)\Gamma\left(\sigma + \epsilon - \varpi - \varpi'\right)} \frac{\Gamma\left(\sigma + \epsilon - \varpi' - \tau\right)}{} x^{\sigma-\varpi-\varpi'+\epsilon-1}. \quad (12) $$

LEMMA 2.2. *Let* $\varpi, \varpi', \tau, \tau', \epsilon, \sigma \in \mathbb{C}$ *such that* $\Re(\epsilon) > 0$ *and*

$$ \Re(\sigma) > \max\{\Re(\tau), \Re(-\varpi - \varpi' + \epsilon), \Re(-\varpi - \tau' + \epsilon)\}. $$

Then

$$\left(I_{-}^{\varpi,\varpi',\tau,\tau',\epsilon}t^{-\sigma}\right)(x) = \frac{\Gamma(-\tau+\sigma)\,\Gamma\left(\varpi+\varpi'-\epsilon+\sigma\right)}{\Gamma\left(\varpi+\tau'-\epsilon+\sigma\right)}\frac{\Gamma\left(\varpi+\varpi'+\tau'-\epsilon+\sigma\right)}{\Gamma(\sigma)\,\Gamma(\varpi-\tau+\sigma)}x^{-\varpi-\varpi'+\epsilon-\sigma}, \quad (13)$$

The main aim of this paper is to apply the generalized operators of fractional calculus for the GMLTF in order to get certain new image formulas.

2.1. Sumudu Transform

The Sumudu transform is widely used to solve various type of problems in science and engineering and it is introduced by Watugala (see [37, 38]). The details of Sumudu transforms, properties, and its applications the interesting readers can be refer to Asiru [39], Belgacem et al. [40], and Bulut et al. [41].

The Sumudu transform over the set functions

$$A=\left\{f(t)\,\middle|\,\exists\, M,\tau_1,\tau_2>0,\left|f(t)\right|<Me^{|t|/\tau_j}\ ,\ \text{if}\ t\in(-1)^j\times[0,\infty)\right\},$$

is defined by

$$G(u)=S\left[f(t);u\right]=\int_0^{\infty}f(ut)\,e^{-t}dt,\ u\in(-\tau_1,\tau_2)\,. \quad (14)$$

The main aim of this study is to establish the generalized fractional calculus operators and the generalized FKEs involving GMLTF.

Theorem 2.1. Let $\eta,\eta',\chi,\chi',\epsilon,\tau,\varpi,\lambda,\gamma\in\mathbb{C},\Re(\kappa)>0,\delta\neq 0,-1,-2,\cdots$, such that $\Re(\tau)>\max\{0,\Re(\eta+\eta'-\chi-\epsilon),\Re(\eta'-\chi')\}$. Then

$$\left(I_{0+}^{\eta,\eta',\chi,\chi',\epsilon}t^{\tau-1}\,{}_pE_{q;\delta}^{\varpi,\lambda;\gamma}(t)\right)(x) = \frac{\Gamma(\delta)\prod_{j=1}^{q}\Gamma(\omega_j)}{\Gamma(\gamma)\prod_{i=1}^{p}\Gamma(\kappa_i)}x^{\tau-\eta-\eta'+\epsilon-1}\times{}_{p+5}\Psi_{q+5}\left[\begin{matrix}(\kappa_i,1)_{1,p},(\gamma,1),(\tau,1),(\tau+\epsilon-\eta-\eta'-\chi,1),\\(\tau+\chi'-\eta',1),(1,1)\\(\omega_j,1)_{1,q},(\delta,1),(\gamma,\varpi),(\tau+\chi',1),(\tau+\epsilon-\eta-\eta',1),\\(\tau+\epsilon-\eta'-\chi,1)\end{matrix}\,\middle|\,x\right].$$

Proof: Applying the definition (7) on the left hand side (l.h.s) of Theorem 2.1,

$$\mathfrak{I}_1=\left(I_{0+}^{\eta,\eta',\chi,\chi',\epsilon}t^{\tau-1}\,{}_pE_{q;\delta}^{\varpi,\lambda;\gamma}(t)\right)(x) = \left(I_{0+}^{\eta,\eta',\chi,\chi',\epsilon}t^{\tau-1}\sum_{r=0}^{\infty}\frac{(\kappa_1)_r\,(\kappa_2)_r\cdots\left(\kappa_p\right)_r}{(\omega_1)_r\,(\omega_2)_r\cdots,\left(\omega_q\right)_r}\frac{(\gamma)_r\,t^r}{(\delta)_r\,\Gamma(\varpi r+\lambda)}\right)(x)$$

Changing the order of integration and summation gives

$$\mathfrak{I}_1=\sum_{r=0}^{\infty}\frac{(\kappa_1)_r\,(\kappa_2)_r\cdots\left(\kappa_p\right)_r}{(\omega_1)_r\,(\omega_2)_r\cdots\left(\omega_q\right)_r}\frac{(\gamma)_r}{(\delta)_r\,\Gamma(\varpi r+\lambda)}\left(I_{0+}^{\eta,\eta',\chi,\chi',\epsilon}t^{\tau+r-1}\right)(x)$$

Applying Lemma 2.1, we get

$$\mathfrak{I}_1=\sum_{r=0}^{\infty}\frac{(\kappa_1)_r\,(\kappa_2)_r\cdots\left(\kappa_p\right)_r}{(\omega_1)_r\,(\omega_2)_r\cdots\left(\omega_q\right)_r}\frac{(\gamma)_r}{(\delta)_r\,\Gamma(\varpi r+\lambda)} \times\frac{\Gamma(\tau+r)}{\Gamma(\tau+r+\epsilon-\eta-\eta'-\chi)\Gamma(\tau+r+\chi'-\eta')}{(\Gamma(\tau+r+\chi')\Gamma(\tau+r+\epsilon-\eta-\eta')}x^{\tau+r-\eta-\eta'+\epsilon-1}.$$

Using $\Gamma(x+\kappa)=(x)_k\Gamma(x)$, we have

$$\mathfrak{I}_1=x^{\tau-\eta-\eta'+\epsilon-1}\frac{\Gamma(\delta)\prod_{j=1}^{q}\Gamma(\omega_j)}{\Gamma(\gamma)\prod_{i=1}^{p}\Gamma(\kappa_i)}\sum_{r=0}^{\infty}\frac{\prod_{i=1}^{p}\Gamma(\kappa_i+r)}{\prod_{j=1}^{q}\Gamma(\omega_j+r)} \times x^r\frac{\Gamma(\gamma+r)\Gamma(\tau+r)\Gamma(\tau+r+\epsilon-\eta-\eta'-\chi)}{\Gamma(\tau+r+\chi'-\eta')\Gamma(1+r)}{\Gamma(1+r)\Gamma(\delta+r)\Gamma(\varpi r+\lambda)\Gamma(\tau+\chi'+r)} \frac{\Gamma(\tau+\epsilon+r-\eta-\eta')}{\Gamma(\tau+\epsilon+r-\eta'-\chi)}$$

In view of (4), we reached the required result. □

Theorem 2.2. Let $\eta,\eta',\chi,\chi',\epsilon,\tau,\varpi,\lambda,\gamma\in\mathbb{C},\Re(\kappa)>0,\delta\neq 0,-1,-2,\cdots$, such that $\Re(\tau)>\max\{\Re(\chi),\Re(-\eta-\eta'+\epsilon),\Re(-\eta-\chi'+\epsilon)\}$. Then

$$\left(I_{-}^{\eta,\eta',\chi,\chi',\epsilon}t^{-\tau}\,{}_pE_{q;\delta}^{\varpi,\lambda;\gamma}(\frac{1}{t})\right)(x) = \frac{\Gamma(\delta)\prod_{j=1}^{q}\Gamma(\omega_j)}{\Gamma(\gamma)\prod_{i=1}^{p}\Gamma(\kappa_i)}x^{-\eta-\eta'+\epsilon-\tau} \times{}_{p+5}\Psi_{q+5}\left[\begin{matrix}(\kappa_i,1)_{1,p},(\gamma,1),(-\chi+\tau,1),\\(\eta+\eta'-\epsilon+\tau,1),(\eta+\chi'-\epsilon+\tau,1),(1,1)\\(\omega_j,1)_{1,q},(\delta,1),(\lambda,\varpi),(\tau,1),\\(\eta-\chi+\tau,1),(\eta+\eta'+\chi'-\epsilon+\tau,1)\end{matrix}\,\middle|\,x\right].$$

Proof: Applying the definition (7) on the left hand side (l.h.s) of Theorem 2.2,

$$\mathfrak{I}_2=\left(I_{-}^{\eta,\eta',\chi,\chi',\epsilon}t^{-\tau}\,{}_pE_{q;\delta}^{\varpi,\lambda;\gamma}(\frac{1}{t})\right)(x) = \left(I_{-}^{\eta,\eta',\chi,\chi',\epsilon}t^{-\tau}\sum_{r=0}^{\infty}\frac{(\kappa_1)_r\,(\kappa_2)_r\cdots\left(\kappa_p\right)_r}{(\omega_1)_r\,(\omega_2)_r\cdots\left(\omega_q\right)_r}\frac{(\gamma)_r\,t^r}{(\delta)_r\,\Gamma(\varpi r+\lambda)}\right)(x)$$

Changing the order of integration and summation gives

$$\mathfrak{I}_2=\sum_{r=0}^{\infty}\frac{(\kappa_1)_r\,(\kappa_2)_r\cdots\left(\kappa_p\right)_r}{(\omega_1)_r\,(\omega_2)_r\cdots\left(\omega_q\right)_r}\frac{(\gamma)_r}{(\delta)_r\,\Gamma(\varpi r+\lambda)}\left(I_{-}^{\eta,\eta',\chi,\chi',\epsilon}t^{-\tau-r}\right)(x)$$

Applying Lemma 2.2, we get

$$\mathfrak{I}_2 = \sum_{r=0}^{\infty} \frac{(\kappa_1)_r (\kappa_2)_r \cdots (\kappa_p)_r}{(\omega_1)_r (\omega_2)_r \cdots (\omega_q)_r} \frac{(\gamma)_r}{(\delta)_r \Gamma(\varpi r + \lambda)} \times \frac{\Gamma(-\chi + \tau + r)\Gamma(\eta + \eta' - \epsilon + \tau + r)}{\Gamma(\eta + \chi' - \epsilon + \tau + r)} \frac{\Gamma(\eta + \chi' - \epsilon + \tau + r)}{\Gamma(\tau + r)\Gamma(\eta - \chi + \tau + r)} x^{-\eta-\eta'+\epsilon-\tau-r}.$$

Using $\Gamma(x + r) = (x)_r \Gamma(x)$, we have

$$\mathfrak{I}_2 = x^{-\eta-\eta'+\epsilon-\tau} \frac{\Gamma(\delta) \prod_{j=1}^{q} \Gamma(\omega_j)}{\Gamma(\gamma) \prod_{i=1}^{p} \Gamma(\kappa_i)} \sum_{r=0}^{\infty} \frac{\prod_{i=1}^{p} \Gamma(\kappa_i + r)}{\prod_{j=1}^{q} \Gamma(\omega_j + r)} \times x^r \frac{\Gamma(\gamma + r)\Gamma(-\chi + \tau + r)\Gamma(\eta + \eta' - \epsilon + \tau + r)}{\Gamma(\delta + r)\Gamma(\varpi r + \lambda)\Gamma(\tau + r)\Gamma(\eta - \chi + \tau + r)} \frac{\Gamma(\eta + \chi' - \epsilon + \tau + r)}{\Gamma(\eta + \eta' + \chi' - \epsilon + \tau + r)}$$

In view of (4), we reached the required result. □

The following corollaries can derive immediately from Theorems 2.1 and 2.2 with the help of Pochhammer symbol

Corollary 2.1. *Let $\delta = \lambda = 1$ in Theorem 2.1, we get*

$$\left(I_{0+}^{\eta,\eta',\chi,\chi',\epsilon} t^{\tau-1} {}_p\mathrm{E}_{q;\delta}^{\varpi,\lambda;\gamma}(t)\right)(x) = \frac{\Gamma(\tau)\Gamma(\tau + \epsilon - \eta - \eta' - \chi)\Gamma(\tau + \chi' - \eta')}{\Gamma(\tau + \chi')\Gamma(\tau + \epsilon - \eta - \eta')} x^{\tau-\eta-\eta'+\epsilon-1} \frac{\Gamma(\tau + \epsilon - \eta' - \chi)\Gamma(\gamma)}{\times {}_{p+4}F_{q+4}\left[\begin{matrix}(\kappa_i, 1)_{1,p}, \nu, \tau, \tau + \epsilon - \eta - \eta' - \chi, \\ \tau + \chi' - \eta'; \\ (\omega_j, 1)_{1,q}, \lambda, \tau + \chi', \tau + \epsilon - \eta - \eta', \\ \tau + \epsilon - \eta' - \chi;\end{matrix}\middle| x\right].}$$

Corollary 2.2. *If $\delta = \lambda = 1$ in Theorem 2.2, then*

$$\left(I_{-}^{\eta,\eta',\chi,\chi',\epsilon} t^{\tau-1} {}_p\mathrm{E}_{q;\delta}^{\varpi,\lambda;\gamma}(\frac{1}{t})\right)(x) = \frac{\Gamma(\tau - \chi)\Gamma(\eta + \eta' - \epsilon + \tau)}{\Gamma(\tau)\Gamma(\eta - \chi + \tau)\Gamma(\eta + \eta' + \chi - \epsilon + \tau)} x^{-\tau-\eta-\eta'+\epsilon-1} \frac{\Gamma(\eta + \chi' - \epsilon + \tau)}{\Gamma(\gamma)} \times {}_{p+4}F_{q+4}\left[\begin{matrix}(\kappa_i, 1)_{1,p}, \gamma, \tau - \chi, \eta + \eta' - \epsilon + \tau, \eta + \chi' \\ -\epsilon + \tau; \\ (\omega_j, 1)_{1,q}, \lambda, \tau, \eta - \chi + \tau, \eta + \eta' \\ -\epsilon + \tau;\end{matrix}\middle| x\right].$$

In the next section, we derived the generalized FKEs and we consider the Sumudu transform methodology to achieve the results.

3. GENERALIZED FRACTIONAL KINETIC EQUATIONS INVOLVING GMLTF

The generalized fractional kinetic equations (FKEs) involving the GMLTF with the Sumudu transform is derived in this section. The FKEs are studied widely in many papers [42–45].

Let $\mathfrak{K} = (\mathfrak{K}_t)$ be the arbitrary reaction defined by a time-dependent quantity. The destruction $\mathfrak{d}$ and production $\mathfrak{p}$ depend on the quantity $\mathfrak{K}$ itself: $\mathfrak{d} = \mathfrak{d}(\mathfrak{K})$ or $\mathfrak{p} = \mathfrak{p}(\mathfrak{K})$ [see [42]]. The fractional differential equation can be expressed by

$$\frac{d\mathfrak{K}}{dt} = -\mathfrak{d}(\mathfrak{K}_t) + \mathfrak{p}(\mathfrak{K}_t), \tag{15}$$

where $\mathfrak{K}_t$ described by $\mathfrak{K}_t(t^*) = \mathfrak{K}(t - t^*), t^* > 0$ (see, [42]). A special case of (15) is

$$\frac{d\mathfrak{K}_i}{dt} = -\mathfrak{c}_i \mathfrak{K}_i(t), \tag{16}$$

with $\mathfrak{K}_i(t = 0) = \mathfrak{K}_0$, $\mathfrak{c}_i > 0$ and the solution of (16) is

$$\mathfrak{K}_i(t) = \mathfrak{K}_0 e^{-\mathfrak{c}_i t}. \tag{17}$$

Performing the integration of (16) leads to

$$\mathfrak{K}(t) - \mathfrak{K}_0 = -\mathfrak{c}\, {}_0\mathfrak{D}_t^{-1} \mathfrak{K}(t), \tag{18}$$

where ${}_0\mathfrak{D}_t^{-1}$ is the particular case of Riemann–Liouville (R-L) integral operator and $\mathfrak{c}$ is a constant. The fractional form of (18) is (see [42])

$$\mathfrak{K}(t) - \mathfrak{K}_0 = -\mathfrak{c}^{\mu}\, {}_0\mathfrak{D}_t^{-\mu} \mathfrak{K}(t), \tag{19}$$

where ${}_0\mathfrak{D}_t^{-\mu}$ is given by

$${}_0\mathfrak{D}_t^{-\mu} f(t) = \frac{1}{\Gamma(\mu)} \int_0^t (t - s)^{\mu-1} f(s)\, ds, \Re(\mu) > 0. \tag{20}$$

Theorem 3.1. For $\varpi, \lambda, \gamma \in \mathbb{C}, \delta \neq 0, -1, -2, \cdots, d > 0, \epsilon > 0$ then the solution of

$$\mathfrak{K}(t) - \mathfrak{K}_0\, {}_p\mathsf{E}_{q;\delta}^{\varpi,\lambda;\gamma}(t) = -d^{\epsilon}\, {}_0\mathfrak{D}_t^{-\epsilon} \mathfrak{K}(t) \tag{21}$$

is given by

$$\mathfrak{K}(t) = \mathfrak{K}_0 \sum_{n=0}^{\infty} \frac{(\kappa_1)_n \ldots (\kappa_p)_n}{(\omega_1)_n \ldots (\omega_q)_n} \frac{(\gamma)_n n!}{(\delta)_n \Gamma(\varpi n + \lambda)} t^{n-1} E_{\epsilon,n}(-d^{\epsilon} t^{\epsilon}) \tag{22}$$

Proof: The Sumudu transform (ST) of the R-L fractional operator is

$$\mathcal{S}\left\{{}_0\mathfrak{D}_t^{\epsilon} g(t); u\right\} = u^{\epsilon} G(u) \tag{23}$$

where $G(u)$ is defined in (14). Now, applying the ST on the both sides of (21) and using (7) and (23), we have

$$\mathcal{S}\{\mathfrak{K}(t); u\} - \mathfrak{K}_0 \mathcal{S}\{{}_p\mathsf{E}_{q;\delta}^{\varpi,\lambda;\gamma}(t); u\} = \mathcal{S}\{-d^{\epsilon}\, {}_0\mathfrak{D}_t^{-\epsilon} \mathfrak{K}(t); u\}, \tag{24}$$

which gives

$$\mathfrak{K}^*(u) = \mathfrak{K}_0\Big(\int_0^\infty e^{-t}\sum_{n=0}^{\infty}\frac{(\kappa_1)_n(\kappa_2)_n\cdots(\kappa_p)_n}{(\omega_1)_n(\omega_2)_n\cdots(\omega_q)_n}\frac{(\gamma)_n(ut)^n}{(\delta)_r\Gamma(\varpi n+\lambda)}dt\Big) - d^\epsilon u^\epsilon \mathfrak{K}*(u), \tag{25}$$

which implies that

$$\mathfrak{K}^*(u)[1+d^\epsilon u^\epsilon] = \mathfrak{K}_0\sum_{n=0}^{\infty}\frac{(\kappa_1)_n(\kappa_2)_n\cdots(\kappa_p)_n}{(\omega_1)_n(\omega_2)_n\cdots(\omega_q)_n}\frac{(\gamma)_n(u)^n}{(\delta)_n\Gamma(\varpi n+\lambda)}\int_0^\infty e^{-t}t^n dt. \tag{26}$$

After some simple calculation, we get

$$\mathfrak{K}^*(u) = \mathfrak{K}_0\sum_{n=0}^{\infty}\frac{(\kappa_1)_n(\kappa_2)_n\cdots(\kappa_p)_n}{(\omega_1)_n(\omega_2)_n\cdots(\omega_q)_n}\frac{(\gamma)_n}{(\delta)_n\Gamma(\varpi n+\lambda)(u^n)n!}\Gamma(n+1)\times\Big\{\sum_{s=0}^{\infty}[(-du)^\epsilon]^s\Big\}. \tag{27}$$

The inverse ST of (27) and using the formula $\mathcal{S}^{-1}\{u^\epsilon;t\} = \frac{t^{\epsilon-1}}{\Gamma(\epsilon)}$, $\Re(\epsilon)>0$ gives

$$\mathfrak{K}(t) = \mathfrak{K}_0\sum_{n=0}^{\infty}\frac{(\kappa_1)_n(\kappa_2)_n\cdots(\kappa_p)_n}{(\omega_1)_n(\omega_2)_n\cdots(\omega_q)_n}\frac{(\gamma)_n}{(\delta)_n\Gamma(\varpi n+\lambda)}\Gamma(n+1)\times\sum_{s=0}^{\infty}(-1)^s d^{\epsilon s}\frac{t^{\epsilon s+n-1}}{\Gamma(\epsilon s+n)}. \tag{28}$$

In view of the Mittag-Leffler function definition, we arrived the needful result. □

Theorem 3.2. For $\varpi,\lambda,\gamma\in\mathbb{C},\delta\neq 0,-1,-2,\cdots,d>0,\epsilon>0$ then the equation

$$\mathfrak{K}(t) - \mathfrak{K}_0{}_p\mathsf{E}_{q;\delta}^{\varpi,\lambda;\gamma}\left(d^\epsilon t^\epsilon\right) = -d^\epsilon{}_0\mathfrak{D}_t^{-\epsilon}\mathfrak{K}(t) \tag{29}$$

have the following solution

$$\mathfrak{K}(t) = \mathfrak{K}_0\sum_{n=0}^{\infty}\frac{(\kappa_1)_n\ldots(\kappa_p)_n}{(\omega_1)_n\ldots(\omega_q)_n}\frac{(\gamma)_n\Gamma(\epsilon n+1)}{(\delta)_n\Gamma(\varpi n+\lambda)}(d)^{\epsilon n}t^{n-1}E_{\epsilon,n}(-d^\epsilon t^\epsilon) \tag{30}$$

Proof: Applying the Sumudu transform on the both sides of (29)

$$\mathcal{S}\{\mathfrak{K}(t);u\} - \mathfrak{K}_0\mathcal{S}\{{}_p\mathsf{E}_{q;\delta}^{\varpi,\lambda;\gamma}\left(d^\epsilon t^\epsilon\right);u\} = \mathcal{S}\{-d^\epsilon{}_0\mathfrak{D}_t^{-\epsilon}\mathfrak{K}(t);u\}, \tag{31}$$

and using (7) and (23), we get

$$\mathfrak{K}^*(u) = \mathfrak{K}_0\Big(\int_0^\infty e^{-t}\sum_{n=0}^{\infty}\frac{(\kappa_1)_n(\kappa_2)_n\cdots(\kappa_p)_n}{(\omega_1)_n(\omega_2)_n\cdots(\omega_q)_n}\frac{(\gamma)_n(ud^\epsilon t^\epsilon)^n}{(\delta)_n\Gamma(\varpi n+\lambda)}dt\Big) - d^\epsilon u^\epsilon\mathfrak{K}(u), \tag{32}$$

which gives

$$\mathfrak{K}(u)[1+d^\epsilon u^\epsilon] = \mathfrak{K}_0\sum_{n=0}^{\infty}\frac{(\kappa_1)_n(\kappa_2)_n\cdots(\kappa_p)_n}{(\omega_1)_n(\omega_2)_n\cdots(\omega_q)_n}\frac{(\gamma)_n u^n d^{\epsilon n}}{(\delta)_n\Gamma(\varpi n+\lambda)}\int_0^\infty e^{-t}t^{\epsilon n}dt, \tag{33}$$

which can be simplified as

$$\mathfrak{K}(u) = \mathfrak{K}_0\sum_{n=0}^{\infty}\frac{(\kappa_1)_n(\kappa_2)_n\cdots(\kappa_p)_n}{(\omega_1)_n(\omega_2)_n\cdots(\omega_q)_n}\frac{(\gamma)_n d^{\epsilon n}}{(\delta)_n\Gamma(\varpi n+\lambda)}\Gamma(\epsilon n+1)\times\Big\{u^n d^{\epsilon n}\sum_{s=0}^{\infty}[(-du)^\epsilon]^s\Big\}. \tag{34}$$

Taking the Sumudu inverse of (34) and using $\mathcal{S}^{-1}\{u^\vartheta;t\} = \frac{t^{\vartheta-1}}{\Gamma(\vartheta)}$, we get

$$\mathfrak{K}(t) = \mathfrak{K}_0\sum_{n=0}^{\infty}\frac{(\kappa_1)_n(\kappa_2)_n\cdots(\kappa_p)_n}{(\omega_1)_n(\omega_2)_n\cdots(\omega_q)_n}\frac{(\gamma)_n d^{\epsilon n}t^{n-1}}{(\delta)_n\Gamma(\varpi n+\lambda)}\Gamma(\epsilon n+1)\times\sum_{s=0}^{\infty}(-1)^s d^{\epsilon s}\frac{t^{\epsilon s}}{\Gamma(\epsilon s+1)}. \tag{35}$$

In view of the definition of the Mittag-Leffler function, we get the required result. □

Theorem 3.3. For $\varpi,\lambda,\gamma\in\mathbb{C},\delta\neq 0,-1,-2,\cdots,d>0,\epsilon>0$ and $a\neq d$ then the equation

$$\mathfrak{K}(t) - \mathfrak{K}_0{}_p\mathsf{E}_{q;\delta}^{\varpi,\lambda;\gamma}\left(d^\epsilon t^\epsilon\right) = -a^\epsilon{}_0\mathfrak{D}_t^{-\epsilon}\mathfrak{K}(t) \tag{36}$$

have the following solution

$$\mathfrak{K}(t) = \mathfrak{K}_0\sum_{n=0}^{\infty}\frac{(\kappa_1)_n\ldots(\kappa_p)_n}{(\omega_1)_n\ldots(\omega_q)_n}\frac{(\gamma)_n\Gamma(\epsilon n+1)}{(\delta)_n\Gamma(\varpi n+\lambda)}(d)^{\epsilon n}t^{n-1}E_{\epsilon,n}(-a^\epsilon t^\epsilon) \tag{37}$$

Proof: Applying the Sumudu transform on the both sides of (36)

$$\mathcal{S}\{\mathfrak{K}(t);u\} - \mathfrak{K}_0\mathcal{S}\{{}_p\mathsf{E}_{q;\delta}^{\varpi,\lambda;\gamma}\left(d^\epsilon t^\epsilon\right);u\} = \mathcal{S}\{-a^\epsilon{}_0\mathfrak{D}_t^{-\epsilon}\mathfrak{K}(t);u\}, \tag{38}$$

and using (7) and (23), we get

$$\mathfrak{K}^*(u) = \mathfrak{K}_0\Big(\int_0^\infty e^{-t}\sum_{n=0}^{\infty}\frac{(\kappa_1)_n(\kappa_2)_n\cdots(\kappa_p)_n}{(\omega_1)_n(\omega_2)_n\cdots(\omega_q)_n}\frac{(\gamma)_n(ud^\epsilon t^\epsilon)^n}{(\delta)_n\Gamma(\varpi n+\lambda)}dt\Big) - a^\epsilon u^\epsilon\mathfrak{K}(u), \tag{39}$$

which gives

$$\mathfrak{K}(\rho)[1+a^\epsilon u^\epsilon]$$

$$= \Re_0 \sum_{n=0}^{\infty} \frac{(\kappa_1)_n (\kappa_2)_n \cdots (\kappa_p)_n}{(\omega_1)_n (\omega_2)_n \cdots (\omega_q)_n} \frac{(\gamma)_n u^n d^{\epsilon n}}{(\delta)_n \Gamma(\varpi n + \lambda)} \int_0^{\infty} e^{-t} t^{\epsilon n} dt, \quad (40)$$

which can be simplified as

$$\Re(u) = \Re_0 \sum_{n=0}^{\infty} \frac{(\kappa_1)_n (\kappa_2)_n \cdots (\kappa_p)_n}{(\omega_1)_n (\omega_2)_n \cdots (\omega_q)_n} \frac{(\gamma)_n d^{\epsilon n}}{(\delta)_n \Gamma(\varpi n + \lambda)} \Gamma(\epsilon n + 1) \times \left\{ u^n d^{\epsilon n} \sum_{s=0}^{\infty} [(-au)^{\epsilon}]^s \right\}. \quad (41)$$

Taking the Sumudu inverse of (41) and using $\mathcal{S}^{-1}\{u^{\vartheta}; t\} = \frac{t^{\vartheta-1}}{\Gamma(\vartheta)}$, we get

$$\Re(t) = \Re_0 \sum_{n=0}^{\infty} \frac{(\kappa_1)_n (\kappa_2)_n \cdots (\kappa_p)_n}{(\omega_1)_n (\omega_2)_n \cdots (\omega_q)_n} \frac{(\gamma)_n d^{\epsilon n} t^{n-1}}{(\delta)_n \Gamma(\varpi n + \lambda)} \Gamma(\epsilon n + 1) \times \sum_{s=0}^{\infty} (-1)^s a^{\epsilon s} \frac{t^{\epsilon s}}{\Gamma(\epsilon s + 1)}. \quad (42)$$

In view of the definition of the Mittag-Leffler function, we get the required result. □

If we take $\delta = 1$ in Theorem 3.1, we get the generalized FKE involving $K-$ function as follows:

Corollary 3.1. *For* $\varpi, \lambda, \gamma \in \mathbb{C}, \delta \neq 0, -1, -2, \cdots, d > 0, \epsilon > 0$ *then*

$$\Re(t) - \Re_0 \, {}_p\mathsf{E}_{q;1}^{\varpi,\lambda;\gamma}(t) = -d^{\epsilon} \, {}_0\mathfrak{D}_t^{-\epsilon} \Re(t) \quad (43)$$

is given by

$$\Re(t) = \Re_0 \sum_{n=0}^{\infty} \frac{(\kappa_1)_n \ldots (\kappa_p)_n}{(\omega_1)_n \ldots (\omega_q)_n} \frac{(\gamma)_n}{\Gamma(\varpi n + \lambda)} t^{n-1} E_{\epsilon,n}(-d^{\epsilon} t^{\epsilon}) \quad (44)$$

If we take $\delta = 1, p = q = 0$ in Theorem 3.1, we have the generalized FKE involving the Prabhakar function:

Corollary 3.2. *For* $\varpi, \lambda, \gamma \in \mathbb{C}, \delta \neq 0, -1, -2, \cdots, d > 0, \epsilon > 0$ *then*

$$\Re(t) - \Re_0 \, {}_0\mathsf{E}_{0;1}^{\varpi,\lambda;\gamma}(t) = -d^{\epsilon} \, {}_0\mathfrak{D}_t^{-\epsilon} \Re(t) \quad (45)$$

is given by

$$\Re(t) = \Re_0 \sum_{n=0}^{\infty} \frac{(\gamma)_n}{\Gamma(\varpi n + \lambda)} t^{n-1} E_{\epsilon,n}(-d^{\epsilon} t^{\epsilon}) \quad (46)$$

If we choose $\delta = 1, p = q = 0$ and $\gamma = 1$ in Theorem 3.1, then the generalized FKE involving the Wiman function:

Corollary 3.3. *For* $\varpi, \lambda \in \mathbb{C}, \delta \neq 0, -1, -2, \cdots, d > 0, \epsilon > 0$ *then*

$$\Re(t) - \Re_0 \, {}_0\mathsf{E}_{0;1}^{\varpi,\lambda;1}(t) = -d^{\epsilon} \, {}_0\mathfrak{D}_t^{-\epsilon} \Re(t) \quad (47)$$

is given by

$$\Re(t) = \Re_0 \sum_{n=0}^{\infty} \frac{1}{\Gamma(\varpi n + \lambda)} t^{n-1} E_{\epsilon,n}(-d^{\epsilon} t^{\epsilon}) \quad (48)$$

If we choose $\delta = 1, p = q = 0$ and $\gamma = 1$ in Theorem 3.1, then we get the generalized FKE involving the Mittag-Leffler function:

Corollary 3.4. *For* $\varpi \in \mathbb{C}, \delta \neq 0, -1, -2, \cdots, d > 0, \epsilon > 0$ *then*

$$\Re(t) - \Re_0 \, {}_0\mathsf{E}_{0;1}^{\varpi,1;1}(t) = -d^{\epsilon} \, {}_0\mathfrak{D}_t^{-\epsilon} \Re(t) \quad (49)$$

is given by

$$\Re(t) = \Re_0 \sum_{n=0}^{\infty} \frac{1}{\Gamma(\varpi n + 1)} t^{n-1} E_{\epsilon,n}(-d^{\epsilon} t^{\epsilon}) \quad (50)$$

Remark 3.1. By choosing the suitable parameters in Theorems 3.2 and 3.3, one can derive the generalized FKEs of GMLTF as similar as above corollaries.

4. CONCLUSION

The generalized fractional integrations of the generalized Mittag-Leffler type function is studied in this paper. The obtained results are expressed in terms of the generalized Wright hypergeometric function and generalized hypergeometric functions. To show the potential application of GMLTF, the solutions of fractional kinetic equations are derived with the help of Sumudu transform. The results obtained in this study have significant importance as the solution of the equations are general and can derive many new and known solutions of FKEs involving various type of special functions.

DATA AVAILABILITY STATEMENT

All datasets generated for this study are included in the article.

AUTHOR CONTRIBUTIONS

The author confirms being the sole contributor of this work and has approved it for publication.

REFERENCES

1. Srivastava HM, Choi J. *Zeta and q-Zeta Functions and Associated Series and Integrals*. Amsterdam; London; New York, NY: Elsevier Science Publishers (2012).
2. Rainville ED. *Special Functions*. New York, NY: Macmillan (1960).
3. Fox C. The asymptotic expansion of generalized hypergeometric functions. *Proc Lond Math Soc.* (1928) **27**:389–400.
4. Kilbas AA, Saigo M, Trujillo JJ. On the generalized Wright function. *Fract Calc Appl Anal.* (2002) **5**:437–60.

5. Wright EM. The asymptotic expansion of integral functions defined by Taylor series. *Philos Trans Roy Soc Lond A*. (1940) **238**:423–51.
6. Wright EM. The asymptotic expansion of the generalized hypergeometric function. *Proc Lond Math Soc.* (1940) **46**:389–408.
7. Mittag-Leffler GM. Sur la representation analytiqie d'une fonction monogene cinquieme note. *Acta Math.* (1905) **29**:101–81.
8. Wiman A. Uber den fundamental satz in der theorie der funktionen E_α (z). *Acta Math.* (1905) **29**:191–201.
9. Rahman G, Baleanu D, Al Qurashi M, Purohit SD, Mubeen S, Muhammad A. The extended Mittag-Leffler function via fractional calculus. *J Nonlinear Sci Appl.* (2017) **10**:4244–53. doi: 10.22436/jnsa.010.08.19
10. Nisar KS, Rahman G, Baleanu D, Mubeen S, Arshad M. The (k,s)-fractional calculus of k-Mittag-Leffler function. *Adv Differ Equat.* (2017) **2017**:118. doi: 10.1186/s13662-017-1176-4
11. Kumar S, Kumar A, Momani S, Aldhaifallah M, Nisar KS. Numerical solutions of nonlinear fractional model arising in the appearance of the stripe patterns in two-dimensional systems. *Adv Differ Equat.* (2019) **2019**:413. doi: 10.1186/s13662-019-2334-7
12. Singh J, Kumar D, Swroop R, Kumar S. An efficient computational approach for time-fractional Rosenau–Hyman equation. *Neural Comput Appl.* (2018) **30**:3063–70. doi: 10.1007/s00521-017-2909-8
13. Bhatter S, Mathur A, Kumar D, Nisar KS, Singh J. Fractional modified Kawahara equation with Mittag–Leffler law. *Chaos Solit Fract.* (2019) **2019**:109508. doi: 10.1016/j.chaos.2019.109508
14. Nisar KS. Fractional integrations of a generalized Mittag-Leffler type function and its application. *Mathematics.* (2019) **7**:1230. doi: 10.3390/math7121230
15. Sharma K. Application of fractional calculus operators to related Areas. *Gen Math Notes.* (2011) **7**:33–40. doi: 10.1142/9789814340250_0005
16. Prabhakar TR. A singular integral equation with a generalized Mittag-Leffler function in the Kernel. *Yokohama Math J.* (1971) **19**:7–15.
17. Srivastava HM, Tomovski Z. Fractional calculus with an integral operator containing a generalized Mittag–Leffler function in the kernel. *Appl Math Comput.* (2009) **211**:198–210. doi: 10.1016/j.amc.2009.01.055
18. Odibat Z, Kumar S. A robust computational algorithm of homotopy asymptotic method for solving systems of fractional differential equations. *J Comput Nonlinear Dyn.* (2019) **14**:081004. doi: 10.1115/1.4043617
19. Singh J, Kumar D, Baleanu D. New aspects of fractional Biswas-Milovic model with Mittag-Leffler law. *Math Model Nat Phenom.* (2019) **14**:303. doi: 10.1051/mmnp/2018068
20. Yang XJ. New general fractional-order rheological models with kernels of Mittag-Leffler functions. *Rom Rep Phys.* (2017) **69**:118.
21. Yang XJ, Gao F, Tenreiro Machado JA, Baleanu D. A new fractional derivative involving the normalized sinc function without singular kernel. *Eur Phys J Spec Top.* (2017) **226**:3567–75. doi: 10.1140/epjst/e2018-00020-2
22. Gao W, Ghanbari B, Baskonus HM. New numerical simulations for some real world problems with Atangana–Baleanu fractional derivative. *Chaos Solit Fract.* (2019) **128**:34–43. doi: 10.1016/j.chaos.2019.07.037
23. Araci S, Rahman G, Ghaffar A, Azeema, Nisar KS. Fractional calculus of extended Mittag-Leffler function and its applications to statistical distribution. *Mathematics.* (2019) **7**:248. doi: 10.3390/math7030248
24. Andrić M, Farid G, Pećarić J. A further extension of Mittag-Leffler function. *Fract Calc Appl Anal.* (2018) 21:1377–95. doi: 10.1515/fca-2018-0072
25. Rahman G, Nisar KS, Choi J, Mubeen S, Arshad M. Formulas for Saigo fractional integral operators with 2F1 generalized k -Struve functions. *Far East J Math Sci.* (2017) **102**:55–66. doi: 10.17654/MS102010055
26. Kumar D, Singh J, Baleanu D. A new analysis of the Fornberg-Whitham equation pertaining to a fractional derivative with Mittag-Leffler-type kernel. *Eur Phys J Plus.* (2018) **133**:70. doi: 10.1140/epjp/i2018-11934-y
27. Choi J, Mubeen S, Nisar KS, Choi J. Certain extended special functions and fractional integral and derivative operators via an extended beta function. *Nonlinear Funct Anal Appl.* (2019) 24:1–13. Available online at: http://nfaa.kyungnam.ac.kr/journal-nfaa
28. Kiryakova V. All the special functions are fractional differintegrals of elementary functions. *J Phys A.* (1977) **30**:5085–103.
29. Miller KS, Ross B. *An Introduction to the Fractional Calculus and Fractional Differential Equations*. New York, NY: Wiley (1993).
30. Srivastava HM, Lin SD, Wang PY. Some fractional-calculus results for the H-function associated with a class of Feynman integrals. *Russ J Math Phys.* (2006) **13**:94–100. doi: 10.1134/S1061920806010092
31. Marichev OI. Volterra equation of Mellin convolution type with a Horn function in the kernel. *Izvest Akad Nauk BSSR Ser Fiziko Mat Nauk.* (1974) **1**:128–9.
32. Saigo M, Maeda N. Editors. More generalization of fractional calculus. Transform methods and special functions. In: *Proceedings of the 2nd International Workshop*, Varna (1996).
33. Baleanu D, Kumar D, Purohit SD. Generalized fractional integrals of product of two H-functions and a general class of polynomials. *Int J Comput Math.* (2016) **93**:1320–9. doi: 10.1080/00207160.2015.1045886
34. Mondal SR, Nisar KS. Marichev-Saigo-Maeda fractional integration operators involving generalized Bessel functions. *Math Probl Eng.* (2014) **2014**:11. doi: 10.1155/2014/274093
35. Purohit SD, Suthar DL, Kalla SL. Marichev-Saigo-Maeda fractional integration operators of the Bessel function. *Le Mat.* (2012) **67**:21–32. doi: 10.4418/2012.67.1.2
36. Kataria KK, Vellaisamy P. The generalized k-Wright function and Marichev-Saigo-Maeda fractional operators. *J Anal.* (2015) **23**:75–87.
37. Watugala GK. Sumudu transform:a new integral transform to solve differential equations and control engineering problems. *Int J Math Edu Sci Tech.* (1993) **24**:35–43.
38. Watugala GK. The Sumudu transform for functions of two variables. *Math Eng Ind.* (2002) **8**:293–302.
39. Asiru MA. Sumudu transform and the solution of integral equation of convolution type. *Int J Math Educ Sci Technol.* (2001) **32**:906–10. doi: 10.1080/002073901317147870
40. Belgacem FBM, Karaballi AA, Kalla SL. Analytical investigations of the Sumudu transform and applications to integral production equations. *J Math Probl Eng.* (2003) **3**:103–18. doi: 10.1155/S1024123X03207018
41. Bulut H, Baskonus HM, Belgacem FB. The analytical solution of some fractional ordinary differential equations by the Sumudu transform method. *Abstr Appl Anal.* (2013) **2013**:6. doi: 10.1155/2013/203875
42. Haubold HJ, Mathai AM. The fractional kinetic equation and thermonuclear functions. *Astrophys Space Sci.* (2000) **327**:53–63. doi: 10.1023/A:1002695807970
43. Saxena RK, Mathai AM, Haubold HJ. On fractional kinetic equations. *Astrophys Space Sci.* (2002) **282**:281–7. doi: 10.1023/A:1021175108964
44. Saxena RK, Mathai AM, Haubold HJ. On generalized fractional kinetic equations. *Phys A.* (2004) **344**:657–64. doi: 10.1016/j.physa.2004.06.048
45. Nisar KS, Purohit SD, Mondal SR. Generalized fractional kinetic equations involving generalized Struve function of the first kind. *J King Saud Univ Sci.* (2016) 28:167–71. doi: 10.1016/j.jksus.2015.08.005

Conflict of Interest: The author declares that the research was conducted in the absence of any commercial or financial relationships that could be construed as a potential conflict of interest.

frontiers in Physics

ORIGINAL RESEARCH
published: 28 February 2020
doi: 10.3389/fphy.2020.00025

New Investigation on the Generalized $\mathcal{K}$-Fractional Integral Operators

Saima Rashid[1], *Zakia Hammouch*[2], *Humaira Kalsoom*[3], *Rehana Ashraf*[4] and *Yu Ming Chu*[5*]

[1] Department of Mathematics, Government College University, Faisalabad, Pakistan, [2] Faculty of Science and Techniques Moulay Ismail University of Meknes, Errachidia, Morocco, [3] School of Mathematical Sciences, Zhejiang University, Hangzhou, China, [4] Department of Mathematics, Lahore College Women University, Lahore, Pakistan, [5] Department of Mathematics, Huzhou University, Huzhou, China

The main objective of this paper is to develop a novel framework to study a new fractional operator depending on a parameter $\mathcal{K} > 0$, known as the generalized $\mathcal{K}$-fractional integral operator. To ensure appropriate selection and with the discussion of special cases, it is shown that the generalized $\mathcal{K}$-fractional integral operator generates other operators. Meanwhile, we derived notable generalizations of the reverse Minkowski inequality and some associated variants by utilizing generalized $\mathcal{K}$-fractional integrals. Moreover, two novel results correlate with this inequality, and other variants associated with generalized $\mathcal{K}$-fractional integrals are established. Additionally, this newly defined integral operator has the ability to be utilized for the evaluation of many numerical problems.

Keywords: Minkowski inequality, fractional integral inequality, generalized $\mathcal{K}$-fractional integrals, holder inequalitiy, generalized Riemann-Liouville fractional integral

2000 Mathematics Subject Classification: 26D15, 26D10, 90C23.

Edited by:
Devendra Kumar,
University of Rajasthan, India

Reviewed by:
Haci Mehmet Baskonus,
Harran University, Turkey
Muhammad Bilal Riaz,
University of the Free State, South Africa
Sushila Rathore,
Vivekananda Global University, India

***Correspondence:**
Yu Ming Chu
chuyuming2005@126.com

Specialty section:
This article was submitted to Mathematical Physics, a section of the journal Frontiers in Physics

Received: *15 December 2019*
Accepted: *27 January 2020*
Published: *28 February 2020*

Citation:
Rashid S, Hammouch Z, Kalsoom H, Ashraf R and Chu YM (2020) New Investigation on the Generalized K-Fractional Integral Operators. Front. Phys. 8:25. doi: 10.3389/fphy.2020.00025

1. INTRODUCTION

Fractional calculus is truly considered to be a real-world framework, for example, a correspondence framework that comprises extravagant interfacing, has reliant parts that are utilized to achieve a bound-together objective of transmitting and getting signals, and can be portrayed by utilizing complex system models (see [1–8]). This framework is considered to be a mind-boggling system, and the units that create the whole framework are viewed as the hubs of the intricate system. An attractive characteristic of this field is that there are numerous fractional operators, and this permits researchers to choose the most appropriate operator for the sake of modeling the problem under investigation (see [9–13]). Besides, because of its simplicity in application, researchers have been paying greater interest to recently introduced fractional operators without singular kernels [2, 14, 15], after which many articles considering these kinds of fractional operators have been presented. These techniques had been developed by numerous mathematicians with a barely specific formulation, for instance, the Riemann-Liouville (RL), the Weyl, Erdelyi-Kober, Hadamard integrals, and the Liouville and Katugampola fractional operators (see [16–18]). On the other hand, there are numerous approaches to acquiring a generalization of classical fractional integrals. Many authors have introduced new fractional operators generated from general classical local derivatives (see [9, 19, 20]) and the references therein. Other authors have introduced a parameter and enunciated a generalization for fractional integrals on a selected space. These are called generalized $\mathcal{K}$-fractional integrals. For such operators, we refer to Mubeen and Habibullah [21] and Singh et al. [22] and the works cited in them. Inspired by these developments, future research can bring revolutionary thinking to provide novelties and produce variants concerning such fractional operators. Fractional integral inequalities are an appropriate device for enhancing the qualitative

and quantitative properties of differential equations. There has been a continuous growth of interest in several areas of science: mathematics, physics, engineering, amongst others, and particularly, initial value problems, linear transformation stability, integral-differential equations, and impulse equations [23–30].

The well-known integral inequality, as perceived in Dahmani [31], is referred to as the reverse Minkowski inequality. In Nisar et al. [32, 33], the authors investigated numerous variants of extended gamma and confluent hypergeometric $\mathcal{K}$-functions and also established Gronwall inequalities involving the generalized Riemann-Liouville and Hadamard $\mathcal{K}$-fractional derivatives with applications. In Dahmani [25], Dahmani explored variants on intervals that are known as generalized $(\mathcal{K}, s)$-fractional integral operators for positive continuously decreasing functions for a certain family of $n(n \in \mathbb{N})$. In Chinchane and Pachpatte [34], the authors obtained Minkowski variants and other associated inequalities by employing Katugampola fractional integral operators. Recently, some generalizations of the reverse Minkowski and associated inequalities have been established via generalized $\mathcal{K}$ fractional conformable integrals by Mubeen et al. in [35]. Additionally, Hardy-type and reverse Minkowski inequalities are supplied by Bougoffa [36]. Aldhaifallah et al. [37], explored several variants by employing the $(\mathcal{K}, s)$-fractional integral operator.

In the present paper, the authors introduce a parameter and enunciate a generalization for fractional integrals on a selected space, which we name generalized $\mathcal{K}$-fractional integrals. Taking into account the novel ideas, we provide a new version for reverse Minkowski inequality in the frame of the generalized $\mathcal{K}$-fractional integral operators and also provide some of its consequences that are advantageous to current research. New outcomes are introduced, and new theorems relating to generalized $\mathcal{K}$-fractional integrals are derived that correlate with the earlier results.

The article is composed as follows. In the second section, we demonstrate the notations and primary definitions of our newly described generalized $\mathcal{K}$-fractional integrals. Also, we present the results concerning reverse Minkowski inequality. In the third section, we advocate essential consequences such as the reverse Minkowski inequality via the generalized $\mathcal{K}$-fractional integral. In the fourth section, we show the associated variants using this fractional integral.

2. PRELUDE

In this section, we demonstrate some important concepts from fractional calculus that play a major role in proving the results of the present paper. The essential points of interest are exhibited in the monograph by Kilbas et al. [20].

Definition 2.1. ([9, 20]) A function $\mathcal{Q}_1(\tau)$ is said to be in $L_{p,u}[0,\infty]$ space if

$$L_{p,u}[0,\infty) = \Big\{\mathcal{Q}_1 : \|\mathcal{Q}_1\|_{L_{p,u}[0,\infty)} = \left(\int_{\upsilon_1}^{\upsilon_2} |\mathcal{Q}_1(\eta)|^p \xi^u d\eta\right)^{\frac{1}{p}} < \infty,\ 1 \le p < \infty,\ u \ge 0\Big\}.$$

For $r = 0$,

$$L_p[0,\infty) = \Big\{\mathcal{Q}_1 : \|\mathcal{Q}_1\|_{L_p[0,\infty)} = \left(\int_{\upsilon_1}^{\upsilon_2} |\mathcal{Q}_1(\eta)|^p d\eta\right)^{\frac{1}{p}} < \infty,\ 1 \le p < \infty\Big\}.$$

Definition 2.2. ([38]) "Let $\mathcal{Q}_1 \in L_1[0,\infty)$ and Ψ be an increasing and positive monotone function on $[0,\infty)$ and also derivative Ψ' be continuous on $[0,\infty)$ and $\Psi(0) = 0$. The space $\chi_{\Psi}^{p}(0,\infty)$ $(1 \le p < \infty)$ of those real-valued Lebesgue measureable functions $\mathcal{Q}_1$ on $[0,\infty)$ for which

$$\|\mathcal{Q}_1\|_{\chi_{\Psi}^{p}} = \Big(\int_0^{\infty} |\mathcal{Q}_1(\eta)|^p \Psi'(\eta) d\eta\Big)^{\frac{1}{p}} < \infty, \quad 1 \le p < \infty$$

and for the case $p = \infty$

$$\|\mathcal{Q}_1\|_{\chi_{\Psi}^{\infty}} = ess \sup_{0 \le \eta < \infty} \big[\Psi'(\eta)\mathcal{Q}_1(\eta)\big]".$$

In particular, when $\Psi(\lambda) = \lambda$ $(1 \le p < \infty)$, the space $\chi_{\Psi}^{p}(0,\infty)$ matches with the $L_p[0,\infty)$-space and, furthermore, if we take $\Psi(\lambda) = \ln\lambda$ $(1 \le p < \infty)$, the space $\chi_{\Psi}^{p}(0,\infty)$ concurs with $L_{p,u}[1,\infty)$-space.

Now, we present a new fractional operator that is known as the generalized $\mathcal{K}$-fractional integral operator of a function in the sense of another function Ψ.

Definition 2.3. Let $\mathcal{Q}_1 \in \chi_{\Psi}^{q}(0,\infty)$, and let Ψ be an increasing positive monotone function defined on $[0,\infty)$, containing continuous derivative $\Psi'(\lambda)$ on $[0,\infty)$ with $\Psi(0) = 0$. Then, the left- and right-sided generalized $\mathcal{K}$-fractional integral operators of a function $\mathcal{Q}_1$ in the sense of another function Ψ of order $\eta > 0$ are stated as:

$$({}^{\Psi}\mathcal{T}_{\upsilon_1^+,\tau}^{\rho,\mathcal{K}}\mathcal{Q}_1)(\lambda) = \frac{1}{\mathcal{K}\Gamma_{\mathcal{K}}(\rho)} \int_{\upsilon_1}^{\lambda} \Psi'(\eta)(\Psi(\lambda) - \Psi(\eta))^{\frac{\rho}{\mathcal{K}}-1}\mathcal{Q}_1(\eta)d\eta, \quad \upsilon_1 < \lambda \tag{2.1}$$

and

$$({}^{\Psi}\mathcal{T}_{\upsilon_2^-,\tau}^{\rho,\mathcal{K}}\mathcal{Q}_1)(\lambda) = \frac{1}{\mathcal{K}\Gamma_{\mathcal{K}}(\rho)} \int_{\lambda}^{\upsilon_2} \Psi'(\eta)(\Psi(\eta) - \Psi(\lambda))^{\frac{\rho}{\mathcal{K}}-1}\mathcal{Q}_1(\eta)d\eta, \quad \lambda < \upsilon_2, \tag{2.2}$$

where $\rho \in \mathbb{C}, \Re(\rho) > 0$, and $\Gamma_{\mathcal{K}}(\lambda) = \int_0^{\infty} \eta^{\lambda-1} e^{-\frac{\eta^{\mathcal{K}}}{\mathcal{K}}} d\eta$, $\Re(\lambda) > 0$ is the $\mathcal{K}$-Gamma function introduced by Daiz and Pariguan [39].

Remark 2.1. Several existing fractional operators are just special cases of (2.1) and (2.2).
(1) Choosing $\mathcal{K} = 1$, it turns into the both sided generalized RL-fractional integral operator [20].
(2) Choosing $\Psi(\lambda) = \lambda$, it turns into the both-sided $\mathcal{K}$-fractional integral operator [21].
(3) Choosing $\Psi(\lambda) = \lambda$ along with $\mathcal{K} = 1$, it turns into the both-sided RL-fractional integral operators.
(4) Choosing $\Psi(\lambda) = \log\lambda$ along with $\mathcal{K} = 1$, it turns into the both-sided Hadamard fractional integral operators [9, 20].
(5) Choosing $\Psi(\lambda) = \frac{\lambda^{\beta}}{\beta}, \beta > 0$, along with $\mathcal{K} = 1$, it turns into the both-sided Katugampola fractional integral operators [17].
(6) Choosing $\Psi(\lambda) = \frac{(\lambda-a)^{\beta}}{\beta}, \beta > 0$ along with $\mathcal{K} = 1$, it turns into the both-sided conformable fractional integral operators defined by Jarad et al. [2].
(7) Choosing $\Psi(\lambda) = \frac{\lambda^{u+\nu}}{u+\nu}$ along with $\mathcal{K} = 1$, it turns into the both-sided generalized conformable fractional integrals defined by Khan et al. [40].

Definition 2.4. Let $\mathcal{Q}_1 \in \chi^{q}_{\Psi}(0,\infty)$, and let Ψ be an increasing positive monotone function defined on $[0,\infty)$, containing continuous derivative $\Psi'(\lambda)$ in $[0,\infty)$ with $\Psi(0) = 0$. Then, the one-sided generalized $\mathcal{K}$-fractional integral operator of a function $\mathcal{Q}_1$ in the sense of another function Ψ of order $\eta > 0$ is stated as:

$$({}^{\Psi}\mathcal{T}^{\rho,\mathcal{K}}_{0^+,\lambda}\mathcal{Q}_1)(\lambda) = \frac{1}{\mathcal{K}\Gamma_{\mathcal{K}}(\rho)}\int_0^{\lambda}\Psi'(\eta)(\Psi(\lambda) - \Psi(\eta))^{\frac{\rho}{\mathcal{K}}-1}\mathcal{Q}_1(\eta)d\eta, \quad \eta > 0, \tag{2.3}$$

where $\Gamma_{\mathcal{K}}$ is the $\mathcal{K}$-Gamma function.

In Set et al. [41] proved the Hermite-Hadamard and reverse Minkowski inequalities for an RL-fractional integral. The subsequent consequences concerning the reverse Minkowski inequalities are the motivation of work finished to date concerning the classical integrals.

Theorem 2.5. Set et al. [41] For $s \geq 1$, let $\mathcal{Q}_1, \mathcal{Q}_2$ be two positive functions on $[0,\infty)$. If $0 < \varsigma \leq \frac{\mathcal{Q}_1(\eta)}{\mathcal{Q}_2(\eta)} \leq \Omega, \lambda \in [\upsilon_1, \upsilon_2]$, then

$$\Big(\int_{\upsilon_1}^{\upsilon_2}\mathcal{Q}_1^s(\lambda)d\lambda\Big)^{\frac{1}{s}} + \Big(\int_{\upsilon_1}^{\upsilon_2}\mathcal{Q}_2^s(\lambda)d\lambda\Big)^{\frac{1}{s}} \leq \frac{1+\Omega(\varsigma+2)}{(\varsigma+1)(\Omega+1)}\Big(\int_{\upsilon_1}^{\upsilon_2}\big(\mathcal{Q}_1+\mathcal{Q}_2\big)^s(\lambda)d\lambda\Big)^{\frac{1}{s}}.$$

Theorem 2.6. Set et al. [41] For $s \geq 1$, let $\mathcal{Q}_1, \mathcal{Q}_2$ be two positive functions on $[0,\infty)$. If $0 < \varsigma \leq \frac{\mathcal{Q}_1(\eta)}{\mathcal{Q}_2(\eta)} \leq \Omega, \lambda \in [\upsilon_1, \upsilon_2]$, then

$$\Big(\int_{\upsilon_1}^{\upsilon_2}\mathcal{Q}_1^s(\lambda)d\lambda\Big)^{\frac{2}{s}} + \Big(\int_{\upsilon_1}^{\upsilon_2}\mathcal{Q}_2^s(\lambda)d\lambda\Big)^{\frac{2}{s}} \geq \Big(\frac{(1+\Omega)(\varsigma+1)}{\Omega} - 2\Big)\Big(\int_{\upsilon_1}^{\upsilon_2}\mathcal{Q}_1^s(\lambda)d\lambda\Big)^{\frac{1}{s}}\Big(\int_{\upsilon_1}^{\upsilon_2}\mathcal{Q}_2^s(\lambda)d\lambda\Big)^{\frac{1}{s}}.$$

In Dahmani [31], introduced the subsequent reverse Minkowski inequalities involving the RLFI operators.

Theorem 2.7. Dahmani [31] For $\rho \in \mathbb{C}$, $\Re(\rho) > 0$, $s \geq 1$, and let $\mathcal{Q}_1, \mathcal{Q}_2$ be two positive functions on $[0,\infty)$ such that, for all $\lambda > 0$, $\mathcal{T}^{\rho}_{\upsilon_1^+}\mathcal{Q}_1^s(\lambda) < \infty$, $\mathcal{T}^{\rho}_{\upsilon_1^+}\mathcal{Q}_2^s(\lambda) < \infty$. If $0 < \varsigma \leq \frac{\mathcal{Q}_1(\lambda)}{\mathcal{Q}_2(\lambda)} \leq \Omega, \eta \in [\upsilon_1, \lambda]$, then

$$\Big(\mathcal{T}^{\rho}_{\upsilon_1^+}\mathcal{Q}_1^s(\lambda)\Big)^{\frac{1}{s}} + \Big(\mathcal{T}^{\rho}_{\upsilon_1^+}\mathcal{Q}_2^s(\lambda)\Big)^{\frac{1}{s}} \leq \frac{1+\Omega(\varsigma+2)}{(\varsigma+1)(\Omega+1)}\Big(\mathcal{T}^{\rho}_{\upsilon_1^+}\big(\mathcal{Q}_1+\mathcal{Q}_2\big)^s(\lambda)\Big)^{\frac{1}{s}}.$$

Theorem 2.8. Dahmani [31] For $\rho \in \mathbb{C}$, $\Re(\rho) > 0$, $s \geq 1$, and let $\mathcal{Q}_1, \mathcal{Q}_2$ be two positive functions on $[0,\infty)$ such that, for all $\lambda > 0$, $\mathcal{T}^{\rho}_{\upsilon_1^+}\mathcal{Q}_1^s(\lambda) < \infty$, $\mathcal{T}^{\rho}_{\upsilon_1^+}\mathcal{Q}_2^s(\lambda) < \infty$. If $0 < \varsigma \leq \frac{\mathcal{Q}_1(\lambda)}{\mathcal{Q}_2(\lambda)} \leq \Omega, \eta \in [\upsilon_1, \lambda]$, then

$$\Big(\mathcal{T}^{\rho}_{\upsilon_1^+}\mathcal{Q}_1^s(\lambda)\Big)^{\frac{2}{s}} + \Big(\mathcal{T}^{\rho}_{\upsilon_1^+}\mathcal{Q}_2^s(\lambda)\Big)^{\frac{2}{s}} \geq \Big(\frac{(1+\Omega)(\varsigma+2)}{\Omega} - 2\Big)\Big(\mathcal{T}^{\rho}_{\upsilon_1^+}\mathcal{Q}_1^s(\lambda)\Big)^{\frac{1}{s}}\Big(\mathcal{T}^{\rho}_{\upsilon_1^+}\mathcal{Q}_2^s(\lambda)\Big)^{\frac{1}{s}}.$$

3. REVERSE MINKOWSKI INEQUALITY VIA GENERALIZED $\mathcal{K}$-FRACTIONAL INTEGRALS

Throughout the paper, it is supposed that all functions are integrable in the Riemann sense. Also, this segment incorporates the essential contribution for obtaining the proof of the reverse Minkowski inequality via the newly described generalized $\mathcal{K}$-fractional integrals defined in section (2.4).

Theorem 3.1. For $\mathcal{K} > 0, \rho \in \mathbb{C}, \Re(\rho) > 0$ and $s \geq 1$, and let two positive functions $\mathcal{Q}_1, \mathcal{Q}_2$ be defined on $[0,\infty)$. Assume that Ψ is an increasing positive monotone function on $[0,\infty)$ having derivative Ψ' and is continuous on $[0,\infty)$ with $\Psi(0) = 0$ such that, for all $\lambda > 0$, ${}^{\Psi}\mathcal{T}^{\rho,\mathcal{K}}_{0^+,\lambda}\mathcal{Q}_1^s(\lambda) < \infty$ and ${}^{\Psi}\mathcal{T}^{\rho,\mathcal{K}}_{0^+,\lambda}\mathcal{Q}_2^s(\lambda) < \infty$. If $0 < \varsigma \leq \frac{\mathcal{Q}_1(\eta)}{\mathcal{Q}_2(\eta)} \leq \Omega$ for $\varsigma, \Omega \in \mathbb{R}^+$ and for all $\eta \in [0, \lambda]$, then

$$\Big({}^{\Psi}\mathcal{T}^{\rho,\mathcal{K}}_{0^+,\lambda}\mathcal{Q}_1^s(\lambda)\Big)^{\frac{1}{s}} + \Big({}^{\Psi}\mathcal{T}^{\rho,\mathcal{K}}_{0^+,\lambda}\mathcal{Q}_2^s(\lambda)\Big)^{\frac{1}{s}} \leq \theta_1\Big({}^{\Psi}\mathcal{T}^{\rho,\mathcal{K}}_{0^+,\lambda}\big(\mathcal{Q}_1+\mathcal{Q}_2\big)^s(\lambda)\Big)^{\frac{1}{s}} \tag{3.1}$$

with $\theta_1 = \frac{\Omega(\varsigma+1)+(\Omega+1)}{(\varsigma+1)(\Omega+1)}$.

Proof: Under the given conditions $\frac{\mathcal{Q}_1(\eta)}{\mathcal{Q}_2(\eta)} \leq \Omega$, $0 \leq \eta \leq \lambda$, it can written as

$$\mathcal{Q}_1(\eta) \leq \Omega\big(\mathcal{Q}_1(\eta) + \mathcal{Q}_2(\eta)\big) - \Omega\mathcal{Q}_1(\eta),$$

which implies that

$$(\Omega+1)^s\mathcal{Q}_1^s(\eta) \leq \Omega^s\big(\mathcal{Q}_1(\eta) + \mathcal{Q}_2(\eta)\big)^s. \tag{3.2}$$

If we multiply both sides of (3.2) by $\frac{1}{\mathcal{K}\Gamma_{\mathcal{K}}(\rho)}\Psi'(\eta)\big(\Psi(\lambda)-\Psi(\eta)\big)^{\frac{\rho}{\mathcal{K}}-1}$ and integrate w.r.t η over $[0,\lambda]$, one obtains

$$\begin{aligned}&\frac{(\Omega+1)^s}{\mathcal{K}\Gamma_{\mathcal{K}}(\rho)}\int_0^\lambda \Psi'(\eta)\big(\Psi(\lambda)-\Psi(\eta)\big)^{\frac{\rho}{\mathcal{K}}-1}\mathcal{Q}_1^s(\eta)d\eta\\&\leq \frac{\Omega^s}{\mathcal{K}\Gamma_{\mathcal{K}}(\rho)}\int_0^\lambda \Psi'(\eta)\big(\Psi(\lambda)-\Psi(\eta)\big)^{\frac{\rho}{\mathcal{K}}-1}\big(\mathcal{Q}_1(\eta)\\&+\mathcal{Q}_2(\eta)\big)^s d\eta. \qquad (3.3)\end{aligned}$$

Accordingly, it can be written as

$$\Big({}^{\Psi}\mathcal{T}^{\rho,\mathcal{K}}_{0^+,\lambda}\mathcal{Q}_1^s(\lambda)\Big)^{\frac{1}{s}}\leq\frac{\Omega}{\Omega+1}\Big({}^{\Psi}\mathcal{T}^{\rho,\mathcal{K}}_{0^+,\lambda}\big(\mathcal{Q}_1+\mathcal{Q}_2\big)^s(\lambda)\Big)^{\frac{1}{s}}. \qquad (3.4)$$

In contrast, as $\varsigma\mathcal{Q}_2(\lambda)\leq\mathcal{Q}_1(\lambda)$, it follows

$$\Big(1+\frac{1}{\varsigma}\Big)^s\mathcal{Q}_2^s(\eta)\leq\Big(\frac{1}{\varsigma}\Big)^s\big(\mathcal{Q}_1(\eta)+\mathcal{Q}_2(\eta)\big)^s. \qquad (3.5)$$

Again, taking the product of both sides of (3.5) with $\frac{1}{\mathcal{K}\Gamma_{\mathcal{K}}(\rho)}\Psi'(\eta)\big(\Psi(\lambda)-\Psi(\eta)\big)^{\frac{\rho}{\mathcal{K}}-1}$ and integrating w.r.t η over $[0,\lambda]$, we obtain

$$\Big({}^{\Psi}\mathcal{T}^{\rho,\mathcal{K}}_{0^+,\lambda}\mathcal{Q}_2^s(\lambda)\Big)^{\frac{1}{s}}\leq\frac{1}{\varsigma+1}\Big({}^{\Psi}\mathcal{T}^{\rho,\mathcal{K}}_{0^+,\lambda}\big(\mathcal{Q}_1+\mathcal{Q}_2\big)^s(\lambda)\Big)^{\frac{1}{s}}. \qquad (3.6)$$

The desired inequality (3.1) can be obtained from 3.4 and 3.6. □

Inequality (3.1) is referred to as the reverse Minkowski inequality related to the generalized $\mathcal{K}$-fractional integral.

Theorem 3.2. For $\mathcal{K}>0,\rho\in\mathbb{C},\Re(\rho)>0$ and $s\geq1$, let two positive functions $\mathcal{Q}_1,\mathcal{Q}_2$ be defined on $[0,\infty)$. Assume that Ψ is an increasing positive monotone function on $[0,\infty)$ having derivative Ψ' and is continuous on $[0,\infty)$ with $\Psi(0)=0$ such that, for all $\lambda>0$, ${}^{\Psi}\mathcal{T}^{\rho,\mathcal{K}}_{0^+,\lambda}\mathcal{Q}_1^s(\lambda)<\infty$ and ${}^{\Psi}\mathcal{T}^{\rho,\mathcal{K}}_{0^+,\lambda}\mathcal{Q}_2^s(\lambda)<\infty$. If $0<\varsigma\leq\frac{\mathcal{Q}_1(\eta)}{\mathcal{Q}_2(\eta)}\leq\Omega$ for $\varsigma,\Omega\in\mathbb{R}^+$ and for all $\eta\in[0,\lambda]$, then

$$\begin{aligned}&\Big({}^{\Psi}\mathcal{T}^{\rho,\mathcal{K}}_{0^+,\lambda}\mathcal{Q}_1^s(\lambda)\Big)^{\frac{2}{s}}+\Big({}^{\Psi}\mathcal{T}^{\rho,\mathcal{K}}_{0^+,\lambda}\mathcal{Q}_2^s(\lambda)\Big)^{\frac{2}{s}}\\&\geq\theta_2\Big({}^{\Psi}\mathcal{T}^{\rho,\mathcal{K}}_{0^+,\lambda}\mathcal{Q}_1^s(\lambda)\Big)^{\frac{1}{s}}\Big({}^{\Psi}\mathcal{T}^{\rho,\mathcal{K}}_{0^+,\lambda}\mathcal{Q}_2^s(\lambda)\Big)^{\frac{1}{s}} \qquad (3.7)\end{aligned}$$

with $\theta_2=\frac{(\varsigma+1)(\Omega+1)}{\Omega}-2$.

Proof: Multiplying 3.4 and 3.6 results in

$$\begin{aligned}&\frac{(\varsigma+1)(\Omega+1)}{\Omega}\Big({}^{\Psi}\mathcal{T}^{\rho,\mathcal{K}}_{0^+,\lambda}\mathcal{Q}_1^s(\lambda)\Big)^{\frac{1}{s}}\Big({}^{\Psi}\mathcal{T}^{\rho,\mathcal{K}}_{0^+,\lambda}\mathcal{Q}_2^s(\lambda)\Big)^{\frac{1}{s}}\\&\leq\Big({}^{\Psi}\mathcal{T}^{\rho,\mathcal{K}}_{0^+,\lambda}\big(\mathcal{Q}_1+\mathcal{Q}_2\big)^s(\lambda)\Big)^{\frac{2}{s}}. \qquad (3.8)\end{aligned}$$

Involving the Minkowski inequality, on the right side of (3.8), we get

$$\begin{aligned}&\frac{(\varsigma+1)(\Omega+1)}{\Omega}\Big({}^{\Psi}\mathcal{T}^{\rho,\mathcal{K}}_{0^+,\lambda}\mathcal{Q}_1^s(\lambda)\Big)^{\frac{1}{s}}\Big({}^{\Psi}\mathcal{T}^{\rho,\mathcal{K}}_{0^+,\lambda}\mathcal{Q}_2^s(\lambda)\Big)^{\frac{1}{s}}\\&\leq\Big(\Big({}^{\Psi}\mathcal{T}^{\rho,\mathcal{K}}_{0^+,\lambda}\mathcal{Q}_1^s(\lambda)\Big)^{\frac{1}{s}}+\Big({}^{\Psi}\mathcal{T}^{\rho,\mathcal{K}}_{0^+,\lambda}\mathcal{Q}_2^s(\lambda)\Big)^{\frac{1}{s}}\Big)^2. \qquad (3.9)\end{aligned}$$

From 3.9, we conclude that

$$\begin{aligned}&\Big({}^{\Psi}\mathcal{T}^{\rho,\mathcal{K}}_{0^+,\lambda}\mathcal{Q}_1^s(\lambda)\Big)^{\frac{2}{s}}+\Big({}^{\Psi}\mathcal{T}^{\rho,\mathcal{K}}_{0^+,\lambda}\mathcal{Q}_2^s(\lambda)\Big)^{\frac{2}{s}}\\&\geq\Big(\frac{(\varsigma+1)(\Omega+1)}{\Omega}-2\Big)\Big({}^{\Psi}\mathcal{T}^{\rho,\mathcal{K}}_{0^+,\lambda}\mathcal{Q}_1^s(\lambda)\Big)^{\frac{1}{s}}\Big({}^{\Psi}\mathcal{T}^{\rho,\mathcal{K}}_{0^+,\lambda}\mathcal{Q}_2^s(\lambda)\Big)^{\frac{1}{s}}.\end{aligned}$$

□

4. CERTAIN ASSOCIATED INEQUALITIES VIA THE GENERALIZED $\mathcal{K}$-FRACTIONAL INTEGRAL OPERATOR

Theorem 4.1. For $\mathcal{K}>0,\rho\in\mathbb{C},\Re(\rho)>0,\ s,r\geq1,\frac{1}{s}+\frac{1}{r}=1$ and let two positive functions $\mathcal{Q}_1,\mathcal{Q}_2$ be defined on $[0,\infty)$. Assume that Ψ is an increasing, positive monotone function on $[0,\infty)$ having derivative Ψ' and is continuous on $[0,\infty)$ with $\Psi(0)=0$ such that, for all $\lambda>0$, ${}^{\Psi}\mathcal{T}^{\eta,\mathcal{K}}_{0^+,\tau}\mathcal{Q}_1^s(\lambda)<\infty$ and ${}^{\Psi}\mathcal{T}^{\rho,\mathcal{K}}_{0^+,\lambda}\mathcal{Q}_2^s(\lambda)<\infty$. If $0<\varsigma\leq\frac{\mathcal{Q}_1(\eta)}{\mathcal{Q}_2(\eta)}\leq\Omega$ for $\varsigma,\Omega\in\mathbb{R}^+$ and for all $\eta\in[0,\lambda]$, then

$$\begin{aligned}&\Big({}^{\Psi}\mathcal{T}^{\rho,\mathcal{K}}_{0^+,\lambda}\mathcal{Q}_1(\lambda)\Big)^{\frac{1}{s}}\Big({}^{\Psi}\mathcal{T}^{\rho,\mathcal{K}}_{0^+,\lambda}\mathcal{Q}_2(\lambda)\Big)^{\frac{1}{r}}\\&\leq\Big(\frac{\Omega}{\varsigma}\Big)^{\frac{1}{sr}}\Big(\Big({}^{\Psi}\mathcal{T}^{\rho,\mathcal{K}}_{0^+,\lambda}\mathcal{Q}_1^{\frac{1}{s}}(\lambda)\mathcal{Q}_2^{\frac{1}{r}}(\lambda)\Big). \qquad (4.1)\end{aligned}$$

Proof: Under the given condition $\frac{\mathcal{Q}_1(\eta)}{\mathcal{Q}_2(\eta)}\leq\Omega,\ 0\leq\eta\leq\lambda$, it can be expressed as

$$\mathcal{Q}_1(\eta)\leq\Omega\mathcal{Q}_2(\eta),$$

which implies that

$$\mathcal{Q}_2^{\frac{1}{r}}(\eta)\geq\Omega^{-\frac{1}{r}}\mathcal{Q}_1^{\frac{1}{r}}(\eta). \qquad (4.2)$$

Taking the product of both sides of (4.2) by $\mathcal{Q}_1^{\frac{1}{s}}(\eta)$, we are able to rewrite it as follows:

$$\mathcal{Q}_1^{\frac{1}{s}}(\eta)\mathcal{Q}_2^{\frac{1}{r}}(\eta)\geq\Omega^{-\frac{1}{r}}\mathcal{Q}_1(\eta). \qquad (4.3)$$

Multiplying both sides of (4.3) with $\frac{1}{\mathcal{K}\Gamma_{\mathcal{K}}(\rho)}\Psi'(\eta)\big(\Psi(\lambda)-\Psi(\eta)\big)^{\frac{\rho}{\mathcal{K}}-1}$ and integrating w.r.t η over $[0,\lambda]$, one obtains

$$\frac{\Omega^{-\frac{1}{r}}}{\mathcal{K}\Gamma_{\mathcal{K}}(\rho)}\int_0^\lambda\Psi'(\eta)\big(\Psi(\lambda)-\Psi(\eta)\big)^{\frac{\rho}{\mathcal{K}}-1}\mathcal{Q}_1(\eta)d\eta$$

$$\geq \frac{1}{\mathcal{K}\Gamma_{\mathcal{K}}(\rho)}\int_0^{\lambda}\Psi'(\eta)\big(\Psi(\lambda) - \Psi(\eta)\big)^{\frac{\rho}{\mathcal{K}}-1}\mathcal{Q}_1^{\frac{1}{s}}(\eta)\mathcal{Q}_2^{\frac{1}{r}}(\eta)d\eta. \quad (4.4)$$

As a consequence, we can rewrite as follows

$$\Omega^{\frac{-1}{sr}}\Big({}^{\Psi}\mathcal{T}^{\rho,\mathcal{K}}_{0^+,\lambda}\mathcal{Q}_1(\lambda)\Big)^{\frac{1}{s}} \leq \big({}^{\Psi}\mathcal{T}^{\rho,\mathcal{K}}_{0^+,\lambda}\mathcal{Q}_1^{\frac{1}{s}}(\lambda)\mathcal{Q}_1^{\frac{1}{r}}(\lambda)\big)^{\frac{1}{s}}. \quad (4.5)$$

Similarly, as $\varsigma\mathcal{Q}_2(\eta) \leq \mathcal{Q}_1(\eta)$, it follows that

$$\varsigma^{\frac{1}{s}}\mathcal{Q}_2^{\frac{1}{s}}(\eta) \leq \mathcal{Q}_1^{\frac{1}{s}}(\eta). \quad (4.6)$$

Again, taking the product of both sides of (4.6) by $\mathcal{Q}_2^{\frac{1}{s}}(\eta)$ and using the relation $\frac{1}{s}+\frac{1}{r}=1$ gives

$$\varsigma^{\frac{1}{s}}\mathcal{Q}_2(\eta) \leq \mathcal{Q}_1^{\frac{1}{s}}(\eta)\mathcal{Q}_2^{\frac{1}{s}}(\eta). \quad (4.7)$$

If we multiply both sides of (4.7) by $\frac{1}{\mathcal{K}\Gamma_{\mathcal{K}}(\rho)}\Psi'(\eta)\big(\Psi(\lambda) - \Psi(\eta)\big)^{\frac{\rho}{\mathcal{K}}-1}$ and integrate w.r.t η over $[0,\lambda]$, we obtain

$$\varsigma^{\frac{1}{sr}}\Big({}^{\Psi}\mathcal{T}^{\rho,\mathcal{K}}_{0^+,\lambda}\mathcal{Q}_2(\lambda)\Big)^{\frac{1}{r}} \leq \big({}^{\Psi}\mathcal{T}^{\rho,\mathcal{K}}_{0^+,\lambda}\mathcal{Q}_1^{\frac{1}{s}}(\lambda)\mathcal{Q}_1^{\frac{1}{r}}(\lambda)\big)^{\frac{1}{r}}. \quad (4.8)$$

Finding the product between (4.5) and (4.8) and using the relation $\frac{1}{s}+\frac{1}{r}=1$, we get the desired inequality (4.1). □

Theorem 4.2. For $\mathcal{K}>0, \rho\in\mathbb{C}, \Re(\rho)>0,\ s,r\geq 1, \frac{1}{s}+\frac{1}{r}=1$, and let two positive functions $\mathcal{Q}_1,\mathcal{Q}_2$ be defined on $[0,\infty)$. Assume that Ψ is an increasing, positive monotone function on $[0,\infty)$ having derivative Ψ' and is continuous on $[0,\infty)$ with $\Psi(0)=0$ such that, for all $\lambda>0$, ${}^{\Psi}\mathcal{T}^{\eta,\mathcal{K}}_{0^+,\tau}\mathcal{Q}_1^s(\lambda)<\infty$ and ${}^{\Psi}\mathcal{T}^{\rho,\mathcal{K}}_{0^+,\lambda}\mathcal{Q}_2^s(\lambda)<\infty$. If $0<\varsigma\leq\frac{\mathcal{Q}_1(\eta)}{\mathcal{Q}_2(\eta)}\leq\Omega$ for $\varsigma,\Omega\in\mathbb{R}^+$ and for all $\eta\in[0,\lambda]$, then

$$\Big({}^{\Psi}\mathcal{T}^{\rho,\mathcal{K}}_{0^+,\lambda}\mathcal{Q}_1(\lambda)\mathcal{Q}_1(\lambda)\Big) \leq \theta_3\Big({}^{\Psi}\mathcal{T}^{\rho,\mathcal{K}}_{0^+,\lambda}\big(\mathcal{Q}_1^s+\mathcal{Q}_2^s\big)(\lambda)\Big) + \theta_4\Big({}^{\Psi}\mathcal{T}^{\rho,\mathcal{K}}_{0^+,\lambda}\big(\mathcal{Q}_1^r+\mathcal{Q}_2^r\big)(\lambda)\Big) \quad (4.9)$$

with $\theta_3=\frac{2^{s-1}\Omega^s}{s(\Omega+1)^s}$ and $\theta_4=\frac{2^{r-1}}{r(\varsigma+1)^r}$.

Proof: Under the assumptions, we have the subsequent identity:

$$(\Omega+1)^s\mathcal{Q}_1^s(\eta) \leq \Omega^s(\mathcal{Q}_1+\mathcal{Q}_2)^s(\eta). \quad (4.10)$$

Multiplying both sides of (4.10) by $\frac{1}{\mathcal{K}\Gamma_{\mathcal{K}}(\rho)}\Psi'(\eta)\big(\Psi(\lambda) - \Psi(\eta)\big)^{\frac{\rho}{\mathcal{K}}-1}$ and integrating w.r.t η over $[0,\lambda]$, one obtains

$$\frac{(\Omega+1)^s}{\mathcal{K}\Gamma_{\mathcal{K}}(\rho)}\int_0^{\lambda}\Psi'(\eta)\big(\Psi(\lambda)-\Psi(\eta)\big)^{\frac{\rho}{\mathcal{K}}-1}\mathcal{Q}_1^s(\eta)d\eta \leq \frac{\Omega^s}{\mathcal{K}\Gamma_{\mathcal{K}}(\rho)}\int_0^{\lambda}\Psi'(\eta)\big(\Psi(\lambda) - \Psi(\eta)\big)^{\frac{\rho}{\mathcal{K}}-1}(\mathcal{Q}_1+\mathcal{Q}_2)^s(\eta)d\eta. \quad (4.11)$$

Accordingly, it can be written as

$${}^{\Psi}\mathcal{T}^{\rho,\mathcal{K}}_{0^+,\lambda}\mathcal{Q}_1^s(\lambda) \leq \frac{\Omega^s}{(\Omega+1)^s}\ {}^{\Psi}\mathcal{T}^{\rho,\mathcal{K}}_{0^+,\lambda}\big(\mathcal{Q}_1+\mathcal{Q}_2\big)^s(\lambda). \quad (4.12)$$

In contrast, as $0<\varsigma\frac{\mathcal{Q}_1(\eta)}{\mathcal{Q}_2(\eta)},\ 0<\eta<\lambda$, it follows

$$(\varsigma+1)^r\mathcal{Q}_2^r(\eta) \leq (\mathcal{Q}_1+\mathcal{Q}_2)^r(\eta). \quad (4.13)$$

Again, taking the product of both sides of (4.13) with $\frac{1}{\mathcal{K}\Gamma_{\mathcal{K}}(\rho)}\Psi'(\eta)\big(\Psi(\lambda) - \Psi(\eta)\big)^{\frac{\rho}{\mathcal{K}}-1}$ and integrating w.r.t η over $[0,\lambda]$, one obtains

$${}^{\Psi}\mathcal{T}^{\rho,\mathcal{K}}_{0^+,\lambda}\mathcal{Q}_2^r(\lambda) \leq \frac{1}{(\varsigma+1)^r}\ {}^{\Psi}\mathcal{T}^{\rho,\mathcal{K}}_{0^+,\lambda}\big(\mathcal{Q}_1+\mathcal{Q}_2\big)^r(\lambda). \quad (4.14)$$

Considering Young's inequality,

$$\mathcal{Q}_1(\eta)\mathcal{Q}_2(\eta) \leq \frac{\mathcal{Q}_1^s(\eta)}{s}+\frac{\mathcal{Q}_2^r(\eta)}{r}. \quad (4.15)$$

If we multiply both sides of (4.15) with $\frac{1}{\mathcal{K}\Gamma_{\mathcal{K}}(\rho)}\Psi'(\eta)\big(\Psi(\lambda) - \Psi(\eta)\big)^{\frac{\rho}{\mathcal{K}}-1}$ and integrate w.r.t η over $[0,\lambda]$, we obtain

$${}^{\Psi}\mathcal{T}^{\rho,\mathcal{K}}_{0^+,\lambda}\big(\mathcal{Q}_1\mathcal{Q}_2\big)(\lambda) \leq \frac{{}^{\Psi}\mathcal{T}^{\rho,\mathcal{K}}_{0^+,\lambda}\mathcal{Q}_1^s(\lambda)}{s}+\frac{{}^{\Psi}\mathcal{T}^{\rho,\mathcal{K}}_{0^+,\lambda}\mathcal{Q}_2^r(\lambda)}{r}. \quad (4.16)$$

Invoking (4.12) and (4.14) into (4.16), we obtain

$$\begin{aligned}&{}^{\Psi}\mathcal{T}^{\rho,\mathcal{K}}_{0^+,\lambda}\big(\mathcal{Q}_1\mathcal{Q}_2\big)(\lambda)\\ &\leq \frac{{}^{\Psi}\mathcal{T}^{\rho,\mathcal{K}}_{0^+,\lambda}\mathcal{Q}_1^s(\lambda)}{s}+\frac{{}^{\Psi}\mathcal{T}^{\rho,\mathcal{K}}_{0^+,\lambda}\mathcal{Q}_2^r(\lambda)}{r}\\ &\leq \frac{\Omega^s}{(\Omega+1)^s}\ {}^{\Psi}\mathcal{T}^{\rho,\mathcal{K}}_{0^+,\lambda}\big(\mathcal{Q}_1+\mathcal{Q}_2\big)^s(\lambda)\\ &+\frac{1}{(\varsigma+1)^r}\ {}^{\Psi}\mathcal{T}^{\rho,\mathcal{K}}_{0^+,\lambda}\big(\mathcal{Q}_1+\mathcal{Q}_2\big)^r(\lambda). \end{aligned} \quad (4.17)$$

Using the inequality $(\mu+\nu)^z \leq 2^{z-1}(\mu^z+\nu^z),\ z>1,\ \mu,\nu>0$, one obtains

$${}^{\Psi}\mathcal{T}^{\rho,\mathcal{K}}_{0^+,\lambda}\big(\mathcal{Q}_1+\mathcal{Q}_2\big)^s(\lambda) \leq 2^{s-1}\ {}^{\Psi}\mathcal{T}^{\rho,\mathcal{K}}_{0^+,\lambda}\big(\mathcal{Q}_1^s+\mathcal{Q}_2^s\big)(\lambda) \quad (4.18)$$

and

$${}^{\Psi}\mathcal{T}^{\rho,\mathcal{K}}_{0^+,\lambda}\big(\mathcal{Q}_1+\mathcal{Q}_2\big)^r(\lambda) \leq 2^{r-1}\ {}^{\Psi}\mathcal{T}^{\rho,\mathcal{K}}_{0^+,\lambda}\big(\mathcal{Q}_1^r+\mathcal{Q}_2^r\big)(\lambda). \quad (4.19)$$

The desired (4.9) can be established from (4.17), (4.18) and (4.19) jointly.

Theorem 4.3. For $\mathcal{K}>0, \rho\in\mathbb{C}, \Re(\rho)>0,\ s,r\geq 1, \frac{1}{s}+\frac{1}{r}=1$ and let two positive functions $\mathcal{Q}_1,\mathcal{Q}_2$ be defined on $[0,\infty)$. Assume that Ψ is an increasing positive monotone function on $[0,\infty)$ having derivative Ψ' and is continuous on $[0,\infty)$ with $\Psi(0)=0$ such that, for all $\lambda>0$, ${}^{\Psi}\mathcal{T}^{\eta,\mathcal{K}}_{0^+,\tau}\mathcal{Q}_1^s(\lambda)<\infty$ and

${}^{\Psi}\mathcal{T}_{0^+,\lambda}^{\rho,\mathcal{K}}\mathcal{Q}_2^s(\lambda) < \infty$. If $0 < \zeta < \varsigma \leq \frac{\mathcal{Q}_1(\eta)}{\mathcal{Q}_2(\eta)} \leq \Omega$ for $\varsigma, \Omega \in \mathbb{R}^+$ and for all $\eta \in [0, \lambda]$, then

$$\begin{aligned}
&\frac{\Omega+1}{\Omega-\zeta}\Big(\mathfrak{J}_{\Psi}^{\lambda}\big(\mathcal{Q}_1(\lambda)-\mathcal{Q}_2(\lambda)\big)\Big)\\
&\leq \Big(\mathfrak{J}_{\Psi}^{\lambda}\mathcal{Q}_1(\lambda)\Big)^{\frac{1}{s}}+\Big(\mathfrak{J}_{\Psi}^{\lambda}\mathcal{Q}_2(\lambda)\Big)^{\frac{1}{s}}\\
&\leq \frac{\varsigma+1}{\varsigma-\zeta}\Big(\mathfrak{J}_{\Psi}^{\lambda}\big(\mathcal{Q}_1(\lambda)-\mathcal{Q}_2(\lambda)\big)\Big)^{\frac{1}{s}}. \qquad (4.20)
\end{aligned}$$

Proof: Using the hypothesis $0 < \zeta < \varsigma \leq \Omega$, we get

$$\begin{aligned}
\varsigma\zeta \leq \Omega\zeta \;&\Rightarrow \varsigma\zeta+\varsigma \leq \varsigma\zeta+\Omega \leq \Omega\zeta+\Omega\\
&\Rightarrow (\Omega+1)(\varsigma-\zeta) \leq (\varsigma+1)(\Omega-\zeta).
\end{aligned}$$

It can be concluded that

$$\frac{\Omega+1}{\Omega-\zeta} \leq \frac{\varsigma+1}{\varsigma-\zeta}.$$

Further, we have that

$$\varsigma-\zeta \leq \frac{\mathcal{Q}_1(\eta)-\zeta\mathcal{Q}_2(\eta)}{\mathcal{Q}_2(\eta)} \leq \Omega-\zeta$$

implies that

$$\frac{\big(\mathcal{Q}_1(\eta)-\zeta\mathcal{Q}_2(\eta)\big)^s}{(\Omega-\zeta)^s} \leq \mathcal{Q}_2^s(\eta) \leq \frac{\big(\mathcal{Q}_1(\eta)-\zeta\mathcal{Q}_2(\eta)\big)^s}{(\varsigma-\zeta)^s}. \qquad (4.21)$$

Again, we have that

$$\frac{1}{\Omega} \leq \frac{\mathcal{Q}_2(\eta)}{\mathcal{Q}_1(\eta)} \leq \frac{1}{\varsigma} \Rightarrow \frac{\varsigma-\zeta}{\zeta\varsigma} \leq \frac{\mathcal{Q}_1(\eta)-\zeta\mathcal{Q}_2(\eta)}{\zeta\mathcal{Q}_1(\eta)} \leq \frac{\Omega-\zeta}{\zeta\Omega}$$

implies that

$$\begin{aligned}
\Big(\frac{\Omega}{\Omega-\zeta}\Big)^s\big(\mathcal{Q}_1(\eta)-\zeta\mathcal{Q}_2(\eta)\big)^s &\leq \mathcal{Q}_1^s(\eta)\\
&\leq \Big(\frac{\varsigma}{\varsigma-\zeta}\Big)^s\big(\mathcal{Q}_1(\eta)-\zeta\mathcal{Q}_2(\eta)\big)^s. \qquad (4.22)
\end{aligned}$$

If we multiply both sides of (4.21) with $\frac{1}{\mathcal{K}\Gamma_{\mathcal{K}}(\rho)}\Psi'(\eta)\big(\Psi(\lambda)-\Psi(\eta)\big)^{\frac{\rho}{\mathcal{K}}-1}$ and integrate w.r.t η over $[0, \lambda]$, we obtain

$$\begin{aligned}
&\frac{1}{\mathcal{K}\Gamma_{\mathcal{K}}(\rho)(\Omega-\zeta)^s}\int_0^{\lambda}\Psi'(\eta)\big(\Psi(\lambda)\\
&-\Psi(\eta)\big)^{\frac{\rho}{\mathcal{K}}-1}\big(\mathcal{Q}_1(\eta)-\zeta\mathcal{Q}_2(\eta)\big)^s d\eta\\
&\leq \frac{1}{\mathcal{K}\Gamma_{\mathcal{K}}(\rho)}\int_0^{\lambda}\Psi'(\eta)\big(\Psi(\lambda)-\Psi(\eta)\big)^{\frac{\rho}{\mathcal{K}}-1}\mathcal{Q}_2^s(\eta)d\eta\\
&\leq \frac{1}{\mathcal{K}\Gamma_{\mathcal{K}}(\rho)(\varsigma-\zeta)^s}\int_0^{\lambda}\Psi'(\eta)\big(\Psi(\lambda)\\
&-\Psi(\eta)\big)^{\frac{\rho}{\mathcal{K}}-1}\big(\mathcal{Q}_1(\eta)-\zeta\mathcal{Q}_2(\eta)\big)^s d\eta.
\end{aligned}$$

Accordingly, it can be written as

$$\begin{aligned}
&\frac{1}{\Omega-\zeta}\Big({}^{\Psi}\mathcal{T}_{0^+,\lambda}^{\rho,\mathcal{K}}\big(\mathcal{Q}_1(\lambda)-\zeta\mathcal{Q}_2(\lambda)\big)^s\Big)^{\frac{1}{s}}\\
&\leq \Big({}^{\Psi}\mathcal{T}_{0^+,\lambda}^{\rho,\mathcal{K}}\mathcal{Q}_1^s(\lambda)\Big)^{\frac{1}{s}}\\
&\leq \frac{1}{\varsigma-\zeta}\Big(\mathfrak{J}_{\Psi}^{\lambda}\big(\mathcal{Q}_1(\lambda)-\zeta\mathcal{Q}_2(\lambda)\big)^s\Big)^{\frac{1}{s}}. \qquad (4.23)
\end{aligned}$$

In a similar way with (4.22), one obtains

$$\begin{aligned}
&\frac{\Omega}{\Omega-\zeta}\Big({}^{\Psi}\mathcal{T}_{0^+,\lambda}^{\rho,\mathcal{K}}\big(\mathcal{Q}_1(\lambda)-\zeta\mathcal{Q}_2(\lambda)\big)^s\Big)^{\frac{1}{s}}\\
&\leq \Big({}^{\Psi}\mathcal{T}_{0^+,\lambda}^{\rho,\mathcal{K}}\mathcal{Q}_1^s(\lambda)\Big)^{\frac{1}{s}}\\
&\leq \frac{\varsigma}{\varsigma-\zeta}\Big({}^{\Psi}\mathcal{T}_{0^+,\lambda}^{\rho,\mathcal{K}}\big(\mathcal{Q}_1(\lambda)-\zeta\mathcal{Q}_2(\lambda)\big)^s\Big)^{\frac{1}{s}}. \qquad (4.24)
\end{aligned}$$

The desired inequality (4.20) can be established by adding (4.23) and (4.24). □

Theorem 4.4. For $\mathcal{K} > 0, \rho \in \mathbb{C}, \Re(\rho) > 0$, $s, r \geq 1, \frac{1}{s}+\frac{1}{r} = 1$ and let two positive functions $\mathcal{Q}_1, \mathcal{Q}_2$ be defined on $[0, \infty)$. Assume that Ψ is an increasing positive monotone function on $[0, \infty)$ having derivative Ψ' and is continuous on $[0, \infty)$ with $\Psi(0) = 0$ such that, for all $\lambda > 0$, ${}^{\Psi}\mathcal{T}_{0^+,\tau}^{\eta,\mathcal{K}}\mathcal{Q}_1^s(\lambda) < \infty$ and ${}^{\Psi}\mathcal{T}_{0^+,\lambda}^{\rho,\mathcal{K}}\mathcal{Q}_2^s(\lambda) < \infty$. If $0 \leq d \leq \mathcal{Q}_1(\eta) \leq \mathcal{D}$ and $0 \leq f \leq \mathcal{Q}_2(\eta) \leq \mathcal{F}$ for $\varsigma, \Omega \in \mathbb{R}^+$ and for all $\eta \in [0, \lambda]$, then

$$\begin{aligned}
&\Big({}^{\Psi}\mathcal{T}_{0^+,\lambda}^{\rho,\mathcal{K}}\mathcal{Q}_1^s(\lambda)\Big)^{\frac{1}{s}}+\Big({}^{\Psi}\mathcal{T}_{0^+,\lambda}^{\rho,\mathcal{K}}\mathcal{Q}_2^s(\lambda)\Big)^{\frac{1}{s}}\\
&\leq \theta_5\Big(\mathfrak{J}_{\Psi}^{\lambda}(\mathcal{Q}_1+\mathcal{Q}_2)^s(\lambda)\Big)^{\frac{1}{s}} \qquad (4.25)
\end{aligned}$$

with $\theta_5 = \frac{\mathcal{D}(d+\mathcal{F})+\mathcal{F}(\mathcal{D}+f)}{(\mathcal{D}+f)(d+\mathcal{F})}$.

Proof: Under the assumptions, it pursues that

$$\frac{1}{\mathcal{F}} \leq \frac{1}{\mathcal{Q}_2(\lambda)} \leq \frac{1}{f}. \qquad (4.26)$$

Taking the product between (4.26) and $0 \leq d \leq \mathcal{Q}_1(\eta) \leq D$, we have

$$\frac{d}{\mathcal{F}} \leq \frac{\mathcal{Q}_1(\lambda)}{\mathcal{Q}_2(\lambda)} \leq \frac{\mathcal{D}}{f}. \qquad (4.27)$$

From (4.27), we get

$$\mathcal{Q}_2^s(\eta) \leq \Big(\frac{\mathcal{F}}{d+\mathcal{F}}\Big)^s\big(\mathcal{Q}_1(\eta)+\mathcal{Q}_2(\eta)\big)^s \qquad (4.28)$$

and

$$\mathcal{Q}_1^s(\eta) \leq \Big(\frac{\mathcal{D}}{f+\mathcal{D}}\Big)^s\big(\mathcal{Q}_1(\eta)+\mathcal{Q}_2(\eta)\big)^s. \qquad (4.29)$$

If we multiply both sides of (4.28) with $\frac{1}{\mathcal{K}\Gamma_{\mathcal{K}}(\rho)}\Psi'(\eta)\big(\Psi(\lambda)-\Psi(\eta)\big)^{\frac{\rho}{\mathcal{K}}-1}$ and integrate w.r.t η over $[0,\lambda]$, we obtain

$$\begin{aligned}&\frac{1}{\mathcal{K}\Gamma_{\mathcal{K}}(\rho)}\int_0^{\lambda}\Psi'(\eta)\big(\Psi(\lambda)-\Psi(\eta)\big)^{\frac{\rho}{\mathcal{K}}-1}\mathcal{Q}_2^s(\eta)d\eta\\&\leq\frac{\mathcal{F}^s}{(d+\mathcal{F})^s\mathcal{K}\Gamma_{\mathcal{K}}(\rho)}\int_0^{\lambda}\Psi'(\eta)\big(\Psi(\lambda)\\&-\Psi(\eta)\big)^{\frac{\rho}{\mathcal{K}}-1}\big(\mathcal{Q}_1(\eta)+\mathcal{Q}_2(\eta)\big)^s d\eta.\end{aligned}$$

Likewise, it can be composed as

$$\Big({}^{\Psi}\mathcal{T}_{0^+,\lambda}^{\rho,\mathcal{K}}\mathcal{Q}_2^s(\lambda)\Big)^{\frac{1}{s}}\leq\frac{\mathcal{F}}{d+\mathcal{F}}\Big({}^{\Psi}\mathcal{T}_{0^+,\lambda}^{\rho,\mathcal{K}}(\mathcal{Q}_1+\mathcal{Q}_2)^s(\lambda)\Big)^{\frac{1}{s}}.\quad(4.30)$$

In the same way with (4.29), we have

$$\Big({}^{\Psi}\mathcal{T}_{0^+,\lambda}^{\rho,\mathcal{K}}\mathcal{Q}_1^s(\lambda)\Big)^{\frac{1}{s}}\leq\frac{\mathcal{D}}{f+\mathcal{D}}\Big({}^{\Psi}\mathcal{T}_{0^+,\lambda}^{\rho,\mathcal{K}}(\mathcal{Q}_1+\mathcal{Q}_2)^s(\lambda)\Big)^{\frac{1}{s}}.\quad(4.31)$$

The desired inequality (4.25) can be established by adding (4.30) and (4.31). □

Theorem 4.5. For $\mathcal{K}>0,\rho\in\mathbb{C},\Re(\rho)>0$, $s\geq1$, and let two positive functions $\mathcal{Q}_1,\mathcal{Q}_2$ be defined on $[0,\infty)$. Assume that Ψ is an increasing positive monotone function on $[0,\infty)$ having derivative Ψ' and is continuous on $[0,\infty)$ with $\Psi(0)=0$ such that, for all $\lambda>0$, ${}^{\Psi}\mathcal{T}_{0^+,\tau}^{\eta,\mathcal{K}}\mathcal{Q}_1^s(\lambda)<\infty$ and ${}^{\Psi}\mathcal{T}_{0^+,\lambda}^{\rho,\mathcal{K}}\mathcal{Q}_2^s(\lambda)<\infty$. If $0<\theta<\varsigma\leq\frac{\mathcal{Q}_1(\eta)}{\mathcal{Q}_2(\eta)}\leq\Omega$ for $\varsigma,\Omega\in\mathbb{R}^+$ and for all $\eta\in[0,\lambda]$, then

$$\begin{aligned}&\frac{1}{\Omega}\Big({}^{\Psi}\mathcal{T}_{0^+,\lambda}^{\rho,\mathcal{K}}\mathcal{Q}_1(\lambda)\mathcal{Q}_2(\lambda)\Big)\\&\leq\frac{1}{(\varsigma+1)(\Omega+1)}\Big({}^{\Psi}\mathcal{T}_{0^+,\lambda}^{\rho,\mathcal{K}}\big(\mathcal{Q}_1+\mathcal{Q}_2\big)^2(\lambda)\Big)\\&\leq\frac{1}{\varsigma}\Big({}^{\Psi}\mathcal{T}_{0^+,\lambda}^{\rho,\mathcal{K}}\mathcal{Q}_1(\lambda)\mathcal{Q}_2(\lambda)\Big).\end{aligned}\quad(4.32)$$

Proof: Using $0<\varsigma\leq\frac{\mathcal{Q}_1(\eta)}{\mathcal{Q}_2(\eta)}\leq\Omega$, it follows that

$$(\varsigma+1)\mathcal{Q}_2(\eta)\leq\mathcal{Q}_1(\eta)+\mathcal{Q}_2(\eta)\leq\mathcal{Q}_2(\eta)(\Omega+1).\quad(4.33)$$

Also, it follows that $\frac{1}{\Omega}\leq\frac{\mathcal{Q}_2(\eta)}{\mathcal{Q}_1(\eta)}\leq\frac{1}{\varsigma}$, which yields

$$\mathcal{Q}_1(\eta)\Big(\frac{\Omega+1}{\Omega}\Big)\leq\mathcal{Q}_1(\eta)+\mathcal{Q}_2(\eta)\leq\mathcal{Q}_1(\eta)\Big(\frac{\varsigma+1}{\varsigma}\Big).\quad(4.34)$$

Finding the product between (4.33) and (4.34), we have

$$\frac{\mathcal{Q}_1(\eta)\mathcal{Q}_2(\eta)}{\Omega}\leq\frac{(\mathcal{Q}_1(\eta)+\mathcal{Q}_2(\eta))^2}{(\varsigma+1)(\Omega+1)}\leq\frac{\mathcal{Q}_1(\eta)\mathcal{Q}_2(\eta)}{\varsigma}.\quad(4.35)$$

If we multiply both sides of (4.28) with $\frac{1}{\mathcal{K}\Gamma_{\mathcal{K}}(\rho)}\Psi'(\eta)\big(\Psi(\lambda)-\Psi(\eta)\big)^{\frac{\rho}{\mathcal{K}}-1}$ and integrate w.r.t η over $[0,\lambda]$, we obtain

$$\begin{aligned}&\frac{1}{\Omega\mathcal{K}\Gamma_{\mathcal{K}}(\rho)}\int_0^{\lambda}\Psi'(\eta)\big(\Psi(\lambda)-\Psi(\eta)\big)^{\frac{\rho}{\mathcal{K}}-1}\mathcal{Q}_1(\eta)\mathcal{Q}_2(\eta)d\eta\\&\leq\theta_6\frac{1}{\mathcal{K}\Gamma_{\mathcal{K}}(\rho)}\int_0^{\lambda}\Psi'(\eta)\big(\Psi(\lambda)-\Psi(\eta)\big)^{\frac{\rho}{\mathcal{K}}-1}(\mathcal{Q}_1(\eta)\\&+\mathcal{Q}_2(\eta))^2d\eta\\&\leq\frac{1}{\varsigma\mathcal{K}\Gamma_{\mathcal{K}}(\rho)}\int_0^{\lambda}\Psi'(\eta)\big(\Psi(\lambda)-\Psi(\eta)\big)^{\frac{\rho}{\mathcal{K}}-1}\mathcal{Q}_1(\eta)\mathcal{Q}_2(\eta)d\eta\end{aligned}$$

with $\theta_6=\frac{1}{(\varsigma+1)(\Omega+1)}$.
Likewise, the required outcome (4.32) can be finished up. □

Theorem 4.6. For $\mathcal{K}>0,\rho\in\mathbb{C},\Re(\rho)>0$, $s\geq1$, and let two positive functions $\mathcal{Q}_1,\mathcal{Q}_2$ be defined on $[0,\infty)$. Assume that Ψ is an increasing positive monotone function on $[0,\infty)$ having derivative Ψ' and is continuous on $[0,\infty)$ with $\Psi(0)=0$ such that, for all $\lambda>0$, ${}^{\Psi}\mathcal{T}_{0^+,\tau}^{\eta,\mathcal{K}}\mathcal{Q}_1^s(\lambda)<\infty$ and ${}^{\Psi}\mathcal{T}_{0^+,\lambda}^{\rho,\mathcal{K}}\mathcal{Q}_2^s(\lambda)<\infty$. If $0<\theta<\varsigma\leq\frac{\mathcal{Q}_1(\eta)}{\mathcal{Q}_2(\eta)}\leq\Omega$ for $\varsigma,\Omega\in\mathbb{R}^+$ and for all $\eta\in[0,\lambda]$, then

$$\begin{aligned}&\Big({}^{\Psi}\mathcal{T}_{0^+,\lambda}^{\rho,\mathcal{K}}\mathcal{Q}_1^s(\lambda)\Big)^{\frac{1}{s}}+\Big({}^{\Psi}\mathcal{T}_{0^+,\lambda}^{\rho,\mathcal{K}}\mathcal{Q}_2^s(\lambda)\Big)^{\frac{1}{s}}\\&\leq2\Big({}^{\Psi}\mathcal{T}_{0^+,\lambda}^{\rho,\mathcal{K}}\mathcal{H}^s\big(\mathcal{Q}_1(\lambda),\mathcal{Q}_2(\lambda)\big)\Big)^{\frac{1}{s}},\end{aligned}\quad(4.36)$$

where $\mathcal{H}\big(\mathcal{Q}_1(\eta),\mathcal{Q}_2(\eta)\big)=\max\Big\{\Omega\big(\frac{\Omega}{\varsigma}+1\big)\mathcal{Q}_1(\lambda)-\Omega\mathcal{Q}_2(\lambda),\frac{(\varsigma+\Omega)\mathcal{Q}_2(\lambda)-\mathcal{Q}_1(\lambda)}{\varsigma}\Big\}$.

Proof: Under the given conditions $0<\varsigma\leq\frac{\mathcal{Q}_1(\eta)}{\mathcal{Q}_2(\eta)}\leq\Omega$, $0\leq\eta\leq\lambda$, can be written as

$$0<\varsigma\leq\Omega+\varsigma-\frac{\mathcal{Q}_1(\eta)}{\mathcal{Q}_2(\eta)},\quad(4.37)$$

and

$$\Omega+\varsigma-\frac{\mathcal{Q}_1(\eta)}{\mathcal{Q}_2(\eta)}\leq\Omega.\quad(4.38)$$

From (4.35) and (4.38), we obtain

$$\mathcal{Q}_2(\eta)<\frac{(\Omega+\varsigma)\mathcal{Q}_2(\eta)-\mathcal{Q}_1(\eta)}{\varsigma}\leq\mathcal{H}\big(\mathcal{Q}_1(\eta),\mathcal{Q}_2(\eta)\big),\quad(4.39)$$

where $\mathcal{H}\big(\mathcal{Q}_1(\eta),\mathcal{Q}_2(\eta)\big)=\max\Big\{\Omega\big(\frac{\Omega}{\varsigma}+1\big)\mathcal{Q}_1(\lambda)-\Omega\mathcal{Q}_2(\lambda),\frac{(\varsigma+\Omega)\mathcal{Q}_2(\lambda)-\mathcal{Q}_1(\lambda)}{\varsigma}\Big\}$.
From hypothesis, it also follows that $0<\frac{1}{\Omega}\leq\frac{\mathcal{Q}_2(\eta)}{\mathcal{Q}_1(\eta)}\leq\frac{1}{\varsigma}$ implies that

$$\frac{1}{\Omega}\leq\frac{1}{\Omega}+\frac{1}{\varsigma}-\frac{\mathcal{Q}_2(\eta)}{\mathcal{Q}_1(\eta)}\quad(4.40)$$

and

$$\frac{1}{\Omega}+\frac{1}{\varsigma}-\frac{\mathcal{Q}_2(\eta)}{\mathcal{Q}_1(\eta)}\leq\frac{1}{\varsigma}. \tag{4.41}$$

From (4.40) and (4.41), we obtain

$$\frac{1}{\Omega}\leq\frac{\left(\frac{1}{\Omega}+\frac{1}{\varsigma}\right)\mathcal{Q}_1(\eta)-\mathcal{Q}_2(\eta)}{\mathcal{Q}_1(\eta)}\leq\frac{1}{\varsigma}, \tag{4.42}$$

which can be composed as

$$\begin{aligned}\mathcal{Q}_1(\eta)&\leq\Omega\Big(\frac{1}{\Omega}+\frac{1}{\varsigma}\Big)\mathcal{Q}_1(\eta)-\Omega\mathcal{Q}_2(\eta)\\&=\frac{\Omega(\Omega+\varsigma)\mathcal{Q}_1(\eta)-\Omega^2\varsigma\mathcal{Q}_2(\eta)}{\varsigma\Omega}\\&=\Big(\frac{\Omega}{\varsigma}+1\Big)\mathcal{Q}_1(\eta)-\Omega\mathcal{Q}_2(\eta)\\&\leq\Omega\Big[\Big(\frac{\Omega}{\varsigma}+1\Big)\mathcal{Q}_1(\eta)-\Omega\mathcal{Q}_2(\eta)\Big]\\&\leq\mathcal{H}\big(\mathcal{Q}_1(\eta),\mathcal{Q}_2(\eta)\big).\end{aligned} \tag{4.43}$$

We can compose from (4.40) and (4.43)

$$\mathcal{Q}_1^s(\eta)\leq\mathcal{H}^s\big(\mathcal{Q}_1(\eta),\mathcal{Q}_2(\eta)\big), \tag{4.44}$$

$$\mathcal{Q}_2^s(\eta)\leq\mathcal{H}^s\big(\mathcal{Q}_1(\eta),\mathcal{Q}_2(\eta)\big). \tag{4.45}$$

Multiplying both sides of (4.44) by $\frac{1}{\mathcal{K}\Gamma_{\mathcal{K}}(\rho)}\Psi'(\eta)\big(\Psi(\lambda)-\Psi(\eta)\big)^{\frac{\rho}{\mathcal{K}}-1}$ and integrating w.r.t η over $[0,\lambda]$, one obtains

$$\begin{aligned}&\frac{1}{\mathcal{K}\Gamma_{\mathcal{K}}(\rho)}\int_0^\lambda\Psi'(\eta)\big(\Psi(\lambda)-\Psi(\eta)\big)^{\frac{\rho}{\mathcal{K}}-1}\mathcal{Q}_1^s(\eta)d\eta\\&\leq\frac{1}{\mathcal{K}\Gamma_{\mathcal{K}}(\rho)}\int_0^\lambda\Psi'(\eta)\big(\Psi(\lambda)-\Psi(\eta)\big)^{\frac{\rho}{\mathcal{K}}-1}\mathcal{H}^s\big(\mathcal{Q}_1(\eta),\mathcal{Q}_2(\eta)\big)d\eta.\end{aligned}$$

Likewise, it can be composed as

$$\Big({}^{\Psi}\mathcal{T}_{0^+,\lambda}^{\rho,\mathcal{K}}\mathcal{Q}_1^s(\lambda)\Big)^{\frac{1}{s}}\leq\Big({}^{\Psi}\mathcal{T}_{0^+,\lambda}^{\rho,\mathcal{K}}\mathcal{H}^s\big(\mathcal{Q}_1(\lambda),\mathcal{Q}_2(\lambda)\big)\Big)^{\frac{1}{s}}. \tag{4.46}$$

Repeating the same procedure as above, for (4.45), we have

$$\Big({}^{\Psi}\mathcal{T}_{0^+,\lambda}^{\rho,\mathcal{K}}\mathcal{Q}_2^s(\lambda)\Big)^{\frac{1}{s}}\leq\Big({}^{\Psi}\mathcal{T}_{0^+,\lambda}^{\rho,\mathcal{K}}\mathcal{H}^s\big(\mathcal{Q}_1(\lambda),\mathcal{Q}_2(\lambda)\big)\Big)^{\frac{1}{s}}. \tag{4.47}$$

The desired inequality (4.36) is obtained from (4.46) and (4.47). □

5. CONCLUSION

This article succinctly expresses the newly defined fractional integral operator. We characterize the strategy of generalized $\mathcal{K}$-fractional integral operators for the generalization of reverse Minkowski inequalities. The outcomes presented in section 3 are the generalization of the existing work done by Dahmani [31] for the RL-fractional integral operator. Also, the consequences in section 3 under certain conditions are reduced to the special cases proved in Set al. [41]. The variants built in section 4 are the generalizations of the existing results derived in Sulaiman [42]. Additionally, our consequences will reduce to the classical results established by Sroysang [43]. Our consequences with this new integral operator have the capacities to be used for the assessment of numerous scientific issues as utilizations of the work, which incorporates existence and constancy for the fractional-order differential equations.

AUTHOR CONTRIBUTIONS

All authors contributed to each part of this work equally, read, and approved the final manuscript.

FUNDING

This work was supported by the Natural Science Foundation of China (Grant Nos. 61673169, 11301127, 11701176, 11626101, 11601485) and the Natural Science Foundation of Huzhou City (Grant No. 2018YZ07).

ACKNOWLEDGMENTS

The authors are thankful to the referees for their useful suggestions and comments.

REFERENCES

1. Goswami A, Singh J, Kumar D, Sushila. An efficient analytical approach for fractional equal width equations describing hydromagnetic waves in cold plasma. *Phys A*. (2019) **524**:563–75. doi: 10.1016/j.physa.2019.04.058
2. Jarad F, Ugrlu E, Abdeljawad T, Baleanu D. On a new class of fractional operators. *Adv Differ Equat*. (2017) **2017**:247. doi: 10.1186/s13662-017-1306-z
3. Kirmani S, Suaib NBS, Raiz MB. Shape preserving fractional order KNR C1 cubic spline. *Eur Phys J Plus*. (2019) **134**:319. doi: 10.1140/epjp/i2019-12704-1
4. Khalil R, Al Horani M, Yousef A, Sababheh M. A new definition of fractional derivative. *J Comput Appl Math*. (2014) **264**:65–70. doi: 10.1016/j.cam.2014.01.002
5. Losada J, Nieto JJ. Properties of a new fractional derivative without singular kernel. *Prog Fract Differ Appl*. (2015) **1**:87–92. doi: 10.12785/pdfa/010202
6. Kumar D, Singh J, Al-Qurashi M, Baleanu D. A new fractional SIRS-SI malaria disease model with application of vaccines, anti-malarial drugs,

and spraying. *Adv. Differ Eqn*. (2019) **2019**:278. doi: 10.1186/s13662-019-2199-9
7. Kumar D, Singh J, Baleanu D. On the analysis of vibration equation involving a fractional derivative with Mittag-Leffler law. *Math Methods Appl Sci*. (2019) **43**:443–57. doi: 10.1002/mma.5903
8. Samko SG, Kilbas AA, Marichev OI. *Fractional Integrals and Derivatives: Theory and Applications*. Gordon and Breach: Yverdon (1993).
9. Podlubny I. Fractional Differential Equation. In: Podlubny I, edtior. *Mathematics in Science and Engineering*. San Diego, CA: Academic Press (1999). p. 1–340.
10. Raiz MB, Zafar AA. Exact solutions for the blood flow through a circular tube under the influence of a magnetic field using fractional Caputo-Fabrizio derivatives. *Math Model Nat Phenom*. (2018) **13**:131. doi: 10.1051/mmnp/2018005
11. Rihan FA, Hashish A, Al-Maskari F, Hussein MS, Ahmed E, Riaz MB, Yafia R. Dynamics of tumor-immune system with fractional-order. *J Tumor Res*. (2016) **2**:109–15.
12. Singh J, Kumar D, Baleanu. New aspects of fractional Biswas-Milovic model with Mittag-Leffler law. *Math Model Nat Phenomena*. (2019) **14**:303. doi: 10.1051/mmnp/2018068
13. Singh J, Kumar D, Baleanu D, Rathore S. On the local fractional wave equation in fractal strings. *Math Methods Appl Sci*. (2019) 42:1588–95. doi: 10.1002/mma.5458
14. Atangana A, Baleanu D. New fractional derivatives with nonlocal and non-singular kernel: theory and application to heat transfer model. *Therm Sci*. (2016) **20**:763–9. doi: 10.2298/TSCI160111018A
15. Caputo M, Fabrizio M. A new definition of fractional derivative without singular kernel. *Prog Fract Differ Appl*. (2015) **1**:73–85. doi: 10.12785/pfda/010201
16. Katugampola UN. A new approach to generalized fractional derivatives. *Bull Math Anal Appl*. (2014) **6**:1–15.
17. Katugampola UN. New fractional integral unifying six existing fractional integrals. *arXiv:1612.08596* (2016).
18. Katugampola UN. Approach to a generalized fractional integral. *Appl Math Comput*. (2011) **218**:860–86. doi: 10.1016/j.amc.2011.03.062
19. Chen H, Katugampola UN. Hermite-Hadamard and Hermite-Hadamard-Fejer type inequalities for generalized fractional integrals. *J Math Anal Appl*. (2017) **446**:1274–91. doi: 10.1016/j.jmaa.2016.09.018
20. Kilbas AA, Srivastava HM, Trujillo JJ. *Theory and Applications of Fractional Differential Equations*. Amsterdam; London; New York, NY: North-Holland Mathematical Studies; Elsevier (North-Holland) Science Publishers (2006).
21. Mubeen S, Habibullah GM. $\mathcal{K}$-Fractional integrals and application. *J Contemp Math Sci*. (2012) **7**:89–94.
22. Set E, Tomar M, Sarikaya MZ. On generalized Gruss type inequalities for $\mathcal{K}$-fractional integrals. *Appl Math Comput*. (2015) **269**:29–34.
23. da Vanterler J, Sousa C, Capelas de Oliveira E. The Minkowski's inequality by means of a generalized fractional integral. *AIMS Ser Appl Math*. (2018) **3**:131–47. doi: 10.3934/Math.2018.1.131
24. Dahmani Z. New inequalities in fractional integrals. *Int J Nonlin Sci*. (2010) **9**:493–7.
25. Dahmani Z. New classes of integral inequalities of fractional order. *Le-Matematiche*. (2014) **2014**:237–47. doi: 10.4418/2014.69.1.18
26. Latif MA, Rashid S, Dragomir SS, Chu YM. Hermite-Hadamard type inequalities for co-ordinated convex and qausi-convex functions and their applications. *J Inequal Appl*. (2019) **2019**:317. doi: 10.1186/s13660-019-2272-7
27. Rashid S, Safdar F, Akdemir AO, Noor MA, Noor KI. Some new fractional integral inequalities for exponentially *m*-convex functions via extended generalized Mittag-Leffler function. *J Inequal Appl*. (2019) **2019**:299. doi: 10.1186/s13660-019-2248-7
28. Rashid S, Jarad F, Noor MA, Kalsoom H. Inequalities by means of generalized proportional fractional integral operators with respect to another function. *Mathematics*. (2020) **7**:1225. doi: 10.3390/math7121225
29. Rashid S, Noor MA, Noor KI, Safdar F, Chu YM. Hermite-Hadamard inequalities for the class of convex functions on time scale. *Mathematics*. (2019) **7**:956. doi: 10.3390/math7100956
30. Rashid S, Latif MA, Hammouch Z, Chu YM. Fractional integral inequalities for strongly h-preinvex functions for a kth order differentiable functions. *Symmetry*. (2019) **11**:1448: doi: 10.3390/sym11121448.
31. Dahmani Z. On Minkowski and Hermite-Hadamard integral inequalities via fractional integral. *Ann Funct Anal*. (2010) **1**:51–8.
32. Nisar KS, Qi F, Rahman G, Mubeen S, Arshad M. Some inequalities involving the extended gamma function and the Kummer confluent hypergeometric $\mathcal{K}$-function. *J Inequal Appl*. (2018) **2018**:135. doi: 10.1186/s13660-018-1717-8
33. Nisar KS, Rahman G, Choi J, Mubeen S, Arshad M. Certain Gronwall type inequalities associated with Riemann-Liouville-$\mathcal{K}$ and Hadamard $\mathcal{K}$-fractional derivatives and their applications. *East Asian Mat J*. (2018) **34**:249–63. doi: 10.7858/eamj.2018.018
34. Chinchane VL, Pachpatte DB. New fractional inequalities via Hadamard fractional integral. *Int J Funct Anal Oper Theory Appl*. (2013) **5**:165–76.
35. Mubeen S, Habib S, Naeem MN. The Minkowski inequality involving generalized k-fractional conformable integral. *J Inequal Appl*. (2019) **2019**:81. doi: 10.1186/s13660-019-2040-8
36. Bougoffa L. On Minkowski and Hardy integral inequalities. *J Inequal Pure Appl. Math*. (2006) **7**:60.
37. Aldhaifallah M, Tomar M, Nisar KS, Purohit SD. Some new inequalities for (k, s)-fractional integrals. *J Nonlin Sci Appl*. (2016) **9**:5374–81.
38. Kacar E, Kacar Z, Yildirim H. Integral inequalities for Riemann-Liouville fractional integrals of a function with respect to another function. *Iran J Math Sci Inform*. (2018) **13**:1–13.
39. Diaz R, Pariguan E. On hypergeometric functions and Pochhammer *k*-symbol. *Divulgaciones Matematicas*. (2007) **15**:179–92.
40. Khan TU, Khan MA. Generalized conformable fractional operators. *J Comput Appl. Math*. (2019) **346**:378–89. doi: 10.1016/j.cam.2018.07.018
41. Set E, Ozdemir M, Dragomir S. On the Hermite-Hadamard inequality and other integral inequalities involving two functions. *J Inequal Appl*. (2010) **2010**:148102. doi: 10.1155/2010/148102
42. Sulaiman WT. Reverses of Minkowski's, Hö}lder's, and Hardy's integral inequalities. *Int J Mod Math Sci*. (2012) **1**:14–24.
43. Sroysang B. More on reverses of Minkowski's integral inequality. *Math Eterna*. (2013) **3**:597–600.

Conflict of Interest: The authors declare that the research was conducted in the absence of any commercial or financial relationships that could be construed as a potential conflict of interest.

frontiers in Physics

ORIGINAL RESEARCH
published: 20 March 2020
doi: 10.3389/fphy.2020.00062

Exact Soliton Solutions to the Cubic-Quartic Non-linear Schrödinger Equation With Conformable Derivative

Hemen Dutta[1]*, *Hatıra Günerhan*[2], *Karmina K. Ali*[3,4] and *Resat Yilmazer*[4]

[1] Department of Mathematics, Gauhati University, Guwahati, India, [2] Department of Mathematics, Faculty of Education, Kafkas University, Kars, Turkey, [3] Department of Mathematics, Faculty of Science, University of Zakho, Zakho, Iraq, [4] Department of Mathematics, Faculty of Science, Firat University, Elazig, Turkey

The research paper aims to investigate the space-time fractional cubic-quartic non-linear Schrödinger equation in the appearance of the third, and fourth-order dispersion impacts without both group velocity dispersion, and disturbance with parabolic law media by utilizing the extended sinh-Gordon expansion method. This method is one of the strongest methods to find the exact solutions to the non-linear partial differential equations. In order to confirm the existing solutions, the constraint conditions are used. We successfully construct various exact solitary wave solutions to the governing equation, for example, singular, and dark-bright solutions. Moreover, the 2D, 3D, and contour surfaces of all obtained solutions are also plotted. The finding solutions have justified the efficiency of the proposed method.

Keywords: the non-linear cubic-quartic Schrödinger equation, conformable derivative, analytical solutions, the extended sinh-Gordon expansion method, solitary wave solutions

OPEN ACCESS

Edited by:
Devendra Kumar,
University of Rajasthan, India

Reviewed by:
Haci Mehmet Baskonus,
Harran University, Turkey
K. S. Nisar,
Prince Sattam Bin Abdulaziz University, Saudi Arabia
Jagdev Singh,
JECRC University, India

***Correspondence:**
Hemen Dutta
hemen_dutta08@rediffmail.com

Specialty section:
This article was submitted to Mathematical Physics, a section of the journal Frontiers in Physics

Received: *29 November 2019*
Accepted: *27 February 2020*
Published: *20 March 2020*

Citation:
Dutta H, Günerhan H, Ali KK and Yilmazer R (2020) Exact Soliton Solutions to the Cubic-Quartic Non-linear Schrödinger Equation With Conformable Derivative. Front. Phys. 8:62. doi: 10.3389/fphy.2020.00062

1. INTRODUCTION AND MOTIVATION

Non-linear partial differential equations have different types of equations, one of them is the non-linear Schrödinger equation (NLSE) that relevant to the classical and quantum mechanics. The non-linear Schrödinger equation is a generalized (1+1)-dimensional version of the Ginzburg-Landau equation presented in 1950 in their study on supraconductivity and has been specifically reported by Chiao et al. [1] in their research of optical beams. In the past several years, various methods have been proposed to obtain the exact optical soliton solutions of the non-linear Schrödinger equation [2–12]. Dispersion and non-linearity are two of the essential components for the distribution of solitons across inter-continental regions. Usually, group velocity dispersion (GVD) level with self-phase modulation in a sensible manner allows these solitons to sustain tall range travel. In fact it might happen that the GVD is tiny and thus totally ignored, in this case the dispersion effect is determined by third and fourth order dispersion effects. Subsequently, this equation has been studied in a variety of ways, such as the Lie symmetry [13], both the $\left(m+\frac{G'}{G}\right)$-improved expansion, and the $\exp\left(-\varphi\left(\xi\right)\right)$ −expansion methods [14], and the semi-inverse variation principle method [4]. In this study, the extended sinh-Gordon expansion method (ShGEM) is applied to the non-linear cubic-quartic Schrödinger equations with the Parabolic law of fractional order, which is given by

$$iD_t^{\alpha}u+i\beta D_x^{3\alpha}u+\gamma D_x^{4\alpha}u+cF\left(|u|^2\right)u=0, \tag{1}$$

where $u(x,t)$ is the complex valued wave function. The operator D^{α} of order α, where $\alpha \in (0, 1]$ is the fractional derivative, the parameters γ and β are real constants, a real-valued algebraic function $F\left(|u|^2\right)$ is p-times continuously differentiable, then

$$F\left(|u|^2\right) \in \bigcup_{m,n=1}^{\infty} C^p\left((-n,n)\times(-m,m):R^2\right). \tag{2}$$

By using the relation of

$$F(u) = c_1 u + c_2 u^2,$$

on Equation (1), we obtain the fractional non-linear Schrödinger equations with Parabolic law as follows:

$$iD_t^{\alpha}u + i\beta D_x^{3\alpha}u + \gamma D_x^{4\alpha}u + \left(c_1|u|^2 + c_2|u|^4\right)u = 0. \tag{3}$$

The extended sinh-Gordon expansion method is intended to a generalization of the sine-Gordon expansion equation because it is based on an auxiliary equation namely the sine-Gordon equation (see previous studies [15, 16] for details). Moreover, different computational and numerical methods have been utilized to constructed new solutions to the non-linear partial differential equations, such as the variable separated method [17], the auxiliary parameters and residual power series method [18], the Bernoulli sub-equation method [19, 20], the modified auxiliary expansion method [21], the homotopy analysis transform method [22–26], the homotopy perturbation sumudu transform method [27], the shooting method with the explicit Runge-Kutta scheme [28, 29], and the Adomian decomposition method [30]. Recently, several fractional operators have been applied to the mathematical models in order to seek their exact solutions, such as the Laplace transform [31, 32], the Nabla operator [33–35].

The outline of paper are organize the paper as follows: A short review of the conformable derivative is presented in section 2. Section 3 deals with the analysis of the ShGEM. In section 4, the method is applied to solve the non-linear Schrödinger equation involving the fractional derivatives with the parabolic law. Eventually, in section 5, we presented our conclusion of this paper.

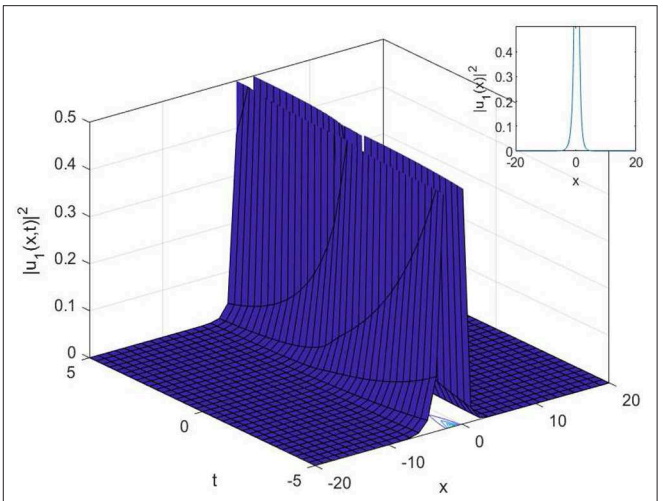

FIGURE 1 | 3D, 2D, and contour surfaces of Equation (26) where $\omega = 0.1,\ c_2 = 0.1,\ \kappa = 2,\ \alpha = 0.8$.

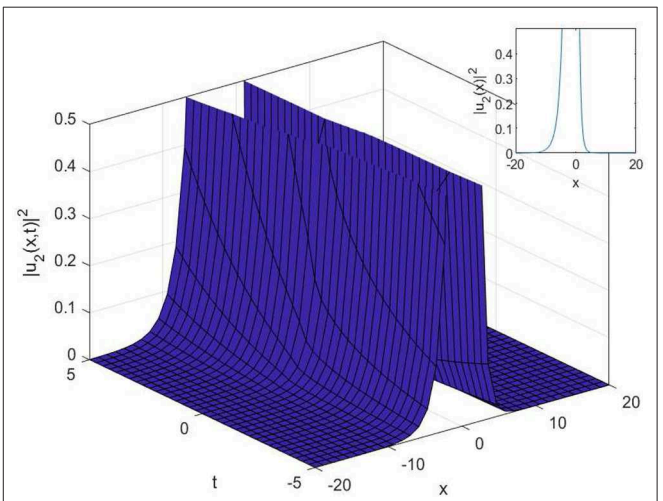

FIGURE 2 | 3D, 2D, and contour surfaces of Equation (28) where $\gamma = 0.5,\ c_2 = 0.2,\ \kappa = 0.4,\ \alpha = 0.7$.

2. BASIC DEFINITIONS

The basic definitions of the conformable derivative of order α are given as follows [36–41]:

Definition 2.1. Assume the function $h:(0,\infty)\to\mathbb{R}$ then, the conformable derivative of h of order α is defined as $D_t^{\alpha}h(t) = \lim_{\varepsilon\to 0}\frac{h\left(t+\varepsilon t^{1-\alpha}\right)-h(t)}{\varepsilon}$, $\forall t>0$, and $0<\alpha\le 1$.

Definition 2.2. Assume that $c \ge 0$ and $t \ge c$, let h be a function defined on $(c, t]$ as well as $\alpha \in \mathbb{R}$. Then, the α-fractional integral of h is given by

$${}_tI_c^{\alpha}h(t) = \int_c^{\alpha}\frac{h(x)}{x^{1-\alpha}}dx, \tag{4}$$

if the Riemann improper integral exists.

Theorem 2.1. *Let $\alpha \in (0,1]$, and $h = h(t)$, $g = g(t)$ be α-conformable differentiable at a point $t > 0$, then:*

$$\begin{aligned} D_t^{\alpha}\left(ah+bg\right) &= aD_t^{\alpha}h + bD_t^{\alpha}g, forall(a,\ b\notin\mathbb{R}).\\ D_t^{\alpha}\left(t^{\lambda}\right) &= \lambda t^{\lambda-\alpha}, forall(\lambda\in\mathbb{R}).\\ D_t^{\alpha}\left(hg\right) &= gD_t^{\alpha}\left(h\right) + hD_t^{\alpha}\left(g\right).\\ D_t^{\alpha}\left(\frac{h}{g}\right) &= \frac{gD_t^{\alpha}\left(h\right) - hD_t^{\alpha}\left(g\right)}{g^2}. \end{aligned} \tag{5}$$

Furthermore, if function h is differentiable, then $D_t^{\alpha}\left(h(t)\right) = t^{1-\alpha}\frac{dh}{dt}$.

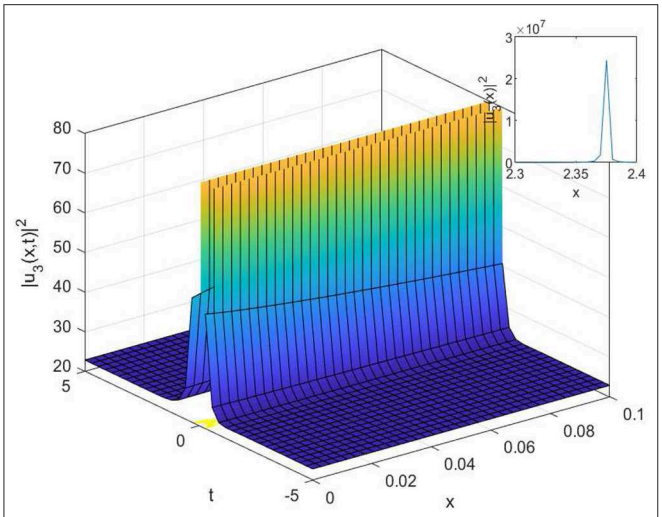

FIGURE 3 | 3D, 2D, and contour surfaces of Equation (30) where $\gamma = 0.5,\ c_1 = 0.7,\ \alpha = 0.9$.

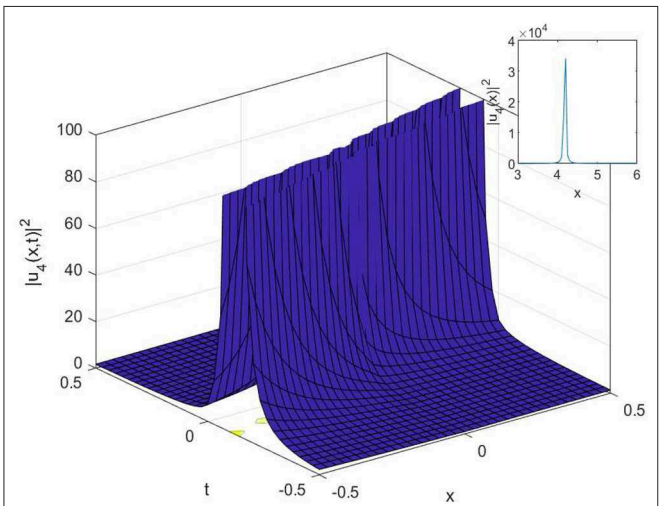

FIGURE 4 | 3D, 2D, and contour surfaces of Equation (32) where $\gamma = 5,\ c_1 = 7,\ \alpha = 0.7$.

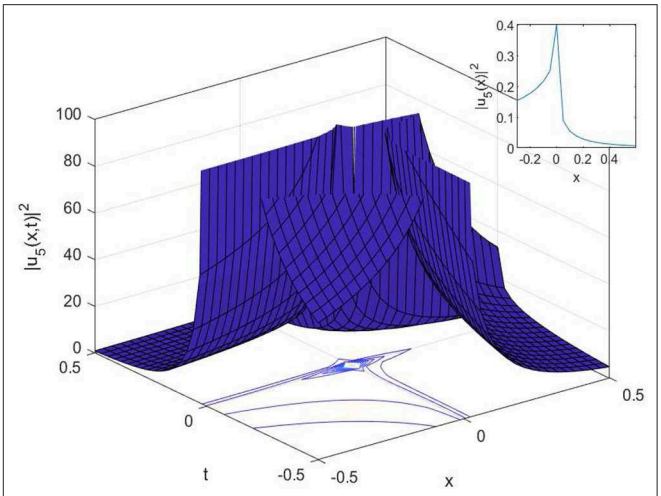

FIGURE 5 | 3D, 2D, and contour surfaces of Equation (34) where $c_1 = 0.2,\ \kappa = 0.4,\ \omega = 6,\ \alpha = 0.4$.

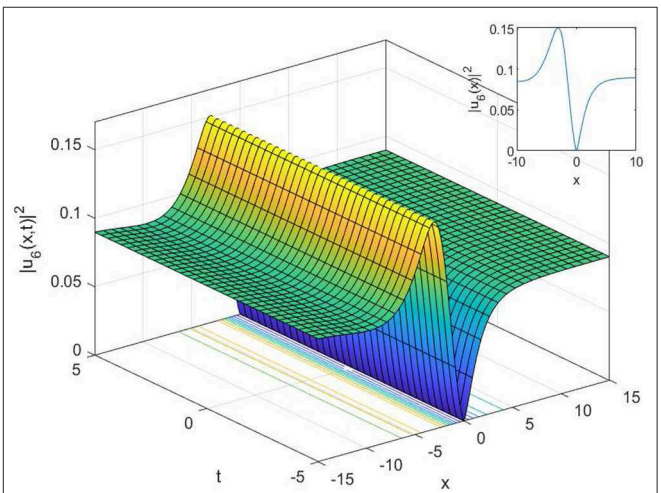

FIGURE 6 | 3D, 2D, and contour surfaces of Equation (36) where $c_2 = 0.2,\ A_1 = 0.3,\ \alpha = 0.7$.

Theorem 2.2. *(see for details pervious research [40]): Let h be a differentiable function and α is order of the conformable derivative. Let g be a differentiable function defined in the range of h, then*

$$D_t^{\alpha}\left(fog\right)(t) = t^{1-\alpha} g(t)^{\alpha-1} g'(t)\, D_t^{\alpha}\left(f(t)\right)_{t=g(t)}, \tag{6}$$

here "prime" is the classical derivatives with respect to t.

3. THE EXTENDED ShGEM

In the current section, we presented the main steps of the e ShGEM (see previous study [42, 43]).

Consider the following fractional non-linear PDE:

$$W\left(D_x^{\sigma} p,\ p^2 D_x^{2\sigma} p,\ D_t^{\upsilon} p,\ D_t^{\upsilon} D_x^{\sigma} p, \ldots\right) = 0, \tag{7}$$

where $p = p(x,t)$.

Consider the wave transformation

$$p(x,t) = \psi(\zeta), \zeta = \frac{x^{\sigma}}{\sigma} - c\frac{t^{\upsilon}}{\upsilon}, \tag{8}$$

by substitute relation Equation (8) into Equation (7), we obtain the following non-linear ODE:

$$P\left(\psi,\ \psi',\ \psi,'' \ \psi^2\psi', \ldots\right) = 0. \tag{9}$$

Consider the trial solution of Equation (9) of the form

$$\psi(\theta) = \sum_{j=1}^{k}\left[A_j \sinh(\theta) + B_j \cosh(\theta)\right]^j + A_0. \tag{10}$$

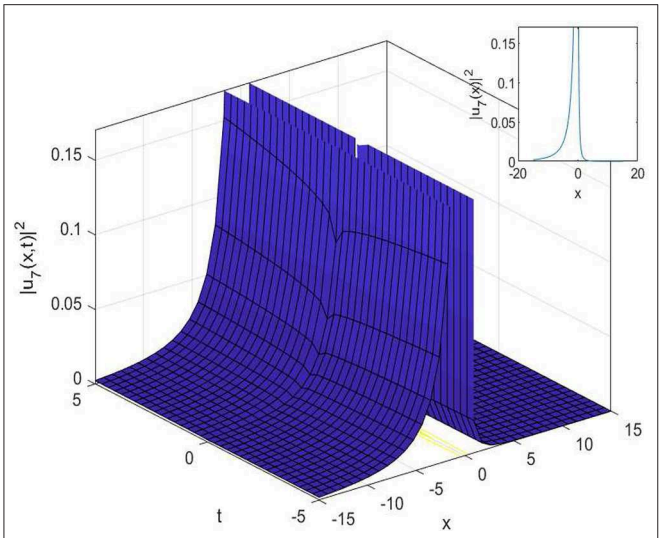

FIGURE 7 | 3D, 2D, and contour surfaces of Equation (38) where $\alpha = 0.3,\ c_1 = 0.5,\ c_2 = 0.2,\ \kappa = 0.4$.

The parameters A_j, B_j, for $(j = 1, 2, \ldots, k)$ and A_0 are real constants, and θ is a function of η that hold the following ODE:

$$\theta' = \sinh(\theta). \tag{11}$$

The homogeneous balance principle is applied on Equation (9) to find the value of k. From the space-time fractional the sinh-Gordon equation, we have (see previous study [15, 16]).

$$D_t{}^{\nu} D_x{}^{\sigma} p = \lambda sinh(p). \tag{12}$$

The exact solutions of Equation (12) may be given as

$$sinh\,(\theta) = \pm\, csch\,(\zeta)\ or\ sinh\,(\theta) = \pm\, isech\,(\zeta), \tag{13}$$

and

$$cosh\,(\theta) = \pm\, coth\,(\zeta)\ or\ cosh\,(\theta) = \pm\, tanh\,(\zeta). \tag{14}$$

Letting solutions of Equation (10) along with Equations (13) and (14) as the form

$$\psi(\zeta) = \sum_{j=1}^{k} \left[\pm iA_j\, \mathrm{sech}\,(\zeta) \pm B_j \tanh(\zeta)\right]^j + A_0, \tag{15}$$

$$\psi(\zeta) = \sum_{j=1}^{k} \left[\pm A_j\, \mathrm{csch}\,(\zeta) \pm B_j \coth(\zeta)\right]^j + A_0. \tag{16}$$

Finding the value of k and then inserting Equations (10) and (12) into Equation (9), we get a system of terms of:

$$sinh^i\,(\theta)\ cosh^j\,(\theta), \tag{17}$$

we gather a group of over-defined non-linear algebraic equations in A_0, A_j, B_j, putting the coefficients of $sinh^i\,(\theta)\ cosh^j\,(\theta)$ to zero, and finding the solutions of acquired system, we gain the values of A_0, A_j, B_j, c_1, c_2, κ, and ω. Putting the values of A_0, A_j, B_j, c_1, c_2, κ, and ω into Equations (15) and (16), we can find the solutions of Equation (7).

4. IMPLEMENT OF THE EXTENDED ShGEM

The implementation of the extended ShGEM to the cubic-quartic non-linear Schrödinger equation with conformable derivative is provided in this section.

Consider the wave transformation

$$u(x,t) = U(\xi)e^{i\theta},\ \xi = \frac{x^\alpha}{\alpha} - \nu\frac{t^\alpha}{\alpha},\ \theta = -\frac{\kappa\, x^\alpha}{\alpha} + \frac{\omega\, t^\alpha}{\alpha}. \tag{18}$$

In Equation (18), $\theta(x,t)$ represents the phase component of the soliton. The ω, κ, ν are the wave number, the soliton frequency, and the soliton velocity, respectively. Substituting wave transformation into Equation (2) and splitting the outcomes equation into real and imaginary parts, we gain

$$-\left(\beta\kappa^3 - \gamma\kappa^4 + \omega\right)U + c_1U^3 + c_2U^5 + 3\beta\kappa U'' - 6\gamma\kappa^2 U'' + \gamma U^{(4)} = 0, \tag{19}$$

$$-\left(3\beta\kappa^2 - 4\gamma\kappa^3 + \nu\right)U' + \beta U^{(3)} - 4\gamma\kappa U^{(3)} = 0. \tag{20}$$

Multiply both sides of Equation (19) by U' and integrate it, we obtain

$$\gamma\left(-\frac{\left(U''\right)^2}{2} + U'''\,U'\right) + \frac{c_1U^4}{4} + \frac{c_2U^6}{6} + 3\gamma\kappa^2\left(U'\right)^2 + \frac{1}{2}U^2\left(-4\gamma\kappa^4 + \gamma\kappa^4 - \omega\right) = 0. \tag{21}$$

From Equation (20), we get constraint conditions $\nu = 4\gamma\kappa^3 - 3\beta\kappa^2$ and $\beta = 4\gamma\kappa$. Balancing the terms $U'''\,U'$ and U^6 yields $\kappa = 1$. With $\kappa = 1$, Equations (10), (16), and (17) change to

$$\psi(\theta) = \left[A_1 \sinh(\theta) + B_1 \cosh(\theta)\right] + A_0, \tag{22}$$

$$\psi(\zeta) = \left[\pm iA_1\, \mathrm{sech}\,(\zeta) \pm B_1 \tanh(\zeta)\right] + A_0, \tag{23}$$

and

$$\psi(\zeta) = \left[\pm m_1\, \mathrm{csch}\,(\zeta) \pm n_1 \coth(\zeta)\right] + n_0, \tag{24}$$

respectively.

Inserting Equation (22) along with Equation (12) into Equation (21), and using constraint conditions provides a non-linear algebraic system. Equaling each coefficient of $sinh^i\,(\theta)\ cosh^j\,(\theta)$ with the same power to zero, and finding the obtained system of algebraic equations, we gain the values of the parameters. Putting the obtained values of the parameters into Equations (23) and (24), give the solutions of Equation (3).

Set 1

$$B_1 = \frac{2^{3/4}3^{1/4}\omega^{1/4}}{\left(c_2\left(-1-6\kappa^2+3\kappa^4\right)\right)^{1/4}},\ c_1 = \frac{\sqrt{\frac{2}{3}}c_2\left(5+3\kappa^2\right)\sqrt{\omega}}{\sqrt{c_2\left(-1-6\kappa^2+3\kappa^4\right)}},$$
$$A_0 = 0,\ \gamma = \frac{\omega}{1+6\kappa^2-3\kappa^4}, A_1 = 0, \tag{25}$$

we get

$$u_1(x,t) = \frac{2^{3/4}3^{1/4}\omega^{1/4}}{\left(c_2\left(-1-6\kappa^2+3\kappa^4\right)\right)^{1/4}} csch\left(\frac{x^\alpha}{\alpha}+\frac{8t^\alpha\kappa^3\omega}{\alpha\left(1+6\kappa^2-3\kappa^4\right)}\right)e^{i\left(-\frac{x^\alpha\kappa}{\alpha}+\frac{t^\alpha\omega}{\alpha}\right)}. \tag{26}$$

Set 2

$$B_1 = \frac{(1+i)\,6^{1/4}\gamma^{1/4}}{{c_2}^{1/4}},\ \omega = \gamma\left(1+6\kappa^2-3\kappa^4\right),$$
$$c_1 = i\sqrt{\frac{2}{3}}\sqrt{\gamma}\sqrt{c_2}\left(5+3\kappa^2\right),\ A_1 = 0,\ A_0 = 0, \tag{27}$$

we get

$$u_2(x,t) = \frac{(1+i)\,6^{1/4}a_2^{1/4}}{{c_2}^{1/4}} csch\left(\frac{x^\alpha}{\alpha}+\frac{8a_2t^\alpha\kappa^3}{\alpha}\right)e^{i\left(-\frac{x^\alpha\kappa}{\alpha}+\frac{a2t^\alpha\left(1+6\kappa^2-3\kappa^4\right)}{\alpha}\right)}. \tag{28}$$

Set 3

$$A_0 = 0,\ A_1 = \frac{4\sqrt{2}\sqrt{\gamma}}{\sqrt{c_1}},\ B_1 = 0,\ c_2 = -\frac{3{c_1}^2}{128\gamma},$$
$$\kappa = -\sqrt{\frac{2}{3}}, \omega = \frac{20\gamma}{3}, \tag{29}$$

we get

$$u_3(x,t) = -\frac{4\sqrt{2}\sqrt{\gamma}}{\sqrt{c_1}}\coth\left(\frac{16\sqrt{\frac{2}{3}}\gamma t^\alpha}{3\alpha}-\frac{x^\alpha}{\alpha}\right)e^{i\left(\frac{20\gamma t^\alpha}{3\alpha}+\frac{\sqrt{\frac{2}{3}}x^\alpha}{\alpha}\right)}. \tag{30}$$

Set 4

$$A_0 = 0,\ A_1 = -\frac{\sqrt{2}\sqrt{\gamma}}{\sqrt{c_1}}, B_1 = \frac{\sqrt{2}\sqrt{\gamma}}{\sqrt{c_1}},\ c_2 = -\frac{3{c_1}^2}{8\gamma},$$
$$\kappa = -\frac{1}{\sqrt{6}}, \omega = \frac{5\gamma}{12}, \tag{31}$$

we get

$$u_4(x,t) = -\frac{\sqrt{2}\sqrt{\gamma}}{\sqrt{c_1}}\left(\coth\left(\frac{2\sqrt{\frac{2}{3}}\gamma t^\alpha}{3\alpha}-\frac{x^\alpha}{\alpha}\right)+\text{csch}\left(\frac{2\sqrt{\frac{2}{3}}\gamma t^\alpha}{3\alpha}-\frac{x^\alpha}{\alpha}\right)\right)\times e^{i\left(\frac{5a2t^\alpha}{12\alpha}+\frac{x^\alpha}{\sqrt{6}\alpha}\right)}. \tag{32}$$

Set 5

$$B_1 = -\frac{2\sqrt{\left(5+3\kappa^2\right)\omega}}{\sqrt{c_1\left(-1-6\kappa^2+3\kappa^4\right)}},\ A_1 = 0,\ A_0 = 0,$$
$$c_2 = \frac{3{c_1}^2\left(-1-6\kappa^2+3\kappa^4\right)}{2\left(5+3\kappa^2\right)^2\omega},\ \gamma = \frac{\omega}{1+6\kappa^2-3\kappa^4}, \tag{33}$$

we obtain

$$u_5(x,t) = \frac{2\sqrt{\left(5+3\kappa^2\right)\omega}}{\sqrt{c_1\left(-1-6\kappa^2+3\kappa^4\right)}} csch\left(\frac{x^\alpha}{\alpha}+\frac{8t^\alpha\kappa^3\omega}{\alpha\left(1+6\kappa^2-3\kappa^4\right)}\right)e^{i\left(-\frac{x^\alpha\kappa}{\alpha}+\frac{t^\alpha\omega}{\alpha}\right)}. \tag{34}$$

Set 6

$$B_1 = A_1, A_0 = 0,\ c_1 = -\frac{4{A_1}^2c_2}{3},\ \gamma = -\frac{2{A_1}^4c_2}{3},$$
$$\omega = -\frac{5{A_1}^4c_2}{18}, \kappa = \frac{1}{\sqrt{6}}, \tag{35}$$

we get

$$u_6(x,t) = \left(-A_1\coth\left(\frac{4\sqrt{\frac{2}{3}}{A_1}^4c_2t^\alpha}{9\alpha}-\frac{x^\alpha}{\alpha}\right)+A_1 csch\left(\frac{4\sqrt{\frac{2}{3}}{A_1}^4c_2t^\alpha}{9\alpha}-\frac{x^\alpha}{\alpha}\right)\right)\times e^{i\left(-\frac{5{A_1}^4c_2t^\alpha}{18\alpha}-\frac{x^\alpha}{\sqrt{6}\alpha}\right)}. \tag{36}$$

Set 7

$$B_1 = \frac{\sqrt{6}\sqrt{c_1}}{\sqrt{c_2\left(5+3\kappa^2\right)}},\ \gamma = -\frac{3{c_1}^2}{2c_2\left(5+3\kappa^2\right)^2},$$
$$\omega = \frac{3{c_1}^2\left(-1-6\kappa^2+3\kappa^4\right)}{2c_2\left(5+3\kappa^2\right)^2},\ A_1 = 0,\ A_0 = 0, \tag{37}$$

we get

$$u_7(x,t) = \frac{\sqrt{6}\sqrt{c_1}}{\sqrt{c_2\left(5+3\kappa^2\right)}} csch\left(\frac{x^\alpha}{\alpha}-\frac{12{c_1}^2t^\alpha\kappa^3}{c_2\alpha\left(5+3\kappa^2\right)^2}\right)e^{i\left(-\frac{x^\alpha\kappa}{\alpha}+\frac{3{c_1}^2t^\alpha\left(-1-6\kappa^2+3\kappa^4\right)}{2c_2\alpha\left(5+3\kappa^2\right)^2}\right)}. \tag{38}$$

5. CONCLUSION

In this article, we have successfully used the extended sinh-Gordon expansion method to solve the problem for the non-linear cubic-quartic Schrödinger equations involving fractional derivatives with the Parabolic law. A traveling wave

transforms in the sense of the comfortable derivative has been used to convert the governing equation into a NODE. The various optical solutions of the studied model have been constructed, for example, the singular soliton solutions as shown in **Figures 1–6**, and the dark-bright soliton solution as seen in **Figure 7**. Comparing our solutions to the results obtained in references [16–18], our findings solutions are new and different. To better analyze the dynamic attitude, and the characteristics of these solutions, the 2D, 3D and counter-surface of all obtained solutions are plotted. The study shows that this method is the effective and appropriate technique for finding the exact solution of the model considered in the paper.

DATA AVAILABILITY STATEMENT

All datasets generated for this study are included in the article/supplementary material.

AUTHOR CONTRIBUTIONS

HD contributed in developing the proofs and edited the article for possible improvement. HG, KA, and RY contributed in developing the main results and proofs. All authors read the final version and approved it.

REFERENCES

1. Chiao RY, Garmire E, Townes CH. Self-trapping of optical beams. *Phys Rev Lett*. (1964) **13**:479–82. doi: 10.1103/PhysRevLett.13.479
2. Arshad M, Seadawy AR, Dianchen Lu. Exact bright–dark solitary wave solutions of the higher-order cubic–quintic nonlinear Schrödinger equation and its stability. *Optik*. (2017) **9**:40–9. doi: 10.1016/j.ijleo.2017.03.005
3. Biswas A, Triki H, Zhou Q, Moshokoa SP, Ullah MZ, Belic M. Cubic–quartic optical solitons in Kerr and power law media. *Optik*. (2017) **144**:357–62. doi: 10.1016/j.ijleo.2017.07.008
4. Biswas A, Arshed S. Application of semi-inverse variational principle to cubic-quartic optical solitons with kerr and power law nonlinearity. *Optik*. (2018) **172**:847–50. doi: 10.1016/j.ijleo.2018.07.105
5. Hosseini K, Samadani F, Kumar D, Faridi M. New optical solitons of cubic-quartic nonlinear Schrödinger equation. *Optik*. (2018) **157**:1101–5. doi: 10.1016/j.ijleo.2017.11.124
6. Houwe A, Hammouch Z, Bienvenue D, Nestor S, Betchewe G, DOKA SY. Nonlinear Schrödingers equations with cubic nonlinearity: M-derivative soliton solutions by $exp(\phi(\xi))$-Expansion method. *Preprints*. (2019). **2019**:2019030114 doi: 10.20944/preprints201903.0114.v1
7. Li HM, Xu YS, Lin J. New optical solitons in high-order dispersive cubic-quintic nonlinear Schrödinger equation. *Commun Theor Phys*. (2004) **41**:829–32. doi: 10.1088/0253-6102/41/6/829
8. Nawaz B, Ali K, Oan Abbas S, Rizvi STR, Zhou Q. Optical solitons for non-Kerr law nonlinear Schrödinger equation with third and fourth order dispersions. *Chin J Phys*. (2019) **60**:133–40. doi: 10.1016/j.cjph.2019.05.014
9. Seadawy AR, Kumar D, Chakrabarty AK. Dispersive optical soliton solutions for the hyperbolic and cubic-quintic nonlinear Schrödinger equations via the extended sinh-Gordon equation expansion method. *Eur Phys J Plus*. (2018) **133**:182. doi: 10.1140/epjp/i2018-12027-9
10. Xie Y, Yang Z, Li L. New exact solutions to the high dispersive cubic–quintic nonlinear Schrödinger equation. *Phys Lett A*. (2018) **382**:2506–14. doi: 10.1016/j.physleta.2018.06.023
11. Wang P, Shang T, Feng L, Du Y. Solitons for the cubic-quintic nonlinear Schrödinger equation with Raman effect in nonlinear optics. *Opt Quant Electron*. (2014) **46**:1117–26. doi: 10.1007/s11082-013-9840-8
12. Srivastava HM, Gnerhan H, Ghanbari B. Exact traveling wave solutions for resonance nonlinear Schrödinger equation with intermodal dispersions and the Kerr law nonlinearity. *Math Meth Appl Sci*. (2019) **42**:7210–21. doi: 10.1002/mma.5827
13. Bansal A, Biswas A, Zhou Q, Babatin MM. Lie symmetry analysis for cubic–quartic nonlinear Schrödinger's equation. *Optik*. (2018) **169**:12–5. doi: 10.1016/j.ijleo.2018.05.030
14. Gao W, Ismael HF, Husien AM, Bulut H, Baskonus HB. Optical soliton solutions of the cubic-quartic nonlinear schrödinger and resonant nonlinear Schrödinger equation with the parabolic law. *Appl Sci*. (2020) **10**:219. doi: 10.3390/app10010219
15. Baskonus HM, Bulut, H, Sulaiman TA. New complex hyperbolic structures to the lonngren-wave equation by using sine-gordon expansion method. *Appl Math Nonlin Sci*. (2019) **4**:129–38. doi: 10.2478/AMNS.2019.1.00013
16. Ali KK, Yilmazer R, Bulut H. Analytical solutions to the coupled Boussinesq–Burgers equations via Sine-Gordon expansion method. In: *4th International Conference on Computational Mathematics and Engineering Sciences (CMES-2019). CMES 2019. Advances in Intelligent Systems and Computing*, Vol. 1111. Cham: Springer. (2020). p. 233–40. doi: 10.1007/978-3-030-39112-6_17
17. Al-Ghafri KS, Rezazadeh H. Solitons and other solutions of (3+1)-dimensional space–time fractional modified KdV–Zakharov–Kuznetsov equation. *Appl Math Nonlin Sci*. (2019) **4**:289–304. doi: 10.2478/AMNS.2019.2.00026
18. Kumar S, Kumar A, Momani S, Aldhaifallah M, Nisar KS. Numerical solutions of nonlinear fractional model arising in the appearance of the stripe patterns in two-dimensional systems. *Adv Differ Equat*. (2019) **2019**:413. doi: 10.1186/s13662-019-2334-7
19. Ismael HF, Bulut H. On the Solitary Wave Solutions to the (2+1)-Dimensional Davey-Stewartson Equations, 4th International Conference on Computational Mathematics and Engineering Sciences (CMES-2019). CMES 2019. Advances in Intelligent Systems and Computing, vol 1111. Springer, Cham. (2020). p. 156–65. doi: 10.1007/978-3-030-39112-6_11
20. Abdulkareem HH, Ismael HF, Panakhov ES, Bulut H. Some novel solutions of the coupled Whitham-Broer-Kaup equations. In: *4th International Conference on Computational Mathematics and Engineering Sciences (CMES-2019). CMES 2019. Advances in Intelligent Systems and Computing*, Vol. 1111. Cham: Springer (2020). p. 200–8. doi: 10.1007/978-3-030-39112-6_14
21. Gao W, Ismael HF, Bulut H, Baskonus HM. Instability modulation for the (2+1)-dimension paraxial wave equation and its new optical soliton solutions in Kerr media. *Phys Scripta*. (2019) **95**. doi: 10.1088/1402-4896/ab4a50
22. Kumar D, Singh J, Purohit SD, Swroop R. A hybrid analytical algorithm for nonlinear fractional wave-like equations. *Math Modell Nat Phen*. (2019) **14**:304. doi: 10.1051/mmnp/2018063
23. Bhatter S, Mathur A, Kumar D, Nisar KS, Singh J. Fractional modified Kawahara equation with Mittag–Leffler law. *Chaos Solit Fract*. (2019) **131**:109508. doi: 10.1016/j.chaos.2019.109508
24. Singh J, Kumar D, Baleanu D. New aspects of fractional Biswas–Milovic model with Mittag-Leffler law. *Math Modell Nat Phen*. (2019) **14**:303. doi: 10.1051/mmnp/2018068
25. Kumar D, Singh J, Baleanu D. On the analysis of vibration equation involving a fractional derivative with Mittag-Leffler law. *Math Methods Appl Sci*. (2020) **43**:443–57. doi: 10.1002/mma.5903
26. Veeresha P, Prakasha DG, Baskonus HM. New numerical surfaces to the mathematical model of cancer chemotherapy effect in caputo fractional derivatives. *AIP Chaos*. (2019) **29**:1–14. doi: 10.1063/1.5074099
27. Goswami A, Singh J, Kumar D. An efficient analytical approach for fractional equal width equations describing hydro-magnetic waves in cold plasma. *Phys A*. (2019) **524**:563–75. doi: 10.1016/j.physa.2019.04.058

28. Ismael HF. Carreau-Casson fluids flow and heat transfer over stretching plate with internal heat source/sink and radiation. *Int J Adv Appl Sci*. (2017) **4**:11–5. doi: 10.21833/ijaas.2017.07.003
29. Ismael HF, Arifin NM. Flow and heat transfer in a Maxwell liquid sheet over a stretching surface with thermal radiation and viscous dissipation. *JP J Heat Mass Transf*. (2018) **15**:847–66. doi: 10.17654/HM015040847
30. Ismael HF, Ali KK. MHD casson flow over an unsteady stretching sheet. *Adv Appli Fluid Mech*. (2017) **20**:533–41. doi: 10.17654/FM020040533
31. Kumar D, Singh J, Al Qurashi M, Baleanu D. A new fractional SIRS-SI malaria disease model with application of vaccines, antimalarial drugs, and spraying. *Adv Differ Equat*. (2019) **2019**:278. doi: 10.1186/s13662-019-2199-9
32. Singh J, Kumar D, Baleanu D, Rathore S. On the local fractional wave equation in fractal strings. *Math Methods Appl Sci*. (2019) **42**:1588–95. doi: 10.1002/mma.5458
33. Ali KK, Yilmazer R. Discrete fractional solutions to the effective mass Schrödinger equation by mean of Nabla operator. *AIMS Math*. (2020) **5**:894–903. doi: 10.3934/math.2020061
34. Ozturk O, Yilmazer R. Solutions of the radial Schrödinger equation in hypergeometric and discrete fractional forms. *Commun Fac Sci Univ Ank Ser A1 Math Stat*. (2019) **68**:833–9. doi: 10.31801/cfsuasmas.481600
35. Yilmazer R, Discrete fractional solution of a non-homogeneous non-Fuchsian differential equations. *Therm Sci*. (2019) **23**:S121–7. doi: 10.2298/TSCI180917336Y
36. Khalil R, Al Horani M, Yousef A, Sababheh M. A new definition of fractional derivative. *J Comput Appl Math*. (2014) **264**:65–70. doi: 10.1016/j.cam.2014.01.002
37. Nisar KS, Rahman G, Khan A. Some new inequalities for generalized fractional conformable integral operators. *Adv Differ Equat*. (2019) **2019**:427. doi: 10.1186/s13662-019-2362-3
38. Nisar KS, Tassaddiq A, Rahman G, Khan A. Some inequalities via fractional conformable integral operators. *J Inequal Appl*. (2019) **2019**:217. doi: 10.1186/s13660-019-2170-z
39. Rahman G, Ullah Z, Khan A, Set E, Nisar KS. Certain Chebyshev-type inequalities involving fractional conformable integral operators. *Mathematics*. (2019) **7**:364. doi: 10.3390/math7040364
40. Abdeljawad T. On conformable fractional calculus. *J Comput Appl Math*. (2015) **279**:57–66. doi: 10.1016/j.cam.2014.10.016
41. Gao W, Yel G, Haci MB, Cattani C. Complex solitons in the conformable (2+1)-dimensional Ablowitz-Kaup-Newell-Segur Equation. *AIMS Math*. (2020) **5**:507–21. doi: 10.3934/math.2020034
42. Xian-Lin X, Jia-Shi T. Travelling wave solutions for Konopelchenko-Dubrovsky equation using an extended sinh-Gordon equation expansion. *Commun Theor Phys*. (2008) **50**:1047. doi: 10.1088/0253-6102/50/5/06
43. Esen A, Sulaiman TA, Bulut H, Baskonus HM. Optical solitons to the space-time fractional (1+1)-dimensional coupled nonlinear Schrödinger equation. *Optik*. (2018) **167**:150–6. doi: 10.1016/j.ijleo.2018.04.015

Conflict of Interest: The authors declare that the research was conducted in the absence of any commercial or financial relationships that could be construed as a potential conflict of interest.

frontiers in Physics

ORIGINAL RESEARCH
published: 31 March 2020
doi: 10.3389/fphy.2020.00054

On the New Wave Behaviors of the Gilson-Pickering Equation

Karmina K. Ali[1,2]*, *Hemen Dutta*[3], *Resat Yilmazer*[2] *and Samad Noeiaghdam*[4,5]

[1] Department of Mathematics, Faculty of Science, University of Zakho, Zakho, Iraq, [2] Department of Mathematics, Faculty of Science, Firat University, Elazig, Turkey, [3] Department of Mathematics, Gauhati University, Guwahati, India, [4] Baikal School of BRICS, Irkutsk National Research Technical University, Irkutsk, Russia, [5] South Ural State University, Chelyabinsk, Russia

In this article, we study the fully non-linear third-order partial differential equation, namely the Gilson-Pickering equation. The $(1/G')$-expansion method, and the generalized exponential rational function method are used to construct various exact solitary wave solutions for a given equation. These methods are based on a homogeneous balance technique that provides an order for the estimation of a polynomial-type solution. In order to convert the governing equation into a nonlinear ordinary differential equation, a traveling wave transformation has been implemented. As a result, we have constructed a variety of solitary wave solutions, such as singular solutions, compound singular solutions, complex solutions, and topological and non-topological solutions. Besides, the 2D, 3D, and contour surfaces are plotted for all obtained solutions by choosing appropriate parameter values.

Keywords: the Gilson-Pickering equation, the $(1/G')$-expansion method, the generalized exponential rational function method, analytic methods, exact solutions

OPEN ACCESS

Edited by:
Devendra Kumar,
University of Rajasthan, India

Reviewed by:
Haci Mehmet Baskonus,
Harran University, Turkey
Amit Goswami,
Jagannath University, India

***Correspondence:**
Karmina K. Ali
karmina.ali@uoz.edu.krd

Specialty section:
This article was submitted to Mathematical Physics, a section of the journal Frontiers in Physics

Received: *12 January 2020*
Accepted: *20 February 2020*
Published: *31 March 2020*

Citation:
Ali KK, Dutta H, Yilmazer R and Noeiaghdam S (2020) On the New Wave Behaviors of the Gilson-Pickering Equation. Front. Phys. 8:54. doi: 10.3389/fphy.2020.00054

1. INTRODUCTION

Nonlinear partial differential equations (NLPDEs) are used to represent a variety of nonlinear physical phenomena in different areas of applied sciences like fluid dynamics, plasma physics, optical fibers, and biology. Among the most profitable strategies for examining such nonlinear physical phenomena is to seek for the exact solutions of NLPDEs [1–5]. In recent years, a variety of effective methods have been implemented to investigate the exact solutions of nonlinear partial differential equations, such as Hirota's bilinear method [6], the Adomian decomposition method [7], the $\exp(-\Phi(\xi))$-expansion method [8], the sine-Gordon expansion method [9], the Bernoulli sub-equation method [10, 11], the shooting method with the fourth-order Runge-Kutta scheme [12, 13], the generalized exponential rational function method [14–18], the modified exponential function method [19], the modified auxiliary expansion method [20], the homotopy perturbation Sumudu transform method [21], the homotopy perturbation transform method [22, 23], and the fractional homotopy analysis transform method [24].

The third-order nonlinear partial differential equation (NLPDE) was introduced in [25] by Gilson and Pickering as

$$u_t - \epsilon u_{xxt} + 2ku_x - uu_{xxx} - \alpha uu_x - \beta u_x u_{xx} = 0, \tag{1}$$

where $\varepsilon, \alpha, \kappa$, and β are non-zero real numbers. Recently, the Gilson-Pickering equation has been investigated using a variety of methods, such as the (G'/G)-expansion method [26], the anstaz method [27], the (G'/G)-expansion method to tanh, the coth, cot, and the logical forms under certain conditions [28], the Bernoulli sub-equation model [29], a not a knot meshless method [30], and the symmetry method [31].

The core of this paper is to investigate the Gilson-Pickering equation using the $(1/G')$-expansion method and the generalized exponential rational function method (GERF).

2. APPLICATIONS OF THE GILSON PICKERING EQUATION

This section presents specific instances of the Gilson Pickering equation and their applications. When $\varepsilon = 1, \alpha = -3$, and $\beta = 2$, Equation (1) gives the Fuchssteiner-Fokas-Camassa-Holm equation, which is a completely integrable nonlinear partial differential equation that arises at different levels of approximation in shallow water theory [32, 33]. When $\varepsilon = 0, \alpha = 1, \kappa = 0$, and $\beta = 3$, Equation (1) reduces to the Rosenau-Hyman equation (RH), which arises in the study of the influence of nonlinear dispersion on the structure of patterns in liquid drops [34]. When $\varepsilon = 1, \alpha = -1, \kappa = 0.5$, and $\beta = 3$, Equation (1) gives the Fronberg-Whitham (FW), which was developed to analyze the qualitative characteristics of wave breakage and admits a wave of the highest height [35–37].

3. THE BASIC CONCEPTS OF THE $(1/G')$-EXPANSION METHOD

In this section, the fundamental steps of the $(1/G')$-expansion method are presented [38, 39]:

Step 1. Let us consider the general form of a two-variable nonlinear partial differential equation (NPDE) as follows:

$$Q(p, p_t, p_x, p_{xx}, ...) = 0, \tag{2}$$

where $p = p(x, t)$, and Q is a partial differential equation.

Step 2. To convert Equation (2) to a nonlinear ordinary differential equation (NODE), we employ the following wave transformation

$$p(x, t) = P(\eta), \ \eta = (x - ht), \tag{3}$$

where h is a scalar. After some procedures, Equation (2) reduces to the following NODE:

$$W(P', P'', P''', ...) = 0, \tag{4}$$

where W is an ordinary differential equation.

Step 3. Assume that Equation (4) has a solution of the form

$$P(\eta) = \sum_{i=0}^{m} a_i \left(\frac{1}{G'}\right)^i, \tag{5}$$

where $a_0, a_1, a_2, ..., a_m$ are scalars to be determined, m is a balance term, and $G = G(\eta)$ satisfies the following second-order linear ODE:

$$G'' + \lambda G' + \mu = 0, \tag{6}$$

where λ *and* μ are scalars.

The solution of Equation (6) is given by

$$G(\eta) = a_0 + a_1 \left(\frac{1}{-\mu/\lambda + be^{-\lambda\eta}}\right). \tag{7}$$

If we convert the algebraic expression given by Equation (7) to a trigonometric function, we can write it as the following:

$$G(\eta) = a_0 + \frac{a_1}{-\frac{\mu}{\lambda} + b\cosh(\lambda\eta) - b\sinh(\lambda\eta)}. \tag{8}$$

Inserting Equation (6) and its necessary derivatives along with Equation (5) into Equation (4) returns the polynomial of $\left(\frac{1}{G'}\right)^i$. Summing the $\left(\frac{1}{G'}\right)^i$ coefficients with the same power and then setting every summation to zero, we get a system of algebraic equations for $a_i, i \geq 0$. Eventually, solving this system simply gives the value of the variables. Putting these values of variables with the value of the balance term m into Equation (4), we can get solutions for Equation (2).

4. THE BASIC CONCEPTS OF THE GERF

In this section, the basic steps of the GERF are presented.

Step1. Let us consider that the general form of a nonlinear partial differential equation is given by:

$$Q(p, p_x, p_t, p_{xx}, ...) = 0, \tag{9}$$

where Q is a partial differential equation.

Suppose that the wave transformation takes the form:

$$p(x, t) = P(\eta), \ \eta = x - ht, \tag{10}$$

where h is a scalar.

Using Equation (10) in Equation (9), we get the nonlinear ordinary differential equation

$$W(P, P', P'', ...) = 0, \tag{11}$$

where W is an ordinary differential equation.

Step 2. Suppose that the solitary wave solutions of Equation (11) are given by:

$$P(\eta) = A_0 + \sum_{K=1}^{m} A_K \varphi(\eta)^K + \sum_{K=1}^{m} B_K \varphi(\eta)^{-K}, \tag{12}$$

where

$$\varphi(\eta) = \frac{r_1 e^{s_1\eta} + r_2 e^{s_2\eta}}{r_3 e^{s_3\eta} + r_4 e^{s_4\eta}}, \tag{13}$$

where r_m, s_m $(1 \leq n \leq 4)$ are real/complex constants, A_0, A_K, B_K are constants to be determined, and m will be determined by the balance principle.

Step 3. Substituting Equation (12) into Equation (11), we get the polynomials that are dependent on Equation (12). By equating the same order terms, we obtain an algebraic system of equations. With the help of computational programs such as Mathematica, Matlab, and Maple, we solve this system and determine the values of A_0, A_K, B_K. Finally one can easily obtain the nontrivial exact solutions of Equation (11).

5. MATHEMATICAL CALCULATION

In this section, the mathematical calculation of the Gilson-Pickering equation is presented.

Consider the Gilson-Pickering equation (Equation 1) stated in section 1. Inserting the wave transformation

$$u = P(\eta), \ \eta = x - ht, \tag{14}$$

into Equation (1), the following NODE can be obtained

$$(2k - h)P' + \epsilon hP''' - PP' - \beta P'P' - \alpha PP' = 0, \tag{15}$$

where $\epsilon, \beta, \alpha, h$, and k are non-zero real numbers.
Integrating Equation (15) once with respect to η and assuming that the integration constant is zero, we have.

$$(2k - h)P + (\epsilon h - P)P'' + \frac{1-\beta}{2}(P')^2 - \frac{\alpha}{2}P^2 = 0. \tag{16}$$

6. IMPLEMENTATION OF THE (1/G′)-EXPANSION METHOD

In this section, the application of the $(1/G')$-expansion method to the Gilson-Pickering equation is presented.

Applying the balance principle, by taking the nonlinear term P^2 and the highest derivative P'' in Equation (16) gives $m = 2$. With $m = 2$, Equation (5) takes the form

$$P(\eta) = a_0 + a_1\left(\frac{1}{G'}\right) + a_2\left(\frac{1}{G'}\right)^2. \tag{17}$$

Inserting Equation (17) and its necessary derivatives into Equation (16), returns the polynomial of $\left(\frac{1}{G'}\right)^i$. Summing the $\left(\frac{1}{G'}\right)^i$ coefficients with the likely power and then setting every summation to zero, we get a system of algebraic equations. Solving this system simply gives the following families of solutions:

Family 1. When

$$\begin{aligned} a_0 &= -\frac{2(h-2k)}{\alpha}, \\ a_1 &= -\frac{12\sqrt{-(h-2k)\alpha}\left(-4k + h(2+\alpha\epsilon)\right)^{3/2}\mu}{\alpha^2\left(-6k + h(3+\alpha\epsilon)\right)}, \\ a_2 &= \frac{12\left(-4k + h(2+\alpha\epsilon)\right)^2\mu^2}{\alpha^2\left(-6k + h(3+\alpha\epsilon)\right)}, \ \lambda = -\frac{\sqrt{-(h-2k)\alpha}}{\sqrt{2h - 4k + h\alpha\epsilon}}, \\ \beta &= -2, \end{aligned} \tag{18}$$

we get

$$\begin{aligned} u_1(x,t) = &\frac{12\left(-4k + h(2+\alpha\epsilon)\right)^2\mu^2}{\alpha^2\left(-6k + h(3+\alpha\epsilon)\right)\left(-\frac{L\mu}{M} + C_1\cosh\left(\frac{M\xi}{L}\right) - C_1\sinh\left(\frac{M\xi}{L}\right)\right)^2} \\ &+ \frac{12M\left(-4k + h(2+\alpha\epsilon)\right)^{3/2}\mu}{\alpha^2\left(-6k + h(3+\alpha\epsilon)\right)\left(-\frac{L\mu}{M} + C_1\cosh\left(\frac{M\xi}{L}\right) - C_1\sinh\left(\frac{M\xi}{L}\right)\right)} \\ &- \frac{2(h-2k)}{\alpha}, \end{aligned} \tag{19}$$

where $M = \sqrt{(-h+2k)\alpha}$, $L = \sqrt{2h - 4k + h\alpha\epsilon}$.

Family 2. When

$$\begin{aligned} &a_0 = 0, a_1 = \frac{12h^{3/2}\sqrt{h-2k}\epsilon^{3/2}\mu}{2k + h(-1+\alpha\epsilon)}, a_2 = \frac{12h^2\epsilon^2\mu^2}{2k + h(-1+\alpha\epsilon)}, \\ &\lambda = \frac{\sqrt{h-2k}}{\sqrt{h}\sqrt{\epsilon}}, \beta = -2, \end{aligned} \tag{20}$$

we get

$$\begin{aligned} u_2(x,t) = &\frac{12h^2\epsilon^2\mu^2}{(2k + h(-1+\alpha\epsilon))\left(-\frac{\sqrt{h}\sqrt{\epsilon}\mu}{\sqrt{h-2k}} + C_1\cosh(S) - C_1\sinh(S)\right)^2} \\ &+ \frac{12h^{3/2}\sqrt{h-2k}\epsilon^{3/2}\mu}{(2k + h(-1+\alpha\epsilon))\left(-\frac{\sqrt{h}\sqrt{\epsilon}\mu}{\sqrt{h-2k}} + C_1\cosh(S) - C_1\sinh(S)\right)}, \end{aligned} \tag{21}$$

where $S = \frac{\sqrt{h-2k}\xi}{\sqrt{h}\sqrt{\epsilon}}$.

Family 3. When

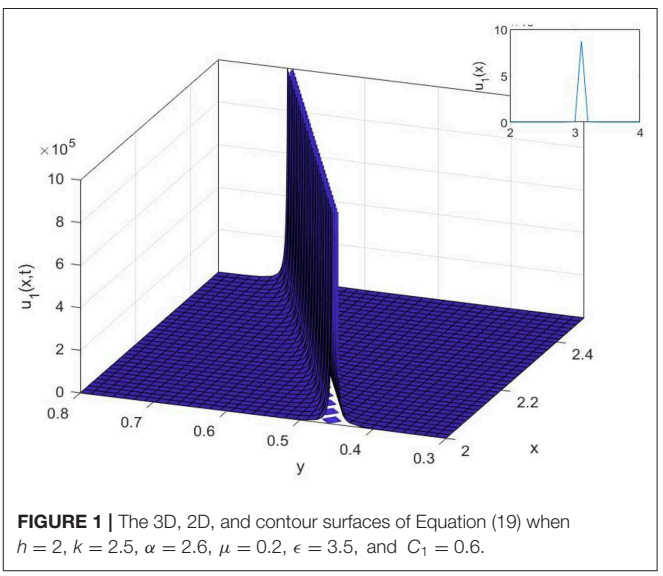

FIGURE 1 | The 3D, 2D, and contour surfaces of Equation (19) when $h = 2$, $k = 2.5$, $\alpha = 2.6$, $\mu = 0.2$, $\epsilon = 3.5$, and $C_1 = 0.6$.

$$a_0 = \frac{4k\epsilon\lambda^2}{\alpha + (2+\alpha\epsilon)\lambda^2},\ a_2 = \frac{\left(\alpha - \lambda^2\right)\left(\alpha + (2+\alpha\epsilon)\lambda^2\right)a_1^2}{24k\alpha\epsilon\lambda^2},$$
$$\mu = \frac{\left(\alpha - \lambda^2\right)\left(\alpha + (2+\alpha\epsilon)\lambda^2\right)a_1}{24k\alpha\epsilon\lambda}, \beta = -2,$$
$$h = \frac{2k\left(\alpha + 2\lambda^2\right)}{\alpha + (2+\alpha\epsilon)\lambda^2}, \tag{22}$$

gives

$$u_3(x,t) = \frac{a_1}{C_1\cosh(\lambda\xi) - C_1\sinh(\lambda\xi) - \frac{(\alpha-\lambda^2)(\alpha+(2+\alpha\epsilon)\lambda^2)a_1}{24k\alpha\epsilon\lambda^2}} + \frac{\left(\alpha - \lambda^2\right)\left(\alpha + (2+\alpha\epsilon)\lambda^2\right)a_1^2}{24k\alpha\epsilon\lambda^2\left(C_1\cosh(\lambda\xi) - C_1\sinh(\lambda\xi) - \frac{(\alpha-\lambda^2)(\alpha+(2+\alpha\epsilon)\lambda^2)a_1}{24k\alpha\epsilon\lambda^2}\right)^2} + \frac{4k\epsilon\lambda^2}{\alpha + (2+\alpha\epsilon)\lambda^2}. \tag{23}$$

Family 4. When

$$a_0 = \frac{4k\epsilon}{1+\alpha\epsilon},\ a_2 = 0,\ \beta = -3,\ \mu = \frac{\mathrm{i}\sqrt{\alpha}\,(1+\alpha\epsilon)\,a_1}{4k\epsilon},$$
$$h = \frac{2k}{1+\alpha\epsilon},\ \lambda = \mathrm{i}\sqrt{\alpha}, \tag{24}$$

we get

$$u_4(x,t) = \frac{4k\epsilon}{1+\alpha\epsilon} + \frac{a_1}{C_1\cos\left(\sqrt{\alpha}\xi\right) - \mathrm{i}C_1\sin\left(\sqrt{\alpha}\xi\right) - \frac{(1+\alpha\epsilon)a_1}{4k\epsilon}}. \tag{25}$$

Family 5. When

$$a_0 = \frac{\mathrm{i}\sqrt{\alpha}a_1}{\mu},\ a_2 = 0,\ \beta = -3,\ h = \frac{\mathrm{i}\sqrt{\alpha}a_1}{2\epsilon\mu},$$
$$k = \frac{\mathrm{i}\sqrt{\alpha}\,(1+\alpha\epsilon)\,a_1}{4\epsilon\mu},\ \lambda = \mathrm{i}\sqrt{\alpha}, \tag{26}$$

we get

$$u_5(x,t) = \frac{\mathrm{i}\sqrt{\alpha}a_1}{\mu} + \frac{a_1}{\frac{\mathrm{i}\mu}{\sqrt{\alpha}} + C_1\cos\left(\sqrt{\alpha}\xi\right) - \mathrm{i}C_1\sin\left(\sqrt{\alpha}\xi\right)}. \tag{27}$$

Family 6. When

$$a_0 = \frac{12h\epsilon\mu + 3\lambda a_1 - \sqrt{-96h\epsilon\lambda\mu a_1 + 9\left(4h\epsilon\mu + \lambda a_1\right)^2}}{24\mu},\ a_2 = \frac{\mu a_1}{\lambda},$$
$$\alpha = \frac{\lambda\left(12h\epsilon\mu - \lambda a_1 + \sqrt{3}\sqrt{48h^2\epsilon^2\mu^2 + \lambda a_1\left(-8h\epsilon\mu + 3\lambda a_1\right)}\right)}{2a_1},$$
$$k = \frac{24h\mu + 12h\epsilon\lambda^2\mu - 3\lambda^3 a_1 + \lambda^2\sqrt{-96h\epsilon\lambda\mu a_1 + 9\left(4h\epsilon\mu + \lambda a_1\right)^2}}{48\mu},$$
$$\beta = -2, \tag{28}$$

we have

$$u_6(x,t) = \frac{\mu a_1}{\lambda\left(-\frac{\mu}{\lambda} + C_1\cosh(\lambda\xi) - C_1\sinh(\lambda\xi)\right)^2} + \frac{a_1}{-\frac{\mu}{\lambda} + C_1\cosh(\lambda\xi) - C_1\sinh(\lambda\xi)} + \frac{12h\epsilon\mu + 3\lambda a_1 - \sqrt{-96h\epsilon\lambda\mu a_1 + 9\left(4h\epsilon\mu + \lambda a_1\right)^2}}{24\mu}. \tag{29}$$

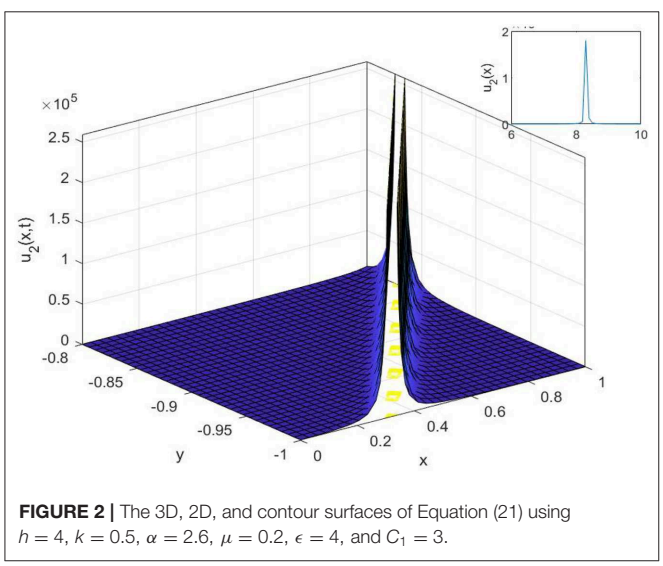

FIGURE 2 | The 3D, 2D, and contour surfaces of Equation (21) using $h = 4$, $k = 0.5$, $\alpha = 2.6$, $\mu = 0.2$, $\epsilon = 4$, and $C_1 = 3$.

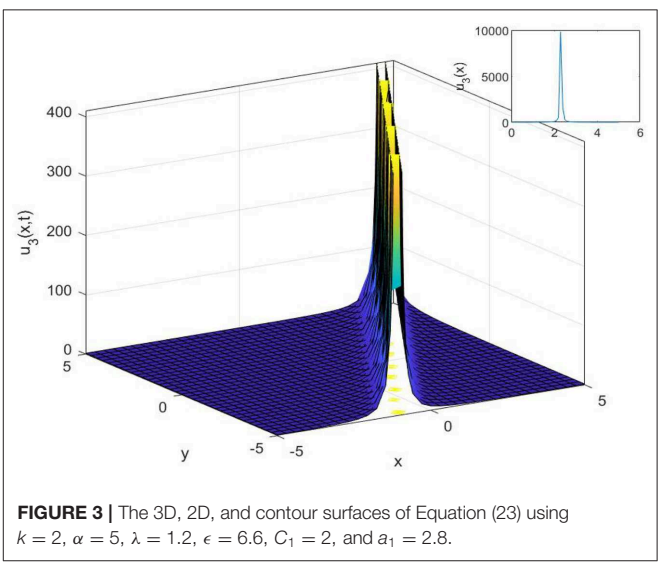

FIGURE 3 | The 3D, 2D, and contour surfaces of Equation (23) using $k = 2$, $\alpha = 5$, $\lambda = 1.2$, $\epsilon = 6.6$, $C_1 = 2$, and $a_1 = 2.8$.

7. IMPLEMENTATION OF THE GERF METHOD

In this section, the application of the GERF method to the Gilson-Pickering equation is presented.

Applying the balance principle, by taking the nonlinear term P^2 and the highest derivative P'' in Equation (16) gives $m = 2$. With $m = 2$, Equation (12) takes the form

$$P(\eta) = A_0 + A_1\varphi(\eta) + \frac{B_1}{\varphi(\eta)} + A_2\varphi(\eta)^2 + \frac{B_2}{\varphi(\eta)^2}, \quad (30)$$

where $\varphi(\eta)$ is given by Equation (13). Following the methodology described above in section 4, we obtain the following nontrivial solutions of Equation (1):

Family 1. When $r_i = \{-2, -1, 1, 1\}$, $s_i = \{0, 1, 0, 1\}$, we get

$$\varphi(\eta) = \frac{-2 - e^{\eta}}{1 + e^{\eta}}, \quad (31)$$

Case 1.

$$A_0 = \frac{A_1(-1+13\alpha)}{18\alpha},\ B_1 = 0,\ A_2 = \frac{A_1}{3},\ B_2 = 0,\ \beta = -2,$$
$$h = \frac{A_1\left(-2+\alpha+\alpha^2\right)}{36\alpha\epsilon},\ k = \frac{A_1(-1+\alpha)(2+\alpha+\alpha\epsilon)}{72\alpha\epsilon}, \quad (32)$$

we get

$$u_7(x,t) = \frac{A_1\left(-2-e^{x-\frac{A_1 t\left(-2+\alpha+\alpha^2\right)}{36\alpha\epsilon}}\right)^2}{3\left(1+e^{x-\frac{A_1 t\left(-2+\alpha+\alpha^2\right)}{36\alpha\epsilon}}\right)^2} + \frac{A_1\left(-2-e^{x-\frac{A_1 t\left(-2+\alpha+\alpha^2\right)}{36\alpha\epsilon}}\right)}{1+e^{x-\frac{A_1 t\left(-2+\alpha+\alpha^2\right)}{36\alpha\epsilon}}} + \frac{A_1(-1+13\alpha)}{18\alpha}, \quad (33)$$

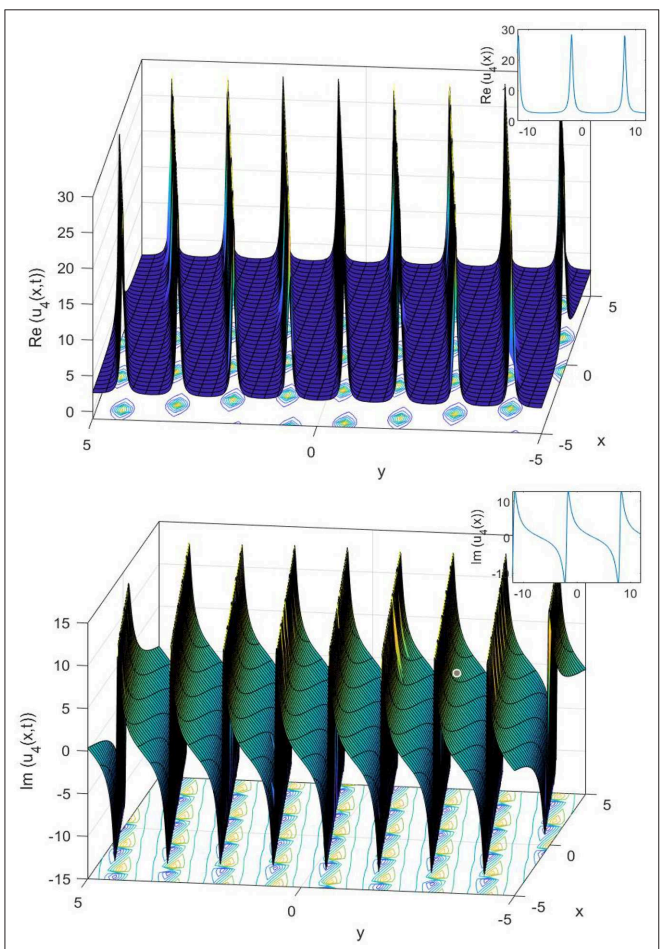

FIGURE 4 | The 3D, 2D, and contour surfaces of Equation (25), using $k = 4.5$, $\alpha = 0.4$, $\epsilon = 0.3$, $C_1 = 0.2$, and $a_1 = 0.8$.

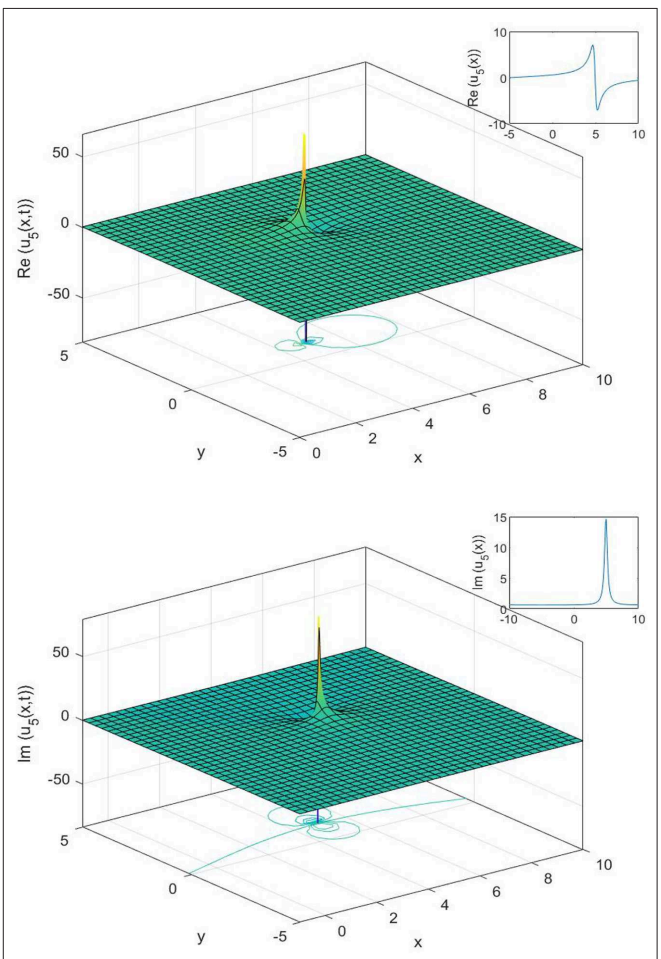

FIGURE 5 | The 3D, 2D, and contour surfaces of Equation (27), using $\mu = 0.4$, $\alpha = 0.1$, $\epsilon = 0.5$, $C_1 = 2$, and $a_1 = 1.5$.

Case 2. When

$$A_0 = -\frac{2\left(h-2k\right)\left(-1+13\alpha\right)}{\left(-1+\alpha\right)\alpha}, A_1 = 0, B_1 = -\frac{72\left(h-2k\right)}{-1+\alpha},$$
$$A_2 = 0, B_2 = -\frac{48\left(h-2k\right)}{-1+\alpha}, \epsilon - \frac{\left(h-2k\right)\left(2+\alpha\right)}{h\alpha}, \beta = -2, \tag{34}$$

we get

$$u_8\left(x,t\right) = -\frac{72\left(1+\mathrm{e}^{-ht+x}\right)\left(h-2k\right)}{\left(-2-\mathrm{e}^{-ht+x}\right)\left(-1+\alpha\right)} - \frac{48\left(1+\mathrm{e}^{-ht+x}\right)^2\left(h-2k\right)}{\left(-2-\mathrm{e}^{-ht+x}\right)^2\left(-1+\alpha\right)} - \frac{2\left(h-2k\right)\left(-1+13\alpha\right)}{\left(-1+\alpha\right)\alpha}. \tag{35}$$

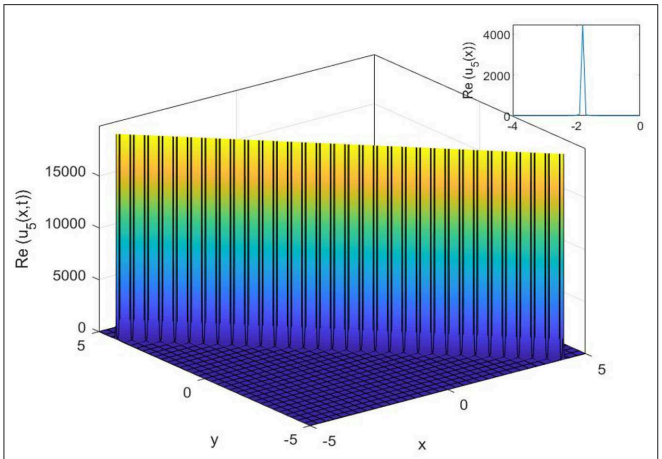

FIGURE 6 | The 3D, 2D, and contour surfaces of Equation (29) using $\mu = 1.5,\ \alpha = 0.4, \epsilon = 0.1, C_1 = 2, a_1 = 0.4,\ h = -1$, and $\lambda = 0.5$.

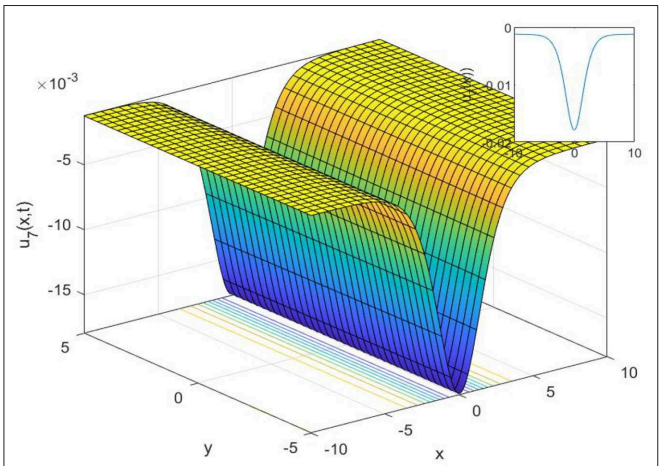

FIGURE 7 | The 3D, 2D, and contour surfaces of Equation (33) using $A_1 = 0.2, \alpha = 0.9$, and $\epsilon = 0.6$.

Family 2. When $r_i = \{-2-i, 2-i, -1, 1\}, s_i = \{i, -i, i, -i\}$ we get

$$\varphi\left(\eta\right) = \frac{\cos\left(\eta\right) + 2\sin\left(\eta\right)}{\sin\left(\eta\right)}, \tag{36}$$

Case 1. When

$$A_0 = \frac{B_1\left(8-13\alpha\right)}{60\alpha}, A_1 = 0, A_2 = 0, B_2 = -\frac{5B_1}{4}, \beta = -2,$$
$$h = -\frac{B_1\left(-8+\alpha\right)\left(4+\alpha\right)}{240\alpha\epsilon}, k = \frac{B_1\left(4+\alpha\right)\left(8+\alpha\left(-1+4\epsilon\right)\right)}{480\alpha\epsilon}, \tag{37}$$

we get

$$u_9\left(x,t\right) = \frac{B_1\left(8-13\alpha\right)}{60\alpha} - \frac{5B_1\sin\left(D\right)^2}{4(\cos\left(D\right)+2\sin\left(D\right))^2} + \frac{B_1\sin\left(D\right)}{\cos\left(D\right)+2\sin\left(D\right)}, \tag{38}$$

where $D = x + \frac{B_1 t(-8+\alpha)(4+\alpha)}{240\alpha\epsilon}$.

Case 2.

$$A_0 = \frac{A_1\left(8-13\alpha\right)}{12\alpha}, B_1 = 0, A_2 = -\frac{A_1}{4}, B_2 = 0, \beta = -2,$$
$$\epsilon - \frac{A_1\left(-8+\alpha\right)\left(4+\alpha\right)}{48h\alpha}, k = \frac{1}{24}\left(12h + A_1\left(4+\alpha\right)\right), \tag{39}$$

we get

$$u_{10}\left(x,t\right) = \frac{A1\left(8-13\alpha\right)}{12\alpha} - A_1\csc\left(ht-x\right)\left(\cos\left(ht-x\right) - 2\sin\left(ht-x\right)\right) - \frac{1}{4}A_1\csc\left(ht-x\right)^2\left(\cos\left(ht-x\right) - 2\sin\left(ht-x\right)\right)^2. \tag{40}$$

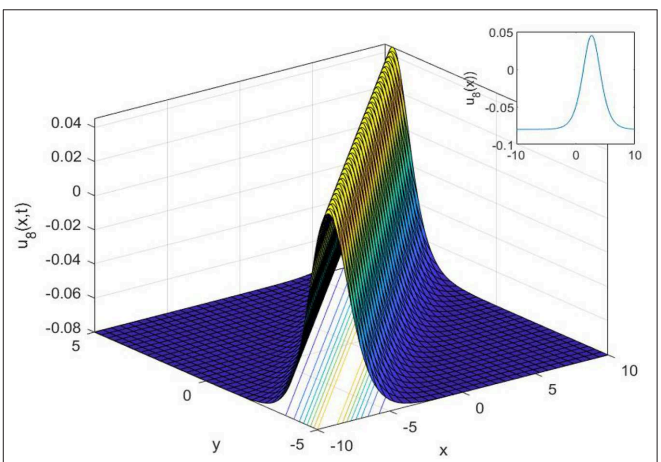

FIGURE 8 | The 3D, 2D, and contour surfaces of Equation (35) using $k = 0.5, \alpha = 25$, and $h = 2$.

Family 3. When $r_i = \{2, 0, 1, 1\}, s_i = \{-1, 0, 1, -1\}$

$$\varphi(\eta) = \frac{\left(\cosh(\eta) - \sinh(\eta)\right)}{\cosh(\eta)}, \tag{41}$$

Case 1. When

$$A_0 = -\frac{A_1(-4+\alpha)}{3\alpha}, B_1 = 0, A_2 = -\frac{A_1}{2}, B_2 = 0, \beta = -2,$$
$$h = -\frac{A_1(-4+\alpha)(8+\alpha)}{24\alpha\epsilon}, k = -\frac{A_1(-4+\alpha)(8+\alpha+4\alpha\epsilon)}{48\alpha\epsilon}, \tag{42}$$

we have

$$u_{11}(x,t) = A_1 Sech(D)\left(\cosh(D) - \sinh(D)\right)\frac{1}{2}A_1 Sech(D)^2\left(\cosh(D) - \sinh(D)\right)^2 - \frac{A_1(-4+\alpha)}{3\alpha}, \tag{43}$$

where $D = x + \frac{A_1 t(-4+\alpha)(8+\alpha)}{24\alpha\epsilon}$.

Case 2.

$$A_0 = -\frac{(h-2k)\left(-4+\sqrt{(-4+\alpha)^2}+\alpha\right)}{(-4+\alpha)\alpha}, B_2 = 0, \beta = -2,$$
$$\epsilon = -\frac{(h-2k)\left(4\left(-4+\sqrt{(-4+\alpha)^2}\right)+\alpha^2\right)}{4h\sqrt{(-4+\alpha)^2}\alpha}, B_1 = 0,$$
$$A_1 = \frac{6(h-2k)}{\sqrt{(-4+\alpha)^2}}, A_2 = -\frac{3(h-2k)}{\sqrt{(-4+\alpha)^2}}, \tag{44}$$

we get

$$u_{12}(x,t) = \frac{6(h-2k)\,sech(ht-x)\left(\cosh(ht-x)+\sinh(ht-x)\right)}{\sqrt{(-4+\alpha)^2}} - \frac{3(h-2k)\,sech(ht-x)^2\left(\cosh(ht-x)+\sinh(ht-x)\right)^2}{\sqrt{(-4+\alpha)^2}} - \frac{(h-2k)\left(-4+\sqrt{(-4+\alpha)^2}+\alpha\right)}{(-4+\alpha)\alpha}. \tag{45}$$

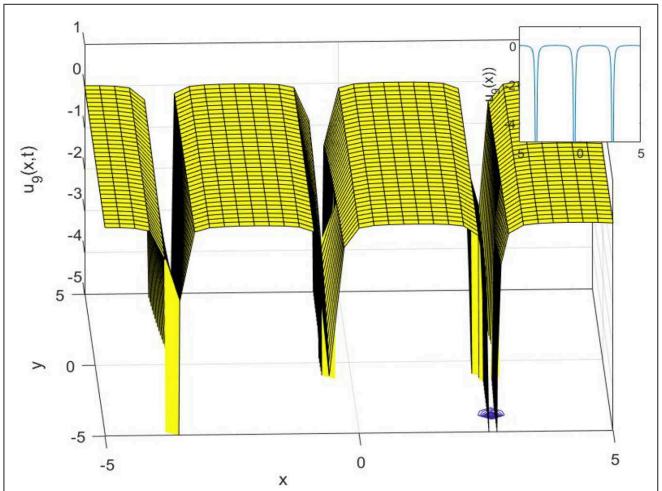

FIGURE 9 | The 3D, 2D, and contour surfaces of Equation (38) using $B_1 = 0.5$, $\alpha = 4$, and $\epsilon = 2$.

8. RESULT AND DISCUSSION

The powerful methods, namely the $(1/G')$ expansion method and the generalized exponential rational function method, are used to construct various analytical solutions for the Gilson-Pickering equation. Some results of the Gilson-Pickering equation have already been reported in the literature. Fan et al.

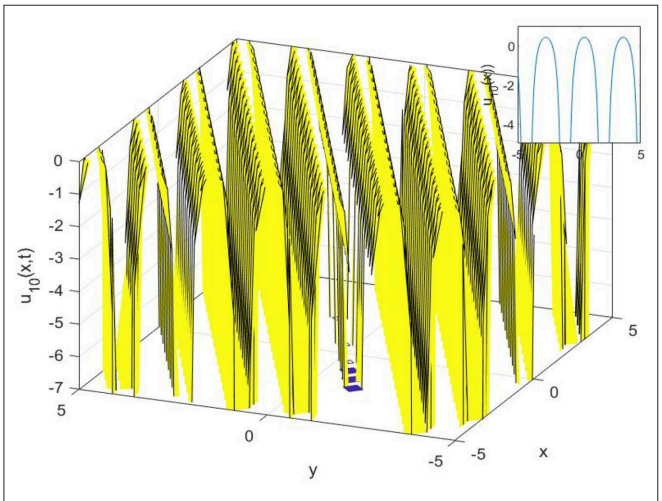

FIGURE 10 | The 3D, 2D, and contour surfaces of Equation (40) using $A_1 = 5$, $\alpha = 4$, and $\epsilon = 2$.

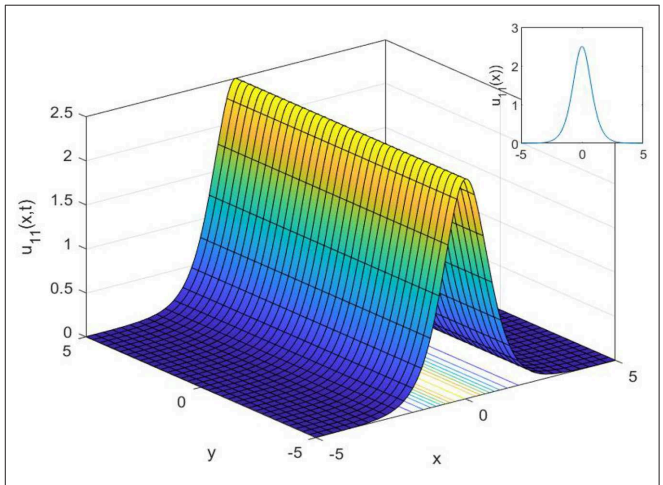

FIGURE 11 | The 3D, 2D, and contour surfaces of Equation (43) using $A_1 = 5$, $\alpha = 4$, and $\epsilon = 2$.

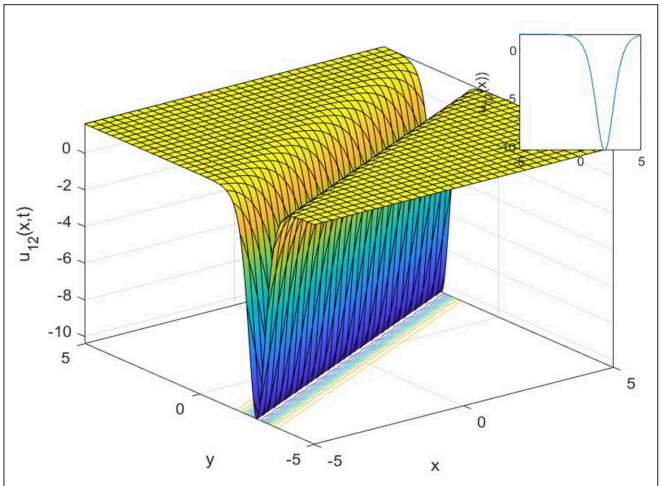

FIGURE 12 | The 3D, 2D, and contour surfaces of Equation (45) using $k = 3$, $\alpha = 5$, and $h = 2$.

[28] used (G'/G) and the ansatz method and found the solitary wave solutions to Equation (1). Baskonus [29] investigated the Gilson-Pickering equation by using the first integral method. Zabihi and Saffarian [30] implemented the simplified (G'/G) expansion method to reveal the hyperbolic, trigonometric function, and rational function solutions. Singla and Gupta [31] reported some new complex soliton solutions to Equation (1) with the aid of the Bernoulli sub-equation function method. Camsssa et al. [32] used a not a knot meshless method to obtain numerical solutions to Equation (1). Fuchssteiner and Fokas [33] performed Lie symmetry analysis and found conservation laws for the space-time fractional Gilson-Pickering equation. In this article, we obtained the singular, compound singular, complex, topological, and non-topological wave solutions to the studied equation. It is known that non-topological solutions detect waves with an intensity lower than the background, topological solutions with such a maximum intensity higher than the background, and singular solutions that are waves with discontinuous derivatives.

9. CONCLUSION

In this study, we have successfully applied the $(1/G')$ expansion method and the generalized exponential rational function method to find new exact solutions for the Gilson-Pickering equation. In order to convert the governing equation into a NODE, a traveling wave transformation has been implemented. Various analytical solutions of the proposed model have been constructed such as singular solutions, as shown in **Figures 1**, **2**, **3**, compound singular solution, as seen in **Figure 4**, complex solution, as seen in **Figure 5**, as well as a singular solution, can be shown in **Figure 6**. The non-topological solution, as shown in **Figure 7**, topological solutions, as shown in **Figure 8**, and compound singular solutions, as seen in **Figures 9**, **10**. Also, topological solution and non-topological solution as seen in **Figures 11**, **12**, respectively. Compared with the results reported in Fan et al. [28], Baskonus [29], Zabihi and Saffarian [30], Singla and Gupta [31], Camsssa et al. [32], and Fuchssteiner and Fokas [33], the solutions obtained are novel. Both methods are efficient for solving complex nonlinear partial differential equations, but, by using the generalized exponential rational function method, we can get more solutions than with the $(1/G')$ expansion method. Furthermore, the 2D, 3D, and contour surfaces are plotted for all obtained solutions by selecting suitable values for the parameters.

DATA AVAILABILITY STATEMENT

All datasets generated for this study are included in the article/supplementary material.

AUTHOR CONTRIBUTIONS

RY and SN suggested the problem first. KA drafted the first version of the problem statement with the help of HD. All authors made several suggestions to make improvements in the problem statement and contributed to the development of solution in their best possible ways.

REFERENCES

1. Osman MS, Abdel-Gawad HI, El Mahdy MA. Two-layer-atmospheric blocking in a medium with high nonlinearity and lateral dispersion. *Results Phys.* (2018) **8**:1054–60. doi: 10.1016/j.rinp.2018.01.040
2. Tariq KU, Younis M, Rezazadeh H, Rizvi STR, Osman MS. Optical solitons with quadratic-cubic nonlinearity and fractional temporal evolution. *Mod Phys Lett B.* (2018) **32**:1850317. doi: 10.1142/S0217984918503177
3. Osman MS, Ghanbari B, Machado JAT. New complex waves in nonlinear optics based on the complex Ginzburg-Landau equation with Kerr law nonlinearity. *Eur Phys J Plus.* (2019) **134**:20. doi: 10.1140/epjp/i2019-12442-4
4. Liu Y, Wen XY, Wang DS. Novel interaction phenomena of localized waves in the generalized (3+ 1)-dimensional KP equation. *Comp Math Appl.* (2019) **78**:1–19. doi: 10.1016/j.camwa.2019.03.005
5. Wang DS, Guo B, Wang X. Long-time asymptotics of the focusing Kundu-Eckhaus equation with nonzero boundary conditions. *J Diff Equat.* (2019) **266**:5209–53. doi: 10.1016/j.jde.2018.10.053
6. Manafian J. Novel solitary wave solutions for the (3+ 1)-dimensional extended Jimbo-Miwa equations. *Comput Math Appl.* (2018) **76**:1246–60. doi: 10.1016/j.camwa.2018.06.018
7. Ismael HF, Ali KK. MHD casson flow over an unsteady stretching sheet. *Adv Appl Fluid Mech.* (2017) **20**:533–41. doi: 10.17654/FM020040533
8. Wei G, Ismael HF, Husien AM, Bulut H, Baskonus HM. Optical soliton solutions of the cubic-quartic nonlinear schrödinger and resonant nonlinear schrödinger equation with the parabolic law. *Appl Sci.* (2020) **10**:219. doi: 10.3390/app10010219
9. Ali KK, Yilmazer R, Bulut H. Analytical solutions to the coupled Boussinesq-Burgers equations via sine-Gordon expansion method. In: Dutta H, Hammouch Z, Bulut H, Baskonus H, editors. *4th International Conference on Computational Mathematics and Engineering Sciences (CMES-2019). CMES*

2019. Advances in Intelligent Systems and Computing, Vol. 1111. Cham: Springer (2020). p. 233–40.
10. Abdulkareem HH, Ismael HF, Panakhov ES, Bulut H. Some novel solutions of the coupled Whitham-Broer-Kaup equations. In: Dutta H, Hammouch Z, Bulut H, Baskonus H, editors. *4th International Conference on Computational Mathematics and Engineering Sciences (CMES-2019). CMES 2019. Advances in Intelligent Systems and Computing*, Vol. 1111. Cham: Springer (2020). p. 200–8.
11. Ismael HF, Bulut H. On the Solitary Wave Solutions to the (2+1)-Dimensional Davey-Stewartson Equations. In: Dutta H, Hammouch Z, Bulut H, Baskonus H, editors. *4th International Conference on Computational Mathematics and Engineering Sciences (CMES-2019). CMES 2019. Advances in Intelligent Systems and Computing*, Vol. 1111. Cham: Springer (2020). p. 156–65.
12. Ismael HF, Arifin NM. Flow and heat transfer in a maxwell liquid sheet over a stretching surface with thermal radiation and viscous dissipation. *JP J Heat Mass Transf*. (2018) **15**:847–66. doi: 10.17654/HM015040847
13. Ali KK, Varol A. Weissenberg and Williamson MHD flow over a stretching surface with thermal radiation and chemical reaction. *JP J Heat Mass Transf*. (2019) **18**:57–71. doi: 10.17654/HM018010057
14. Osman MS, Ghanbari B. New optical solitary wave solutions of Fokas-Lenells equation in presence of perturbation terms by a novel approach. Optik. (2018) **175**:328–33. doi: 10.1016/j.ijleo.2018.08.007
15. Ghanbari B, Osman MS, Baleanu D. Generalized exponential rational function method for extended Zakharov-Kuzetsov equation with conformable derivative. *Mod Phys Lett A*. (2019) **34**:1950155. doi: 10.1142/S0217732319501554
16. Ghanbari B, Baleanu D. A novel technique to construct exact solutions for nonlinear partial differential equations. *Eur Phys J Plus*. (2019) **134**:506. doi: 10.1140/epjp/i2019-13037-9
17. Ghanbari B, Nauman R. An analytical method for soliton solutions of perturbed Schrödinger's equation with quadratic-cubic nonlinearity. *Mod Phys Lett B*. (2019) **33**:1950018. doi: 10.1142/S0217984919500180
18. Ghanbari B. Abundant soliton solutions for the Hirota-Maccari equation via the generalized exponential rational function method. *Mod Phys Lett B*. (2019) **33**:1950106. doi: 10.1142/S0217984919501069
19. Wei G, Ismael HF, Mohammed SA, Baskonus HM, Bulut H. Complex and real optical soliton properties of the paraxial non-linear Schrödinger equation in Kerr media with M-fractional. *Front Phys*. (2019) **7**:197. doi: 10.3389/fphy.2019.00197
20. Wei G, Ismael HF, Bulut H, Baskonus HM. Instability modulation for the (2+1)-dimension paraxial wave equation and its new optical soliton solutions in Kerr media. *Phys Script*. (2020) **95**:035207. doi: 10.1088/1402-4896/ab4a50
21. Goswami A, Singh J, Kumar D. An efficient analytical approach for fractional equal width equations describing hydro-magnetic waves in cold plasma. *Phys A*. (2019) **524**:563–75. doi: 10.1016/j.physa.2019.04.058
22. Goswami A, Singh J, Kumar D. Numerical simulation of fifth order KdV equations occurring in magneto-acoustic waves. *Ain Shams Eng J*. (2018) **9**:2265–73. doi: 10.1016/j.asej.2017.03.004
23. Kumar D, Singh J, Purohit SD, Swroop R. A hybrid analytical algorithm for nonlinear fractional wave-like equations. *Math Model Nat Phenomena*. (2019) **14**:304. doi: 10.1051/mmnp/2018063
24. Bhatter S, Mathur A, Kumar D, Singh J. A new analysis of fractional Drinfeld-Sokolov-Wilson model with exponential memory. *Phys A*. (2020) **537**:122578. doi: 10.1016/j.physa.2019.122578
25. Gilson C, Pickering A. Factorization and Painlevé analysis of a class of nonlinear third-order partial differential equations. *J Phys A Math Gen*. (1995) **28**:2871. doi: 10.1088/0305-4470/28/10/017
26. Ebadi G, Kara AH, Petkovic MD, Biswas A. Soliton solutions and conservation laws of the Gilson-Pickering equation. *Waves Random Comp Media*. (2011) **21**:378–85. doi: 10.1080/17455030.2011.569036
27. Ismail A. Exact and explicit solutions to nonlinear evolution equations using the division theorem. *Appl Math Comput*. (2011) **217**:8134–9. doi: 10.1016/j.amc.2011.02.098
28. Fan X, Yang S, Zhao D. Travelling wave solutions for the Gilson-Pickering equation by using the simplified G/G-expansion method. *Int J Nonlin Sci*. (2009) **8**:368–73.
29. Baskonus HM. Complex soliton solutions to the Gilson-Pickering model. *Axioms*. (2019) **8**:18. doi: 10.3390/axioms 8010018
30. Zabihi F, Saffarian M. A not-a-knot meshless method with radial basis functions for numerical solutions of Gilson-Pickering equation. *Eng Comput*. (2018) **34**:37–44. doi: 10.1007/s00366-017-0519-9
31. Singla K, Gupta RK. Space-time fractional nonlinear partial differential equations: symmetry analysis and conservation laws. *Nonlin Dyn*. (2017) **89**:321–31. doi: 10.1007/s11071-017-3456-7
32. Camsssa R, Holm DD, Hyman JM. An integrable shallow water equation with peaked solitons. *Phys Rev Lett*. (1993) **71**:1661–4. doi: 10.1103/PhysRevLett.71.1661
33. Fuchssteiner B, Fokas AS. Symplectic structure, their biicklund transformations and hereditary symmetries. *Physica*. (1981) **4**:47–66. doi: 10.1016/0167-2789(81)90004-X
34. Rosenau P, Hyman J. Compactons: solitons with finite wavelength. *Phys Rev Lett*. (1993) **93**:564–7. doi: 10.1103/PhysRevLett.70.564
35. Fornberg B, Whitham G. A numerical and theoretical study of certain nonlinear wave phenomena. *Philos Trans R Soc Lond A*. (1978) **289**:373–404. doi: 10.1098/rsta.1978.0064
36. Whitham G. Variational methods and applications to water waves. *Proc R Soc Lond A*. (1967) **299**:6–25. doi: 10.1098/rspa.1967.0119
37. Whitham G. *Linear and Nonlinear Waves*. New York, NY: Wiley (1974).
38. Yokus A, Doğan K. Conservation laws and a new expansion method for sixth order Boussinesq equation. In: *AIP Conference Proceedings*, Vol. 1676. Antalya: AIP Publishing (2015). p. 020062. doi: 10.1063/1.4930488
39. Yokus A. An expansion method for finding traveling wave solutions to nonlinear PDEs. *Istanbul Ticaret Üniversitesi Fen Bilimleri Dergisi*. (2015) **14**:65–81.

Conflict of Interest: The authors declare that the research was conducted in the absence of any commercial or financial relationships that could be construed as a potential conflict of interest.

frontiers in Physics

ORIGINAL RESEARCH
published: 17 April 2020
doi: 10.3389/fphy.2020.00087

On Optical Solitons of the Fractional (3+1)-Dimensional NLSE With Conformable Derivatives

Zeliha Korpinar[1], *Fairouz Tchier*[2] *and Mustafa Inc*[3,4]*

[1] Department of Administration, Faculty of Economic and Administrative Sciences, Mus Alparslan University, Muş, Turkey, [2] Department of Mathematics, King Saud University, Riyadh, Saudi Arabia, [3] Department of Mathematics, Science Faculty, Firat University, Elâzığ, Turkey, [4] Department of Medical Research, China Medical University Hospital, China Medical University, Taichung, Taiwan

In this article, the fractional (3+1)-dimensional nonlinear Shrödinger equation is analyzed with kerr law nonlinearity. The extended direct algebraic method (EDAM) is applied to obtain the optical solitons of this equation with the aid of the conformable derivative. Optical solitons are investigated for this equation with the aid of the EDAM after the nonlinear Shrödinger equation transforms an ordinary differential equation using the wave variables transformation.

Keywords: optical solitons, nonlinear Shrödinger equation, conformable derivative, Kerr law nonlinearity, the extended direct algebraic method

OPEN ACCESS

Edited by:
Wen-Xiu Ma,
University of South Florida,
United States

Reviewed by:
Aly R. Seadawy,
Taibah University, Saudi Arabia
Kashif Ali,
COMSATS Institute of Information Technology, Pakistan

***Correspondence:**
Mustafa Inc
minc@firat.edu.tr

Specialty section:
This article was submitted to Mathematical Physics, a section of the journal Frontiers in Physics

Received: *11 November 2019*
Accepted: *11 March 2020*
Published: *17 April 2020*

Citation:
Korpinar Z, Tchier F and Inc M (2020) On Optical Solitons of the Fractional (3+1)-Dimensional NLSE With Conformable Derivatives. Front. Phys. 8:87. doi: 10.3389/fphy.2020.00087

INTRODUCTION

Over the past few decades, there have been many studies on optical solitons [1–10]. The nonlinear wave process can be viewed in several scientific fields, such as optical fiber, quantum theory, plasma physics, fluid dynamics [11, 12], etc. Solitons are one pulse forms which are created due to the proportion between nonlinearity and wave stage speed dispersal impacts in the system. The envelope soliton, which holds both fast and slow vibrations, performs for nonlinearity proportions with the wave group dispersal impacts in the physical systems. The envelope soliton is controlled by a small field adjusted wave package whose dynamics are controlled via the nonlinear Schrödinger equation (NSE) [1–12]. The analytical solutions of these NPDEs plays a significant part in the analysis of nonlinear phenomena. Over the past few decades, numerous methods were developed to obtain analytical solutions of NPDEs such as the inverse scattering method [13], the Sine—cosine function method [14], the tanh-expansion method, and the Kudryashov-expansion method [15], etc.

There has also been considerable interest and significant theoretical improvements in fractional calculus, applied in many fields, and in fractional differential equations and its applications [16–25]. Nonlinear fractional partial differential equations (FPDEs) are a special type of NPDEs. Several studies have discussed these equations. Additionally, FPDEs are significant in several analyses because of the iterative reporting and the probability explanation process in water wave hypothesis, nonlinear optics, fluid dynamics, plasma physics, optical fiber, quantum mechanics, signal processing, and so on. Several researchers have investigated the wave solutions of NPDEs with the aid of some mathematical algorithms. Besides, one advantage of the conformable fractional derivative is that it is easy to apply [26–34].

The conformable derivative of order $\alpha \in (0,1)$ is defined as the following expression [28]

$$ {}_tD^{\alpha} f(t) = \lim_{\vartheta \to 0} \frac{f(t + \vartheta t^{1-\alpha}) - f(t)}{\vartheta}, \ \ f:(0,\infty) \to \mathrm{R}. $$

A few properties for the conformable derivative are given by [28, 31].

$$ \begin{aligned} a)_t D^{\alpha} t^{\eta} &= \eta t^{\alpha-\eta}, \quad \forall \alpha \in \mathrm{R}, \\ b)_t D^{\alpha}(fg) &= f_t D^{\alpha} g + g_t D^{\alpha} f, \\ c)_t D^{\alpha}(fog) &= t^{1-\alpha} g'(t) f'(g(t)), \\ d)_t D^{\alpha}(\frac{f}{g}) &= \frac{g_t D^{\alpha} f - f_t D^{\alpha} g}{g^2}. \end{aligned} $$

Recently, there have been about the conformable model of fractional computations [25–33].

The (3+1)-dimensional dependent NLSE is given by:

$$ iq_t + \nabla^2 q + \lambda F(|q|^2) q = 0. \tag{1.1} $$

in [10–12], there are analyzed symmetry reductions for the $(3+1)$-dimensional NLSE.

Then, Equation (1.1) can be scripted for fractional (3+1)-dimensional NLSE with conformable derivatives as:

$$ iD_t^{\alpha} q + \nabla^2 q + \lambda F(|q|^2) q = 0, \ t > 0, \ \ 0 < \alpha \leq 1. \tag{1.2} $$

where F is a real-valued function and has the fluency of the complex function $F(|q|^2)q : C \to C$. When the $F(|q|^2)q$ is k times continuously differentiable, the following situation can be written,

$$ F(|q|^2) q \in \bigcup_{m,n=1}^{\infty} C^k((-n,n) \times (-m,m); R^2). $$

For Kerr law nonlinearity, Equation (1.2) is converted to

$$ iD_t^{\alpha} q + \nabla^2 q + \lambda |q|^2 q = 0, \ t > 0, \ \ 0 < \alpha \leq 1. \tag{1.3} $$

In (1.3), the first expression describes the evolution condition, the second expression, describes the dispersal in x, y, and z directions while the third expression describes nonlinearity. Solitons are the consequence of an attentive adjust between dispersal and nonlinearity.

In this work, we analyze the fractional (3+1)-dimensional nonlinear Shrödinger's equation with the aid of a conformable derivative operator to find solitons using the extended direct algebraic method (EDAM) [8, 26].

This method is a powerful in solving nonlinear evolution equations and it can be applied to solve the above mentioned equations. This has led to the innovation of many modern techniques to solve these equations. There are several advantages and disadvantages of this modern method. Although a closed type soliton solution can be found with the aid of this process, the disadvantage of this method is that this technique cannot calculate the conserved quantities of nonlinear evolution equations.

DESCRIPTION FOR THE EXTENDED DIRECT ALGEBRAIC METHOD

Suppose the general nonlinear partial differential equation,

$$ U(q, q_t^{(\alpha)}, q_x, q_y, q_z, q_t^{(2\alpha)}, q_{xx}, , ...) = 0. \tag{2.1} $$

where $q = q(x,y,z)$, U is a polynomial in $q = q(x,y,z,t)$ and the x, y, z, t define the partial fractional derivatives.

- Assume the traveling wave transformation:

$$ q(x,y,z,t) = v(\phi), \qquad \phi = x\cos\xi + y\cos\kappa + z\cos\chi + Q\frac{t^{\alpha}}{\alpha}, \tag{2.2} $$

where $\cos^2\xi + \cos^2\kappa + \cos^2\chi = 1$.

With the aid of (2.2) wave transformation, Equation (2.1) is changed into an ordinary differential equation for $v(\phi)$:

$$ B(v, v_{\phi}, v_{\phi\phi}, v_{\phi\phi\phi}, ...) = 0. \tag{2.3} $$

where the sub-indices define the ordinary derivatives with respect to ϕ.

- Suppose the solution of Equation (2.3),

$$ v(\phi) = \sum_{j=0}^{M} a_j G^j(\phi), \tag{2.4} $$

where $a_M \neq 0$ and $G(\phi)$ can be satisfied as follows:

$$ G'(\phi) = \ln(E)(fG^2(\phi) + gG(\phi) + h), \ \ E \neq 0, 1, \tag{2.5} $$

where f, g, h are arbitrary constants.

- M is obtained by balancing between the highest order derivatives and the nonlinear terms in Equation (2.3).
- First, Equation (2.4) and Equation (2.5) are placed into Equation (2.3). Then each coefficient of the polynomials are synchronized to zero ve algebraic equations of a_j $(j = 1, 2, ..., M)$, Q and f, g, h are obtained.
- The obtained system is solved and parameters a_j $(j = 1, 2, ..., M)$ and Q are found. Thus, solutions of Equation (2.3) are found.

Where a few specific solutions of Equation (2.3) are given by;

1) When $\Psi = g^2 - 4hf < 0$ and $f \neq 0$,

$$ \begin{aligned} G_1(\phi) &= -\tfrac{g}{2f} + \tfrac{\sqrt{-\Psi}}{2f} \tan_E(\tfrac{\sqrt{-\Psi}}{2}\phi), \\ G_2(\phi) &= -\tfrac{g}{2f} + \tfrac{\sqrt{-\Psi}}{2f} \cot_E(\tfrac{\sqrt{-\Psi}}{2}\phi), \end{aligned} $$

2) When $\Psi = g^2 - 4hf > 0$ and $f \neq 0$,

$$ G_3(\phi) = -\frac{g}{2f} + \frac{\sqrt{\Psi}}{2f}(-\tanh_E(\sqrt{\Psi}\phi) \pm i\sqrt{\Delta\Omega}\sec h_E(\sqrt{\Psi}\phi)), $$

$$ G_4(\phi) = -\frac{g}{2f} + \frac{\sqrt{\Psi}}{2f}(-\coth_E(\sqrt{\Psi}\phi) \pm \sqrt{\Delta\Omega}\csc h_E(\sqrt{\Psi}\phi)), $$

3) When $fh > 0$ and $g = 0$,

$$\begin{aligned} G_5(\phi) &= \sqrt{\tfrac{h}{f}}(\tan_E(2\sqrt{hf}\phi) \pm \sqrt{\Delta\Omega}\sec_E(2\sqrt{hf}\phi)), \\ G_6(\phi) &= \sqrt{\tfrac{h}{f}}(-\cot_E(2\sqrt{hf}\phi) \pm \sqrt{\Delta\Omega}\csc_E(2\sqrt{hf}\phi)), \end{aligned}$$

4) When $fh < 0$ and $g = 0$,

$$\begin{aligned} G_7(\phi) &= -\sqrt{-\tfrac{h}{f}}\tanh_E(\sqrt{-hf}\phi), \\ G_8(\phi) &= -\sqrt{-\tfrac{h}{f}}\coth_E(\sqrt{-hf}\phi), \end{aligned}$$

5) When $g = 0$ and $f = h$,

$$G_9(\phi) = \frac{1}{2}(\tan_E(\frac{h}{2}\phi) - \cot_E(\frac{h}{2}\phi)).$$

6) When $g = 0$ and $f = -h$,

$$G_{10}(\phi) = -\frac{1}{2}(\tanh_E(\frac{h}{2}\phi) + \coth_E(\frac{h}{2}\phi)).$$

7) When $g^2 = 4hf$,

$$G_{11}(\phi) = -2h\frac{g\phi\ln(E)+2}{g^2\phi\ln(E)}.$$

8) When $g \neq 0$ and $h = 0$,

$$G_{12}(\phi) = -\frac{\Delta g}{f(\cosh_E(g\phi) - \sinh_E(g\phi) + \Delta)},$$

Remark. The generalized trigonometric and hyperbolic functions are defined as Ghosh and Nandy [13];

$$\begin{aligned} \sin_E(\phi) &= \tfrac{\Delta E^{i\phi} - \Omega E^{-i\phi}}{2i}, \cos_E(\phi) = \tfrac{\Delta E^{i\phi} + \Omega E^{-i\phi}}{2}, \\ \tan_E(\phi) &= -i\tfrac{\Delta E^{i\phi} - \Omega E^{-i\phi}}{\Delta E^{i\phi} + \Omega E^{-i\phi}}, \cot_E(\phi) = i\tfrac{\Delta E^{i\phi} + \Omega E^{-i\phi}}{\Delta E^{i\phi} - \Omega E^{-i\phi}}, \\ \sec_E(\phi) &= \tfrac{2}{\Delta E^{i\phi} + \Omega E^{-i\phi}}, \csc_E(\phi) = \tfrac{2i}{\Delta E^{i\phi} - \Omega E^{-i\phi}} \\ \sinh_E(\phi) &= \tfrac{\Delta E^{\phi} - \Omega E^{-\phi}}{2}, \cosh_E(\phi) = \tfrac{\Delta E^{\phi} + \Omega E^{-\phi}}{2}, \\ \tanh_E(\phi) &= \tfrac{\Delta E^{\phi} - \Omega E^{-\phi}}{\Delta E^{\phi} + \Omega E^{-\phi}}, \coth_E(\phi) = \tfrac{\Delta E^{\phi} + \Omega E^{-\phi}}{\Delta E^{\phi} - \Omega E^{-\phi}}, \\ \sec h_E(\phi) &= \tfrac{2}{\Delta E^{\phi} + \Omega E^{-\phi}}, \csc h_E(\phi) = \tfrac{2}{\Delta E^{\phi} - \Omega E^{-\phi}}. \end{aligned}$$

where ϕ is an independent variable, $\Delta \neq 0$ and $\Omega \neq 0$ are called deformation parameters.

SOLUTIONS OF TIME FRACTIONAL (3+1)-DIMENSIONAL NLSE WITH KERR LAW NONLINEARITY USING CONFORMABLE DERIVATIVES

Now, suppose the wave variable transform:

$$\begin{aligned} q(x,y,z,t) &= e^{i(a(x\cos\xi + y\cos\kappa + z\cos\chi) + w\frac{t^\alpha}{\alpha})}v(\phi), \\ \phi &= x\cos\xi + y\cos\kappa + z\cos\chi + Q\tfrac{t^\alpha}{\alpha}, \end{aligned} \quad (3.1)$$

By placing Equation (3.1) into Equation (1.3) and taking the properties of conformable time fractional derivatives into account, the following nonlinear equation is obtained,

$$v''(\phi) + \lambda v(\phi)^3 - (a^2 + w)v(\phi) = 0, \quad (3.2)$$

with $Q = -2a$.

Suppose the solution of Equation (3.2) is expressed as a finite series. We can write this solution as follows,

$$v(\phi) = \sum_{k=0}^{M} a_k G^k(\phi) \quad (3.3)$$

where $G(\phi)$ satisfies Equation (2.5), $\phi = x\cos\xi + y\cos\kappa + z\cos\chi + Q\frac{t^\alpha}{\alpha}$ and a_k for $k = \overline{1, M}$ are values to be described.

With the aid of balance $v''(\phi)$ with $v(\phi)^3$ in Equation (3.3), is found $M = 1$.

We can write the solution of Equation (3.3) in the following form:

$$v(\phi) = a_0 + a_1 G(\phi), \quad (3.4)$$

First, Equation (3.4) and Equation (2.5) are placed into the Equation (3.2). Then each coefficient of the $G(\phi)$ synchronized to zero ve from algebraic equations and the following values are found:

$$\begin{aligned} a_0 &= \tfrac{ig\ln(E)}{\sqrt{2\lambda}}, a_1 = \tfrac{i\sqrt{2}f\ln(E)}{\sqrt{\lambda}}, \\ w &= -a^2 - \tfrac{1}{2}(g^2 - 4fh)\ln^2(E). \end{aligned} \quad (3.5)$$

The solutions of Equation (1.3) are found as follows; ($\Upsilon = e^{i(a(x\cos\xi + y\cos\kappa + z\cos\chi) - (a^2 + \frac{1}{2}(g^2 - 4fh)\ln^2(E))\frac{t^\alpha}{\alpha})}$ and $\Psi = g^2 - 4hf$)

1) When $\Psi < 0$ and $f \neq 0$, the singular periodic solutions are obtained as follows

$$\begin{aligned} q_1 &= \Upsilon(\tfrac{ig\ln(E)}{\sqrt{2\lambda}} + \tfrac{i\sqrt{2}f\ln(E)}{\sqrt{\lambda}}(-\tfrac{g}{2f} + \tfrac{\sqrt{-\Psi}}{2f}\tan_E(\tfrac{\sqrt{-\Psi}}{2}\phi))), \\ q_2 &= \Upsilon(\tfrac{ig\ln(E)}{\sqrt{2\lambda}} + \tfrac{i\sqrt{2}f\ln(E)}{\sqrt{\lambda}}(-\tfrac{g}{2f} + \tfrac{\sqrt{-\Psi}}{2f}\cot_E(\tfrac{\sqrt{-\Psi}}{2}\phi))), \end{aligned}$$

2) When $\Psi > 0$ and $f \neq 0$, the singular soliton solutions are obtained as follows

$$\begin{aligned} q_3 &= \Upsilon(\tfrac{ig\ln(E)}{\sqrt{2\lambda}} + \tfrac{i\sqrt{2}f\ln(E)}{\sqrt{\lambda}}(-\tanh_E(\sqrt{\Psi}\phi) \\ &\quad \pm i\sqrt{\Delta\Omega}\sec h_E(\sqrt{\Psi}\phi))), \\ q_4 &= \Upsilon(\tfrac{ig\ln(E)}{\sqrt{2\lambda}} + \tfrac{i\sqrt{2}f\ln(E)}{\sqrt{\lambda}}(-\coth_E(\sqrt{\Psi}\phi) \\ &\quad \pm\sqrt{\Delta\Omega}\csc h_E(\sqrt{\Psi}\phi))), \end{aligned}$$

3) When $g = 0$ and $fh > 0$, the singular periodic solutions are obtained as follows

$$\begin{aligned} q_5 &= \Upsilon(\tfrac{ig\ln(E)}{\sqrt{2\lambda}} + \tfrac{i\sqrt{2}f\ln(E)}{\sqrt{\lambda}}(\sqrt{\tfrac{h}{f}}(\tan_E(2\sqrt{hf}\phi) \\ &\quad \pm\sqrt{\Delta\Omega}\sec_E(2\sqrt{hf}\phi)))), \\ q_6 &= \Upsilon(\tfrac{ig\ln(E)}{\sqrt{2\lambda}} + \tfrac{i\sqrt{2}f\ln(E)}{\sqrt{\lambda}}(\sqrt{\tfrac{h}{f}}(-\cot_E(2\sqrt{hf}\phi) \\ &\quad \pm\sqrt{\Delta\Omega}\csc_E(2\sqrt{hf}\phi)))), \end{aligned}$$

4) When $g = 0$ and $fh < 0$, the singular and dark soliton solutions are obtained as follows

$$q_7 = \Upsilon\left(\frac{ig\ln(E)}{\sqrt{2\lambda}} + \frac{i\sqrt{2f}\ln(E)}{\sqrt{\lambda}}\left(-\sqrt{-\frac{h}{f}}\tanh_E\left(\sqrt{-hf}\phi\right)\right)\right),$$
$$q_8 = \Upsilon\left(\frac{ig\ln(E)}{\sqrt{2\lambda}} + \frac{i\sqrt{2f}\ln(E)}{\sqrt{\lambda}}\left(-\sqrt{-\frac{h}{f}}\coth_E\left(\sqrt{-hf}\phi\right)\right)\right),$$

5) When $g = 0$ and $f = h$, the singular periodic solution is obtained as follows

$$q_9 = \Upsilon\left(\frac{ig\ln(E)}{\sqrt{2\lambda}} + \frac{i\sqrt{2f}\ln(E)}{\sqrt{\lambda}}\left(\frac{1}{2}\left(\tan_E\left(\frac{h}{2}\phi\right) - \cot_E\left(\frac{h}{2}\phi\right)\right)\right)\right),$$

6) When $g = 0$ and $f = -h$, the combined soliton solution is obtained as follows

$$q_{10} = \Upsilon\left(\frac{ig\ln(E)}{\sqrt{2\lambda}} + \frac{i\sqrt{2f}\ln(E)}{\sqrt{\lambda}}\left(-\frac{1}{2}\left(\tanh_E\left(\frac{h}{2}\phi\right) + \coth_E\left(\frac{h}{2}\phi\right)\right)\right)\right),$$

7) When $g^2 = 4hf$, the rational solution is obtained as follows

$$q_{11} = \Upsilon\left(\frac{ig\ln(E)}{\sqrt{2\lambda}} + \frac{i\sqrt{2f}\ln(E)}{\sqrt{\lambda}}\left(-2h\frac{\phi\ln(E)g + 2}{g^2\phi\ln(E)}\right)\right),$$

8) When $h = 0$ and $g \neq 0$, the singular soliton is obtained as follows

$$q_{12} = \Upsilon\left(\frac{ig\ln(E)}{\sqrt{2\lambda}} + \frac{i\sqrt{2f}\ln(E)}{\sqrt{\lambda}}\left(-\frac{\Delta g}{f\left(\cosh_E(g\phi) - \sinh_E(g\phi) + \Delta\right)}\right)\right),$$

GRAPHICAL EXPRESSION OF THE SOLUTIONS

In this section we draw 2D and 3D graphics for some of the solutions obtained in the previous section. We obtained these graphics using Matlab. In **Figures 1**, **2**, we show some numerical models and q_1 and q_4. 3D plots are drawn for $-10 \leq x \leq 10$, $-10 \leq t \leq 10$. 2D plots are drawn for $x = 0.1$.

The above graphics were drawn for $h = 1, f = 2, g = 1, E = 2.7, a = 0.5, \lambda = 2, \xi = \kappa = \frac{\pi}{2}, \alpha = 0.8, \Delta = \Omega = 1$ in (a) and for $h = 1, f = -1, g = 0, E = 2.7, a = 0.5, \lambda = 2, \xi = \kappa = \frac{\pi}{2}, \alpha = 0.8, \Delta = \Omega = 1$ in (b).

We obtained the sum of solutions found for the fractional (3+1)-dimensional NLSE with kerr law nonlinearities via the conformable fractional derivative operator. In addition, we presented some graphics of solutions in **Figures 1**, **2**.

CONCLUSION

In this article, the EDAM is applied to find new soliton solutions for the (3+1)-dimensional NLSE with kerr law

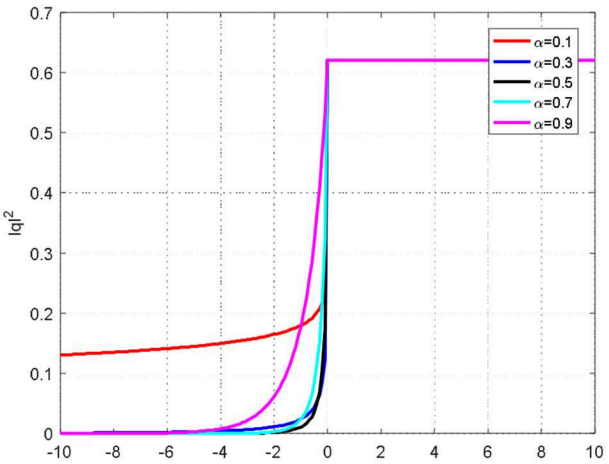

FIGURE 2 | The 2D graphic of the (3+1)-dimensional NLSE with kerr law non-linearities for a different value of α.

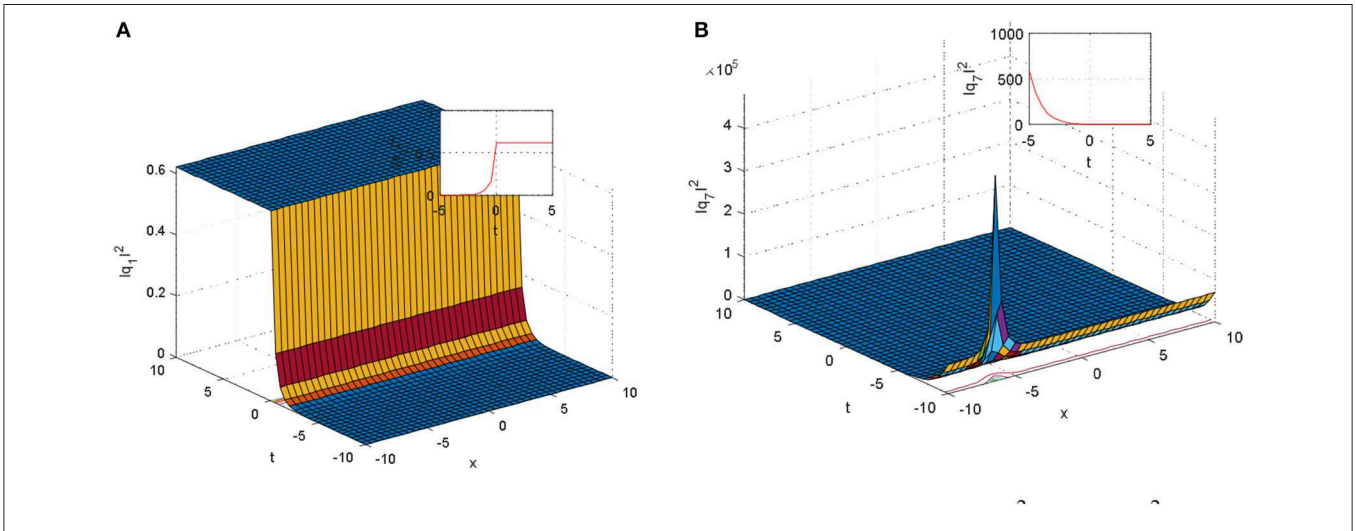

FIGURE 1 | The surface and 2D graphic for the **(A)** $|q_1|^2$, **(B)** $|q_7|^2$.

nonlinearities, with the aid of the conformable fractional derivative operator. The dark, bright, and combined optical solitons are obtained. There are 12 different situations in these solutions. The existence of solutions obtained from these functions are all stipulated through limitation states that are also listed in addition to the solutions. Some interesting figures are also presented in **Figures 1**, **2**. The method applied in this article is appropriate to investigate several problems that are face in the fields of engineering and science.

AUTHOR CONTRIBUTIONS

All authors listed have made a substantial, direct and intellectual contribution to the work, and approved it for publication.

ACKNOWLEDGMENTS

The authors extend their appreciation to the Deanship of Scientific Research at King Saud University for funding this work through research group no (RG-1440-010).

REFERENCES

1. Osman MS, Lu D, Khater MMA. A study of optical wave propagation in the nonautonomous Schrodinger-Hirota equation with power-law nonlinearity. *Results Phys*. (2019) **13**:102157. doi: 10.1016/j.rinp.2019.102157
2. Inc M, Korpinar ZS, Al Qurashi MM, Baleanu D. A new method for approximate solution of some nonlinear equations: residual power series method. *Adv Mech Eng*. (2016) **8**:1–7. doi: 10.1177/1687814016644580
3. Khater MMA, Attia RAM, Lu D. Explicit lump solitary wave of certain interesting (3+ 1)-dimensional waves in physics via some recent traveling wave methods. *Entropy*. (2019) **21**:397. doi: 10.3390/e21040397
4. Jana S, Konar S. A new family of Thirring type optical spatial solitons via electromagnetic induced transparency. *Phys Lett A*. (2007) **362**:435–38. doi: 10.1016/j.physleta.2006.10.043
5. Bhrawy AH, Abdelkawy MA. Computational study of some nonlinear shallow water equations. *Cent Eur Phys J*. (2013) **11**:518–25. doi: 10.2478/s11534-013-0197-1
6. Bhrawy AH, Abdelkawy MA. Integrable system modeling shallow water waves: Kaup–Boussinesq shallow water system. *Indian Phys J*. (2013) **87**:665–71. doi: 10.1007/s12648-013-0260-1
7. Biswas A, Milovic D. Optical solitons in 1+2 dimensions with non-Kerr law nonlinearity, *Eur Phys Spec Top J*. (2009) **173**:81–6. doi: 10.1140/epjst/e2009-01068-8
8. Rezazadeh H. New solitons solutions of the complex Ginzburg-Landau equation with Kerr law nonlinearity. *Optik*. (2018) **167**:218–27. doi: 10.1016/j.ijleo.2018.04.026
9. Triki H, Wazwaz AM. Combined optical solitary waves of the Fokas-Lenells equation. *Waves Random Complex Media*. (2017) **27**:587–93. doi: 10.1080/17455030.2017.1285449
10. Inc M, Isa Aliyu A, Yusuf A, Baleanu D. Optical solitons and modulation instability analysis with (3+1)-dimensional nonlinear Shrödinger equation. *Superlattices Microstruct*. (2017) **112**:296–302. doi: 10.1016/j.spmi.2017.09.038
11. Seadawy AR. Stability analysis solutions for nonlinear three-dimensional modified Korteweg–de Vries–Zakharov–Kuznetsov equationin a magnetize delectron–positron plasma. *Phys A*. (2016) **455**:44–51. doi: 10.1016/j.physa.2016.02.061
12. Seadawy AR. Three-dimensional weakly nonlinear shallow water waves regime and its traveling wave solutions. *Int J Comput Methods*. (2018) **15**:1850017. doi: 10.1142/S0219876218500172
13. Ghosh S, Nandy S. Inverse scattering method and vector higher order non-linear Schrödinger equation. *Nucl Phys B*. (1999) **561**:451–66. doi: 10.1016/S0550-3213(99)00484-8
14. Irwaq IA, Alquran M, Jaradat I, Baleanu D. New dual-mode Kadomtsev–Petviashvili model with strong–weak surface tension: analysis and application. *Adv Diff Equat*. (2018) **2018**:433. doi: 10.1186/s13662-018-1893-3
15. Alquran M, Jaradat I, Baleanu D. Shapes and dynamics of dual-mode Hirota–Satsuma coupled KdV equations: exact traveling wave solutions and analysis. *Chin J Phys*. (2019) **58**:49–56. doi: 10.1016/j.cjph.2019.01.005
16. Alquran M, Al-Khaled K, Sivasundaram S, Jaradat HM. Mathematical and numerical study of existence of bifurcations of the generalized fractional Burgers-Huxley equation. *Nonlinear Stud*. (2017) **24**:235–44.
17. Jaradat I, Alquran M, Al-Khaled K. An analytical study of physical models with inherited temporal and spatial memory. *Eur Phys J Plus*. (2018) **133**:162. doi: 10.1140/epjp/i2018-12007-1
18. Ali M, Alquran M, Jaradat I. Asymptotic-sequentially solution style for the generalized Caputo time-fractional Newell-Whitehead-Segel system. *Adv Diff Equat*. (2019) **2019**:70. doi: 10.1186/s13662-019-2021-8
19. Imran MA, Aleem M, Riaz MB, Ali R, Khan I. A comprehensive report on convective flow of fractional (ABC) and (CF) MHD viscous fluid subject to generalized boundary conditions. *Chaos Solitons Fractals*. (2019) **118**:274–89. doi: 10.1016/j.chaos.2018.12.001
20. Asif NA, Hammouch Z, Riaz MB, Bulut H. Analytical solution of a Maxwell fluid with slip effects in view of the Caputo-Fabrizio derivative. *Eur Phys J Plus*. (2018) **133**:272. doi: 10.1140/epjp/i2018-12098-6
21. Riaz MB, Zafar AA. Exact solutions for the blood flow through a circular tube under the influence of a magnetic field using fractional Caputo-Fabrizio derivatives. *Mathem Model Nat Phenom*. (2018) **13**:14. doi: 10.1051/mmnp/2018005
22. Korpinar ZS, Inc M. Numerical simulations for fractional variation of (1+ 1)-dimensional Biswas-Milovic equation. *Optik*. (2018) **166**:77–85. doi: 10.1016/j.ijleo.2018.02.099
23. Tchier F, Inc M, Korpinar ZS, Baleanu D. Solution of the time fractional reaction-diffusion equations with residual power series method. *Adv Mech Eng*. (2016) **8**:1–10. doi: 10.1177/1687814016670867
24. Korpinar Z. On numerical solutions for the Caputo-Fabrizio fractional heat-like equation. *Thermal Sci*. (2018) **22**:87–95. doi: 10.2298/TSCI170614274K
25. Alquran M, Jaradat I, Al-Shara S, Awawdeh F. A new simplified bilinear method for the n-soliton solutions for a generalized FmKdV equation with time-dependent variable coefficients. *Int J Nonlinear Sci Num Simul*. (2015) **16**:259–69. doi: 10.1515/ijnsns-2014-0023
26. Rezazadeh H, Tariq H, Eslami M, Mirzazadeh M, Zhou Q. New exact solutions of nonlinear conformable time-fractional Phi-4 equation. *Chin J Phys*. (2018) **56**:2805–16. doi: 10.1016/j.cjph.2018.08.001
27. Korkmaz A. Explicit exact solutions to some one dimensional conformable time fractional equations. *Waves Random Complex Media*. (2019) **29**:124–37. doi: 10.1080/17455030.2017.1416702
28. Khalil R, Al Horani M, Yousef A, Sababheh M. A new definition of fractional derivative. *J Comput Appl Math*. (2014) 264:65–70. doi: 10.1016/j.cam.2014.01.002
29. Eslami M, Rezazadeh H. The first integral method for Wu-Zhang system with conformable time-fractional derivative. *Calcolo*. (2016) **53**:475–85. doi: 10.1007/s10092-015-0158-8
30. Çenesiz Y, Baleanu D, Kurt A, Tasbozan O. New exact solutions of Burgers' type equations with conformable derivative. *Waves Random Complex Media*. (2017) **27**:103–16. doi: 10.1080/17455030.2016.1205237
31. Eslami M, Khodadad FS, Nazari F, Rezazadeh H. The first integral method applied to the Bogoyavlenskii equations by means of conformable fractional derivative. *Opt Quant Electron*. (2017) **49**:391. doi: 10.1007/s11082-017-1224-z

32. Rezazadeh H, Manaan J, Khodadad FS, Nazari F. Traveling wave solutions for density-dependent conformable fractional diffusion-reaction equation by the rst integral method and the improved $tan(\varphi(\xi)/2)$-expansion method. *Opt Quant Electron*. (2018) **50**:12. doi: 10.1007/s11082-018-1388-1
33. Hosseini, Mayeli P, Ansari R. Bright and singular soliton solutions of the conformable time-fractional Klein-Gordon equations with different nonlinearities. *Waves Random Complex Media*. (2018) **28**:426–34. doi: 10.1080/17455030.2017.1362133
34. Ali M, Alquran M, Jaradat I, Baleanu D. Stationary wave solutions for new developed two-waves fifth-order Korteweg-de Vries equation. *Adv Diff Equat*. (2019) **2019**:263. doi: 10.1186/s13662-019-2157-6

Conflict of Interest: The authors declare that the research was conducted in the absence of any commercial or financial relationships that could be construed as a potential conflict of interest.

frontiers in Applied Mathematics and Statistics

ORIGINAL RESEARCH
published: 22 April 2020
doi: 10.3389/fams.2020.00007

Criteria of Existence for a *q* Fractional *p*-Laplacian Boundary Value Problem

Lakhdar Ragoub[1]*, *Fairouz Tchier*[2] *and Ferdous Tawfiq*[2]

[1] Mathematics Department, University of Prince Mugrin, Medina, Saudi Arabia, [2] Mathematics Department, King Saud University, Riyadh, Saudi Arabia

This paper is devoted to establishing some criteria for the existence of non-trivial solutions for a class of fractional q-difference equations involving the *p*-Laplace operator, which is nowadays known as Lyapunov's inequality. The method employed for it is based on a construction of a Green's function and its maximum value. Parallel to this result, it is worth mentioning that the Hartman-Wintner inequality for the *q*-fractional *p*-Laplace boundary value problem is also provided. It covers all previous results known in the literature on the fractional case as well as that on the classical ordinary case. The non-existence of non-trivial solutions to the q-difference fractional p-Laplace equation subject to the Riemann-Liouville mixed boundary conditions will obey such integral inequalities. The tools mainly rely on an integral form of the solution construction of a Green function corresponding to the considered problem and its properties as well as its maximum value in consideration where the kernel is the Green's function. The example that we consider here for applying this result is an eigenvalue fractional problem. To be more specific, we provide an interval where an appropriate Mittag-Leffler function to the given eigenvalue fractional boundary problem has no real zeros.

2010 Mathematics Subject Classification: 34A08, 34A40, 26D10, 33E12

Keywords: Lyapunov's inequality, *q*-fractional integral, Green's function, *p*-Laplacian, mixed boundary conditions

OPEN ACCESS

Edited by:
Mustafa Inc,
Firat University, Turkey

Reviewed by:
HongGuang Sun,
Hohai University, China
Marin I. Marin,
Transilvania University of Braşov, Romania

***Correspondence:**
Lakhdar Ragoub
radhkla@hotmail.com

Specialty section:
This article was submitted to Mathematical Physics, a section of the journal Frontiers in Applied Mathematics and Statistics

Received: *30 November 2019*
Accepted: *24 February 2020*
Published: *22 April 2020*

Citation:
Ragoub L, Tchier F and Tawfiq F (2020) Criteria of Existence for a q Fractional p-Laplacian Boundary Value Problem. Front. Appl. Math. Stat. 6:7. doi: 10.3389/fams.2020.00007

1. INTRODUCTION

The field of fractional calculus and its applications to the class of partial differential equations, as well as ordinary equations, gained a rapid development. Interesting fractional results turn, in general, on the existence and non-existence of solutions. Such kinds of fractional equations come from different disciplines in sciences, covering medical and engineering matters. Techniques used in this kind of work recourse mainly to the use of Green's function and its corresponding maximum values, which is not always an easy approach. The fractional differential equations with the p-Laplacian operator involves this mathematical tool. However, to overcome this kind of difficulty, another approach can be taken, namely the use of the Cauchy-Schwarz inequality and related inequalities as holders. Different aspects have been considered by many different researchers in this respect. They have treated the existence of either a single or multiple solutions for linearity, but there have been few cases for non-linearity. In addition to this, the manner to extend these results to a general case with more a general operator seems non-evident and requires a thorough analysis of the maximum value of Green's functions. This paper is devoted to tackling this problem with the *p*-Laplace operator using the Green's function method for the non-linearity case.

Some results focusing on the existence of positive solutions of boundary value problems for a class of fractional differential equations with the p-Laplacian operator have been raised in previous papers (see [1–22] and the references therein). Ren and Chen [15] and Su et al. [17] established the existence of positive solutions to four-point boundary value problems for non-linear fractional differential equations with the p-Laplacian operator. However, for papers on this line concerning the q-difference type of fractional problems, we refer the reader to references [1–4, 8–12, 15, 18, 19, 19–33].

It is worthy of notice that the q-fractional calculus was introduced by Jackson [30, 31], as the reader may observe in consulting the article of Ernst [28], where he attributed the work to Jackson.

Accordingly, we mention the recent developments related to this subject (see [5, 12, 13, 32, 34–46]) and the references therein.

For multiple solutions for the non-linear case, we refer to the work done by El-Shahed and Al-Askar [47], whereas Graef et al. [48] deal with positive solutions by applying different methods.

The first result came from Liapunov [6], in the second ordinary differential equation. It was shown that if u is a non-trivial solution of

$$\begin{cases} u''(t) + q(t)u(t) = 0, \quad a < t < b \\ u(a) = u(b) = 0, \end{cases}$$

where $a < b$, a and b are two real constants, and the function $q \in C([a,b];\mathbb{R})$, then the function q must satisfy the following integral inequality:

$$\int_a^b |q(t)|\, dt > \frac{4}{b-a}. \tag{1}$$

After this result, several extensions are derived from this one, and consequently, analogous inequalities are obtained for a class of fractional differential equations subject to different kind of boundary conditions (see [5, 12–14, 29, 32, 34–36, 39–41, 44, 45, 49, 50]). However, concerning the fractional q-difference boundary value problem, it was shown in Jleli and Samet [42] that a non-trivial solution of

$$\begin{cases} {}_aD_q^{\alpha}u(t) + Q(t)(t)u(t) = 0, \quad t \in (a,b),\ q \in [0,1),\ 1 < \alpha \le 2, \\ u(a) = 0, \quad u(b) = 0, \end{cases} \tag{2}$$

where ${}_aD_q^{\alpha}$ denotes the fractional q-derivative of Riemann-Liouville type [43, 51], and $Q:[a,b] \to \mathbb{R}$ is a continuous function, exists if the following integral inequality

$$\int_a^b (s-a)^{\alpha-1}(b-(qs+(1-q)a)_a{}^{(\alpha-1)}\, |Q(s)|\, {}_ad_qs \ge \Gamma(\alpha)(b-a)^{\alpha-1} \tag{3}$$

is satisfied.

In the opinion of the authors, there are no articles dealing with these types of inequalities for the study of non-trivial solutions for the p-Laplacian operator involving the q-fractional case. We therefore fill the gap in the literature with this paper.

Our result generalizes that one investigated in Jleli and Samet [42].

In this work, we aim to investigate the following q-fractional boundary value problem with the p Laplace operator

$$\begin{cases} {}_aD_q^{\beta}(\phi_p({}_aD_q^{\alpha}u(t)) + Q(t)\phi_p(u(t)) = 0, \quad t \in (a,b), \\ u(a) = 0, \quad u(b) = Au(\xi), \\ {}_aD_q^{\alpha}(a) = 0, \quad {}_aD_q^{\alpha}u(b) = B\,{}_aD_q^{\alpha}u(\delta), \end{cases} \tag{4}$$

where ${}_aD_q^{\alpha}$, ${}_aD_q^{\beta}$ are the fractional q-derivative of the Riemann-Liouville type with $1 < \alpha, \beta < 2$, $0 \le A, B \le 1$, $0 < \xi, \delta < 1$, $\phi_p(s) = |s|^{p-2}s$, $p > 1$, $\phi_p^{-1} = \phi_r$, $\frac{1}{p} + \frac{1}{r} = 1$, and $Q:[a,b] \to \mathbb{R}$ is a continuous function on $[a,b]$.

We prove that the necessary condition of the existence of non-trivial solutions of (4) is the following:

$$1 \le \left(\int_a^b \tilde{G}_q(s)\, {}_ad_qs\right)\left(\int_a^b \tilde{H}_q(s)\, {}_ad_qs\right), \tag{5}$$

where $\tilde{G}_q(s)$ and $\tilde{H}_q(s)$ are defined respectively by

$$\tilde{G}_q(s) := \frac{1}{\Gamma_q(\alpha)}\frac{q(s-a)^{(\alpha-1)}}{(b-a)^{\alpha-1}}\left(b-(qs+(1-q)a)\right)_a^{(\alpha-1)} + \frac{Ag(\xi,(qs+(1-q)a)(b-a)^{\alpha-1}}{\gamma}, \tag{6}$$

$$\tilde{H}_q(s) := \frac{1}{\Gamma_q(\beta)}\frac{q(s-a)^{(\beta-1)}}{(b-a)^{\beta-1}}\left(b-(qs+(1-q)a)\right)_a^{(\beta-1)} + \frac{A\,h(\xi,(qs+(1-q)a)(b-a)^{\beta-1}}{\bar{\gamma}}, \tag{7}$$

where

$$\gamma := (b-a)^{\alpha-1} - A\,(\xi-a)^{\alpha-1},$$

and

$$\bar{\gamma} := (b-a)^{\beta-1} - b(\delta-a)^{\beta-1}.$$

Besides, we show that from this inequality derive several existing previous results in the literature as well as the standard Lyapunov inequality (1): those of Hartman and Wintner [52], Ferreira [39], and so on.

2. DEFINITIONS AND LEMMAS

In this section, we adopt the main tools that will be needed in the subsequent sections; these belong to q fractional calculus. Notations, definitions and lemmas are recalled in order to cover the goal of this paper, whereas, for consistency, we conserve the same notations for q fractional material as adopted in Jleli and Samet [42].

Let $q \in (0,1)$, $N_0 = \{0,1,2,\dots\}$, and define

$$[a]_q = \frac{q^a - 1}{q-1}, \quad a \in \mathbb{R}.$$

The similar q formula to the power $(a-b)^n$ with $n \in N_0$ is

$$(a-b)^0 = 1, \qquad (a-b)^n = \prod_{k=0}^{n-1}(a - bq^k), \quad n \in N,\ a,b \in \mathbb{R}.$$

More generally, if $\alpha \in \mathbb{R}$, then

$$(a-b)^\alpha = a^\alpha \prod_{n=0}^{\infty} \frac{a - bq^n}{a - bq^{\alpha+n}}.$$

For the particular case when $b = 0$, we note $a^{(\alpha)} = a^\alpha$. Also, the similar q formula to the power function $(x-y)^n$, with $n \in N_0$ is

$$\begin{aligned}(x-y)_a^{(0)} &= 1, \quad (x-y)_a^{(k)} \\ &= \prod_{i=0}^{k-1}\left((x-a) - (y-a)q^i\right),\ k \in N,\ (x,y) \in \mathbb{R}^2.\end{aligned}$$

For the general case, when $\gamma \in \mathbb{R}$, then

$$\begin{aligned}(x-y)_a^{(\gamma)} &= (x-a)^\gamma \prod_{i=0}^{k-1}\left(\frac{(x-a) - (y-a)q^i}{(x-a) - (y-a)q^{\gamma+i}}\right), \quad (8)\\ &= (x-a)^\gamma \prod_{i=0}^{k-1}\left(\frac{1 - q^i\frac{(y-a)}{(x-a)}}{1 - q^{\gamma+i}\frac{(y-a)}{(x-a)}}\right)\\ &= (x-a)^\gamma \left(1 - q\frac{(y-a)}{(x-a)}\right).\end{aligned}$$

It has the following properties

- $(t-s)_q^{(\beta+\gamma)} = (t-s)_q^{(\beta)}(t-qs)_q^{(\gamma)}$
- $(at-as)_q^{(\beta)} = a^\beta\,(t-s)_q^{(\beta)}$.

When derivatives are involved, it holds:

- $(t-a)^\alpha \geq (t-b)^\alpha$, for $a \leq b \leq t$, and $\alpha > 0$.

We define the q-Gamma function by

$$\Gamma_q(x) = \frac{(1-q)_0^{(x-1)}}{(1-q)^{x-1}}, \quad x \in R\backslash\{0,-1,-2,-3,\dots\}.$$

In particular one has

$$\Gamma_q(x+1) = [x]_q\Gamma_q(x),\ \forall x > 0,\ \Gamma_q(1) = 1.$$

Here and further, we recall some properties of the q-fractional derivative of a function f defined on $[a,b]$, $a < b$, to $\mathbb{R}$.

The q-fractional derivative of a function $f:[a,b] \to \mathbb{R}$, is defined by

$$({}_aD_q f)(t) = \frac{f(t) - f(qt + (1-q)a)}{(1-q)(t-a)},\ t \neq a,$$

and

$$({}_aD_q f)(a) = \lim_{t\to a}({}_aD_q f)(t).$$

Remark:
By using the following changes:

$$q := \frac{x-a}{y-a},$$

it is easy to conclude that if $({}_aD_q f)(t) \leq 0$ (respectively, $({}_aD_q f)(t) \geq 0$) then f is decreasing (respectively, f is increasing).

Remark:
If f is differentiable in (a,b) then

$$\lim_{q\to 1^-}(aD^q f)(t) = f'(t).$$

The q-fractional derivative of a function $f:[a,b] \to \mathbb{R}$ of higher order is defined by

$$({}_aD_q^0 f)(t) = f(t), \quad \text{and} \quad ({}_aD_q^n f)(t) = ({}_aD_q({}_aD_q^{n-1}f)(t)),\ n \in N.$$

The q-derivative of a product and a quotient of functions f and g defined on $[a,b]$ follows as

$$\left({}_aD_q fg\right)(t) = f(t)({}_aD_q g)(t) + g(qt + (1-q)a)({}_aD_q f)(t),$$

and

$${}_aD_q\frac{f}{g})(t) = \frac{({}_aD_q f)(t)g(t) - ({}_aD_q g)(t)f(t)}{g(t)g(qt + (1-q)a)}.$$

Lemma 2.1. [44] *For $t,s \in [a,b]$, the following formulas hold:*

$${}_t({}_aD_q(t-s)_a^{(\gamma)}) = [\gamma]_q(t-s)_a^{(\gamma-1)},$$

and

$${}_s({}_aD_q(t-s)_a^{\gamma}) = -[\gamma]_q(t-(qs+(1-q)a))_a^{\gamma-1},$$

where ${}_i({}_aD_q)$ denotes the q-derivative with respect to the variable i.

Remark :
If $\gamma > 0$, $a \leq b \leq t$, then

$$(t-a)_0^{(\gamma)} \geq (t-b)_0^{(\gamma)}.$$

Next, we recall the q-integral of a function f defined on $[a,b]$, $a < b$, to $\mathbb{R}$ and its properties.

The q-integral of a function $f:[a,b] \to R$ is defined by

$$\begin{aligned}({}_aI_q^0 f)(t) &= \int_a^t f(s)\,{}_ad_q s = (1-q)(t-a)\Sigma_{i=0}^{\infty}q^i f(q^i t\\ &\quad + (1-q)a),\ t \in [a,b].\end{aligned}$$

One may see that the above series is convergent if f is continuous.

If $a < c < b$, then the following integral equality is satisfied

$$\int_c^t f(s)\,{}_a d_q s + \int_a^t f(s)\,{}_a d_q s = \int_a^c f(s)\,{}_a d_q s,\ t \in [a,b].$$

The following two relations are also satisfied

$$({}_aI_q^0 f)(t) = f(t), \quad \text{and } ({}_aI_q^n f)(t) = {}_a I_q({}_aI_q^{n-1} f)(t),\ n \in N.$$

An essential and important theorem that is known for the classical ordinary case is also valid for the fractional one; it is the fundamental theorem of calculus. Once applied to the fractional operator, we get

$$({}_aD_q\,{}_aI_q f)(t) = f(t) - f(a)$$

if the continuity of the function f is provided. When the continuity of f is avoided, we obtain

$$({}_aD_q\,{}_aI_q f)(t) = f(t).$$

Another crucial integration that is very useful in dealing with non-existence of solutions for a class of fractional boundary value problems is the integration by parts. It follows as

$$\int_a^b f(s)({}_aD_q g)(s)\,{}_a d_q s = [f(t)g(t)]_{t=a}^{t=b} - \int_a^b g(qs + (1-q)a)({}_aD_q f)(s)\,{}_a d_q s.$$

The rule of q-integration by parts is also expressed by (see [24])

$$\int_0^a g(t)D_q f(t)\,d_q t = fg(a) - \lim_{n\to+\infty} fg(aq^n) - \int_0^a D_q g(t) f(qt)\,d_q t. \tag{9}$$

If and g are q-regular at zero, then the limit on the right-hand-side of (9) can be replaced by $(fg)^{\cdot}(0)$. (For more details, see [24]).

In what follows, we define the q-fractional Riemann-Liouville integral of a function f defined on $[a,b]$ as follows

$$({}_aI_q^0 f)(t) = f(t).$$

Let us assume that f and g are two functions defined on $[a,b]$ such that $f \le g$, then the following properties are satisfied

$$\int_a^b f(s)_a d_q s \le \int_a^b g(s)_a d_q s,$$

and

$$\int_a^b f(s)_a d_q s \le \int_a^b |f|(s)_a d_q s.$$

As auxiliary results, we need to use the following two lemmas. The reader may consult [23, 30, 31] for more details.

Lemma 2.2. [30, 50] *Let $f:[a,b] \to \mathbb{R}$ be a continuous function. Then*

$$(i)\ {}_aD_q^\alpha({}_aI_q^\alpha f)(t) = f(t),\ \alpha > 0,\ t \in [a,b],$$
$$(ii)\ {}_aI_q^\alpha\,{}_aI_q^\beta f(t) = {}_a I_q^{\alpha+\beta} f(t),\ \alpha,\beta > 0,\ t \in [a,b].$$

Lemma 2.3. [30, 50] *Let $\alpha > p-1$ and p be a positive integer. The following then holds:*

$$({}_aI_q^\alpha)\,{}_aD_q^p f(x) = ({}_aD_q^p)_a I_q^\alpha f(x) - \Sigma_{k=0}^{p-1} \frac{(t-a)^{\alpha-p+k}}{\Gamma_q(\alpha+k-p+1)}\,{}_a D_q^k f(a).$$

2.1. Results and Consequences

The method that we would like to apply here consists of getting an equivalent integral representation of the non-trivial solution of the considered fractional boundary value problem. It therefore necessitates an appropriate construction of the Green function, which plays a crucial role in getting Lyapunov's inequalities.

In order to reduce the q fractional boundary value problem (4) to an equivalent integral equation, an auxiliary result is needed. It is formulated in the following Lemma.

Lemma 2.4. *Let $u \in AC([a,b])$. The unique non-trivial solution of the q fractional boundary value problem*

$$\begin{cases} {}_aD_q^\alpha u(t) + Q(t)z(t) = 0, & t \in (a,b), \\ u(a) = 0, \quad u(b) = Au(\epsilon), \end{cases}$$

where $1 < \alpha < 2$, $a < \epsilon < b$, and $0 \le A \le 1$, is then given by

$$u(t) = \int_a^b G(t, \left(qs + (1-q)a\right) z(s)Q(s)\,{}_a d_q s, \tag{10}$$

$$G(t,s) = g(t,s) + \frac{Ag(\epsilon,s)(t-a)^{\alpha-1}}{(b-a)^{\alpha-1} - A(\epsilon-a)^{\alpha-1}}, \tag{11}$$

where

$$\Gamma_q(\alpha)g(t,s) = \begin{cases} \frac{(t-a)^{\alpha-1}}{(b-a)^{\alpha-1}}(b-a)^{\alpha-1}(b-s)^{\alpha-1} - (t-s)^{\alpha-1}, \\ \quad a \le s \le t, \\ \\ \frac{(t-a)^{\alpha-1}}{(b-a)^{\alpha-1}}(b-s)^{\alpha-1}, \qquad t \le s \le b. \end{cases} \tag{12}$$

Proof. We apply Lemma 2.3 in order to reduce the fractional boundary value problem (4) to an equivalent integral one

$$u(t) = -{}_aI_q^\alpha\, u(t) + c_1(t-a)^{\alpha-1} + c_2(t-a)^{\alpha-2}, \tag{13}$$

where c_1, c_2 are real constants.

From $u(a) = 0$ and (4), we get $c_2 = 0$. Therefore, the general solution of (4) is given by

$$u(t) = -{}_aI_q^\alpha\, u(t) + c_1(t-a)^{\alpha-1}$$

$$= -\int_a^t \frac{(t-\left(qs+(1-q)a\right))_a^{(\alpha-1)}}{\Gamma_q(\alpha)} Q(s)z(s)_a d_q s + c_1(t-a)^{\alpha-1}.$$

From (14), we deduce that

$$u(b) = -\int_a^b \frac{(b-\left(qs+(1-q)a\right))_a^{(\alpha-1)}}{\Gamma_q(\alpha)} Q(s)z(s)_a d_q s + c_1(b-a)^{\alpha-1}, \tag{14}$$

and

$$u(\epsilon) = -\int_a^\epsilon \frac{(\epsilon-\left(qs+(1-q)a\right))_a^{(\alpha-1)}}{\Gamma_q(\alpha)} Q(s)z(s)_a d_q s, + c_1(\epsilon-a)^{\alpha-1}. \tag{15}$$

Now, the boundary condition $u(b) = Au(\epsilon)$ yields

$$c_1 = \int_a^b \frac{(b-\left(qs+(1-q)a\right))_a^{(\alpha-1)}}{\gamma\Gamma_q(\alpha)} Q(s)u(s)_a d_q s \tag{16}$$

$$- \int_a^\epsilon \frac{A(\epsilon-\left(qs+(1-q)a\right))_a^{(\alpha-1)}}{\gamma\Gamma_q(\alpha)} Q(s)u(s)_a d_q s, \tag{17}$$

where

$$\gamma := (b-a)^{\alpha-1} - A(\epsilon-a)^{\alpha-1}.$$

Thus, the non-trivial solution of (4) is uniquely given by

$$\begin{aligned} u(t) &= -\int_a^t \frac{(t-\left(qs+(1-q)a\right))_a^{(\alpha-1)}}{\Gamma_q(\alpha)} Q(s)z(s)_a d_q s \\ &+ \int_a^b \frac{(t-a)^{\alpha-1}(b-\left(qs+(1-q)a\right))_a^{(\alpha-1)}}{\gamma\Gamma_q(\alpha)} Q(s)z(s)_a d_q s \\ &- \int_a^\epsilon \frac{A(t-a)^{\alpha-1}(\epsilon-\left(qs+(1-q)a\right))_a^{(\alpha-1)}}{\gamma\Gamma_q(\alpha)} Q(s)z(s)_a d_q s \\ &= -\int_a^t \frac{(t-\left(qs+(1-q)a\right))_a^{(\alpha-1)}}{\Gamma_q(\alpha)} Q(s)z(s)_a d_q s \\ &+ \int_a^b \frac{(t-a)^{\alpha-1}(b-\left(qs+(1-q)a\right))_a^{(\alpha-1)}}{\gamma\Gamma_q(\alpha)} Q(s)z(s)_a d_q s, \\ &+ \int_a^b \frac{A(t-a)^{\alpha-1}(\epsilon-\left(qs+(1-q)a\right))_a^{(\alpha-1)}}{\gamma\Gamma_q(\alpha)} Q(s)z(s)_a d_q s \\ &- \int_b^\epsilon \frac{A(t-a)^{\alpha-1}(\epsilon-\left(qs+(1-q)a\right))_a^{(\alpha-1)}}{\gamma\Gamma_q(\alpha)} Q(s)z(s)_a d_q s \\ &= \int_a^b G(t,s)Q(s)z(s)_a d_q s, \end{aligned} \tag{18}$$

where the Green function G is defined in (11) and (12), and the proof is finished.

Lemma 2.5. *Let $u \in AC[a,b]$. The q fractional boundary value problem*

$$\begin{cases} {}_aD_q^\beta(\phi_p({}_aD_q^\alpha u(t))) + Q(t)z(t) = 0, \quad t \in (a,b), \\ u(a) = 0, \quad u(b) = Au(\epsilon), \\ {}_aD_q^\alpha(a) = 0, \quad {}_aD_q^\alpha u(b) = B\,{}_aD_q^\alpha u(\delta),, \end{cases} \tag{19}$$

$1 < \alpha,\ \beta < 2,,\ a < \epsilon < b$, *and* $0 \le A,\ B \le 1$, *then admits a non-trivial unique solution defined by*

$$u(t) = \int_a^b G(t,\left(qs+(1-q)a\right))\,\phi_r \left(\int_a^b H(s,\left(q\tau+(1-q)a\right))z(\tau)Q(\tau)d_q\tau\right) d_q s, \tag{20}$$

where $G(t,s)$ is defined in (11), (12) *and*

$$H(t,s) := h(t,s) + \frac{(B)^{p-1}h(\delta,s)(t-a)^{\alpha-1}}{(b-a)^{\beta-1} - (\delta-a)^{\beta-1}}, \tag{21}$$

where

$$\Gamma_q(\alpha)h(t,s) = \begin{cases} \frac{(t-a)^{\beta-1}}{(b-a)^{\beta-1}}(b-s)^{\beta-1} - (t-s)^{\beta-1}, & a \le s \le t, \\ \frac{(t-a)^{\beta-1}}{(b-a)^{\beta-1}}(b-s)^{\beta-1}, & t \le s \le b. \end{cases} \tag{22}$$

Proof. We use Lemma 2.4 in order to reduce the fractional differential Equation (4) to an equivalent integral one

$$\phi_p({}_aD_q^\alpha u(t)) = ({}_aD_q^\beta u(t)) + c_3(t-a)^{\beta-1} + c_4(t-a)^{\beta-2}. \tag{23}$$

In view of the boundary condition ${}_aD_q u(a) = 0$ and (23), we obtain $c_4 = 0$. Hence the non-trivial solution of the fractional boundary value (4) is given by

$$\begin{aligned} \phi_p({}_aD_q^\alpha u(t)) &= ({}_aD_q^\beta u(t)) + c_3(t-a)^{\beta-1} \\ &= \int_a^t \frac{(t-\left(qs+(1-q)a\right)_a)^{(\beta-1)}}{\Gamma_q(\beta)} Q(s)z(s)\,{}_a d_q s \\ &+ c_3(t-a)^{\beta-1}. \end{aligned} \tag{24}$$

Now in light of (24), we get

$$\begin{aligned} \phi_p({}_aD_q^\alpha u(b)) &= \int_a^b \frac{(b-\left(qs+(1-q)a\right))_a^{(\beta-1)}}{\Gamma_q(\beta)} Q(s)z(s)\,{}_a d_q s \\ &+ c_3(b-a)^{\beta-1}, \end{aligned} \tag{25}$$

$$\begin{aligned} \phi_p({}_aD_q^\alpha u(\delta)) &= \int_a^\delta \frac{(\delta-\left(qs+(1-q)a\right))_a^{(\beta-1)}}{\Gamma_q(\beta)} Q(s)z(s)\,{}_a d_q s \\ &+ c_3(\delta-a)^{\beta-1}. \end{aligned} \tag{26}$$

By the boundary condition ${}_aD_q^\alpha u(b) = B\,{}_aD_q^\alpha u(\delta)$ yields

$$c_3 = \int_a^b \frac{(b-\left(qs+(1-q)a\right)_a)^{(\beta-1)}}{\left((b-a)^{\beta-1} - b^{p-1}(\delta-a)^{\beta-1}\right)\Gamma_q(\beta)} Q(s)z(s)\,{}_a d_q s$$

$$
\begin{aligned}
&- \int_a^{\delta} \frac{(\delta - \left(qs + (1-q)a\right))_a^{(\beta-1)}}{\left((b-a)^{\beta-1} - b^{p-1}(\delta-a)^{\beta-1}\right)\Gamma_q(\beta)} Q(s)z(s)\,{}_a d_q s. \\
&= \frac{1}{\bar{\gamma}} \left(\int_a^b \frac{(b - \left(qs + (1-q)a\right))_a^{(\beta-1)}}{\Gamma_q(\beta)} Q(s)z(s)\,{}_a d_q s \right) \\
&- \frac{1}{\bar{\gamma}} \left(\int_a^{\delta} \frac{(\delta - \left(qs + (1-q)a\right))_a^{(\beta-1)}}{\Gamma_q(\beta)} Q(s)z(s)\,{}_a d_q s \right), \quad (27)
\end{aligned}
$$

where

$$
\bar{\gamma} := \left((b-a)^{\beta-1} - b^{p-1}(\delta-a)^{\beta-1}\right).
$$

One may observe that, in a similar way to Lemma 2.4, we get

$$
\phi_p({}_a D_q^{\alpha} u(t) = - \int_a^b H(t, \left(qs + (1-q)a\right))_a Q(s)z(s)\,{}_a d_q s. \quad (28)
$$

Thus, the given fractional boundary value problem (4) may be re-written equivalently as

$$
\begin{aligned}
({}_a D_q^{\alpha} u(t) + \phi_r \left(\int_a^b H(t, \left(qs + (1-q)a\right))_a Q(s)u(s)\,{}_a d_q s \right) &= 0, \quad t \in (a,b), \\
u(a) = 0, \quad u(b) &= Au(\delta).
\end{aligned}
$$

Again by Lemma 2.4, the non-trivial solution of (4) is uniquely given by

$$
\begin{aligned}
u(t) = \int_a^b G(t, \left(qs + (1-q)a\right))\phi_r \\
\left(\int_a^b H(s, q\tau) z(\tau) Q(\tau)_a d_q \tau \right)\,{}_a d_q s. \quad (29)
\end{aligned}
$$

The proof of the desired result is achieved.

Next we shall focus on finding the properties of the Green functions as well as their maximum principle. In order to do so, we express this fact in the following lemma.

Lemma 2.6. *Let $u \in C[a,b]$. The Green functions G and H defined respectively in* (11), (12) *and* (21), (22) *are then continuous and satisfy*

$$
\begin{aligned}
&(a)\ G(t, \left(qs + (1-q)a\right)) \geq 0, \text{ and } H(t, \left(qs + (1-q)a\right)_a) \geq 0, \\
&\quad \forall\ (t,s) \in [a,b] \times [a,b], \quad (30) \\
&(b)\ G(t, qs + (1-q)a) \leq G(s, (qs + (1-q)a)), \text{ and} \quad (31) \\
&\quad H(t, qs + (1-q)a)) \leq H((qs + (1-q)a), (qs + (1-q)a)) \\
&\quad \forall\ (t,s) \in [a,b] \times [a,b],
\end{aligned}
$$

$1 < \alpha,\ \beta < 2,\ a < \epsilon < b$, *and* $0 \leq A,\ B \leq 1$.

Proof. Before starting the proof of Lemma 2.6, let us mention that γ and $\bar{\gamma}$ are positive, since $a < \epsilon,\ \delta < b$, and $0 \leq A,\ B \leq 1$.

We consider

$$
G(t,s) = g(t,s) + \frac{Ag(\epsilon, s)(t-a)^{\alpha-1}}{(b-a)^{\alpha-1} - A(\epsilon-a)^{\alpha-1}}. \quad (32)
$$

Let us differentiate $g(t,s)$ defined in (12) with respect to t, for $s \leq t$, by

$$
\Gamma_q(\alpha) g(t,s) = \begin{cases} \frac{(t-a)^{\alpha-1}}{(b-a)^{\alpha-1}}(b-s)^{\alpha-1} - (t-s)^{\alpha-1}, & a \leq s \leq t, \\ \frac{(t-a)^{\alpha-1}}{(b-a)^{\alpha-1}}(b-s)^{\alpha-1}, & t \leq s \leq b. \end{cases} \quad (33)
$$

$$
\begin{aligned}
t_{({}_a D_q} g(t,s) &= t_{({}_a D_q}((t-a)^{\alpha-1}) \frac{(b-s)_a^{(\alpha-1)}}{(b-a)^{\alpha-1}} \\
&\quad - t_{({}_a D_q}((t-s)_a^{(\alpha-1)}, \\
&= \frac{[\alpha-1]_q}{\Gamma_q(\alpha)} \left((b-s)_a^{(\alpha-1)} (t-a)^{\alpha-2} \right) \\
&\quad - (t-s)_a^{(\alpha-2)} \left((t-a)^{\alpha-2} \right) \\
&= \frac{[\alpha-1]_q}{\Gamma_q(\alpha)} (t-a)^{\alpha-2} \left((1 - \frac{s-a}{b-a})_0^{\alpha-1} \right) \\
&\quad - (t-a)^{\alpha-2} \left((1 - \frac{s-a}{t-a})_0^{\alpha-2} \right) \\
&\leq \frac{[\alpha-1]_q}{\Gamma_q(\alpha)} (t-a)^{\alpha-2} \left((1 - \frac{s-a}{b-a})_0^{\alpha-1} \right) \\
&\quad - \left((1 - \frac{s-a}{b-a})_0^{\alpha-2} \right), \quad (34)
\end{aligned}
$$

which is non-positive, since $a < s < t < b$.
Therefore, the function g is decreasing in its argument t, and the following inequality is satisfied

$$
\begin{aligned}
0 &= g(b, qs + (1-q)a) \quad (35) \\
&\leq g(t, qs + (1-q)a) \\
&\leq g(qs + (1-q)a), qs + (1-q)a).
\end{aligned}
$$

To this end, one may conclude that the right-hand-side of (35) may be expressed as

$$
\begin{aligned}
g(qs + (1-q)a), qs + (1-q)a) = \frac{1}{\Gamma_q(\alpha)} (\frac{q(s-a)}{b-a})^{\alpha-1} \\
\left(b - ((qs + (1-q)a)_a\right)_a^{(\alpha-1)}. \quad (36)
\end{aligned}
$$

Thus, $G(t, ((qs + (1-q)a))_a)$ is non-negative and satisfies

$$
\begin{aligned}
G(t, ((qs + (1-q)a))_a) &\leq \max_{a \leq t \leq b} G(t, (qs + (1-q)a)) \\
&= \max_{a \leq t \leq b} (g(t, (qs + (1-q)a)) \\
&\quad + \frac{Ag(\epsilon, (qs + (1-q)a)(t-a)^{\alpha-1}}{\gamma}) \\
&\leq \frac{1}{\Gamma_q(\alpha)} \frac{q(s-a)^{(\alpha-1)}}{(b-a)^{\alpha-1}} \left(b - ((qs + (1-q)a)\right)_a^{(\alpha-1)} \\
&\quad + \frac{Ag(\epsilon, (qs + (1-q)a)_a (b-a)^{\alpha-1}}{\gamma} := \tilde{G}_q(s). \quad (37)
\end{aligned}
$$

For $t \leq s$, G is defined by

$$
G(t,s) = g(t,s) + \frac{Ag(\epsilon, s)(t-a)^{\alpha-1}}{(b-a)^{\alpha-1} - A(\epsilon-a)^{\alpha-1}}, \quad (38)
$$

where

$$\Gamma_q(\alpha)g(t,s) = \frac{(t-a)^{\alpha-1}}{(b-a)^{\alpha-1}}(b-s)^{\alpha-1}. \quad (39)$$

Similarly to above, we make differentiation with respect to t, and then we get

$${}_t({}_aD_q g(t,s)) = \frac{[\alpha-1]_q}{\Gamma_q(\alpha)}\left(\left(1-\frac{s-a}{b-a}\right)_a^{\alpha-1}(t-a)^{\alpha-2}\right), \quad (40)$$

which is non-negative, and consequently the function g is non-decreasing in its argument t. We have

$$\begin{aligned} 0 &= g(a, qs+(1-q)a) \quad (41)\\ &\le g(t, qs+(1-q)a)\\ &\le g(s, qs+(1-q)a), \end{aligned}$$

where $g(s, qs+(1-q)a) = \frac{(q(s-a))^{(\alpha-1)}}{(b-a)^{\alpha-1}}\left(b-((qs+(1-q)a)\right)_a^{(\alpha-1)}$.

Now, to prove the inequality involving H, we consider $H(t,s)$ defined in $(21)-(22)$ by

$$H(t,s) := h(t,s) + \frac{(B)^{p-1}h(\delta,s)(t-a)^{\beta-1}}{(b-a)^{\beta-1}-(B)^{p-1}(\delta-a)^{\beta-1}}, \quad (42)$$

$$\Gamma_q(\alpha)h(t,s) = \begin{cases} \frac{(t-a)^{\beta-1}}{(b-a)^{\beta-1}}(b-s)^{\beta-1}-(t-s)^{\beta-1}, & a\le s\le t,\\ \frac{(t-a)^{\beta-1}}{(b-a)^{\beta-1}}(b-s)^{\beta-1}, & t\le s\le b. \end{cases} \quad (43)$$

For $t \le s$, we have

$$\begin{aligned} \Gamma_q(\alpha)h(t,(qs+(1-q)a)_a &= \frac{(t-a)^{\beta-1}}{(b-a)^{\beta-1}}(b-(qs+(1-q)a))_a^{(\beta-1)}\\ &\le \frac{(s-a)^{(\beta-1)}}{(b-a)^{\beta-1}}(b-(qs+(1-q)a))_a{}^{(\beta-1)}\\ &:= \Gamma_q(\alpha)\,h(s,(qs+((1-q)a)). \end{aligned} \quad (44)$$

For $t \ge s$, we consider

$$\begin{aligned} \Gamma_q(\alpha)h(t,(qs+(1-q)a)_a &= \frac{(t-a)^{\beta-1}}{(b-a)^{\beta-1}}(b-(qs+(1-q)a))_a{}^{(\beta-1)}\\ &- (t-(qs+(1-q)a))_a{}^{(\beta-1)}. \end{aligned} \quad (45)$$

We claim that $h(t,(qs+(1-q)a)_a)$ is non-negative too. It is sufficient to replace $\alpha-1$ by $\beta-1$ in all the steps of the proof of Lemma 2.6 (b), and we get the same result. So the proof is omitted, since it is similar to that of Lemma 2.6. Therefore

$$\begin{aligned} 0 &= h(a,(qs+(1-q)a))\\ &\le h(t,(qs+(1-q)a))\\ &\le h(s,(qs+(1-q)a)). \end{aligned}$$

Likely, one may conclude that the right-hand-side $h(s,(qs+(1-q)a))$ appearing in the previous inequality may be expressed as

$$h(s,(qs+(1-q)a)) = \frac{1}{\Gamma_q(\beta)}\left(\frac{q(s-a)}{b-a}\right)^{\beta-1}\left(b-(qs+(1-q)a)\right)_a^{(\beta-1)}. \quad (46)$$

Thus, $H(t,(qs+(1-q)a))$ is non-negative and satisfies

$$\begin{aligned} H(t,(qs+(1-q)a)) &\le \max_{a\le t\le b} H(t,(qs+(1-q)a))\\ &= \max_{a\le t\le b}\Big(h(t,(qs+(1-q)a))\\ &\quad + \frac{Ah(\delta,(qs+(1-q)a)_a(t-a)^{\beta-1}}{\bar\gamma}\Big)\\ &\le \frac{1}{\Gamma_q(\beta)}\frac{q(s-a)^{(\beta-1)}}{(b-a)^{\beta-1}}\\ &\quad \left(b-((qs+(1-q)a)\right)_a^{(\beta-1)}\\ &\quad + \frac{Ah(\delta,(qs+(1-q)a)_a(b-a)^{\beta-1}}{\bar\gamma}\\ &:= \tilde H_q(s). \end{aligned} \quad (47)$$

The main result of this paper, which is a Lyapunov's inequality for a q- fractional difference p-Laplacian boundary value problem (4), will be formulated in the next theorem. We state and prove it in light of the previous lemmas.

Theorem 2.1. *Assume that u is a non-trivial solution of the q fractional boundary value problem*

$$\begin{cases} {}_aD_q^{\beta}(\phi_p({}_aD_q^{\alpha}\phi_p(u(t))) + Q(t)\phi_p(u(t)) = 0, \quad t\in(a,b),\\ u(a)=0, \quad u(b)=Au(\epsilon),\\ {}_aD_q^{\alpha}(a)=0, \quad {}_aD_q^{\alpha}u(b)=B\,{}_aD_q^{\alpha}u(\delta), \end{cases} \quad (48)$$

where ${}_aD_q^{\alpha}$, ${}_aD_q^{\beta}$ are the fractional q-derivative of the Riemann-Liouville type with $1<\alpha,\ \beta<2$, $0\le A,\ B\le 1$, $a<\epsilon,\ \delta<b$, $\phi_p(s)=|s|^{p-2}s$, $p>1$, $\phi_p^{-1}=\phi_r$, $\frac{1}{p}+\frac{1}{r}=1$, and $Q:[a,b]\to R$ is a continuous function on $[a,b]$.

The following integral inequality is then satisfied

$$1 \le \left(\int_a^b \tilde G_q(s)\,{}_ad_qs\right)\left(\int_a^b \tilde H_q(s)\,|Q(s)|\,{}_ad_qs\right)^{r-1}, \quad (49)$$

where $\tilde G_q(s)$, and $\tilde H_q(s)$ are defined in (37) *and* (49)*, respectively.*

Proof. Let us define the norm of u, where u is a non-trivial solution of the q-fractional difference boundary value problem (4) by

$$||u|| := \max_{t\in[a,b]}|u(t)|.$$

Then, in view of Lemma 2.5, the non-trivial solution $u \in AC([a,b],\mathbb{R})$ may be re-written for all $t\in[a,b]$ as follows

$$u(t) = \int_a^b G(t,qs+(1-q)a)\phi_q \quad (50)$$

$$\left(\int_a^b H(s,q\sigma)+(1-q)a)\,Q(\sigma)\phi_p(u(\sigma))\,{}_ad_q\sigma\right)\,{}_ad_qs.$$

We then deduce

$$\begin{aligned}|u(t)| &\le \int_a^b |G(t,qs+(1-q)a))|\,|\phi_q\left(\int_a^b H(s,\sigma)\,Q(\sigma)\phi_p(u(\sigma))\,{}_ad_q\sigma\right)|\,{}_ad_qs\\ &= \int_a^b |G(t,qs+(1-q)a))| \qquad (51)\\ &\quad |\left(\int_a^b H(s,q\sigma)+(1-q)a)\,Q(\sigma)\phi_p(u(\sigma))\,{}_ad_q\sigma\right)|^{r-1}\,{}_ad_qs\\ &= \int_a^b |G(t,qs+(1-q)a))|\\ &\quad |\left(\int_a^b |H(s,q\sigma)+(1-q)a)\,Q(\sigma)|\,||u||_a^{p-1}d_q\sigma\right)|^{r-1}\,{}_ad_qs\\ &= \int_a^b |G(t,s)|||u||^{\frac{p-1}{r-1}}\left(\int_a^b |H(s,q\sigma)+(1-q)a)|\,|Q(\sigma)|\,{}_ad_q\sigma\right)^{r-1}\,{}_ad_qs.\end{aligned}$$

Based on the non-triviality of the solution u and the fact that p and r are conjugates, one may observe that

$$1\le\int_a^b |G(t,qs+(1-q)a)|\,{}_ad_qs\left(\int_a^b |H(s,q\sigma)+(1-q)a)|\,|Q(\sigma)|\,{}_ad_q\sigma\right)^{r-1}.$$

Due to Lemma 2.5 and Lemma 2.6, it holds that

$$1\le\int_a^b \tilde{G}_q(s)\,{}_ad_qs\left(\int_a^b \tilde{H}_q(s)\,|Q(\sigma)|\,{}_ad_q\sigma\right)^{r-1}.$$

To this end, it is worth noticing that, by letting q to 1^-, we retrieve the following integral inequality due to Hartman and Wintner (see [52])

$$\int_a^b (s-a)(b-s)|Q(s)|\,ds\ \ge\ (b-a).$$

Due to this fact, the obtained integral inequality (49) may be viewed as the q-fractional integral Hartman and Wintner inequality for the p-Laplacian case. However, it is easy for the reader to get an analogous result to this fundamental inequality by considering $p=2,\alpha=2$, and $q\to\ 1^-$.

Several types of Lyapunov's inequality were derived from Theorem 2.1. Hereafter, we formulate and express all of them in the following corollaries. We shall focus on covering both cases, ordinary differential equations and fractional differential equations. In addition, we illustrate this Theorem by giving an example. It consists of getting the interval of non-zeros of an appropriate eigenvalue fractional boundary value problem.

Let us start with the first result derived from Theorem 2.1.

Corollary 2.1. *Suppose that u is a non-trivial solution of the q fractional boundary value problem*

$$\begin{cases} {}_aD_q^\beta(\phi_p({}_aD_q^\alpha u(t)) + Q(t)\phi_p(u(t))=0, \quad t\in(a,b),\\ u(a)=0,\quad u(b)=A\,u(\epsilon),\\ {}_aD_q^\alpha(a)=0,\quad {}_aD_q^\alpha u(b)=B\,{}_aD_q^\alpha u(\delta),,\end{cases}\qquad(52)$$

where ${}_aD_q^\alpha$, ${}_aD_q^\beta$ are the fractional q-derivative of Riemann-Liouville type with $1<\alpha,\ \beta<2$, $0\le A,\ B\le 1$, $a<\epsilon,\ \delta<b$, $\phi_p(s)=|s|^{p-2}s$, $p>1$, $\phi_p^{-1}=\phi_r$, $\frac{1}{p}+\frac{1}{r}=1$, and $Q:[a,b]\to R$ is a continuous function on $[a,b]$.

The following integral inequality is then satisfied

$$1\le\frac{1}{\Gamma_q(\alpha)}\frac{A}{\gamma}(\epsilon-a)^{(\alpha-1)}\frac{1}{\Gamma_q(\beta)}\frac{B^{p-1}}{\bar{\gamma}}(\delta-a)^{\beta-1}(b-a)\left(\int_a^b |Q(s)|\,{}_ad_qs\right)^{r-1}.\qquad(53)$$

Proof. It is sufficient to let $q\to 0^+$ and consider two cases: $t\le s$ and $s\le t$. In the first case, $\tilde{G}_q(t,s)$ and $\tilde{H}_q(t,s)$ defined in (37) and (47) tend to zero. In the second case, they take the following form

$$\tilde{G}_q(t,s):=\frac{A(\epsilon-a)^{\alpha-1}}{\gamma}\ \text{and}\ \tilde{H}_q(t,s)::=\frac{B^{p-1}(\delta-a)^{\beta-1}}{\bar{\gamma}},$$

and we get the result of this corollary.

Corollary 2.2. *Suppose that u is a non-trivial solution of the q fractional boundary value problem*

$$\begin{cases} {}_aD_q^\beta(\phi_p({}_aD_q^\alpha u(t)) + Q(t)\phi_p(u(t))=0, \quad t\in(a,b),\\ u(a)=0,\quad u(b)=A\,u(\epsilon),\\ {}_aD_q^\alpha(a)=0,\quad {}_aD_q^\alpha u(b)=B\,{}_aD_q^\alpha u(\delta),\end{cases}\qquad(54)$$

where ${}_aD_q^\alpha$, ${}_aD_q^\beta$ are the fractional q-derivative of the Riemann-Liouville type with $1<\alpha,\ \beta<2$, $0\le A,\ B\le 1$, $a<\epsilon,\ \delta<b$, $\phi_p(s)=|s|^{p-2}s$, $p>1$, $\phi_p^{-1}=\phi_r$, $\frac{1}{p}+\frac{1}{r}=1$, and $Q:[a,b]\to R$ is a continuous function on $[a,b]$.

The following integral inequality is then satisfied

$$\begin{aligned}1\ \le\ &\left(\int_a^b \frac{1}{\Gamma_q(\alpha)}(\frac{s-a}{b-a})^{\alpha-1}(b-s)^{\alpha-1}\,{}_ad_qs\right.\\ &\left.+\int_a^b \frac{A}{\gamma}g(\epsilon,s)(b-a)^{\alpha-1}\,{}_ad_qs\right)\\ &\left(\int_a^b \frac{1}{\Gamma_q(\beta)}(\frac{s-a}{b-a})^{\beta-1}(b-s)^{\beta-1}\,|Q(s)|\,{}_ad_qs\right.\\ &\left.+\int_a^b \frac{B^{p-1}}{\bar{\gamma}}h(\delta,s)(b-a)^{\beta-1}\,|Q(s)|\,{}_ad_qs\right)^{r-1}.\end{aligned}$$

Proof. The result is achieved by letting $q\ \to\ 1^-$ in (49).

Remarks:

- The result of this corollary (Corollary 2.2) represents a Hartman-Wintner inequality for the q-fractional difference p-Laplacian boundary value problem (54). For the particular case when $A = B = 0$ and $\alpha = \beta$, we obtain

$$\int_a^b (s-a)^{\alpha-1}(b-s)^{\alpha-1}Q(s)ds \geq \Gamma(\alpha)(\frac{4}{b-a})^{\alpha-1}.$$

- When $\alpha = \beta = 2$, we retrieve the necessary condition of existence of non-trivial solutions investigated by Lyapunov for the second ordinary differential equation subject to the Dirichlet boundary conditions, and therefore one may conclude that if the non-trivial solution corresponding to this problem exists, then the non-trivial solution of (54) exists too, and vice-versa.

  Indeed, in that case, for $\alpha = \beta = 2$, we find:

$$\frac{4}{b-a} \leq \int_a^b (s-a)(b-s)\,|Q(s)|\,ds.$$

  Now we focus on a second mixed-order differential inequality by taking $\alpha = \beta = 2$. For the next derived result from Theorem 2.1, we provide an important inequality that is very useful. This is the arithmetic-geometric-harmonic inequality. It says that:

$$(s-a)(b-s) \leq \frac{(b-a)^2}{4}.$$

Corollary 2.3. *Suppose that u is a non-trivial solution of the q fractional boundary value problem*

$$\begin{cases} {}_aD_q^{\beta}(\phi_p({}_aD_q^{\alpha}u(t))) + Q(t)\phi_p(u(t)) = 0, \quad t \in (a,b), \\ u(a) = 0, \quad u(b) = A\,u(\epsilon), \\ {}_aD_q^{\alpha}(a) = 0, \quad {}_aD_q^{\alpha}u(b) = B\,{}_aD_q^{\alpha}u(\delta), \end{cases} \tag{55}$$

where ${}_aD_q^{\alpha}$, ${}_aD_q^{\beta}$ are the fractional q-derivative of the Riemann-Liouville type with $1 < \alpha,\ \beta < 2$, $0 \leq A,\ B \leq 1$, $a < \epsilon,\ \delta < b$, $\phi_p(s) = |s|^{p-2}s$, $p > 1$, $\phi_p^{-1} = \phi_r$, $\frac{1}{p} + \frac{1}{r} = 1$, and $Q{:}[a,b] \to R$ is a continuous function on $[a,b]$.

The following integral inequality is then satisfied

$$1 \leq \left(\int_a^b \frac{1}{\Gamma(\alpha)}\frac{(b-a)^{2(\alpha-1)}}{4^{\alpha-1}}\,ds + \int_a^b \frac{A}{\gamma}g(\epsilon,s)(b-a)^{\alpha-1}\,ds\right)$$
$$\left(\int_a^b \frac{1}{\Gamma(\beta)}(\frac{(b-a)^{2(\beta-1)}}{4^{\beta-1}}\,|Q(s)|\,ds + \int_a^b \frac{B^{p-1}}{\bar{\gamma}}h(\delta,s)(b-a)^{\beta-1}\,|Q(s)|\,ds\right)^{r-1}.$$

Proof. We use the result of Corollary 2.2 by considering the arithmetic-geometric-harmonic inequality, and we get the desired result. Now we focus on a second mixed-order differential inequality by taking $\alpha = \beta = 2$, $p = 2$ and therefore $r = 2$, since p and r are conjugates.

Corollary 2.4. *Suppose that u is a non-trivial solution of the fractional q-difference boundary value problem*

$$\begin{cases} {}_aD''({}_aD''u(t) + Q(t)u(t) = 0, \quad t \in (a,b), \\ u(a) = 0, \quad u(b) = A\,u(\epsilon), \\ {}_aD''(a) = 0, \quad {}_aD''u(b) = B\,{}_aD''u(\delta), \end{cases} \tag{56}$$

where ${}_aD''$, ${}_aD''$ are the fractional derivative of the Riemann-Liouville type of order 2, $0 \leq A,\ B \leq 1$, $a < \epsilon,\ \delta < b$, and $Q{:}[a,b] \to R$ is a continuous function on $[a,b]$.

The following integral inequality is then satisfied

$$1 \leq \left(\int_a^b (\frac{s-a}{b-a})(b-s)\,ds + \int_a^b \frac{A}{\gamma}g(\epsilon,s)(b-a)\,ds\right)$$
$$\left(\int_a^b (\frac{s-a}{b-a})(b-s)\,|Q(s)|\,ds + \int_a^b \frac{B}{\bar{\gamma}}h(\delta,s)(b-a)\,|Q(s)|\,ds\right),$$

where g and h are defined in (12) and (22), respectively (with $\alpha = \beta = 2$), and γ and $\bar{\gamma}$ are defined by

$$\gamma := (b-a) - A(\epsilon - a), \text{ and } \bar{\gamma} := (b-a) - B^{p-1}(\delta - a).$$

Proof. We set $\alpha = \beta = 2$, $p = r = 2$, and we let $q \to 1^-$ in Corollary 2.2, and the desired result is therefore established.

Remark:

The result obtained in Corollary 2.4 is more general than the Hartman Wintner inequality. For the particular case when $A = B = 0$, we get the classical Hartman-Wintner inequality.

Corollary 2.5. *Suppose that u is a non-trivial solution of the fractional boundary value problem*

$$\begin{cases} {}_aD''({}_aD''u(t) + Q(t)u(t) = 0, \quad t \in (a,b), \\ u(a) = 0, \quad u(b) = 0, \\ {}_aD''u(a) = 0, \quad {}_aD''u(b) = 0, \end{cases} \tag{57}$$

where ${}_aD''$, ${}_aD''$ are the fractional derivative of the Riemann-Liouville type of order 2, and $Q{:}[a,b] \to \mathbb{R}$ is a continuous function on $[a,b]$.

The following integral inequality is then satisfied

$$\frac{4}{b-a} \leq \int_a^b (s-a)(b-s)|Q(s)|\,ds. \tag{58}$$

Proof. It is sufficient to use the arithmetic-geometric-harmonic inequality to the conclusion of Corollary 2.4 and set $A = B = 0$, and the result will follow.

Corollary 2.6. *Suppose that u is a non-trivial solution of the fractional boundary value problem*

$$\begin{cases} {}_aD''({}_aD''u(t) + Q(t)u(t) = 0, \quad t \in (a,b), \\ u(a) = 0, \quad u(b) = 0, \\ {}_aD''(a) = 0, \quad {}_aD''u(b) = 0, \end{cases} \tag{59}$$

where ${}_aD''$, ${}_aD''$ are the fractional derivative of the Riemann-Liouville type of order 2, and $Q{:}[a,b] \to R$ is a continuous function on $[a,b]$.

The following integral inequality is then satisfied

$$\left(\frac{4}{b-a}\right)^2 \leq \int_a^b |Q(s)|ds. \tag{60}$$

Proof. Similarly to the above, we apply two times the arithmetic-geometric-harmonic inequality to the result of Corollary 2.4, and the desired result is achieved.

3. ON AN INTERVAL OF REAL ZEROS OF THE MITTAG-LEFFLER FUNCTION

In this section, we are interested in getting the interval of real zeros of the following Mittag-Leffler function [43]:

$$E_\alpha(\lambda) = \Sigma_{k=0}^{\infty} \frac{\lambda^k}{\Gamma(k\alpha+\beta)}, \quad \lambda, \beta \in \mathbb{C}, \text{ and } Re(\alpha) > 0,$$

where C denotes the set of complex numbers, and $R(\alpha)$ is the real part of α. The key tool in proving this result consists of an appropriate integral inequality of the following fractional boundary value problem.

Theorem 3.1. *Let u be a non-trivial solution of*

$$\begin{aligned} &{}_0D^\alpha({}_0D^\alpha(u(t))) + \lambda u(t) = 0, \quad 0 < t < 1, \quad 1 < \alpha \leq 2, \\ &u(0) = 0, \ u(1) = 0, \end{aligned}$$

$$ {}_0D^\alpha u(0) = 0, \ {}_0D^\alpha u(1) = 0, \tag{61}$$

then $|\lambda| \geq (\Gamma(\alpha)4^{\alpha-1})^2$.

Proof. We apply Corollary 2.3 with $A = B = 0$, $\alpha = \beta$, $p = 2$, $r = 2$, and $a = 0$, $b = 1$. We obtain

$$|\lambda| \geq (\Gamma(\alpha)4^{\alpha-1})^2,$$

and the proof is completed.

DATA AVAILABILITY STATEMENT

All datasets generated for this study are included in the article/supplementary material.

AUTHOR CONTRIBUTIONS

All authors listed have made a substantial, direct and intellectual contribution to the work, and approved it for publication.

FUNDING

FTc and FTa extend their appreciation to the Deanship of Scientific Research at King Saud University for funding this work through Research Group no. RG-1440-010.

REFERENCES

1. Chai G. Positive solutions for boundary value problem of fractional differential equation with p-Laplacian operator. *Bound Value Probl*. (2012) **2012**:18. doi: 10.1186/1687-2770-2012-18
2. El-Shahed M, Hassan HA. Positive solutions of q-difference equation. *Proc Am Math Soc*. (2010) **138**:1733–8. doi: 10.1090/S0002-9939-09-10185-5
3. Ferreira RAC. Nontrivial solutions for fractional q-difference boundary value problems, *Electron J Qual Theory Differ Equat*. (2010) **70**:1–10. doi: 10.14232/ejqtde.2010.1.70
4. Ferreira RAC. Positive solutions for a class of boundary value problems with fractional q-differences. *Comput Math Appl*. (2011) **61**:367–73. doi: 10.1016/j.camwa.2010.11.012
5. Ferreira RAC. On a Lyapunov-type inequality the zeros of a certain Mittag-Leffler function. *J Math Anal Appl*. (2014) **412**:1058–63. doi: 10.1016/j.jmaa.2013.11.025
6. Liapunov AM. Problème général de la stabilityé du movement. *Ann Fac Sci Univ Toulouse*. (1907) **2**:203–407.
7. Liang S, Zhang J. Existence and uniqueness of positive solutions for three-point boundary value problem with fractional q-differences. *J Appl Math Comput*. (2012) **40**:277–88. doi: 10.1007/s12190-012-0551-2
8. Liu X, Jia M. Multiple solutions for fractional differential equations with nonlinear boundary conditions. *Comput Math Appl*. (2010) **59**:2880–6. doi: 10.1016/j.camwa.2010.02.005
9. Marin M, Nicaise S. Existence and stability results for thermoelastic dipolar bodies with double porosity. *Continuum Mech. Thermodyn*. (2016) **28**:1645–57. doi: 10.1007/s00161-016-0503-4
10. Marin M, Baleanu D, Vlase S. Effect of microtemperatures for micropolar thermoelastic bodies. *Struct Eng Mech*. (2017) **61**:381–7. doi: 10.12989/sem.2017.61.3.381
11. Marin M, Craciun EM. Uniqueness results for a boundary value problem in dipolar thermoelasticity to model composite materials. *Compos B Eng*. (2017) **126**:27–37. doi: 10.1016/j.compositesb.2017.05.063
12. Pachpatte BG. Lyapunov type integral inequalities for certain differential equations. *Georgian Math J*. (1997) **4**:139–48. doi: 10.1023/A:1022930116838
13. Podlubny I. *Fractional Differential Equations*. San Diego, CA: Academic Press (1999).
14. Rong J, Bai C. Lyapunov-type inequality for a fractional differential equation with fractional boundary conditions. *Adv Differ Equat*. (2015) **2015**:10. doi: 10.1186/s13662-015-0430-x
15. Ren T, Chen X. Positive solutions of fractional differential equation with p-Laplacian operator. *Abstr Appl Anal*. (2013) **2013**:789836. doi: 10.1155/2013/789836
16. Samko SG, Kilbas AA, Marichev OI. *Fractional Integrals and Derivatives, Theory and Applications*. Yverdon: Gordon and Breach (1993).
17. Su Y, Li Q, Liu X. Existence criteria for positive solutions of p-Laplacian fractional differential equations with derivative terms. *Adv Differ Equat*. (2013) **2013**:119. doi: 10.1186/1687-1847-2013-119
18. Tariboon J, Ntouyas SK. Quantum integral inequalities on finite intervals. *J Inequal Appl*. (2014) **2014**:121. doi: 10.1186/1029-242X-2014-121
19. Tariboon J, Ntouyas SK, Agarwal P. New concepts of fractional quantum calculus and applications to impulsive fractional q-difference equations. *Adv Differ Equat*. (2015) **2015**:18. doi: 10.1186/s13662-014-0348-8
20. Wang J, Xiang H, Liu Z. Upper and lower solutions method for a class of singular fractional boundary value problems with p-Laplacian operator. *Abstr Appl Anal*. (2010) **2010**:971824. doi: 10.1155/2010/971824
21. Wu W, Zhou X. Eigenvalue of fractional differential equations with p-Laplacian operator. *Discrete Dyn Nat Soc*. (2013) **2013**:137890. doi: 10.1155/2013/137890
22. Yao S, Wang G, Li Z, Yu L. Positive solutions for three-point boundary value problem of fractional differential equation with p-Laplacian operator. *Discrete Dyn Nat Soc*. (2013) **2013**:376938. doi: 10.1155/2013/376938
23. Agarwal RP. Certain fractional q-integrals and q-derivatives. *Proc Camb Philos Soc*. (1969) **66**:365–70. doi: 10.1017/S0305004100045060
24. Annaby MH, Mansour ZS. *q-Fractional Calculus and Equations, Lecture Notes in Mathematics 2056*. Berlin: Springer-Verlag (2012).

25. Anastassiou GA. On right fractional calculus. *Chaos Solit Fract*. (2009) **42**:365–76. doi: 10.1016/j.chaos.2008.12.013
26. Al-Salam WA. Some fractional q-integrals and q-derivatives. *Proc Edinb Math Soc*. (1966/1967) **15**:135140. doi: 10.1017/S0013091500011469
27. Atici FM, Eloe PW. Fractional q-calculus on a time scale. *J Nonlinear Math Phys*. (2007) **14**:333–44. doi: 10.2991/jnmp.2007.14.3.4
28. Ernst T. *The History of q-Calculus a New Method*. UUDM Report 2000:16. Department of Mathematics, Uppsala University (2000).
29. Jleli M, Ragoub L, Samet B. On a Lyapunov-type inequality for a fractional differential equation under a Robin boundary condition. *J Funct Spaces*. (2015) **2015**:468536. doi: 10.1155/2015/468536
30. Jackson FH. On q-functions and a certain difference operator. *Trans R Soc Edinb*. (1909) **46**:253–81. doi: 10.1017/S0080456800002751
31. Jackson FH. On q-definite integrals. *Q Pure J Appl Math*. (1910) **41**:193–203.
32. Pachpatte BG. *Mathematical Inequalities*. North Holland Mathematical Library. Elsevier (2005).
33. Rajkovic PM, Marinkovic SD, Stankovic MS. On q-analogues of Caputo derivative and Mittag-Leffler function. *Fract Calc Appl Anal*. (2007) **10**:359–73. Available online at: http://eudml.org/doc/11332
34. Aktas MF. Lyapunov-type inequalities for a certain class of n-dimensional quasilinear systems. *Electron J Differ Equat*. (2013) **67**:18.1. doi: 10.1016/j.camwa.2012.02.019
35. Cakmak D. Lyapunov-type integral inequalities for certain higher order differential equations. *Appl Math Comput*. (2010) **216**:368–73. doi: 10.1016/j.amc.2010.01.010
36. Cakmak D. On Lyapunov-type inequality for a class of nonlinear systems. *Math Inequal Appl*. (2013) **16**:101–8. doi: 10.7153/mia-16-07
37. Cheng SS. A discrete analogue of the inequality of Lyapunov. *Hokkaido Math J*. (1983) **12**:105–12. doi: 10.14492/hokmj/1381757783
38. El-Shahed M. Positive solutions for boundary value problem of nonlinear fractional differential equation. *Abstr Appl Anal*. (2007) **2007**:10368. doi: 10.1155/2007/10368
39. Ferreira RAC. A Lyapunov-type inequality for a fractional boundary value problem. *Fract Calc Appl Anal*. (2013) **16**:978–84. doi: 10.2478/s13540-013-0060-5
40. He X, Tang XH. Lyapunov-type inequalities for even order differential equations. *Commun Pure Appl Anal*. (2012) **11**:465–73. doi: 10.3934/cpaa.2012.11.465
41. Jleli M, Samet B. On a Lyapunov-type inequality for a fractional differential equation with a mixed boundary condition. *Math Inequal Appl*. (2015) **18**:443–51. doi: 10.7153/mia-18-33
42. Jleli M, Samet B. A Lyapunov-type inequality for a fractional q-difference boundary value problem. *J Nonlinear Sci Appl*. (2016) **9**:1965–76. doi: 10.22436/jnsa.009.05.03
43. Kilbas AA, Srivastava HM, Trujillo JJ. *Theory and Applications of Fractional Differential Equations, Vol. 204 of North-Holland Mathematics Studies*. Amsterdam: Elsevier (2006).
44. Kwong MK. On Lyapunov's inequality for disfocality. *J Math Anal Appl*. (1981) **83**:486–94. doi: 10.1016/0022-247X(81)90137-2
45. Pachpatte BG. On Lyapunov-type inequalities for certain higher order differential equations. *J Math Anal Appl*. (1995) **195**:527–36. doi: 10.1006/jmaa.1995.1372
46. Ma J, Yang J. Existence of solutions for multi-point boundary value problem of fractional q-difference equation. *Electron J Qual Theory Differ Equat*. (2011) **92**:1–10. doi: 10.14232/ejqtde.2011.1.92
47. El-Shahed M, Al-Askar FMA. Multiple positive solutions for nonlinear second boundary value problems. *Int Math Forum*. (2010) **5**:769–74.
48. Graef JR, Kong L, Kong Q. Application of the mixed monotone operator method to fractional boundary value problems. *Fract Differ Calc*. (2012) **2**:87–98. doi: 10.7153/fdc-02-06
49. Eliason SB. A Lyapunov inequality for a certain nonlinear differential equation. *J Lond Math Soc*. (1970) **2**:524–7. doi: 10.1112/jlms/2.Part_3.461
50. Parhi N, Panigrahi S. On Liapunov-type inequality for third-order differential equations. *J Math Anal Appl*. (1999) **233**:445–60. doi: 10.1006/jmaa.1999.6265
51. Liu Y, Lu L. A class of fractional p-Laplacian integro-differential equations in Banach spaces. *Abstr Appl Anal*. (2013) **2013**:398632. doi: 10.1155/2013/398632
52. Hartman P, Wintner A. On an oscillation criterion of Liapounoff. *Am J Math*. (1951) **73**:885–90. doi: 10.2307/2372122

Conflict of Interest: The authors declare that the research was conducted in the absence of any commercial or financial relationships that could be construed as a potential conflict of interest.

frontiers in Physics

ORIGINAL RESEARCH
published: 07 May 2020
doi: 10.3389/fphy.2020.00073

Optical Solutions of Schrödinger Equation Using Extended Sinh–Gordon Equation Expansion Method

Amna Irshad[1†], *Naveed Ahmed*[1†], *Umar Khan*[2†], *Syed Tauseef Mohyud-Din*[3†], *Ilyas Khan*[4*†] *and El-Sayed M. Sherif*[5,6]

[1] Department of Mathematics, Faculty of Sciences, HITEC University, Taxila, Pakistan, [2] Department of Mathematics and Statistics, Hazara University, Mansehra, Pakistan, [3] University of Multan, Multan, Pakistan, [4] Faculty of Mathematics and Statistics, Ton Duc Thang University, Ho Chi Minh City, Vietnam, [5] Center of Excellence for Research in Engineering Materials (CEREM), King Saud University, Al-Riyadh, Saudi Arabia, [6] Electrochemistry and Corrosion Laboratory, Department of Physical Chemistry, National Research Centre, Dokki, Egypt

In this paper, we investigated the non-linear Schrödinger equation (NLS) to extract optical soliton solutions by implementing the extended Sinh–Gordon equation expansion method (ShGEEM). Optical soliton solutions included bright, dark, combined bright-dark, singular soliton combined singular soliton solutions, and singular periodic wave solutions. Our new results have been compared to these in the literature. Also, graphical analysis was presented with 3D and contour graphs to understand the physics of obtained solutions.

Keywords: extended Sinh-Gordon equation expansion method (ShGEEM), optical soliton, non-linear Schrödinger equation, exact solutions, singular soliton solution

OPEN ACCESS

Edited by:
Xiao-Jun Yang,
China University of Mining and Technology, China

Reviewed by:
Haci Mehmet Baskonus,
Harran University, Turkey
Carlo Cattani,
University of Tuscia, Italy

***Correspondence:**
Ilyas Khan
ilyaskhan@tdtu.edu.vn

[†]*These authors have contributed equally to this work*

Specialty section:
This article was submitted to Mathematical Physics, a section of the journal Frontiers in Physics

Received: *04 October 2019*
Accepted: *03 March 2020*
Published: *07 May 2020*

Citation:
Irshad A, Ahmed N, Khan U, Mohyud-Din ST, Khan I and Sherif E-SM (2020) Optical Solutions of Schrödinger Equation Using Extended Sinh–Gordon Equation Expansion Method. Front. Phys. 8:73. doi: 10.3389/fphy.2020.00073

INTRODUCTION

In recent years, soliton propagation in non-linear optical fiber has become the most extensive topic of research in the field of non-linear sciences. In non-linear optical fiber, the study of the non-linear Schrödinger equation (NLS) plays an important role in order to understand the dynamical behavior of optical soliton. NLS helps to provide exact soliton solutions in non-linear fiber optics. During the last few years, in the study of optical solitons, many new research developments have taken place, which is a great achievement in the field of soliton [1–15]. However, there are a lot of problems that need to be solved.

Many new methods have been developed to tackle complicated problems in a very smooth manner and provide exact soliton solutions of these problems such as the modified simple equation method [16, 17], the extended trial equation method [18, 19], the $\tan(\frac{\phi(\xi)}{2})$-expansion method [20, 21], and many others.

In this paper, our main focus is the study of NLS [22]. This equation has large physical importance in non-linear optics.

$$iV_t - V_{xx} + 2|V|^2V - 2\sigma^2V = 0, \quad i = \sqrt{-1}, \tag{1}$$

where $V(x,t)$ is a complex function and σ is a constant. It should also be noted that, for $\sigma = 0$, Equation (1) reduces to the non-Kerr law non-linearity as

$$V_t - V_{xx} + 2|V|^2V = 0, \quad i = \sqrt{-1} \tag{2}$$

To study Equation (1), we consider the following wave transformation:

$$V(x,t) = p(\xi)\, e^{i\phi(x,t)}, \xi = \rho x - \upsilon t,\ \varphi = -kx + \varpi t + \theta \quad (3)$$

where $\varphi(x,t)$ is the phase component, and k, ϖ, θ, *and* υ represent the frequency, wave number, phase constant, and velocity of the soliton. By substituting Equation (3) into Equation (1), we obtain the following real and imaginary equations:

$$\left(\frac{d^2}{d\xi^2}\varphi(\xi)\right)\rho^2 + \phi(\xi)\left(k^2 - 2\sigma^2 - \varpi\right) - 2(\phi(\xi))^3 = 0, \quad (4)$$

$$\upsilon = 2k\rho, \quad (5)$$

ALGORITHM OF EXTENDED ShGEEM

To describe the mechanism of the extended Sinh–Gordon equation method (SGEM) for differential equations, we consider the equation [23]

$$\Upsilon_{xt} = \varrho \sinh(\Upsilon), \quad (6)$$

where $\Upsilon = \Upsilon(x,t)$ and ϱ is a nonzero constant.

Applying the traveling wave transformation $\Upsilon(x,t) = \Phi(\zeta)$, $\zeta = \lambda(x - \mu t)$, to Equation (6), we acquire the following form of non-linear ODE:

$$\Phi'' = -\frac{\varrho}{\lambda^2\mu}\sinh(\Phi), \quad (7)$$

where $\Phi = \Phi(\zeta)$, λ is a wave number, and μ is the velocity of the traveling wave. By applying the integration procedure, Equation (7) can be found in a simplified form:

$$\left[\frac{\left(\Phi'\right)}{2}\right]^2 = -\frac{\varrho}{\lambda^2\mu}\sinh^2\left(\frac{\Phi}{2}\right) + r, \quad (8)$$

where r is the constant of integration. Setting $v(\zeta) = \frac{\Phi}{2}$, and $\theta = -\frac{\varrho}{\lambda^2\mu}$, into Equation (8) yields

$$v'(\zeta) = \sqrt{\theta \sinh^2(v) + r}, \quad (9)$$

Equation (9) has the following set of solutions, by substituting different values for given parameters θ and r.

Set I:

If we substitute $r = 0$, $\theta = 1$ in Equation (9), we obtain

$$v'(\zeta) = \sin h(v), \quad (10)$$

Simplifying Equation (10), we acquire the following solutions:

$$\sin h(v(\zeta)) = \pm csch(\zeta), \quad or \quad \sin h(v(\zeta)) = \pm isech(\zeta), \quad (11)$$

and

$$\cos h(v(\zeta)) = \pm coth(\zeta), \ or\ \cos h(v(\zeta)) = \pm tanh(\zeta)!, \quad (12)$$

where $i = \sqrt{-1}$.

Set II:

If we substitute $r = 1$, $\theta = 1$ in Equation (9), we have the following equation:

$$v'(\zeta) = \cos h(v), \quad (13)$$

After simplification in Equation (13), we have the following solutions:

$$\sin h(v(\zeta)) = \tan(\zeta), \quad or \quad \sin h(v(\zeta)) = -cot(\zeta), \quad (14)$$

and

$$\cos h(v(\zeta)) = \pm sec(\zeta), \quad or \quad \cos h(v(\zeta)) = \pm tan(\zeta), \quad (15)$$

To obtain the different wave solutions of non-linear partial differential equations (NPDEs), we consider the equation in the following form:

$$\complement(\Upsilon, \Upsilon_t, \Upsilon_x, \Upsilon_{xx}, \Upsilon_{xt}, \Upsilon_{tt}, \ldots) = 0, \quad (16)$$

Step I: By using wave transformation $\Upsilon(x,t) = \Phi(\zeta)$, $\zeta = \lambda(x - \mu t)$, we first transform Equation (16) into the following NODE:

$$H\left(\Phi, \Phi', \Phi'', \Phi^2\Phi', \ldots\right) = 0, \quad (17)$$

Step II: We suppose that Equation (17) has a new ansatz solution in the following form:

$$\Phi(v) = \sum_{\kappa=1}\left[\mathcal{B}_\kappa sinh(v(\zeta)) + A_\kappa cosh(v(\zeta))\right]^\kappa + \mathring{A}_0, \quad (18)$$

where $\mathring{A}_0$, $\mathring{A}_\kappa$, $\mathcal{B}_\kappa$, $(\kappa = 1, \ldots, n)$ are constants to be determined later. The value of can be determined by balancing the highest order dispersive term with the non-linear term in Equation (17).

Step III: We substitute Equation (18) for the fixed value of in Equation (17) to obtain a polynomial form of equation in $v'^f sinh^g(v) cosh^\iota(v), \left(f = 0, 1\ and\ g, \iota = 0, 1, 2 \ldots\ldots\right)$. We get the system of algebraic equations by equating the coefficients of $v'^f sinh^g(v) cosh^\iota(v)$ to be all zero. We extract the values of coefficients $\mathring{A}_0$, $\mathring{A}_\kappa$, $\mathcal{B}_\kappa, \lambda$, μ by solving the system of algebraic equations with the help of MAPLE 2016.

Step IV: Substituting the values of $\mathring{A}_0$, $\mathring{A}_\kappa$, $\mathcal{B}_\kappa$, μ in Equations (19)–(22), we obtain the following wave solutions to the non-linear Equation (16):

$$\Phi(\zeta) = \sum_{\kappa=1}^{N}\left[\pm\mathcal{B}_\kappa isech(\zeta) \pm \mathring{A}_\kappa \tanh(\zeta)\right]^\kappa + \mathring{A}_0, \quad (19)$$

$$\Phi(\zeta) = \sum_{\kappa=1}^{N}\left[\pm\mathcal{B}_\kappa csch(\zeta) \pm \mathcal{B}_\kappa \coth(\zeta)\right]^\kappa + \mathring{A}_0, \quad (20)$$

$$\Phi(\zeta) = \sum_{\kappa=1}^{N}\left[\mathcal{B}_\kappa \sec(\zeta) + \mathring{A}_\kappa \tan(\zeta)\right]^\kappa + \mathring{A}_0, \quad (21)$$

and

$$\Phi(\zeta) = \sum_{\kappa=1}^{N} \left[\mathcal{B}_\kappa \csc(\zeta) - \mathring{A}_\kappa \cot(\zeta)\right]^\kappa + \mathring{A}_0, \quad (22)$$

APPLICATION OF EXTENDED ShGEEM TO EQUATION (1)

In this section, Extended ShGEEM [24–29] is implemented to Equation (1).

Considering a homogeneous balance between Φ'' and Φ^3 in Equation (4) yields $N = 1$. And setting the value of N in Equations (18)–(22), we obtain

$$\Phi(v) = \mathcal{B}_1 sinh(v(\zeta)) + \mathring{A}_1 cosh(v(\zeta)) + \mathring{A}_0, \quad (23)$$
$$\Phi(\zeta) = \pm\mathcal{B}_1 isech(\zeta) \pm \mathring{A}_1 tanh(\zeta) + \mathring{A}_0, \quad (24)$$
$$\Phi(\zeta) = \pm\mathcal{B}_1 csch(\zeta) \pm \mathring{A}_1 coth(\zeta) + \mathring{A}_0, \quad (25)$$
$$\Phi(\zeta) = \pm\mathcal{B}_1 sec(\zeta) + \mathring{A}_1 tan(\zeta) + \mathring{A}_0, \quad (26)$$
$$\Phi(\zeta) = \pm\mathcal{B}_1 csc(\zeta) - \mathring{A}_1 cot(\zeta) + \mathring{A}_0, \quad (27)$$

Substituting Equation (23) together with its derivatives in Equation (4), we get a polynomial equation in $v'^f sinh^g(v) cosh^\iota(v), (f = 0, 1 \text{ and } g, \iota = 0, 1, 2 \ldots\ldots)$. Using some hyperbolic identities, we acquire a system of algebraic equations by setting the coefficients of $v'^f sinh^g(v) cosh^\iota(v)$ equal to zero. After simplifying the system of equations, we obtain the values of $\mathring{A}_0$, $\mathring{A}_\kappa$, $\mathcal{B}_\kappa, \rho, k, \lambda$ with the help of Maple 16. Subsisting all the values of $\mathring{A}_0$, $\mathring{A}_\kappa$, $\mathcal{B}_\kappa, \rho, k, \lambda$ in any of Equations (24)–(27), we found numerous different types of soliton solutions of Equation (1).

Result I:

$$\mathring{A}_0 = 0, \ \mathring{A}_1 = \pm\frac{1}{2}\rho, \mathcal{B}_1 = \pm\frac{1}{2}\rho, \varpi = k^2 + \frac{1}{2}\rho^2 - 2\sigma^2, \quad (28)$$

Result II:

$$\mathring{A}_0 = 0, \ \mathring{A}_1 = 0, \ \mathcal{B}_1 = \pm\rho, \ \varpi = k^2 - \rho^2 - 2\sigma^2, \quad (29)$$

Result III:

$$\sigma^2 \mathring{A}_0 = 0, \ \mathring{A}_1 = \pm\rho, \ \mathcal{B}_1 = 0, \ \varpi = k^2 + 2\rho^2 - 2\sigma^2, \quad (30)$$

Result IV:

$$\mathring{A}_0 = 0, \ \mathring{A}_1 = 0 \ , \ \mathcal{B}_1 = \pm\rho, \quad \rho = \sqrt{k^2 - 2\sigma^2 - \varpi}, \quad (31)$$

Result V:

$$\mathring{A}_0 = 0, \ \mathring{A}_1 = \rho \ , \mathcal{B}_1 = 0, \ \rho = \frac{1}{2}\sqrt{-2k^2 + 4\sigma^2 + 2\varpi}, \quad (32)$$

Result VI:

$$\mathring{A}_0 = 0, \ \mathring{A}_1 = \frac{1}{2}\rho, \mathcal{B}_1 = \frac{1}{2}\rho, \rho = \sqrt{-2k^2 + 4\sigma^2 + 2\varpi}, \quad (33)$$

Result VII:

$$\mathring{A}_0 = 0, \ \mathring{A}_1 = \mp\frac{1}{2}\rho, \mathcal{B}_1 = \pm\frac{1}{2}\rho, \varpi = k^2 - \frac{1}{2}\rho^2 - 2\sigma^2, \quad (34)$$

Result VIII:

$$\mathring{A}_0 = 0, \ \mathring{A}_1 = \frac{1}{2}\rho, \ \mathcal{B}_1 = \frac{1}{2}\rho, \ \rho = \sqrt{2k^2 - 4\sigma^2 - 2\varpi}, \quad (35)$$

Substituting the values of the above given results in Equations (24)–(27), we get the following solutions.

Case I: Bright Optical Solitons

Substituting the values of the parameters given in Results II and IV into Equation (24):

$$V_1(x,t) = \pm i\rho sech\left(\rho x - 2tk\rho\right) e^{i\left(-kx + t\left(k^2 - \rho^2 - 2\sigma^2\right) + \theta\right)}, \quad (36)$$
$$V_2(x,t) = \pm i\sqrt{k^2 - 2\sigma^2 - \varpi}\ \text{sech}\left(-2tk\sqrt{k^2 - 2\sigma^2 - \varpi} + \sqrt{k^2 - 2\sigma^2 - \varpi}x\right) \times e^{i(-kx + t\varpi + \theta)} \quad (37)$$

where $\left(k^2 - 2\sigma^2 - \varpi\right) > 0$, for valid solutions.

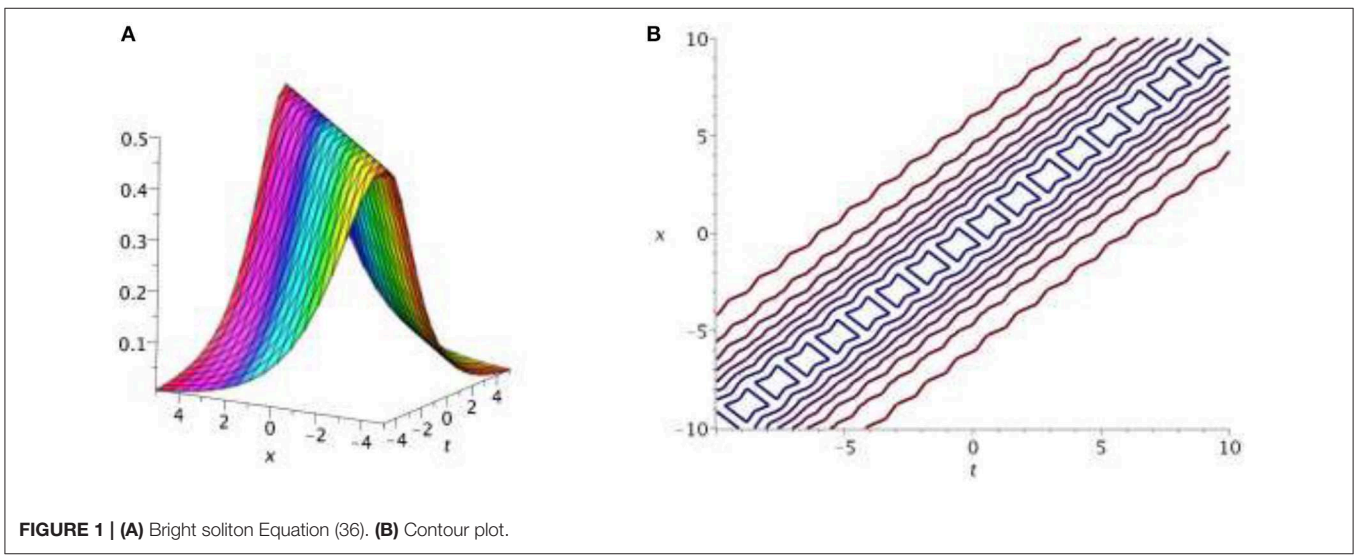

FIGURE 1 | (A) Bright soliton Equation (36). **(B)** Contour plot.

Case II: Dark Optical Solitons

Substituting the values of the parameters given in Results III and V into Equation (24):

$$V_3(x,t) = \pm\rho \tanh\left(-2tk\rho + \rho x\right) e^{i\left(-kx+t\left(k^2+2\rho^2-2\sigma^2\right)+\theta\right)}, \quad (38)$$

$$V_4(x,t) = \left(\tanh\left(-tk\sqrt{-2k^2+4\sigma^2+2\varpi} + \frac{\frac{1}{2}\sqrt{-2k^2+4\sigma^2+2\varpi}}{2\sqrt{-2k^2+4\sigma^2+2\varpi}\,x}\right)\right) e^{i(-kx+t\varpi+\theta)} \quad (39)$$

where $\left(-2k^2+4\sigma^2+2\varpi\right) > 0$, for valid solutions.

Case III: Combined Dark-Bright Optical Soliton Solutions

Using the values of the parameters given in Results I and VI into Equation (24):

$$V_5(x,t) = \pm\frac{1}{2}\rho\left(isech\left(\rho x - 2tk\rho\right) + \tanh\left(\rho x - 2tk\rho\right)\right) e^{i\left(-kx+t\left(k^2+\frac{1}{2}\rho^2-2\sigma^2\right)+\theta\right)}, \quad (40)$$

$$V_6(x,t) = \left(\operatorname{sech}\left(-2tk\sqrt{2\varpi-2k^2+4\sigma^2} + \sqrt{2\varpi-2k^2+4\sigma^2}\,x\right)\right) + \left(\tanh\left(-2tk\sqrt{2\varpi-2k^2+4\sigma^2} + \sqrt{2\varpi-2k^2+4\sigma^2}\,x\right)\right) \times e^{i(-kx+t\varpi+\theta)}. \quad (41)$$

where $\left(2\varpi - 2k^2 + 4\sigma^2\right) > 0$, for valid solutions.

Case IV: Singular Soliton Solutions

Using the values of the parameters given in Results II, III, IV, and V into Equation (25):

$$V_7(x,t) = \pm\rho csch(-2tk\rho + \rho x) e^{i\left(-kx+t\left(k^2-\rho^2-2\sigma^2\right)+\theta\right)}, \quad (42)$$

$$V_8(x,t) = \pm\rho \coth(-2tk\rho + \rho x) e^{i\left(-kx+t\left(k^2+2\rho^2-2\sigma^2\right)+\theta\right)} \quad (43)$$

$$V_9(x,t) = \pm\sqrt{k^2-2\sigma^2-\varpi}\, csch(-2tk\sqrt{k^2-2\sigma^2-\varpi}$$

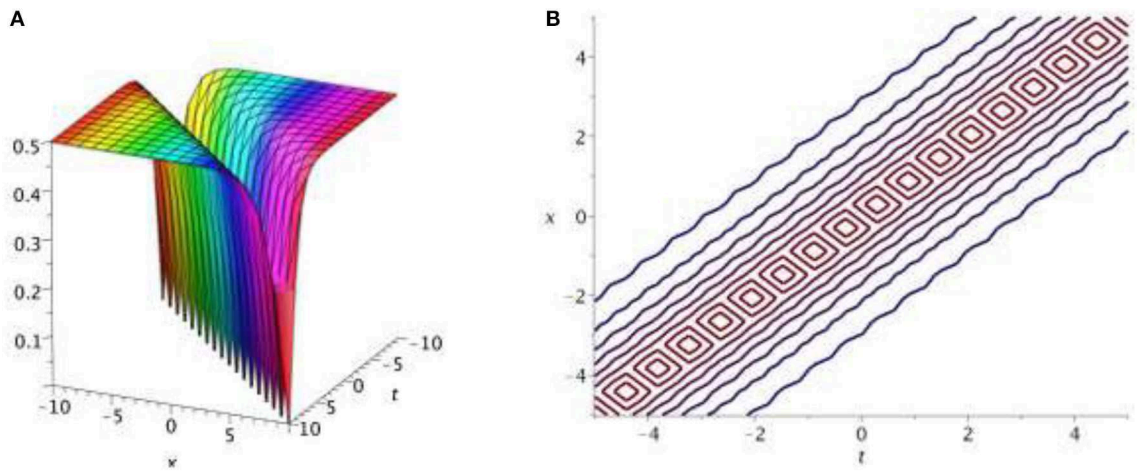

FIGURE 2 | (A) Dark soliton solution Equation (38). **(B)** Contour plot.

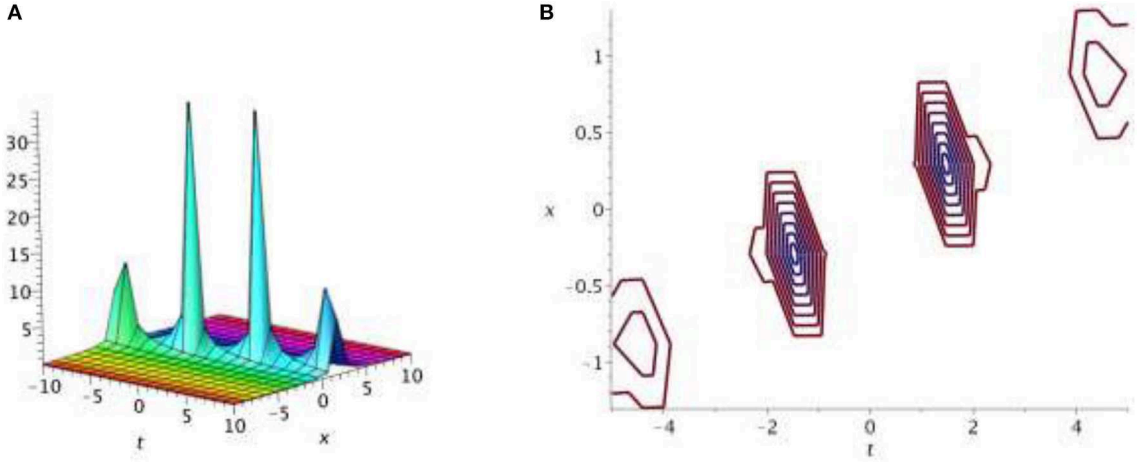

FIGURE 3 | (A) Singular solution Equation (43). **(B)** Contour plot.

$$+\sqrt{k^2-2\sigma^2-\varpi}\,x)\;\times e^{i(-kx+t\varpi+\theta)} \tag{44}$$

where $\left(k^2-2\sigma^2-\varpi\right)>0$, for valid solutions.

$$V_{10}(x,t) = \left(\coth\left(-tk\sqrt{2\varpi-2k^2+4\sigma^2}+\tfrac{1}{2}\sqrt{2\varpi-2k^2+4\sigma^2}\,x\right)\right) \times e^{i(-kx+t\varpi+\theta)}, \tag{45}$$

where $\left(2\varpi-2k^2+4\sigma^2\right)>0$, for valid solutions.

Case V: Combined Singular Solitons

Substituting the values of the parameters given in Results I and VI into Equation (25):

$$V_{11}(x,t) = \pm\left(\frac{1}{2}\rho\,csch\left(-2tk\rho+\rho x\right)-\frac{1}{2}\rho\coth\left(-2tk\rho+\rho x\right)\right) \times e^{i(-kx+t(k^2+\frac{1}{2}\rho^2-2\sigma^2)+\theta)}, \tag{46}$$

$$V_{12}(x,t) = \left(\begin{array}{c}\frac{1}{2}\sqrt{-2k^2+4\sigma^2+2\varpi}\\ \times csch\left(-2tk\sqrt{-2k^2+4\sigma^2+2\varpi}+\sqrt{-2k^2+4\sigma^2+2\varpi}\,x\right)\\ +\frac{1}{2}\sqrt{-2k^2+4\sigma^2+2\varpi}\\ \times\coth\left(-2tk\sqrt{-2k^2+4\sigma^2+2\varpi}+\sqrt{-2k^2+4\sigma^2+2\varpi}\,x\right)\end{array}\right) \times e^{i(-kx+t\varpi+\theta)}, \tag{47}$$

where $\left(-2k^2+4\sigma^2+2\varpi\right)>0$, for valid solutions.

Case VI: Singular Periodic Wave Solitons

Substituting the values of the parameters given in Result VII into Equations (26), (27):

$$V_{13}(x,t) = \frac{1}{2}\rho\left(\pm\sec\left(-2tk\rho+\rho x\right)\mp\tan\left(-2tk\rho+\rho x\right)\right) e^{i(-kx+t(k^2-\frac{1}{2}\rho^2-2\sigma^2)+\theta)}, \tag{48}$$

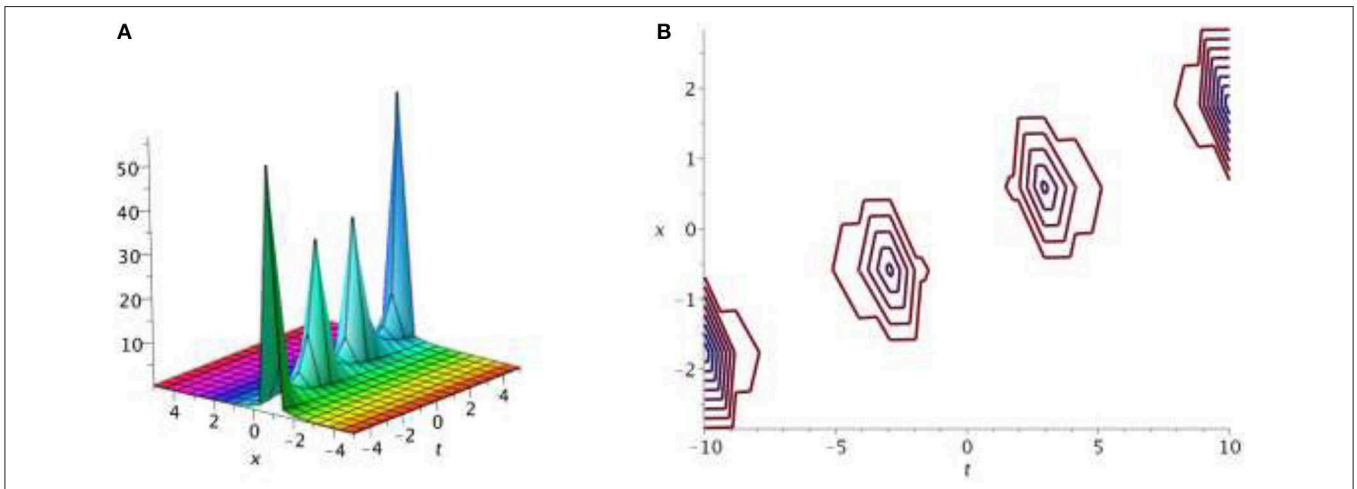

FIGURE 4 | (A) Combined singular solution Equation (47). **(B)** Contour plot.

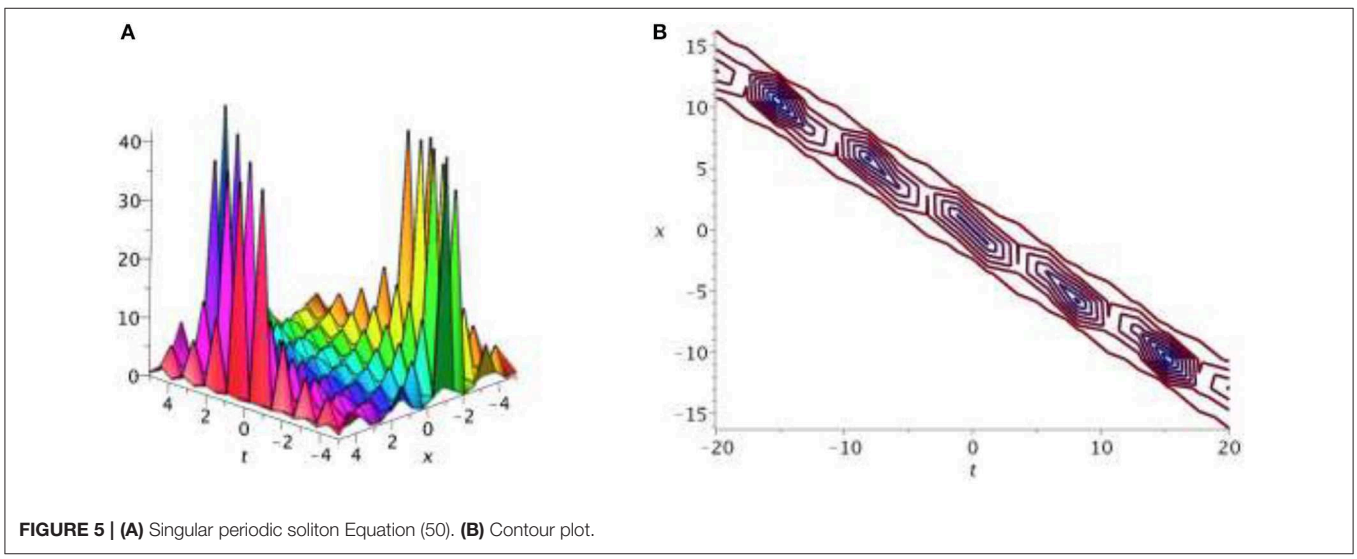

FIGURE 5 | (A) Singular periodic soliton Equation (50). **(B)** Contour plot.

$$V_{14}(x,t) = \left(\begin{pmatrix} \frac{1}{2}\sqrt{2k^2-4\sigma^2-2\varpi} \\ \times \sec\left(-2tk\sqrt{2k^2-4\sigma^2-2\varpi}+\sqrt{2k^2-4\sigma^2-2\varpi}x\right) \\ +\frac{1}{2}\sqrt{2k^2-4\sigma^2-2\varpi} \\ \times \tan\left(-2tk\sqrt{2k^2-4\sigma^2-2\varpi}+\sqrt{2k^2-4\sigma^2-2\varpi}x\right) \end{pmatrix}\right) \times e^{i(-kx+t\varpi+\theta)}, \quad (49)$$

where $\left(2k^2-4\sigma^2-2\varpi\right) > 0$, for valid solutions.

Substituting the values of the parameters given in Result VIII into Equations (26), (27):

$$V_{15}(x,t) = \frac{1}{2}\left(\pm\rho\csc\left(-2tk\rho+\rho x\right)\pm\rho\cot\left(-2tk\rho+\rho x\right)\right) e^{i(-kx+t(k^2-\frac{1}{2}\rho^2-2\sigma^2)+\theta)}, \quad (50)$$

$$V_{16}(x,t) = \left(\begin{pmatrix} \frac{1}{2}\sqrt{2k^2-4\sigma^2-2\varpi} \\ \csc\left(-2tk\sqrt{2k^2-4\sigma^2-2\varpi}+\sqrt{2k^2-4\sigma^2-2\varpi}x\right) \\ -\frac{1}{2}\sqrt{2k^2-4\sigma^2-2\varpi} \\ \cot(-2tk\sqrt{2k^2-4\sigma^2-2\varpi}+\sqrt{2k^2-4\sigma^2-2\varpi}x) \end{pmatrix}\right) \times e^{i(-kx+t\varpi+\theta)}, \quad (51)$$

where $\left(2k^2-4\sigma^2-2\varpi\right) > 0$, for valid solutions.

GRAPHS AND DISCUSSIONS

In this section, we presented some of our obtained solutions in the following figures.

Solutions V_1, V_2 of Equation (1) depict the bright optical soliton solutions. **Figure 1** represents the 3D surface of the bright soliton solution of Equation (36) with a contour plot for given parametric values $\rho = 0.5$, $\theta = 0.5$, $\sigma = 0.5$, $k = 0.5$.

Solutions V_3, V_4 of Equation (1) show the dark optical soliton solutions. **Figure 2** represents the 3D surface of the dark optical soliton solution of Equation (38) with a contour plot for given parametric values $\rho = 0.5$, $\theta = 0.5$, $\sigma = 0.5$, $k = 0.5$.

Figures 3, **4** represent the singular and combined singular soliton solutions of Equation (1), obtained from solutions of V_8 *and* V_{12}[Equations (38), (47)] for $\rho = 0.065$, $\theta = 1$, $\sigma = 0.09$, $k = 0.095$ and $\varpi = 0.05$, $\theta = 5$, $\sigma = 0.05$, $k = 0.09$.

Solutions V_{13}, V_{14}, V_{15}, V_{16} of Equation (1) represent the singular periodic wave solutions. **Figure 5** illustrates the 3D surface of the singular periodic wave solution of Equation (50) with a contour plot for given parametric values $\rho = 2.5$, $\theta = 0.2$, $\sigma = 0.2$, $k = 7.5$. For convenience, some other figures are not reported.

COMPARISONS

In Cheemaa and Younis [22], Nadia Cheema and Muhammad Younis investigated the traveling wave solutions of NLSE by applying the extended Fan sub-equation method. The obtained solutions V_3, V_4, V_8, V_{10}, V_{11}, V_{12}, V_{15}, V_{16} in this paper are equivalent to the solutions q_1, q_2, q_6, q_{15}, q_{16}. found in Cheemaa and Younis [22] for non-linear Schrödinger's equation. The extended Sinh–Gordon equation expansion method provides a large variety of optical soliton solutions [24–29]. By means of the extended Sinh–Gordon equation expansion method, we found some new more generalized exact solutions. Therefore, these new exact solutions are not reported before for this equation in the literature.

CONCLUSIONS

We have implemented the extended Sinh–Gordon equation expansion method to solve the non-linear Schrodinger equation for exact optical soliton solutions. The types of solutions we reported include singular periodic wave solutions, bright, dark, combined bright-dark, singular, and combined singular soliton solutions. The non-linear Schrodinger equation is one of the very major equations arising in the field of optic fibers. Its new solutions are expected to help engineers and scientists working in the field. It is worth mentioning that the solutions obtained by us are more generalized. That is, we have recovered not only many already existing solutions but also many unreported solutions. These new solutions are expected to help scientists working in the fields of optic fiber to understand the phenomenon governed by the non-linear Schrodinger equation. All the solutions have been verified for their exactness. Wherever the reported solutions have been recovered, they have been compared with their counterparts in the literature.

DATA AVAILABILITY STATEMENT

The datasets generated for this study are available on request to the corresponding author.

AUTHOR CONTRIBUTIONS

The formulation of the problem was done by UK and AI. Non-dimensionalization of the nanofluid models by using invertible transformations done by NA. Mathematical analysis and the graphical results plotted and discussed by SM-D and IK. E-SS revised the whole manuscript and checked the typo mistakes.

ACKNOWLEDGMENTS

Researchers Supporting Project number (RSP-2019/33), King Saud University, Riyadh, Saudi Arabia.

REFERENCES

1. Khalique CM, Mhlanga IE. Travelling waves and conservation laws of a. (2+1)-dimensional coupling system with Korteweg-de Vries equation. *Appl Math Nonlinear Sci.* (2018) **3**:241–54. doi: 10.21042/AMNS.2018.1.00018
2. Biswas A, Yildirim Y, Yasar E, Triki H, Alshomrani AS, Ullah MZ, et al. Optical soliton perturbation with Gerdjikov–Ivanov equation by modified simple equation method. *Optik.* (2018) **157**:1235–40. doi: 10.1016/j.ijleo.2017.12.101
3. Eskitaşçioglu EI, Aktaş MB, Baskonus HM. New complex and hyperbolic forms for Ablowitz–Kaup–Newell–Segur wave equation with fourth order.

Appl Math Nonlinear Sci. (2019) **4**:93–100. doi: 10.2478/AMNS.2019.1.00010
4. Mathobo M, Atangana A. Analysis of exact groundwater model within a confined aquifer: new proposed model beyond the Theis equation. *Eur Phys J Plus.* (2018) **133**:415. doi: 10.1140/epjp/i2018-12205-9
5. Inc M, Aliyu AI, Yusuf A, Baleanu D. Optical solitons for biswas-milovic model in nonlinear optics by sine-gordon equation method. *Optik.* (2018) **157**:267–74. doi: 10.1016/j.ijleo.2017.11.061
6. Biswas A, Yildirim Y, Yasar E, Triki H, Alshomrani AS, Ullah MZ, et al. Optical soliton perturbation for complex Ginzburg–Landau equation with modified simple equation method. *Optik.* (2018) **158**:399–415. doi: 10.1016/j.ijleo.2017.12.131
7. Biswas A, Yildirim Y, Yasar E, Zhou Q, Moshokoa SP, Belic M. Optical solitons for Lakshmanan–Porsezian–Daniel model by modified simple equation method. *Optik.* (2018) **160**:24–32. doi: 10.1016/j.ijleo.2018.01.100
8. Biswas A, Yildirim Y, Yasar E, Triki H, Alshomrani AS, Ullah MZ, Zhou Q, Moshokoa SP, Belic M, Optical soliton perturbation with full nonlinearity for Kundu–Eckhaus equation by modified simple equation method. *Optik.* (2018) **157**:1376–80. doi: 10.1016/j.ijleo.2017.12.108
9. Biswas A, Yildirim Y, Yasar E, Zhou Q, Moshokoa SP, Belic M. Optical soliton perturbation with resonant nonlinear schrödinger's equation having full nonlinearity by modified simple equation method. *Optik.* (2018) **160**:33–43. doi: 10.1016/j.ijleo.2018.01.098
10. Tariq KU, Seadawy AR. Optical soliton solutions of higher order nonlinear Schrödinger equation in monomode fibers and its applications. *Optik.* (2018) **154**:785–98. doi: 10.1016/j.ijleo.2017.10.063
11. Jawad AJM, Abu-AlShaeer MJ, Biswas A, Zhou Q, Moshokoa S, Belic M. Optical solitons to Lakshmanan-Porsezian-Daniel model for three nonlinear forms. *Optik.* (2018) **160**:197–202. doi: 10.1016/j.ijleo.2018.01.121
12. Jawad AJM, Abu-AlShaeer MJ, Majid FB, Biswas A, Zhou Q, Belic M. Optical soliton perturbation with exotic non-Kerr law nonlinearities. *Optik.* (2018) **158**:1370–9. doi: 10.1016/j.ijleo.2017.12.184
13. Bulut H, Sulaiman TA, Baskonus HM, Aktürk T. On the bright and singular optical solitons to the $(2+1)$-dimensional NLS and the Hirota equations. *Opt Quantum Electron.* (2018) **50**:134. doi: 10.1007/s11082-018-1411-6
14. Baskonus HM, Bulut H, Atangana A. On the complex and hyperbolic structures of the longitudinal wave equation in a magneto-electro-elastic circular rod. *Smart Mater Struct.* (2016) **25**:1–8. doi: 10.1088/0964-1726/25/3/035022
15. Amkadni M, Azzouzi A, Hammouch Z, On the exact solutions of laminar MHD flow over a stretching flat plate. *Commun Nonlinear Sci.* (2008) **13**:359–68. doi: 10.1016/j.cnsns.2006.04.002
16. Arnous AH, Ullah MZ, Asma M, Moshokoa SP, Zhou Q, Mirzazadeh M, et al. Dark and singular dispersive optical solitons of Schrödinger–Hirota equation by modified simple equation method. *Optik.* (2017) **136**:445–50. doi: 10.1016/j.ijleo.2017.02.051
17. El-Borai MM, El-Owaidy HM, Ahmed HM, Arnous AH, Moshokoa S, Biswas A, et al. Dark and singular optical solitons with spatio-temporal dispersion using modified simple equation method. *Optik.* (2017) **130**:324–31. doi: 10.1016/j.ijleo.2016.10.105
18. Biswas A, Ekici M, Sonmezoglu A, Triki H, Zhou Q, Moshokoa SP, et al. Dispersive optical solitons with differential group delay by extended trial equation method. *Optik.* (2018) **158**:790–98. doi: 10.1016/j.ijleo.2017.12.193
19. Foroutan M, Zamanpour I, Manafian J. Applications of IBSOM and ETEM for solving the nonlinear chains of atoms with long-range interactions. *Eur Phys J Plus.* (2017) **132**:421. doi: 10.1140/epjp/i2017-11681-7
20. Manafian J, Lakestani M. Abundant soliton solutions for the Kundu–Eckhaus equation via $\tan[\varphi(\xi)]$-expansion method. *Optik.* (2016) **127**:5543–51. doi: 10.1016/j.ijleo.2016.03.041
21. Ahmed N, Irshad A, Mohyud-Din ST, Khan U. Exact solutions of perturbed nonlinear schrödinger's equation with kerr law nonlinearity by improved tan(2) -expansion method. *Opt Quantum Electron.* (2018) **50**:1–27. doi: 10.1007/s11082-017-1314-y
22. Cheemaa N, Younis M. New and more general traveling wave solutions for nonlinear schrödinger equation. *Waves Random and Complex Media.* (2016) **26**:30–41. doi: 10.1080/17455030.2015.1099761
23. Yan Z. A sinh-Gordon equation expansion method to construct doubly periodic solutions for nonlinear differential equations. *Chaos Solitons Fractals.* (2003) **16**:291–7. doi: 10.1016/S0960-0779(02)00321-1
24. Cattani C, Sulaiman TA, Baskonus HM, Bulut H. Solitons in an inhomogeneous Murnaghan's rod. *Eur Phys J Plus.* (2018) **133**:228. doi: 10.1140/epjp/i2018-12085-y
25. Baskonus HM, Sulaiman TA, Bulut H. On the new wave behavior to the Klein–Gordon–Zakharov equations in plasma physics. *Indian J Phys.* (2019) **93**:393–9. doi: 10.1007/s12648-018-1262-9
26. Cattani C, Sulaiman TA, Baskonus HM, Bulut H. On the soliton solutions to the Nizhnik-Novikov-Veselov and the Drinfel'd-Sokolov systems. *Opt Quantum Electron.* (2018) **50**:138. doi: 10.1007/s11082-018-1406-3
27. Bulut H, Sulaiman TA, Baskonus HM. Dark, bright optical and other solitons with conformable space-time fractional second-order spatiotemporal dispersion. *Optik.* (2018) **163**:1–7. doi: 10.1016/j.ijleo.2018.02.086
28. Bulut H, Sulaiman TA, Baskonus HM, Rezazadeh H, Eslami M, Mirzazadeh M. Optical solitons and other solutions to the conformable space–time fractional Fokas–Lenells equation. *Optik.* (2018) **172**:20–7. doi: 10.1016/j.ijleo.2018.06.108
29. Baskonus HM, Sulaiman TA, Bulut H. Bright, dark optical and other solitons to the generalized higher-order NLSE in optical fibers. *Opt Quantum Electr.* (2018) **50**:253. doi: 10.1007/s11082-018-1522-0

Conflict of Interest: The authors declare that the research was conducted in the absence of any commercial or financial relationships that could be construed as a potential conflict of interest.

frontiers in Physics

ORIGINAL RESEARCH
published: 15 May 2020
doi: 10.3389/fphy.2020.00131

An Efficient Analytical Technique for Time-Fractional Parabolic Partial Differential Equations

Muhammad Mustahsan[1], *H. M. Younas*[1], *S. Iqbal*[2], *Sushila Rathore*[3]*, *Kottakkaran Sooppy Nisar*[4] *and Jagdev Singh*[5]

[1] Department of Mathematics, The Islamia University of Bahawalpur, Bahawalpur, Pakistan, [2] School of Systems and Technology, University of Management and Technology, Lahore, Pakistan, [3] Department of Physics, Vivekananda Global University, Jaipur, India, [4] Department of Mathematics, College of Arts and Sciences, Prince Sattam Bin Abdulaziz University, Wadi Aldawaser, Saudi Arabia, [5] Department of Mathematics, JECRC University, Jaipur, India

In this work, we examine time-fractional fourth-order parabolic partial differential equations with the aid of the optimal homotopy asymptotic method (OHAM). The 2nd order approximate results obtained by using the suggested scheme are compared with the exact solution. It has been noted that the results achieved via OHAM have a large convergence rate for the problems. The solutions are graphically analyzed, and the relative errors are presented in tabular form.

Keywords: approximate solutions, fractional calculus, TFPPDE, OHAM, convergence

OPEN ACCESS

Edited by:
Mustafa Inc,
Firat University, Turkey

Reviewed by:
Haci Mehmet Baskonus,
Harran University, Turkey
Mehmet Yavuz,
Necmettin Erbakan University, Turkey

***Correspondence:**
Sushila Rathore
sushila.jag@gmail.com

Specialty section:
This article was submitted to Mathematical Physics, a section of the journal Frontiers in Physics

Received: *12 February 2020*
Accepted: *06 April 2020*
Published: *15 May 2020*

Citation:
Mustahsan M, Younas HM, Iqbal S, Rathore S, Nisar KS and Singh J (2020) An Efficient Analytical Technique for Time-Fractional Parabolic Partial Differential Equations. Front. Phys. 8:131. doi: 10.3389/fphy.2020.00131

INTRODUCTION

The physical behaviors of fractional order differential and integral equations have been studied in fractional calculus (FC). Fractional calculus deals with more general behavior than classical calculus. However, in the present era FC has got more attention for its vast applications in many fields such as science and engineering. Spanier and Oldham [1], Podlubny [2], and Miller and Rose [3], have studied this subject in detail and developed the theoretical explanation of the subject. During the last few decades, a large number of researchers have noted that the role of fractional differential or integral operators are unavoidable in representing the characteristics of physical phenomena like traffic flow, viscoelasticity, fluid flow, signal processing, etc., [4–10]. Many processes and equipment have been efficiently explained by FC. Furthermore, comparative studies have been done for fractional and total differential models. In conclusion, the fractional models are more effective than classical models. Fourth ordered linear PDE

$$\partial_t^2 v(s,t) + \mu\, \partial_s^4 v(s,t) = h(s,t), \tag{1}$$

is very important in engineering and modern science. Bridge slabs, floor systems etc. are examples of fourth order PDEs. Where v is the beam transversal displacement, μ the is ratio of flexural stiffness to mass per unit length, t is the time, s is the space variable and h is the dynamic deriving force acting on unit mass.

In this study, the problem of undamped transverse vibrations of a flexible straight beam is considered. The support of the beam does not contribute to the strain energy of the system. The mathematical model of the problem is expressed in the form of the following time-fractional fourth-order parabolic partial differential equation as

$$\partial_t^\alpha v(s,t) + \mu\, \partial_s^4 v(s,t) = f(s,t),\ s \in [0,1],\ t > 0, 1 < \alpha \leq 2, \tag{2}$$

where ∂_t and ∂_s represents the partial derivatives with respect to t and s, respectively. The initial and boundary conditions are

$$\begin{aligned} v(s;0) = g_0,\ v_t(s;0) = g_1, \\ v(0;t) = f_0,\ v_t(s;0) = f_1, \\ v_{ss}(0;t) = p_0, v_{ss}(1;t) = p_1, \end{aligned} \tag{3}$$

where ∂_t^α denotes the fractional order derivative operator, $v(s,t)$ is the displacement of the beam in s direction, μ is the ratio of flexural stiffness to mass per unit length, t the is time, s is the space variable and $f(s,t)$ is the dynamic deriving force acting on per unit mass, and $g_0(s), g_1(s), f_0(t), f_1(t), p_0(t)$ and $p_1(t)$ are continuous functions.

The concept of homotopy has been merged with perturbation in order to solve non-linear problems. Liao [11] conducted the basic work by utilizing the homotopy analysis method (HAM). He [12] presented the homotopy perturbation method and its applications. Marinca et al. [13–15] developed a novel computational scheme known as OHAM. The OHAM established a convergence criteria similar to HAM, but OHAM is more flexible. In various research papers Iqbal et al. [16–18] and Sarwar et al. [19, 20] have demonstrated the usefulness extension and trust of this technique and have achieved trustworthy solutions. In this paper, the Idea of OHAM has been explained. It gives logical, trustworthy solutions to linear and non-linear mathematical model fractional orders.

Very recently, some new definitions of fractional derivatives have been introduced and many physical medical problems have been modeled based on fractional derivatives, e.g., the SIRS-SI model describes the transmission of malaria disease [21]. The fractional extension of partial differential equations occurring in physical sciences was studied by Dubey et al. [22]. Other real-life problems with fractional calculus can be seen in a recent work by Gao et al. [23].

The homotopy asymptotic method (HAM) is also effective in solving a differential equation. Some result work comprises linear and nonlinear fractional differential equations considering different constraints without a singular kernel [24, 25]. The model shows that OHAM/HAM guarantee good approximation and better convergence rate than other numerical techniques.

The paper is structured as follows: The basic definition of fractional calculus is given in Section Basic Definitions. The method is described in Section Solution Procedure of OHAM. Section Solutions of Fractional Models of Parabolic PDEs gives the model problems and detailed results. Section Discussion of Results provides a discussion of the results. The conclusion is outlined in Section Conclusions.

BASIC DEFINITIONS

Let $g(t),\ t > 0$ is a function of real value considered to be in space $c_\lambda,\ \lambda \in R$, which is very useful for the study in FC. If there exists, $p > \lambda$ is a real number such that $g(t) = t^p g_1(t)$, where $g_1(t) \in c(0,\infty)$, supposed to be in space c_λ^m if and only if $g^m \in c_\lambda, m \in N$.

Definition 2.1. Riemann-Liouville form of integral operator of a function $g \in c_\lambda$, of fractional order $\beta > 0, \lambda \geq -1$ is expressed as

$${}^{RL}D_{a,t}^{-\beta} g(t) = \frac{1}{\Gamma(\beta)} \int_a^t (t-\lambda)^{\beta-1} g(\lambda)\, d\lambda,\ t > 0, \beta > 0,$$

$$k-1 < \beta < k,\ k \in Z^+ \tag{4}$$

Definition 2.2. Riemann-Liouville form of integral operator of a function$g(t)$ of fractional order $\beta > 0$ is given as

$${}^{RL}D_{a,t}^{\beta} g(t) = \frac{1}{\Gamma(n-\beta)} \frac{d^k}{dt^k} \int_a^t (t-\lambda)^{k-\beta-1} g(\lambda)\, d\lambda,\ t > 0, \beta > 0,$$

$$k-1 < \beta < k,\ k \in Z^+. \tag{5}$$

Definition 2.3. The Caputo fractional derivative of order $\beta > 0$ is expressed as

$${}^{C}D_{a,t}^{\beta} g(t) = \frac{1}{\Gamma(n-\beta)} \int_a^t (t-\lambda)^{k-\beta-1} g^{(k)}(\lambda)\, d\lambda,\ t > 0, \beta > 0,$$

$$k-1 < \beta < k,\ k \in Z^+. \tag{6}$$

If $j-1 < \beta < j$, and $g \in c_\lambda^m,\ \lambda \geq -1$, then

$${}^{RL}D_{a,t}^{-\beta} \left({}^{C}D_{a,t}^{\beta} g(t) \right) = g(t) - \sum_{i=0}^{j-1} g^i(a) \frac{(t-a)^j}{\Gamma(i+1)}, t > 0. \tag{7}$$

SOLUTION PROCEDURE OF OHAM

Based on the OHAM scheme [18, 19], we will extend this approach for time-fractional parabolic partial differential equations (TFPPDE) in the subsequent steps.

Step I. Write the governing time fractional order parabolic equation in the subsequent way

$$Q(v(s,\ t)) - f(s,\ t) = 0;\ s \in [0,1],\ t > 0. \tag{8}$$

Ω is domain. Equation (8) is bifurcated in to $Q(v) = J(v) + T(v)$. In this expression J is a fractional component and T is a non-fractional component. $J_i = \frac{\partial^\alpha \Phi_i(s,t)}{\partial t^\alpha}, i \geq 0, T_i = \frac{\partial^4 \varphi}{\partial s^4},\ i \geq 0.$

Step II. Develop an optimal homotopy for time-fractional partial deferential equation (TFPDE), $\varphi(s,t;p) : \Omega \times [0,1] \to R$ which satisfies

$$(1-p)(J(v) - f(s,t)) - H(s,p;c)(Q(v) - f(s,t)) = 0. \tag{9}$$

In Equation (9) $p \in [0,1]$ and $s \in \Omega$ is a parameter, for $p \neq 0, H(s,p;c)$ is a non-zero auxiliary function and $H(0,p;c) = 0$ when p increases in the interval $[0,1]$ the solution $\varphi(s,t)$ guarantees the rapidly convergent to the exact solution.

$$\begin{aligned} H(s,\ p;\ c) = {} & pj_1(s,\ c_i) + p^2 j_2(s,\ c_i) + p^3 j_3(s, c_i) + \ldots \\ & + p^m j_m(s,\ c_i), \end{aligned} \tag{10}$$

Where the auxiliary convergence control parameters are $c_i, i = 0, 1, 2, 3, ..., m$ and $J_i(s), i = 0, 1, 2, 3, ..., m$ can be a function on the variables. The $J_m(s, c_i)$ may be selected in the form of polynomial, exponential and so on. It is very important to note that the crucial step is to select an appropriate function as the convergence rate depends on the initial guess of the solutions.

Step III. Expand $\varphi(s,t;p,c)$ in Taylor's series for p to develop an approximate result as

$$\varphi(s,t;p,c_i) = v_0(s,t) + \sum_{j=1}^{m} v_k(s,t;c_i)\, p^j, 1 \le i \le m. \quad (11)$$

It has been clarified that the rate of convergence of the (11) depends upon auxiliary constants c_i. If the Equation (11), at p = 1 is convergent, then one has:

$$\tilde{v}(s,t;p,c_i) = v_0(s,t) + \sum_{j=1}^{m} v_k(s,t;c_i). \quad (12)$$

Step IV. Compare the coefficients of identical powers p after substituting Equations (11) in (9), we can get 0th, 1st, 2nd and higher order problems if needed.

$$p^0 : J_0 - f(s,t) = 0. \quad (13)$$

$$p^1 : J_0 - J_1 + f(s,t) - c_1(J_0 + T_1 - f(s,t)) = 0. \quad (14)$$

$$p^2 : J_2 - J_1 - c_1(J_1 + T_0) - c_2(T_0 - f(s,t)) = 0. \quad (15)$$

$$p^3 : J_3 - J_2 - c_1(J_2 + T_2) - c_2(J_1 + T_1) - c_3(J_0 + T_0 - f(s,t)) = 0. \quad (16)$$

And so on

Step V. Substitute Equations (12) in (8), the outcome will be residual.
Create the $\delta(c_i)$

$$\delta(c_i) = \int_0^t \int_\Omega R^2(s,t;c_i) ds dt.$$

Residual of Problem Is R

Convergence auxiliary control (c_i) constants can be acquired as follows.

$$\frac{\partial \delta}{\partial c_1} = \frac{\partial \delta}{\partial c_2} = \ldots = \frac{\partial \delta}{\partial c_m} = 0. \quad (17)$$

If $R(s;j_i) = 0$ then $v(s;j_i) = 0$ must be exact solution of the TFPDE. Normally it does not happen for non-linear problems.
Step VI. Using the convergence auxiliary control constants in Equation (12), we can develop an approximate solution.

Step VII. Accuracy of the technique is presented as
Error norm L_2

$$\left\| v^{exact} - v_n \right\| = \sqrt{\frac{b-a}{n} \sum_{i=0}^{N} \left| v^{exact} - v_n \right|^2}. \quad (18)$$

Error normL^∞

$$\left\| v^{exact} - v_n \right\| = \left| v_i^{exact} - (v_n)_i \right|. \quad (19)$$

SOLUTIONS OF FRACTIONAL MODELS OF PARABOLIC PDES

In the current section, we take the two examples and solve them with the aid of OHAM and demonstrate the accuracy, validity, and suitability of the suggested computational scheme.

Example 1

Let us take the fourth order TFPPDE of the form

$$\frac{\partial^\alpha v(s,t)}{\partial t^\alpha} + \frac{\partial^4 v(s,t)}{\partial s^4} = \left(\pi^4 - 1\right) \sin \pi s \cos t.$$
$$s \in [0,1], t > 0, \mu = 1, 1 < \alpha \le 2. \quad (20)$$

Initial conditions (ICs)

$$v(s,0) = \sin \pi s,\ v_t(s,0) = 0.$$

Boundary conditions (BCs)

$$v(0,t) = 0, v_{ss}(0,t) = 0.$$
$$v(1,t) = 0, v_{ss}(1,t) = 0.$$

Exact solution of problem is

$$v(s,t) = \cos t \sin \pi s \quad (21)$$

Compare the coefficients of equal powers of embedding parameter p, after substituting $\phi(s,p)$ in to optimal homotopy equation to get zero-order, 1st-order, and 2nd-order and higher-order series problems.

$$p^0 : \frac{\partial^\alpha v_0(s,t)}{\partial t^\alpha} = 0, \quad (22)$$

$$p^1 : \left(\cos(t) \sin(\pi s) + \pi^4 \cos(t) \sin(\pi s) - \frac{\partial^4 v_0(s,t)}{\partial s^4} - \frac{\partial^\alpha v_0(s,t)}{\partial t^\alpha}\right) c_1 - \frac{\partial^\alpha v_0(s,t)}{\partial t^\alpha} + \frac{\partial^\alpha v_1(s,t)}{\partial t^\alpha} = 0,$$

$$p^2 : \left(-\cos(t) \sin(\pi s) + \pi^4 \sin(\pi s) \cos(t) - \frac{\partial^4 v_0(s,t)}{\partial s^4} - \frac{\partial^\alpha v_0(s,t)}{\partial t^\alpha}\right) c_2 \quad (23)$$

$$- c_1 \left(\frac{\partial^\alpha v_0(s,t)}{\partial t^\alpha} + \frac{\partial^\alpha v_1(s,t)}{\partial t^\alpha} \right) - \frac{\partial^\alpha v_1(s,t)}{\partial t^\alpha} + \frac{\partial^\alpha v_2(s,t)}{\partial t^\alpha} = 0. \quad (24)$$

After implementing the step-5 of sec-3 on Equations (22–24), we get following zero-order, 1st-order and 2nd-order results:

$$v_0(s,t) = \sin(\pi s), \quad (25)$$

$$v_1(s,t) = \frac{c_1(\pi^4 - \frac{1}{4}(1+\pi^4)(-t^2)) \sin(\pi s) t^\alpha}{\Gamma(\alpha+1)}, \quad (26)$$

$$v_2(s,t) = \frac{((1+\pi^4)c_1(c_1+1) + (\pi^4 - 1)c_2) \sin(\pi s) t^{\alpha+2}}{4\Gamma(\alpha+1)} + \frac{\pi^8 c_1^2 \sin(\pi s) t^{2\alpha} + \frac{\pi^4(1+\pi^4)(\alpha+2)c_1^2 \sin(\pi s) t^{2\alpha+2}}{8(2\alpha+1)}}{\Gamma(2\alpha+1)} + \frac{\pi^4 c_1(c_1+1) \sin(\pi s) t^\alpha}{\Gamma(\alpha+1)} + \frac{\pi^4 c_2 \sin(\pi s) t^\alpha}{\Gamma(\alpha+1)}. \quad (27)$$

After using Equations (25–27), we get the second order solution as follows

$$v(s,t) = \frac{1}{8}\sin(\pi s)\left(\frac{\pi^4 c_1^2\left((\alpha+2)t^2+\pi^4\left(16\alpha+(\alpha+2)t^2+8\right)\right)t^{2\alpha}}{\Gamma(2\alpha+2)} + \frac{2\left(c_1(c_1+2)\left(t^2+\pi^4\left(t^2+4\right)\right)+c_2\left(\pi^4\left(t^2+4\right)-t^2\right)\right)t^{\alpha}}{\Gamma(\alpha+1)} + 8\right). \quad (28)$$

Example 2

We take the 4rth-order TFPPDE of the form

$$\frac{\partial^{\alpha} v(s,t)}{\partial t^{\alpha}} + \frac{\partial^4 v(s,t)}{\partial s^4} = \left(\pi^4 - 1\right) e^t sin\pi s, \quad s \in [0,\,1],\ t > 0,\ \mu = 1,\ 1 < \alpha \le 2. \quad (29)$$

Initial conditions

$$v(s,\,0) = \sin(\pi s),\ v_t(s,\,0) = \sin(\pi s).$$

Boundary conditions

$$v(0,\,t) = 0,\ v_{ss}(0,\,t) = 0,$$
$$v(1,t) = 0,\ v_{ss}(1,t) = 0.$$

Exact solution is

$$v(s,\,t) = e^t \sin(\pi s). \quad (30)$$

Compare the coefficients of like powers of embedding parameter p, after substituting $\phi(s,\,p)$ in to optimal homotopy equation to get zero-order, 1st-order, 2nd-order and higher-order (if needed) deformed problems as under:

$$p^0 \ : \quad \frac{\partial^{\alpha} v_0(s,\,t)}{\partial t^{\alpha}} = 0, \quad (31)$$

$$p^1 \ : \quad \left(e^t \sin(\pi s) + e^t \pi^4 \sin(\pi s) - \frac{\partial^4 v_0(s,\,t)}{\partial s^4} - \frac{\partial^{\alpha} v_0(s,\,t)}{\partial t^{\alpha}}\right) c_1 - \frac{\partial^{\alpha} v_0(s,\,t)}{\partial t^{\alpha}} + \frac{\partial^{\alpha} v_1(s,\,t)}{\partial t^{\alpha}} = 0, \quad (32)$$

$$p^2 \ : \quad \left(e^t \sin(\pi s) + \pi^4 \sin(\pi s)\cos(t) - \frac{\partial^4 v_0(s,\,t)}{\partial s^4} - \frac{\partial^{\alpha} v_0(s,\,t)}{\partial t^{\alpha}}\right) c_2 - c_1\left(\frac{\partial^4 v_1(s,\,t)}{\partial s^4} + \frac{\partial^{\alpha} v_1(s,\,t)}{\partial t^{\alpha}}\right) - \frac{\partial^{\alpha} v_1(s,\,t)}{\partial t^{\alpha}} + \frac{\partial^{\alpha} v_2(s,\,t)}{\partial t^{\alpha}} = 0. \quad (33)$$

After implementing the step-5 of sec-3 on Equations (31–33), we develop the following zero-order, 1st-order and 2nd-order results.

$$v_0(s,\,t) = t\sin(\pi s) + \sin(\pi s), \quad (34)$$

$$v_1(s,\,t) = \frac{\sqrt{\pi} c_1 t^{\alpha} \sin(\pi s)\left(2\pi^{\frac{7}{2}}(\alpha+t+1) - \left(1+\pi^4\right)2^{-\alpha}\left(\frac{2t^2}{4} + \frac{t^2 t}{4}\right)\Gamma(\alpha+2)\right)}{2\,\Gamma(\alpha+2)}, \quad (35)$$

$$v_2(s,\,t) = \frac{1}{8}t^{\alpha}\sin(\pi s)\left(\frac{8\pi^8 c_1^2 t^{\alpha+1}}{\Gamma(2\alpha+2)} - \frac{\pi^{\frac{9}{2}}\left(1+\pi^4\right)2^{1-\alpha}c_1^2\,\Gamma(\alpha+3)t^{\alpha+2}}{\Gamma(2\alpha+3)} - \frac{\pi^{\frac{9}{2}}\left(1+\pi^4\right)2^{-\alpha}c_1^2\,\Gamma(\alpha+4)t^{\alpha+3}}{\Gamma(2\alpha+4)} + \frac{8\pi^8 c_1^2 t^{\alpha}}{\Gamma(2\alpha+1)} + \frac{8\left(c_1^2+c_1+c_2\right)\left(\frac{\pi^4(\alpha+t+1)-\frac{1}{4}\left(1+\pi^4\right)t^3}{\alpha+1} - \frac{1}{4}\left(1+\pi^4\right)t^2\right)}{\Gamma(\alpha+1)}\right). \quad (36)$$

After using Equations (34–36), we get the second order solution as follows:

$$\begin{aligned} v(s,\,t) &= \frac{1}{8}\sin(\pi s)\left(-\frac{2^{-\alpha}c_1 t^{\alpha}\left(2^{\alpha+1}\left(t^2+\pi^4\left(t^2-8\right)\right)(\alpha+t+1) + \left(1+\pi^4\right)\sqrt{\pi}(t+2)t^2\,\Gamma(\alpha+2)\right)}{\Gamma(\alpha+2)}\right. \\ &- \frac{2c_2\left(t^2+\pi^4\left(t^2-4\right)\right)(\alpha+t+1)t^{\alpha}}{\Gamma(\alpha+2)} \\ &+ c_1^2 t^{\alpha}\left(-\frac{\pi^{\frac{9}{2}}\left(1+\pi^4\right)2^{-\alpha}\,\Gamma(\alpha+3)(4\alpha+(\alpha+3)t+6)t^{\alpha+2}}{\Gamma(2\alpha+4)}\right. \\ &+ \frac{8\pi^8\left(2\alpha+t+1\right)t^{\alpha}}{\Gamma(2\alpha+2)} \\ &\left.\left. - \frac{2\left(t^2+\pi^4\left(t^2-4\right)\right)(\alpha+t+1)}{\Gamma(\alpha+2)}\right) + 8t + 8\right). \end{aligned} \quad (37)$$

DISCUSSION OF RESULTS

In the last section, a detailed algorithm for OHAM is presented for parabolic equations of arbitrary fractional order, and a description is designed for the examples in the above section which gives remarkably valid results for the TFPPDEs without domain discretization. OHAM does not require any higher order solutions to initiate the process.

In the **Tables 1A, 2A** for examples 1 and 2 represent the values of auxiliary constants c_1 and c_2 for distinct values of $\alpha, \alpha = 1.5,\ 1.75$, and 2. **Tables 1B**, **2B** for examples 1 and 2 represent the approximate and exact solutions with absolute error for distinct values of α at fixed time $t = 0.01$, and also error norms of example 1 are $L_2 = 2.48306 \times 10^{-5}, L_{\infty} = 1.11348 \times 10^{-5}$ and error norms of example 2 are $L_2 = 3.76272 \times 10^{-7}, L_{\infty} = 1.68732 \times 10^{-7}$, which demonstrates the validity and accuracy of the suggested scheme.

Figures 1, **2**, **4** for example 1 represent the exact solution, approximate result and absolute error for fixed value $\alpha = 2$. **Figure 3** for example 1 represents the 2D results for different values of α, $\alpha = 1.5, 1.75$ and 2 at fixed value of $t = 0.01$. **Figures 5**, **6**, **8** for example 2 represent the exact solution, approximate result and absolute error for fixed value $\alpha = 2$. **Figure 7** for example 2 represents the 2D results for different

TABLE 1A | Shows the order of solution of problem-1 with α.

α	*c*1	*c*2
1.5	−0.00023970059767714635	−0.004433615478664607
1.75	−0.00036010106878677054	−0.005492424284324476
2.0	−0.0005420552371218715	−0.006893703812240392

TABLE 2A | Shows the order of solution of problem-2 with α.

α	*c*1	*c*2
1.5	−0.0008721941975312075	0.009452825526087602
1.75	−0.0007319603747448314	0.01166646474774557
2.0	0.00034649675001248057	0.01303912473486976

TABLE 1B | Shows the solutions and absolute error of problem-1 for various values of α.

S	α = 1.5	α = 1.75	α = 2	Exact	Abs. Error
0	0	0	0	0	0
$\frac{\pi}{10}$	0.834054	0.834255	0.834322	0.834313	9.29844×10^{-6}
$\frac{\pi}{5}$	0.919509	0.91973	0.919804	0.919794	1.02511×10^{-5}
$\frac{3\pi}{10}$	0.179665	0.179708	0.179722	0.17972	2.00299×10^{-6}
$\frac{2\pi}{5}$	−0.721436	−0.72161	−0.721668	−0.72166	8.04292×10^{-6}
$\frac{\pi}{2}$	−0.975017	−0.975252	−0.97533	−0.975319	1.087×10^{-5}
$\frac{3\pi}{5}$	−0.353478	−0.353563	−0.353592	−0.353588	3.94074×10^{-6}
$\frac{7\pi}{10}$	−0.585323	0.585646	0.585511	0.58550	6.52546×10^{-6}
$\frac{4\pi}{5}$	0.998771	0.999012	0.999092	0.58550	1.11348×10^{-5}
$\frac{9\pi}{10}$	0.515779	0.515904	0.515945	0.515939	5.75016×10^{-6}
π	−0.430146	−0.43025	−0.430284	−0.43028	4.79548×10^{-6}

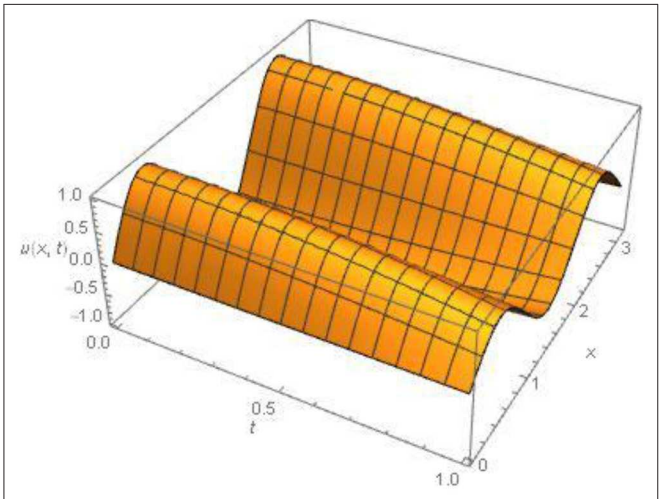

FIGURE 1 | Surface of Exact solution for TFPPDE (20) with α = 2.

TABLE 2B | Shows the solution and absolute error of problem-2 for distinct values of α.

S	α = 1.5	α = 1.75	α = 2	Exact	Abs. Error
0	0	0	0	0	0
$\frac{\pi}{10}$	0.835204	0.835192	0.835189	0.835189	1.40905×10^{-7}
$\frac{\pi}{5}$	0.920776	0.920763	0.92076	0.92076	1.55341×10^{-7}
$\frac{3\pi}{10}$	0.179912	0.17991	0.179909	0.179909	3.03524×10^{-8}
$\frac{2\pi}{5}$	−0.72243	−0.72242	−0.722418	−0.722418	1.21879×10^{-7}
$\frac{\pi}{2}$	−0.976361	−0.976347	−0.976344	−0.976344	1.64719×10^{-7}
$\frac{3\pi}{5}$	−0.353965	−0.35396	−0.353959	−0.353959	5.97163×10^{-8}
$\frac{7\pi}{10}$	0.586129	0.586121	0.586119	0.586119	9.8884×10^{-8}
$\frac{4\pi}{5}$	1.00015	1.00013	1.00013	1.00013	1.68732×10^{-7}
$\frac{9\pi}{10}$	0.51649	0.516483	0.516481	0.516481	8.71354×10^{-8}
π	−0.430739	−0.430733	−0.430732	−0.430732	7.26686×10^{-8}

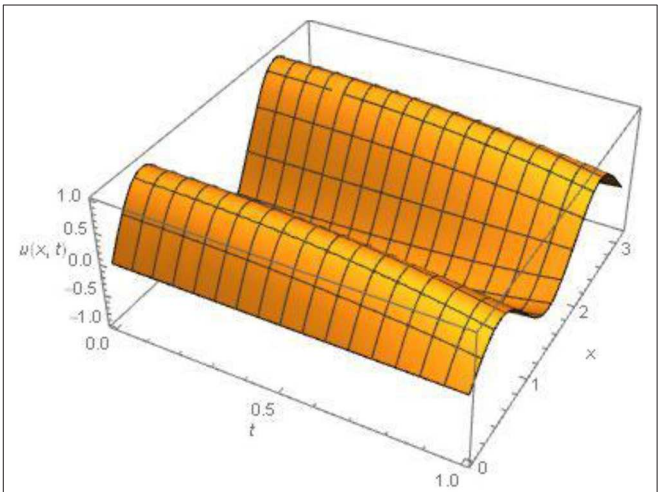

FIGURE 2 | Surface of Approximate solution for TFPPDE (20) with α = 2.

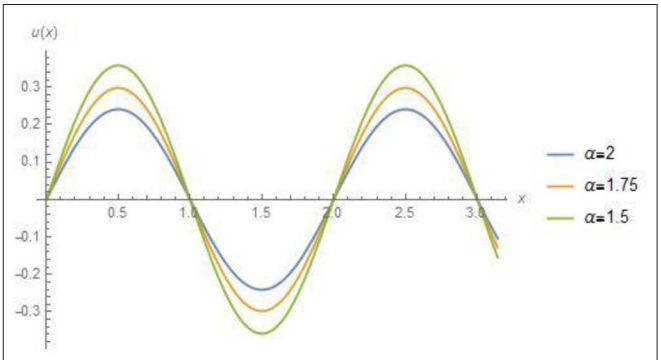

FIGURE 3 | Approximate solutions for TFPPDE (20) for distinct values of α = 1.5, 1.75, 2.

values of α, $\alpha = 1.5, 1.75$ and 2 at fixed value of $t = 0.01$. All the above figures indicate the accuracy, suitability and effectiveness of the suggested algorithm. It is clear that as we proceed along the domain, we obtain consistent validity. In the above discussion (**Tables 1B**, **2B**) show an excellent agreement between the approximate and exact solutions.

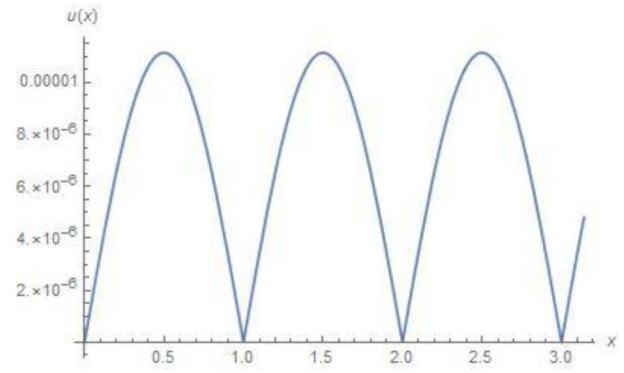

FIGURE 4 | Absolute error for TFPPDE (20) at $\alpha = 2$.

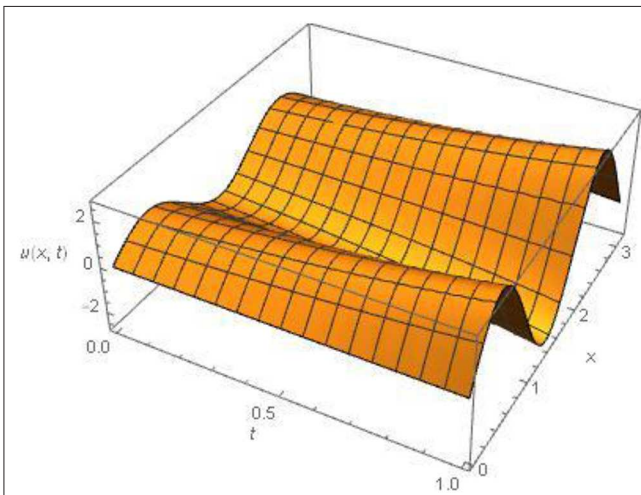

FIGURE 5 | Surface of Exact solution for TFPPDE (29) with $\alpha = 2$.

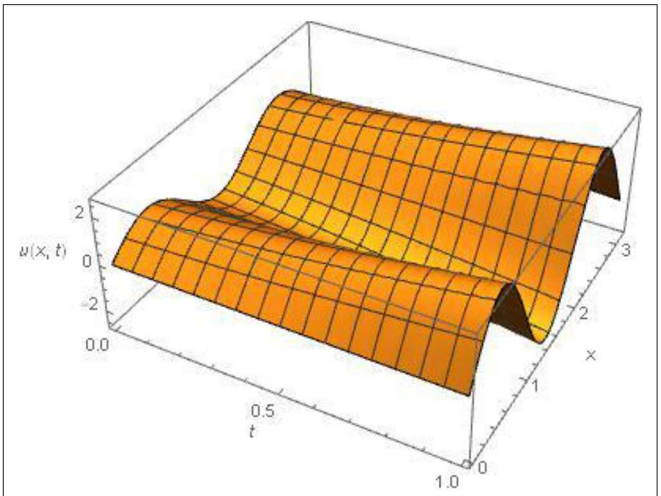

FIGURE 6 | Surface of Approximate solution for TFPPDE (29) with $\alpha = 2$.

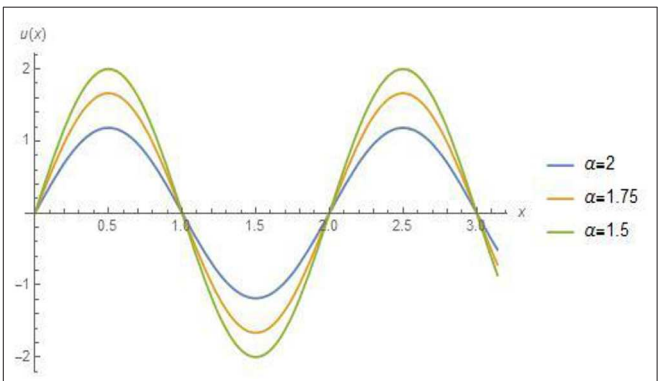

FIGURE 7 | Approximate solutions of TFPPDE (29) for distinct values of $\alpha = 1.5, 1.75, 2$.

CONCLUSIONS

In this work, the TFPDE are examined by a semi-analytical scheme. The problems in hand are solved by OHAM. OHAM is incredibly effective for fractional order parabolic partial differential equations. The solutions obtained from OHAM are smooth enough to be compared with the exact solutions. The graphical reviews show the smoothness of the solutions. The error estimations with the exact solutions are of order 10^{-6}. The tabular and graphical reviews of the solutions and errors are presented for different values of $1 < \alpha \leq 2$ which are convergent. L^2 error and L^∞ error norms are calculated which show the error bounds. The error bound is of order 10^{-7}. This is incredibly excellent.

This article focuses on the approximate solution of the parabolic equation which has many applications in engineering and physical sciences. The contribution of this article is 3-fold: first, we briefly defined the concept of fractional derivative, then developed the mathematical model. In the last step we implemented OHAM to find the solution of the model. The results are graphically represented and shown in tabular form to show the novelty and credibility of our method. In the future, we are interested in implementing OHAM on the system of fractional order partial differential equations in a more general way.

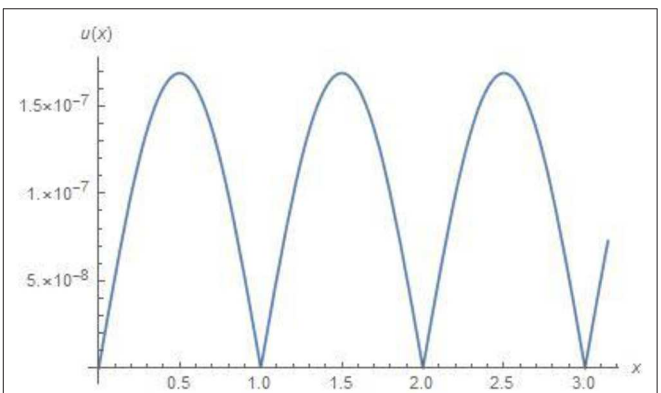

FIGURE 8 | Absolute error for TFPPDE (29) at $\alpha = 2$.

DATA AVAILABILITY STATEMENT

All datasets generated for this study are included in the article/supplementary material.

AUTHOR CONTRIBUTIONS

All authors listed have made a substantial, direct and intellectual contribution to the work, and approved it for publication.

REFERENCES

1. Oldham KB, Spanier J. *The Fractional Calculus*. New York, NY: Academic Press (1974).
2. Podlubny I. *Fractional Differential Equations*. New York, NY: Academic Press (1999).
3. Miller KS, Ross B. *An Introduction to the Fractional Calculus and Fractional Differential Equations*. New York, NY: Wiley (1993).
4. Kumar D, Singh J, Tanwar K, Baleanu D. A new fractional exothermic reactions model having constant heat source in porous media with power, exponential and Mittag-Leffler Laws. *Int J Heat Mass Transfer.* (2019) **138**:1222–7. doi: 10.1016/j.ijheatmasstransfer.2019.04.094
5. Kumar D, Singh J, Baleanu D. On the analysis of vibration equation involving a fractional derivative with Mittag-Leffler law. *Math Methods Appl Sci.* (2019) **43**:443–57. doi: 10.1002/mma.5903
6. Bhatter S, Mathur A, Kumar D, Singh J. A new analysis of fractional Drinfeld–Sokolov–Wilson model with exponential memory. *Physica A.* (2020) **537**:122578. doi: 10.1016/j.physa.2019.122578
7. Kumar D, Singh J, Purohit SD, Swroop R. A hybrid analytical algorithm for nonlinear fractional wave-like equations. *Math Model Nat Phenom.* (2019) **14**:304. doi: 10.1051/mmnp/2018063
8. Singh J, Kumar D, Baleanu D. New aspects of fractional Biswas-Milovic model with Mittag-Leffler law. *Math Model Nat Phenom.* (2019) **14**:303. doi: 10.1051/mmnp/2018068
9. Goswami A, Singh J, Kumar D, Sushila. An efficient analytical approach for fractional equal width equations describing hydro-magnetic waves in cold plasma. *Physica A*. (2019) **524**:563–75. doi: 10.1016/j.physa.2019.04.058
10. Goswami A, Singh J, Kumar D, Gupta S, Sushila. An efficient analytical technique for fractional partial differential equations occurring in ion acoustic waves in plasma. *J Ocean Eng Sci.* (2019) **4**:85–99. doi: 10.1016/j.joes.2019.01.003
11. Liao SJ. *On the Proposed Homotopy Analysis Technique for Nonlinear Problems and Its Applications* (Ph. D. Dissertation). Shanghai Jio Tong University, Shanghai, China (1992).
12. He JH. An approximation solution technique depending upon an artificial parameter. *Commun Nonlinear Sci Numerical Simul.* (1998) **3**:92–7. doi: 10.1016/S1007-5704(98)90070-3
13. Marinca V, Herisanu N. The optimal homotopy asymptotic method for solving Blasius equation. *Appl Math Comput.* (2014) **231**:134–9. doi: 10.1016/j.amc.2013.12.121
14. Marinca V, Herisanu N. Application of homotopy asymptotic method for solving non-linear equations arising in heat transfer, I, Comm. *Heat Mass Transfer.* (2008) **35**:710–5. doi: 10.1016/j.icheatmasstransfer.2008.02.010
15. Marinca V, Herisanu N. Determination of periodic solutions for the motion of a particle on a rotating parabola by means of the optimal homotopy asymptotic method, *J Sound Vib.* (2010) **329**:1450–9. doi: 10.1016/j.jsv.2009.11.005
16. Iqbal S, Idrees M, Siddiqui AM, Ansari AR. Some solutions of the linear and nonlinear Klein Gordon equations using the optimal homotopy asymptotic method. *Appl Math Comput.* (2010) **216**:2898–909. doi: 10.1016/j.amc.2010.04.001
17. Iqbal S, Javed A. Application of optimal homotopy asymptotic method for the analytic solution of singular Lane-Emden type equation. *Appl Math Comput.* (2011) **217**:7753–61. doi: 10.1016/j.amc.2011.02.083
18. Iqbal S, Sarwar F, Rafiq M, Mufti Siddique I. Use of optimal homotopy asymptotic method for fractional order nonlinear Fredholm integro-differential equations. *Sci Int*. (2015) **27**:3033−40.
19. Sarwar S, Salem Alkhalaf. Iqbal S, Zahid MA. A note on optimal homotopy asymptotic method for the solutions of fractional order heat-and wave-like partial differential equations. *Comp Math Appl.* (2015) **70**:942–53. doi: 10.1016/j.camwa.2015.06.017
20. Sarwar S, Rashidi MM. Approximate solution of two term fractional order diffusion, wave diffusion and telegraph models arising in mathematical physics using optimal homotopy asymptotic method. *Waves Random Complex Media.* (2016) **26**:365–82. doi: 10.1080/17455030.2016.1158436
21. Kumar D, Singh J, Al Qurashi M, Baleanu D. A new fractional SIRS-SI malaria disease model with application of vaccines, antimalarial drugs, and spraying. *Adv Differ Equ.* (2019) **2019**:278. doi: 10.1186/s13662-019-2199-9
22. Dubey VP, Kumar R, Kumar D, Khan I, Singh J. An efficient computational scheme for nonlinear time fractional systems of partial differential equations arising in physical sciences. *Adv Diff Eq.* (2020) **2020**:46. doi: 10.1186/s13662-020-2505-6
23. Gao W, Yel G, Baskonus HM, Cattani C. Complex solitons in the conformable (2+1)-dimensional Ablowitz-Kaup-Newell-Segur equation. *AIMS Math.* (2020) 5:507–21. doi: 10.3934/math.2020034
24. Yavuz M. Characterizations of two different fractional operators without singular kernel. *Math Model Nat Phenom.* (2019) **14**:302. doi: 10.1051/mmnp/2018070
25. Keten A, Yavuz M, Baleanu D. Nonlocal Cauchy problem via a fractional operator involving power kernel in Banach spaces. *Fractal Fract.* (2019) **3**:27. doi: 10.3390/fractalfract3020027

Conflict of Interest: The authors declare that the research was conducted in the absence of any commercial or financial relationships that could be construed as a potential conflict of interest.

frontiers in Physics

ORIGINAL RESEARCH
published: 05 June 2020
doi: 10.3389/fphy.2020.00181

New Soliton Applications in Earth's Magnetotail Plasma at Critical Densities

Hesham G. Abdelwahed [1], Mahmoud A. E. Abdelrahman [2,3], Mustafa Inc [4,5]* and R. Sabry [1,6]*

[1] Department of Physics, College of Science and Humanities, Prince Sattam Bin Abdulaziz University, Al-Kharj, Saudi Arabia, [2] Department of Mathematics, College of Science, Taibah University, Medina, Saudi Arabia, [3] Department of Mathematics, Faculty of Science, Mansoura University, Mansoura, Egypt, [4] Department of Mathematics, Faculty of Science, Firat University, Elaziğ, Turkey, [5] Department of Medical Research, China Medical University Hospital, China Medical University, Taichung, Taiwan, [6] Department of Physics, Faculty of Science, Damietta University, New Damietta, Egypt

New plasma wave solutions of the modified Kadomtsev Petviashvili (MKP) equation are presented. These solutions are written in terms of some elementary functions, including trigonometric, rational, hyperbolic, periodic, and explosive functions. The computational results indicate that these solutions are consistent with the MKP equation, and the numerical solutions indicate that new periodic, shock, and explosive forms may be applicable in layers of the Earth's magnetotail plasma. The method employed in this paper is influential and robust for application to plasma fluids. In order to depict the propagating soliton profiles in a plasma medium, the MKP equation must be solved at critical densities. In order to achieve this, the Riccati-Bernoulli sub-ODE technique has been utilized in solutions. The research findings indicate that a number of MKP solutions may be applicable to electron acoustics appearing in the magnetotail.

AMS subject classifications: 35A20, 35A99, 35C07, 35Q51, 65Z05

Keywords: MKP equation, explosive solutions, Riccati-Bernoulli sub-ODE method, plasma applications, magnetotail

OPEN ACCESS

Edited by:
Manuel Asorey,
University of Zaragoza, Spain

Reviewed by:
Yilun Shang,
Northumbria University,
United Kingdom
Babak Shiri,
Neijiang Normal University, China

****Correspondence:***
Hesham G. Abdelwahed
h.abdelwahed@psau.edu.sa;
hgomaa_eg@hotmail.com
Mustafa Inc
minc@firat.edu.tr

Specialty section:
This article was submitted to Mathematical Physics, a section of the journal Frontiers in Physics

Received: *04 March 2020*
Accepted: *27 April 2020*
Published: *05 June 2020*

Citation:
Abdelwahed HG, Abdelrahman MAE, Inc M and Sabry R (2020) New Soliton Applications in Earth's Magnetotail Plasma at Critical Densities. Front. Phys. 8:181. doi: 10.3389/fphy.2020.00181

1. INTRODUCTION

The existence of electron acoustic solitary excitations (EAs) in plasmas has been noticed in laboratories [1, 2]. Different observations in space have confirmed propagations of EAs in magnetospheres, auroral zones, broadband electrostatic noise (BEN), heliospheric shock, and geomagnetic tails [3–10]. The concept of EAs was generated by Fried and Gould [11]. It is principally an acoustic-type of wave with inertia given by the mass of cold electrons and restoring force expressed by hot electron thermal pressure [12]. Abdelwahed et al. [10] inspected the modulation of characteristics of EAs in non-isothermal electron plasmas [13] using a time-fractional modified non-linear equation. Pakzad studied [14] cylindrical EAs by hot non-extensive electrons, and found through numerical simulations that the spherical amplitude is greater than the cylindrical in EAs. Non-thermal critical geometrical EA plasmas were studied using a Gardner-type equation in Shuchy et al. [15]. Contributions of solitons to science have been discussed in many research works, some of which may be listed as [16–23]. The observed BEN emission bursts in auroras and the Earth's magnetotail regions indicate small and large amplitude electric fields with some explosive and rational domains at critical density. These wave structures appear to be prevalent in some parts of these regions [16, 17]. Therefore, we aim to obtain the solutions that confirm the existence of the electrostatic field in our model.

Let us consider the non-linear partial differential equation

$$H(\varphi, \varphi_x, \varphi_t, \varphi_{xx}, \varphi_{xt}, \varphi_{tt}, ...) = 0, \tag{1.1}$$

where $\varphi(x,t)$ is an unknown function. Using the wave transformation

$$\varphi(x,t) = \varphi(\xi), \quad \xi = kx - ct, \tag{1.2}$$

Equation (1.1) is converted to an ODE:

$$E(\varphi, \varphi', \varphi'', \varphi''', ...) = 0. \tag{1.3}$$

Many models in physics, fluid mechanics, and engineering are written in the form of (1.1), and this form may be transformed into the ODE:

$$\alpha_1\varphi'' + \alpha_2\varphi^3 + \alpha_3\varphi = 0, \tag{1.4}$$

(see for instance [24–35], and so on). Equation (1.3) is quite significant and useful in our computations, and we employ a robust and unified method known as the Riccatti-Bernoulli (RB) sub-ODE method [36]. The RB sub-ODE method has been used as a box solver for many systems of equations arising in applied science and physics. There are other powerful analytical methods that solve such ODEs; an important example is the Lie algebra method (see [37, 38]).

Next, we describe the RB sub-ODE method briefly.

2. THE RB SUB-ODE METHOD

According to the RB sub-ODE method [36], the solution of Equation (1.3) is

$$\varphi' = a\varphi^{2-m} + b\varphi + c\varphi^m, \tag{2.1}$$

where a, b, c, and n are constants that will be determined later. From Equation (2.1), we get

$$\begin{aligned}\varphi'' &= ab(3-m)\varphi^{2-m} + a^2(2-m)\varphi^{3-2m} + mc^2\varphi^{2m-1}\\ &+bc(m+1)\varphi^m + (2ac+b^2)\varphi,\end{aligned} \tag{2.2}$$

$$\begin{aligned}\varphi''' = \varphi'[&ab(3-m)(2-m)\varphi^{1-m} + a^2(2-m)(3-2m)\varphi^{2-2m}\\ &+ m(2m-1)c^2\varphi^{2m-2} + bcn(m+1)\varphi^{m-1} + (2ac+b^2)].\end{aligned} \tag{2.3}$$

The solitary solutions $\varphi_i(\xi)$ of Equation (2.1) are given by

1. At $m = 1$

$$\varphi(\xi) = \varsigma e^{(a+b+c)\xi}. \tag{2.4}$$

2. At $m \neq 1$, $b = 0$, and $c = 0$

$$\varphi(\xi) = \left(a(m-1)(\xi+\varsigma)\right)^{\frac{1}{m-1}}. \tag{2.5}$$

3. At $m \neq 1$, $b \neq 0$, and $c = 0$

$$\varphi(\xi) = \left(\frac{-a}{b} + \varsigma e^{b(m-1)\xi}\right)^{\frac{1}{m-1}}. \tag{2.6}$$

4. At $m \neq 1$,$a \neq 0$, and $b^2 - 4ac < 0$

$$\varphi(\xi) = \left(\frac{-b}{2a} + \frac{\sqrt{4ac-b^2}}{2a}\tan\left(\frac{(1-m)\sqrt{4ac-b^2}}{2}(\xi+\varsigma)\right)\right)^{\frac{1}{1-m}} \tag{2.7}$$

and

$$\varphi(\xi) = \left(\frac{-b}{2a} - \frac{\sqrt{4ac-b^2}}{2a}\cot\left(\frac{(1-m)\sqrt{4ac-b^2}}{2}(\xi+\varsigma)\right)\right)^{\frac{1}{1-m}}. \tag{2.8}$$

5. At $m \neq 1$,$a \neq 0$, and $b^2 - 4ac > 0$

$$\varphi(\xi) = \left(\frac{-b}{2a} - \frac{\sqrt{b^2-4ac}}{2a}\coth\left(\frac{(1-m)\sqrt{b^2-4ac}}{2}(\xi+\varsigma)\right)\right)^{\frac{1}{1-m}} \tag{2.9}$$

and

$$\varphi(\xi) = \left(\frac{-b}{2a} - \frac{\sqrt{b^2-4ac}}{2a}\tanh\left(\frac{(1-m)\sqrt{b^2-4ac}}{2}(\xi+\varsigma)\right)\right)^{\frac{1}{1-m}}. \tag{2.10}$$

6. At $m \neq 1$, $a \neq 0$, and $b^2 - 4ac = 0$

$$\varphi(\xi) = \left(\frac{1}{a(m-1)(\xi+\varsigma)} - \frac{b}{2a}\right)^{\frac{1}{1-m}}. \tag{2.11}$$

2.0.1. Bäcklund Transformation

If $\varphi_{r-1}(\xi)$ and $\varphi_r(\xi)(\varphi_r(\xi) = \varphi_r(\varphi_{r-1}(\xi)))$ are the solutions of Equation (2.1), we have

$$\begin{aligned}\frac{d\varphi_r(\xi)}{d\xi} &= \frac{d\varphi_r(\xi)}{d\varphi_{r-1}(\xi)}\frac{d\varphi_{r-1}(\xi)}{d\xi}\\ &= \frac{d\varphi_r(\xi)}{d\varphi_{r-1}(\xi)}(a\varphi_{r-1}^{2-m} + b\varphi_{r-1} + c\varphi_{r-1}^m),\end{aligned}$$

namely

$$\frac{d\varphi_r(\xi)}{a\varphi_r^{2-m} + b\varphi_r + c\varphi_r^m} = \frac{d\varphi_{r-1}(\xi)}{a\varphi_{r-1}^{2-m} + b\varphi_{r-1} + c\varphi_{r-1}^m}. \tag{2.12}$$

Integrating Equation (2.12) once with respect to ξ, we get the Bäcklund transformation of Equation (2.1) as follows:

$$\varphi_r(\xi) = \left(\frac{-cL_1 + aL_2\left(\varphi_{r-1}(\xi)\right)^{1-m}}{bL_1 + aL_2 + aL_1\left(\varphi_{r-1}(\xi)\right)^{1-m}}\right)^{\frac{1}{1-m}}, \tag{2.13}$$

where L_1 and L_2 are arbitrary constants. Equation (2.13) gives the infinite solutions of Equations (2.1) and (1.1).

3. UNIFIED SOLVER

In this section, we will describe the practical implementation of the concept of a unified solver.

$$\alpha_1\varphi'' + \alpha_2\varphi^3 + \alpha_3\varphi = 0, \tag{3.1}$$

Substituting Equation (2.2) into Equation (3.1), we obtain

$$\alpha_1\left(ab(3-m)\varphi^{2-m}+a^2(2-m)\varphi^{3-2m}+mc^2\varphi^{2m-1}+bc(m+1)\varphi^m+(2ac+b^2)\varphi\right)+\alpha_2\varphi^3+\alpha_3\varphi=0\,. \quad (3.2)$$

Making $m=0$, Equation (3.2) is reduced to

$$\alpha_1(3abu^2+2a^2\varphi^3+bc+(2ac+b^2)\varphi)+\alpha_2\varphi^3+\alpha_3\varphi=0. \quad (3.3)$$

Setting each coefficient of $\varphi^i(i=0,1,2,3)$ to zero, we get

$$\alpha_1 bc=0, \quad (3.4)$$
$$\alpha_1(2ac+b^2)+\alpha_3=0, \quad (3.5)$$
$$3\alpha_1 ab=0, \quad (3.6)$$
$$2\alpha_1 a^2+\alpha_2=0. \quad (3.7)$$

Solving Equations (3.4)–(3.7) yields

$$b=0\,, \quad (3.8)$$
$$c=\mp\frac{\alpha_3}{\sqrt{-2\alpha_1\alpha_2}}, \quad (3.9)$$
$$a=\pm\sqrt{\frac{-\alpha_2}{2\alpha_1}}. \quad (3.10)$$

Hence, we present the following possible cases for solutions of Equations (3.1) and (1.1).

1. When $b=0$ and $c=0$ ($\alpha_3=0$), the solution of Equation (3.1) is

$$\varphi_1(x,t)=\left(\mp\sqrt{\frac{-\alpha_2}{2\alpha_1}}\,(\xi+\varsigma)\right)^{-1}, \quad (3.11)$$

where ς is an arbitrary constant.

2. When $\frac{\alpha_3}{\alpha_1}<0$, substituting Equations (3.8)–(3.10) and (1.2) into Equations (2.7) and (2.8), the trigonometric function solutions of Equation (1.1) are then given by

$$\varphi_{2,3}(x,t)=\pm\sqrt{\frac{\alpha_3}{\alpha_2}}\,tan\left(\sqrt{\frac{-\alpha_3}{2\alpha_1}}\,(\xi+\varsigma)\right) \quad (3.12)$$

$$\varphi_{4,5}(x,t)=\pm\sqrt{\frac{\alpha_3}{\alpha_2}}\,cot\left(\sqrt{\frac{-\alpha_3}{2\alpha_1}}\,(\xi+\varsigma)\right), \quad (3.13)$$

where ς is an arbitrary constant.

3. When $\frac{\alpha_3}{\alpha_1}>0$, substituting Equations (3.8)–(3.10) and (1.2) into Equations (2.9) and (2.10), the hyperbolic function solutions of Equation (1.1) are,

$$\varphi_{6,7}(x,t)=\pm\sqrt{\frac{-\alpha_3}{\alpha_2}}\,tanh\left(\sqrt{\frac{\alpha_3}{2\alpha_1}}\,(\xi+\varsigma)\right) \quad (3.14)$$

and

$$\varphi_{8,9}(x,t)=\pm\sqrt{\frac{-\alpha_3}{\alpha_2}}\,coth\left(\sqrt{\frac{\alpha_3}{2\alpha_1}}\,(\xi+\varsigma)\right), \quad (3.15)$$

where ς is an arbitrary constant.

4. MATHEMATICAL MODEL

We use stretched $\tau=\epsilon^3 t,\ \xi=\epsilon(x-\lambda t),\ \eta=\epsilon^2 y$, where ϵ is an arbitrarily small number and λ is the speed of EA. Elwakil et al. [17] examined two-dimensional propagation of EAs in plasma with cold fluid of electrons and two different ion temperatures within the framework of Poisson equations:

$$\frac{\partial^2\boldsymbol{\phi}}{\partial x^2}+\frac{\partial^2\boldsymbol{\phi}}{\partial y^2}=(n_e-n_{il}-n_{ih}), \quad (4.1)$$

$$n_{il}=\mu\exp(\frac{-\phi}{\nu\beta+\mu}),\ n_{ih}=\gamma\exp(\frac{-\beta\,\phi}{\nu\beta+\mu}). \quad (4.2)$$

where T_l is the low ion temperature at equilibrium density μ, T_h is the high ion temperature at equilibrium density γ, and $\beta=\frac{T_l}{T_h}$. The computational results indicate that the system reaches critical density μ_c which makes non-linearity vanish. At $\mu=\mu_c$, the modified KP equation was given:

$$\frac{\partial}{\partial\xi}\left(\frac{\partial}{\partial\tau}\phi+G\phi^2\frac{\partial}{\partial\xi}\phi+R\frac{\partial^3}{\partial\xi^3}\phi\right)+Q\frac{\partial^2}{\partial\eta^2}\phi=0$$

with

$$\mu_c=\frac{\beta^2\lambda^4-\lambda^4\pm(\beta-1)\lambda^2\sqrt{\beta^2\lambda^4+2\beta\lambda^4+\lambda^4-12\beta}-6\beta^2+6\beta}{2\left(-3\beta^2+6\beta-3\right)}, \quad (4.3)$$

$$G=\frac{1}{2}\lambda(-\frac{3\nu\beta^2}{2(\mu+\beta\nu)^2}-\frac{3\mu}{2(\mu+\beta\nu)^2}-\frac{3}{\lambda^4}), \quad (4.4)$$

$$R=\frac{\lambda^3}{2}, Q=\frac{\lambda}{2}.$$

We use a similarity transformation in the form:

$$\chi=L\xi+M\eta-\tau(\upsilon_1+\upsilon_2), \quad (4.5)$$
$$\phi(\chi)=\phi(x,y,t) \quad (4.6)$$
$$\tau=t, \quad (4.7)$$

where L and M are *directional cosines* of x and y axes.

The MKP equation transformed to the ODE form is:

$$-3(\nu-s)\phi+\delta\,\phi^3+3\,\sigma\frac{d^2\phi}{d\chi^2}=0. \quad (4.8)$$

Equation (4.8) gives a stationary soliton in the form of

$$\phi_c=\sqrt{6(\frac{\nu-S}{\delta})}\,\mathrm{sech}\left(\frac{\sqrt{\frac{\nu-S}{\delta}}}{\sqrt{\frac{\sigma}{\delta}}}\chi\right), \quad (4.9)$$

$$S=\frac{M^2Q}{L}-u, \quad (4.10)$$
$$\delta=GL, \sigma=RL^3, \quad (4.11)$$

where u and v are traveling speeds in both directions.

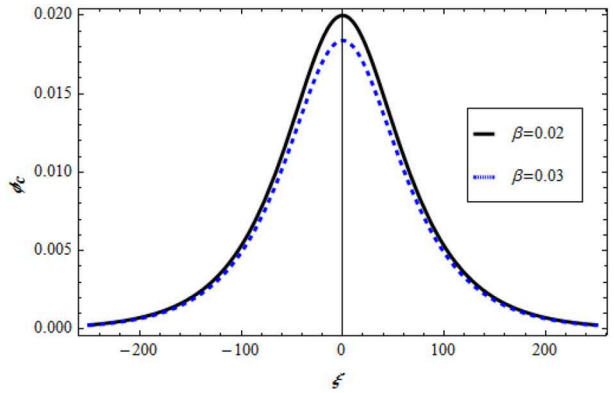

FIGURE 1 | Variation of ϕ_c against χ, β for $u = 0.01, v = 0.01, L = 0.95$.

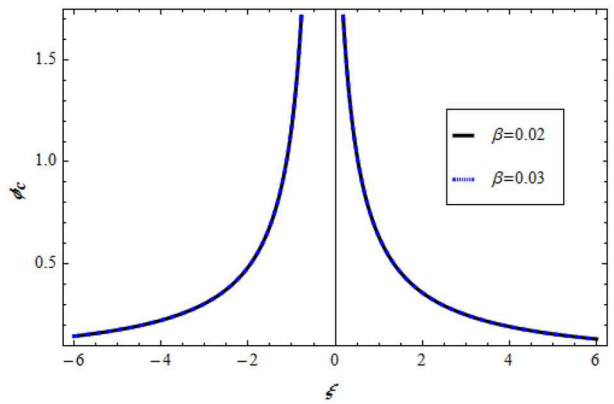

FIGURE 2 | Variation of rational ϕ_c against χ, β for $u = 0.01$, $v = 0.01$, $L = 0.95$.

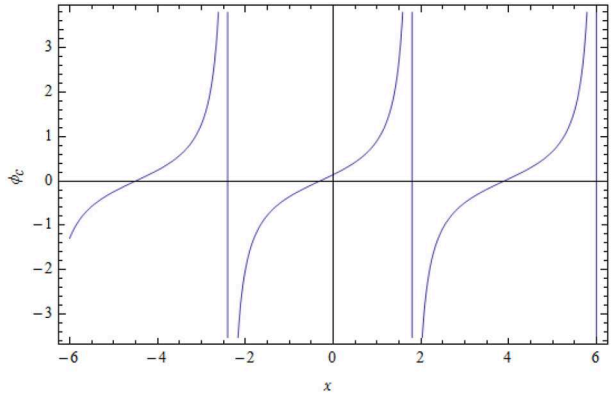

FIGURE 3 | Variation of periodic ϕ_c against χ for $\beta = 0.05$, $u = 0.02$, $v = 0.5$, $L = 0.92$.

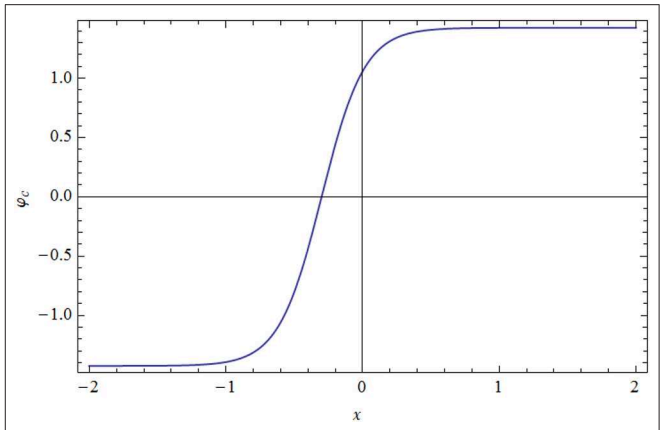

FIGURE 4 | Variation of shock ϕ_c against χ for $\beta = 0.02$, $u = 0.02$, $v = 0.5$, $L = 0.5$.

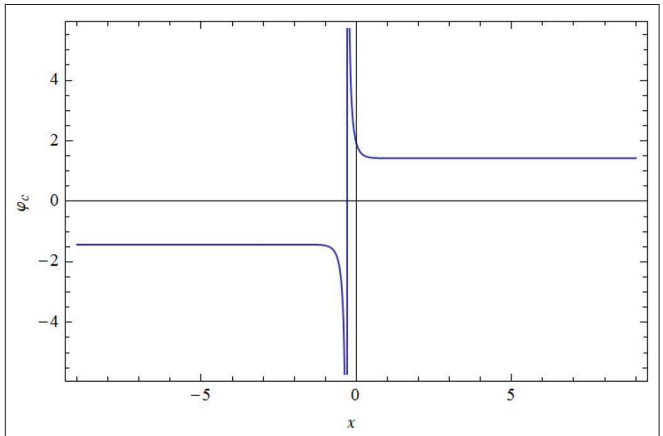

FIGURE 5 | Variation of explosive shock ϕ_c against χ for $\beta = 0.02$, $u = 0.02$, $v = 0.5$, $L = 0.5$.

5. RESULTS AND DISCUSSION

Comparing Equation (4.8) with the general form (3.1) gives $\alpha_1 = 3\sigma$, $\alpha_2 = \delta$, and $\alpha_3 = -3(\upsilon - s)$. According to the unified solver given in section 3, solutions of Equation (4.8) are expressed as follows.

5.1. Rational Function Solutions: (When $\upsilon = s$)

The rational solutions of Equation (4.8) are.

$$\phi_{1,2}(x,t) = \left(\mp\sqrt{\frac{-\delta}{6\sigma}}\,(\chi + \varsigma)\right)^{-1}. \tag{5.1}$$

5.2. Trigonometric Function Solution: (When $\frac{\upsilon - s}{\sigma} > 0$)

The trigonometric solutions of Equation (4.8) are

$$\phi_{3,4}(x,t) = \pm\sqrt{\frac{-3(\upsilon - s)}{\delta}}\,tan\left(\sqrt{\frac{\upsilon - s}{2\sigma}}(\chi + \varsigma)\right) \tag{5.2}$$

and

$$\phi_{5,6}(x,t) = \pm\sqrt{\frac{-3(\upsilon - s)}{\delta}}\, cot\left(\sqrt{\frac{\upsilon - s}{2\sigma}}(\chi + \varsigma)\right). \quad (5.3)$$

5.3. Hyperbolic Function Solution: (When $\frac{\upsilon - s}{\sigma} < 0$)

The hyperbolic solutions of Equation (4.8) are.

$$\phi_{7,8}(x,t) = \pm\sqrt{\frac{3(\upsilon - s)}{\delta}}\, tanh\left(\sqrt{\frac{s - \upsilon)}{2\sigma}}(\chi + \varsigma)\right) \quad (5.4)$$

and

$$\phi_{9,10}(x,t) = \pm\sqrt{\frac{3(\upsilon - s)}{\delta}}\, coth\left(\sqrt{\frac{s - \upsilon}{2\sigma}}(\chi + \varsigma)\right). \quad (5.5)$$

Two-dimensional propagation of solitary non-linear EAs has been examined in a plasma mode using parameters related to sheet layers of plasmas of the Earth's magnetotail [16, 17]. At a certain ion density value called the criticality value, the equation obtained cannot describe the mode. Hence, the new stretching produced by the MKP equation describes the critical system under investigation. Equation (4.9) represents a soliton with stationary behavior, as shown in **Figure 1**. At the critical point, many solitary forms are concerned with the behavior of EAs using the Riccati-Bernoulli solver for the MKP equation.

Solution (5.1) is a solitary wave type called explosive type, which has rapidly increasing amplitude, as depicted in **Figure 2**. Solution (5.2) has a blow-up periodic shape, as shown in **Figure 3**. Dissipative behaviors are also produced in **Figures 4**, **5**. In the solution of (5.4), the shock wave is propagated in the medium, as shown in **Figure 4**. Finally, the explosive shock profile is obtained for solution (5.5), as shown in **Figure 5**.

6. CONCLUSIONS

We have devoted major effort to examining the adequate description of the new type solutions at critical density in plasma layers of the Earth's magnetotail. The application of perturbation theory leads to the modified MKP equation. An RB sub-ODE solver gives new solitary excitations for the MKP equation, including periodic, explosive, and shock types. The new explosive shocks represent the wave motion of plasma solitons. Moreover, these new exact solitonic and other solutions to the MKP equation supply guidelines for the classification of the new types of waves according to the model parameters and can introduce the following types: (a) solitary and hyperbolic solutions, (b) periodic solutions, (c) explosive solutions, (d) rational solutions, (e) shock waves, and (f) explosive shocks. The application of this model could be used in the verification of the broadband and observations of magnetotail electrostatic waves.

DATA AVAILABILITY STATEMENT

The datasets generated for this study are available on request to the corresponding author.

AUTHOR CONTRIBUTIONS

All authors listed have made a substantial, direct and intellectual contribution to the work, and approved it for publication.

FUNDING

This project was supported by the deanship of scientific research at Prince Sattam Bin Abdulaziz University under the research project No. 10259/01/2019.

REFERENCES

1. Henry D, Treguier JP. Propagation of electronic longitudinal modes in a non-Maxwellian plasma. *J Plasma Phys*. (1972) **8**:311–9. doi: 10.1017/S0022377800007169
2. Ikezawa S, Nakamura Y. Observation of electron plasma waves in plasma of two-temperature electrons. *J Phys Soc Jpn*. (1981) **50**:962–7. doi: 10.1143/JPSJ.50.962
3. Dubouloz N, Pottelette R, Malingre M, Treumann RA. Generation of broadband electrostatic noise by electron acoustic solitons. *Geophys Res Lett*. (1991) **18**:155–8. doi: 10.1029/90GL02677
4. Singh SV, Lakhina GS. Generation of electron-acoustic waves in the magnetosphere. *Planet Space Sci*. (2001) **49**:107–14. doi: 10.1016/S0032-0633(00)00126-4
5. Dubouloz N, Treumann R, Pottelette R, Malingre MJ. Turbulence generated by a gas of electron acoustic solitons. *Geophys Res*. (1993) **98**:17415–22. doi: 10.1029/93JA01611
6. Gill TS, Kaur H, Bansal S, Saini NS, Bala P. Modulational instability of electron-acoustic waves: an application to auroral zone plasma. *Eur Phys J D*. (2007) **41**:151–6. doi: 10.1140/epjd/e2006-00198-7
7. Demiray H. Modulation of electron-acoustic waves in a plasma with kappa distribution. *Phys Plasmas*. (2016) **23**:032109. doi: 10.1063/1.4943279
8. Devanandhan S, Singh SV, Lakhina GS, Bharuthram R. Electron acoustic waves in a magnetized plasma with kappa distributed ions. *Phys Plasmas*. (2012) **19**:082314. doi: 10.1063/1.4743015
9. Williams G, Verheest F, Hellberg MA, Anowar MGM, Kourakis I. A Schamel equation for ion acoustic waves in superthermal plasmas. *Phys Plasmas*. (2014) **21**:092103. doi: 10.1063/1.4894115
10. Abdelwahed HG. Higher-order corrections to broadband electrostatic shock noise in auroral zone. *Phys Plasmas*. (2015) **22**:092102. doi: 10.1063/1.4929793
11. Fried BD, Gould RW. Longitudinal ion oscillations in a hot plasma. *Phys Fluids*. (1961) **4**:139. doi: 10.1063/1.1706174
12. Watanabe K, Taniuti T. Electron-acoustic mode in a plasma of two-temperature eelectrons. *J Phys Soc Jpn*. (1977) **43**:1819–20. doi: 10.1143/JPSJ.43.1819
13. Abdelwahed HG, El-Shewy EK, Mahmoud AA. Cylindrical electron acoustic solitons for modified time-fractional nonlinear equation. *Phys Plasmas*. (2017) **24**:082107. doi: 10.1063/1.4996569
14. Pakzad HR. Cylindrical and spherical electron acoustic solitary waves with nonextensive hot electrons. *Phys Plasmas*. (2011) **18**:082105. doi: 10.1063/1.3622207
15. Shuchy ST, Mannan A, Mamun AA. Cylindrical and spherical electron-acoustic Gardner solitons and double layers in a two-electron-temperature plasma with nonthermal

ions. *JETP Lett*. (2012) **95**:282. doi: 10.1134/S0021364012060094
16. Matsumoto H, Kojima H, Miyatake T, Omura Y, Okada M, Nagano I, et al. Electrostatic solitary waves (ESW) in the magnetotail: BEN wave forms observed by GEOTAIL. *Geophys Res Lett*. (1994) **21**:2915. doi: 10.1029/94GL01284
17. Elwakil SA, El-hanbaly AM, El-Shewy EK, El-Kamash IS. Electron acoustic soliton energy of the Kadomtsev-Petviashvili equation in the Earth's magnetotail region at critical ion density. *Astrophys Space Sci*. (2014) **349**:197–203. doi: 10.1007/s10509-013-1613-0
18. Aliyu AI, Li Y, Qi L, Inc M, Baleanu D, Alshomrani AS. Lump-type and bell-shaped soliton solutions of the time-dependent coefficient Kadomtsev-Petviashvili equation. *Front Phys*. (2020) **7**:242. doi: 10.3389/fphy.2019.00242
19. Abdo NF. Effect of non Maxwellian distribution on the dressed electrostatic wave and energy properties. *J Taibah Univ Sci*. (2017) **11**:617–22. doi: 10.1016/j.jtusci.2016.06.001
20. El-Shewy EK, Abdelwahed HG, Abdo NF, Yousef MS. On the modulation of ionic velocity in electron-positron-ion plasmas. *J Taibah Univ Sci*. (2017) **11**:1267–74. doi: 10.1016/j.jtusci.2017.03.003
21. Alharbi AR, Almatrafi MB. Numerical investigation of the dispersive long wave equation using an adaptive moving mesh method and its stability. *Results Phys*. (2020) **16**:1028702. doi: 10.1016/j.rinp.2019.102870
22. Alharbi AR, Abdelrahman MAE, Almatrafi MB. Analytical and numerical investigation for the DMBBM equation. *Comput Model Eng Sci*. (2020) **122**:743–56. doi: 10.32604/cmes.2020.07996
23. Abdelrahman MAE, Almatrafi MB, Alharbi AR. Fundamental solutions for the coupled KdV system and its stability. *Symmetry*. (2020) **12**:429. doi: 10.3390/sym12030429
24. Abdelrahman MAE, Sohaly MA. The development of the deterministic nonlinear PDEs in particle physics to stochastic case. *Results Phys*. (2018) **9**:344–50. doi: 10.1016/j.rinp.2018.02.032
25. Abdelrahman MAE, Sohaly MA. On the new wave solutions to the MCH equation. *Indian J Phys*. (2019) **93**:903–11. doi: 10.1007/s12648-018-1354-6
26. Abdelrahman MAE, Sohaly MA. Solitary waves for the nonlinear Schrödinger problem with the probability distribution function in stochastic input case. *Eur Phys J Plus*. (2017) **132**:339. doi: 10.1140/epjp/i2017-11607-5
27. Abdelrahman MAE, Moaaz O. New exact solutions to the dual-core optical fibers. *Indian J Phys*. (2019) **94**:705–11. doi: 10.1007/s12648-019-01503-w
28. Abdelrahman MAE, Sohaly MA, Alharbi A. The new exact solutions for the deterministic and stochastic (2+1)-dimensional equations in natural sciences. *J Taibah Univ Sci*. (2019) **13**:834–43. doi: 10.1080/16583655.2019.1644832
29. Wazwaz AM. A sine-cosine method for handling nonlinear wave equations. *Math Comput Model*. (2004) **40**:499–508. doi: 10.1016/j.mcm.2003.12.010
30. Baskonus HM, Bulut H. New wave behaviors of the system of equations for the ion sound and Langmuir waves. Waves Random Complex Media. (2016) **26**:613–25. doi: 10.1080/17455030.2016.1181811
31. Liu C. Exact solutions for the higher-order nonlinear Schrödinger equation in nonlinear optical fibres. *Chaos Solit Fract*. (2005) **23**:949–55. doi: 10.1016/S0960-0779(04)00345-5
32. Zhang S. Exp-function method for solving Maccari's system. *Phys Lett A*. (2007) **371**:65–71. doi: 10.1016/j.physleta.2007.05.091
33. El Achab A, Amine A. A construction of new exact periodic wave and solitary wave solutions for the 2D Ginzburg-Landau equation. *Nonlinear Dyn*. (2017) **91**:995–9. doi: 10.1007/s11071-017-3924-0
34. Hosseini K, Kumar D, Kaplan M, Bejarbaneh EY. New exact traveling wave solutions of the unstable nonlinear Schrödinger equations. *Commun Theor Phys*. (2017) **68**:761–7. doi: 10.1088/0253-6102/68/6/761
35. Bulut H, Sulaiman TA, Baskonus HM. Optical solitons to the resonant nonlinear Schrödinger equation with both spatio-temporal and inter-modal dispersions under Kerr law nonlinearity. *Optik*. (2018) **163**:49–55. doi: 10.1016/j.ijleo.2018.02.081
36. Yang XF, Deng ZC, Wei Y. A Riccati-Bernoulli sub-ODE method for nonlinear partial differential equations and its application. *Adv Differ Equat*. (2015) **1**:117–33. doi: 10.1186/s13662-015-0452-4
37. Shang Y. A Lie algebra approach to susceptible-infected-susceptible epidemics. *Electron J Differ Equat*. (2012) **2012**:1–7.
38. Shang Y. Lie algebraic discussion for affinity based information diffusion in social networks. *Open Phys*. (2017) **15**:705–11. doi: 10.1515/phys-2017-0083

Conflict of Interest: The authors declare that the research was conducted in the absence of any commercial or financial relationships that could be construed as a potential conflict of interest.

frontiers in Physics

ORIGINAL RESEARCH
published: 08 October 2020
doi: 10.3389/fphy.2020.00293

An Efficient Numerical Technique for Solving Time-Fractional Generalized Fisher's Equation

Abdul Majeed[1], *Mohsin Kamran*[1], *Muhammad Abbas*[2]* *and Jagdev Singh*[3]

[1] Division of Science and Technology, Department of Mathematics, University of Education Lahore, Lahore, Pakistan, [2] Department of Mathematics, University of Sargodha, Sargodha, Pakistan, [3] Department of Mathematics, Jaipur Engineering College & Research Centre (JECRC) University, Jaipur, India

This paper extends the existing Fisher's equation by adding the source term and generalizing the degree β of the non-linear part. A numerical solution of a modified Fisher's equation for different values of β using the cubic B-spline collocation scheme is also investigated. The fractional derivative in a time dimension is discretized in Caputo's form based on the $L1$ formula, while cubic B-spline basis functions are used to interpolate the spatial derivative. The non-linear part in the model is linearized by the modified formula. The efficiency of the proposed scheme is examined by simulating four test examples with different initial and boundary conditions. The effect of different parameters is discussed and presented in tables and graphics form. Moreover, by using the Von Neumann stability formula, the proposed scheme is shown to be unconditionally stable. The results of error norms reflect that the present scheme is suitable for non-linear time fractional differential equations.

Keywords: cubic B-spline (CBS) collocation scheme, time fractional modified Fisher equation, Caputo derivative, stability analysis, error norms

OPEN ACCESS

Edited by:
Xiao-Jun Yang,
China University of Mining and Technology, China

Reviewed by:
Haci Mehmet Baskonus,
Harran University, Turkey
Harendra Singh,
Indian Institute of Technology (BHU), India

***Correspondence:**
Muhammad Abbas
muhammad.abbas@uos.edu.pk

Specialty section:
This article was submitted to Mathematical and Statistical Physics, a section of the journal Frontiers in Physics

Received: *17 March 2020*
Accepted: *29 June 2020*
Published: *08 October 2020*

Citation:
Majeed A, Kamran M, Abbas M and Singh J (2020) An Efficient Numerical Technique for Solving Time-Fractional Generalized Fisher's Equation. Front. Phys. 8:293. doi: 10.3389/fphy.2020.00293

1. INTRODUCTION

Fractional calculus-based models have been used in different fields of engineering and science. In the last few years, fractional differential equations have been widely used. The main advantage of using fractional order differential equation is its non-local property in mathematical modeling. During the twentieth century, the authors [1–3] added a significant amount of research in the area of fractional calculus. The applications can be seen in different branches of science and engineering, such as finance [4], nano-technology [5], electrodynamics [6], and visco-elasticity. Fisher's equation is commonly used in epidemics and bacteria, branching Brownian motion, neolithic transitions and chemical kinetics [7–9]. The spatial and temporal propagation of a virile gene in an infinite medium has been explained by Fisher [10]. Several numerical methods for differential equations with Riemann-Liouville and Caputo sense fractional order derivatives have been applied and analyzed [11–13].

The time-fractional Fisher's equation used in Baranwal et al. [14] has been modified in this paper in two different ways: (1) by introducing the source term or (2) by generalizing the non-linear power.

The modified form of time fractional Fisher's equation is:

$$\frac{\partial^\alpha Z(r,t)}{\partial t^\alpha} - \nu\frac{\partial^2 Z(r,t)}{\partial r^2} - Z(r,t)(1-Z^\beta(r,t)) = f(r,t),\ \ a \le r \le b,\ \ 0 < \alpha \le 1,\ \ t \ge 0, \quad (1.1)$$

with the initial condition

$$Z(r,0) = \psi(r), \qquad a \le r \le b, \quad (1.2)$$

and the boundary conditions

$$Z(a,t) = \psi_1(t), \quad Z(b,t) = \psi_2(t), \qquad t \ge 0, \quad (1.3)$$

where ν is a parameter of viscosity.
The Caputo and Riemann-Liouville fractional derivatives have a wide range of applications [15–17]. The Caputo derivative is used in this work:

$$\frac{\partial^\alpha Z(r,t)}{\partial t^\alpha} = \begin{cases} \frac{1}{\Gamma(q-a)}\int_0^t \frac{\partial^q Z(r,s)}{\partial t^q}(t-s)^{q-\alpha-1}ds, & q-1 < \alpha < q, \\ \frac{\partial^q Z(r,t)}{\partial t^q}, & q = \alpha. \end{cases}$$

The Caputo derivative is discretized by the $L1$ formula [18]:

$$\left.\frac{\partial^\alpha h}{\partial t^\alpha}\right| t_n = \frac{1}{(\Delta t)^\alpha \Gamma(2-\alpha)}\sum_{k=0}^{n-1}\lambda_k^\alpha [h(t_{n-k}) - h(t_{n-k-1})] + O(\Delta t), \quad (1.4)$$

where $\lambda_k = (k+1)^{1-\alpha} - k^{1-\alpha}$.

In this paper, we generalized the linearization formula used in [19]:

$$(Z^\beta)_j^{n+1} = \beta Z_j^{n+1}(Z^{\beta-1})_j^n - (\beta-1)(Z^\beta)_j^n, \quad (1.5)$$

where β is a positive integer.

The numerical and analytical solution of fractional order PDEs play an important role in explaining the characteristics of non-linear problems that arise in everyday life. In the literature, researchers applied various techniques for the numerical solutions of Fisher's equation. Baranwal et al. [14] introduced an analytic algorithm for solving non-linear time-fractional reaction diffusion equations based on the variational iteration method (VIM) and Adomian decomposition method (ADM). Wazwaz and Gorguis [20] implemented ADM for the analytic study of Fisher's equation. Homotopy perturbation sumudu transform method has been applied for solving fractional non-linear dispersive equations by Abedle-Rady et al. [21]. Gupta and Saha Ray [22] implemented two methods. Haar wavelet method and the optimal homotopy asymptotic method (OHAM) for the numerical solutions of arbitrary order PDE, such as Burger-Fisher's and generalized Fisher's equations. Cherif et al. [23] solved space-fractional Fisher's equation using classical HPM. Khader and Saad [24] proposed a numerical solution for solving the space-fractional Fisher's equation using Chebyshev spectral collocation technique. Rawashdeh [25] introduced the fractional natural decomposition method (FNDM) to find the analytical and approximate solutions of the non-linear time-fractional Harry Dym equation and the non-linear time-fractional Fisher's equation. Singh [26] introduced an efficient computational method for the approximate solution of a non-linear Lane-Emden-type equation. The numerical solution of fractional vibration equation of large membrane has been investigated in Singh [27] by Jacobi polynomial. The authors in [28] employed the cubic B-spline method for the numerical simulations of time fractional Burgers' and Fisher's equation. Singh et al. [29] constructed a q-homotopy analysis transform method for solving time and space-fractional coupled Burgers' equation. Najeeb et al. [30] used HPM for the analytical solution of time-fractional reaction-diffusion equation. Majeed et al. [28] used B-spline at non-uniform for the construction of craniofacial fractures.

In this paper, we have presented a cubic B-spline (CBS) algorithm for numerical simulation of the time-fractional generalized Fisher's equation. Caputo's time fractional derivative based on the $L1$ scheme has been discretized by finite difference formula, whereas spatial derivatives are discretized by CBS functions. The present approach is novel for the numerical results of fractional order PDEs and, to the best of our knowledge, any spline solution of the time-fractional generalized Fisher's equation has never yet been studied. Moreover, this scheme is equally effective for homogeneous and non-homogeneous boundary conditions.

This article has been presented in the following manner. Section 2 evolves a brief description of temporal discretization, cubic B-spline functions and spatial discretization. In section 4, the stability of the proposed algorithm has been discussed. The discussion on numerical results of four test problems has been reported in section 5. Concluding remarks of this work are given in section 6.

2. DESCRIPTION OF THE METHOD

Let us consider the interval $[a,b]$ is sub divided into N finite elements of equal spacing h determined by the knots r_j, $j = 0,1,2,3.....,N$ such that $a = r_0 < r_1 < r_2 \ldots < r_{N-1} < r_N = b$. The cubic B-spline basis function at the grid points is defined as

$$\phi_j(r) = \frac{1}{6h^3}\begin{cases} (r-r_j)^3, & \text{if } r \in [r_j, r_{j+1}), \\ h^3 + 3h^2(r-r_{j+1}) & \\ +3h(r-r_{j+1})^2 - 3(r-r_{j+1})^3, & \text{if } r \in [r_{j+1}, r_{j+2}], \\ h^3 + 3h^2(r_{j+3}-r) & \\ +3h(r_{j+3}-r)^2 - 3(r_{j+3}-r)^3, & \text{if } r \in [r_{j+2}, r_{j+3}], \\ (r_{j+4}-r)^3, & \text{if } r \in [r_{j+3}, r_{j+4}). \end{cases} \quad (2.1)$$

From the above basis, the approximation solution $Z_N(r,t)$ can be written in terms of linear combination of cubic B-spline base function as follows

$$Z_N(r,t) = \sum_{j=-1}^{N+1}\Upsilon_j(t)\phi_j(r), \quad (2.2)$$

where $\Upsilon_j(t)'s$ are the unknowns to be determined. Four consecutive cubic B-splines are used to construct each element $[r_j, r_{j+1}]$. The values of cubic B-splines and its derivatives at the

TABLE 1 | Coefficients of CBS and its derivative at the nodes r_j.

$Z_N(r,t)$	Υ_{j-1}	Υ_j	Υ_{j+1}
$Z_j = Z(r_j)$	$\frac{1}{6}$	$\frac{4}{6}$	$\frac{1}{6}$
$Z'_j = Z'(r_j)$	$\frac{-1}{2h}$	0	$\frac{1}{2h}$
$Z''_j = Z''(r_j)$	$\frac{1}{h^2}$	$\frac{-2}{h^2}$	$\frac{1}{h^2}$

nodal points are given in **Table 1**. The variation of $Z_N(r,t)$ over the typical component $[r_j, r_{j+1}]$ is given by

$$Z_N(r_j,t_n) = \sum_{m=j-1}^{j+1} \Upsilon_m(t)\phi_m(r_m). \tag{2.3}$$

By plugging the approximation values given in **Table 1** into Equation (2.3) at (r_j, t_n), The Equation (1.1) yields the following set of fractional order ordinary differential equations.

$$\begin{aligned}&[(\Upsilon^{\bullet}_{j-1}(t) + 4\Upsilon^{\bullet}_{j}(t) + \Upsilon^{\bullet}_{j+1}(t))/6] - \frac{\nu}{h^2}[\Upsilon_{j-1} - 2\Upsilon_j + \Upsilon_{j+1}]\\ &-[(\Upsilon_{j-1} + 4\Upsilon_j + \Upsilon_{j+1})/6][1 - ((\Upsilon_{j-1} + 4\Upsilon_j + \Upsilon_{j+1})/6)^{\beta}]\\ &= f(r_j,t_n).\end{aligned} \tag{2.4}$$

Here, $\bullet$ represents αth order fractional derivative with respect to time. After some simplification, a recurrence relation for Equation (1.1) with $\beta = 3$ can be written as

$$\begin{aligned}&\Upsilon^{n+1}_{j-1}\left[\frac{\gamma}{6} - \frac{1}{2h^2} - \frac{1}{12} + \frac{2}{1296}(T_m)^3\right]\\ &+\Upsilon^{n+1}_{j}\left[\frac{4\gamma}{6} + \frac{1}{h^2} - \frac{1}{3} + \frac{8}{1296}(T_m)^3\right]\\ &+\Upsilon^{n+1}_{j+1}\left[\frac{\gamma}{6} - \frac{1}{2h^2} - \frac{1}{12} + \frac{2}{1296}(T_m)^3\right]\\ &= \Upsilon^{n}_{j-1}\left[\frac{\gamma}{6} + \frac{1}{2h^2} + \frac{1}{12}\right] + \Upsilon^{n}_{j}\left[\frac{4\gamma}{6} - \frac{1}{h^2} + \frac{1}{3}\right]\\ &+\Upsilon^{n}_{j+1}\left[\frac{\gamma}{6} + \frac{1}{2h^2} + \frac{1}{12}\right] - \frac{1}{1296}(T_m)^4 + f(r_j,t_n)\\ &-\left(\gamma\sum_{k=0}^{n-1}\lambda_k[((\Upsilon^{n-k-1}_{j-1} - \Upsilon^{n-k}_{j-1}) + 4(\Upsilon^{n-k-1}_{j} - \Upsilon^{n-k}_{j})\right.\\ &\left.+(\Upsilon^{n-k-1}_{j+1} - \Upsilon^{n-k}_{j+1}))/6] + \rho^{n+1}_{\Delta t}\right),\end{aligned} \tag{2.5}$$

where $\lambda_k = [(k+1)^{1-\alpha} - k^{1-\alpha}]$, $T_m = \Upsilon^n_{j-1} + 4\Upsilon^n_j + \Upsilon^n_{j+1}$, $\gamma = \frac{(\Delta t)^{-\alpha}}{\Gamma(2-\alpha)}$. Moreover, the truncation error $\rho^{n+1}_{\Delta t}$ is bounded as

$$|\rho^{n+1}_{\Delta t}| \le \varpi(\Delta t)^{2-\alpha}, \tag{2.6}$$

where ϖ is a real constant.

Lemma 2.1. *The coefficients λ_k in (2.5) possess the following characteristics* [31]*:*

- $\lambda_k > 0$ *and* $\lambda_0 = 1$, $k = 1:1:n$,
- $\lambda_0 > \lambda_1 > \lambda_2 > ... > \lambda_k, \lambda_k \to 0$ *as* $k \to \infty$,
- $\sum_{k=0}^{n}(\lambda_k - \lambda_{k+1}) + \lambda_{n+1} = (1-\lambda_1) + \sum_{k=1}^{n-1}(\lambda_k - \lambda_{k+1}) + \lambda_n = 1$.

Equation (2.5) is modified as

$$\begin{aligned}\Upsilon^{n+1}_{j-1}\alpha_0 \;&+\; \Upsilon^{n+1}_{j}\alpha_1 + \Upsilon^{n+1}_{j+1}\alpha_0 = \Upsilon^{n}_{j-1}(n_1) + \Upsilon^{n}_{j}(n_2)\\ &+\; \Upsilon^{n}_{j+1}(n_1) - \frac{1}{1296}(T_m)^4 + f(r_j,t_n)\\ &-\left(\gamma\sum_{k=1}^{n-1}\lambda_k[((\Upsilon^{n-k-1}_{j-1} - \Upsilon^{n-k}_{j-1}) + 4(\Upsilon^{n-k-1}_{j} - \Upsilon^{n-k}_{j})\right.\\ &+\; \left.(\Upsilon^{n-k-1}_{j+1} - \Upsilon^{n-k}_{j+1}))/6] + \rho^{n+1}_{\Delta t}\right),\end{aligned} \tag{2.7}$$

where $\alpha_0 = \frac{\gamma}{6} - \frac{1}{2h^2} - \frac{1}{12} + \frac{2}{1296}(T_m)^3$, $\alpha_1 = \frac{4\gamma}{6} + \frac{1}{h^2} - \frac{1}{3} + \frac{8}{1296}(T_m)^3$, $n_1 = \frac{\gamma}{6} + \frac{1}{2h^2} + \frac{1}{12}$ and $n_2 = \frac{4\gamma}{6} - \frac{1}{h^2} + \frac{1}{3}$

From (2.7), the system of $N+1$ linear equation with $N+3$ unknown parameters $(\Upsilon_{-1}, \Upsilon_0, \Upsilon_1, \ldots, \Upsilon_{N+1})^T$ can be obtained. To acquire unique solution of the system, two extra equations are needed. For this purpose, given boundary conditions are used. Thus, the system of linear equations for expression (2.7) becomes

$$PY^{n+1} = QY^n. \tag{2.8}$$

$$Y^n = (\Upsilon^n_{-1}, \Upsilon^n_0, \Upsilon^n_1, \ldots, \Upsilon^n_{N+1})^T.$$

where

$$P = \begin{bmatrix} \frac{1}{6} & \frac{4}{6} & \frac{1}{6} & 0 & \cdots & 0 & 0 & 0\\ \alpha_0 & \alpha_1 & \alpha_0 & 0 & \cdots & 0 & 0 & 0\\ \vdots & \vdots & \vdots & \vdots & \ddots & \vdots & \vdots & \vdots\\ 0 & 0 & 0 & 0 & \cdots & \alpha_0 & \alpha_1 & \alpha_0\\ 0 & 0 & 0 & 0 & \cdots & \frac{1}{6} & \frac{4}{6} & \frac{1}{6} \end{bmatrix}. \tag{2.9}$$

3. INITIAL VECTOR

For the initial vector, the initial and boundary conditions of the problem under consideration will help to compute the initial vector $Y^0 = (\Upsilon^0_{-1}, \Upsilon^0_0, \Upsilon^0_1, \ldots, \Upsilon^0_{N+1})^T$. The approximation (2.2) therefore becomes

$$Z_N(r,0) = \sum_{j=-1}^{N+1} \Upsilon_j(0)\phi_j(r).$$

To determine Υ^0, the approximation for the derivatives of the initial and boundary conditions is as follows [32]:

- $(Z_r)^k_j = g'(r_j)$ for $j = 0,\ N$
- $(Z)^0_j = g(r_j)$ for $j = 0, 1, 2, ..., N$

This gives the following $(N+3)\times(N+3)$ matrix system:

$$\begin{bmatrix} \frac{-1}{2h} & 0 & \frac{1}{2h} & 0 & \cdots & 0 & 0 & 0\\ \frac{1}{6} & \frac{4}{6} & \frac{1}{6} & 0 & \cdots & 0 & 0 & 0\\ \vdots & \vdots & \vdots & \vdots & \ddots & \vdots & \vdots & \vdots\\ 0 & 0 & 0 & 0 & \cdots & \frac{1}{6} & \frac{4}{6} & \frac{1}{6}\\ 0 & 0 & 0 & 0 & \cdots & \frac{-1}{2h} & 0 & \frac{1}{2h} \end{bmatrix} \begin{bmatrix} \Upsilon^0_{-1}\\ \Upsilon^0_0\\ \vdots\\ \Upsilon^0_{N+1} \end{bmatrix} = \begin{bmatrix} g'(r_0)\\ g(r_0)\\ \vdots\\ g(r_N)\\ g'(r_N) \end{bmatrix}$$

4. STABILITY ANALYSIS

The von Neumann analysis is frequently used to determine the requirements of stability, as it is usually simple to apply in a simple way. The solution in single Fourier mode is defined as

$$\Upsilon_j^n = \Upsilon^k e^{i\eta jh}, \tag{4.1}$$

where $i = \sqrt{-1}$. The approximation solution of generalized Fisher's equation (2.7) can be written as

$$\begin{aligned}\Upsilon_{j-1}^{n+1}(\alpha_0) + \Upsilon_j^{n+1}(\alpha_1) + \Upsilon_{j+1}^{n+1}(\alpha_0) &= \Upsilon_{j-1}^n(n_1) + \Upsilon_j^n(n_2) \\ &+ \Upsilon_{j+1}^n(n_3) - \frac{1}{1296}(T_m)^4 \\ &+ f(r_j, t_n) - \gamma \sum_{k=1}^{n-1} \lambda_k^\alpha [((\Upsilon_{j-1}^{n-k+1} - \Upsilon_{j-1}^{n-k}) \\ &+ 4(\Upsilon_j^{n-k+1} - \Upsilon_j^{n-k}) + (\Upsilon_{j+1}^{n-k+1} - \Upsilon_{j+1}^{n-k}))/6].\end{aligned} \tag{4.2}$$

where $n_1 = \frac{\gamma}{6} + \frac{1}{2h^2} + \frac{1}{12}$, $n_2 = \frac{4\gamma}{6} - \frac{1}{h^2} + \frac{1}{3}$, $n_3 = \frac{\gamma}{6} + \frac{1}{2h^2} + \frac{1}{12}$, $T_m = \Upsilon_{i-1}^n + 4\Upsilon_i^n + \Upsilon_{i+1}^n$.
Substituting (4.1) into (4.2), we get

$$\begin{aligned}&\Upsilon^{k+1} e^{i\eta(j-1)h}(\alpha_0) + \Upsilon^{k+1} e^{i\eta(j)h}(\alpha_1) + \Upsilon^{k+1} e^{i\eta(j+1)h}(\alpha_0) \\ &= \Upsilon^k e^{i\eta(j-1)h}(n_1) \\ &+ \Upsilon^k e^{i\eta(j)h}(n_2) + \Upsilon^k e^{i\eta(j+1)h}(n_3) - \frac{1}{1296}(T_m)^4 + f(r,t) \\ &- \sum_{k=1}^{n-1} \lambda_k^\alpha [((\Upsilon^{n-k+1} e^{i\eta(j-1)h} \\ &- \Upsilon^{n-k} e^{i\eta(j-1)h}) + 4(\Upsilon^{n-k+1} e^{i\eta(j)h} - \Upsilon^{n-k} e^{i\eta(j)h}) \\ &+ (\Upsilon^{n-k+1} e^{i\eta(j+1)h} - \Upsilon^{n-k} e^{i\eta(j+1)h}))/6].\end{aligned}$$

$$\begin{aligned}&\Upsilon^{k+1}[e^{i\eta(j-1)h}(\alpha_0) + e^{i\eta(j)h}(\alpha_1) + e^{i\eta(j+1)h}(\alpha_0)] \\ &= \Upsilon^k [e^{i\eta(j-1)h}(n_1) + e^{i\eta(j)h}(n_2) \\ &+ e^{i\eta(j+1)h}(n_3)] - \frac{1}{1296}(T_m)^4 + f(r,t) \\ &- \sum_{k=1}^{n-1} \lambda_k^\alpha [(\Upsilon^{n-k+1} e^{i\eta(j-1)h} - \Upsilon^{n-k} e^{i\eta(j-1)h} \\ &+ 4\Upsilon^{n-k+1} e^{i\eta(j)h} - 4\Upsilon^{n-k} e^{i\eta(j)h} + \Upsilon^{n-k+1} e^{i\eta(j+1)h} \\ &- \Upsilon^{n-k} e^{i\eta(j+1)h})/6].\end{aligned}$$

$$\begin{aligned}\Upsilon^{k+1} = &\frac{\Upsilon^k e^{i\eta(j)h}[e^{-i\eta h}(n_1) + n_2 + e^{i\eta h}(n_3)] - \frac{1}{1296}(T_m)^4 e^{-i\eta jh} + f(r,t)e^{-i\eta jh}}{e^{i\eta(j)h}[e^{-i\eta h}(\alpha_0) + \alpha_1 + e^{i\eta h}(\alpha_0)]} \\ &- \frac{\sum_{k=1}^{n-1} \lambda_k^\alpha [\Upsilon^{n-k+1} e^{i\eta jh}(e^{-i\eta h} + 4 + e^{i\eta h}) - \Upsilon^{n-k} e^{-i\eta jh}(e^{-i\eta h} + 4 + e^{i\eta h})]}{e^{i\eta(j)h}[e^{-i\eta h}(\alpha_0) + \alpha_1 + e^{i\eta h}(\alpha_0)]}.\end{aligned}$$

By inserting values of α_0, α_1 and n_1, n_2, n_3 in above expression, we have

$$\begin{aligned}\Upsilon^{k+1} = &\frac{\Upsilon^k[\frac{\gamma}{3}(\cos\eta h + 3) + \frac{1}{6h^2}(\cos\eta h - 6) + \frac{1}{6}(\cos\eta h + 2)] - \frac{1}{1296}(T_m)^4 e^{-i\eta jh}}{\frac{\gamma}{3}(\cos\eta h + 3) - \frac{1}{6h^2}(\cos\eta h - 6) - \frac{1}{6}(\cos\eta h + 2) + \frac{3}{216}(T_m)^2(\cos\eta h + 3)} \\ &+ \frac{f(r,t)e^{-i\eta jh} - \sum_{k=1}^{n-1} \lambda_k^\alpha [2\cos\eta h + 4(\Upsilon^{n-k+1} - \Upsilon^{n-k})]}{\frac{\gamma}{3}(\cos\eta h + 3) - \frac{1}{6h^2}(\cos\eta h - 6) - \frac{1}{6}(\cos\eta h + 2) + \frac{3}{216}(T_m)^2(\cos\eta h + 3)}.\end{aligned}$$

The applied scheme is stable if augment factor $|\Upsilon^{k+1}| \leq 1$, and, from the above expression, we can observe that value of numerator is lesser than denominator for the values of γ, η, h. The scheme become unstable as the approximations grows in magnitude.

$$\Upsilon^{k+1} \leq \Upsilon^k,$$

$$\Upsilon^{k+1} \leq 1.$$

The above result thus reflects that scheme is unconditionally stable.

5. APPLICATIONS AND DISCUSSION

This section presents some examples with different initial and boundary conditions. The numerical results are presented graphically and numerically in figures and tables. The error norms L^2 and L^∞ are computed to analyze the precision of the suggested technique as

$$L^2 = \| Z_{exact} - Z_{approx} \|_2 \simeq \sqrt{h \sum_{j=0}^{n} | (Z_j)_{exact} - (Z_j)_{approx} |^2},$$

$$L^\infty = \| Z_{exact} - Z_{approx} \|_\infty \simeq max_j | (Z_j)_{exact} - (Z_j)_{approx} | .$$

In this manuscript we used, MATLAB 2015b on $Intel^R CORE^{TM} i5$ CPU with 8GB RAM and 64-bit operating system (window 7) for numerical simulations.

Example 5.1. Consider the fractional order Fisher's equation (1.1) for $\beta = 3$ subject to

$$\frac{\partial^\alpha Z(r,t)}{\partial t^\alpha} - \nu \frac{\partial^2 Z(r,t)}{\partial r^2} - Z(r,t)(1 - Z^3(r,t)) = f(r,t). \tag{5.1}$$

$$IC: \; Z(r,0) = 0, \quad 0 \leq r \leq 1.$$

$$BCs: \; Z(0,t) = t^{2\alpha}, \quad Z(1,t) = 0, \quad t \geq 0.$$

and the source term

$$\begin{aligned}f(r,t) = \exp(2r)(1 - r^2)t^\alpha \frac{\Gamma(2\alpha + 1)}{\Gamma(1 + \alpha)} - 2\nu t^{2\alpha}(1 - 4r - 2r^2)\exp(2r) \\ -[t^{2\alpha}(1 - r^2)\exp(2r)][1 - (t^{2\alpha}(1 - r^2)\exp(2r))^3].\end{aligned}$$

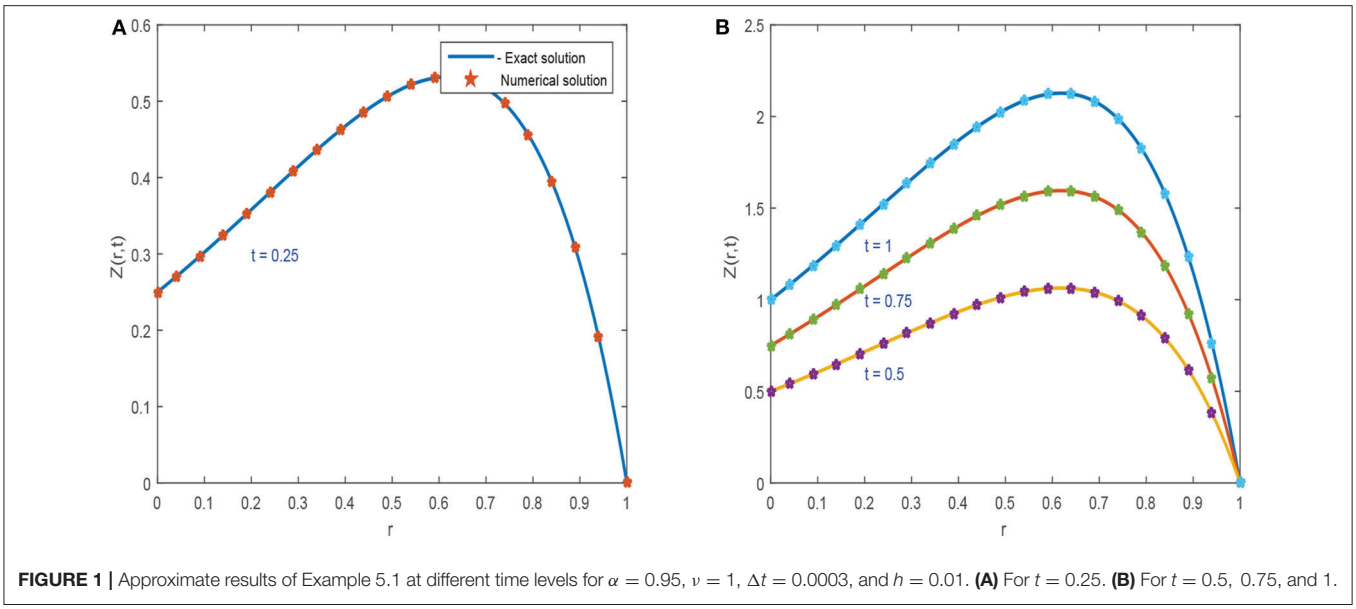

FIGURE 1 | Approximate results of Example 5.1 at different time levels for $\alpha = 0.95$, $\nu = 1$, $\Delta t = 0.0003$, and $h = 0.01$. **(A)** For $t = 0.25$. **(B)** For $t = 0.5,\ 0.75$, and 1.

The approximate solution (2.3) can be written in piecewise form:

$$Z(r,t_n) = \Upsilon_{j-3}\phi_{3,j-3}(r) + \Upsilon_{j-2}\phi_{3,j-2}(r) + \Upsilon_{j-1}\phi_{3,j-1}(r) + \Upsilon_j\phi_{3,j}(r), \qquad r \in [r_j, r_{j+1}). \quad (5.2)$$

$$Z_N(r,1) = \begin{cases} r^3 - 0.64r^2 - 0.805r + 0.99997, & r \in [0, 0.1), \\ 0.56667r^3 - 0.51r^2 - 0.818r + 1.0004, & r \in [0.1, 0.2), \\ 16.75r^3 - 10.22r^2 + 1.124r + 0.87093, & r \in [0.2, 0.3), \\ 0.11667r^3 - 0.195r^2 - 0.8945r + 1.0068, & r \in [0.3, 0.4), \\ -0.033333r^3 - 0.015r^2 - 0.9665r + 1.0165, & r \in [0.4, 0.5), \\ -0.066667r^3 + 0.035r^2 - 0.9915r + 1.0206, & r \in [0.5, 0.6), \\ -0.05r^3 + 0.005r^2 - 0.9735r + 1.017, & r \in [0.6, 0.7), \\ -0.033333r^3 - 0.03r^2 - 0.949r + 1.0113, & r \in [0.7, 0.8), \\ -3546.6r^3 + 8511.7r^2 - 6810.3r + 1816.8, & r \in [0.8, 0.9), \\ 10640.0r^3 - 29793.0r^2 + 27664.0r - 8525.4, & r \in [0.9, 1). \end{cases} \quad (5.3)$$

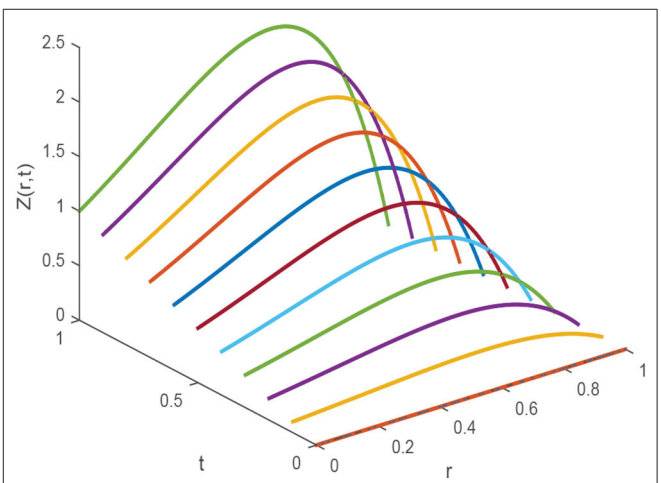

FIGURE 2 | 3D image of numerical solution of Example 5.1 for $t \in [0, 1]$, $\alpha = 0.25$, $\nu = 1$, $\Delta t = 0.0003$, and $h = 0.01$.

The exact solution of (5.1) is $Z(r,t) = t^{2\alpha}(1 - r^2)\exp(2r)$.

Figures 1, **2** explores the comparison of CBS solution with exact solution for Example 5.1 for different parameters. **Figure 1A** shows the 2-dimensional preview of approximate and exact results for $t = 0.25$ with $\alpha = 0.95$, $h = 0.01$, $\Delta t = 0.0003$ and $\nu = 1$. The graph illustrates that exact and approximate outcomes are indiscriminately similar to each other. **Figure 1B** cites the action of solution obtained for Equation (5.1) with $\alpha = 0.95$, $h = 0.01$, $\nu = 1$ and for various time steps $t = 0.5$, 0.75, and 1 with $\Delta t = 0.0003$. It is clear from the graph that both solutions are overlapping. Three dimensional preview has been given in **Figure 2**. While the influence of α has been discussed for distinct Brownian motion, i.e, $\alpha = 0.25$, 0.5, and 0.98 in **Figure 3**. It can be observed that as the value of α increases, the solution profile decreases and as $\alpha \to 1$, the numerical solution tends to overlap the exact solution. The comparison of numerical and exact outcomes is expressed in **Table 2**, which shows that both results are consistent with each other and are accurate up to 5 decimal places. The numerical results for α variation is presented in **Table 3**. It is clear from tabular data that both results strongly agree with each other, and the accuracy of the scheme is examined by the error norms as shown in **Table 4**.

Example 5.2. The fractional order Fisher's equation (1.1) for $\beta = 3$ can be written as:

$$\frac{\partial^\alpha Z(r,t)}{\partial t^\alpha} - \nu\frac{\partial^2 Z(r,t)}{\partial r^2} - Z(r,t)(1 - Z^3(r,t)) = f(r,t). \quad (5.4)$$

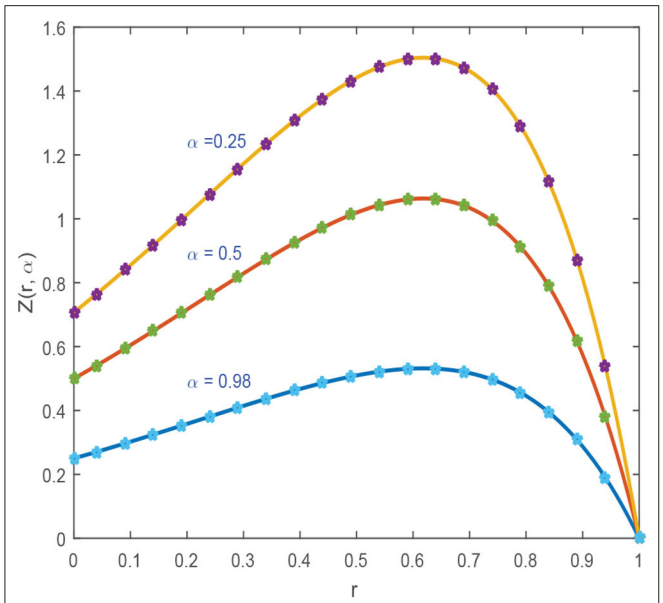

FIGURE 3 | Numerical solution of Example 5.1 for various values of $\alpha = 0.25,\ 0.5,$ *and* $0.98,\ \nu = 1,\ \Delta t = 0.0003$, and $h = 0.01$.

TABLE 2 | The comparison of results for Example 5.1 at different time level.

$t = 0.5$		$t = 0.75$		$t = 1$	
Exact	**Approximate**	**Exact**	**Approximate**	**Exact**	**Approximate**
0.5	0.5	0.750	0.750	1	1
0.5937599	0.5937573	0.89063992	0.8906763	1.1875199	1.1875187
0.7047480	0.7047441	1.05712208	1.0571243	1.409496	1.4094943
0.8179162	0.8179136	1.22687444	1.2268714	1.635832	1.6358312
0.9248351	0.9248321	1.38725275	1.3872564	1.849670	1.8496765
1.0123601	1.0123537	1.51854022	1.5185531	2.024720	2.0247276
1.0607632	1.0607532	1.59114490	1.5911456	2.121526	2.1215213
1.0412254	1.0412256	1.56183822	1.5618331	2.082450	2.0824589
0.9124889	0.9124764	1.36873341	1.3687335	1.824977	1.8249795
0.6164085	0.6164432	0.92461286	0.92461257	1.2328171	1.2328141
0	0	0	0	0	0

with

$$IC:\ Z(r,0) = r^2\exp(2r), \quad 0 \le r \le 1.$$

$$BCs:\ Z(0,t) = 0, \quad Z(1,t) = \exp(2)(1+t^2), \quad t \ge 0.$$

source term is

$$f(r,t) = \frac{2r^2t^{2-\alpha}\exp(2r)}{\Gamma(3-\alpha)} - 2\nu(1+t^2)(1+4r+2r^2)\exp(2r) - [(1+t^2)r^2\exp(2r)][1-((1+t^2)r^2\exp(2r))^3].$$

The Exact solution of Example 5.2 is $Z(r,t) = (1+t^2)r^2\exp(2r)$. **Figures 4**, **5** plot the 2D and 3D preview of exact and approximate solutions of Example 5.2. The graph shown in **Figure 4A** demonstrates that the approximate solution at $t = 0.25$, $\alpha = 0.95$, $h = 0.01$, $\Delta t = 0.0003$, and $\nu = 1$ is compatible with exact solution. **Figure 4B** shows the effect of various time steps $t = 0.5,\ 0.75$, and 1 on the solution profile. It is clear from the graphics that exact and numerical solutions have identical behavior for fixed value of $\alpha = 0.95$. The comparison of exact and approximate results is presented in **Table 5**, which clearly shows that both solutions are very close to each other and have negligible errors. **Figure 5** give 3D preview of approximate solution. To examine the accuracy of the present technique, error norms are computed and shown in **Table 6**.

TABLE 3 | The comparison of results for Example 5.1 at different values of α and $t = 0.5$.

$\alpha = 0.25$		$\alpha = 0.5$		$\alpha = 0.98$	
Exact	**Approximate**	**Exact**	**Approximate**	**Exact**	**Approximate**
0.7071067	0.7071043	0.5	0.5	0.25	0.25
0.8397033	0.8397012	0.5937599	0.5937568	0.2968799	0.2968754
0.9966642	0.9966601	0.7047480	0.7047454	0.3523740	0.3523721
1.1567083	1.1567231	0.8179163	0.8179164	0.4089581	0.4089512
1.3079144	1.3079221	0.9248351	0.9248123	0.4624175	0.4624121
1.4316934	1.4316932	1.0123601	1.0123342	0.5061800	0.5061321
1.5001458	1.5001456	1.0607632	1.0607612	0.5303816	0.5303802
1.4725151	1.4725148	1.0412254	1.0412245	0.5206127	0.52061012
1.2904542	1.2904532	0.9124889	0.9124893	0.4562444	0.4562432
0.8717333	0.8717312	0.6164085	0.6164123	0.3082042	0.3082011
0	0	0	0	0	0

TABLE 4 | Computation of error norms for Example 5.1.

t	L^2 *norm*	L^∞ *norm*	**CPU time**
0.5	3.923×10^{-6}	3.470×10^{-5}	0.0821
0.75	2.900×10^{-3}	3.638×10^{-5}	0.1201
1	1.489×10^{-6}	8.900×10^{-6}	0.1601

The approximate solution (2.3) can be written in piecewise form:

$$Z(r,t_n) = \Upsilon_{j-3}\phi_{3,j-3}(r) + \Upsilon_{j-2}\phi_{3,j-2}(r) + \Upsilon_{j-1}\phi_{3,j-1}(r) + \Upsilon_j\phi_{3,j}(r), \qquad r \in [r_j, r_{j+1}). \quad (5.5)$$

$$Z_N(r,1) = \begin{cases} -5.4667r^3 + 0.9700r^2 + 14.08r + 0.000033333, & r \in [0, 0.1), \\ -4.2667r^3 + 0.61r^2 + 14.116r - 0.0011667, & r \in [0.1, 0.2), \\ -221.05r^3 + 130.68r^2 - 11.898r + 1.7331, & r \in [0.2, 0.3), \\ -1.4667r^3 - 1.395r^2 + 14.614r - 0.04415, & r \in [0.3, 0.4), \\ 5.35r^3 - 9.575r^2 + 17.887r - 0.48042, & r \in [0.4, 0.5), \\ -1.6333r^3 + 0.9r^2 + 12.649r + 0.3925, & r \in [0.5, 0.6), \\ 56.233r^3 - 103.26r^2 + 75.145r - 12.107, & r \in [0.6, 0.7), \\ -104.25r^3 + 233.76r^2 - 160.77r + 42.939, & r \in [0.7, 0.8), \\ 587.43r^3 - 1426.3r^2 + 1167.3r - 311.2, & r \in [0.8, 0.9), \\ -1846.6r^3 + 5145.5r^2 - 4747.4r + 1463.2, & r \in [0.9, 1). \end{cases} \quad (5.6)$$

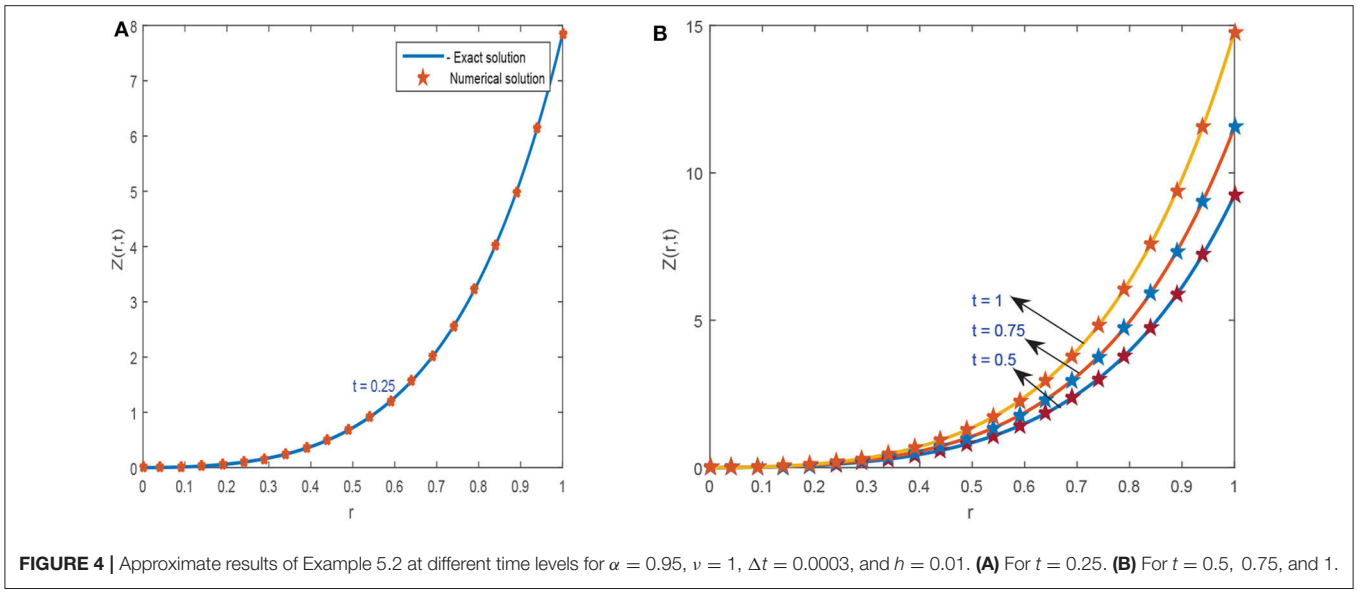

FIGURE 4 | Approximate results of Example 5.2 at different time levels for $\alpha = 0.95$, $\nu = 1$, $\Delta t = 0.0003$, and $h = 0.01$. **(A)** For $t = 0.25$. **(B)** For $t = 0.5,\ 0.75$, and 1.

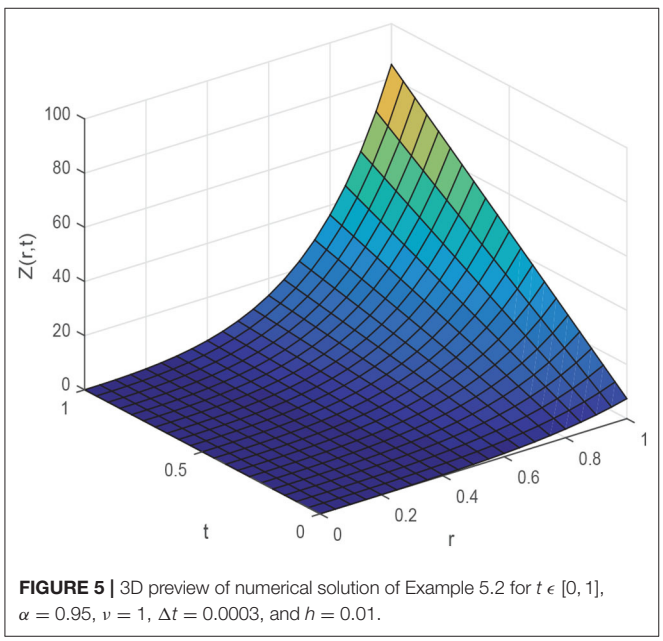

FIGURE 5 | 3D preview of numerical solution of Example 5.2 for $t \in [0, 1]$, $\alpha = 0.95$, $\nu = 1$, $\Delta t = 0.0003$, and $h = 0.01$.

TABLE 5 | Numerical results for Example 5.2.

$t = 0.5$		$t = 0.75$		$t = 1$	
Exact	**Approximate**	**Exact**	**Approximate**	**Exact**	**Approximate**
0	0	0	0	0	0
0.0121218	0.0121321	0.0151522	0.0151433	0.0193949	0.0193932
0.0659855	0.0659843	0.0824819	0.0824654	0.1055769	0.1055759
0.1877572	0.1877576	0.2346966	0.2346753	0.3004116	0.3004116
0.4147524	0.4147527	0.5184405	0.5184425	0.6636038	0.6636021
0.7996699	0.7996642	0.9995874	0.9995841	1.2794718	1.2794717
1.4160595	1.4160543	1.7700744	1.7700722	2.2656953	2.2656943
2.3655633	2.3655421	2.9569541	2.9569543	3.7849013	3.7849021
3.7874724	3.7874722	4.7343405	4.7343421	6.0599558	6.0599533
5.8712990	5.8712976	7.3391238	7.3391242	9.3940785	9.3940752
9.2363201	9.2363212	11.545400	11.545410	14.778112	14.7781113

TABLE 6 | Error norms for Example 5.2.

t	L^2 *norm*	L^∞ *norm*	**CPU time**
0.5	2.49×10^{-6}	2.12×10^{-5}	0.0842
0.75	3.05×10^{-6}	2.13×10^{-5}	0.1252
1	5.105×10^{-7}	3.3×10^{-6}	0.1665

Example 5.3. For $\beta = 2$, the time fractional Fisher's equation becomes

$$\frac{\partial^\alpha Z(r,t)}{\partial t^\alpha} - \nu \frac{\partial^2 Z(r,t)}{\partial r^2} - Z(r,t)(1 - Z^2(r,t)) = f(r,t). \quad (5.7)$$

$$IC:\ Z(r,0) = 0, \quad 0 < r < 1,$$

$$BCs:\ Z(0,t) = 0, \quad Z(1,t) = 0, \quad t \geq 0.$$

The source term

$$f(r,t) = \frac{24t^{4-\alpha}}{\Gamma(5-\alpha)} \sin(2\pi r) + 4\pi^2 t^4 \sin(2\pi r) - (t^4 \sin(2\pi r))(1 - t^4 \sin(2\pi r)).$$

Exact solution for above conditions is

$$Z(r,t) = t^4 \sin(2\pi r).$$

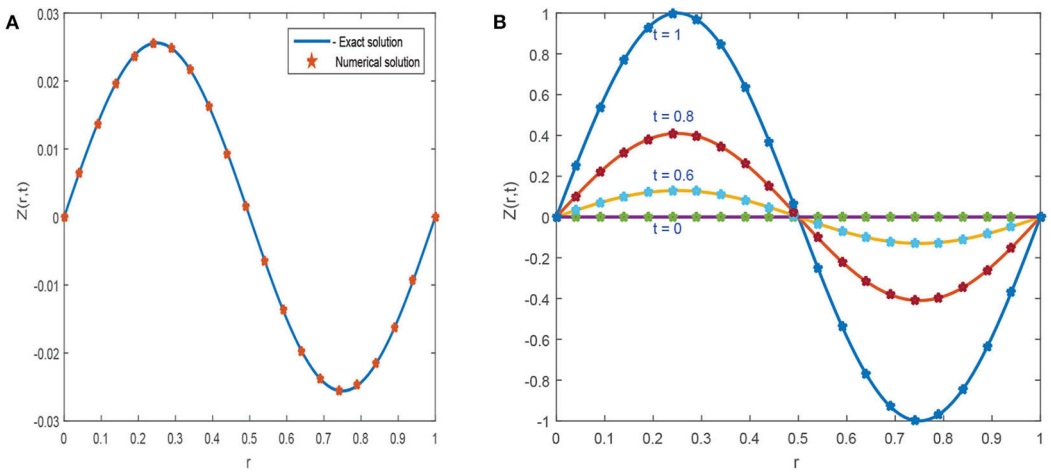

FIGURE 6 | Numerical solution of Example 5.3 for variation in time at $\alpha = 0.96$, $\nu = 1$, $h = 0.01$, $\Delta t = 0.0001$, and $\beta = 1$. **(A)** For $t = 0.25$. **(B)** For $t = 0,\ 0.5,\ 0.75,$ and 1.

TABLE 7 | Comparison of exact and numerical findings of Example 5.3 at various time stages.

$t = 0.6$		$t = 0.8$		$t = 1$	
Exact	**Approximate**	**Exact**	**Approximate**	**Exact**	**Approximate**
0	0	0	0	0	0
0.06925	0.06925	0.21951	0.21952	0.5358	0.5358
0.12044	0.12043	0.38072	0.387087	0.92972	0.92974
0.12556	0.12543	0.39661	0.39665	0.9687	0.96854
0.08257	0.08258	0.26105	0.26126	0.63743	0.63782
0.008124	0.008321	0.02577	0.02573	0.06254	0.06258
-0.069443	-0.069432	-0.21942	-0.21946	-0.53582	-0.53543
-0.120415	-0.120325	-0.38083	-0.38072	-0.92982	-0.92984
-0.125432	-0.125412	-0.39662	-0.39663	-0.96841	-0.96872
-0.082581	-.082573	-0.26149	-0.26144	-0.63723	-0.63712
0	0	0	0	0	0

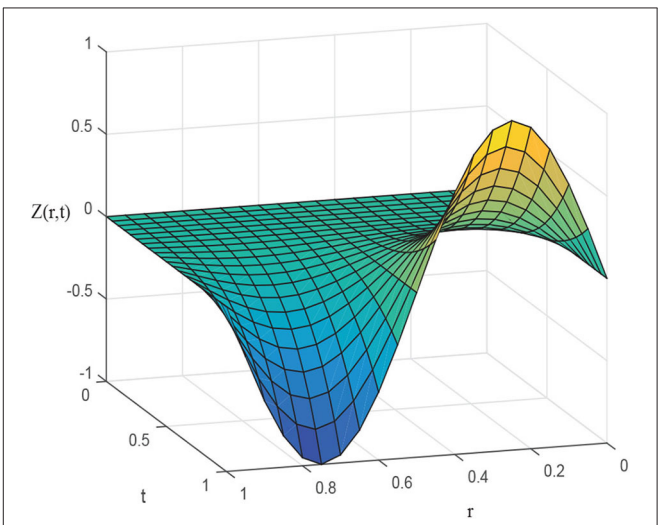

FIGURE 7 | 3D image of approximate results of Example 5.3 for $t \in [0, 1]$, $\alpha = 0.96$, step size $h = 0.01$, $\Delta t = 0.0001$, and $\nu = 1$.

TABLE 8 | Comparison of error norms of Example 5.3.

t	L^2 *norm*	L^∞ *norm*	CPU time
0.6	2.541×10^{-5}	1.97×10^{-4}	0.0930
0.8	6.371×10^{-4}	6.366×10^{-3}	0.1203
1	5.383×10^{-5}	3.9×10^{-4}	0.1561

Thus, the approximate solution (2.3) can be written in piecewise form:

$$Z(r, t_n) = \Upsilon_{j-3}\phi_{3,j-3}(r) + \Upsilon_{j-2}\phi_{3,j-2}(r) + \Upsilon_{j-1}\phi_{3,j-1}(r) + \Upsilon_j\phi_{3,j}(r), \quad r \in [r_j, r_{j+1}). \tag{5.8}$$

$$Z_N(r,1) = \begin{cases} -17815.0r^3 + 3562.9r^2 + 0.008r - 23.753, & r \in [0, 0.1), \\ 5938.2r^3 - 3562.9r^2 + 712.59r - 47.506, & r \in [0.1, 0.2), \\ 0.033333r^3 - 0.045r^2 + 0.0195r - 0.00085, & r \in [0.2, 0.3), \\ -0.025r^2 + 0.0155r - 0.00058333, & r \in [0.3, 0.4), \\ 1490.3r^3 - 1788.4r^2 + 715.36r - 95.38, & r \in [0.4, 0.5), \\ -4470.7r^3 + 7153.2r^2 - 3755.4r + 649.75, & r \in [0.5, 0.6), \\ 4470.8r^3 - 8941.7r^2 + 5901.5r - 1281.6, & r \in [0.6, 0.7), \\ -1490.1r^3 + 3576.4r^2 - 2861.1r + 762.98, & r \in [0.7, 0.8), \\ 0.016667r^3 + 0.005r^2 - 0.0425r + 0.020917, & r \in [0.8, 0.9), \\ -0.033333r^3 + 0.14r^2 - 0.164r + 0.057367, & r \in [0.9, 1). \end{cases} \tag{5.9}$$

Figure 6A, displays the numerical and exact solution of Example 5.3 for $t = 0.4$, $\alpha = 0.96$, $h = 0.01$ and $\Delta t = 0.0001$. The graphics illustrate that numerical and exact solutions are obviously shown to be indiscriminately comparable to one another. The effect of time concentrations $t = 0.6$, 0.8, and 1 is studied and presented in **Figure 6B** keeping other parameters constant. It can be seen from graphics that both solutions have symmetrical conduct and their corresponding numerical data are presented in **Table 7**, which demonstrates that both results are accurate and have negligible error. **Figure 7** plots three-dimensional solution and results of error norms is given in **Table 8**.

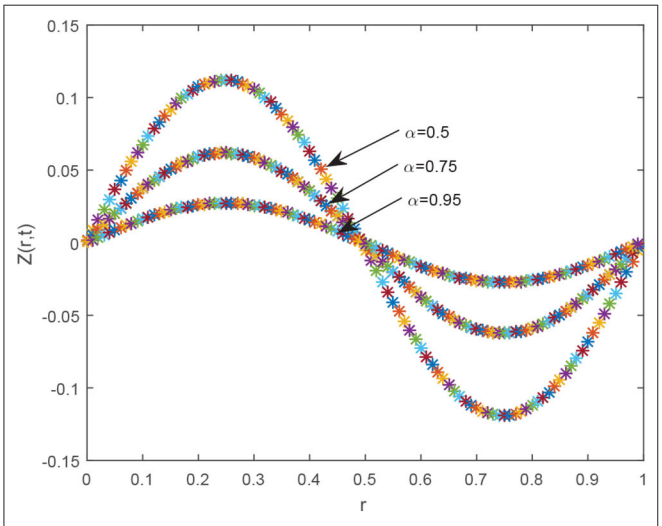

FIGURE 8 | Approximate results of Example 5.3 for $\alpha = 0.5,\ 0.75$ *and* 0.95, $h = 0.01$, $\Delta t = 0.0001$, and $\nu = 1$.

The influence of Brownian motion, i.e, $\alpha = 0.25,\ 0.75$, on solution curve is displayed in **Figure 8**. The identical behavior of solution curves demonstrates that for smaller values of α, the solution profile is away from the exact result and as $\alpha \to 1$, the approximate and exact solution tends to overlap.

Example 5.4. Fisher's equation with fractional order for $\beta = 1$ with $f(r,t) = 0$, is

$$\frac{\partial^{\alpha} Z(r,t)}{\partial t^{\alpha}} - \nu \frac{\partial^2 Z(r,t)}{\partial r^2} - Z(r,t)(1 - Z(r,t)) = f(r,t). \quad (5.10)$$

$$with\ IC:\ Z(r,0) = \sigma^*, \quad 0 \le r \le 1.$$

The exact solution of the model for $\alpha = 1$ is,

$$Z(r,t) = \frac{\exp(t)\sigma^*}{1 - \sigma^* + \sigma^* \exp(t)}.$$

The graphical illustration of exact and numerical solutions for Example 5.4 are shown in **Figure 9**. **Figure 9A** shows compatibility of exact and numerical results for $h = 0.01$, $\Delta t = 0.02$, $\alpha = 1$, and $\sigma^* = 0.25$. The multiple curves for exact and numerical solutions for various values of $\sigma^* = 0.5, 0.7$, and 0.9 are shown in **Figure 9B**. The comparison of exact and approximate solutions acquired by the proposed scheme is expressed in **Table 9**. The tabular data demonstrate that both solutions are compatible with each other for various values of σ^*. **Table 10** demonstrates the error norms.

6. CONCLUDING REMARKS

In this study, cubic B-spline (CBS) scheme has been successfully implemented to acquire numerical solution of

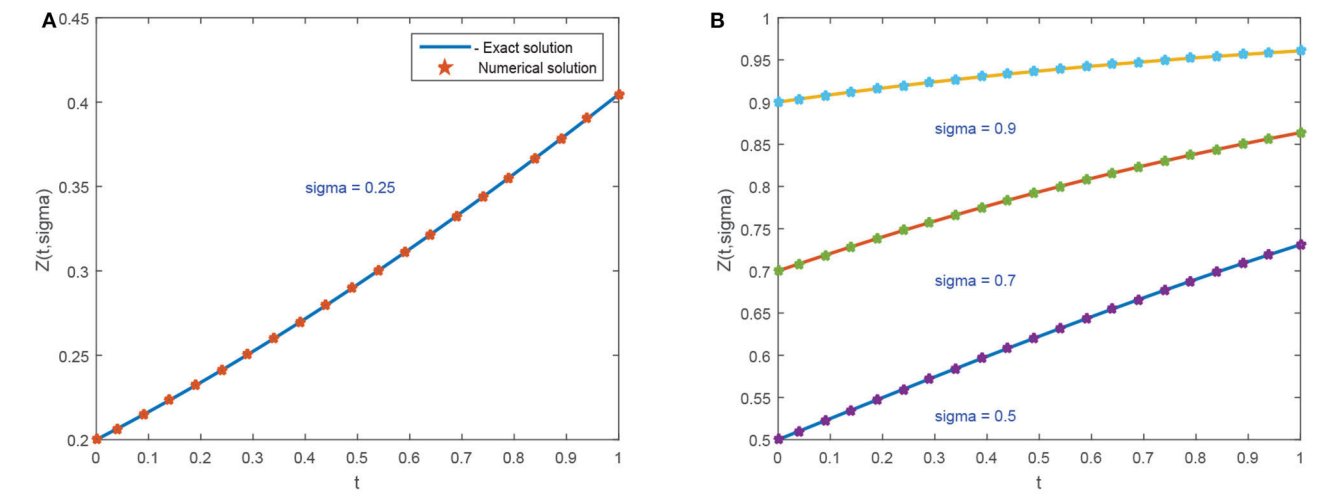

FIGURE 9 | Numerical results of Example 5.4 for various values of σ^* and $\alpha = 1$, $\Delta t = 0.02$, and $h = 0.01$. **(A)** For $\sigma^* = 0.25$. **(B)** For $\sigma^* = 0.5,\ 0.7$, and 0.9.

TABLE 9 | Exact and numerical results of Example 5.4 at different values of σ^*.

$\sigma^* = 0.5$		$\sigma^* = 0.7$		$\sigma^* = 0.9$	
Exact	**Approximate**	**Exact**	**Approximate**	**Exact**	**Approximate**
0.5	0.5	0.7	0.7	0.9	0.9
0.5224848	0.5224743	0.7185535	0.7185432	0.9078134	0.9078432
0.5473576	0.5473321	0.7383282	0.7383321	0.9158479	0.9158980
0.5719961	0.5719883	0.7571831	0.7571743	0.9232413	0.9232421
0.5962826	0.5961235	0.7750933	0.7750653	0.9300348	0.9300343
0.6201064	0.6201432	0.7920452	0.7920876	0.9362685	0.9362651
0.6433651	0.6433321	0.8080358	0.8080213	0.9419815	0.9419821
0.6659669	0.6659442	0.8230715	0.8230342	0.9472112	0.9472131
0.6878313	0.6878321	0.8371669	0.8371321	0.9519936	0.9519527
0.7088901	0.7088870	0.8503435	0.8503876	0.9563626	0.9563984
0.7310585	0.7310572	0.8638095	0.8638451	0.9607296	0.9607481

TABLE 10 | Comparison of error norms.

σ^*	L^2 *norm*	L^∞ *norm*	**CPU time**
0.5	1.706×10^{-5}	1.591×10^{-4}	0.0811
0.75	9.38×10^{-6}	4.4×10^{-5}	0.1209
1	8.192×10^{-6}	5.01×10^{-5}	0.1606

a time-fractional modified Fisher's equation for $\beta = 2$ and 3. The temporal derivative is discretized in the Caputo's sense by means of $L1$ formula, whereas CBS functions have been used for spatial derivative. The results acquired by the proposed scheme are presented in the form of tables and graphics. Following are the main outcomes of this study.

1. The existing Fisher's model has been modified by adding source term and by increasing integer power of non-linear term.
2. The influence of α parameter has been studied for different values and observed that, as the value of α increases gradually, the solution profile $Z(r, t)$ tends toward exact solution. The numerical solution overlaps the exact solution as α approaches 1 as shown in figures.
3. The numerical behavior of the proposed model with different initial and boundary conditions has been observed at different time levels.
4. The comparison of exact and numerical results displayed in graphics reveals that both results show symmetrical behavior and their corresponding numerical data presented in tables clearly elaborate consistency of the results.
5. The results of the study regarding stability of the presented scheme show that proposed scheme is unconditionally stable.

Moreover, the accuracy and efficiency of the proposed scheme is quantified by computing error norms and the numerical results reflect that the proposed scheme is applicable for non-linear time fractional generalized Fisher's equation.

AUTHOR CONTRIBUTIONS

All authors listed have made a substantial, direct and intellectual contribution to the work, and approved it for publication.

REFERENCES

1. Caputo M. *Elasticita e Dissipazione*. Bologna: Zanichelli (1969).
2. Miller KS, Ross B. *An Introduction to Fractional Calculus and Fractional Differential Equations*. New York, NY: Wiley (1993).
3. Liao SJ. Homotopy analysis method: a new analytic method for nonlinear problems. *Appl Math Mech*. (1998) **19**:957–62. doi: 10.1007/BF02457955
4. Scalar E, Gorenflo R, Mainardi F. Fractional calculus and continuous time finance. *Phys A*. (2000) **284**:376–84. doi: 10.1016/S0378-4371(00)00255-7
5. West BJ, Turalskal M, Grigolini P. Fractional calculus ties the microscopic and macroscopic scales of complex network dynamics. *New J Phys*. (2015) **17**:045009. doi: 10.1088/1367-2630/17/4/045009
6. Tarasov VE. Fractional vector calculus and fractional Maxwell's equations. *Ann Phys*. (2008) **323**:2756–78. doi: 10.1016/j.aop.2008.04.005
7. Rossa J, Villaverdeb AF, Bangab JR, Vazquezc S, Moranc F. A generalized Fisher equation and its utility in chemical kinetics. *Proc Natl Acad Sci USA*. (2010) **107**:12777–81. doi: 10.1073/pnas.1008257107
8. Ammerman AJ, Cavalli-Sforza LL. *The Neolithic Transition and the Genetics of Population in Europe*. Princeton, NJ: Princeton University Press (1984).
9. Kerke VM. Results from variants of the Fisher equation in the study of epidemics and bacteria. *Phys A*. (2004) **342**:242–8. doi: 10.1016/j.physa.2004.04.084
10. Fisher RA. The wave of advance of advantageous genes. *Ann Eugen*. (1937) **7**:355–69. doi: 10.1111/j.1469-1809.1937.tb02153.x
11. Podlubny I. *Fractional Differential Equations, Vol. 198 of Mathematics in Science and Engineering*. San Diego, CA: Academic Press (1999).
12. Odibat Z. Approximation of fractional integrals and caputo fractional derivatives. *Appl Math Comput*. (2006) **178**:527–33. doi: 10.1016/j.amc.2005.11.072
13. Baleanu D, Diethelm K, Scalas E, Trujillo JJ. *Fractional Calculus Models and Numerical Methods, Vol. 3 of Series on Complexity, Nonlinearity and Chaos*. Singapore: World Scientific (2012).
14. Baranwal VK, Pandey RK, Tripathi MP, Singh OP. An analytic algorithm for time fractional nonlinear reaction diffusion equation based on a new iterative method. *Commun Nonlin Sci Numer Simul*. (2012) **17**:3906–21. doi: 10.1016/j.cnsns.2012.02.015
15. Yang XJ, Machado JAT, Baleanu D. Anomalous diffusion models with general fractional derivatives within the kernels of the extended Mittag Leffler type functions. *Rom Rep Phys*. (2017) **69**:120. Available online at:http://hdl.handle.net/20.500.12416/1850
16. Yang XJ. Fractional derivatives of constant and variable orders applied to anomalous relaxation models in heat-transfer problems. *Therm Sci*. (2017) **21**:116–71. doi: 10.2298/TSCI161216326Y
17. Yang XJ, Machado JAT, Cattani C, Gao F. On a fractal LC-electric circuit modeled by local fractional calculus. *Commun Nonlinear Sci Numer Simul*. (2017) **47**:200–6. doi: 10.1016/j.cnsns.2016.11.017
18. Alaattin E, Ucar Y, Yagmurlu N, Tasbozan O. A Galerkin finite element method to solve fractional diffusion and fractional diffusionwave equations. *Math Model Anal*. (2013) **18**:260–73. doi: 10.3846/13926292.2013.783884
19. Rubin SG, Graves RA. *Cubic Spline Approximation for Problems in Fluid Mechanics*. Washington, DC: NASA TR R-436 (1975).
20. Wazwaz AM, Gorguis A. An analytic study of Fishers equation by using Adomian decomposition method. *Appl Math Comput*. (2004) **154**:609–20. doi: 10.1016/S0096-3003(03)00738-0

21. Abedle-Rady AS, Rida SZ, Arafa AAM, Adedl-Rahim HR. Approximate analytical solutions of the fractional nonlinear dispersive equations using homotopy perturbation Sumudu transform method. *Int J Innov Sci Eng Technol*. (2014) **19**:257–67.
22. Gupta AK, Ray SS. On the solutions of fractional Burgers Fisher and generalized Fishers equations using two reliable methods. *Int J Math Math Sci*. (2014) **2014**:682910. doi: 10.1155/2014/682910
23. Cherif MH, Belghaba K, Zaine D. Homotopy perturbation method for solving the fractional Fishers equation. *Int J Anal Appl*. (2016) **101**:916.
24. Khader MM, Saad KM. A numerical approach for solving the fractional Fisher equation using Chebyshev spectral collocation method. *Chaos Solit Fract*. (2018) **110**:169177. doi: 10.1016/j.chaos.2018.03.018
25. Rawashdeh MS. The fractional natural decomposition method: theories and applications. *Math Methods Appl Sci*. (2016) **40**:2362–76. doi: 10.1002/mma.4144
26. Singh H. An efficient computational method for the approximate solution of nonlinear Lane-Emden type equations arising in astrophysics. *Astrophys Space Sci*. (2018) **363**:71. doi: 10.1007/s10509-018-3286-1
27. Singh H. Approximate solution of fractional vibration equation using Jacobi polynomials. *Appl Math Comput*. (2018) **317**:85–100. doi: 10.1016/j.amc.2017.08.057
28. Majeed A, Piah ARM, Rafique M, Abdullah JY, Rajion ZA. NURBS curves with the application of multiple bones fracture reconstruction. *Appl Math Comput*. (2017) **315**:70–84. doi: 10.1016/j.amc.2017.05.061
29. Singh J, Kumar D, Swroop R. Numerical solution of timeand space-fractional coupled Burgers equations via homotopy algorithm. *Alex Eng J*. (2016) **552**:1753–63. doi: 10.1016/j.aej.2016.03.028
30. Najeeb AK, Ayaz F, Jin L, Ahmet Y. On approximate solutions for the time-fractional reaction-diffusion equation of Fisher type. *Int J Phys Sci*. (2011) **6**:2483–96.
31. Sayevand K, Yazdani A, Arjang F. Cubic B-spline collocation method and its application for anomalous fractional diffusion equations in transport dynamic systems. *J Vib Control*. (2016) **22**:2173–86. doi: 10.1177/1077546316636282
32. Dag I, Irk D, Saka B. A numerical solution of Burgers equation using cubic B-splines. *Appl Math Comput*. (2005) **163**:199–211. doi: 10.1016/j.amc.2004.01.028

Conflict of Interest: The authors declare that the research was conducted in the absence of any commercial or financial relationships that could be construed as a potential conflict of interest.

The reviewer HS declared a past co-authorship with one of the authors JS to the handling editor.

Frontiers in Physics

Investigates complex questions in physics to understand the nature of the physical world

Addresses the biggest questions in physics, from macro to micro, and from theoretical to experimental and applied physics.

Discover the latest Research Topics

See more →

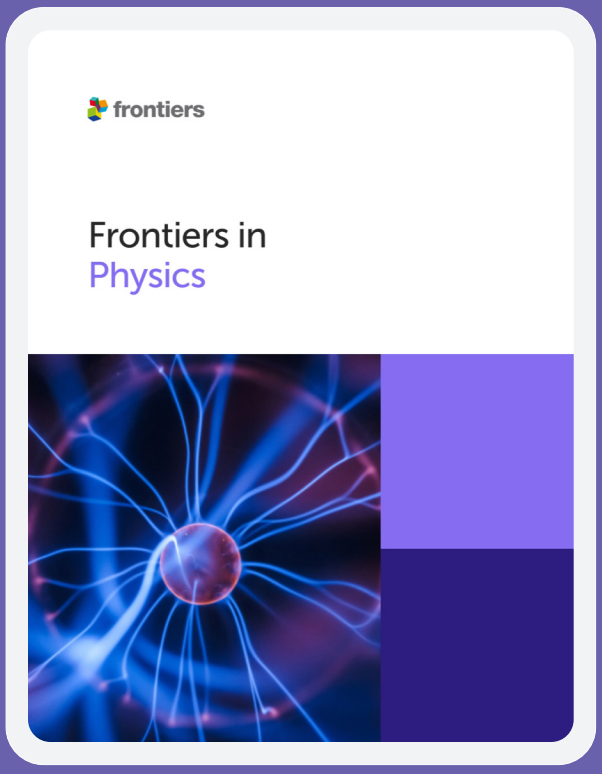

Frontiers

Avenue du Tribunal-Fédéral 34
1005 Lausanne, Switzerland
frontiersin.org

Contact us

+41 (0)21 510 17 00
frontiersin.org/about/contact